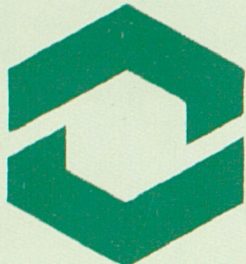


# European cooperation in the field of scientific and technical research

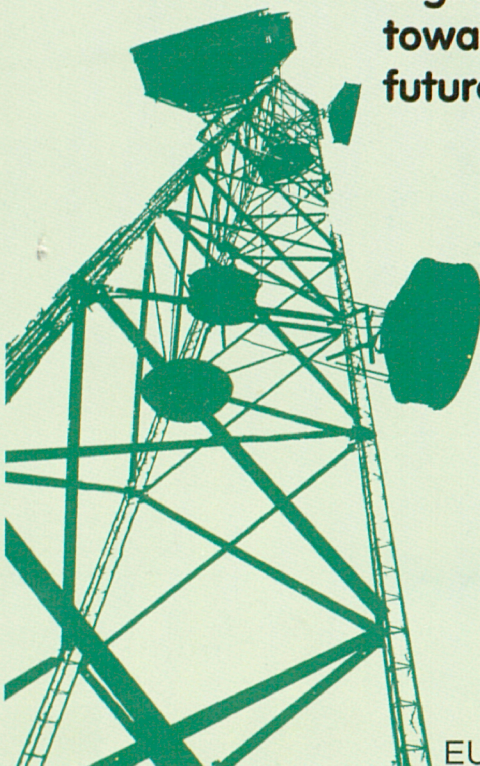
## COST telecommunications



### COST Action 231

Digital mobile radio  
towards  
future generation systems

Final report



EUR 18957

Austria  
Belgium  
Croatia  
Czech Republic  
Denmark  
Estonia  
Finland  
France  
Germany  
Greece  
Hungary  
Iceland  
Ireland  
Italy  
Luxembourg  
Malta  
Norway  
Poland  
Portugal  
Romania  
Slovakia  
Slovenia  
Spain  
Sweden  
Switzerland  
The Netherlands  
Turkey  
United Kingdom



European  
Commission

**European Commission**  
**Directorate General XIII — Information Society: Telecommunications,  
Markets, Technologies — Innovation and Exploitation of Research**  
**Directorate G**  
**Rue de la Loi, 200**  
**B-1049 Brussels, Belgium**

**Tel:** (32-2) 29 902 35  
**Fax:** (32-2) 296 29 81  
**E-mail:** Cost@bxl.dg13.cec.be  
<http://www.cordis.lu/cost/src/telecom.htm>

European Commission

# **COST Action 231**

## **Digital mobile radio towards future generation systems**

**Final report**

Directorate-General  
Telecommunications, Information society, Information Market,  
and Exploitation of Research

1999

EUR 18957

## **LEGAL NOTICE**

Neither the European Commission nor any person acting on behalf of the Commission is responsible for the use which might be made of the following information.

A great deal of additional information on the European Union is available on the Internet. It can be accessed through the Europa server (<http://europa.eu.int>).

Cataloguing data can be found at the end of this publication.

Luxembourg: Office for Official Publications of the European Communities, 1999

ISBN 92-828-5416-7

© European Communities, 1999

Reproduction is authorised provided the source is acknowledged.

*Printed in Belgium*

PRINTED ON WHITE CHLORINE-FREE PAPER

# **DIGITAL MOBILE RADIO TOWARDS FUTURE GENERATION SYSTEMS**

## **COST 231 Final Report**

*This book presents the European COST Action 231 view on the evolution of mobile radio towards next generation systems.*

*COST 231 during its six year life has produced a number of Temporary Documents (TDs). Reference to such documents, whenever possible, has been avoided throughout the book by replacing them with references to papers and articles published in the open literature and originated from them. However, when reference is made to a TD, the reader should be aware that the document could be obtained either directly from the authors or by COST Telecom Secretariat and the COST 231 Chairman, at the following addresses:*

<b>COST Telecom Secretariat</b>	<b>Eraldo Damosso</b>
<b>BU-9, 2/94</b>	<b>CSELT S.p.A</b>
<b>200, rue de la Loi</b>	<b>Via G. Reiss Romoli, 274</b>
<b>B-1049 Brussels</b>	<b>I-10148 Turin</b>
<b>Fax: +32 2 296 2981</b>	<b>Fax: +39 11 228 5577</b>
<b>E-mail:</b>	<b>E-mail:</b>
<b><i>COST@postman.dg13.cec.be</i></b>	<b><i>eraldo.damosso@cselt.it</i></b>



---

## Editors' Preface

It is rather difficult to consider a new publication on mobile radio as an actual novel book, due to the proliferation of literature and contributions on this subject. Nevertheless, the turbulence of the environment and the fast development of mobile communications world tend to make any publication rapidly obsolete and subsequently a dissemination of up-to-date information is required. In such a context, this book may be considered as an excellent synthesis of the fresh achievements resulting from the activities carried out during the past six years by a huge number of European experts in different areas of wireless communications. The contributors come from about a hundred of different Institutions, such as public and private operators, universities, research bodies, manufacturers, involved at various levels in COST Action 231, "*Evolution of Land Mobile Radio (including personal) Communications*", aimed at identifying the most likely migration paths from current cellular networks towards next generation universal systems.

The book, which summarises the most significant results obtained by such a group of distinguished experts, covers a wide range of topics, starting from radio system aspects (investigating and comparing various access, modulation and coding schemes), going through propagation issues (considering measurements, models and simulation tools related to different environments, from macro- to micro- and pico-cell coverage), to end with broadband communications services (i.e., services requiring a capacity greater than that of the basic ISDN services), which involve a large spectrum of new telecom technologies at high microwave and millimetre wave bands for short range applications. Accordingly, the ambitious goal of this book is on one side to give a general overview of the ongoing researches in Europe to support the deployment of trans-European and world-wide systems and the development of specifications for future generation systems currently in progress within standardisation bodies. In addition, on the other side, the objective is to present novel approaches to face problems that such development may pose, and in several cases to suggest solutions which have been made possible only by the continuous interactions among the members of the Action and the stimulating discussions occurred within the three Working Groups created by the Management Committee.

In fact, COST, "European Co-operation in the field of Scientific and Technical research", is a framework for the preparation and implementation of European projects involving applied scientific research, within European Countries (but not limited to the European Union Member States) having signed the so-called "COST Treaty". Such COST framework was used to set up specific "projects", within several activity domains, from Agriculture to Chemistry, Environment, Food technology, Medical research, Meteorology, Transport, etc. Recently events in Central and Eastern Europe have made the original list of members somewhat

obsolete: COST now involves 26 states, but the principles have remained mostly unchanged, and each signatory enjoys the same rights and privileges within COST. This is in agreement with the spirit of the initiative, which is to stimulate "cross-fertilisation" across all the organisations having interests in a given field. Financing of researches is in fact provided by each member state (and very often by each organisation involved in the Projects), while the co-ordination costs are funded by both the participating countries and the European Commission. A special feature of all COST Actions is the complete freedom of participation of each country involved: any COST country can join any Action by signing the "Memorandum of Understanding" (MoU), which is the formal basis of each Action.

In such a context, COST Telecommunications Actions have an important role to play in the development of our networked society. They should be proactive in the challenging times presented by these rapid changes: not only COST must be at the forefront of research, but it also must ensure that the broad international collaborative perspective be maintained. COST Actions have to investigate those technologies most appropriate to the future environment, so as to minimise potential duplication of research and maximise the size of the eventual marketplace. COST Telecommunications in fact involve research topics that are strategic to the development of the information society. These areas include radio and optical communications, signal processing, future user requirements, to name but a few.

As said before, COST Actions are funded nationally either by the member states or the participating institutions, in contrast to other European researches, such as RACE Projects in the recent past and ACTS projects nowadays, which are funded by the European Union. Such a voluntary form of collaboration which does not require an "*a priori*" agreed overall research policy, in conjunction with the "*bottom-up*" principle which distinguishes all COST Actions, allowed in particular COST 231 to focus on several themes of personal communications, on the only condition that the activities are approved by the internal Management Committee which is responsible for administering the Action.

As a matter of fact, this is not a book for students or a text for senior level or advanced graduate courses, although its completeness and the comprehensive approach to the world of mobile and personal communications might make it useful also for this specific purpose. The original intention of COST 231 Management Committee was to address a much wider audience, not limited to the scientific/technical level, but including also operators, manufacturers and regulatory bodies at the managing level, in order to bear witness of what an heterogeneous group working on a pure voluntary basis, but stimulated by common aims and interests, can obtain in a free environment. Furthermore, a not negligible result could also to provide all the potential players in the mobile radio scenario with suitable guidelines and tools for a correct understanding of what are the most likely and fruitful current paths in the somewhat confusing (but intriguing) situation. In this respect, as editors of this book, we are proud to introduce a work which can be considered at least at the same level of an outstanding forerunner, COST Action 207, which played a unique role in supporting the Group Spécial Mobiles in their work

that led to the definition (and subsequent world-wide implementation) of the Global System for Mobile Communications (GSM).

A special acknowledgement is made to the invaluable work of the vast group of contributors, authors and co-editors, whose commitment to the common cause made it possible to edit the text, notwithstanding the difficulties in reaching a sufficient degree of harmonisation of the contents and avoiding at the same time any drawback due to potential duplication or overlapping. Many thanks in particular to the former Chairman, Mr. P. Porzio Giusto, the Vice-Chairman, Mr. G. de Brito, to the Working Groups Chairmen (Prof. J. Bach Andersen, Prof. S.K. Barton, Mr. R.J. Goodwin, Mr. P. Porzio Giusto, Prof. P.A. Watson) for their co-ordination efforts and the excellent management work during the entire life of the Action. The edition of this book was initiated by Eraldo Damosso, which unfortunately could not finish it, due to health problems, hence being terminated by Luis M. Correia and taking much more time than it was supposed to; as a consequence, some chapter editors had to be replaced in the middle of the editing process, and new ones had to be found - to those who accepted the challenging task of finishing the edition of chapters in difficult circumstances a special word of acknowledgement. Finally, last but not least, our sincere thanks to the whole COST 231 Management Committee for submitting contributions which served as a basis for this book and for the useful discussions which resulted into a significant improvement of the original text.

*Eraldo Damosso  
(Chairman, COST 231)  
Luis M Correia*



---

## Table of Contents

<b>Editors' Preface</b>	<b>v</b>
<b>Table of Contents</b>	<b>ix</b>
<b>List of Figures</b>	<b>xv</b>
<b>List of Tables</b>	<b>xxv</b>
<b>List of Acronyms</b>	<b>xxix</b>
<b>Introduction</b>	<b>1</b>
<b>1 COST 231 in the European Telecommunication Environment</b>	<b>5</b>
1.1 The Evolutionary Vision of Mobile Communications in Europe	5
1.2 System Migration Prerequisites	10
1.2.1 Frequency Allocations and Spectrum Efficiency	10
1.2.2 Enabling Technologies and Advanced Service Provision	14
1.2.3 Terrestrial/Satellite Mobile Networks Integration	16
1.2.4 Standardisation	17
1.3 Medium/Long-Term Action Perspectives	18
1.3.1 Objectives and Participation	18
1.3.2 Liaisons with European Research and Specification Bodies	19
1.3.3 Action Activities	19
1.4 Outline of the Contents	20
1.4.1 Narrowband & Wideband Communications	20
1.4.2 Broadband Communications	23
1.5 References	25
<b>2 Radio Channel Characterisation</b>	<b>27</b>
2.1 Characteristics of Radio Channels	28
2.1.1 Field Direction-Delay-Spread Function	28
2.1.2 Space-Dependent Channel Impulse Response	30
2.1.3 Time-Dependent Channel Response	31
2.1.4 The Sources of Randomness	32
2.1.5 Characterisation of the Small-Scale/Short-Term Fluctuations	33
2.1.6 Characterisation of the Large-Scale Fluctuations of the Channel	42
2.2 Measurement Techniques - Channel Sounders	44
2.2.1 Pulse Sounders	45
2.2.2 Time Domain Sounders	45
2.2.3 Frequency Domain Sounders	50
2.3 Propagation Measurements and their Analysis	51
2.3.1 The Need for Propagation Measurements	51

2.3.2 Objectives of the COST 231 Propagation Measurements	51
2.3.3 Narrowband and Wideband Measurements	52
2.3.4 Analysis of Propagation Measurements	53
2.3.5 Indoor Measurements	53
2.3.6 Outdoor Measurements	57
2.3.7 Fading and Path Loss Characteristics	57
2.3.8 Results for Frequency Selectivity in Different Environments	58
2.3.9 Determination of Directions-of-Arrival	60
<b>2.4 Propagation Modelling for the Simulation of the Radio Channel</b>	<b>61</b>
2.4.1 Radio Channel Simulation	61
2.4.2 Long Term Area Simulations	62
2.4.3 Narrowband System Simulations	63
2.4.4 Wideband System Simulations	63
2.4.5 UMTS Simulators	66
2.4.6 Hardware Channel Simulators	68
<b>2.5 References</b>	<b>71</b>
<b>3 Antennas and Antenna Diversity</b>	<b>79</b>
<b>3.1 Antenna Design</b>	<b>80</b>
3.1.1 Extremely Wideband Antennas	80
3.1.2 Millimetre-Wave Antennas	82
3.1.3 Internal Antennas for Handsets	85
<b>3.2 Base Station Antenna Relations</b>	<b>86</b>
3.2.1 Angular Relations between BS-Antennas and Radio Environment	86
3.2.2 Environmental Influence on Perceived Antenna Pattern	88
3.2.3 Adaptive Base Station Antenna Arrays	91
<b>3.3 Antennas for Portables</b>	<b>92</b>
3.3.1 Antenna Performance	92
3.3.2 Antenna Configurations for Reducing Body Loss	94
<b>3.4 Mobile and Base Station Diversity Techniques</b>	<b>96</b>
3.4.1 Diversity Domains	96
3.4.2 Base Station Antenna Diversity for Outdoor Environments	98
3.4.3 Base Station Diversity for Indoor Environments	100
3.4.4 Mobile Antenna Diversity	101
3.4.5 Wideband Correlation	102
<b>3.5 Combining Techniques</b>	<b>102</b>
3.5.1 Gain and Complexity for Different Combining Techniques	103
3.5.2 Influence of the Time-Variant Channel	104
<b>3.6 Macro and Micro-Diversity Gain</b>	<b>105</b>
3.6.1 Macro Diversity	105
3.6.2 Micro Diversity	107
3.6.3 Wideband Diversity Performance	110
<b>3.7 References</b>	<b>110</b>

<b>4 Propagation Prediction Models</b>	<b>115</b>
<b>4.1 General Considerations</b>	<b>115</b>
<b>4.2 Geographical Information for Propagation Modelling &amp; Simulation</b>	<b>117</b>
4.2.1 Canonical Scattering Problems	117
4.2.2 Acquisition of Geographical Data	120
4.2.3 Accuracy of Data	121
4.2.4 Model Evaluation	121
4.2.5 Manipulation of Geographical Data	122
4.2.6 Exchange of Measurement and Geographic Information	123
<b>4.3 Propagation Mechanisms</b>	<b>124</b>
4.3.1 General	124
4.3.2 Propagation Mechanisms in Ray Theory	127
4.3.3 Other Propagation Mechanisms	131
4.3.4 Main Propagation Mechanisms	132
<b>4.4 Propagation Models for Macro-Cells</b>	<b>134</b>
4.4.1 Semideterministic and Empirical Models for Urban Areas	134
4.4.2 Influence of Vegetation	140
4.4.3 Modelling of Large-Scale Terrain Variations	140
4.4.4 Estimation of Time Dispersion	145
4.4.5 General Models	147
<b>4.5 Propagation Models for Small- and Micro-Cells</b>	<b>149</b>
4.5.1 General	149
4.5.2 Two-Dimensional Models for Below Roof-Top Propagation	150
4.5.3 Two-Dimensional Models for Over Roof-Top Propagation	153
4.5.4 Three-Dimensional Models for Arbitrary Base-Station Heights	155
4.5.5 Overview about the Prediction Models	158
4.5.6 Comparison with Path Loss Measurements at 947 MHz	158
<b>4.6 Building Penetration</b>	<b>167</b>
4.6.1 Introduction and Definitions	167
4.6.2 Building Penetration Loss at Line of Sight Conditions	169
4.6.3 Penetration Loss at Non Line of Sight Conditions	171
4.6.4 General Building Penetration Model	174
<b>4.7 Indoor Propagation Models</b>	<b>175</b>
4.7.1 General	175
4.7.2 Empirical Narrow-Band Models	176
4.7.3 Empirical Wide-Band Models	179
4.7.4 Modelling the Time Fluctuations of the Indoor Channel	181
4.7.5 Deterministic Models	183
4.7.6 Comparison of the Performance of the Path Loss Models	186
<b>4.8 Tunnels, Corridors and Other Special Environments</b>	<b>190</b>
4.8.1 Tunnels	190
4.8.2 Loss Models and Coverage	191
4.8.3 Leaky Feeders	194
4.8.4 Railway Environment and High-Speed Trains	195
4.8.5 Scaled-Model Measurements	196
<b>4.9 References</b>	<b>197</b>

<b>5 Research into Performance and Enhancements of Second Generation Systems: GSM and DECT</b>	<b>209</b>
<b>5.1 General Considerations</b>	<b>209</b>
<b>5.2 On Antenna and Frequency Diversity in GSM</b>	<b>210</b>
5.2.1 The GSM Test Profiles	210
5.2.2 The GSM TCH/FS Transmission Mode	212
5.2.3 GSM Link Tests	213
5.2.4 Frequency Diversity	214
5.2.5 Antenna Diversity	216
5.2.6 Antenna Diversity Performance Results	219
<b>5.3 Capacity Study of a Frequency Hopping GSM Network</b>	<b>222</b>
5.3.1 Conventional Fixed Frequency Reuse Schemes	222
5.3.2 Frequency Reuse on Hopping TCH Carriers	223
5.3.3 Impact of Allocated Frequency Spectrum	224
5.3.4 Results from GSM Network Simulations	225
5.3.5 Interference Gain from Fractional Loading	228
5.3.6 Potential Capacity Gain from Smart Antenna Systems	230
<b>5.4 The DECT Standard</b>	<b>232</b>
5.4.1 General	232
5.4.2 The DECT Standard and its Challenges	232
<b>5.5 A Physical and Medium Access Layer DECT Testbed</b>	<b>235</b>
5.5.1 Modelling of a DECT Wireless Link	235
5.5.2 The DECT Testbed	235
<b>5.6 Propagation Studies for DECT Environments</b>	<b>237</b>
5.6.1 Measurement Results	237
5.6.2 Channel Models	239
<b>5.7 Basic Performance of DECT</b>	<b>241</b>
<b>5.8 DECT Radio Performance Enhancement</b>	<b>246</b>
5.8.1 Standard Spatial Diversity: Switch and Selection Techniques	246
5.8.2 Diversity Techniques in Dynamic Channels	249
5.8.3 Equalisation Techniques for DECT	251
5.8.4 An Advanced DECT Receiver Concept	253
<b>5.9 A DECT Field Trial in a Multipath Environment</b>	<b>255</b>
5.9.1 The Measurement Equipment	257
5.9.2 Førde Measurements	258
5.9.3 Conclusions from Field Trial and Measurements	261
<b>5.10 Traffic Capacity for the DECT System</b>	<b>263</b>
5.10.1 WPBX Application	263
5.10.2 RLL Application	269
<b>5.11 References</b>	<b>276</b>
<b>6 Advanced Radio Interface Techniques and Performance</b>	<b>285</b>
<b>6.1 Modulation and Channel Coding</b>	<b>287</b>
6.1.1 Linear Modulation	287
6.1.2 Continuous Phase Modulation	291

6.1.3 Performance of MSK in Time Dispersive Channels	294
6.1.4 Trellis Coded Modulation	297
<b>6.2 Equalisation</b>	<b>300</b>
6.2.1 Convergence of Classical Adaptive Algorithm	300
6.2.2 Advanced Equaliser Techniques	300
6.2.3 Joint Diversity and Equalisation Techniques	301
<b>6.3 Enhanced TDMA</b>	<b>305</b>
6.3.1 TDMA Enhancements	305
6.3.2 Capacity Comparisons	309
6.3.3 Summary	311
<b>6.4 CDMA</b>	<b>312</b>
6.4.1 DS-CDMA	312
6.4.2 FH-CDMA	326
6.4.3 Hybrid DS/SFH CDMA	327
<b>6.5 CDMA with Multi-User Detection</b>	<b>331</b>
6.5.1 Joint Detection CDMA	331
6.5.2 Joint Parameter Estimation and Data Detection	334
6.5.3 CDMA with Interference Cancellation	336
<b>6.6 Hybrid TDMA/CDMA</b>	<b>340</b>
6.6.1 TDMA/SFH	340
6.6.2 JD-CDMA	340
6.6.3 CTDMA	341
<b>6.7 Multicarrier Techniques</b>	<b>343</b>
6.7.1 OFDM with Guard Time	343
6.7.2 OFDM without Guard Time	345
6.7.3 OFDM-CDMA	345
<b>6.8 MAC Protocols</b>	<b>350</b>
<b>6.9 References</b>	<b>353</b>
<b>7 Potential Radio Interface Subsystems</b>	<b>361</b>
<b>7.1 Advanced TDMA Mobile Access</b>	<b>361</b>
7.1.1 Design Rationale	361
7.1.2 Radio Access System Model	362
7.1.3 Transport Technique	364
7.1.4 ATDMA Control System	369
7.1.5 Logical Channels	372
7.1.6 Evaluation and Recommendations	373
<b>7.2 A CDMA Air-Interface for Mobile Access</b>	<b>374</b>
7.2.1 Project Rationale	374
7.2.2 Service Requirements for UMTS	374
7.2.3 Assessment of DS and FH CDMA for UMTS	374
7.2.4 Test Bed Specifications & Design Issues	378
7.2.5 Validation and Test Bed Performance	383
7.2.6 Conclusions	385
<b>7.3 Code Time Division Multiple Access</b>	<b>386</b>
7.3.1 Design Rationale	386

7.3.2 System Description	386
7.3.3 System Performance	391
7.3.4 Service Provision	393
7.3.5 Chip Rates, Spreading Factors, Symbol Rates and Bit Rates	395
7.3.6 Compatibility with GSM	399
<b>7.4 Joint Detection CDMA</b>	<b>400</b>
7.4.1 Design Rationale	400
7.4.2 System Description	402
<b>7.5 References</b>	<b>410</b>
 <b>8 Broadband Systems</b>	 <b>415</b>
<b>8.1 Introduction</b>	<b>415</b>
8.1.1 Infra-Red Safety	416
8.1.2 Millimetre Wave Safety and Technology	417
<b>8.2 Material Characterisation</b>	<b>418</b>
8.2.1 Measurement Methods	418
8.2.2 Measurement Results and Parameter Estimation	420
8.2.3 Isolation and Transmission of Building Materials	423
<b>8.3 Indoor Radio Channel</b>	<b>425</b>
8.3.1 Narrowband Measurements	425
8.3.2 Wideband Measurements	429
8.3.3 Statistical Modelling	432
8.3.4 Deterministic Modelling	435
<b>8.4 Outdoor Radio Channel</b>	<b>438</b>
8.4.1 Path Loss Modelling	439
8.4.2 Wideband Characterisation	442
<b>8.5 Transmission Performance Evaluation</b>	<b>446</b>
8.5.1 Early Performance Predictions	446
8.5.2 Spread Spectrum	447
8.5.3 Multicarrier Modulation	449
8.5.4 Antenna Diversity	449
8.5.5 Adaptive Equalisation	451
8.5.6 HIPERLAN	452
8.5.7 Channel Coding	454
<b>8.6 Network Performance Evaluation</b>	<b>455</b>
8.6.1 Centralised Control Based on Pooling	455
8.6.2 Centralised Control Based on Random Access	458
8.6.3 Distributed Networks	459
<b>8.7 Summary</b>	<b>463</b>
<b>8.8 References</b>	<b>464</b>
 <b>Annex I: List of Participating Entities</b>	 <b>469</b>
<b>Annex II: List of Editors/Contributors</b>	<b>473</b>

---

## List of Figures

Fig. 1.1	Evolution towards third/fourth generation systems with reference to RACE and ACTS programmes.	8
Fig. 1.2	WARC-92 frequency allocations to mobile services (1.6-2.5 GHz).	11
Fig. 1.3	General scheme of a multiple access to radio channel within a cell.	14
Fig. 1.4	Evolution timeline towards personal communications and multimedia services.	24
Fig. 2.1	Geometrical situation considered.	29
Fig. 2.2	Definition of the direction $\Omega$ and its associated unit vectors.	29
Fig. 2.3	Schematic of a time domain pulse sounder.	49
Fig. 2.4	Measured path loss as a function of distance between transmitter and receiver in a typical office building.	56
Fig. 2.5	Impulse response along a run of 300m in a micro cellular environment.	58
Fig. 2.6	Cumulative distributions of received power levels for 5 MHz, 1 MHz and 500 kHz bandwidth, evaluated from a micro cellular NLOS measurement.	59
Fig. 2.7	Delay-Doppler scattering function for a micro cellular NLOS situation.	60
Fig. 2.8	FIR filter implementation of a channel simulator.	65
Fig. 2.9	General structure of the CODIT channel emulator.	70
Fig. 3.1	Cross-section of a conical monopole antenna.	80
Fig. 3.2	Monopole antenna no. 1.	81
Fig. 3.3	Monopole antenna no. 2.	81
Fig. 3.4	SWR of monopole no. 1.	82
Fig. 3.5	SWR of monopole no. 2.	82
Fig. 3.6	Co-polarisation pattern of monopole antenna no. 1.	82
Fig. 3.7	Co-polarisation pattern of monopole antenna no. 2.	82
Fig. 3.8	Radiation pattern of the circular patch antenna.	83
Fig. 3.9	Geometry of biconical horn antenna.	83
Fig. 3.10	Measured and theoretical radiation pattern in the elevation plane.	84

Fig. 3.11	Radiation-coupled dual-L antenna mounted on top of the shielding case of a cordless telephone.	85
Fig. 3.12	Pattern influence of a mast placed 30 cm behind 8-element colinear array.	88
Fig. 3.13	Elevation pattern influence of roof 3 m below antenna (detail near the main lobe).	88
Fig. 3.14	Expected and measured relative angular level decrease for azimuthal shaped antenna pattern.	89
Fig. 3.15	Angular scattering function at a BS, i.e., PDP versus angle.	90
Fig. 3.16	Measured RSSI for sector antennas normalised by measured RSSI omnidirectional dipoles.	91
Fig. 3.17	The VSWR as a function of frequency for the FS-PIFA both for the handset used in speaking position and in standby.	93
Fig. 3.18	The radiation pattern for the handset <i>without</i> a model of the human head and hand.	95
Fig. 3.19	The radiation pattern for the handset <i>with</i> a model of the human head and hand.	95
Fig. 3.20	Average autocorrelation of the instantaneous rms delay spread versus separation in indoor environments at 1800 MHz.	102
Fig. 3.21	Diversity gain for a narrowband system with RSSI selection and for a wideband system with switch or selection combining based on RSSI and/or CRC as a function of the normalised combining rate.	104
Fig. 3.22	Cumulative distribution of the log-normal long-term fading, with standard deviations 5 and 10 dB.	106
Fig. 3.23	Cumulative distribution of the short-term fading, using two branch selection diversity with the correlation coefficients 0, 0.3, 0.7 and 1.	109
Fig. 4.3.1	Simulation of wave propagation.	126
Fig. 4.3.2	Ray theory.	126
Fig. 4.3.3	The first Fresnel zone.	127
Fig. 4.3.4	Propagation phenomena.	133
Fig. 4.4.1	Typical propagation situation in urban areas and definition of parameters used in the COST-WI model.	136
Fig. 4.4.2	Definition of the street orientation angle $\phi$ .	137
Fig. 4.4.3	Terrain profile at "Hjonrringvej".	143
Fig. 4.4.4	Measurement and prediction by the MFIE-method for the terrain profile "Hjonrringvej" at 970 MHz.	144
Fig. 4.4.5	Measurement and prediction by the MFIE-method for the terrain profile "Hjonrringvej" at 1900 MHz.	144

Fig. 4.4.6	Measured and predicted scattering functions using the Telekom model.	147
Fig. 4.4.7	Measured and predicted impulse responses in a hilly terrain using the IHE-receiver-near-range model at 947 MHz.	148
Fig. 4.5.1	Ray tracing within a vertical and a transverse Tx-Rx plane.	158
Fig. 4.5.2	Munich test site with measurement routes and transmitter location.	160
Fig. 4.5.3	Comparison between measured and predicted path loss along route Metro200.	163
Fig. 4.5.4	Comparison between measured and predicted path loss along route Metro201.	164
Fig. 4.5.5	Comparison between measured and predicted path loss along route Metro202.	165
Fig. 4.6.1	Definition of grazing angle $\theta$ and distances D, S and d.	169
Fig. 4.6.2	Non line of sight scenario when the external antenna is located above the building height.	172
Fig. 4.6.3	Non line of sight scenario when the external antenna is located below the building height.	172
Fig. 4.6.4	Relevant propagation paths into a building.	174
Fig. 4.7.1	Overall average power delay profiles in three configurations.	180
Fig. 4.7.2	Simulated receiver trajectory, and estimated and theoretical normalised power Doppler profile.	182
Fig. 4.7.3	2D view of the reception sphere.	184
Fig. 4.7.4	Ray launching.	184
Fig. 4.7.5	Map of the 2 <sup>nd</sup> floor of the office building with marked base and mobile locations.	186
Fig. 4.7.6	Performance of empirical and ray optical propagation models at 856 MHz in 4 successive floors.	189
Fig. 4.7.7	Performance of empirical and ray optical propagation models at 1800 MHz in 4 successive floors.	189
Fig. 4.8.1	Delay spread in a corridor versus Tx-Rx separation.	191
Fig. 4.8.2	Signal strength in a naturally rough tunnel at 960 MHz as compared to ray tracing.	192
Fig. 4.8.3	Measured signal level in a road tunnel and fitted model.	193
Fig. 4.8.4	Signal level in tunnel with compensated leaky feeder cable.	194
Fig. 4.8.5	Booster concept to cover confined areas.	195
Fig. 4.8.6	Speed profile synchronisation information and signal level along high-speed train line "TGV Paris-Lille".	196
Fig. 5.1	GSM specified power delay profiles.	210

Fig. 5.2	Normalised signal-strength distribution for the three GSM specified profiles.	211
Fig. 5.3	Schematic flow diagram of the TCH/FS transmission and receiving path.	212
Fig. 5.4	Frame Erasure Rate as a function of C/I for Cyclic Frequency Hopping.	215
Fig. 5.5	Block diagram of matched filter and soft decision combining.	217
Fig. 5.6	A GSM normal burst with indication of the signal-strength period $k$ and the switching time $m$ .	219
Fig. 5.7	Delayed signal combining of GSM signals.	219
Fig. 5.8	Simulated antenna diversity gain for various diversity algorithms.	220
Fig. 5.9	Simulated antenna diversity gain for various diversity algorithms.	221
Fig. 5.10	The instantaneous CIR of two mobiles during a period of 520 bursts.	226
Fig. 5.11	Maximum capacity per site as a function of frequency reuse factor K for a network with 36 TCH carriers.	228
Fig. 5.12	FER as a function of mean CIR for a fractionally loaded network.	229
Fig. 5.13	DECT frame and DECT slot structures.	233
Fig. 5.14	Basic arrangement of the DECT testbed.	236
Fig. 5.15	Measured impulse responses, wideband received power and delay spread in the two diversity branches.	238
Fig. 5.16	Error floor with adaptive sampling.	244
Fig. 5.17	Switch and selection diversity configurations.	247
Fig. 5.18	Burst Failure Rate for a two path Rayleigh fading channel with delay spread of 200 ns.	248
Fig. 5.19	Performance of different diversity arrangements on uplink and downlink directions as a function of portable speed.	249
Fig. 5.20	Timing diagram for RSSI measurements on two antennas during the preamble.	250
Fig. 5.21	Magnitude of the autocorrelation of the S-filed subsequence starting at bit 17 with length 11.	252
Fig. 5.22	Delay spread performance of the non-coherent equaliser.	253
Fig. 5.23	Førde measurement routes 1-3.	258
Fig. 5.24	Førde measurement routes 5-6.	259
Fig. 5.25	BER versus delay spread from Førde.	261
Fig. 5.26	Frame architecture for one DECT duplex bearer.	263
Fig. 5.27	Reference building.	264
Fig. 5.28	Three unsynchronised systems in the building.	264
Fig. 5.29	Offered traffic per RFP with three systems in the building.	265
Fig. 5.30	Performance with diversity in a mixed voice-data scenario.	267

Fig. 5.31	Performance with diversity in a mixed voice-data scenario.	268
Fig. 5.32	Some typical scenarios for the RLL application.	270
Fig. 5.33	Typical frame architecture of the CRFP unit.	271
Fig. 5.34	Typical frame architecture of the REP unit.	272
Fig. 5.35	Example of the interlacing procedure.	273
Fig. 5.36	The two simulation scenarios considered.	273
Fig. 5.37	GOS versus the Erlang/RFP in case of 1 RFP and 1 REP.	274
Fig. 5.38	GOS versus the Erlang/RFP in case of 1 RFP and 2 REPs.	274
Fig. 5.39	Distribution of the occupied slots at the RFP.	275
Fig. 6.1	Effect of gain imbalances.	290
Fig. 6.2	Effect of phase imbalances.	290
Fig. 6.3	MAMSK and MAQMSK signal constellation diagrams.	292
Fig. 6.4	Performance of QMSK, GMSK and $\pi/4$ -QPSK signal in Rayleigh fading channel with cochannel interference.	292
Fig. 6.5	Comparison of the signature areas for constant bandwidth as a function of $\tau/T_{\text{symbol}}$ compensated for the different bandwidth efficiencies.	293
Fig. 6.6	Error performance of coherent multi-h CPM ( $h_1 = 2/4$ , $h_2 = 3/4$ ) in an urban area, without diversity, with selection div. and post detection div..	294
Fig. 6.7	Error probability of MSK in a 10-path fading channel.	296
Fig. 6.8	Bit error rate for FH-TCM-8-DPSK with normalised frequency hopping separation as a parameter.	298
Fig. 6.9	Structure of a vector decision-feedback equaliser for M-ary orthogonal signals.	301
Fig. 6.10	Performance of vector decision-feedback equalisation using a two path channel model.	302
Fig. 6.11	Performance of DFSE with diversity in the HT50 channel.	303
Fig. 6.12	Performance of joint diversity and DFE equalisation as a function of the normalised delay spread.	304
Fig. 6.13	Architecture of ATDMA adaptive transport interface.	307
Fig. 6.14	Spectral efficiency of adaptive TDMA.	307
Fig. 6.15	Information theoretic capacity of single-cell systems.	310
Fig. 6.16	Simulation results for IS-95 downlink with channel 1(Frankfurt measurements) and channel 2 (Darmstad measurements).	314
Fig. 6.17	Uplink capacity as a function of power control imperfection for three values of the processing gain.	315
Fig. 6.18	Performance of low pass filtered DS-CDMA.	316
Fig. 6.19	Effective processing gain of DS-CDMA systems using GMSK.	317

Fig. 6.20	Number of users against propagation factor $\alpha$ , with outage probability 1 % and various propagation standard deviation factors $\sigma$ .	319
Fig. 6.21	$C/I$ ratio vs. number of users per cell computed at an outage probability of 10 %, for both a single and a multicell system with the base stations equipped with omnidirectional antennas, in a rural area and in an urban area, when power control is applied and when it is not applied.	320
Fig. 6.22	Maximum number of users per site vs. processing gain computed for a multicell system equipped with omnidirectional antennas, 120 degree and 60 degree sector antennas, in a rural area and in an urban area, when power control is applied.	320
Fig. 6.23	Maximum number of users per site vs. processing gain computed for a multicell system equipped with 120 degree sector antennas, in a rural area, with power control.	321
Fig. 6.24	Maximum number of users per site vs. processing gain computed for a multicell system equipped with 120 degree sector antennas, in an urban area, with power control.	321
Fig. 6.25	$T_a$ versus $\delta_l$ for UDC with $M_1 = 1, M_2 = 5$ .	323
Fig. 6.26	$T_a$ versus $\delta_l$ for TRS with $M_1 = 1, M_2 = 5$ .	323
Fig. 6.27	The correlation signal detection scheme.	323
Fig. 6.28	Block diagram of the proposed DLL.	325
Fig. 6.29	Normalised jitter for rectangular and Nyquist pulses in terms of SIR.	327
Fig. 6.30	Hybrid DS/SFH, DS and SFH with (23,12) Golay coding.	329
Fig. 6.31	Delay performance of hybrid DS/SFH with BPSK modulation, using a measured and analytical channel model.	330
Fig. 6.32	BER performance of the ZF-BLE, MMSE-BLE, ZF-BDFE and MMSE-BDFE.	334
Fig. 6.33	Bit error probability of user 1 as a function of the signal-to-noise ratio in the presence of 5 interfering users.	335
Fig. 6.34	Bit error probability of user 1 for constant $\gamma_i = 8$ dB and various interference levels.	335
Fig. 6.35	Receiver structure.	338
Fig. 6.36	Performance comparison of the different receiver types.	339
Fig. 6.37	Diversity approaches in cellular systems.	341
Fig. 6.38	OFDM transmitter and receiver.	343
Fig. 6.39	Performance of OFDM in the Bad Urban channel for various speeds.	344
Fig. 6.40	BER for $N_c/N_t = 15/2$ , $N_u = 3$ users and channels with 2 paths per user and matched filtering only, interference cancellation only, and JEIC.	346

Fig. 6.41	Bit error rate as a function of $E_b/N_0$ for $N_r/N_t = 15/2$ , and $N_u = 3$ over one-path asynchronous channels.	347
Fig. 6.42	Illustration of the near-far resistance for $N_r/N_t = 15/2$ , and $N_u = 3$ over one-path asynchronous channels.	348
Fig. 6.43	BER as a function of the average $E_b/N_0$ for different OFDM-CDMA equalisation algorithms under Rayleigh fading conditions.	349
Fig. 7.1.1	ATDMA functional model.	363
Fig. 7.1.2	ATDMA protocol model.	364
Fig. 7.1.3	Example of an adaptive transport chain for a downlink traffic channel.	365
Fig. 7.1.4	Generic burst structure.	365
Fig. 7.1.5	PRMA++ uplink.	371
Fig. 7.1.6	Relationship between Traffic and Associated channels.	373
Fig. 7.2.1	Performance comparison of DS and FH CDMA.	375
Fig. 7.2.2	LINK CDMA channel structure.	378
Fig. 7.2.3	Partitioning of LINK CDMA test bed.	380
Fig. 7.2.4	MS demodulator.	381
Fig. 7.2.5	Coherent Rake receiver for uplink.	382
Fig. 7.2.6	Uplink BER measurements with the channel simulator.	384
Fig. 7.3.1	CTDMA example for $K = 3$ users.	387
Fig. 7.3.2	Block diagram of a CTDMA system.	388
Fig. 7.3.3	Example of a multipath channel impulse response $h(t)$ with absolute delay $\tau_A$ and excess delay $\tau_E$ .	389
Fig. 7.3.4	CTDMA transmitter, noisy multipath channel, and CTDMA receiver.	390
Fig. 7.3.5	CTDMA error performance for the COST 207 RA100 channel model.	392
Fig. 7.3.6	Rates overview of a generalised CTDMA system.	393
Fig. 7.3.7	Rates examples of a generalised CTDMA system.	396
Fig. 7.3.8	CTDMA chip rates $R_C$ , spreading factors $L$ and encoded symbol rates $R_S$ for $Q = 1, 2$ and $4$ orthogonal WH families.	397
Fig. 7.3.9	CTDMA chip rates $R_C$ and encoded symbol rates $R_S$ for a fixed spreading factor $L = 32$ and $Q = 1, 2$ and $4$ orthogonal WH families.	398
Fig. 7.4.1	Hybrid multiple access schemes.	402
Fig. 7.4.2	Uplink frame structure of the JD-CDMA mobile radio system concept.	403
Fig. 7.4.3	Uplink burst structure of the JD-CDMA mobile radio system concept.	404

Fig. 7.4.4	Burst structure of an uplink transmitter of the JD-CDMA mobile radio system concept.	404
Fig. 7.4.5	Base station receiver of the JD-CDMA mobile radio system concept.	406
Fig. 7.4.6	Downlink frame structure of the JD-CDMA mobile radio system concept.	408
Fig. 7.4.7	Downlink burst structure of the JD-CDMA mobile radio system concept.	409
Fig. 8.2.1	Measurement setups for power measurements.	419
Fig. 8.2.2	Multiple reflections within a slab.	421
Fig. 8.3.1	Path-loss versus distance at 1.7 and 60 GHz.	426
Fig. 8.3.2	Measured DOA distributions in a laboratory.	427
Fig. 8.3.3	Direction of arrival from Doppler spectrum.	427
Fig. 8.3.4	Measured DOA distributions (CNET).	428
Fig. 8.3.5	Setup for wideband measurements.	430
Fig. 8.3.6	NRP in the large rooms, hall and corridor.	431
Fig. 8.3.7	Cumulative distributions of RDS in large rooms, hall and corridor.	432
Fig. 8.3.8	Example of measured impulse response.	433
Fig. 8.3.9	Example of an average PDP.	434
Fig. 8.3.10	Simulated antenna setups.	436
Fig. 8.3.11	Results for the low reflective environment with "sec-sec" setup and obstructed LOS.	437
Fig. 8.3.12	Results for the low reflective environment with "sec-sec" setup and 5° pointing error.	437
Fig. 8.3.13	Results for the low reflective room with "bic-bic" setup under LOS and OBS conditions.	438
Fig. 8.4.1	Comparison between measured and simulated power in a city tunnel at 60 GHz.	439
Fig. 8.4.2	Street plan and sample CIR for "street A".	444
Fig. 8.4.3	Comparison between ray-tracing and measurements of statistical parameters.	445
Fig. 8.5.1	DS and SFH performance.	447
Fig. 8.5.2	Irreducible BER vs. NDS.	448
Fig. 8.5.3	BER for DS-multitone without and with equalisation for different numbers of tones.	449
Fig. 8.5.4	Scheme of proposed BPSK receiver with quasi-coherent signal combining.	450
Fig. 8.5.5	Average probability of bit error versus normalised maximum bit rate for various number of forward taps.	451

Fig. 8.5.6	Outage probability vs. SIR, simplified channel model.	453
Fig. 8.5.7	System block diagram.	454
Fig. 8.5.8	The BER performance vs. $E_b/N_0$ for concatenated and multiplexed coding schemes (soft decision).	454
Fig. 8.6.1	Upstream information structure.	456
Fig. 8.6.2	Downstream information structure.	457
Fig. 8.6.3	Throughput of slotted non-persistent ISMA.	459
Fig. 8.6.4	COMB scheme.	460
Fig. 8.6.5	EY-NPMA.	461
Fig. 8.6.6	Throughput with hidden nodes.	461
Fig. 8.6.7	RTS/CTS protocol.	462



---

## List of Tables

Tab. 2.1	Characteristics of pulse compression channel sounders contributed to COST 231.	46
Tab. 2.2	Indoor environment categories.	54
Tab. 2.3	Description of indoor measurement data.	55
Tab. 3.1	Average received power obtained from measurements.	93
Tab. 3.2	Cross-correlation $\rho$ , versus antenna separation $\Delta s$ .	101
Tab. 3.3	Fading margins and diversity gain of the long-term fading using two antenna separations in indoor environment.	106
Tab. 3.4	Macrodiversity fading margin $M_{99}$ and gain $G_D$ for the log-normal fading component with standard deviation 5, 8 and 10 dB, for three correlation levels between two branches.	107
Tab. 3.5	Estimated fading margins and diversity gain by selection of strongest signal measured in two separate branches.	108
Tab. 3.6	Simulated levels of fading margins and the corresponding diversity gain versus envelope correlation for the short-term fading with five different Ricean K-factors.	109
Tab. 4.1.1	Definition of cell types.	116
Tab. 4.4.1	Methods to consider large-scale terrain variations.	141
Tab. 4.4.2	Comparison of different propagation models.	145
Tab. 4.5.1	Small- and micro-cell prediction models: an overview.	159
Tab. 4.5.2	Performance of the propagation models at 947 MHz.	166
Tab. 4.7.1	Wall types for the multi-wall model.	177
Tab. 4.7.2	Results for model coefficients for path loss models at 1800 MHz.	178
Tab. 4.7.3	Delay spread and PDP shape in different environments.	180
Tab. 4.7.4	Material parameters	185
Tab. 4.7.5	Performance of the models for single floor propagation.	187
Tab. 4.7.6	Performance of the models for multi-floor propagation.	188
Tab. 4.8.1	Observed power levels and coverage lengths in an Euro-standard two-lane road tunnel.	193
Tab. 5.1	Simulation results for Cyclic Frequency Hopping.	216

Tab. 5.2	Required C/I for a FER of 2% for different antenna diversity techniques.	220
Tab. 5.3	Required $E_b/N_0$ for a FER of 2% for different antenna diversity techniques.	221
Tab. 5.4	The number of available TCH carriers per cell for various spectrum allocations and frequency reuse factors.	224
Tab. 5.5	Maximum relative load of a GSM cell at a 2% hard blocking level.	225
Tab. 5.6	The parameters of the GSM network simulation.	225
Tab. 5.7	The maximum load of a FH GSM network limited by co-channel interference.	227
Tab. 5.8	Maximum capacity of various reuse factors for a network with 36 TCH carriers.	227
Tab. 5.9	Personal capacity increase of a random FH GSM network using $K=1/3$ frequency reuse and adaptive antenna arrays.	230
Tab. 5.10	Important parameters of the DECT standard.	234
Tab. 5.11	Comparative performance of DECT receivers.	254
Tab. 5.12	Environment characteristics and system planning aspects of the DECT field trial at Førde.	256
Tab. 5.13	Measurements from Førde.	260
Tab. 5.14	Traffic capacity for different system scenarios.	266
Tab. 5.15	Traffic evaluation in a mixed voice-data scenario.	268
Tab. 5.16	Traffic evaluation in a mixed voice-data scenario.	269
Tab. 6.1	Coding gains for rate 1/2 convolutional coding with 10 ms partial block interleaving in dependence on different normalised Doppler frequencies and diversity-orders.	287
Tab. 6.2	Upper bound of the channel rejection with a maximum error of 3 dB.	289
Tab. 6.3	Summary of code rates and required $E_b/N_0$ for $\text{BER}=10^{-3}$ (Rayleigh fading channel).	297
Tab. 6.4	Coding gains of Trellis coded 8-PSK compared to uncoded QPSK.	297
Tab. 6.5	Spectrum efficiency in a cellular network.	299
Tab. 6.6	Spectral efficiencies (bit/Hz/cell) of various multiple access schemes.	311
Tab. 6.7	Mean time between two consecutive losts of lock under different channel conditions using DLL shown in Fig. 6.28.	325
Tab. 6.8	Comparison of the maximum throughput $S$ normalised on the offered traffic $G$ of the hybrid DS/SFH system with Q-, B- and D-PSK.	329

<b>Tab. 7.1.1</b>	Transport parameters for static adaptation.	366
<b>Tab. 7.1.2</b>	Summary of mode characteristics for 64 kb/s low delay service.	368
<b>Tab. 7.1.3</b>	Summary of mode characteristics for 64 kb/s long delay service.	368
<b>Tab. 7.2.1</b>	Air interface parameters.	379
<b>Tab. 7.4.1</b>	Important system parameters of the uplink.	405
<b>Tab. 8.2.1</b>	Characteristics of building materials at mmw.	422
<b>Tab. 8.2.2</b>	Wall thicknesses for specific values of isolation.	424
<b>Tab. 8.3.1</b>	Wideband measurement environments.	430
<b>Tab. 8.4.1</b>	Power-distance decay rate at mmw in outdoor scenarios.	441
<b>Tab. 8.4.2</b>	Main figures from the wideband measurements.	443



---

## List of Acronyms

ACCH	<u>A</u> sso <u>c</u> iated <u>C</u> ontrol <u>C</u> hannel
ACF	<u>A</u> uto- <u>C</u> orrelation <u>F</u> unction
ACI	<u>A</u> djacent- <u>C</u> hannel <u>I</u> nterference
ACTS	<u>A</u> dvanced <u>C</u> ommunications <u>T</u> echnologies and <u>S</u> ervices
ADC	<u>A</u> nalogue to <u>D</u> igital <u>C</u> onverter
ADPCM	<u>A</u> daptive <u>D</u> ifferential <u>P</u> ulse <u>C</u> ode <u>M</u> odulation
AMPS	<u>A</u> dvanced <u>M</u> obile <u>P</u> hone <u>S</u> ystem
ATDMA	<u>A</u> dvanced TDMA
ATDMA	<u>A</u> dvanced TDMA <u>M</u> obile <u>A</u> ccess (RACE project)
ATM	<u>A</u> synchronous <u>T</u> ransfer <u>M</u> ode
AWGN	<u>A</u> dditive <u>W</u> hite <u>GN</u> oise
BCCH	<u>B</u> roadcast <u>C</u> ontrol <u>C</u>
BDFE	<u>B</u> lock <u>D</u> ecision <u>F</u> eedback <u>E</u> qualiser
BER	<u>B</u> it <u>E</u> rror <u>R</u> ate
B-ISDN	<u>B</u> roadband ISDN
BLE	<u>B</u> lock <u>L</u> inear <u>E</u> qualiser
BPSK	<u>B</u> inary PSK
BS	<u>B</u> ase <u>S</u> tation
BTS	<u>B</u> ase <u>T</u> ransceiver <u>S</u> tation
CCI	<u>C</u> o- <u>g</u> hannel <u>I</u> nterference
CDF	<u>C</u> umulative <u>D</u> istribution <u>F</u> unction
CDMA	<u>C</u> ode <u>D</u> ivision <u>M</u> ultiple <u>A</u> ccess
CENELEC	<u>C</u> omité <u>E</u> uropéen de <u>N</u> ormalisation <u>É</u> lectronique
CEPT	<u>C</u> onference of <u>E</u> uropean <u>P</u> ostal and <u>T</u> elecommunications <u>A</u> dministrations
CF	<u>C</u> orrelation <u>F</u> unction
CG	<u>C</u> onjugate <u>G</u>
CIR	<u>C</u> arrier to <u>I</u> nterference <u>R</u> atio
CIR	<u>C</u> hannel <u>I</u> mpulse <u>R</u> esponse
CNR	<u>C</u> arrier to <u>N</u> oise <u>R</u> atio
CODIT	<u>C</u> ode <u>D</u> ivision <u>T</u> estbed for UMTS (RACE project)
COST	European <u>C</u> o-operation in the Field of <u>ST</u>

CPM	<u>C</u> ontinuous <u>P</u> hase <u>M</u> odulation
CR	<u>C</u> hannel <u>R</u> esponse
CRC	<u>C</u> yclic <u>R</u> edundancy <u>C</u> heck
CSMA/CD	<u>C</u> arrier <u>S</u> ense <u>M</u> ultiple <u>A</u> ccess with <u>C</u> ollision <u>D</u> etection
CTS	<u>C</u> lear <u>t</u> o <u>S</u> end
CW	<u>C</u> ontinuous <u>W</u> ave
DAC	<u>D</u> igital to <u>A</u> nalogue <u>C</u> onverter
DCA	<u>D</u> ynamic <u>CA</u> llocation
DCS	<u>D</u> igital <u>CS</u> ystem
DECT	<u>D</u> igital <u>E</u> nhanced <u>C</u> ordless <u>Telecommunications</u>
DFE	<u>D</u> ecision <u>F</u> eedback <u>E</u> qualiser
DFE	<u>D</u> ecision <u>F</u> eedback <u>E</u> stimation
DFSE	<u>D</u> ecision <u>F</u> eedback <u>S</u> equence <u>E</u> stimation
DLC	<u>D</u> ata <u>L</u> ink <u>C</u> ontrol
DOA	<u>D</u> irection <u>o</u> f <u>A</u> rrival
DPSK	<u>D</u> ifferential <u>P</u> SK
DS	<u>D</u> irect <u>S</u> equence
DSP	<u>D</u> igital <u>S</u> ignal <u>P</u> rocessing
DTX	<u>D</u> iscontinuous <u>Transmission</u>
EGC	<u>E</u> qual <u>GCombining</u>
EMC	<u>E</u> lectromagnetic <u>Compatibility</u>
ERC	<u>E</u> uropean <u>Radiocommunications <u>Committee</u></u>
ERMES	<u>E</u> uropean <u>Radio <u>MS</u></u>
ERO	<u>E</u> uropean <u>Radiocommunications <u>O</u>ffice</u>
ETSI	<u>E</u> uropean <u>Telecommunications <u>SI</u></u>
ETSI/RES	<u>E</u> TSI / <u>Radio <u>E</u>quipment &amp; <u>Systems</u></u>
ETSI/SMG	<u>E</u> TSI / <u>SMG</u>
FCA	<u>F</u> ixed <u>CA</u>
FDD	<u>F</u> requency <u>DD</u>
FDDSF	<u>F</u> ield <u>DDSF</u>
FDM	<u>F</u> requency <u>DM</u>
FDMA	<u>F</u> requency <u>DMultiple <u>A</u></u>
FEC	<u>F</u> orward <u>ECorrection</u>
FER	<u>F</u> rame <u>ER</u>
FH	<u>F</u> requency <u>H</u>
FIR	<u>F</u> inite <u>I</u> mpulse <u>Response</u>
FM	<u>F</u> requency <u>Modulation</u>

FPLMTS	<u>F</u> uture <u>P</u> ublic <u>L</u> and <u>M</u> obile <u>T</u> elecommunication <u>S</u> ystems
FS	<u>F</u> ull-rate <u>S</u> peech
GEO	<u>G</u> eosynchronous <u>O</u> rbit
GMSK	<u>G</u> aussian <u>M</u> SK
GO	<u>G</u> eometrical <u>O</u> ptics
GOS	<u>G</u> rade <u>o</u> f <u>S</u> ervice
GSM	<u>G</u> lobal <u>S</u> ystem for <u>M</u> obile <u>C</u> ommunications
HCA	<u>H</u> ybrid <u>C</u> hannel <u>A</u> llocation
HEO	<u>H</u> igh <u>E</u> lliptical <u>O</u> rbit
HIPERLAN	<u>H</u> igh <u>P</u> erformance <u>R</u> adio <u>L</u> AN
HS	<u>H</u> alf-rate <u>S</u> peech
HT	<u>H</u> illy <u>T</u>
IBC	<u>I</u> ntegrated <u>B</u> roadband <u>C</u> ommunications
IC	<u>I</u> nterference <u>C</u> ancellation
IMT-2000	<u>I</u> nternational <u>M</u> obile <u>Telecommunications - 2000</u>
IN	<u>I</u> ntelligent <u>N</u> etwork
INIRC	<u>I</u> nternational <u>N</u> on- <u>I</u> onising <u>Radiation <u>Committee</u></u>
IR	<u>I</u> nfra <u>R</u> ed
IR	<u>I</u> mpulse <u>Response</u>
IRPA	<u>I</u> nternational <u>R</u> adio <u>Protection <u>A</u>sociation</u>
ISDN	<u>I</u> ntegrated <u>S</u> ervices <u>D</u> igital <u>N</u> etwork
ISI	<u>I</u> nter- <u>S</u> ymbol <u>I</u> nterference
ISM	<u>I</u> ndustrial, <u>S</u> cientific and <u>M</u> edical (frequency bands)
ISMA	<u>I</u> nhibit <u>S</u> ense <u>M</u> ultiple <u>A</u> ccess
ITU	<u>I</u> nternational <u>Telecommunications <u>Unnion</u></u>
ITU-R	ITU - <u>R</u> adiocommunications sector
JD	<u>J</u> oint <u>D</u> etection
LAN	<u>L</u> ocal <u>A</u> rea <u>N</u> etwork
LEO	<u>L</u> ow <u>E</u> arth <u>O</u> rbit
LINC	<u>L</u> inear <u>AN</u> on-linear <u>Components</u>
LMS	<u>L</u> east <u>M</u> ean <u>S</u> quare
LOS	<u>L</u> ine- <u>o</u> f- <u>S</u> ight
LT	<u>L</u> ong <u>T</u> erm
MAC	<u>M</u> edium <u>A</u> ccess <u>C</u> ontrol
MAMSK	<u>M</u> ulti- <u>A</u> mplitude MSK
MAQMSK	<u>M</u> ulti- <u>A</u> mplitude QMSK
MAVT	<u>M</u> obile <u>A</u> udio <u>V</u> isual <u>Terminal (RACE project)</u>

MBS	<u>M</u> obile <u>B</u> roadband <u>S</u> ystem
MBS	<u>M</u> obile <u>B</u> roadband <u>S</u> ystem (RACE project)
MLSE	<u>M</u> aximum <u>LS</u> equence <u>E</u> stimator
MMSE	<u>M</u> inimum <u>M</u> ean <u>S</u> quare <u>E</u> rror
MoM	<u>M</u> ethod <u>o</u> f <u>M</u> oments
MONET	<u>M</u> obile <u>N</u> etwork (RACE project)
MoU	<u>M</u> emorandum <u>o</u> f <u>U</u> nderstanding
MPSK	<u>M</u> ultilevel PSK
MQAM	<u>M</u> ultilevel QAM
MRC	<u>M</u> aximal <u>R</u> atio <u>C</u> ombining
MS	<u>M</u> obile <u>S</u> tation
MSK	<u>M</u> inimum <u>S</u> hift <u>K</u> eying
MTLL	<u>M</u> ean <u>T</u> ime to <u>L</u> oose <u>L</u> ock
MUSIC	<u>M</u> ultiple <u>S</u> ignal <u>C</u> lassification
NEC	<u>N</u> umerical <u>E</u> lectromagnetic <u>C</u> ode
NLOS	<u>N</u> on-LOS
NRP	<u>N</u> ormalised <u>R</u> eceived <u>P</u> ower
OFDM	<u>O</u> rthogonal <u>F</u> requency <u>D</u> ivision <u>M</u> ultiplexing
OLOS	<u>O</u> bstructed LOS
PAP	<u>P</u> ower <u>A</u> ngular <u>P</u> rofile
PCMCIA	<u>P</u> ersonal <u>C</u> omputer <u>M</u> odule <u>C</u> ard <u>I</u> ndustry <u>A</u> sociation
PCS	<u>P</u> ersonal <u>C</u> ommunication <u>S</u> ervices
PDA	<u>P</u> ersonal <u>D</u> igital <u>A</u> ssistant
PDP	<u>P</u> ower <u>D</u> elay <u>P</u> rofile
PIC	<u>P</u> ersonal <u>I</u> ntelligent <u>C</u> ommunicator
PIFA	<u>P</u> lanar <u>I</u> nverted <u>F</u> Antenna
PRMA	<u>P</u> acket <u>R</u> eservation <u>M</u> ultiple <u>A</u> ccess
PSK	<u>P</u> hase <u>S</u> hift <u>K</u> eying
PSTN	<u>P</u> ublic <u>S</u> witched <u>T</u> elephone <u>N</u> etwork
QAM	<u>Q</u> uadrature <u>A</u> mplitude <u>M</u> odulation
QC	<u>Q</u> uasi <u>C</u> oherent
QMSK	<u>Q</u> uadrature MSK
QOS	<u>Q</u> uality <u>o</u> f <u>S</u> ervice
QPSK	<u>Q</u> uaternary PSK
RA	<u>R</u> ural <u>A</u> rea
RACE	<u>R</u> esearch and <u>T</u> echnology <u>D</u> evelopment in <u>A</u> dvanced <u>C</u> ommunication <u>T</u> echnologies in <u>E</u>
RDS	<u>R</u> M斯 <u>D</u> elay <u>S</u> pread

RF	<u>R</u> adio <u>Frequency</u>
RLL	<u>R</u> adio <u>L</u> ocal <u>L</u> oop
RLS	<u>R</u> ecursive <u>L</u> east <u>S</u> quare
RMS	<u>R</u> oot <u>M</u> ean <u>S</u> quare
RS	<u>R</u> emote <u>S</u> tation
RS	<u>R</u> eed <u>S</u> olomon
RSSI	<u>R</u> eciever <u>S</u> ignal <u>S</u> trength <u>I</u> ndicator
RTS	<u>R</u> equest <u>t</u> o <u>S</u> end
RX	<u>R</u> ecevier
SAINT	<u>S</u> atellite <u>I</u> ntegration in the Future Mobile Network (RACE project)
SAR	<u>S</u> pecific <u>A</u> bsoption <u>R</u> ate
SAW	<u>S</u> urface <u>A</u> coustic <u>W</u> ave
SC	<u>S</u> election <u>C</u> ombining
SCPC	<u>S</u> ingle <u>C</u> hannel per <u>C</u> arrier
SDMA	<u>S</u> pace <u>D</u> ivision <u>M</u> ultiple <u>A</u> ccess
SFH	<u>S</u> low <u>Frequency <u>H</u>opping</u>
SIP	<u>S</u> pectral <u>I</u> ncremental <u>P</u> ropagation
SNR	<u>S</u> ignal to <u>N</u> oise <u>Ratio</u>
ST	<u>S</u> hort <u>T</u> erm
SWR	<u>S</u> tanding <u>W</u> ave <u>Ratio</u>
TCH	<u>T</u> raffic <u>C</u> hannel
TCM	<u>T</u> rellis <u>C</u> oded <u>M</u> odulation
TDD	<u>T</u> ime <u>D</u> ivision <u>D</u> uplex
TDMA	<u>T</u> ime <u>D</u> ivision <u>M</u> ultiple <u>A</u> ccess
TSUNAMI	<u>T</u> echnology in <u>S</u> mart <u>A</u> ntennas for <u>Universal <u>A</u>dvanced <u>M</u>obile <u>I</u>nfrastructure (RACE project)</u>
TU	<u>T</u> ypical <u>U</u> rban
TX	<u>T</u> ransmitter
UMTS	<u>U</u> niversal <u>M</u> obile <u>T</u> elecommunications <u>S</u> ystem
UPT	<u>U</u> niversal <u>P</u> ersonal <u>T</u> elecommunications
VAD	<u>V</u> oice <u>A</u> ctivity <u>D</u> etection
VDFE	<u>V</u> ector <u>D</u> ecision <u>Feedback <u>E</u>qualiser</u>
VLSI	<u>V</u> ery <u>L</u> arge <u>S</u> cale <u>I</u> ntegration
VSWR	<u>V</u> oltage <u>SWR</u>
WARC	<u>W</u> orld <u>A</u> dministrative <u>R</u> adio <u>C</u> onference
WHO	<u>W</u> orld <u>H</u> ealth <u>O</u> rganisation
WLAN	<u>W</u> ireless <u>L</u> AN
WPBX	<u>W</u> ireless <u>P</u> rivate <u>B</u> ranch <u>E</u> xchange

WSSUS	<u>Wide-Sense-Stationary Uncorrelated Scattering</u>
XPD	<u>Cross Polarisation Discrimination</u>
ZF	<u>Zero Forcing</u>





---

*"It is dangerous to put limits on wireless"*

**Guglielmo Marconi (1932)**

*"What is now wired will become wireless and virtually everything now transmitted over the airwaves will be wired"*

**Nicholas Negroponte ( MIT Media Laboratory)**

## Introduction

**Eraldo Damosso, CSELT, Italy**

It is widely and unanimously acknowledged that Telecommunications will play a role of strategic importance in the future of both developed and developing countries. In the European Commission's vision, a reasonable scenario for the near and long-term future services which should be offered to the customer, could be depicted according to the following approximate time schedule:

- 1990-1995: Deployment of ISDN
- 1995-2000: Implementation of IBC (Integrated Broadband Communications)
- 2000-2005: Emergence of Personal Communications Services, with a full integration of user mobility and Intelligent Network
- 2005-2010: Photonic Network implementation at all network levels

In the above scenario four major requirements are to be met by future telecommunication networks: high transport capacity (high speed, multimedia services), access and addressing flexibility (full user mobility, customised services, multi-purpose communications), network intelligence ("ad hoc" service creation, personalised performance, bandwidth on demand), service quality (reliability, security, communication integrity).

As to the third issue in the list, the publication of the Green Paper by the European Commission on April 1994 [1] and the following decision by the Council on July 1994 [2] on the adoption of a specific research and technological programme, emphasise the importance of the mobile and personal communications in shaping the future information environment on a world-wide basis. The Green Paper, in particular, and the subsequent public consultation (and concertation) process may be considered as a first basic step in preparing the total liberalisation of the telecommunications market within the European Union, effective by January 1998, promoting the migration towards personal services and stimulating the implementation of trans-European networks, with a progressive disappearance of the traditional distinction between fixed and mobile networks. In this context, Personal Communication Services (PCS) are intended as a set of capabilities providing a mixture of terminal and personal mobility and may be considered as a service that

may be run transparently on top of different networks, offering personalised access to communication services and facilities to people on the move. Access to the service is by a mobile-radio (referred to as terminal mobility) or any wired terminal (referred to as personal mobility) using coded means to personalise the right of access: the key requirements for the success will be the availability of ubiquity of access by users travelling across large geographical areas and related administrative domains. Notwithstanding the vagueness of any possible definition of PCS, the user expectations seem to be for a sort of family or continuum of wireless communications services at lower power and with more, smaller cell sites than cellular; some services will be feature-rich and therefore are presumed to be more costly; other, more modest offerings, will perhaps be less costly.

Such a vision is strongly supported by current mobile communications market analyses which indicate that Europe is mobile aware and entering the consumer market. The most successful estimates suggest a penetration greater than 10%. To achieve such high penetration levels will require broadening the general user community and at the same time offering more advanced and different services. Even if personal communications services are likely to be based initially on combinations of existing systems such as GSM, DCS@1800 and DECT, ultimately they should be carried most economically via a single integrated technology concept, the so-called UMTS (Universal Mobile Telecommunications System). Although incompatibility is the essential weakness between today's cellular, paging, cordless and mobile data services, their strength lies in their responsiveness to customer demand in a variety of different public and private market sectors with an element of service-creation flexibility and standardisation of the individual system-access technology. With the UMTS implementation, all the potential aspects of mobility would be fully accommodated:

- *Access (or Local) Mobility*, based on use of radio technologies, typical of cordless systems;
- *Terminal Mobility*, typical of current (and future) mobile cellular systems, based on mobility management capabilities at the fixed and/or mobile network levels;
- *Personal Mobility*, which is the main feature of the UPT (Universal Personal Telecommunications) service concept, aimed at providing the user with personalised services through a personal identity number and a specific user profile.

The development of UMTS is therefore an opportunity both to exploit the spectrum resources in the 2 GHz band and to converge the presently separate mobile services into a more unified and universal system solution in multi-operator environments. UMTS is in fact a multi-function, multi-service, multi-application digital system that will use future technology to provide personal mobile telecommunications that support universal roaming, offer broadband multi-media services and have a much larger user base than current mobile networks. In particular, the current work of ETSI relating to integration of GSM-DECT and GSM-DCS@1800 is paving the way to the evolution towards multimode transceivers and as such is relevant to the introduction of UMTS. Furthermore, UMTS is designed to have both terrestrial and satellite components, with a suitable degree of commonality between them, including the radio interfaces. Therefore, it is of paramount importance that the

progressive migration from second to third generation systems, expected to start at the turn of the century, must be undertaken while ensuring that the current user markets will perceive such a service evolution as relatively seamless, attractive and natural.

## References

- [1] CEC DGXIII, *Towards the Personal Communications Environment: Green Paper on a common approach in the field of mobile and personal communications in the European Union*, COM(94)145, Apr. 1994
- [2] Council of the European Union, *Decision on a specific programme of research and technological development and demonstration in the area of Advanced Communications Technologies and Services (1994-1998)*, July 1994



---

## COST 231 in the European Telecommunications Environment

**Eraldo Damosso, CSELT, Italy**

With the emergence of second generation cellular mobile and cordless systems, the first steps have been taken towards a ubiquitous universal personal mobile communications network. Since 1988 Europe has conducted pre-normative UMTS research within the RACE programme, as well as in other European Community frameworks and in the context of national programmes, to explore technological options and to carry out basic research in collaboration with service providers, network operators and equipment manufacturers. However, the vision within the past RACE Mobile Projects and current ACTS Workplan developed under the 1994-98 4<sup>th</sup> Framework for European Research (as well as within the various standardisation bodies), is now one of total universality; universal in coverage and accessibility, but coupled with universal service provision in terms of scope, capability and availability. Personalised communication services over UMTS will exploit its bearer and teleservice capabilities: a wide variety of UMTS-supported services and applications are foreseen. Services include speech, video and data at various bit rates and these are expected to provide a wide range of user-group applications, including provision of interactivity. This will lead to a gradual blurring of distinctions that now exist between fixed and mobile services, in parallel with the development of the Intelligent Network(s). To enable UMTS to enter service successfully, clear technical guidelines have to be developed, regarding in particular the level of UMTS support of ATM (Asynchronous Transfer Mode) technology on IBC networks, the compatibility of UMTS and fixed-network architecture and intelligent functionality, the level of integration of the satellite components of UMTS, the multi-service convergence philosophy of the UMTS radio air-interface(s).

### **1.1 The evolutionary vision of mobile communications in Europe**

While UMTS is a system to be deployed at the turn of the century, work towards defining 4<sup>th</sup> generation Mobile Broadband Systems (MBS), for use beyond 2005, is already necessary from now. It is indeed of strategic importance to meet the requirements for wireless communication with very high throughput and to develop

the industrial capability to produce the necessary system components. Also essential is the investigation and definition of system aspects, radio access schemes, network management issues, integration with IBC, etc.

Although most basic and system technologies have been already developed for the implementation of wideband digital mobile networks and their inter-operability with the fixed network, what is still to be done for a true UMTS and MBS implementation may be in principle listed as follows:

- a full functional integration between mobile and fixed networks and a provision on mobile networks of all services which, more or less, are already available at the fixed level;
- a sound characterisation of the radio channel properties in the 2 GHz band;
- feasibility studies and development of new (universal) mobile terminals;
- basic studies for mobile broadband communication at millimetre waves, including propagation aspects, network architectures, RF and IF components, intelligent antennas and the integration with satellite networks;
- an exhaustive and well assessed test bed demonstration of UMTS/MBS facilities and capabilities;
- the definition of the relevant standards at a worldwide level.

The above vision embraces the inter-operability of fixed, mobile and mobile-satellite networks when supporting personal communications facilities. UMTS and MBS must, therefore, be locked into this convergence process towards access-independent, universal, personal communications. The European pre-eminence in digital mobile radio (Europe's world leading position in the implementation of digital mobile technologies is unquestionable) has made the Union a major actor in this field: Europe has historic strength in the domain, has technical competence, large home markets comprising sophisticated users, competent service providers, and equipment manufacturers competitive on a world-wide level. Unlike other countries, like US and Japan however, it suffers from a fragmentation of activity across the different Member States and its nationally based companies and organisations. Without a rationalisation of the efforts in this area it losing its position to the global competition; such a rationalisation should carefully take into due account the three kinds of economy which affect the policies and strategies of the major telecommunications players in the world market: scale, scope and integration.

"Economy of scale" is the classic advantage of mass production; "Economy of scope" reflects the additional benefit to the user of having the same service widely available; finally, the "Economy of integration" reflects the advantage of sharing facilities and the benefit for the user of combining services to meet specific needs. To do this, Europe's assets need to be fully mobilised to become effective in ensuring the exploitation of the three economies mentioned above and the whole process should hopefully be user oriented, in order to ensure that the technology

development activities respond quickly to changes in economic and social conditions and to new scientific discoveries and breakthroughs.

Furthermore, mobility and the proliferation of either portable and laptop computers or Personal Digital Assistants (PDA), together with potential cost savings in avoiding the wiring or re-wiring of buildings, are driving forces for the introduction of wireless Local Area Networks (LANs), which can transfer data and share resources without physically connecting them. These have received most attention from equipment manufacturers because they represent two of the fastest-growing segments of the computer industry, LANs and mobile computing. Although in Europe the activities at ETSI are aiming towards the standardisation of a stand-alone wireless LAN, next generation mobile systems must consider a system integrated wireless LAN as one of its key functionalities. Such integration concept requires the design of high-performance pico-cells, capable to support the requirements for high-rate local data communication: important issues to be addressed are frequency allocation/selection, bandwidth efficient coding schemes, specification of medium access protocols and link control, as well as connectivity aspects related to the backbone wired or wireless communications networks. Different working environments (e.g. office, production line, storehouse) have different requirements, which concern security, range, health aspects, transmission rate, re-using of frequencies, cost, maintenance, penetration ability, etc. The status of WLANs is presently that they are mainly used for data distribution and specified to IEEE 802.11 standard for use in the North American ISM frequency band. Other standards are in preparation, e.g. ETSI RES-10, and there are several proprietary systems; specific characteristics include:

- limited transmission distance (20-100 m);
- high capacity local pico-cell for voice and data with high throughput;
- un-regulated and uncoordinated operation of multiple WLAN in the same service area;
- propagation and channel models (< 20 GHz, optical, LED);
- propagation and channel models (60 GHz, optical, laser);
- advanced baseband signal processing.

In the above context, Fig. 1.1 presents the schematic flow [1] of the evolution of current (or next) systems/services towards the third/fourth generation ones, highlighting the role of the Community, through RACE and ACTS works.

As a matter of fact, particular attention was paid in Europe in the recent past to radio aspects of third generation systems (for both narrow and broadband services), and related propagation issues (measurements and modelling techniques); in the process towards personal communications, a key topic is the selection of the access technique, due to its impact on several other system aspects: the two major competitors are (Advanced) TDMA and CDMA schemes, as known. Moreover, within the European Community, it is of strategic importance that the efforts

pursued at a national level be complemented on a much larger scale by Community funded projects, aimed at the development not only of a Pan-European market, but also of world markets.

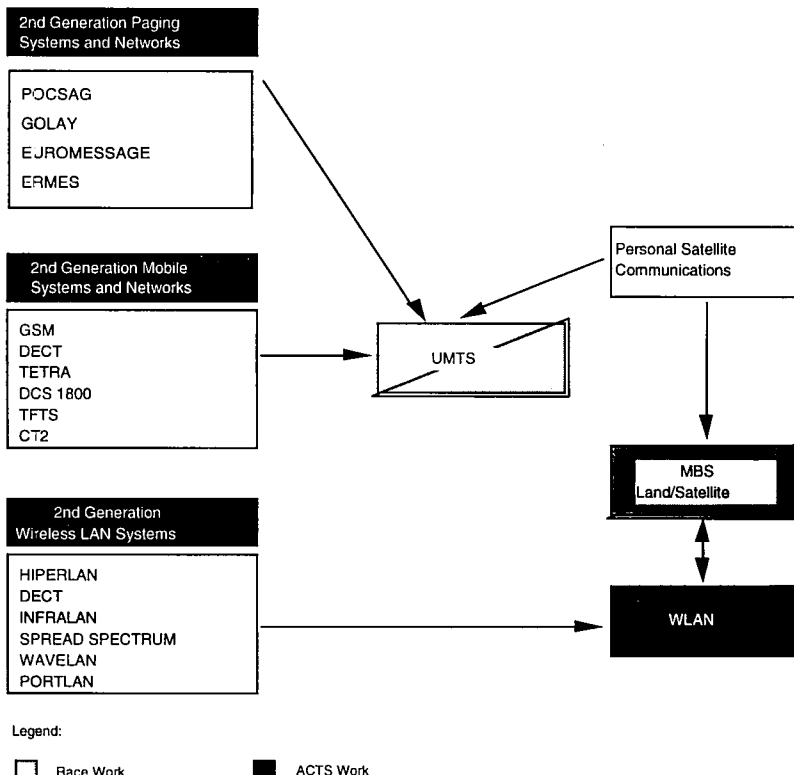


Fig. 1.1 - Evolution towards third/fourth generation systems with reference to RACE and ACTS programmes.

To these purposes, in 1992 two RACE (Research and Technology development in Advanced Communications Technologies in Europe) Projects have been set up by the European Community, e.g. CoDiT-UMTS (UMTS Code Division Testbed) and ATDMA (Advanced TDMA Mobile Access), to get optimised system architectures and compare their performance in a global environment. In addition, other RACE Mobile Projects were launched on related subjects, within the framework of the Mobile Project Line of the Community, namely: MONET (Mobile Network), MBS (Mobile Broadband System), MAVT (Mobile Audio Visual Terminal), SAINT (Satellite Integration in the Future Mobile Network), TSUNAMI (Technology in

Smart Antennas for Universal Advanced Mobile Infrastructure). Concurrent activities in the field of standardisation are in progress within ETSI (the European Telecommunications Standards Institute), to address third generation mobile systems and services under the label of UMTS, with a special focus on radio interfaces and network aspects, but worth noting are also the work of CEPT (Conference of European Postal and Telecommunications Administrations) and ERC/ERO (European Radiocommunications Committee /Office) regarding frequency allocations, the work of CENELEC (Comité Européen de Normalisation ÉLECTronique) on radiation health hazards and the activities of the GSM-MoU (Memorandum of Understanding), insofar as they may be a precursor to a UMTS-MoU.

It is expected that future requirements for personal communications will reach unprecedented levels, and the demand for a Personal Communications Space will require radically new, expanded and spectrum-efficient networks, infrastructures and equipment. As a consequence, the work of the new-born ACTS Projects will mainly focus on operational trials and on the technological aspects of integrated fixed and mobile broadband networks that have a direct bearing on the provision of enhanced personal communication services. Such trials should validate the wireless subsystem and network components in a variety of environments (office, residential, factory); they are expected to demonstrate cost/effective applications and services in the above environments, validate the integration and interworking of heterogeneous mobile networks and fixed network entities and, on the other, support for the radio connection through the various layers of the air-interfaces, proving their effectiveness. The ACTS Projects will also involve the development and proving of maintenance procedures, reliability testing and end-to-end quality-of-service management. The work will contribute to the development of common specifications and standards, as well as to the identification of new market opportunities and needs for changes in regulatory procedures and equipment specifications.

Such evolutionary scenario means that conformity, or at least compatibility, across network interfaces of all the necessary call, signalling and control procedures and protocols should be granted. It will also be necessary to conform to certain network functional arrangements and transmission requirements; in addition, the efficiency of the three technological platforms (UMTS, MBS, and WLANs) must also be proven in offering new opportunities for advanced mobile services. There is a need to establish the application feasibility of these services; a major issue in this context is continuity of services across different radio environments: in-building pico-cells, outdoor micro-cells, small and macro-cells, delivered by networks of widely differing capabilities. The technological feasibility of underlying mobile telecommunications technologies, for acceptable bearer capability, quality of service, general system fit-for-purpose, interworking and integration requirements, etc., should be identified through system oriented demonstrators taking place using UMTS, MBS and broadband Wireless LANs system platforms, in order to perform a fine tuning of the technologies themselves to achieve the desired functionality.

## 1.2 System migration prerequisites

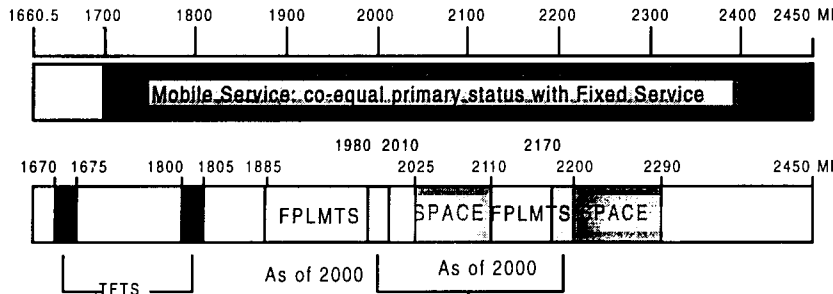
The above transition to third/fourth generation systems is fundamentally based on several prerequisites:

- Frequency Allocations and Spectrum Efficiency
- Enabling Technologies and Advanced Service Provision
- Terrestrial/Satellite Mobile Networks Integration
- Standardisation

### 1.2.1 Frequency Allocations and Spectrum Efficiency

The question of overcrowding in the frequency spectrum is an old one. As each year passes, new services and new users are demanding a share of this limited natural resource; the problem may be alleviated (and this is the case of mobile communications) through the adoption of new techniques enabling higher and higher frequencies to be brought into use, the utilisation of dual polarisation, directional or smart antennas, improved modulation methods, better filtering techniques and computer aided frequency planning. Nevertheless, demand for spectrum is still growing, leading to a rather strong congestion in some parts of it; taking into account any existing constraint (of technical, economical, social or political nature), both internationally recognised frequency allocation procedures and rules, and the subsequent work for maximising the spectral efficiency of the available resources appear to be essential. Frequency spectrum availability should no longer be an issue for mobile and personal communications, in a medium-term perspective at least, since the Final Acts of the 1992 World Administrative Radio Conference (WARC-92) extended the frequency bands allocated to a wide range of mobile terrestrial and mobile satellite services in the range below 3 GHz.

In most cases, the above services have been given the status of worldwide primary services (or at least on regional basis), with particular reference to FPLMTS (Future Public Land Mobile Telecommunication Systems) or IMT-2000 (International Mobile Telecommunications-2000, which is the recently suggested new name) [2]. WARC-92 decisions will present a variety of challenges in the design and definition of future services and systems and are schematically represented in Fig. 1.2 for the 1670-2450 MHz band: there is also much more room for future growth even at higher frequencies, because several existing fixed service bands above 4400 MHz have been allocated to the mobile service on a primary basis.



Also the Satellite Component as of 2005

*TFTS* = Terrestrial Flight Telephone System

*FPLMTS* = Future Public Land Mobile Telecommunication Systems

*SPACE* = Space Research, Space Operation, Earth Exploration Satellite Services

Fig. 1.2 - WARC-92 Frequency Allocations to Mobile Services (1.6 - 2.5 GHz).

The most significant result was the promotion of mobile services to the co-equal primary status with fixed services in the above frequency range; this is in full agreement with the spirit of the 14 ECP (European Common Proposals) submitted by CEPT, after a formal agreement amongst 31 European administrations (including several eastern countries), reached after a consultation process led by ERC and ERO. The WARC-92 decisions in the mobile area may be summarised as follows:

- Allocation of a given frequency band (on a world-wide basis) to Personal Communications under the title of FPLMTS, with 230 MHz (including space segments) around 2 GHz;
- Allocation of additional spectrum for mobile satellite services (terrestrial, maritime, aeronautical) with up to 100 MHz for big LEO satellite services (Low Earth Orbiting) below 2 GHz and up to 10 MHz for little LEO, below 1 GHz
- Spectrum allocation to APC (Aeronautical Public Correspondence) systems, taking into account the different needs (and reservations) of Europe, US and Japan

The primary status condition will facilitate the implementation at a worldwide level of a number of European mobile systems, such as DECT, DCS@1800, ERMES, DSRR (Digital Short Range Radio), without significant constraints. Concurrently, the allocation of a given spectrum segment to FPLMTS (215 MHz for Europe, in the 1885-2025 and 2110-2200 MHz bands, in order to take into account the needs of already existing systems such as DECT and DCS@1800), will pave the way to the 3rd generation systems standardisation bodies (although with some limitations, due to the foreseen dates of entering into force). Furthermore, it will enable them to

define specifications and develop the relevant technologies for personal communications on regional and international paths, including less populated and developing countries, where traditional communication structures do not grant an adequate coverage. On the other hand, it should be pointed out that at the same time demands for spectrum for other service applications and non-civil uses are changing and must also be carefully recognised: for example, it is estimated that over 30% of the spectrum range 30-960 MHz is typically currently allocated in Europe for governmental (and chiefly military) use (a similar proportion holds for the frequency range up to 3 GHz) [3]. Therefore, the problems of release/sharing of frequencies or of funding user migration on re-farming of frequencies are of crucial importance for a sound frequency spectrum management.

For Europe in particular, it is worth noting that, since from its inception, ERO activities have been directed to study the radio spectrum usage, promoting the DS1 (Detailed Spectrum Investigation) programme [4 a,b], in co-operation with ECTEL (European Telecommunications and Professional Electronic Industry), whose main goal is to arrive at a well established Frequency Allocations Table for Europe by June 2008; the first phase, regarding the frequency range between 3400 MHz and 105 GHz was settled in 1993, while a second phase (29.7 to 960 MHz) is being concluded during 1995. This work should ensure administrations, industry, broadcasters, service providers, operators and users derive the maximum benefit from the frequency allocations decided at ITU level and is of course in full agreement with the EC policy (as outlined by the European Commission [3]), aimed at the introduction of a single market in which competitive supply opportunities exist, together with a technical harmonisation which ensures maximum compatibility and inter-operability of telecommunications through Europe.

When allocations and assignments (by licensing authorities) have been performed, the question of effective usage of spectrum resources arises, in order to maximise the spectral efficiency of the service under examination. From a quite general standpoint, protection against potentially interfering services may be increased with a proper selection of the available system design parameters. In very general terms, the following measure may be used for quantifying the effective spectrum usage of a system [5]:

$$U = B \cdot S \cdot T \quad (1.1)$$

where  $B$  is the frequency bandwidth,  $S$  the geometric space and  $T$  the time, all denied to other potential user of the same resources. The quantity  $S$ , in particular (usually an area) may be interpreted in some cases as a volume or as an angular sector around a point, whilst in other situation may lose one dimension, as in the case of the geostationary orbit. In case of mobile services, all the above quantities must be taken into account simultaneously and optimised for an effective spectrum management. Once the measure of the spectrum usage is known (according to the previous expression) the actual spectrum efficiency must be evaluated, since the spectrum usage  $U$ , by itself, tells nothing about the efficiency of use; again from a general point of view, a ratio between the information transferred within the system and the above measure  $U$  of the usage may be defined, according to the equation:

$$E = M / U \quad (1.2)$$

where  $U$  has been previously discussed and  $M$  could be the system information transmission capacity (bit/s), the number of radio channels per unit length (or area), or even an equivalent macro-indicator, such as the service area size, the investment revenue, etc.

According to [5], considerable work is needed to transform such general concepts into calculated values for any particular service. In case of mobile communications the above measure may be specialised (irrespective of system characteristics), as:

$$\eta = (N \cdot B) / W \quad (1.3)$$

in which  $N$  is the potential number of users that could be served with the expected quality,  $B$  is the bit-rate of a single digital signal and  $W$  the total available bandwidth for serving the territory. No matter which multiple access scheme is adopted (see Fig. 1.3 for a general schematic representation, with  $n$  transmitters and  $n$  receivers), one can conventionally introduce an equivalent bandwidth dedicated to a single channel, denoted by  $W_0$ ; it is then possible to factorise in the following way:

$$\eta = \frac{B}{W_0} \cdot \frac{N}{W / W_0} = \frac{B}{W_0} \cdot \frac{N}{M} = \eta_f \cdot \eta_s \quad (1.4)$$

where  $\eta_f$  is a measure of the frequency efficiency (depending on the modulation/demodulation technique and coding), while  $\eta_s$  is a measure of the space efficiency, strongly depending on the channel reuse in the territory to be served and the modulation robustness to interference contributions (once the spatial filtering effects, due to both propagation losses and the possible use of directive antennas are taken into account). In practice,  $\eta_f$  and  $\eta_s$  are mutually dependent and what is important is just the combination of both; furthermore, according to the measure  $U$  of spectrum utilisation, a third term should be added to the above equation, to account for the time efficiency too (depending, for a fixed quality, on blocking probability and mean waiting time).

However, time efficiency, as previously defined, has a minor impact on global efficiency; without loosing generality,  $N$  may be then considered as the number of users simultaneously active on the territory (thanks to the cellular structure), while  $M$  is the number that each cell could accommodate, when completely isolated from one another.

Finally, in order to allow comparisons not depending on cell size, a normalised efficiency could be defined, as:

$$\eta_M = \frac{\eta}{N_c} \quad (1.5)$$

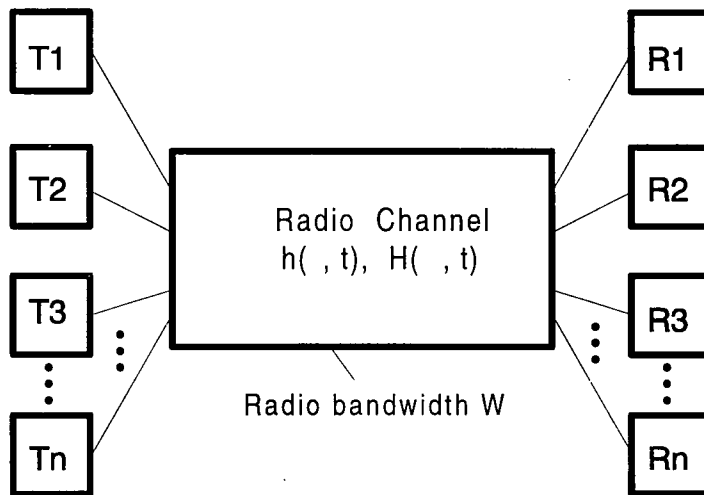


Fig. 1.3 - General scheme of a multiple access to radio channel within a cell.

where  $N_c$  is the number of cells required for an adequate coverage of the service area: according to the selected multiple access technique, the above quantity  $\eta_M$  will take different forms, depending on the orthogonality properties of the adopted scheme (and the related vulnerability to interferences). Further discussions of the relative advantages and drawbacks of different candidate solutions in terms of spectral efficiency are out of the scope of this introductory chapter and will be more extensively addressed afterwards.

### 1.2.2 Enabling Technologies and Advanced Service Provision

The adequacy of enabling technologies is self-evident from the existing hardware implementations which are widespread in use, and from the numerous articles and conference papers devoted to highlight technological developments aimed at future implementations, namely, smaller, lighter and more power efficient hand-held terminals.

Since new generation mobile communication systems should support over a seamless radio infrastructure not only the different service offerings of the second generation ones, but also a much wider range of broadband services (data, voice, video, multimedia), novel multiple-access techniques should be developed for example, together with associated coding and compression technologies, to meet the requirements for a reliable and secure transfer of very large volumes of information at speeds commensurate with those of fixed broadband networks. The overall objective is an improved efficiency of information transfer per unit bandwidth, of frequency re-use planning tools and related channel allocation techniques.

A major application of UMTS is in fact to support data communications for a range of bit rates up to 2 Mbit/s; furthermore, new information systems will be developed that will cover both mobile and fixed workstations. For mobile environments the service providers industry also requires standardised application interfaces: portable workstations are getting smaller and they are often equipped with communication interfaces for mobile and cordless systems. One trend is to integrate the portable computer and mobile telephone into a single unit; this requires adaptive terminal operation, capable to accommodate heterogeneous air-interface characteristics and to optimise the distribution of intelligence between fixed and mobile entities, in order to manage seamless migration among different radio environments. Taking into account the rapid developments occurring in the field of microelectronics, we can expect that the technology will enable the development of Intelligent Multimode Terminals that will provide a full range of service options in the future generations of mobile communication systems and be downwards compatible with current second generation systems too. Finally, as far as the terminals themselves are concerned, the objective is to achieve enhanced performance with reductions in size, weight and battery re-charge frequency.

The enabling technology domain also includes new adaptive (smart) antennas: use of adaptive directional antennas in the context of mobile communications (for base-stations, mobile terminal environments and furthermore indoor and outdoor applications) has been receiving growing attention. Novel developments in fact promise improved frequency re-use, higher protection against interferences, and better overall system capacity, together with a decrease in implementation costs. Coupling these techniques to, and optimised with, sophisticated digital signal processing technology will allow an adaptive, flexible and power efficient transceiver system.

A specific category of user is the personal roamer, operating in developing as well as in developed countries: to provide telecommunication services to these categories of users will require the internetworking and service support of fixed and mobile satellite or terrestrial systems that support narrow and broadband services. Individual requirements may demand handover between terrestrial and satellite systems with terminal equipment capable of accessing both: certain international organisations and large multinational corporations in fact need fixed, temporary fixed and mobile communications and often such organisations operate in developing countries with no telecommunications infrastructure. It is indeed of strategic importance to meet the requirements for wireless communication with very high throughput and to develop the industrial capability to produce the necessary system components: even more, in order to achieve the required high bit rates (up to 155 Mbit/s), it is necessary to consider high frequency spectrum resources. In this context, research to determine the optimum spectrum allocation (either in the K- or Ka-band, or in the 60 GHz region, where two sub-bands at 62-63 GHz and 65-66 GHz have been identified) is needed. MBS-like systems will provide novel multi-media and video mobile telecommunication applications, including applications appropriate to wireless, office, broadband systems.

### 1.2.3 Terrestrial/Satellite Mobile Networks Integration

In recent years there has been significant evidence that personal communications will evolve as hybrid fixed/mobile/satellite networks: system concepts have been developed to cater to specific markets, but conventional satellite designs appear not to be able to provide economical service to hand-held terminals, thus different concepts have emerged. Specifically, geosynchronous orbit satellites (GSO) operating at the Ka-band (20-40 GHz) or low earth orbit (LEO) and highly elliptical orbit (HEO) are contenders to provide the order of magnitude increase in communication capacity required for operation of extremely small terminals used in mobile communication networks. Congestion in currently used frequency bands and the demand for small earth stations is bringing EHF satellite communications to the point of economical viability, even if signal deteriorations due to hydrometeors and vegetation/building blocking phenomena are major drawbacks. In this perspective, the satellite component of MBS, as with UMTS, has to be carefully investigated: in principle, satellites in all the above mentioned different orbits are capable of offering operation to hand-held terminals, but with varying degrees of propagation delays and associated satellite and ground network complexity. The selection of a particular orbit will be a trade-off of these parameters. Compared with cellular systems, the satellite component of UMTS/MBS will be limited by the number of users it can support; there may also be limitations in the range of services it can economically offer to customers. However, they will have significant role to play due to the ability to serve economically very large areas: this should enable them to complement terrestrial UMTS/MBS with global roaming, and possibly to support introduction of some services ahead of a terrestrial infrastructure. Satellite components may also provide fixed links from one UMTS/MBS network, say in a developing country, to the Intelligent Network (IN) of developed countries (interconnection of UMTS/MBS islands); this may help the roll-out of the IN or provide economy where traffic is low. Another important application in this area is the use of a local satellite gateway where direct access to the space segment with the personal communicators is not feasible.

Relevant to the work in this area are the developments taking place in the world, under different schemes and constellations, such as IRIDIUM, GLOBALSTAR, INMARSAT P21, ESA-ARTES, etc. In this framework, the European RACE SAINT project and COST Action 227 (Integrated Space/Terrestrial Mobile Networks), both aiming at evaluating and identifying the requirements for integrating satellites into future personal mobile telecommunications are of paramount importance. This process of Fixed, Mobile & Satellite Network Integration will involve fundamental investigation of the essential network architectures, networking principles, functionality disposition, signalling and control procedures, together with protocols and terminal located functionality, that leads to the definition of efficient and economic network architectures which are mutually compatible: the essential functional, transmission and operating characteristics of each network must be recognised and accommodated by the linked networks.

### 1.2.4 Standardisation

Standardisation seems to be the area of slowest progress: while there is general agreement that global standards are in everybody's interest for the inter-operability of regional telecommunication networks of various kind in order to provide the customer with new universally accepted and available services, some difficulties still seem to exist in the co-operation between regional and international bodies. It may be worthwhile noting that ISDN standardisation has required approximately 15 years and the ATM standard is under development by about 5 years; this in spite of the fact that, on average, telecommunications have developed up to now more than 50% of all existing standards in all possible activity fields at a world-wide level. Standardisation needs a spontaneous consensus from all interested parties, nobody excluded, in some cases on very specific solutions: current procedures (and the relevant structures of specification bodies) appear to be rather cumbersome and no longer adequate to the actual objectives and market requirements, which are the unique real independent variable of the global system. A lack of a suitable and timely answer from the standardisation world would probably lead to pragmatic approaches, such as de facto world-wide standards (INTERNET is a significant example), built up on the ground of market requirements, technology availability and large multi-national companies willing, aimed at actual proprietary solutions, without any a priori agreement.

In this respect, recent initiatives taking place in Japan, North America and within the European Community indicate that to meet the challenges of globalisation and international competition, very significant effort must be devoted to the development of personal telecommunications networks, products and services. In Europe, the European Telecommunications Standards Institute (ETSI) established an "ad-hoc" Group on Universal Mobile Telecommunications System, now SMG5 (Subgroup 5 of the "Special Mobile Group"), which focused on the critical points to be studied for systems suitable for providing personal communications services to people on the move. The main goal of the Group is the definition of the services that can be potentially delivered by radio, with particular reference to access and terminal mobility aspects. This work has a very close relationship with concurrent ITU-R specification activities on FPLMTS [6] and ITU-T studies on UPT (Universal Personal Telecommunications), which is a service concept, aiming at the provision of a full personal mobility. Other regional standardisation bodies are currently active in the same field: the T1 Committee in US and TTC in Japan are two major examples, together with other organisations from Korea (TTA), Australia (ATSC) and Canada (TSACC) [7].

The recent reorganisation of ITU will undoubtedly stimulate progressively closer co-ordination between the various standardisation efforts. In fact, tight relationships among the various regional bodies dealing with third generation systems are warmly supported: this is reflected in a recent draft new ITU Opinion [8] which urges the ITU to make every effort to persuade regional and national authorities to support the Radiocommunication Sector in an explicit manner in its development of Recommendations on FPLMTS and strongly encourage regional organisations to

work together towards a single world-wide standard: the co-ordination of the regional bodies within world-wide standardisation mechanisms is a first positive answer. Their grouping formerly in the Interregional Telecommunications Standards Conference (ITSC) and now around its successor, the Global Standards Collaboration (GSC), should result into an effective and efficient supervision of standards-making management, by means of voluntary exchange of information among their members, thus complementing ITU international activities, minimising the potential risks of overlap and/or duplication of work, and, on the whole, increasingly shaping the world of telecommunications. Accordingly, there is a need to continue, if not accelerate, contributions from any interested institution to standardisation bodies on all aspects regarding UMTS.

## 1.3 Medium/long-term Action perspectives

In the particular field of mobile radio (or personal communications), the above co-operative approach will facilitate the implementation of a smooth transition from the second generation (not compatible) systems to the universal third generation one: COST 231 most ambitious aim was to act as a focal point within such a process.

### 1.3.1 Objectives and Participation

The objectives of the Project were, among others [9], to identify the characteristics of third generation mobile and personal radio systems currently under specification, and to provide design methods and coverage models for their implementation: this involves studies on digital transmission techniques. Propagation studies were concurrently carried on in the UHF band for modelling and simulation of the transmission channel, and establishing prediction methods for attenuation (shadowing, penetration losses, etc.) and multipath effects in large, small and indoor cells. For the long-term period, communications systems for broadband services (i.e., services requiring a capacity greater than that of the basic ISDN services) have been studied, which involve a large spectrum of new telecom technologies at millimetre wave and infrared bands. Then, COST 231 research programme covered a wide spectrum of land mobile communications aspects, with a major emphasis on personal communications systems that in the near future will provide voice and data communications through small, cheap, handportable radio terminals.

**Participating Countries and Entities.** Currently, 20 signatory Countries participate at the M.C. meetings: Austria, Belgium, Czech Republic, Denmark, Finland, France, Germany, Greece, Ireland, Italy, The Netherlands, Norway, Poland, Portugal, Slovenia, Spain, Sweden, Switzerland, Turkey, United Kingdom. COST 231 M.C. meets three times a year, usually on invitation by Administrations, Research Institutes or Universities; more than 80 people usually attend the meetings, from some 70 participating entities (Research Institutes, PTTs, Manufacturers, Universities), as listed in Annex 1.

### 1.3.2 Liaisons with European research and specification bodies

The COST 231 Project started on 6 April 1989 [10] and, formerly scheduled to expire on April 1993, was extended to 5 April 1996, with a three year extension, aimed on one hand to fully support ETSI in its standardisation activities of UMTS, on the other to investigate, for the long-term period, communications systems for broadband services, as well as the relevant propagation characteristics in the appropriate frequency bands (from high microwaves to millimetre waves), taking into account channel limitations and impairments.

Accordingly, COST 231 work in this stimulating context can be envisaged to complement the research activities carried out within international and regional bodies and, by definition, had a synergistic relationship with both ETSI standardisation activities on UMTS and ITU studies on FPLMTS and UPT.

As a matter of fact, in addition to the relationships with most RACE Projects, a number of liaisons with several regional or international bodies (ITU-R SG3, ITU-R TG8/1, ETSI-SMG2, ETSI-SMG5, ETSI-RES02, ETSI-RES03, ETSI-RES10, UK Technical Working Party on Mobile Propagation, UK LINK CDMA Project, URSI) were established by COST Action 231, and were fostered through exchange of documents and participation to meetings: "ad-hoc" rapporteurs are appointed.

### 1.3.3 Action activities

According to the objectives, the major goals were to identify the characteristics of radio systems and provide design methods and coverage models for their implementation [11]. Propagation studies have been carried on for modelling and establishing prediction methods for attenuation (shadowing, penetration losses, etc.) and multipath effects in large, small and indoor cells. For the medium-long-term period, most items concerning future mobile and personal telecommunication systems were examined: narrowband and wideband techniques, coding and access schemes, prediction methods for micro- and pico-cellular applications. COST 231, due to its nature and commitment to basic researches, had the freedom to consider and compare several promising alternatives, in addition to those addressed for example by RACE Projects, with particular reference to broadband services and related technological problems.

The work has been split into three main areas, allocated to three working groups:

- WG1 - Radio System Aspects
- WG2 - UHF Propagation
- WG3 - Broadband Applications

WG1 focused its work on system options and techniques for future third generation standards; the work of WG1 was seen to complement the various RACE Projects, and also to provide significant results for the ETSI SMG5 Group. Particularly important are the contributions looking at multiple access techniques (CDMA,

TDMA, etc.), and the work in new modulation and coding techniques. Three types of CDMA systems were examined in detail, namely DS-CDMA, FH-CDMA, Hybrid SFH/DS-CDMA, together with related problems of interference suppression, spectrum sharing and integrated voice/data services.

WG2 covered the mobile channel characteristics at frequencies between 900 MHz and 3 GHz. Particular attention was given to outdoor measurements and modelling (macro and micro-cells), by developing both statistical and electromagnetic prediction methods, taking into account the effects of system parameters, such as base station antenna height and directivity, site location and environment. Increasingly, the emphasis has been on outdoor short-range, indoor propagation and building penetration, in the perspective of finding suitable planning tools for micro- and pico-cellular environments.

WG3 dealt with both propagation (at microwave and mm-waves) and system aspects. The group concentrated on high data rate ( $>10$  Mbit/s) short range communication in the indoor environment, both from a theoretical (modelling and simulation) and experimental standpoint, using millimetre wave radio frequencies ( $>30$  GHz) where there is adequate bandwidth available. Attention has also been paid to outdoor environments and infrared wavelengths, with particular reference to High Performance Radio Local Area Networks (HIPERLAN), considering typical classes of application. Attention was also given to the safety aspects for both millimetre wave and infrared radiation and to study the performance of possible system configurations for wireless optical systems (and relevant constraints).

## 1.4 Outline of the Contents

According to previous statements, this book covers two main broad areas, respectively dealing with systems for narrowband/wideband communications operating at around 2 GHz, and systems for broadband communications operating at high microwave and millimetre wave bands. Such division appears to be as the most appropriate one, taking into account the potential solutions envisaged for the future [12].

### 1.4.1 Narrowband & Wideband Communications

Mobile system planning is a very broad process that is related to technical aspects on one hand and economic aspects on the other hand. Consequently, there are two main research areas: Simulation Tools and System Planning. Simulation Tools allow to evaluate the performance of a system and to optimise the parameters to meet the specified service or application requirements; the simulation of a system or of a sub-system is based on techniques capable to describe both the systems and the environment, and take into account channel models, mobility models, traffic models, service and application models, etc. As to the second area, System Planning is a specific structured methodology to plan entire communication systems: rather than to consider technical details, as it is the previous case, it deals with economic aspects

and overall performance, reliability, efficiency, capacity capability and acceptance aspects for specified services and applications. COST 231 mainly focused on the first area, with particular reference to the identification of the propagation channel properties and relevant software and hardware simulation techniques: this is reflected in the contents of Chapter 2 (Radio Channel Characterisation). In fact, to characterise a mobile radio channel and establish prediction methods, the first step is to measure it with sufficient accuracy. Third generation of digital cellular systems will have a larger bandwidth than current systems and will be operated in various environments. As a consequence, the investigation of propagation phenomena needs channel sounders able to measure the frequency selective behaviour of the channel by means of either the impulse response or the transfer function in at least the system bandwidth, and to cope with different constraints according to the environment, in terms of maximum excess delay, time resolution, etc. Of course, usual field strength measurements are still needed for path-loss modelling and planning purposes, but the techniques are rather well known; therefore, wideband measurements were given a special attention. Furthermore, measurements of the Direction-of-Arrival (DOA) of multipath components are also a relatively new feature which is important in order to validate prediction methods based on ray tracing (or, more generally, ray-optical methods) and to find good physical models, capable of describing propagation effects like diffraction and scattering by buildings and street corners. Chapter 2, again, concentrates on all the above topics.

In Chapter 3 (Antennas and Antenna Diversity) COST 231 studies on antennas for both base stations and portable terminals are included, and diversity techniques (including combining strategies) are examined, with a discussion of the improvements achievable using macro- or micro-diversity techniques. A particular attention is given to low-absorption (and reduced health hazards) hand-portable applications, together with the investigation of antennas configuration, as well; this would allow to identify the implementation of small-sized equipment and to optimise the relevant link performance. Finally, the advantages of using directive and adaptive (smart) antennas are addressed, stressing the significant achievable improvements, in comparison with antenna systems currently in use, based on either fixed pattern antennas or single space-diversity switching techniques.

In the field of propagation, prediction methods and related data base management were investigated, considering outdoor large cells, outdoor small cells, outdoor micro-cells (short range applications), in-building pico-cells and outdoor/indoor propagation (including penetration losses and attenuation phenomena due to internal walls, floors and ceilings). Overlaid and three-dimensional cellular coverage structures were also examined, including suitable modelling of the wave propagation and application examples (coverage structure for large and small indoor areas, multi-storey buildings, etc.). In fact, in order to evaluate the performance of a system and to optimise the relevant parameters by means of a simulation tool, a sound knowledge is required of the various propagation mechanisms and of the specific approach to be adopted for a given environment. Chapter 4 (Propagation Prediction Models) addresses such issues, together with models for coverage of special environments, such as tunnels: this is particularly important for communication

services with trains. Working with terrestrial cellular networks (using a common standard) would provide the railroad operator and passenger with means of communicating across state boundaries. Tunnels require ad hoc coverage solutions, but at the frequencies envisaged for UMTS operation the ratio of tunnel cross-section and wavelength encourages natural wave propagation within the tunnel, with considerable cost savings, by using antenna systems instead of leaky feeders. In addition, the velocity of some trains exceeds the presently specified capabilities of cellular networks; therefore, the effect of high speed (in combination with the environmental conditions of rail tracks, cuttings, tunnels, etc.) on the reliability of digital transmission was subject of investigation.

In order to identify the most suitable radio access methods for the future Universal Mobile Telecommunications System, advanced transmission techniques must be studied. Continuing studies on modulation methods, multiple access, adaptive channel equalisation, coding, diversity techniques, etc. have been carried out, considering the need for adapting the bit rates to service requirements and channel conditions. Radio Subsystem Aspects Group started its activities examining the performance of 2nd generation systems; a special attention, as described in Chapter 5 (GSM and DECT Systems), was paid to DECT: one good example has been the performance assessment of DECT in different reference scenarios, in the presence of significant delay spreads. Also GSM radio-link performance under selective frequency propagation conditions was investigated, and improvement by using either frequency hopping or antenna diversity was addressed, as well.

Increasingly the emphasis has been on system options and techniques for 3rd generation standards; a special attention was devoted to study Advanced Radio Interface Techniques and Performance (Chapter 6). As far as multiple access techniques are concerned, researches were directed towards Advanced TDMA methods and several Spread Spectrum and CDMA schemes, such as Direct Sequence (DS) CDMA, Frequency Hopping (FH) CDMA, Hybrid Slow Frequency Hopping/Direct Sequence CDMA Systems, CDMA with interference suppression. Concurrently, Chapter 6 present COST 231 studies in the field of coding, modulation and equalisation: a number of equalisers are examined, with particular reference to Viterbi Equalisation with Non-Coherent Modulation, Joint Equalisation, Impulse Response Estimation, Block Decision Feedback Equalisation. Recently, there has been much progress in the research of fast algorithms applicable for adaptive equalisers and echo cancellors: COST 231 work concentrated also on massively parallel structures and VLSI simulation of fast parallel adaptive echo cancellors based on FIR filtering. Finally, Medium Access Control (MAC) protocols and (dynamic) channel allocation strategies are discussed, together with handover capabilities, allowable cell size, maximum mobile speed, roaming capabilities, coexistence with other systems sharing the same frequency bands.

Potential Radio Interface Subsystems for UMTS are examined in Chapter 7; specific different approaches are discussed in detail (Advanced TDMA, DS-CDMA, CTDMA and JD-CDMA), and the relevant performance and spectrum efficiencies assessed for the candidate solutions. Hybrid systems, in particular, appear to be

attractive, because they can combine the advantages of both direct sequence and frequency hopping systems, while avoiding some of their disadvantages. Moreover, such systems offer the possibility to increase the system capacity and may also use shorter spread spectrum code sequences and hopping patterns, thus reducing the overall acquisition time. On the other hand, a drawback of hybrid systems is the increased complexity in their transmitters and receivers: a careful investigation on these topics was carried out. Furthermore, since interference in CDMA could be a limiting feature unless optimum power control is guaranteed, if the impact of imperfect power control has to be reduced adequate CDMA system capacity can only be obtained by applying methods of interference suppression. Such methods can be subdivided into interference cancellation (IC) and joint detection (JD). Both are examined: the potential of the latter, in particular, seems to be very promising and is analysed in a section of Chapter 7.

### 1.4.2 Broadband Communications

The communication landscape of the future will be characterised on one side by a heterogeneous set of networks, including B-ISDN, N-ISDN, usual telephone lines, wireless techniques (including radio in the local loop), and LAN-standards. Wireless voice/data transmission in particular has become an important factor in communication techniques and it is used to develop a new generation of Wireless LANs: as known, the use of the radio transmission technology for LANs will provide an alternative to the cabling of offices and industrial plants. In this scenario, HIPERLAN could play a dominant role: WG3 activities to support ETSI Committee RES-10 in developing a standard for a HIgh PErfomance Radio LAN are worth noting. HIPERLAN, which has been recently assigned spectrum by CEPT/ERC in the 5 GHz and 17 GHz bands for specific use (even if on a non-protected from and non-interference to basis), plans to distinguish itself from earlier spread spectrum products by the large bandwidth (with a target of about 20 Mbit/s) and its time-bounded service capability (aimed at multimedia applications). Furthermore, HIPERLAN should also be able to support ad hoc networking of highly portable PCs, (such as laptops, note-books, pen-books), including full-scale Personal Intelligent Communicators (PICs) and Personal Digital Assistants (PADs) [13], as a result of the technological merger of mobile telecommunications, computer technology and consumer electronics. Functionally these personal communicators are a combination of a portable computer and a cellular telephone thereby giving the user the facilities of data transmission, fax, electronic mail, paging, voice telephony as well as the capability to organise and manipulate information (agenda/scheduler). In Fig. 1.4 a feasible timeline evolution is reported, as excerpted from [1], in terms of potential deliverable services (from voice to multimedia), and related transmission rates.

Accordingly, the majority of HIPERLAN applications are envisaged to be extensions of wired LANs, providing transport of asynchronous data and real time voice and image streams, granting access facilities to public networks with efficient

internetworking, and allowing multiple networks co-existence without the need of frequency planning and co-ordination.

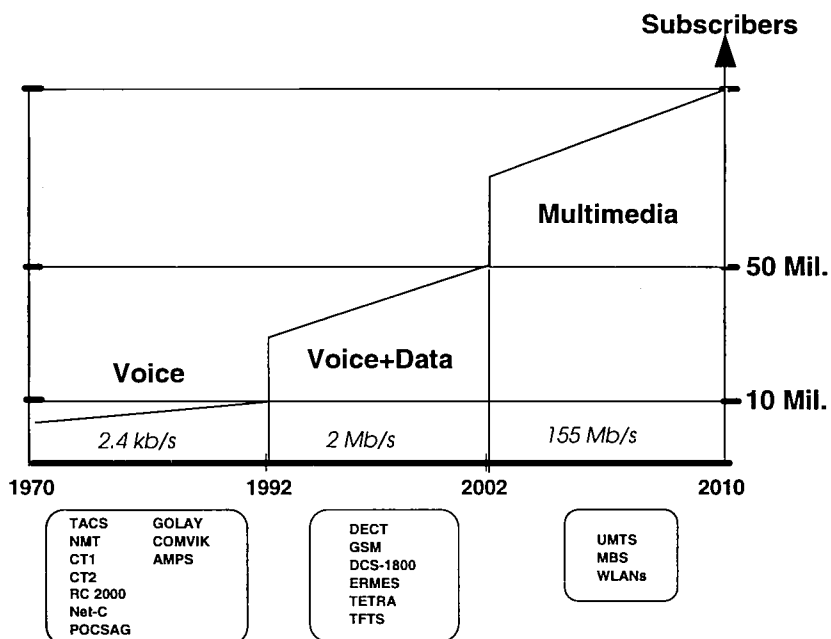


Fig. 1.4 - Evolution timeline towards personal communications and multimedia services.

Of course, HIPERLAN will provide mobility (at least for pedestrian or indoor vehicle speeds), and security (comparable to that of traditional LANs), preventing eavesdropping and ensuring protection against unwanted data injection. Different environments (office, production, storehouse) have different requirements, which concern security, range, health aspects, transmission rate, re-using of frequencies, cost, maintenance, penetration ability, etc. In this respect, the studies on broadband communications carried out in COST Action 231 were directed towards systems operating in the quasi-millimetre band, although this does not rule out considerations of other bands (IR, Infrared) in the light of any future developments, taking also into account the similarities between IR and mm-wave systems at the physical level. Both system aspects and propagation studies in the radio-frequency and optical field have been dealt with, considering communications within buildings with one cell per room, taking advantage of the natural (atmospheric) and man-made shielding effects, cellular coverage of indoor areas (office and industrial buildings) with indoor base stations, coverage of indoor areas from external base stations,

communications from inside a building to a mobile outside, local-area broadband radio networks and outdoor millimetre-wave cellular coverage. The studies concentrated on material characterisation, modulation schemes, non-ideal receivers (especially carrier recovery), to include the effects of co-channel interference and evaluate the application of DS-CDMA and frequency hopping techniques. Transmission performance evaluation, using both simulations and field trials, covered several aspects, such as outage probability evaluation, analytical models for frequency selective channel, adaptive equalisation, OFDM systems and CDMA systems, and dynamic channel allocation. All the above topics are considered in Chapter 8 (Broadband Communications); in the same chapter a variety of medium access control protocols, with a particular attention to the HIPERLAN features are discussed. Analytical models for multipath fading, shadowing, near-far-effect in the mm-wave communication systems to evaluate network performance are then examined, together with the study of suitable protocols for high data rate and for voice and data integration.

## 1.5 References

- [1] CEC DG XIII, *ACTS Workplan (Requirements and Options in Advanced Communications Technologies and Services)*, Draft Version 4.0, Brussels, Belgium, June 1994
- [2] ITU, *Final Acts of the World Administrative Radio Conference for dealing with frequency allocations in certain parts of the spectrum (WARC-92)*, Geneva, Switzerland, 1992
- [3] CEC DGXIII, *Study on analysis of new methods of frequency allocation in the Member States and comparative analysis of recent developments in this field - Final Report*, London, UK, July 1993
- [4a] ERO, *Detailed Spectrum Investigation - First Phase: 3400 MHz to 105 GHz*, Copenhagen, Denmark, Mar. 1993
- [4b] ERO, *Detailed Spectrum Investigation - Phase II: 29.7 MHz to 960 MHz (the trends and preliminary views)*, Prague, Czech Republic, Nov. 1994
- [5] ITU-R, SG1 (Spectrum Management), Rep. 662-3, *Definition of spectrum use and efficiency*, CCIR XVII Plenary Assembly, Vol. 1, Düsseldorf, Germany, 1990
- [6] ITU-R, SG8 (Mobile, Radiodetermination, Amateur and related Satellite Services), Rec. 687, *Future Public Land Mobile Telecommunication systems (FPLMTS)*, CCIR XVII Plenary Assembly, Vol. 8, Düsseldorf, Germany, 1990
- [7] K. Habara, "Co-operation in Standardisation", *IEEE Comm. Magazine*, Vol. 32, No. 1, Jan. 1994, pp. 78-84
- [8] ITU-Radiocommunication Assembly, *Study Group 8 Chairman's Report*, Doc. 8/1001, Nov. 1993
- [9] G. de Brito, "Overview of the activities of the Project COST 231", in *Proc. of ICUPC'93 - 2nd International Conference on Universal Personal Communications*, Ottawa, Canada, Oct. 1993

- [10] COST Doc. 262/88, *COST 231 Project Draft Memorandum of Understanding*, Brussels, Belgium, Dec. 1988
- [11] COST Doc. TD(93)79 Rev.1, *Interim Report*, Limerick, Ireland, Sep. 1993
- [12] P. Porzio Giusto, "Mobile and Personal Communications", in *Proc. of Symp. on New Frontiers for the European COST in Telecommunications*, Rome, Italy, Oct. 1992
- [13] S.K. Barton, "HIPERLAN, the high performance local area network", in *Proc. of COST 235/231 Joint Workshop*, Prague, Czech Republic, Apr. 1994

## Radio Channel Characterisation

**Jørgen Bach Andersen, Aalborg University, Denmark**

The properties of the time varying, frequency dispersive radio channel used for mobile and personal communications are important to know for several reasons. There are scientific reasons for understanding the phenomena involved, and there are practical reasons for being able to design optimal communications networks which have the best possible signal strength and quality for a multi-user situation. In COST 231 Working Group 2 on UHF propagation a number of collaborative results have been achieved, which are described in Chapters 2, 3 and 4.

Specifically, Chapter 2 focuses on the theoretical basis for describing the instantaneous and average quantities are given, as well as measurement techniques and results, and methods for simulating the mobile channel.

In the following Chapter 3, novel results for antennas are described, both for the base station and the portable unit. For the base station diversity systems play an important role, both micro- and macro diversity, while for the portable antennas problems like absorption in the user have been addressed.

Finally, Chapter 4 describes the results of modelling the pathloss and time dispersion for rural, micro cells and indoor situations. It is especially significant that a number of theoretical models have been compared with the same reference experimental situation, making comparisons possible. In the last section, models for penetration into buildings and propagation in special environments (such as tunnels) have been addressed.

## 2.1 Characteristics of radio channels

**Bernard Fleury, Swiss Federal Institute of Technology, Switzerland**

In the mobile radio environment, a part of the electromagnetic energy radiated by the antenna of the transmitting station reaches the receiving station by propagating through different paths. Along these paths, interactions which are commonly referred to as propagation mechanisms, may occur between the electromagnetic field and various objects. Possible interactions are specular reflection on large plane surfaces, diffuse scattering from surfaces exhibiting small irregularities or from objects of small size, transmission through dense material like walls or floors, shadowing by obstacles like trees, etc. The attributes small and large are to be understood here with respect to the wavelength. A detailed description of these propagation mechanisms is given in Chapter 4, Section 4.3.

During the last few years, attention in the research field of propagation prediction and to some extent in the area of propagation simulation has been increasingly focused on issues concerning the resolution of the electric field with respect to both the propagation delay and the incidence direction (cf. e.g. [1], [2]). The characterisation given below accounts for this development in the sense that it relies on the notion of the field direction-delay-spread function.

### 2.1.1 Field Direction-Delay-Spread Function

For the subsequent discussion it is worth regarding the impinging waves as being radiated by sources which are distributed in the surroundings of the receiver. Due to the different positions of these sources, the resulting electric field at the receiver position is spread both in time and in direction. The dispersive nature of the environment is characterised by the location-dependent direction-delay-spread function (DDSF)  $\vec{E}(\vec{z}, \Omega, \tau)$  of the electric field vector. Here,  $\vec{z}$  denotes the receiver position with respect to an arbitrary co-ordinate system with origin  $O_{ref}$  (see Fig. 2.1). The element  $\Omega$  of the sphere  $S$  of arbitrary radius uniquely characterises the incidence direction (see Fig. 2.2) and  $\tau$  stands for the delay variable. The spherical co-ordinates  $\phi$  (longitude) and  $\theta$  (colatitude) uniquely determine the direction  $\Omega$ , and conversely.

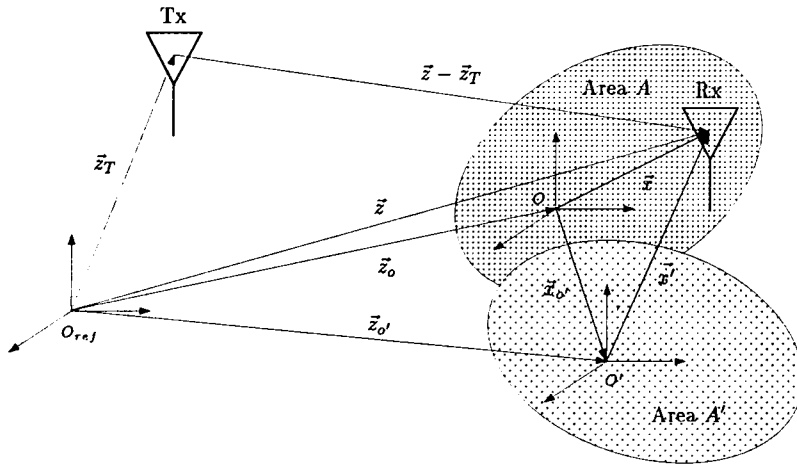


**Fig. 2.1** Geometrical situation considered.

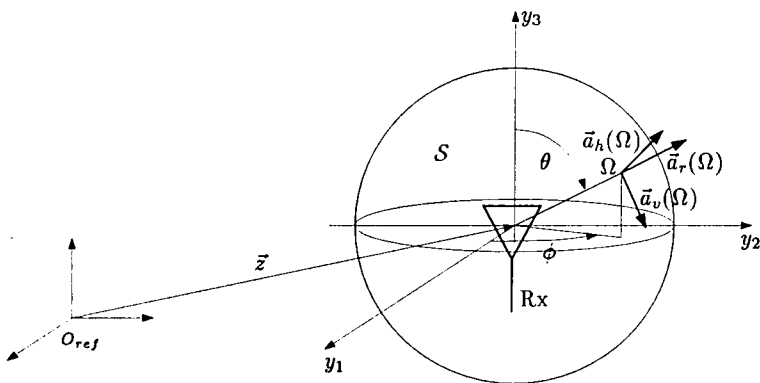


**Fig. 2.2** Definition of the direction  $\Omega$  and its associated unit vectors  $\vec{a}_r(\Omega)$ ,  $\vec{a}_h(\Omega)$ ,  $\vec{a}_v(\Omega)$ .

**Assumption 1:** The receiver is located in the far-field region of the radiating sources. As a consequence, the impinging waves are transverse electromagnetic. Their electric field vector  $\vec{E}(\vec{z}, \Omega, \tau)$  lies in the plane spanned by the unit normal vectors  $\vec{a}_h(\Omega)$

and  $\vec{a}_v(\Omega)$ . Accordingly, denoting with  $E_{h|v}(\vec{z}, \Omega, \tau)$  the horizontal + vertical component of  $\vec{E}(\vec{z}, \Omega, \tau)$ , the following relationships may be written:  
 $\vec{E}(\vec{z}, \Omega, \tau) = E_h(\vec{z}, \Omega, \tau)\vec{a}_h(\Omega) + E_v(\vec{z}, \Omega, \tau)\vec{a}_v(\Omega)$ . Then, let  
 $E(\vec{z}, \Omega, \tau) := [E_h(\vec{z}, \Omega, \tau), E_v(\vec{z}, \Omega, \tau)]^T$  be the field DDDSF (FDDSF) at location  $\vec{z}$ , where  $[\cdot]^T$  stands for the transposition operation. Depending on the kind of interactions along the propagation paths, the FDDSF may embody a coherent and a diffuse part, i.e., it can be written as

$$E(\vec{z}, \Omega, \tau) = E_c(\vec{z}, \Omega, \tau) + E_d(\vec{z}, \Omega, \tau), \quad (2.1)$$

where  $E_d(\vec{z}, \Omega, \tau)$  is a regular vector-valued function, while  $E_c(\vec{z}, \Omega, \tau)$  is a sum of weighted Dirac measures:

$$E_c(\vec{z}, \Omega, \tau) = \sum_{j=1}^{J(\vec{z})} E_j(\vec{z}) \delta(\Omega - \Omega_j(\vec{z})) \delta(\tau - \tau_j(\vec{z})). \quad (2.2)$$

The FDDSF can also be decomposed into a sum of components each being contributed by a specific radiating source:

$$E(\vec{z}, \Omega, \tau) = \sum_{\ell=1}^{L(\vec{z})} E_\ell(\vec{z}, \Omega, \tau). \quad (2.3)$$

As the location changes over small areas not larger than some tens of the wavelength, the components in (2.3) exhibit rapid fluctuations in amplitude and phase which are called small-scale variations or small-scale fading. As the receiver moves over larger areas, the distance and the direction of the radiating sources vary with respect to its instantaneous location. Consequently, their corresponding component in the FDDSF drifts in the  $(\Omega, \tau)$ -space as a function of  $\vec{z}$ . Moreover, some radiating sources may be partly obstructed or disappear while new ones may arise, e.g., in transition regions from a line-of-sight (LOS) to a non-line-of-sight (NLOS) situation or vice-versa. Thus, some components in (2.3) may be attenuated or vanish and new ones may appear. The variations due to location changes over wider areas are called large-scale fluctuations or large-scale fading.

## 2.1.2 Space-Dependent Channel Impulse Response

The radio channel incorporates the propagation medium as well as the transmitting and receiving antennas. Its response is given up to a proportionality constant  $C$  which

depends on the antenna characteristics from integrating the FDDSF weighted by the antenna field pattern with respect to the direction:

$$h(\vec{z}, \tau) := C \int f(\Omega)^T E(\vec{z}, \Omega, \tau) d\Omega.$$

Here,  $f(\Omega)$  is the electric field pattern of the receiving antenna, i.e.,  $f(\Omega) = [f_h(\Omega), f_v(\Omega)]^T$ . The channel impulse response (CIR) is equal to  $\frac{1}{P_r} h(\vec{z}, \tau)$ , where  $P_r$  is the power at the input of the transmitter antenna. According to common practice,  $h(\vec{z}, \tau)$  is also referred to as the CIR in the sequel. It essentially retains the features of the FDDSF regarding the short-term and large-scale fluctuations and its decomposition into a coherent and a diffuse part as

$$h(\vec{z}, \tau) = h_c(\vec{z}, \tau) + h_d(\vec{z}, \tau) \quad (2.4)$$

with 
$$h_c(\vec{z}, \tau) = C \sum_{j=1}^{J(\vec{z})} f(\Omega_j(\vec{z}))^T E_j(\vec{z}) \delta(\tau - \tau_j(\vec{z})) \quad \text{and}$$

$h_d(\vec{z}, \tau) = C \int f(\Omega)^T E_d(\vec{z}, \Omega, \tau) d\Omega$  or into the sum of the components corresponding to the radiating sources according to  $h(\vec{z}, \tau) = \sum_{\ell=1}^{L(\vec{z})} h_\ell(\vec{z}, \tau)$  with

$$h_\ell(\vec{z}, \tau) = C \int f(\Omega)^T E_\ell(\vec{z}, \Omega, \tau) d\Omega. \quad (2.5)$$

### 2.1.3 Time-Dependent Channel Response

When the receiver moves along a trajectory  $\vec{z}(t)$ , the channel varies with time. Its time-variant response is given as

$$h(t, \tau) := h(\vec{z}(t), \tau). \quad (2.6)$$

Notice that strictly speaking the widely used expression time-variant impulse response is not appropriate for  $h(t, \tau)$  because this function is not the response of the channel to an impulse at a certain instant. The time fluctuations of the channel response (CR) which result from the small-scale and large-scale variations are referred to as short-term and long-term variations or fading, respectively. Studies of the time-variant radio channel traditionally rely on the assumption that the temporal fluctuations exclusively

result from receiver displacements with constant velocity, i.e., the receiver trajectory is of the form

$$\vec{z}(t) = \vec{z}_0 + \vec{v}t. \quad (2.7)$$

In this case,  $h(t, \tau)$  reflects up to the time scaling factor  $\|\vec{v}\|$  the spatial behaviour of  $h(\vec{z}, \tau)$  along the straight line precisely given in the parametric form (2.7). Movements with constant velocity are realistic in the outdoor environment where the receiver is mounted in a vehicle. In this case, the Doppler rates caused by the vehicle accelerations can be neglected in comparison to the experienced Doppler shifts. In contrast to this, movements of human beings are slower but more irregular. They exhibit continuous changes in their direction and rapidity so that the model (2.7) does not apply anymore. Recently, the time-variant behaviour of the radio channel has been investigated when the receiver is assumed to perform a Brownian motion [3], [4] or a displacement generated by a stochastic model whose development relies on experimental studies of human arm movements [3]. Despite the close relationship between  $h(\vec{z}, \tau)$  and  $h(t, \tau)$  described by (2.6), the spatial and temporal behaviour of the channel may substantially differ due to the irregularities of the trajectory  $\vec{z}(t)$  [5].

Other sources than receiver displacement may cause the radio channel to become time-variant. For example, shadowing, absorption or scattering may be caused by moving vehicles in an outdoor environment or persons in an indoor environment. The resulting fast variations due to changes of the multipath interference pattern contribute to the ST fluctuations of the channel, while the variations due to shadowing can be embodied in its LT fading [5]. Time variations also arise from changing the orientation of the receiver antenna [6], due to its usually non-isotropic field pattern, and from the time fluctuations of the electrical properties of the scattering objects like fluorescent tubes [7].

The term CR is also used in the sequel to refer to  $h(\vec{z}, \tau)$  when the underlying discussion concerns  $h(\vec{z}, \tau)$  and  $h(t, \tau)$  without distinction.

## 2.1.4 The Sources of Randomness

Radio environments may have extremely different geographical and electrical features, e.g., indoor and outdoor environments, which in turn may lead to basically different dominant propagation mechanisms. For that reason, categories of environments have been identified within which the propagation scenarios are expected to be quite similar. These categories are characterised by the cell type, i.e., macro-, micro-, and picocells, and the area type (urban, suburban, rural, etc. for macrocells). However, variability remains between the environments within a given

category, such as in the arrangement, the mean height, and the electrical properties of the buildings in an urban area, which can be conceived as a source of randomness. Moreover, the features of a specific environment in a given category usually cannot be entirely described. Especially, the geometrical and electrical properties of the objects interacting with the electromagnetic field can only be specified up to a certain level of accuracy. This indeterminateness can also be viewed as an additional cause of randomness. A third source of randomness is the indeterminateness with regard to the specification of the receiver position or of the factors leading to time variations. Even receiver movements with constant velocity are usually not completely described. The velocity is usually specified but not the starting point or even the direction of the motion. The three sources above contribute to make the FDDSF and therefore the CRs random.

### 2.1.5 Characterisation of the Small-Scale/Short-Term Fluctuations

**Model Assumptions.** The following assumption is made to describe the behaviour of the FDDSF and the CRs over small areas.

**Assumption II:** Uniform unattenuated plane waves are impinging in a neighbourhood of the receiver position.

Let  $O$  denote an arbitrary local reference point in this area (see Fig. 2.1). The location of  $O$  with respect to  $O_{ref}$  and the receiver position with respect to  $O$  are described by the vectors  $\vec{z}_o$  and  $\vec{x}$ , respectively. Then, the FDDSF can be written as

$$E(\vec{x}, \Omega, \tau) = \exp\{j2\pi\lambda^{-1}\langle \vec{a}_r(\Omega) | \vec{x} \rangle\} E(\Omega, \tau + c^{-1}\langle \vec{a}_r(\Omega) | \vec{x} \rangle), \quad (2.8)$$

where  $E(\Omega, \tau)$  is the FDDSF at  $O$ , i.e.,  $E(\Omega, \tau) := E(\vec{z}_o, \Omega, \tau)$ ,  $\langle \cdot | \cdot \rangle$  is the scalar product,  $\lambda$  and  $c$  denote the wavelength and the velocity of light, respectively. The terms  $2\pi\lambda^{-1}\langle \vec{a}_r(\Omega) | \vec{x} \rangle$  and  $c^{-1}\langle \vec{a}_r(\Omega) | \vec{x} \rangle$  in (2.8) describe the spatial dependency of the phase and the delay, respectively, of the impinging waves. With (2.8) the CIR  $h(\vec{x}, \tau)$  becomes

$$h(\vec{x}, \tau) = C \int \exp\{j2\pi\lambda^{-1}\langle \vec{a}_r(\Omega) | \vec{x} \rangle\} f(\Omega)^T E(\Omega, \tau + c^{-1}\langle \vec{a}_r(\Omega) | \vec{x} \rangle) d\Omega. \quad (2.9)$$

**Assumption III:** The term  $c^{-1}\langle \vec{a}_r(\Omega) | \vec{x} \rangle$  in (2.9) is discarded.

Hence, the variation of the propagation delays due to the modification of the propagation path lengths is neglected. This assumption is realistic provided that the

receiver position is not too far from  $O$  in the sense that the product of  $\|\vec{x}\|$  times the signal bandwidth is much smaller than  $C$ . Under Assumption III,  $E(\vec{x}, \Omega, \tau)$ ,  $h(\vec{x}, \tau)$ , and  $h(t, \tau)$  simplify to

$$E(\vec{x}, \Omega, \tau) = \exp\{j2\pi\lambda^{-1}\langle\vec{a}_r(\Omega)|\vec{x}\rangle\}E(\Omega, \tau), \quad (2.10)$$

$$h(\vec{x}, \tau) = C \int \exp\{j2\pi\lambda^{-1}\langle\vec{a}_r(\Omega)|\vec{x}\rangle\} f(\Omega)^T E(\Omega, \tau) d\Omega, \quad (2.11)$$

$$h(t, \tau) = C \int \exp\{j2\pi\lambda^{-1}\langle\vec{a}_r(\Omega)|\vec{x}(t)\rangle\} f(\Omega)^T E(\Omega, \tau) d\Omega,$$

respectively.

### **WSSUS Property**

*Assumption IV:* The FDDSF at  $O$  is a realisation of an orthogonal stochastic measure or using Bello's terminology [8] of an uncorrelated process in  $(\Omega, \tau)$ .

Assumption IV is a mathematical formulation of the fact that the electric fields of waves impinging from different directions or exhibiting different delays are uncorrelated. Using Bello's formalism, this statement reads

$$E[E(\Omega, \tau)^* E(\Omega', \tau')^T] = E[E(\Omega, \tau)^* E(\Omega, \tau)^T] \delta(\Omega' - \Omega) \delta(\tau' - \tau) \quad (2.12)$$

In the above expression  $E[\cdot]$  and  $[\cdot]^*$  denote the expectation and the complex conjugation, respectively. The form of the right-hand side in (2.12) suggests that  $E(\Omega, \tau)$  and  $E(\Omega', \tau')$  are uncorrelated unless  $(\Omega', \tau') = (\Omega, \tau)$ . Bello's formalism may lead to inconsistencies such as for example when one tries to evaluate both sides in (2.12) for  $(\Omega', \tau') = (\Omega, \tau)$ . These difficulties arise because  $E(\Omega, \tau)$  is not a regular process. A rigorous mathematical approach consists of regarding  $E(\Omega, \tau)$  as a generalised process, i.e., as a random distribution over an appropriate space of test functions defined on the  $(\Omega, \tau)$ -space. However, working within the framework of distribution theory requires a high mathematical background, especially to avoid the pitfalls arising from the use of the above formalism. An alternative, more accessible mathematical framework exists within which  $E(\Omega, \tau)$  is conceived as a stochastic measure [9], [10], [3]. The latter assigns a number to any not "too wild" subset of the  $(\Omega, \tau)$ -space in the same way as does for example a probability measure. A stochastic measure differs from a measure by the fact that the assigned number is not deterministic but random. Within this framework, (2.12) states that the stochastic measure  $E(\Omega, \tau)$  is orthogonal and that the term denoted by

$E\left[E(\Omega, \tau)^* E(\Omega, \tau)^T\right]$  is its structure matrix [9]. In the sequel, the notation by Bello will be retained despite its shortcomings to make the treatment more accessible. However, all the derived results reported here using Bello's formalism have been checked to have a mathematically rigorous counterpart within the linear theory of random processes [9]. The matrix

$$F(\Omega, \tau) := E\left[E(\Omega, \tau)^* E(\Omega, \tau)^T\right] = \begin{bmatrix} E\left[\left|E_h(\Omega, \tau)\right|^2\right] & E\left[E_h(\Omega, \tau)^* E_v(\Omega, \tau)\right] \\ E\left[E_v(\Omega, \tau)^* E_h(\Omega, \tau)\right] & E\left[\left|E_v(\Omega, \tau)\right|^2\right] \end{bmatrix}$$

can be referred to as the wideband coherence matrix of the electric field in the sense of [11] or in Bello's terminology as the field direction-delay-scattering matrix at location  $\Omega$ .

From (2.10) and (2.12) it follows that

$$E\left[E(\vec{x}, \Omega, \tau)^* E(\vec{x} + \vec{\Delta}x, \Omega, \tau')^T\right] = \exp\left\{j2\pi\vec{\kappa}^1 \langle \vec{a}_r(\Omega) | \vec{\Delta}x \rangle\right\} F(\Omega, \tau) \delta(\Omega' - \Omega) \delta(\tau' - \tau) \quad (2.13)$$

The right-hand side above depends on the location only through the lag  $\vec{\Delta}x$ . Thus, in addition to being uncorrelated in  $(\Omega, \tau)$ ,  $E(\vec{x}, \Omega, \tau)$  is also wide-sense-stationary (WSS) in  $\vec{x}$ . It immediately follows from (2.11) and (2.13) that the space-variant CIR is also WSS in  $\vec{x}$  and uncorrelated in  $\tau$ , i.e.,

$$E\left[h(\vec{x}, \tau)^* h(\vec{x} + \vec{\Delta}x, \tau')\right] = Q(\vec{\Delta}x, \tau) \delta(\tau' - \tau)$$

with

$$\begin{aligned} Q(\vec{\Delta}x, \tau) &= E\left[h(\vec{x}, \tau)^* h(\vec{x} + \vec{\Delta}x, \tau)\right] \\ &= |C|^2 \int \exp\left\{j2\pi\vec{\kappa}^1 \langle \vec{a}_r(\Omega) | \vec{\Delta}x \rangle\right\} f(\Omega)^H F(\Omega, \tau) f(\Omega) d\Omega, \end{aligned} \quad (2.14)$$

where  $[\cdot]^H$  is the Hermitian operator, i.e.,  $[\cdot]^T := \left[[\cdot]^*\right]^T$ . In Bello's terminology,  $Q(\vec{\Delta}x, \tau)$  is referred to as the delay cross-power spectral density function. A more suggestive expression is wideband spatial correlation function (CF). Thus, under the assumptions stated above the radio channel is wide-sense-stationary and uncorrelated-scattering (WSSUS). The propagation environment when regarded as a "device" which generates the FDDSF also exhibits the WSSUS property.

If *Assumption III* is removed, i.e., if the location dependency of the propagation delay is taken into account, then  $E(\bar{x}, \Omega, \tau)$  and  $h(\bar{x}, \tau)$  still remain WSS but are no longer uncorrelated in  $(\Omega, \tau)$  and  $\tau$ , respectively [4]. In this case, the propagation environment and the channel are WSS in  $\bar{x}$  but not US in  $(\Omega, \tau)$  and  $\tau$ , respectively.

Applying the same rationale as above to the time-variant CR yields

$$E[h(t, \tau)^* h(t + \Delta t, \tau')] = E[h(t, \tau)^* h(t + \Delta t, \tau)] \delta(\tau' - \tau) \quad (2.15)$$

with

$$E[h(t, \tau)^* h(t + \Delta t, \tau)] = |C|^2 \int E[\exp\{j2\pi\lambda^{-1}\langle \bar{a}_r(\Omega) | \bar{x}(t + \Delta t) - \bar{x}(t) \rangle\}] f(\Omega)^H F(\Omega, \tau) f(\Omega) d\Omega \quad (2.16)$$

The expectation in the right-hand side term is taken with respect to the random vectors  $\bar{x}(t + \Delta t)$  and  $\bar{x}(t)$ . From (2.15),  $h(t, \tau)$  is uncorrelated in  $\tau$ . Furthermore, it is WSS in  $t$  if, and only if, the expectation in (2.16) does not depend on this variable. In particular, this condition holds for a receiver displacement with constant velocity (2.7). Indeed, for such a movement the expectation above reduces to

$$E[\exp\{j2\pi\lambda^{-1}\langle \bar{a}_r(\Omega) | \bar{x}(t + \Delta t) - \bar{x}(t) \rangle\}] = \exp\{j2\pi\lambda^{-1}\langle \bar{a}_r(\Omega) | \bar{v} \rangle \Delta t\}.$$

The term  $\lambda^{-1}\langle \bar{a}_r(\Omega) | \bar{v} \rangle$  is the Doppler shift of a wave with incidence direction  $\Omega$ . The random movements mentioned in Section 2.1.3 also lead to a time-variant CR which is WSS in  $t$  [3].

**Assumption V:** For the random motion considered in the sequel the expectation in (2.16) does not depend on  $t$ .

The function

$$Q(\Delta t, \tau) := E[h(t, \tau)^* h(t + \Delta t, \tau)] \quad (2.17)$$

is called the wideband time CF of the channel.

The time-variant transfer function of the channel is the partial Fourier transform of  $h(t, \tau)$  with respect to  $\tau$ :

$$H(t, f) := \int \exp\{-j2\pi\tau\} h(t, \tau) d\tau. \quad (2.18)$$

The fact that  $h(t, \tau)$  is WSS in  $t$  and uncorrelated in  $\tau$  implies that  $H(t, f)$  is WSS, and conversely. The autocorrelation function (ACF) of  $H(t, f)$

$$R(\Delta t, \Delta f) := E[H(t, f)^* H(t + \Delta t, t + \Delta f)] \quad (2.19)$$

is the time-frequency CF of the channel. According to the Bochner-Khinchin Theorem [9,Theorem 2, p. 208] there exists a uniquely defined measure  $P(\tau, \nu)$  such that

$$R(\Delta t, \Delta f) = \int \int \exp\{j2\pi(\nu\Delta t - \tau\Delta f)\} P(\tau, \nu) d\tau d\nu. \quad (2.20)$$

The measure  $P(\tau, \nu)$  is called the delay-Doppler-scattering function of the channel. The wideband CF is related to  $R(\Delta t, \Delta f)$  and  $P(\tau, \nu)$  according to

$$R(\Delta t, \Delta f) = \int \exp\{-j2\pi\tau\Delta f\} Q(\Delta t, \tau) d\tau \quad (2.21)$$

and

$$Q(\Delta t, \tau) = \int \exp\{j2\pi\nu\Delta t\} P(\tau, \nu) d\nu, \quad (2.22)$$

respectively. In the above discussion, attention is intentionally focused exclusively on the characterising functions of WSSUS systems which have been the object of experimental investigations in the COST 231 action. A comprehensive treatment of the characterisation of linear time-variant systems is given in [8].

**Time Dispersion and Frequency Selectivity.** Setting  $\bar{\Delta}x = 0$  in (2.14) or  $\Delta t = 0$  in (2.17) yields the delay-scattering function or power delay profile of the channel:

$$\begin{aligned} P(\tau) &:= E[|h(\vec{x}, \tau)|^2] = Q(\bar{\Delta}x, \tau) \Big|_{\bar{\Delta}x=0} \\ &= E[|h(t, \tau)|^2] = Q(\Delta t, \tau) \Big|_{\Delta t=0}. \end{aligned} \quad (2.23)$$

From (2.14) and (2.22),  $P(\tau)$  can also be obtained as

$$P(\tau) = |C|^2 \int f(\Omega)^H F(\Omega, \tau) f(\Omega) d\Omega = \int P(\tau, \nu) d\nu.$$

For theoretical investigation and simulation purposes,  $P(\tau)$  is frequently assumed to behave according to

$$P(\tau) = \frac{P}{\sigma_r} \exp\left\{-\frac{\tau}{\sigma_r}\right\}, \quad (2.24)$$

where  $P$  is the mean received power

$$P := |C|^2 \int \int f(\Omega)^H F(\Omega, \tau) f(\Omega) d\tau d\Omega = \int P(\tau) d\tau = \int \int P(\tau, v) d\tau dv \quad (2.25)$$

and  $\sigma_\tau$  denotes the delay spread subsequently defined. The adequacy of this choice is questioned in [12] considering that the power decays as a function of the distance according to a power law with an exponent which typically takes a value in the range 2 to 5 (see Chapter 4). The power delay profile has been theoretically investigated considering a conceptual situation where scatterers are independently and uniformly distributed in space and the same power decay exponent is used for each propagation path. In this model, the tail of the power delay profile asymptotically obeys a power law. Estimated delay scattering functions obtained from measurements in rural areas exhibit a similar behaviour with a power decay exponent equal to 3.5.

The instantaneous delay spread which is defined as

$$(\sigma_\tau)_i(\vec{x}) := \sqrt{\frac{1}{P_i(\vec{x})} \int [\tau - (\mu_\tau)_i(\vec{x})]^2 |h(\vec{x}, \tau)|^2 d\tau}$$

provides a measure of the width of  $|h(\vec{x}, \tau)|$ . In the expression above,  $P_i(\vec{x})$  is the instantaneous received power

$$P_i(\vec{x}) := \int |h(\vec{x}, \tau)|^2 d\tau \quad (2.26)$$

and the instantaneous mean delay  $(\mu_\tau)_i(\vec{x})$  is the centre of gravity of  $|h(\vec{x}, \tau)|^2$ :

$$(\mu_\tau)_i(\vec{x}) := \frac{1}{P_i(\vec{x})} \int \tau |h(\vec{x}, \tau)|^2 d\tau.$$

The delay spread is defined as

$$\sigma_\tau := \sqrt{\frac{1}{P} \int [\tau - \mu_\tau]^2 P(\tau) d\tau}. \quad (2.27)$$

This quantity gives a measure of the width of the delay-scattering function  $P(\tau)$ . In (2.27),  $\mu_\tau$  is the mean delay defined as

$$\mu_\tau := \frac{1}{P} \int \tau P(\tau) d\tau. \quad (2.28)$$

Theoretical investigations [14] have shown that the delay spread  $\sigma_\tau$  and the expectation of the instantaneous delay spread  $E[(\sigma_\tau)_i(\vec{x})]$  may be quite different for

the Gaussian two-path channel. Here, the expectation is with respect to the random process  $h(\bar{x}, \tau)$ . Simulations indicate that this difference decreases towards 0 as the number of components in the CIR increases.

The delay spread is not an appropriate dispersion parameter for assessing the performance of modems with finite equaliser depth since it does not directly relate to the delay window which the equaliser is capable to cope with. For this reason [13, 30] proposed the following two more suitable parameters. The interference ratio  $Q_D$  is defined as the maximum ratio (in dB) between the power inside and that outside a delay interval of a fixed length  $D$ :

$$Q_D := 10 \log \left\{ \max \left\{ \frac{\int_{W} P(\tau) d\tau}{P - \int_{W} P(\tau) d\tau} : W = \text{delay interval of leng } D \right\} \right\}.$$

The delay window  $W_q$  is the minimum delay interval such that the ratio between the power inside and outside it equals a fixed ratio  $q$  (in dB):

$$W_q := \min \left\{ W = \text{delay interval} : 10 \log \left\{ \frac{\int_{W} P(\tau) d\tau}{P - \int_{W} P(\tau) d\tau} \right\} = q \right\}.$$

For GSM,  $q$  and  $D$  are chosen to be 9dB and 16μs corresponding to the tolerable interference level and delay window. It has been confirmed in [60] and [61] that these parameters predict link performance better than the delay spread.

Time dispersion causes frequency selectivity, i.e., fluctuations of the amplitude of  $H(t, f)$  when  $f$  changes. The frequency CF of the channel is defined to be

$$R(\Delta f) := E \left[ H(t, f)^* H(t, f + \Delta f) \right] = R(\Delta t, \Delta f) \Big|_{\Delta t=0}.$$

According to (2.19) and (2.22), the following identities hold:

$$R(\Delta f) = \int \exp \{-j2\pi\tau\Delta f\} P(\tau) d\tau.$$

The coherence bandwidth is a quantity which describes the width of the main lobe of the absolute value of the frequency CF. It is defined for a given coherence level  $\rho \in [0, 1]$  as

$$B_\rho := \begin{cases} \arg \min \left\{ \Delta f \geq 0 : \frac{1}{P} |R(\Delta f)| < \rho \right\}; \rho \in (0,1] \\ \lim_{\rho \rightarrow 0} B_\rho \end{cases}; \rho = 0 \quad (2.29)$$

An uncertainty relation exists between the delay spread and the coherence bandwidth [15] stating that the product of these quantities is lower-bounded according to

$$\sigma_\tau B_\rho \geq \frac{1}{2\pi} \arccos(\rho). \quad (2.30)$$

Moreover, the lower bound is attained if, and only if, the delay-scattering function is of the form  $P(\tau) = \frac{P}{2} [\delta(\tau - \tau_1) + \delta(\tau - \tau_2)]$ , in which case  $\sigma_\tau = |\tau_2 - \tau_1|/2$ .

The average link quality of a non-equalised system like DECT is closely related to the average delay spread, whereas the instantaneous delay spread does not characterise the instantaneous (burst) link performance of such a system. Indeed, the latter parameter does not provide any information about the actual position of the fades in the frequency domain. In [116] it has been found that the link quality depends on whether an instantaneous fade is present in the system bandwidth  $B_s$  or not. This observation has motivated the introduction of the frequency magnitude variation parameter [116] which is defined as

$$V_{B_s} := \frac{\max \{H(f) : f \in B_s\}}{\min \{H(f) : f \in B_s\}}.$$

The advantage of this frequency domain parameter is that it can be determined using only the actual system bandwidth.

**Doppler Dispersion and Time Selectivity.** The Doppler-scattering function or power Doppler profile and the time CF of the channel are defined to be

$$P(\nu) := \int P(\tau, \nu) d\tau \quad (2.31)$$

and

$$R(\Delta t) := E \left[ H(t, f)^* H(t + \Delta t, f) \right] = R(\Delta t, \Delta f) \Big|_{\Delta f=0}, \quad (2.32)$$

respectively. It follows from (2.20) that

$$R(\Delta t) = \int \exp\{j2\pi\nu\Delta t\} P(\nu) d\nu.$$

Let us assume that the receiver is moving with constant velocity (see (2.7)) and that the radiating sources are randomly selected in the following way: (1) the locations are independently and uniformly distributed in space, (2) the radiated powers are independently and identically distributed with finite expectation, and (3) the locations and the radiated powers are independent random variables. Then,  $P(\nu)$  coincides with the well-known Clarke's spectrum [16]

$$P(\nu) = \begin{cases} \frac{P}{\pi \sqrt{\nu_D^2 - \nu^2}} ; |\nu| < \nu_D \\ 0 ; \text{otherwise} \end{cases}, \quad (2.33)$$

where  $\nu_D := \|\bar{v}\| / \lambda$  is the maximal Doppler shift. The power Doppler profiles which are obtained experimentally in a specific environment usually have a shape different from (2.33). The reason is that the assumptions stated above are rarely satisfied. Actually, the Clarke's spectrum has to be regarded as an average power Doppler profile over many environments considering a fixed velocity magnitude  $\|\bar{v}\|$ . As postulated in [5] and shown in [3] (see also Section 4.7.4), when the receiver performs irregular movements in a random manner, then the resulting power Doppler profiles are basically different from those arising due to movements with constant velocity.

The mean average Doppler shift  $\mu_\nu$ , the Doppler spread  $\sigma_\nu$ , and the coherence time  $T_\rho$  are defined by replacing the delay-scattering function and the frequency CF by the Doppler-scattering function and the time CF, respectively, in the defining equations (2.28), (2.27), and (2.29). An uncertainty relation similar to (2.30) also exists between  $\sigma_\nu$  and  $T_\rho$ .

**Discrete Channel Model.** This model relies on the assumption that the FDDSF and therefore the space-variant CIR only embrace the coherent part in (2.1) and (2.4), respectively. Provided that Assumptions I and II hold,

$$\begin{aligned} E(\vec{x}, \Omega, \tau) &= E_c(\vec{x}, \Omega, \tau) \\ &= \sum_{j=1}^J E_j \exp\left\{j2\pi\tilde{\lambda}^1\langle\bar{a}_r(\Omega_j)|\vec{x}\rangle\right\} \delta(\Omega - \Omega_j) \delta\left(\tau - (\tau_j - c^{-1}\langle\bar{a}_r(\Omega_j)|\vec{x}\rangle)\right) \\ h(\vec{x}, \tau) &= h_c(\vec{x}, \tau) \\ &= \sum_{j=1}^J h_j \exp\left\{j2\pi\tilde{\lambda}^1\langle\bar{a}_r(\Omega_j)|\vec{x}\rangle\right\} \delta\left(\tau - (\tau_j - c^{-1}\langle\bar{a}_r(\Omega_j)|\vec{x}\rangle)\right) \end{aligned}$$

with  $h_j := Cf(\Omega_j)^T E_j$ , so that the time-variant CR reads in this case

$$h(t, \tau) = \sum_{j=1}^J h_j \exp\left\{j2\pi\lambda^{-1}\langle \bar{a}_r(\Omega_j) | \bar{x}(t) \rangle\right\} \delta\left(\tau - \left(\tau_j - c^{-1}\langle \bar{a}_r(\Omega_j) | \bar{x}(t) \rangle\right)\right)$$

Under Assumption III, the three sums above simplify to

$$E(\bar{x}, \Omega, \tau) = \sum_{j=1}^J E_j \exp\left\{j2\pi\lambda^{-1}\langle \bar{a}_r(\Omega_j) | \bar{x} \rangle\right\} \delta(\Omega - \Omega_j) \delta(\tau - \tau_j),$$

$$h(\bar{x}, \tau) = \sum_{j=1}^J h_j \exp\left\{j2\pi\lambda^{-1}\langle \bar{a}_r(\Omega_j) | \bar{x} \rangle\right\} \delta(\tau - \tau_j),$$

$$h(t, \tau) = \sum_{j=1}^J h_j \exp\left\{j2\pi\lambda^{-1}\langle \bar{a}_r(\Omega_j) | \bar{x}(t) \rangle\right\} \delta(\tau - \tau_j).$$

A sufficient condition for the WSSUS property to be satisfied, i.e., for Assumption IV to hold, is that the waves' parameters  $\{\Omega_j, \tau_j, E_j\}$  are randomly selected in such a way that the field vectors  $\{E_j\}$  are uncorrelated with zero mean and finite covariance and, moreover, are independent of the incident characteristics  $\{\Omega_j, \tau_j\}$ .

## 2.1.6 Characterisation of the Large-Scale Fluctuations of the Channel

**Path Loss and Shadowing Effects.** Computing the average of  $P_i(\bar{z})$  in (2.26) over a small domain  $A(\bar{z})$  around  $\bar{z}$  to cancel out the SS fluctuations yields the averaged received power

$$\langle P \rangle(\bar{z}) := \frac{1}{\text{Vol}[A(\bar{z})]} \int_{A(\bar{z})} P_i(\bar{y}) d\bar{y}, \quad (2.34)$$

with  $\text{Vol}[A]$  denoting the volume of the domain  $A$ . This average can also be computed considering a surface or a line rather than a volume. Let  $h_{A(\bar{z})}(\bar{x}, \tau)$  denote the SS characterisation of the space-variant CIR over  $A(\bar{z})$  as presented in Section 2.1.5. According to (2.25) the mean received power is given as

$$P(\bar{z}) := \mathbb{E}\left[\int_{A(\bar{z})} |h_{A(\bar{z})}(\bar{x}, \tau)|^2 d\tau\right] = \int P_{A(\bar{z})}(\tau) d\tau.$$

If the assumptions made in Sections 2.1.5 are realistic over  $A(\vec{z})$ , then  $\langle P \rangle(\vec{z})$  is close to  $P(\vec{z})$ . The ratio  $\langle P \rangle(\vec{z}) / P_T$  expressed in dB is decomposed into the sum

$$-\left[\langle P \rangle(\vec{z}) / P_T\right]_{\text{dB}} = L(\vec{z}) + \Delta L(\vec{z}), \quad (2.35)$$

where  $L(\vec{z})$  is the path loss and  $\Delta L(\vec{z})$  describes the fluctuations of the averaged received power around  $L(\vec{z})$  which result from shadowing effects. Prediction models for  $L(\vec{z})$  are presented in Chapter 4. Usually,  $\Delta L(\vec{z})$  is assumed to be a realisation of a Gaussian process entirely specified by its ACF.

**Transitions Between Areas with Different Propagation Configurations.** The space-variant CIR corresponding to a transition from an area  $A$  to another one  $A'$  (see Fig. 2.1) with possibly different propagation configurations, such as encountered in a transition from a LOS to a NLOS situation, can be built up from the SS characterisation of the CIRs over  $A$  and  $A'$  according to

$$h_{A \rightarrow A'}(\vec{x}, \tau) = (1 - b(\vec{x}))h_A(\vec{x}, \tau) + b(\vec{x})h_{A'}(\vec{x} - \vec{x}_o, \tau).$$

Here,  $b(\vec{x})$  is a smooth unit step function which increases from 0 to 1 over the transition domain from  $A$  to  $A'$ . Situations where specific components  $h_\ell(\vec{x}, \tau)$  of the CIR (see (2.5)) vanish or appear can be handled in the same way as above by multiplying them either with  $(1 - b_\ell(\vec{x}))$  or  $b_\ell(\vec{x})$  where  $b_\ell(\vec{x})$  is a function similar to  $b(\vec{x})$ .

**Fluctuations of the Propagation Delays.** As the receiver moves over large areas, the propagation paths change so that the components  $E_\ell(\vec{z}, \Omega, \tau)$  and  $h_\ell(\vec{z}, \tau)$  of the FDDSF (see (2.3)) and the space-variant CIR (see (2.5)), respectively, drift on the  $\tau$ -axis as  $\vec{z}$  varies. One way to account for this effect consists of removing Assumption III and computing the FDDSF and the CIR from (2.8) and (2.9), respectively.

**Fluctuations of the Incidence Directions.** As the receiver location changes over wide areas, the direction of the radiating sources with respect to its position varies. As a consequence, the components  $E_\ell(\vec{z}, \Omega, \tau)$  of the FDDSF (see (2.3)) move in the  $\Omega$ -space. Assumption II does not allow to account for this effect. Modifications of the incidence direction as a function of the position can be taken into account by assuming that spherical rather than plane waves are impinging in a neighbourhood of the receiver. Hitherto, no publication seems to be available which addresses this issue.

## 2.2 Measurement Techniques - Channel Sounders

Jean-Claude Bic, CNET, France Telecom, France

The first step to characterise the radio mobile channel is to obtain reliable measurements. The quality of the prediction models depends crucially on the measured data. COST 231 is aimed at the third generation of digital cellular systems which will occupy a larger bandwidth either in TDMA or CDMA access than the current systems and will be operated in various environments. As a consequence the investigation of propagation needs channel sounders able to measure the variability and frequency selective behaviour of the channel by means of either the Impulse Response (IR) or the transfer function in at least the system bandwidth. The sounder will also have to cope with different constraints according to the environment, maximum excess delay, time resolution, etc., and must demonstrate a sufficient flexibility. Of course, field strength measurements are still needed for path-loss modelling and planning purposes but the techniques are rather well-known and the following sections will be focused on the wideband measurements techniques. Since the beginning of the COST 231 project, measurements have been carried out with many channel sounders. They have been designed according to different techniques but they could be classified in three main categories: pulse sounding, time domain (pulse compression) and frequency domain techniques.

The main performance of a sounder is given by:

- the maximum duration of the measured IR for delay range;
- the bandwidth or equivalently the time resolution to discriminate between two echoes;
- the dynamic range to detect an echo out of the noise level;
- the acquisition rate to measure successive IRs for Doppler analysis;

Measurements of the Direction of Arrival are also a new feature which is important to validate prediction methods based on ray tracing and different devices have been added to sounders, in order to perform this kind of [17-21].

### 2.2.1 Pulse sounders

They are very simple to implement and give a good resolution but they suffer from the need of high peak-to-mean power ratio. Several of them have been implemented mostly for indoor measurements where high transmitted power is not critical:

- the pulse sounder of the Aalborg University [22] with a pulse width of 100 ns performs measurements in office buildings;
- the pulse sounder [23, 24] operated by VTT has a pulse-width of about 8 ns and a dynamic range of 25 dB;
- the pulse sounder of Telecom Denmark [25] with a 80-ns resolution has been used in indoor office, shopping centre and railway station;
- the pulse sounder [26, 27] of DeTeMobil used in picocell and microcell measurements for DECT has a dynamic range less than 20 dB;
- the pulse sounder developed by Telefonica [28] with pulse width range from 40 to 200 ns and repetition rate from 1 to 100  $\mu$ s.

### 2.2.2 Time domain sounders

The main characteristics of the pulse compression channel sounders that contributed to COST 231 are given in Table 2.1. Several "classical" channel sounders based on PN sequences at the transmitter and sliding correlation at the receiver either by analogue or digital means have been widely used for IR measurements especially within the framework of second generation systems like GSM and DECT. They have good performances in terms of resolution but relatively poor in terms of maximum acquisition rate and they provide only the amplitude of the IR.

- the Swiss-PTT RCS-900 (Real-time Channel Sounder) [29,30] SAW correlator with a 3 MHz 3-dB bandwidth has been used for measurements in Texas in high-rise buildings environment [31]; a new device called Universal Channel Analyser [32] has been developed incorporating the sounders RCS-900 and RCS-1900 and offers real-time analyses in addition to measurements;
- the Bellcore sounder [33] with a 25 MHz 3 dB-bandwidth is based on the sliding correlator approach has been operated indoor measurements where Doppler effects are not so important. It has also been used by Aalborg University to investigate polarisation diversity [34] and antenna diversity after some improvements [35];
- the BT sounder [36] has a time resolution of 50 ns and delays up to 12.75 ms with a dynamic range of about 31 dB, but limited to 4 IR/s;

- the Lund University sounder [37] is derived from the sliding correlator approach by direct conversion at the receiver to obtain a high resolution of 10 ns. A cable is used between the transmitter and the receiver for indoor measurements.

**Tables 2.1** Characteristics of pulse compression channel sounders contributed to COST 231

Country	Austria	Denmark	France	Germany	Germany
Institution	University of Wien	University of Aalborg	CNET	DBP Telekom University of Erlangen	DBP Telekom University of Erlangen
Equipment	DCCS 1800			RUSK 400	RUSK 5000
Frequency range (MHz)	1800	980	900, 2200	890..960	50..1000
Bandwidth (MHz)	15		12.5/25/50	0.4	5.75
peak output power (W)	1	10			
excitation	PNS	PNS	PNS	mod. PNS	mod. PNS
Sequence length (symbols)	7.. 1023	511	127, 255, 511	127	1023
Chiprate (Msymbol/s)	30	50	15	1	10
Modulation	BPSK	BPSK	BPSK	DSB-AM	VSB-AM
Max. duration of IR (us)	34	51	34	127	102.3
Time resolution of IR (us)	0.05	0.02	0.067	3.5	0.24
Max. Acquisition rate (IR/S)	8	> 20	800	44	42 (208)**
Total dynamic range (dB)	>80	100			
Instant. dyn. range (dB)	>28	> 40	>30	>35	>30
Sensitivity (dBm)	-101			-110	-100
Correlation technique	digital correlation	sliding correlation (digital)	Postprocess. inverse filtering	unbiased ML estimation via cyclic inverse filter	unbiased ML estimation via cyclic inverse filter
COST 231 TD Nr. (yy)-nn	93-88	93-08	90-31	90-40/41/75	92-09

Country	Germany	Germany	Ireland	Italy	Norway
Institution	MEDAV	Siemens	Trinity College	CSELT	Telenor R&D
Equipment	RUSK X				
Frequency range (MHz)	900..1800	870-980 1805-1880	980, 1808	2000	900 and 1700
Bandwidth (MHz)	0.1.. 6.0	5, 10, 20	10	100	1, 2, 4, 8
peak output power (W)			35 (average)	0.3	20
Excitation	Chirp	Digital signal (low crest factor)	PNS/Chirp	PNS	Chirp
Sequence length (symbols)	128, 256, 512, 1024	BT = 256, 512, 1024	*	511, 2047	128
Chiprate (Msymbol/s)	10		*BT=256	50 MHz	
Modulation	DSB-AM	DSB-AM	*Vector mod.	BPSK	(leave open)
Max. duration of IR (us)	102.4	102.4	25.6	10.6 - 41.3	16 - 128
Time resolution of IR (us)	0.23		0.1	0.02	0.125 - 1
Max. Acquisition rate (IR/S)	39 (390)**	1000	1000	> 4000	15
Total dynamic range (dB)		100	--	60 (adjust.)	> 80
Instant. Dyn. range (dB)	>35	40	50	> 30	> 30
Sensitivity (dBm)	-115		-115	-92	-121 -148 <sup>1</sup>
Correlation technique	unbiased ML estimation via cyclic inverse filter	unbiased ML estimation (matched filter + sidelobe canc.)	mismatched filtering	Coherent demodulation and cross-correlation	Multiplication in frequency domain
COST 231 TD Nr. (yy)-nn	94-125	95 - 128	93-48, 94-29	94-19	92-62

Country	Norway	Spain	Switzerland	Switzerland	UK
Institution	Telenor R&D	AlcatelSESA/UPC	Swiss PTT	ETH CTL Zurich	British Telecom
Equipment			RCS 900	RCS/RCA900 /1980	
Frequency range (MHz)	1950 - 59 GHz	900, 1900	760..1000	900, 1980	1800
Bandwidth (MHz)	6.25, 12.5, 25, 50, 100, 200	100	3	1-560	50
Peak output power (W)	0.3 or 10	0.1, 1		20	
Excitation	Chirp	PNS	Barker PNS	PNS	PNS
Sequence length (symbols)	64 to 8192	127, 511, 1023	13	127, 255, 511, 1023, 2047	255
Chiprate (Msymbol/s)		50	1.66	1-120	20
Modulation	(leave open)	BPSK	BPSK	BPSK	BPSK
Max. duration of IR (us)	0.32 - 164	2.5, 10.2, 20.4	80	1-2047	12.75
Time resolution of IR (us)	0.005 - 0.16	0.04	0.6	0.008-1	0.05
Max. Acquisition rate (IR/S)	728	40, 9, 4	7	744	4
Total dynamic range (dB)	> 80	70	70	60	
Instant. dyn. range (dB)	> 30	> 25	>25	45	>31
Sensitivity (dBm)	-110 -153 <sup>2</sup>	- 90	-102	-75	
Correlation technique	Multiplication in frequency dom.	Sliding analogue correlator	Correlation by SAW device	Analogue correlation	Sliding SAW correlation dev.
COST 231 TD Nr. (yy)-nn	95-57	95-05	89-41, 91-45	89-39, 90-79, 91-89	90-83

\* Vector modulation of two DDS channels, BT product is given instead of sequence length

\*\* Burst mode of 256 Irs

1 Dependant on measurement bandwidth and number of averaged sweeps before correlation takes place

2 Dependant on measurement bandwidth, sequence length and number of averaged sweeps before correlation takes place

Moreover, the need for better performance and for a greater flexibility to characterise a large variety of environment, both indoor and outdoor, have led to the design of new time-domain sounders, as shown in Fig. 2.3.

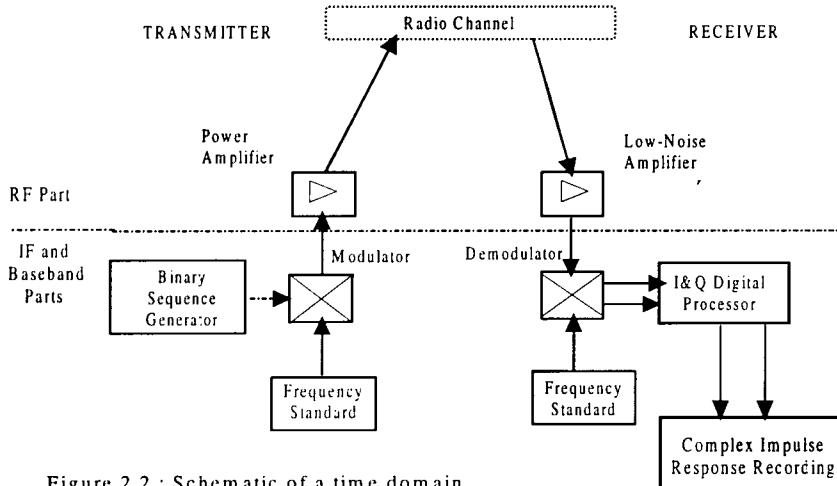


Figure 2.2 : Schematic of a time domain pulse sounder

**Fig. 2.3** Schematic of a time domain pulse sounder

Most of them are based on transmitting a BPSK-modulated binary sequence periodic or not [38] having special correlation properties (PN sequence, generally). Digital processing is usually performed at the receiver, by correlation or inverse filtering of in-phase and quadrature sampled IRs and the Complex IR is obtained. The transmitter and receiver are accurately synchronised by means of very stable clocks and usually can be used both in the 900 MHz and 1.8 GHz bands. They have been widely used especially for measurements performed in RACE II projects ATDMA and CODIT [39-41]:

- RUSK "family": RUSK-5000 [41,42] designed by DBP Telekom is an improvement of the RUSK 400 built for GSM purposes [43-46]. It performs correlation of 1023-bit pseudo noise signals transmitted in a TV-bandwidth of 5.75 MHz. The digital processing give an instantaneous dynamic range better than 30 dB. RUSK X is a further extension of the former one with a carrier frequency ranging from 0.9 to 1.8 GHz and a bandwidth up to 6 MHz utilised in RACE project ATDMA [40].
- Lastly, RUSK SX [47] has been designed with respect to microcell and indoor picocells. Its resolution is 15 ns for indoor, due to a bandwidth of 120 MHz.

- The CNET sounder [41, 48-49] processes the received samples of the IR by inverse filtering to improve dynamic range and resolution and it has an adjustable 3dB-bandwidth up to 50 MHz and a sequence length up to 511 bits.
- The sounder developed at the Swiss Federal Institute of Technology [39, 50-56] and used in the RACE project 2020 CODIT has a very large bandwidth of 560 MHz, a PN-sequence up to 2043 bits and analogue correlation at the receiver. The maximum measurable Doppler shift is about 370 Hz.
- The Siemens sounder is based on the method of optimal estimation which avoided the correlation sidelobes. Especially designed test sequences guarantee measurements with low intermodulation in the transmitter amplifier [57-59].
- The CSELT sounder [39, 117], using a software receiver, performed outdoor and indoor measurements in the CODIT project in a bandwidth of 20 MHz.
- The Trinity College sounder [62] uses the mismatched filter principle to improve the noise gain of the receiver and a low-crest factor signal at the transmitter [63].
- The Direct-Conversion Channel Sounder (DCCS 1800) from Technical University of Vienna [64] has a 50 ns time resolution and a maximum excess delay of 34  $\mu$ s.
- The Alcatel SESA sounder [65] was designed and built by UPC team with a 40 ns resolution to operate in indoor as well as in urban, suburban and rural environments.
- The sounder developed by Telenor R&D in 1991 [66] and the improved sounder developed in 1993 [67, 68] are based on the frequency sweep technique frequently used in radars. In the receiver a digital signal processor performs an operation corresponding to a correlation in the time domain. Although the principle is slightly different, i.e. the carrier is modulated with a bit sequence giving a frequency sweep as the output waveform, it can be considered as a pulse compression technique. It has also been used for measurements in the 60 GHz band (see Chapter 8, Section 8.4).
- The Aalborg University sounder [120] is based on a digital sliding correlator principle, allowing for programmable sweeping windows less than the PN-sequence length, thus allowing for faster acquisition rates than corresponding sliding correlators sounders. The minimum time resolution is 20 ns.

### 2.2.3 Frequency domain sounders

Network analysers can also be used for indoor measurements where it is possible to synchronise transmit and receive sides by means of a cable [39, 69-70]. They achieve rather easily large bandwidths (i.e., 200 MHz for the Telefonica-Ericsson analyser used in CODIT) and are more often used to characterise wideband propagation in the millimetre band than in UHF-VHF bands (see Chapter 8, Section 8.2).

## 2.3 Propagation measurements and their analysis

**Gerhard Kadel, Deutsche Telekom, Germany**

### 2.3.1 The need for propagation measurements

The radio propagation channel is a very important and a very critical component for mobile radio communications systems. Therefore, the detailed analysis of the radio channel is of basic importance for the design of future mobile communications systems as well as for the optimisation and extension of existing systems. Due to the complexity of the propagation phenomena and due to the statistical nature of the radio channel parameters, a reliable channel characterisation can only be based on appropriate channel measurements.

### 2.3.2 Objectives of the COST 231 propagation measurements

Within COST 231 a huge amount of propagation measurements were performed in the 900-MHz bands and 1800-MHz bands in a large variety of different environments ranging from pico cells and micro cells to macro cells. Different measurement techniques, which are described in the previous sections, were used. Much attention was paid to indoor investigations and to urban micro cellular investigations because these cell types will be particularly important for future UMTS systems with high capacity demands. The propagation measurements had the following objectives:

- characterisation of the channel for all types of indoor and outdoor environments relevant for current and future mobile services,
- investigation of transitions between different environments (e.g., transition between line-of-sight (LOS) and non-line-of-sight (NLOS) conditions, penetration),
- measurement of the channel conditions as function of all important factors having an influence on the channel (e.g., antenna heights, antenna patterns, base station locations, bandwidths, etc.),

- generation of data bases for (wideband) propagation modelling (software and hardware channel simulators including "stored channels"), as described in Section 2.4,
- provision of propagation data for the development, verification and optimisation of propagation prediction models as described in Chapter 4,
- investigation of performance and coverage of mobile radio systems by determination of related channel parameters out of measurements (e.g., interference ratio for GSM or delay spread for DECT) in order to determine system performance on the basis of channel characteristics [91,92],
- measurement of channel characteristic for special services (e.g., mobile services for high-speed trains).

According to the different objectives described above, different approaches for the classification of measurements were used. Measurements were categorised as function of the cell size (e.g., pico, micro, macro cells), as function of the base station visibility (LOS, NLOS), as function of terrain undulations (flat, hilly, etc.), as function of building or vegetation density, as function of the mobile speed (from stationary to high speed trains), etc..

### **2.3.3 Narrowband and wideband measurements**

The mobile radio channel within a certain bandwidth of interest can be completely characterised by its complex time-variant impulse responses (Eq. (2.6)) or equivalently its time-variant transfer function (Eq. (2.18)). The measurement equipment must be able to record the impulse responses with a sufficient length in time and to fulfil the sampling theorem with respect to the Doppler shift (i.e. record at least two impulse responses per wavelength). For system related investigations (e.g., simulations with stored channel data) a measurement bandwidth equal to the system bandwidth is sufficient. For the development of (wideband) deterministic or statistical propagation models, a very large bandwidth for channel measurements is desirable in order to gain as much details as possible which help to understand the propagation phenomena (e.g., identification of scatterer locations) and to support the modelling approaches.

However, propagation measurements with large bandwidths produce a huge amount of data. Therefore, narrowband measurements which can be carried out and handled much simpler, are appropriate if only narrowband information is required. This is particularly the case for all types of pathloss modelling.

### 2.3.4 Analysis of propagation measurements

In order to generate a common platform for the analysis and exchange of propagation data, file formats are required which are equipment independent and contain all data necessary for the various methods of data analysis. Within COST 231 two file formats were used for wideband channel data: the binary "Universal Measurement File (UMF)", format developed by Technical University of Vienna and the "RACE Level2 Format" [71] which is an ASCII format developed within the RACE ATDMA project and adopted by COST 231.

Propagation measurements contain noise. Effective methods of noise reduction are required for reliable evaluation of radio channel parameters. Particularly the parameter delay spread is very sensitive for noise components at large excess delays of the impulse responses. For wideband measurements, noise thresholds, derived either from sections of measured impulse responses containing only noise or deduced from back-to-back calibration measurements, were developed to reduce the impact of noise.

From propagation measurements various channel parameters were evaluated (see Section 2.1 for definitions):

- average path loss and its short-term and long-term fluctuations,
- time variance,
- frequency selectivity,
- directions of arrivals (DOA).

In general, all channel parameters show large variations of their absolute values for different environments and rapid fluctuations.

### 2.3.5 Indoor measurements

Indoor propagation measurements have been carried out in the 900- and 1800-MHz range in order to develop and test the indoor propagation models presented in Chapter 4, Section 4.7. The measurements have been conducted by Alcatel Sesa, Swiss Federal Institute of Technology Zürich (ETH), Ericsson Radio Systems, France Telecom (CNET), Technical University of Catalonia (UPC), Technical University of Vienna (TUW), University of Lund and VTT Information technology. The emphasis of the research has been on office buildings which constitute the main application area of wireless indoor communication systems. Also some shopping centres and factory environments have been under study.

The indoor environments have been divided into four categories as described in Table 2.2. A small number of categories has been included in order to obtain clearly different propagation characteristics between the categories and in order to have sufficient amount of measurement data for each category. General information of the measurements carried out by the various organisations is given in Table 2.3.

**Table 2.2** Indoor environment categories

Environment category	Description
Dense (D)	Environments with small rooms; typically an office where each employee has one's own room; mostly NLOS (Non-line-of-sight) conditions.
Open (O)	Environments with large rooms; typically an office where one room is shared by several employees; mostly LOS (Line-of-sight) or OLOS (Obstructed-line-of-sight) conditions.
Large (L)	Environments consisting of very large rooms; typically a factory hall, shopping centre or airport building; mostly LOS or OLOS conditions.
Corridor (C)	Transmitter and receiver along the same corridor; LOS condition

Despite of the different measurement methods and equipment, some common rules were followed in performing the measurements. The overall goal was that the measurement configuration corresponds, as much as possible, to a real communication system, involving a stationary station (base station) and a mobile station.

The base station was located on a central position in the building and the mobile station was moved into several positions within the coverage area of the base station. The base station height from floor varied between 1.5 m and 3 m. Omni-directional antennas with 1.3-2.2 dB gain were used. The transmitter power was 10 to 30 dBm. The polarisation was vertical in all of the measurements.

Averaged path loss values are required for the development of narrow-band models. These were obtained by averaging the received signal level and then calculating the path loss from Eq. (2.34). An example of measured path loss within an office building is shown in Figure 2.4.

**Table 2.3** Description of indoor measurement data (NB=narrow-band, WB=wide-band)

Organisati on	Frequency band(MHz)	Categ.	Numb. of meas.		Data and building description
			NB	WB	
Alcatel [72]	1900	DC	871 <sup>1)</sup>		2 office buildings, meas. in several floors.
ETH [80]	900	OCL		40000 <sup>3)</sup>	subway station, airport, large office, factory
Ericsson [73]	900	DOL	100-500 <sup>6)</sup>		4 office buildings, airport, convention centre, casino, hospital, underground, parking garage
CNET [74]	900 900 1800	D D D	- 548 <sup>1)</sup> 548 <sup>1)</sup>		Office building without furniture in six floors Office building
Lund [75]	1800	DOL	735000 <sup>2)</sup>	3397 <sup>3)</sup>	Office building(NB&WB), shopping centre (NB) and exhibition centre (NB)
TUW [76]	1800	DOC	229 <sup>5)</sup>	36 <sup>4)</sup>	Office building
UPC [77]	900 1800	DLC DLC	400 <sup>1)</sup>	35 <sup>4)</sup>	2 office buildings
VTT [78]	900 1800	DOL DOL	325 <sup>1)</sup> 488 <sup>1)</sup>	82 <sup>4)</sup>	8 office buildings (NB), 2 office buildings (NB&WB), underground hall (NB&WB), factory hall (NB)

<sup>1)</sup> Number of averaged measurement points<sup>2)</sup> Number of samples<sup>3)</sup> Number of instantaneous power delay profiles (PDPs)<sup>4)</sup> Number of averaged PDPs<sup>5)</sup> Number of 1-30 m long measurement routes<sup>6)</sup> Number of measurement loops in each building

The used number of samples was 10 to 50 and the averaging length was 1-6 wavelengths in most of the measurements. In Ericsson's measurements the averaging was performed along a loop covering typically a small room. The considerably shorter averaging length compared to outdoor measurements is appropriate because of the high variability of the indoor environment.

The wide-band results given in Chapter 4, Section 4.7 are expressed in terms of average delay spreads in different environments. These values were obtained by averaging over all the individual measurements of each environment category.

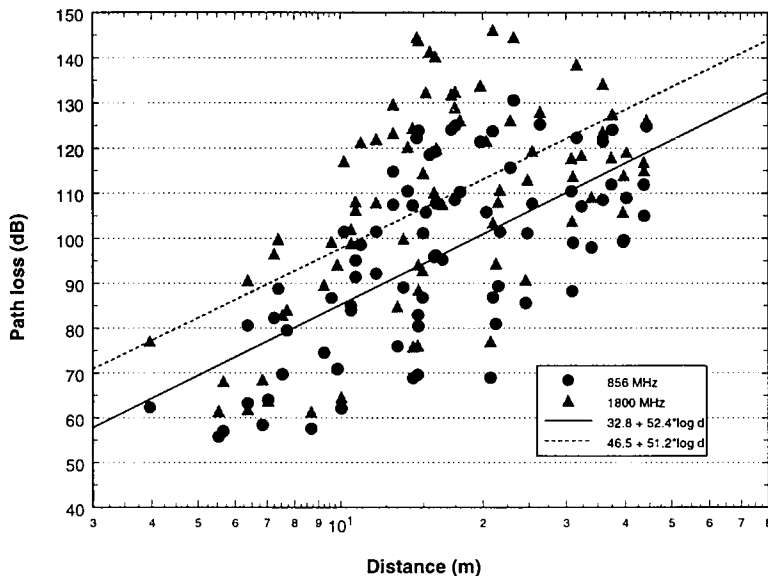


**Fig. 2.4** Measured path loss as a function of distance between transmitter and receiver in a typical office building. Receiver has been in the 4th floor and transmitter has been moved to measurement points in floors 0-4.

The delay spread was calculated from the measured power delay profile (PDP) (Eq. (2.23)) by using Eq. (2.27). The PDP was measured in time-domain either by using a spread-spectrum channel sounder [76,79-80] or using pulse techniques [78]. Frequency domain measurements by a network analyser and a Fourier transform were used in [81] to obtain the PDP.

Wideband polarisation state behaviour of the radio channel has been investigated in [121] at 1800 MHz. The conclusion is that the radio channel has chaotic polarisation behaviours both in the spatial and temporal domain. Average XP (cross-polarisation figures) have been found to 8.7 and 4 dB, outdoors and indoors, respectively.

Also indoor measurements aiming for the determination of directions-of-arrival (DOAs) were carried out. In [82] a measurement concept based on coherent wide band measurement in time domain was presented. The DOAs of dominant signal components at subsequent time slots were calculated by using the Maximum

Likelihood optimisation. Alternative DOA algorithms are presented in [83]. In [84] narrow-band measurements and a synthetic aperture technique are used. The DOA distribution was solved either by using normal beam forming methods or the high resolution MUSIC (Multiple Signal Classification) method.

### 2.3.6 Outdoor measurements

For the outdoor propagation measurements performed in the framework of COST 231 special emphasis was dedicated to path loss and frequency selectivity. For wideband UMTS systems aiming for high data rates, the frequency selectivity in outdoor environments will have a major impact on system performance.

**Measurement example.** In Fig. 2.5 a typical result from a wideband outdoor measurement run in a micro cellular environment is given [96]. The shape of the PDPs are plotted along a run of 300 m. Each line in the three dimensional plot represents an average over 3 m. In the first part of the run there was LOS between transmitter and receiver, in the second part there was NLOS due to shadowing from buildings. The transmitter height was 11 m, the receiver antenna height was 2 m. The average distance between transmitter and receiver was about 200 m.

### 2.3.7 Fading and path loss characteristics

From narrowband and wideband measurements the short term and long term fluctuations of the received power were evaluated. For the determination of the long-term fading the fast fluctuations were eliminated by averaging over a gliding window having a length of 10 to 50 wavelength. The average path loss is ranging from about 50 dB for micro cells with short LOS paths up to about 150 dB for the edges of large macro cells. It depends mainly on the distance between transmitter and receiver, the building density and the heights of base station and mobile station antennas. Guiding effects in micro cellular street canyons with LOS may result in path loss values which are up to 4 dB lower compared to free space propagation if both the transmitter and receiver antenna are well below the roof tops of the surrounding buildings [89]. In general, the path loss is increasing by 25 dB to 30 dB while moving from micro cells with LOS to micro cells with NLOS conditions [94,96].

The increase of path loss with distance varies generally between 20 dB per decade for free space conditions and may exceed 50 dB per decade for NLOS situations with very high building densities. The path loss values are in the order of 6 to 10 dB larger for the 1800-MHz range than for the 900-MHz range [122]. The time variance of the fast fading depends mainly on the carrier frequency and on the speed of the mobile. It can be described for narrowband measurements by the power Doppler profile according to Eq. (2.31) and for wideband measurements by the delay-Doppler scattering function according to Eq. (2.20). The statistical distribution of the short-term fluctuations depend on the existence of dominant propagation paths and on the measurement bandwidth with respect to the coherence bandwidth of the channel (Eq. (2.29)).

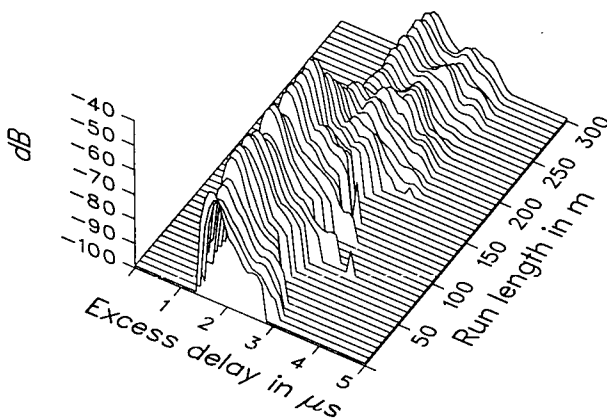


**Fig. 2.5** Impulse responses along a run of 300 m in a micro cellular environment

For narrowband transmission, LOS conditions are resulting in Rice fading instead of Rayleigh fading for NLOS situations. The fast fading of the wideband received power in a given environment is reduced with increasing system bandwidth because multipath gain can be exploited by wideband systems. However, the problem of intersymbol interference is increasing with bandwidth. In Fig. 2.6 the cumulative distributions and the standard deviations of the received power levels are shown for three different bandwidths. These curves were evaluated from micro cellular NLOS measurements.

### 2.3.8 Results for frequency selectivity in different environments

The frequency selectivity of the channel was evaluated from wideband measurements. It was characterised by different parameters, e.g., delay spread, delay window (see Section 2.1.5), interference ratio, notch depth. The largest frequency selectivity have been observed in Alpine regions [99, 100] and mountainous coastal districts, especially in Norwegian and Faroese fjords [97, 98, 60].

The statistical distribution of the delay spreads results in 9th decile values as high as about 10  $\mu$ s. The delay windows containing 90% of the total signal energy of the impulse responses reach 9th-decentile values of up to 35  $\mu$ s. Careful selection of base station sites, antenna heights and antenna radiation patterns, e.g., directional antennas or down-tilt patterns are means to reduce the frequency selectivity in this specific environment. The frequency selectivity of the mobile radio channel is significantly lower for rural areas in flat terrain and areas characterised by rolling hills. The 9th deciles of the delay spread distributions are much smaller than 5  $\mu$ s and the delay windows do not exceed a length of about 12  $\mu$ s in 90% of the locations.

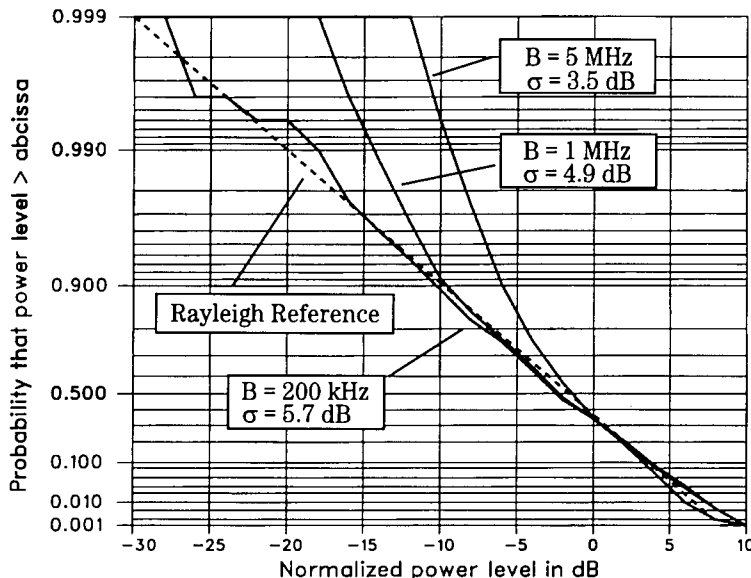


Fig. 2.6 Cumulative distributions of received power levels for 5 MHz, 1 MHz and 200 kHz bandwidth, evaluated from a micro cellular NLOS measurement.

A large variation of the duration of impulse responses was also observed in urban areas characterised by dense, inhomogeneous building structures. Very short as well as rather long excess delays occur. Delay windows larger than 20  $\mu$ s have been measured where the direct path is heavily obstructed and a good view towards prominent reflectors exists from the base station as well as from the mobile station.

The frequency selectivity as function of the cell size and base station antenna height was investigated. A reduction of the delay spread from 5  $\mu$ s to 1.7  $\mu$ s was noticed when the cell radius was reduced from 3 km to 600 m. If base-station antenna heights are reduced from above to below roof-top levels, an increase of the path loss was obtained, while the delay spread did not change significantly. The analysis of the shape of the power delay profiles resulted in increased attenuation of the direct path with decreasing antenna height while the delayed portions of the impulse responses scattered by prominent reflectors remain approximately unchanged. This phenomenon explains also the drawbacks of path-loss models which take into account only the direct path especially if they are applied to antenna heights below roof-top levels.

In micro cells the delay spread for LOS situations is in the range between 20 ns for small street canyons and 200 ns for large squares. For micro cellular NLOS conditions the delay spread is significantly larger. It may exceed values of 1  $\mu$ s. The

comparison of the measurements gained in the 900-MHz and the 1800-MHz bands showed that in general no difference between frequency selectivity in the two frequency ranges has to be expected.

### 2.3.9 Determination of directions-of-arrival (DOA)

In order to obtain a better understanding of the propagation mechanism and to test advanced propagation models, e.g., ray tracing techniques, evaluations of the DOAs of the received signals at different delays were performed. DOAs were determined on the basis of measurements realising a synthetic antenna array (linear, circular, matrix, etc.) [93]. From wideband measurements, the DOA analysis in connection with the excess delay information and in connection with digital terrain information was used to identify scatterer locations. If only power delay profiles are available, scatterer locations can also be estimated from the evolution of the excess delays versus a certain run length. A synthetic aperture antenna, realised by two-dimensional mechanical motion of a scanning antenna mounted on the roof of a van, was used for the determination of the angle-of-arrival distribution at the mobile. Alternatively, the DOAs have been estimated from the evaluation of delay-Doppler scattering function (Eq. (2.20)), processed from impulse responses measured at a spatial separation less than half of a wavelength.

In Fig. 2.7 the delay-Doppler scattering function evaluated from a wideband micro cellular propagation measurement in a NLOS situation is plotted [96]. It can be recognised that the DOAs are widely spread for the different excess delays.

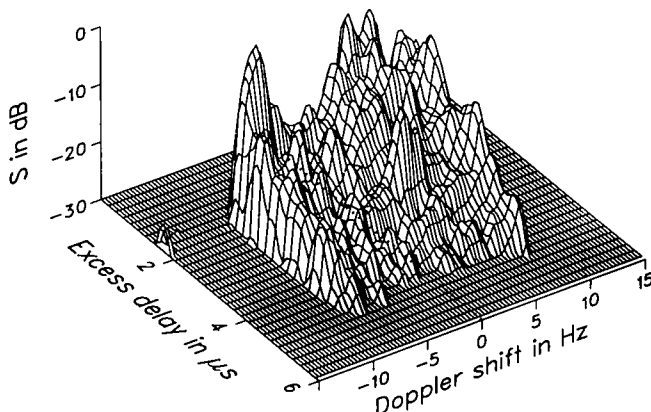


**Fig. 2.7** Delay-Doppler scattering function for a micro cellular NLOS situation.

The evaluation of DOAs from delay-Doppler scattering functions needs no extra measurement facilities, but it is restricted by a left-right ambiguity of the DOAs, because it is based only on a one-dimensional scanning of the received radio waves. DOAs of the direct path are often widespread due to scattering in the vicinity of the mobile whereas distant echoes arrive within a smaller angular distribution, e.g., as result of waves guided within a street canyon. The locations and reflection coefficients of scatterers in the terrain can be estimated from the DOAs and excess delays in case of reasonable free line-of-sight to the scatterers. This is a useful method to improve prediction methods which use terrain data bases.

A large DOA measurement campaign using mechanically rotated antenna has been used by [118]; for further details see section 3.2.

## 2.4 Propagation Modelling for the Simulation of the Radio Channel

**Jose Jimenez and Victor Perez, Telefonica I+D, Spain**

### 2.4.1 Radio Channel Simulation

Radio channel characterisation is an essential element in the design and testing of any communication system. Since computer simulation techniques are the most common way of checking performance, it is not surprising that channel characterisation plays a central role in COST 231 activities. A large number of contributions include a section on the channel model used for simulation. In a second phase, adjustment and testing play also an essential role. The design and implementation of a circuit element which mimics channel behaviour (channel emulator) is also a basic step in the design and optimisation process.

The radio propagation channel can be envisaged as an element transforming input signals into output signals. It can be considered as a filter but with time varying characteristics. Mathematically, the response  $y(t)$  of this element to an input signal  $x(t)$  can be described as the convolution integral

$$y(t) = \int_{-\infty}^{\infty} x(t - \tau) \cdot h(t, \tau) \cdot d\tau \quad (2.36)$$

being  $h(t, \tau)$  the channel impulse response, where  $t$  is the conventional time dimension which gives the variability of the impulse responses, and  $\tau$  the time delay which characterises the dispersion of the environment. Different approaches are possible to find such an element. The more direct is to provide a collection of "Stored Channels" based on actually measured impulse response characteristics representing the situation

on a specific environment. The second, is to use a Synthetic Channel Model based on the behaviour of the propagation process. The first, which has the advantage of the evident relation to reality, can be inadequate due to the complexity and also to the distortion introduced in the measuring and storing process. The second will only be as good as the theory behind it.

In any case, the simulation of the radio channel has to be considered from a system point of view. A narrowband system requires a different simulation method than a wideband one. Furthermore, the simulation of some system aspects leads to employ different radio channel approaches, for example, a diversity performance analysis, uses a different model than that employed for the optimum evaluation of the parameters for a modulation scheme. Taking this fact into account, in general terms, simulations within COST 231 have aimed at the following objectives:

- *Long term area simulations.* This has been the case of studies to evaluate signalling performances, coverage studies, cellular efficiency, etc. This type of simulation usually employs simple channels with attenuators. They are modelled by means of a simple dependence with the transceiver position.
- *Narrowband system simulations.* Those studies consider transceiver performance rather than overall system performance, and have been very frequent in the COST 231, for example for the evaluation of new modulation techniques, optimised transceiver architectures, and of singular importance, some simple studies of DECT performance, use of diversity, etc. In those cases, relatively simple AWGN, Rayleigh or Ricean channels are commonly employed
- *Wideband system simulations.* This is the most interesting case, and frequently, the tapped delay channel has been employed. There is a large variety in complexity depending on the use: from the simpler two path Rayleigh channel to the very elaborate models proposed for UMTS simulations.

This section is mainly focused in simulation for the third case. The analysis is concentrated in systems operating in the 900 MHz and 1800 MHz band, leaving for a different chapter the consideration of Broadband systems, including wideband LAN.

#### **2.4.2 Long term area simulations**

In order to test general system features, such as system capacity, or the performance and consistency of signalling or power control schemes, it is frequent to employ a conceptually simple deployment scheme. The propagation channel is modelled as an attenuator which depends, among other parameters, on the distance TX-RX, and that intends to predict the average field. A log-normal random variability is usually added

to emulate the effects of shadowing. This very simple scheme is complicated, in more elaborate programming, by consideration of the environment layout, particularly when calculating the capacity and performance results over indoors or microcell environments. This has been the case for the comparison of the ATDMA and CODIT projects performed in SIG5 “Special Interest Group 5 Common Testing Requirements” [103].

There is a relative large number of researchers using tools of this type, most of them working over regular and indefinite planes, as for example the simulation package Cellsim, which follows essentially the structure described above. It has been employed for DECT evaluation studies in indoor scenarios, GSM cellular capacity evaluation, and CDMA. Recent adaptations of the tool have been utilised for UMTS. There are also some commercial packages (Opnet, Bones) which could be adapted for that type of simulation.

#### 2.4.3 Narrowband system simulations

For initial testing of modulation schemes or new access techniques, two basic approaches have been taken: 1) Use of the AWGN model, and 2) Use of a Rayleigh or Ricean Channel (with only 1 tap). Those channel models are very simple but effective for initial analysis and they have been frequently used in academic research inside COST 231. However, though in mobile environments the second one responds more adequately to reality than the first one, they are appropriate only for narrowband systems, hence for most of the systems that have been studied during the COST 231 action, they are incomplete and require to introduce time delay dispersion (wideband) effects.

#### 2.4.4 Wideband system simulations

*Simple wideband simulation - 2 path Rayleigh model.* A more elaborate model than the narrowband approach uses a two (rarely three) path simulation (equation 2.37), usually each path having Rayleigh (or Rice) statistics. This model is usually sufficient for many cases and has been extensively employed through COST 231, specially for optimisation and evaluation of MSK and GMSK modulation schemes, but also for OFDM, M-PSK, M-QAM, CPM and TCM. It has also been used for the analysis of CDMA access techniques, (use of Joint Detection, Interference Cancellation, etc.). The number of COST 231 references would be very extensive.

$$h(t, \tau) = a_0(t) \cdot \delta(\tau) + a_1(t) \cdot \delta(\tau - \tau_1) \quad (2.37)$$

This model is also the favourite for the DECT system evaluation, which has been object of extensive studies in COST 231. The use of a 6 taps delay line channel emulator has also been normal during the COST 231 research activities.

**WSSUS models.** When a detailed investigation of a communication system is required, the channel is simulated by means of a time varying filter, in fact, a generalisation of the two (to six) path models mentioned above. The theory of time

varying filters has been developed originally by Zadeh, but it is in a paper by Bello [8], where the Wide Sense Stationary Uncorrelated Scattering model (WSSUS) is introduced and analysed. This model is fully determined by a two dimensional scattering function in terms of the echo delay  $\tau$  due to multipath and the Doppler frequency  $f_d$  due to the mobile movement.

**Software simulation. Implementation aspects.** The search for an effective simulation approach is summarised in [104]. In that work, instead of the conventional formula,

$$h(t, \tau) = \sum_{n=1}^N \beta_n(t) \cdot e^{j\phi_n(t)} \cdot \delta(\tau - \tau_n(t)) \quad (2.38)$$

which is directly translated into a filter, and where the measured impulse response functions allow directly to define the random variables  $\beta_n$ ,  $\phi_n$  and  $\tau_n$ , an alternative formulation is obtained, where the scattering function can be used by considering the marginal pdf's of the delay  $\tau$ , and Doppler  $f_d$  functions, obtained from the measured characteristics:

$$h(t, \tau) = \lim_{N \rightarrow \infty} \frac{1}{\sqrt{N}} \sum_{n=1}^N e^{j(\phi_n + 2\pi f_d n t)} \cdot \delta(\tau - \tau_n) \quad (2.39)$$

This approach seems to be simpler and more economic in computational terms, though it is not so easily connected to the more intuitive “filter like” realisation. Most of the practical models make use, however, of the equation 2.38, which allows to implement the convolution of the signal with the impulse response functions by means of a FIR filter. There exist different alternatives to get the coefficients (delays and complex amplitudes) of the filter, and have been commented in the introduction. When an extensive provision of measurements is available, the functions may be processed and converted in “Stored Channels” to be used by the FIR. The advantage is clear: the fidelity to a real situation. However, the drawback is that the simulations are limited in the length (as the measurement is), the behaviour is not easy to control, and the dependence with measurements may become onerous.

More frequent is the usage of “Synthetic Models”, where the measurements are utilised to get typical parameters for the simulations. With this technique, some fidelity in the emulation of the real channels may be lost, but on the contrary, the main drawbacks of the usage of “Stored Channels” is overcome. The main objective of a synthetic model is usually to get the complex coefficients of the FIR filter in real time, i.e. following a given Doppler spectrum pattern. For this purpose, different alternatives can be envisaged: the first is the classical and widely used method of low-pass filtering two in-quadrature AWGN sequences, in order to get a Rayleigh process with the expected Doppler variation (Classical, Gaussian), like in the COST 207 approach. Another method is based on the interference of phasors obtained randomly from given distributions based on the physical phenomenon, like in the RACE CODIT project [105] (see equation 2.40). Finally, the literature offers other methods

like the one proposed in [106], aimed at a more accurate description of the Doppler spectrum by using fast Fourier algorithms. Regardless of the method used, there are other aspects to take into account in the implementation of a simulator (HW or SW). The time variant complex impulse response functions defined in equation 2.36 cannot be used directly due to the discrete nature of a digital filtering process. This fact is important for designing simulators with tapped delay lines (FIR filters). Generally speaking, some aspects must be taken into account when treating with these functions, and are originated by the limited number of taps, the bandwidth of the signal, the normalisation of the filter coefficients and the interpolation technique of these coefficients.

For some applications, the channel has to be power normalised in order to keep the signal mean power after a convolution process. This is necessary, for example in AWGN simulations, where the noise power is calculated as a fraction of the signal. The normalisation is achieved in a “natural” way if the scatterers that contribute to the impulse responses are uncorrelated and the sum of their powers equals 1 [105]. However, when a tapped delay line like the one shown in the figure 2.8 is used, it is also required that the coefficients  $g_n(t)$  are obtained adequately.

This scheme introduces delays at a rate  $1/T$  equal to the signal sampling rate, therefore it requires a bandlimited filter with a bandwidth greater than or equal to the one of the signal. The coefficients must be obtained from formulas like 2.38, 2.39 or 2.41, which are actually non bandlimited, by a low-pass filtering and sampling.

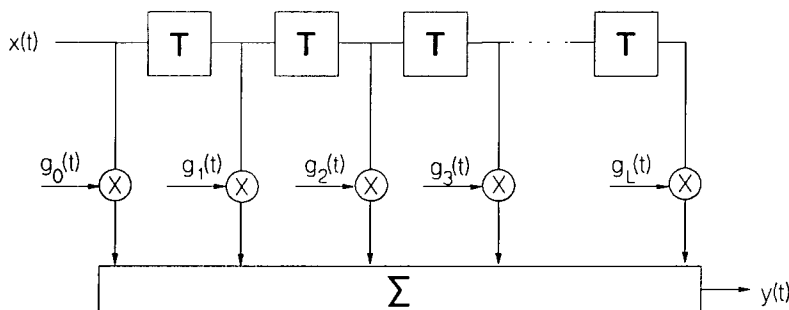


**Figure 2.8** FIR filter implementation of a channel simulator

Ideal low-pass filtering, i.e. the use of a sync function yields an infinite number of coefficients, which is not feasible. In practice, for most of the power delay profiles the energy is concentrated in a few number of taps, therefore, if an adequate truncation of the coefficients is performed, the channel function will behave as expected and the power normalisation will be achieved. However, it has to be kept in mind that the truncation depends on the autocorrelation characteristics of the input signal and the

number of side lobes considered, and can affect seriously to the accuracy of the results [105].

There exists a different and easy approach for obtaining a correct normalisation of the output signal, which consists on performing a previous measurement of the mean power by running the simulation with much lower sampling rates for the overall simulation length.

Other aspect that may influence in the final results, is related to the kind of interpolation used to update the coefficients of the filter. As the maximum Doppler deviation is usually much smaller than the sampling rate of the system  $1/T$ , the coefficients are calculated only every  $KT$  seconds, i.e. the values at the system sampling rate are interpolated. It has been proved that for practical situations, a linear interpolation allows to get a good accuracy [105].

***Other approaches.*** Other approaches consist in building a Time Frequency Linear Filter. The process uses frequency responses measurements instead of impulse responses. More recently a procedure to rationalise the otherwise somewhat heuristic process for the generation of the WSSUS model based on measurement has been proposed in [107,108] and its findings reported and discussed within COST. The procedure uses the collected measurements and follows a well defined algorithm to determine both the number and characteristics of the taps used in the equivalent transversal filter. In some cases, most usually when high frequencies are involved but also for DECT analysis, a ray tracing model is used. This type of model is very frequent for coverage prediction but has also been used for simulation and performance evaluation for wideband systems in some cases. Generally a very simple (square room) structure is proposed. The received signal is composed of the -several- rays starting at the emitter and ending at the receiver. This procedure also allows for the inclusion of the rays delays. Furthermore, there is considerable work in some issues, varying from the definition of better simulation approaches, to the analysis of the applicability of WSSUS assumptions in some environments. In this area, there has been some interest to overcome some of the theoretical limitations of the WSSUS model, particularly as connected to indoor environments, where the validity may be discussed due to the near-field effects of the antennas, the small dimensions of most of the objects, the intrinsic deterministic characteristics of the man-made structures, etc.[109]. Directly applicable are the investigations on the suitability of the WSSUS model when the mobile has not a constant velocity. Several movement patterns are proposed and analysed in [110]. The conclusions suggest that the use of the WSSUS model in -particularly- indoor environments, may be quite risky. This aspect has also been considered in the CODIT project, where a collection of modulation formulas are suggested to simulate varying environments, particularly for corner crossings.

#### 2.4.5 UMTS simulators

The development of UMTS (RACE II projects) required a more detailed description of the wideband channel, than the one suggested by COST 207 Action for the GSM

system. Two projects, ATDMA and CODIT, devoted some efforts to the definition of new propagation models. Since close contact between those projects and COST 231 Action has been established, a summary of the simulation models is given in this subsection.

**COST 207 approach.** As indicated, WSSUS models are the most frequently employed in COST 231. The models actually employed depended mostly on the relative bandwidth of the system as compared to the delay spread. The starting point for COST 231 has been the wideband models proposed by COST 207 for the GSM system [13]. That model has proved to be very powerful and, at the same time very simple to use, because it consists of a few figures which are easily provided for simulation. COST 207 provided a collection of suggested channels for testing rural and urban (hilly and non hilly) environments, with implementations of 6 or 12 taps. The basic elements (settings) for the channel simulation are:

- Tap delay values following different profiles.
- Tap mean power and Rayleigh distribution (eventually, for the first ray, a Rice distribution is used).
- Doppler Spectrum types (4): Classical [16], Gaussian (two different types) and Rice (Classical + Direct ray).

GSM COST 207 models have been used as a reference for many measurements and utilised to perform a large amount of theoretical and performance studies. Their applicability is not restricted to GSM but they also have been used for analysing different modulation techniques, access schemes and for the study of diversity. There has been some work presented in the Action on the original GSM channels - to correct mistakes and to clarify some points -, and during the time span of COST 231, new sets of parameters based on measurements have been produced. For example, a very comprehensive measurement campaign, performed by the Norwegian Administration has produced new parameters, following the rules of COST 207, for smoothly rolling farmland, rolling farmland and forest, valleys, mountainous areas and fjords, coastal terrain, suburban and urban terrain. COST 207 models have also been introduced into a number of commercially available simulation tools (COSSAP, SPW).

There has also been some research on the applicability of COST 207 models to the investigation of SFH gain in ATDMA environments. Those studies show a number of difficulties when a six tap model is used for the evaluation of large band effects, such as frequency hopping. The problem is the frequency correlation of the channel which is distinctly different in the model and in measurements. This opens a new research area not covered for the moment.

**ATDMA simulator.** ATDMA [111] followed two complementary approaches, mentioned above: Stored Measured Channels and Synthetic Channels. For every scenario (indoors, micro and macro cell) a large number of measurements were driven (more than 500 files in some cases) leading to the definition of a *typical channel* and a

collection of (two or three) *atypical channels*. Those recorded responses can be used either directly -stored channels- or by means of synthetic channels.

The synthetic channels are defined in similar terms of those of COST 207 but, instead of using a standard filter (Class) for the description of the Doppler spectrum, a stored function -based on actual measurements- is produced.

**CODIT simulator.** CODIT [105, 112] has based its initial work on some theoretical studies and measurements reported in [113,114]. CODIT activities were mostly aimed at the development of a synthetic model for WSSUS. The model was then extended to non-WSSUS scenarios, by means of some modulating functions in the filter coefficients. For the WSSUS, the *scattering function* modelling was utilised as starting point. A large number of scattering functions were analysed and a comprehensive environment classification produced. Even though CODIT uses the conventional FIR approach, both the statistics of the amplitude and Doppler Spectrum of the coefficients are different from those used in COST 207. The simulation of those parameters also differs since they are not based on a filtering process but on a Montecarlo simulation. Every scatterer laid in a given environment will contribute to the total field perceived at a given spatial location in a given time with a number  $N_{\text{waves}}$  of scattered waves, each of which is characterised by its amplitude  $a_{il}$ , its phase deviation  $\varphi_{il}$ , and the angle of incidence of the wave relative to the velocity vector of the mobile,  $\alpha_{il}$ . Some other parameters are involved such as the wavelength of transmission, the time  $t$ , and the vehicle speed  $v$ . The total contribution due to the  $i$ -th scatterer looks like

$$E_{si}(t) = a_{io} \cdot e^{j\left(\varphi_{io} + \frac{2\pi}{\lambda} vt \cdot \cos(\alpha_{io})\right)} + \sum_{l=1}^N a_{il} \cdot e^{j\left(\varphi_{il} + \frac{2\pi}{\lambda} vt \cdot \cos(\alpha_{il})\right)} \quad (2.40)$$

The total field perceived at a given spatial location in a given time can be obtained as the addition of the contributions due to every scatterer. The contributions of  $M$  scatterers travelling through radioelectrical paths of different lengths will not arrive aligned in time, but exhibiting a certain delay (time dispersion) with respect to the line-of-sight ray:

$$h(t, \tau) = \sum_{i=1}^M E_{si}(t) \cdot \delta(\tau - \tau_i) \quad (2.41)$$

## 2.4.6 Hardware Channel simulators

There has been relatively less activity in the hardware simulation front. Most contributions in this area have been based on acceptance test reports. As an example,

several channel emulators designed to emulate dual GSM channels as defined in GSM 05.05 [115], were reported inside the Action. Those acceptance tests have been useful not only for the manufacturing company, but also for other groups working in COST 231. The study of the DECT system was sometimes performed by means of channel emulators, complemented by actual measurements with a laboratory equipment that could generate time dispersed signals. The essential idea was to utilise tap delay lines with transmitting antennas. Other researchers employed controlled propagation areas where reflectors were carefully located. This kind of work can be better dealt under system evaluation or in -controlled- field test. A digital hardware quadrature baseband sounder based on fast FIR-processors has been developed by Aalborg University [119], with a throughput bandwidth of 1.2 MHz. The different Doppler spectra associated with each FIR tap are down-loadable from a PC. Due to this flexible approach, both simulated and measured (stored channel) Doppler spectra can be used.

ATDMA and CODIT have developed hardware channel simulators for use in their real time testbeds. They have been designed using a time variant transversal filter. The filter coefficients, in the CODIT case, are simulated with the process described above instead of using the conventional Rayleigh filtering technique. ATDMA relies on the use of stored channels, besides to the capability of generating synthetic responses.

**CODIT channel emulator.** This channel emulator has been designed for coping with most of the UMTS environments, thus it is able to work in different propagation conditions - different power delay profiles - with high bit rates.

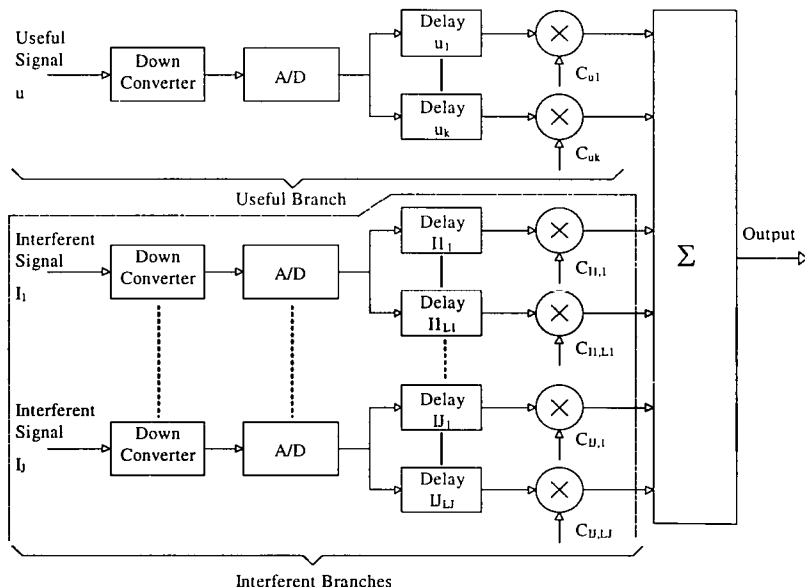


**Figure 2.9** General structure of the CODIT Channel Emulator

The main characteristic is the flexibility, which provides the capability to emulate both outdoor and indoor environments and co-channel interfering signals (this is compulsory in a CDMA system) affected by different or equal channel models. A schematic diagram of the FIR filter is shown in Fig. 2.9.

A FIFO memory is introduced in every tap branch simulating a programmable tap delay line, in order to keep the ability to emulate very different channel behaviours with a limited number of different tap branches. Two circuits (besides the RF stages) are identified:

- *Control circuit.* By means of multiplexer circuits, the signals are selectively introduced in one of the  $J+1$  available branches (different filters), each one comprising  $L_i$  taps. This allows to set the filter structure as function of the inputs used: if there are  $J$  interfering signals, and the total number of available taps is  $N$ , the useful signal will have  $(N-L_1-L_2-\dots-L_J)$  assigned taps. The CODIT channel emulator has 20 taps, 3 inputs and 2 outputs (to provide up and down link simultaneously), thus up to 2 interfering signals can be used with 6 possible branches.
- *Basic tap circuit.* To guarantee that all the filter coefficients which are computed in a sequential way in the DSP processor change simultaneously, a latch circuit has been introduced in every tap. These coefficients are fed to a FIFO memory from a file generated by adequate software tools, and then are real time interpolated by the DSP processor. A complex multiplier completes the tap circuit.

## 2.5 References

- [1] T. Bull, M. Barrett, R. Arnott, "Technology in smart antennas for universal advanced mobile infrastructure (TSUNAMI) - an overview", in *Proc. of the RACE Mobile Communications Summit*, (Cascais, Portugal), (Nov. 22-24), pp. 88-97, 1995.
- [2] D. J. Cichon, "Ray optical modelling of wave-propagation in urban micro and pico cells" (in German : "Strahlenoptische Modellierung der Wellenausbreitung in urbanen Mikro- und Pikofunkzellen"), in *Forschungsberichte aus dem Institut fuer Hochfrequenztechnik und Elektronik der Universitaet Karlsruhe*, vol. 8, ISSN 0942-2935, Ph.D. Thesis, University of Karlsruhe, Faculty of Electrical Engineering, 1994.
- [3] B. Fleury, D. Dahlhaus, "Investigations on the time variations of the wide-band radio channel for random receiver movements", in *Proc. of the IEEE Third Int. Symp. on Spread Spectrum Techniques and Applications (ISSSTA '94)*, (Oulu, Finland), pp. 631-636, July 1994.
- [4] T. Huschka, "Correlations of time-variant impulse responses in an indoor environment", in *Proc. IEEE Vehicular Techn. Conf. VTC' 95*, (Chicago), 1995.
- [5] COST 231 TD(89) 030 L. Olsson, "On the fading of radiowaves above 0.5 GHz indoor"
- [6] D. C. Cox, "Antenna diversity performance in mitigating the effects of portable radio telephone orientation and multipath propagation", *IEEE Trans. Commun.*, vol. COM-31, pp. 620-628, May 1983.
- [7] P. Melancon and J. Lebel, "Effects of fluorescent lights on signal fading characteristics for indoor radio channels", *Electronics Letters*, vol. 28, pp. 1740-1741, Aug. 1992.
- [8] P.A. Bello, "Characterization of randomly time-variant linear channels", *IEEE Trans. Commun. Syst.*, vol. CS-11, pp. 360-393, Dec. 1963.
- [9] I. I. Gihman and A. V. Skorohod, *The Theory of Stochastic Processes*. Springer, 1974.
- [10] S. L. Lauritzen, C. Thommesen, and J. Bach Andersen, "A stochastic model in mobile communications", *Stochastic Processes and their Applications*, vol. 36, pp. 165-172, 1990.
- [11] R. Collin, F. Zucker, *Antenna Theory*, vol. 1, McGraw Hill, 1969.
- [12] J. Bach Andersen, P. Eggers, "A heuristic model of power delay profiles in landmobile communications", in *Proc. URSI Symposium on Electromagnetic Theory*, (Sydney, Australia), pp. 55-57, Aug. 1992.
- [13] J.-P. de Weck, J. Ruprecht, B. Nemsic, H. Bühler, "Sounding radio channels for 1.8 GHz personal communications systems", in *Proc. VTC '92*, Denver Col., USA, May 10-12, 1992, pp. 490-493.
- [14] A. F. Molisch, "Statistical properties of the RMS delay spread of mobile radio channels with independent Rayleigh-fading paths", *IEEE Trans. Veh. Technol.*, Feb. 1996.

- [15] B. Fleury, "An uncertainty relation for WSS processes with an application to WSSUS systems", *IEEE Tran. Commun.*, (Accepted for publication).
- [16] W. C. Jakes, ed., *Microwave Mobile Communications*. New York: John Wiley & Sons, 1974.
- [17] Matthews P.A., Mohebbi B. : "Direction of Arrival and Building Scatter at UHF", Proc. ICAP 91, Part 1, pp. 147 - 150, 1991
- [18] COST 231 TD(91)035 Antti Koivumaki "Direction Diversity Measurements at 900 MHz"
- [19] COST 231 TD (92)0 24 A. Lévy "Time Structures of the Urban Mobile Channel"
- [20] COST 231 TD(92)061 Jaakko Lähteenmäki "High-resolution Direction-of-arrival measurements"
- [21] COST 231 TD(92)065 P.A. Matthews and A. Hairi Abu Bakar "Direction of arrival of radio signals within buildings"
- [22] COST 231 TD(90)028 Jens Jakobsen "Radio Propagation Measurements in two Office Buildings"
- [23] COST 231 TD(90)039 Jaakko Lähteenmäki "Measurements and Modelling for Indoor Power Delay Profile"
- [24] COST 231 TD(91)034 Jaakko Lähteenmäki "More Wide-Band Measurements at 1.7 GHz"
- [25] COST 231 TD(91)0 29 P.C. Andersen et al. "Delay Spread Measurements at 2 GHz"
- [26] COST 231 TD(93)097 U. Kauschke " Wideband Path Loss and Delay Spread Measurements in a NLOS situation"
- [27] Kauschke U. : "Wideband Indoor Channel Measurements for DECT Transmitter Positioned Inside and Outside Office Buildinds", Proc. PIMRC'94 and WIN, The Hague Sept. 1994, Vol. IV pp 1070 - 1074
- [28] COST 231 TD(94)013 F. Jimenez, J.M. Hernando, R. Herradon "Wideband and Narrowband characterization in microcellular and picocellular environments"
- [29] COST 231 TD(89)0 41 " Real-Time Channel Sounder (RCSS 900)"
- [30] de Weck J.P., Ruprecht J. "Real-time ML estimation of very frequency-selective multipath channels", Proceedings GLOBECOM'90, vol. 3, pp 2045-2050, 1990
- [31] Berg J.E., Mattson A., Ruprecht J. and de Weck J.P., "Specular reflections from high-rise buildings in 900 MHz cellular systems, "Proceedings of the 41st IEEE Veh. Technology, 1991
- [32] COST 231 TD(95)030 J. Ruprecht, H. Bühler, T. Klemenschits " Universal Channel Analyser: a Hardware/software Concept to measure and Analyse Mobile radio Channels"
- [33] COST 231 TD(90)014 M. J. Devasivatham "Multi-Frequency Radiowave Propagation Measurements in the Portable Radio Environment"
- [34] COST 231 TD(92)122 P.E. Mogensen "Wideband Polarization Diversity Measurements for Wireless Personal Radio communications"

- [35] COST 231 TD(93)008 P. Eggers, J. Toftgard "Initial results on wideband base-station antenna diversity for in-and outdoor pico-cell environments"
- [36] Gürdenli E., Huisch P.W. : "Propagation measurements and modelling for digital cellular radio systems", British Telecom Technical Journal, vol. 8, N° 1, pp. 44-56, Jan.
- [37] COST 231 TD(94)080 P. Karlsson, L. Olsson "Time Dispersion Measurement System for Radio Propagation at 1800 MHz and Results from Typical Indoor Measurements"
- [38] COST 231 TD(90)009 " Real-Time ML-Estimation of very Frequency-Selective Multipath Channels"
- [39] COST 231 TD(94)019 J. Jimenez "Propagation activities and simulation models in CODIT (RACE 2020) project"
- [40] COST 231 TD(94)068 M. Grigat "Wideband measurement techniques and data evaluation"
- [41] Barbot J.P., Bic J.C., Gollreiter R., Grigat M., Kadel G., Lévy A.J., Lorenz R.W., Mohr W., Strasser G. : Channel Characterization for Advanced TDMA Mobile Access", Proc. Race Mobile Telecommunications Workshop, Metz 1993, pp. 378 -384
- [42] Kadel G., Lorenz R.W. : "Wideband propagation measurements of the mobile radio channel", Proc. ISAP' 92 Sapporo 1992, pp. 81-84
- [43] COST 231 TD(90)041 R.W. Lorenz "First results of measurements using a digital channel sounder with a bandwidth matched to the GSM system"
- [44] COST 231 TD(90)075 R.W Lorenz, G. Kadel " Evaluation of propagation measurements using RUSK 400, a digital- sounder matched to the GSM bandwidth"
- [45] Martin U., Reng R., Schüssler H.W. and Schwarz K., : "Determination of wideband impulse responses", Proc. URSI International Symposium on Signals Systems and Electronics 1989, pp. 393-396
- [46] Hermann H., Martin U., Reng R., Schüssler H.W. and Schwarz K., : "High resolution channel measurement for mobile radio", Proc. EUSIPCO-90 Conference, Barcelona Sept.1990, pp. 1903-1906
- [47] Kauschke U. : "Propagation Measurements with RUSK SX and Simulations for a typical DECT Scenario in Urban Streets", Proc. 2nd Joint COST 227/231 Workshop on Mobile and Personal Com. Florence, April 1995, pp. 255-266
- [48] COST 231 TD(95)021 J. Wiart, P. Pajusco, A. Lévy, J.C. Bic "Analysis of Microcellulars Wideband Measurements in Paris"
- [49] Levy A.J., Rossi J.P., Barbot J.P. and J. Martin, "An improved channel sounding technique applied to wideband mobile 900 MHz propagation measurments", Proc. of the 40th IEEE Vehicular Technology Conference, Orlando 1990
- [50] E. Zollinger, "Measured inhouse radio wave propagation characteristics for wideband communication systems", 8 th European Conference on Electrotechnics, EUROCON'88, pp 314-317, June 13-17, 1988; Stockholm, Sweden

- [51] A. Radovic, E. Zollinger, "Measured time-variant characteristics of radio channels in the indoor environment," Mobile Radio Conference 1991, MRC'91, pp 267-274, November 13-15, 1991, Nice, France.
- [52] E. Zollinger, "Verfahren zur Bestimmung der komplexen Enveloppe von Eingangszeitdispersionsfunktionen linearer, zeitvariante Zweitore" (*Method for the determination of the complex envelope of the impulse response of linear, time-variant two-port networks*), Patentanmeldung, Amtl. Aktenzeichen : 3431/91-1, November 22, 1991, ASCOM Tech AG, Bern.
- [53] E. Zollinger, "Indoor wave propagation and analysis techniques", Workshop WMFG on "Field Theoretical Problems for Wireless Technology", 1995 IEEE MTT-S International Symposium, May 15, 1995, Orlando, FL, USA.
- [54] P. de Weeck, P. Merki, R. Klingler, A. Radovic, E. Zollinger and U. Dersch (Editor J.F. Wagen), "Wideband mobile radio channel measurement and modelling", International Commsphere'91 Symposium, pp. 8.1.1-8.1-10, Dec. 15-19, 1991, Herzliya, Israel.
- [55] E. Zollinger, "Methods for determining complex envelopes of impulse responses of linear time variant two-ports" (in German : "Verfahren zur Bestimmung der komplexen Enveloppe von Stossantworten linearer, zeitvariante Zweitore"), Patentschrift A5, CH 682262 A5, August 13, 1993, ASCOM Tech AG, Bern
- [56] E. Zollinger, "Methods for measuring mobile radio channels", Tutorial E, 1994 International Zurich Seminar on Digital Communications, March 8-11, 1994, ETH Zurich, Switzerland.
- [57] Felhauer T., Baier P., König W. and Mohr W. : "Optimum Spread Spectrum Signals for Wideband Channel Sounding", Electronics letters, Vol. 29, N° 6, pp. 563-564, March 1993
- [58] Felhauer T., Baier P., König W. and Mohr W. : "Optimized Wideband System for Unbiased Mobile Radio Channel Sounding with Periodic Spread Spectrum DSIGnals", IEICE Transactions on Communications, Vol E76-B, N° 8, pp. 1016-1029, August 1993
- [59] COST 231TD (95)J28 W. Mohr, B. Steiner, P. Weber "The Siemens Mobile Channel Sounder"
- [60] P. Eggers, C. Jensen, A. Oprea, K. Davidsen, M. Danielsen, "Assessment of GSM link quality dependence on radio dispersion in rural environments", in Proc. VTC '92, Denver Col., USA, May 10-12, 1992, pp. 532-535.
- [61] G. Kadel, "Determination of the GSM system performance from wideband propagation measurements", in Proc. VTC '92, Denver Col., USA, May 10-12, 1992, pp. 540-545.
- [62] COST 231 TD(93)048 Albert Molina, Peter Cullen, Paul Fannin "A Digital Wideband Mobile Radio Channel Sounder"
- [63] Molina A., Fannin P; : "Accuracy and Dynamic Range Improvement of Bandpass Impulse Response Measurements with pseudo-random noise", Electronics Letters, Vol. 27, N° 19. Sept. 1991, pp. 1755 - 1756
- [64] COST 231 TD(93)088 R. Gahleitner, Th. Klemenschits, R. Stepanek "First results of a Direct-Conversion channel sounder (DCCS1800) recorded in a road tunnel"

- [65] COST 231 TD(95)005 P. Bartolomé "Wideband Measurements in Outdoor Environments"
- [66] COST 231 TD(90)027 R.H. Rækken "Description of the Norwegian Impulse Response Measurements"
- [67] Løvnes G., Paulsen S.E., Rækken R.H. : "Wideband propagation measurements at 900 MHz and 1.7 GHz in macrocells", Proc. ISAP 92, Sapporo, pp. 77-80
- [68] Rækken R.H. , Eskedal B.E. : "DECT performance in multipath environments", Proc. Nordic Radio Symposium 1995 (NRS'95), Saltsjöbaden, Sweden, April 1995
- [69] COST 231 TD(91)071 S. Ruiz-Boqué et al."Indoor wideband channel characterization (900 and 1800 MHz) by means of a network analyzer"
- [70] COST 231 TD(93)089 J. Jimenez, M. Pizarroso, V. Perez, U. Dersch "CODIT Measurement Campaign : Wideband Indoor Measurements"
- [71] Gollreiter, R. (editor): Channel models Issue 2. RACE ATDMA Document R2084/ESG/CC3/DS/P/029/b1, May 15th, 1994.
- [72] P. Bartolomé, "Indoor propagation models validation," *COST 231 Temporary documents*, TD(93)51, Barcelona 1993.
- [73] C. Törnevik, J.-E. Berg, F Lotse, "900 MHz propagation measurements and path loss models for different indoor environments," *Proceedings of 43rd IEEE VTC-93*, New Jersey, USA, 1993.
- [74] J. Wiart, "Indoor electromagnetic wave propagation measurements and modelling," *COST 231 Temporary documents*, TD(94)24, Lisbon , January 1994.
- [75] P. Karlsson, "Indoor radio propagation for personal communications services," dissertation, University of Lund, 1995
- [76] R. Gahleitner, "Radio wave propagation in and into urban buildings," dissertation, Technical University of Vienna, 1994.
- [77] S. Ruiz-Boqué, M Ballart, C. Clúa, R Agustí, "Propagation models for indoor mobile communications," *COST 231 Temporary documents*, TD(91)14, Florence 1991.
- [78] J. Lähteenmäki, "Radiowave propagation in office buildings and underground halls," *Proc. of European Microwave Conference*, Espoo 1992, pp. 377-382.
- [79] P. Karlsson, L. Olsson, "Time dispersion measurement system for radio propagation at 1800 MHz and results from typical indoor environments," *Proc. of 44th IEEE Vehicular Technology Conference*, 1793-1797, 1994.
- [80] U. Dersch, E. Zollinger, "Propagation mechanisms in micro cell and indoor environments," *Transactions on Vehicular Technology*, Vol. 43, Nov. 1994, No. 4, pp. 1058-1066.
- [81] S. Ruiz-Boqué, R. Agustí, J. Peréz, "Indoor wideband channel characterization (900 and 1800 MHz) by means of a network analyzer, *COST 231 Temporary documents*, TD(91)71, Lund 1991.

- [82] J. Lähteenmäki, "Determination of dominant signal paths for indoor radio channels at 1,7 GHz," *Proc. of the 4th International Symposium on Personal, Indoor and Mobile Radio Communications*, Yokohama 1993, pp. 392-396.
- [83] J. Fuhl, Virtual-Image-Array Single-Snapshot (VIASS) algorithm for direction-of-arrival estimation of coherent signals, COST 231 Temporary Documents, TD(95)23, Bern, January 1995.
- [84] A. H. Abubakar and P. A. Matthews, " Direction of arrival of radio signals inside and outside buildings," *Proc. of IEEE 44th Vehicular Technology Conference*, June 8-10, 1994, Stockholm, Sweden, pp. 1754-1756.
- [85] U. Dersch, E. Zollinger, "Propagation measurements in micro cell and indoor environments," *The 4th Int. symposium on Personal, Indoor and Mobile Radio Communications (PIMRC'93)*, pp. 191-195, Yokohama, Sept. 8-11, 1993, Japan.
- [86] U. Dersch, J. Troger, E. Zollinger, "Multiple reflections of radio waves in a corridor," *IEEE Trans. Antennas and propagation*, vol 42, no. 11, pp. 1571-1574, Nov. 1994.
- [87] E. Zollinger, "Indoor wave propagation and analysis techniques," *1995 IEEE MTT-S Int. Symposium, May 15, 1995, Orlando, FL, USA*.
- [88] Barbot, J.P., Bic, J.C., Gollreiter, R., Grigat, M., Kadel, G., Levy, A.J., Lorenz, R.W., Mohr, W., Strasser, G.: Channel Characterisation for advanced TDMA Mobile Access. Proceedings of the RACE Mobile Telecommunications Workshop, Metz, 16-18 June 1993, pp. 378-384.
- [89] Jakoby, R., Liebenow, U.: Modelling of radiowave propagation in microcells. Proceedings of the 9th International Conference on Antennas and Propagation ICAP'95, Vol. 2, Eindhoven, April 1995, pp. 377-380.
- [90] Liebenow, U., Kuhlmann, P.: Theoretical investigations and wideband measurements on wave propagation in hilly terrain. Proceedings of the IEEE Vehicular Technology Conference (VTC), Stockholm 1994, pp. 1803-1806.
- [91] Kadel, G. and Lorenz, R.W.: Mobile propagation measurements using a digital channel sounder with a bandwidth matched to the GSM-system. Proceedings of the seventh International Conference on Antennas and Propagation (ICAP 91). IEE Conf. Publ. 333, 1991, pp. 496-499.
- [92] Lorenz, R.W. and Kadel, G.: Propagation measurements using a digital channel sounder matched to the GSM-bandwidth. ICC'91, Denver, USA, 1991, pp. 548-552.
- [93] Lorenz, R.W. and Kadel, G.: Digital channel sounder for remote sensing of scatterers in mobile radio environment. AGARD Conference Proceedings 502 (1991), pp. 34.1-34.9.
- [94] Kadel, G. and Lorenz, R.W.: Wideband propagation measurements of the mobile radio channel. Proceedings of the International Symposium on Antennas and Propagation (ISAP 92). Sapporo 1992, pp. 81-84.
- [95] Kadel, G., Lorenz, R.W.: Wideband characterization of the mobile radio channel and its impact on system performance. Abstracts of the XXIVth URSI General Assembly, Kyoto, Japan (1993), p.1.

- [96] Kadel, G., Lorenz, R.W.: Impact of the radio channel on the performance of digital mobile communication systems. Proceedings of the Sixth International Symposium on Personal, Indoor and Mobile Communications (PIMRC), Toronto, September 1995, pp. 419-423.
- [97] G. Løvnes, S. E. Paulsen and R. H. Rækken: "UHF radio channel characteristics. Part one: Multipath Propagation and Description of the NTR channel sounder", Kjeller, Telenor R&D, 1991, ISBN 82-423-0172-7.
- [98] G. Løvnes, S. E. Paulsen and R. H. Rækken: "UHF radio channel characteristics. Part two: Wideband propagation measurements in large cells", Kjeller, Telenor R&D, 1992, ISBN 82-423-0214-6.
- [99] Nemsic, B., deWeck, J.-P., Bühler, H., Ergoth, T.: Wideband radio channel characteristics in alpine regions, Electron. Lett. 27 (1991), 717-719.
- [100] Nemsic, B., Bühler, H., Bonek, E.: Assessment of wideband radio channels in alpine regions using PICAM, Proc. 41<sup>st</sup> IEEE Vehicular Techn. Conf., St. Louis, Mai 1991, 491-495.
- [101] Bühler, H., Nemsic, B.: PICAM: A PC based cellular network planning software package, Proc. IEEE Meditarr. Electrotechn. Conf. MELECON 91, Ljubljana, Mai 1991, 643-646.
- [102] Gahleitner, R., Bonek, E.: 900 and 1800 MHz wave penetration into urban buildings, Proc. XXIVth General Assembly of URSI, Kyoto, Japan, Sept. 1993, 557, paper CBEF-2.
- [103] M. Pizarroso, J. Jimenez Ed. "Preliminary Evaluation of ATDMA and CODIT System Concepts". MPLA/TDE/SIG5/DS/P/001/b1.
- [104] P. Hocher. "A Statistical Discrete Time Model for the WSSUS Multipath Channel". IEEE Transactions on VT, vol 41, No. 4, Nov. 1992.
- [105] J. Jimenez, V. Pérez, Ed. "Final propagation model" CEC RACE CODIT R2020/TDE/PS/DS/P/040/b1.
- [106] P.M. Crespo and J. Jiménez, "Computer Simulation of Radio Channels Using a Harmonic Decomposition Technique". IEEE Tr. on VT, vol. 44, No. 3, Aug 95.
- [107] U. Martin, "Modelling the Mobile Radio Channel by Echo Estimation" Frequenz 48 (1994) 9-10
- [108] U Martin, "Echo Estimation - Deriving Simulation Models for the Mobile Radio Channel" Conf. Proc. IEEE VT95 Chicago, July 95.
- [109] U. Dersch, "Physical Modelling of Macro, Micro and Inhouse Cell Mobile Radio Channels", PIMRC Oct. 1992, Boston.
- [110] T. Huschka "Correlations of Time Variant Impulse Responses in an Indoor Environment". Proc. of the 45 IEEE VT Conf, July 1995
- [111] R. Gollreiter Ed, "Channel Models. Issue 2", CEC RACE R2084/ESG/CC3/DS/P/029/b1.

- [112] F. Casadevall, A. Gellonch, J. Olmos, G. Femenias. "Channel Emulator for CoDiT project". RACE Mobile Communications Summit, Cascais, Portugal, Nov. 1995
- [113] W.R. Braun, U. Dersch. "A Physical Mobile Radio Channel Model", IEEE Trans. Veh. Technology. Vol 40, No.2 May. 1991.
- [114] U. Dersch and R. Ruegg "Simulation of the time and Frequency Selective Outdoor Mobile Radio Channel". IEEE Trans. on VT. Vol 42, No. 3, August 1993.
- [115] ESTSI prETS 300 577 GSM 05.05, Digital cellular telecommunications system (Phase2); Radio transmission and reception, August 1996, 8<sup>th</sup> Edition
- [116] G. Kadel, "Simulation of the DECT system using wideband channel data measured in two diversity branches", in *Proc. 2nd Int. Conf. on Univ. Pers. Com.*, Ottawa, Canada, Oct. 1993, pp. 546-550
- [117] F. Gatti, F. Tallone, "Propagation measurements in wideband mobile channels", in *Proc. XIII IMEKO World Congress - From Measurement to Innovation*, Turin, Italy, September 1994
- [118] P.C.F. Eggers, G.F. Pedersen, K. Olesen, "Multi sensor propagation", RACE II-TSUNAMI deliverable R2108/AUC/WP3.1/DS/I/046/b1, D.3.1.1., August 1994
- [119] S. Pedersen, "Real Time Hardware Radio Channel Simulator", in *Proc. Nordic Radio Symposium* (NRS'92), Aalborg, Denmark, June 1992, pp. 191-194
- [120] P.C.F. Eggers, C. Jensen, A.M. Oprea, "Assessment of GSM-link quality dependence on radio dispersion in rural environments", in *Proc. Nordic Radio Symposium* (NRS'92), Aalborg, Denmark, June 1992, pp. 19-22
- [121] J. Toftgård, P.C.F. Eggers, "Experimental characterization of the polarization state dynamics of personal communication radio channels", in *Proc. IEEE VTC'93*, Secaucus, NJ, USA, May 1993, pp. 65-69
- [122] P.E. Mogensen, P. Eggers, C. Jensen, J. Bach Andersen, "Urban area radio propagation measurements at 955 and 1845 MHz for small and micro cells", in *Proc. Globecom '91*, Phoenix, AZ, USA, December 1991, pp. 1297-1302

## Antennas and antenna diversity

Patrick C.F. Eggers, CPK, Denmark

The antennas are the outermost components in the transmission chain which are deterministically describable and physically manufacturable. However the network performance of the antennas is not dependant on the antenna alone, but on the interaction between antenna and radio environment. This causing the network performance evaluation of the antenna system to be of a stochastic nature. The primary task for the antenna is

- connection

that is seeing to that any information is conveyed from transmitter to receiver. Equally import are the possibilities to include the antenna to

- suppress or repair media impairments

There are three major areas that have been considered when using antennas for compensating for the impairments of the mobile radio channel:

- noise suppression through antenna gain and effectivity
- temporal fading and interference suppression through multiport antenna diversity
- spatially selective interference suppression through adaptive antenna directivity

The following sections discuss the design and application of antenna elements and systems to meet these tasks. The first section 3.1 covers physical and electrical design of antenna elements mainly used for propagation experiments. Section 3.2 covers the interaction between base station antennas and the radio environment, which influence the perceived antenna diagram. Design criteria for antennas for handportables and influences on human body absorption, are discussed in section 3.3. This both through efficiency and absorption by the human head. The remainder sections 3.4 to 3.6 focus on three key areas in antenna diversity. That is the antenna system structure, the use of an antenna system via combiners and lastly the expected gain in terms of radio channel parameters.

## 3.1 Antenna design

Ernst Zollinger, IMST, Germany

### 3.1.1 Extremely wideband antennas

*Design of a wideband conical monopole antenna*

Fig.3.1 depicts the cross-section of an extremely wideband conical monopole antenna that was developed for radio channels measurements

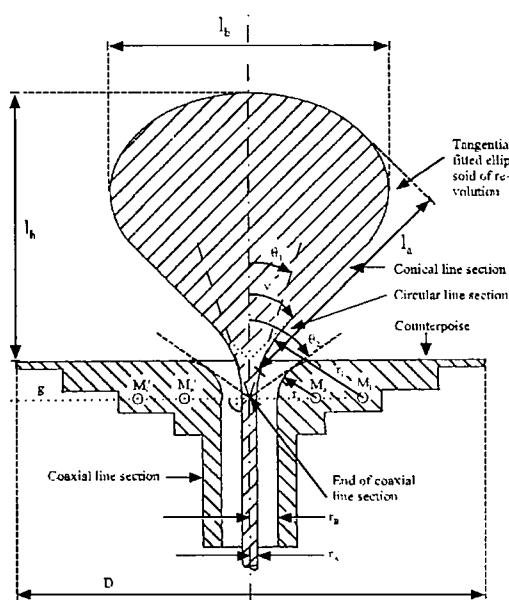


**Fig.3.1** Cross-section of a conical monopole antenna

frequency  $f_L$  for which the length  $l_a$  of the conical section become smaller than approximately  $l_a = c/(4f_L) = \lambda_L/4$  where  $c$  denotes the vacuum speed of light and  $\lambda_L$  the wavelength. For  $f_L = 600$  MHz the length  $l_a$  has to be  $> 12.5$  cm. According to [2], the shape of the upper part of the conical antenna section has a strong influence in achieving good performance of the antenna at the lower cut-off frequency  $f_L$ . In agreement with [2] and [3], experiments showed that a strongly rounded upper part of this section will substantially decrease the SWR at the feeding point of the antenna at  $f_L$ . An ellipsoid of revolution, a hemisphere, a cylindrical superstructure or a combination of the above is well suited for this purpose.

[1]. The feeding point impedance  $Z_{CO}$  of the monopole antenna can be matched to the intrinsic impedance  $Z_{CA}$  of the feeding coaxial cable by choosing angle  $\nu$  accordingly.

$$Z_{CO} = \left( Z_0 / 2\pi\sqrt{\epsilon_r} \right) \ln(\cot(\nu/2))$$

$$Z_{CA} = \left( Z_0 / 2\pi\sqrt{\epsilon_r} \right) \ln(r_B/r_A)$$

$Z_0$  denotes the intrinsic impedance of free space,  $r_A$  and  $r_B$  are the radii of the inner and outer conductor of the feeding cable, respectively, and  $\epsilon'_r$  is the real part of the complex relative permittivity of the dielectric between the two conductors.

This antenna behaves like an inhomogeneous, open line at low frequencies. Therefore, it is hardly possible to ensure the required performance below a

According to these shapes different length-to-diameter ratios  $l_h/l_b$  are obtained. In agreement with [2] widest bandwidth was obtained with a length-to-diameter ratio in the range of 0.9 to 1.1. The transition zone between the coaxial line and the conical structure of the antenna is important in achieving a low reflection coefficient at high frequencies. The theory for this problem is well known and can be found in [2] and [3]. The solution is a circular line which is obtained by stringing together conical lines with continuously increasing aperture angles while keeping the intrinsic impedance  $Z_{CI}$  constant. For a reflection free transition between the coaxial and the circular line as well as between the circular and the conical line, the corresponding intrinsic impedances must coincide, i.e.  $Z_{CA} = Z_{CI}$  and  $Z_{CI} = Z_{CO}$ . To fulfil the first equation, the centres  $M_i$  and  $M_a$  of the curvature of the circular line must be on the plane that is perpendicular to the symmetry axis of the antenna. This plane is indicated in Fig. 3.1 by the dotted line  $g$ . The corresponding radii  $r_i$  and  $r_a$  are given by  $r_i = r_d(r_B/r_A) + (r^2_B - r^2_A)/2r_A$ . The diameter  $D$  of the counterpoise affects the electromagnetic field in the near- and far-field zone of the antenna, the impedance  $Z_{CO}$ , the reflection coefficient and the SWR at the feeding point. Because the transfer function of this antenna has a high-pass characteristic, the SWR increases sharply at the lower cut-off frequency  $f_L = 600$  MHz (Fig. 3.4 and Fig. 3.5). Based on the results outlined in [4] for thin  $\lambda/4$ -monopole,  $D/\lambda_L$  should be  $\approx 0.9$  for a  $\text{SWR} < 1.25$  and  $\approx 0.4$  for a  $\text{SWR} < 1.5$ . Therefore,  $D = 0.426$  m and  $D = 0.259$  m have been selected for antenna no. 1 and 2, respectively.

*Properties of the wideband conical monopole antenna.*

Two wideband monopole antennas have been built (Fig. 3.2 and Fig. 3.3) [1].

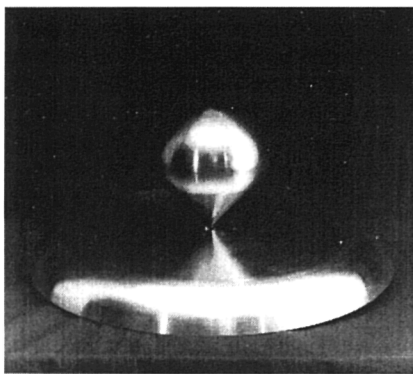


Fig. 3.2 Monopole antenna no. 1.

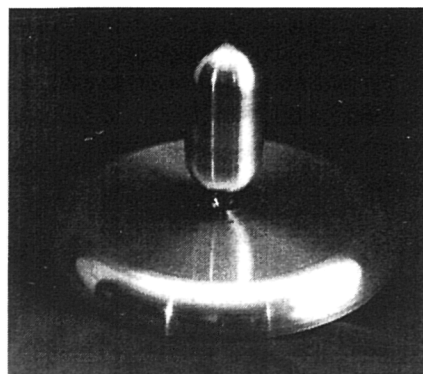
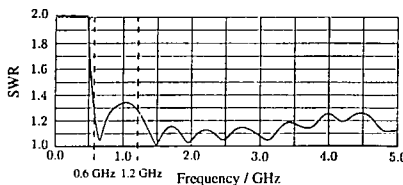


Fig. 3.3 Monopole antenna no. 2.

Their SWR are shown in Fig. 3.4 and Fig. 3.5 for frequencies between DC and 5 GHz. Extremely wideband measurements showed that the bandwidths of antenna 1 and 2 are 15 GHz and 8 GHz, respectively, if  $\text{SWR} < 1.9$  is the criterion.

The co-polarisation patterns of the two antennas have been measured at 1.5 GHz (Fig. 3.6 and Fig. 3.7). For vertical polarisation of the measured antenna  $\theta_A$  denotes the angle with respect to the vertical axis.



**Fig. 3.4** SWR of monopole no. 1.

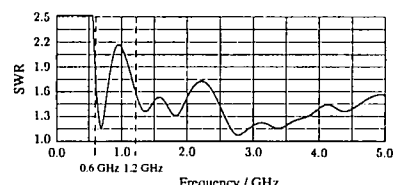


**Fig. 3.5** SWR of monopole no. 2.

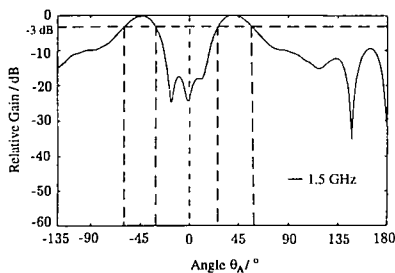


**Fig. 3.6** Co-polarisation pattern of monopole antenna no. 1.

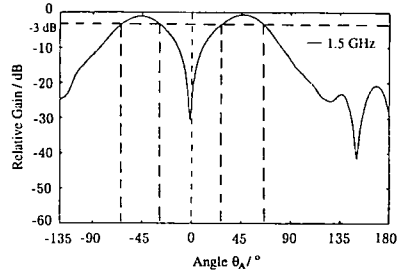


**Fig. 3.7** Co-polarisation pattern of the monopole antenna no. 2.

### 3.1.2 Millimetre-wave antennas

#### *General Considerations*

In mobile systems, small size, low power consumption, conservative exposure limits of less than  $1 \text{ mW/cm}^2$  [5]<sup>1</sup> and low prices are essential requirements. At millimetre-

<sup>1</sup> Currently everything indicates that the limits to be standardised will be adopted from the IRPA/INIRC (International Non-Ionizing Radiation Committee of the International Radiation Protection Association) „Interim guidelines on limits of exposure to RF fields“ [5]. According to a statement of the IRPA these limits are based on a summary and an assessment of scientific works that have been published by the UNEP/WHO (United Nations Environment Program / World Health Organisation) in the „Environmental Health Criteria“ series.

(mm)-waves, where the link budget is a critical issue, antennas with more than 10 dB gain providing uniform cell coverage are needed.

### Patch antennas

Patch antennas printed on top of a PCMCIA card, which protrudes a few centimetres outside of the computer case are suited for ad hoc radio LAN systems where portable computers communicate peer-to-peer.

To obtain circular symmetrical radiation patterns with a null at zenith, and maximum radiation in the plane of the PCMCIA card, a circular patch antennas operated in the  $\text{TM}_{02}$  mode has been designed and tested ([6], [7], [8]). At the operation frequency, a patch antenna can be viewed as a resonator. Following [9], the resonant frequency  $f_r$  of the  $\text{TM}_{02}$  mode circular patch antenna is given by  $f_r = f_0\sqrt{1+D}$ ,  $f_0 = 3.832/2\pi\sqrt{\mu_0\varepsilon_I}$ ,  $D = (2d\varepsilon/\pi\varepsilon_I a)[\ln(\pi a/2d) + 1.7726]$ ,

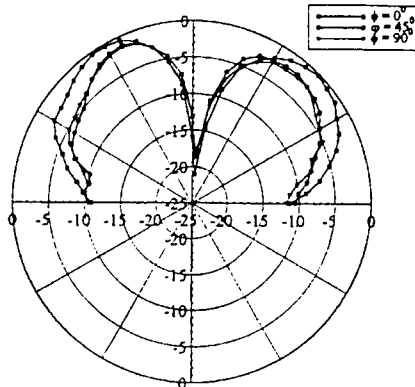


**Fig. 3.8** Radiation pattern of the circular patch antenna.

the permittivity  $\varepsilon_I = \varepsilon_0\varepsilon_{rI}$  of the dielectric with  $\varepsilon_0$  the permittivity of the vacuum, the radius  $a$  of the patch and the substrate thickness  $d$ . The modification factor  $\Delta$  represents the contribution of the stray field at the antenna edge. For the prototype, a substrate with a relative permittivity of 2.55 and  $d = 3$  mm was used resulting in  $a = 2.05$  cm. A SWR  $\leq 2.0$  has been obtained within a frequency range of 5.1 GHz to 5.42 GHz. The radiation patterns are depicted in Fig. 3.8 for different plane-cuts where  $\phi = 0$  represents the plane passing through the feed point.

### Waveguide antennas

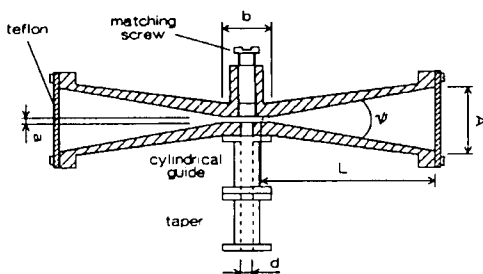


**Fig. 3.9** Geometry of biconical horn antenna.

Near uniform cell coverage may be achieved with a conical horn antenna (Fig. 3.9) [10]. It consists of a radial line with spacing  $a = 2.0$  mm and diameter  $b$ , a circular waveguide with an interior diameter of  $d = 3.5$  mm, a biconical horn of length  $L$ , and an aperture of

width  $A$ . An omnidirectional radiation pattern in the azimuthal plane is obtained if the radial line is excited with a circularly polarised  $TE_{11}$  mode in the circular waveguide.

The polarisation is horizontal for  $\lambda/2 < a < \lambda$  and vertical for  $a < \lambda/2$  where  $\lambda$  denotes the free space wavelength [11]. The radiation pattern in the elevation plane is determined by the parameters  $L$  and  $A$ . Provided that the differences of the phases in the aperture are smaller than  $90^\circ$ , the magnitude of the electric field pattern can be calculated by the methods described for sectored horns excited with the  $TE_{01}$  mode [12]. Excellent agreement between theoretical and measured results have been obtained for the radiation pattern depicted in Fig. 3.10.

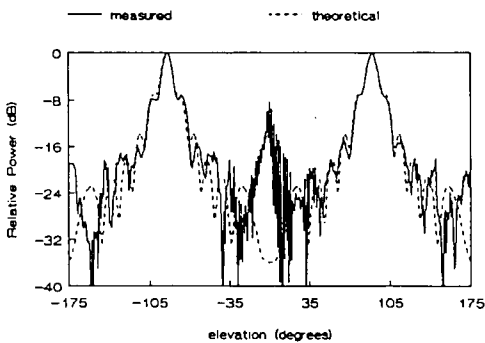


**Fig. 3.10** Measured and theoretical radiation pattern in the elevation plane [10].

### Dielectric antennas

Dielectric antennas are suitable for mm-wave applications because they are structurally simple and easy to fabricate. Two types of dielectric leaky-wave antennas are of particular interest: tapered dielectric-rod and periodic dielectric antennas. The first is a surface wave antenna radiating in the forward direction. Periodic dielectric antennas consist of a leaky-wave guide created either with a periodic surface perturbation or by generating a leaking propagation mode in the structure.

Both structures can be designed to radiate almost to broadside, i.e. orthogonal to the antenna axis. The most important design parameters are the leakage coefficient  $\alpha$  which describes the radiated power per unit length and the phase coefficient  $\beta$  which is determined by the overall effective permittivity  $\epsilon_{\text{eff}}$  of the dielectric antenna. Both parameters strongly depend on the height of the dielectric but only slightly on the thickness of the periodic surface perturbation.

Compared to microstrip travelling mode antennas, the beam pointing angle of dielectric antennas is strongly frequency-dependent: up to  $40^\circ$  per 10% variation of the frequency. This feature could be used in a WLAN FDMA/SCPC concept using DCA for a mobile unit in a given azimuth direction of the antenna beam. More information on both types of dielectric antennas can be found in [13].

Dielectric lens antennas directly fed by the waveguide are compact in size, easily assembled and therefore appropriate for mass production. Depending on the shape of the lens near uniform cell coverage can be obtained [14], [15], [16].

### 3.1.3 Internal antennas for hand sets

Internal antennas are applied in a growing number of mobile communication systems due to design advantages, serviceability and price ([17], [18]). The new radiation-coupled dual-L antenna presented in [19], [20] offers at least 50% higher bandwidth compared to an inverted-F antenna of equal height  $H$  (Fig. 3.11) [21]. Its resonant wavelength  $\lambda_0$  is determined by the geometrical parameters  $L$  and  $H$ :  $L + H = \lambda/4$ . The dimensions of the antenna have been optimised using the 333 segment wire-grid model of the program NEC in conjunction with the program AutoCAD.<sup>®2</sup>

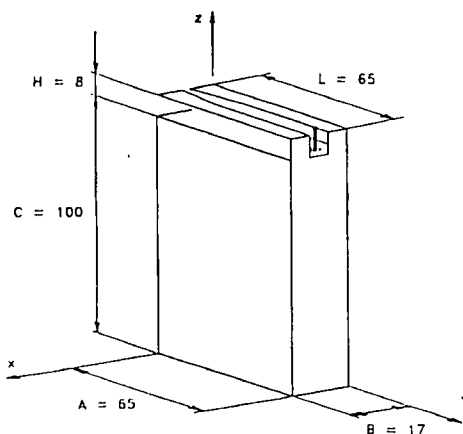


**Fig. 3.11** Radiation-coupled dual-L antenna mounted on top of the shielding case of a cordless telephone [19], [20].

The radiation patterns of the antenna have been measured with a test transmitter powered by the original battery pack of the cordless telephone inside the shielding case, which in turn was put into a plastic case. For the wire-grid model the radiation patterns were calculated. Since NEC did not allow to model the influence of the plastic case, the patterns were calculated for frequencies that corresponded to 914 MHz and 954 MHz when the plastic case was absent, i.e. at 970 MHz and 1010 MHz. Particularly for the dominating polarisation the calculated radiation patterns compare well with the measurements.

<sup>2</sup> Registered trademark of Autodesk, Inc.

## 3.2 Base station antenna relations

**Patrick C.F. Eggers, CPK, Denmark**

In the current cellular systems the base station (BS) antennas are mainly mast-mounted omni directional or sector antennas with respect to the azimuthal plane. The use of collinear arrays lead to increased gain by reducing the elevation beamwidth. Beam tilting and shaping of the elevation pattern are used to attempt control of cell contours. Adaptive antenna arrays have been suggested to suppress interference via spatial filtering in an SDMA scheme. The effectiveness of such antenna arrangements are closely linked with the directional properties of the radio environment as sensed at the BS site. Models exist for the angular BS environments with respect to spatial fading [22],[23],[24]. But only little work [25] has been presented, dealing with basic angular domain fading and antenna relations. The following subsections will expand on the radio propagation description in the previous chapter, to include the directional information at the BS and its influence on perceived antenna characteristics.

### 3.2.1 Angular relations between BS-antennas and radio environments

Basically 2D circular relations in either azimuth or elevation are sufficient for most outdoor small and macro cell applications. In the following we consider small scale relations (mobile station (MS) movements over a few wave lengths ( $\lambda$ ) between antenna diagram 'a' and the environment diagram 'e'. Thus the environment diagram can be considered stationary.

#### 2D circular antenna environment relations

When rotating a BS antenna with directional amplitude radiation pattern  $a(\phi)$  in a circle around azimuth, the measured complex voltage response  $m(\phi)$  is [26]

$$m(\phi, d) = \oint e(\phi, d) \cdot a(\phi - \phi)d\phi = R_{e,a} \cdot (\phi, d) \quad (3.1)$$

which can be expressed as a correlation  $R$  between the antenna amplitude response and the angular environment diagram  $e(\phi)$ . The MS movement is represented in a displacement variable  $d$ . The angular frequency relation  $\tilde{m}(\omega_\phi, \omega_d) = \tilde{e}(\omega_\phi, \omega_d) \cdot \tilde{a}^*(-\omega_\phi)$ , follows from the correlation theorem. Assuming uncorrelated scattering (US) identical relations hold for the mean power diagrams  $M = \langle |m|^2 \rangle$  [27]. It follows that standard frequency domain (inverse Wiener) filtering techniques can be used to suppress the measurement antenna's influence on the measured responses [27], [28], yielding an estimated environment response  $\tilde{E}(\omega_\phi) = \tilde{M}(\omega_\phi) \cdot \tilde{F}(\omega_\phi)$ . The application of this technique to angular pattern processing was introduced by the RACE II project TSUNAMI [28], [27], using an enhanced inverse filter  $\tilde{F}(\omega_\phi) = \tilde{W}(\omega_\phi) \cdot \tilde{A}^*(\omega_\phi) / (|\tilde{A}(\omega_\phi)|^2 + \alpha \cdot \text{NRS}(\omega_\phi))$ .  $\text{NSR}(\omega_\phi) = \tilde{N}(\omega_\phi) / \tilde{E}(\omega_\phi)$  is the noise to signal ratio,  $\tilde{W}(\omega_\phi)$  is a reshaping window and  $\alpha$  is a scalar  $< 1$ , chosen to under estimate the noise [29]

### *Angular correlations*

The angular autocorrelation properties are of interest as they represent angle diversity correlation properties, leaning themselves to adaptive beam operations like for example jitter diversity [30]. We have [26]

$$S_{m12}(\omega_\varphi) = \tilde{m}_1(\omega_\varphi) \cdot \tilde{m}_2^*(\omega_\varphi) = S_{e12}(\omega_\varphi) \cdot S_{a12}^*(-\omega_\varphi) \quad (3.2)$$

Also from the correlation theorem we have

$$R_{m12}(\varphi) = \oint_{\phi} m_1(\phi) \cdot m_2^*(\phi - \varphi) d\phi = F^{-1}[S_{m12}(\omega_\varphi)] = R_{e12}(\varphi) \otimes R_{a12}^*(\varphi) \quad (3.3)$$

Thus the angular correlation function is described by a convolution between the individual correlation functions of the environment and antenna [26]. This correlation expression is general with respect to orientation angle and This correlation is different from those derived for the temporal or spatial fading responses caused by a moving MS [31]. Those type of correlations are orientation specific and thus relevant to the fixed beam operations discussed in section 3.4 to 3.6. Wide sense stationarity (WSS) has been assumed for the previously mentioned angular correlations. Note that this may be more difficult to satisfy for angular than for spatial fading, in particular if the environment is very selective, i.e. it has a narrow beamwidth distribution.

### *Angular diversity coherence measures.*

The complex auto correlation coefficient function is  $\rho(\bullet) = R(\bullet)/R(0)$ , due to the previous US assumption. In case of pure angle diversity we can define an angular coherence beamwidth  $ABW_{0.7} = \varphi|_{|\rho(\varphi)|^2=0.7}$  [26]. This beamwidth is the coherence measure of the angular fading experienced by a BS antenna sweeping in the angular domain. It is also possible to define pattern and space coherence measures for the angular fading [26].

### *Quantitative angular spreading parameters*

First and second order moments of the mean power response have been proposed [26] for a statistical description of the small scale angular environment mean direction and spreading. An angle of a defined Centre of gravity can be used as an unambiguous estimate of the mean angle [27].

A transform of the angular mean power pattern from a circular to a linear representation (power angular profile PAP [26]), provides analogy to the power delay profile (PDP) in the temporal domain. Similar dispersion parameter definitions can be applied to the PAP, as those commonly used for the PDP [32]. The angular spread  $S_\varphi$  follows from [33] as the standard deviation of the PAP, analogue to the delay spread on the PDP. Similar to the delay spread properties, variance subtraction can be used

to suppress the influence of the antenna on the measurement  $S_{E_\varphi}^2 = S_{M_\varphi}^2 - S_{A_\varphi}^2$  [26]. The only difference compared to the delay spread case, comes in a sign change concerning the mean angle relation,  $\overline{\varphi}_E = \overline{\varphi}_M + \overline{\varphi}_A$ . A requirement to apply these properties to the PAP, is that the environment pattern is well confined around the mean angle.

A parameter reflecting the large scale angular spreading of the environment is the effective sidelobe level [27].

#### *Antenna gain*

The effective BS antenna gain saturates when increasing the directivity [30]. Namely when the antenna becomes more selective than the environment. Then the increased directivity is counter-balanced by less received environment power, due to spatial filtering.

### 3.2.2 Environmental influence on perceived antenna pattern

#### *Pattern distortions by nearfield disturbances*

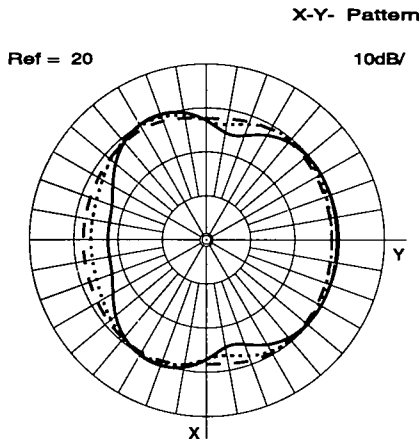


**Fig. 3.12** Pattern influence of a mast placed 30 cm behind 8-element collinear array [34]. Mast diameter very small (dashed), 5cm (dotted) and 10 cm (solid).

where cell splitting is extensively used to gain capacity. Small-cell antenna systems are often placed on roof tops without the clearance found at mast mount macro cell sites.

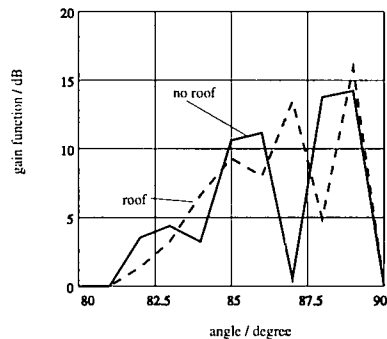


**Fig. 3.13** Elevation pattern influence of roof 3m below antenna (detail near the main lobe) [34]. Roof (dashed) and no roof (solid).

Antenna mountings and other objects in the near field cause pattern distortions. This becomes particularly important

Using the method of moments (MoM) [34] has performed simulations of an 900 MHz collinear array BS antenna subject to nearfield disturbances. The findings are that the azimuthal pattern is distorted less than 2 dB if the antenna mast distance is 1m for a 10 cm thick mast. For a spacing of 30 cm the mast influence is noticeable as seen in Fig. 3.12. Pattern distortion of the mounting rods are found negligible. For a typical small cell antenna at 30 m height above ground, there can be around 10 dB pattern difference whether placed on a 27 m roof or on a free standing mast. This is particularly the case for the main beam area which is also the most critical in determining cell boundaries, see Fig. 3.13. The building influence is indifferent to the exact material parameters, (difference < 3dB):

However the effect found on the BS antennas, stresses the importance of not uncritically applying free space patterns to network planning tools, especially for small cell applications.

#### *Experimental description of sharp gradient pattern shaped antennas*

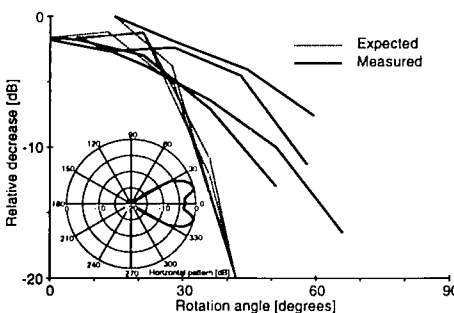


**Fig. 3.14** Expected and measured relative angular level decrease for azimuthal shaped antenna pattern [36].

urements rotating the shaped antenna in 15° steps,), see Fig. 3.14.

From the previous subsection, we have that the perceived pattern is a correlation between antenna and environment. Thus it seems that the azimuthal environment spreading is so wide that the shaping details are 'blurred' by the environment, whereas the spreading in elevation is so compact that the effect of the elevation shaped antenna is still noticeable. This can be explained with the relative low angle of incidence in the elevation plane, where any scattering area around the MS will be perceived strongly compressed in elevation, whereas the azimuthal extension is more dependant on the MS to BS range.

Beam tilting and shaping can be used to enhance cell border definition. Free space properties of a sharp gradient shaped elevation pattern antenna, have proven efficient in small cell urban environments [31]. Shaping of sharp azimuth gradients at the cell edges should ideally provide a more even illumination of a sector and decrease spillover between sectors [35], [36]. However in the azimuthal case the free space shaping is not reflected in an similarly perceived pattern in a small-cell urban environment [36] (900 MHz mea-

### *Experimental description of narrow beamwidth antennas*

Directional BS experiments at 1.8 GHz have been reported by [27],[28], performed under TSUNAMI. A dual branch wideband sounder has been used together with a 1.9 m dual polarised patch array at the BS. Test were performed with range lengths up 2.5 km. One test used a fixed MS and a rotating BS beam. In this case the small scale angular antenna response was recorded (see Fig. 3.15.) It is seen how the received energy is scattered both in delay and angle and thus makes it difficult to associate a main beam direction between MS and BS.

Main conclusion of these tests are, that when comparing main beam responses of highly directional antennas to omnidirectional antennas:

- Delay spread reduction about a factor two or more
- Increase in polarisation purity (XPD) by a few dB

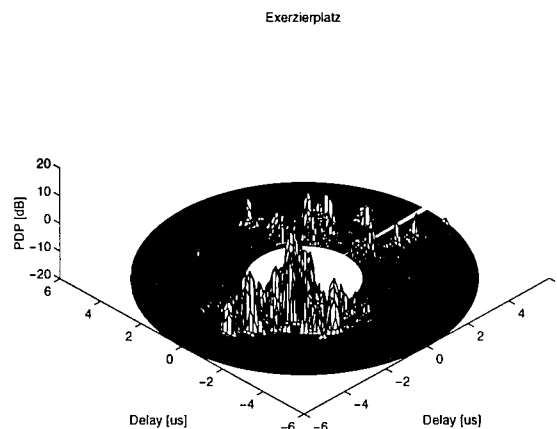


**Fig. 3.15** Angular scattering function at a BS, i.e. PDP versus angle.

environment spreading function), which results in

- Reduction of perceived antenna sidelobe suppression to about 10 dB in urban small cell environments, (20 dB in open rural areas)

The absolute environment XPD figures (around 6dB urban and 12dB rural) sets limits to the worthwhile XPD to target in design of dual polarisation antenna systems.

A second test used a fixed BS beam and a MS driving through boresight, thus revealing the large scale perceived BS antenna pattern. The most important information gained from this test is the distortion of the free space antenna pattern (correlation with the envi-

These findings are also supported by urban microcell measurements on a DECT testbed by [37] and shown in Fig. 3.16. The shoulders of the measured antenna response

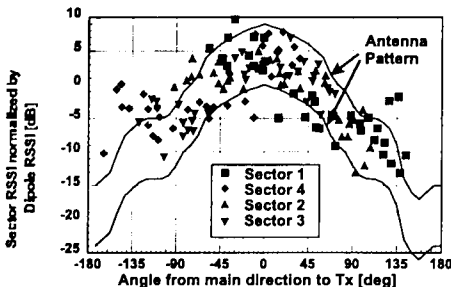


**Fig. 3.16** Measured RSSI for sector antennas normalised by measured RSSI for omnidirectional dipoles [37].

environment, will not give any return in terms of gain in system performance.

### 3.2.3 Adaptive base station antenna arrays

#### *Hardware adaptive antenna testbeds*

A real-time hardware adaptive antenna testbed, based on a DECT radio interface and digital baseband beamforming, is developed by TSUNAMI [38]. The antenna array consists of 8 dual polarised wideband patch antennas[39].

#### *Algorithms*

The algorithms used in the TSUNAMI tests can be grouped into:

- Beam oriented (SDMA, grid of beams, beam jitter)
- Signal combination (selection, maximum ratio etc. diversity)

The first group deals with beam approaches and leans it self to spatial tracking of a MS and possible providing nulls in directions of interferers. These techniques can be applied both on up- and down-link as they mostly rely on mean direction to the MS which is fairly slowly varying. Contrary, the signal combinations approaches which rely on complex weights optimisation on small scale channel variations (optimum combining etc.), only seem feasible in up-link applications, even in TDD systems [40].

The TSUNAMI testbed provided early demonstrations of real-time SDMA-like operation (two users supported, that occupy same frequency and time slot) using MUSIC in LOS environments (note that in time dispersive environments this algorithm will have strong difficulties) [41].

are about -10 dB whereas the free space pattern (solid line) drops below -15 dB when over 90° from bore-sight. This degradation in effective sidelobe level has importance for SDMA capacity calculations as the environments set a limit to the spatial interference suppression one can expect from an antenna in a traditional beam oriented operation. On the other hand the same limit eases sidelobe suppression requirements of the antenna beam design itself. Bettering the free space sidelobe suppression below that supported by the environment, will not give any return in terms of gain in system performance.

Furthermore the testbed also showed real-time functionality of newer type antenna diversity, namely angular domain jitter diversity [30],[42].

Using 3D UTD simulation of indoor propagation environments (7m x 200m x 160m total) [43], the angular distribution and dependence of PDP's is predicted. This used in a 10-20Mb/s 1.8 GHz adaptive antenna system simulation, using a circular array and direct matrix inversion (DMI) as adaptation scheme. Conclusion are that 8 elements are needed to bring BER's below  $10^{-3}$  and that BER's rise to about  $10^{-2}$  when decreasing array diameters from 2 to  $0.5\lambda$ .

High resolution algorithms like 2D ESPRIT can estimate azimuth and elevation concurrently [44]. In a strongly elevation dispersive environment (as for example indoors), failing to estimate elevation can cause errors up to 40° in the azimuthal estimate [44]. This will though hardly be a problem for outdoor macro cell base station situations.

For beam oriented approaches, a few guidelines can be set when designing the antenna aperture

- Size: for beam jittering, so possible 3 dB array beamwidth is less than minimum expected 3 dB beamwidth of the environment [30]. For beam gridding or SDMA operation, the array beamwidth can be much larger, depending on the number of users to support within a sector.
- Number of elements: enough when a sidelobe level suppression better than about 20 dB (open rural terrain) or about 10 dB (urban environment) can be reached [28].

For signal combination approaches, the requirement on element spacing is port decorrelation (see section 3.6) and the number of elements depends on the number of interferers to suppress [40].

### **3.3 Antennas for portables**

**Gert F. Pedersen, CPK, Denmark**

Most antennas for portables today are external wire antennas, typically half-wave dipoles but also quarter waves and partly helical types in order to make them smaller and better matched. The half-wave dipole antenna is a good candidate for portables in respect of antenna performance, but there are practical problems with external antennas and most work in COST231 has therefore been on internal antennas.

For the design of integrated antennas there are two main goals. One is to obtain high antenna performance due to the limited power available, the other goal is to reduce the absorption in the human head. These goals are not necessarily mutually exclusive, which has been demonstrated by an antenna design in [45].

#### **3.3.1 Antenna performance**

An integrated antenna with high performance is characterised by large bandwidth and low volume. The polarisation of the antenna is also important due to the cross

polarisation arising from different environments. It is preferable if the antenna design is unaffected by a change in the physical dimension of the handset, whereby reuse of the antenna is possible.

To fulfil this the current must be concentrated near the antenna and not distributed throughout the entire handset. Also the physical location of the antenna is important. If it is placed very near to parts of the human body high losses will result. A quarter wave monopole on top of the handset will give large antenna currents distributed all over the handset, because the handset and antenna act as an asymmetrical dipole. This results in relative high antenna currents placed just under the plastic cover a few millimetres from the users head/hand, and high losses follows.

In a frequency division duplex system, the bandwidth of an antenna needs only to cover the up and down link band and not the guard band, in order to keep the volume low [45]. The relative bandwidth requirements for GSM/DCS-1800/NMT900 changes from 7.6% to 5.4%. It is important to design a good average match for the handset used in speaking position and in standby, see Fig. 3.17

Low volume to bandwidth ratio is important when considering internal antennas and

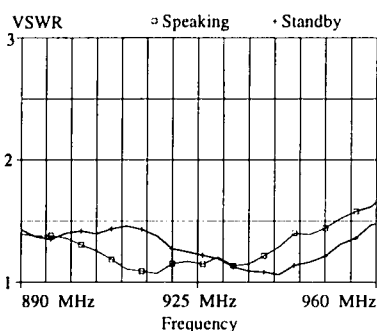


**Fig. 3.17** The VSWR as a function of frequency for the FS-PIFA both for the handset used in speaking position and in standby [45].

the Radiation Coupled Dual-L Antenna is a good example of an integrated antenna with high bandwidth to volume ratio [18].

The performance of an integrated antenna should be found by comparing it to other antennas using the conditions where the antennas are used. Most present handportables for GSM/NMT900 use a half wavelength whip antenna. It is therefore used as reference antenna in measurements of average received power from a BS using the handsets in normal speaking position [45]. These measurements have been carried out in natural user environments. From the field test average received power is calculated and the results are tabulated for three types of environment.

Measurement	Environment	Dipole	FS-PIFA
Average received power	Indoor	0dB (-85.58dBm)	-1.85dB
	Around buildings	0dB (-76.10dBm)	-2.2dB
	Inside moving car	0dB (-69.45dBm)	-2.77dB

**Table 3.1** Average received power obtained from measurements. The figures in brackets are average received power in dBm, the other figures are average received power relative to the dipole in dB.

In all measurements, the handset is used as the receiver, and a fixed GSM- channel (BCCH, channel 94 at 953.8MHz) from a BS is used as “transmitter”. Although the instantaneous power changes, the average power remains constant, as no power control is employed at the base station for this channel. The results of the gain measurements are shown in Table 3.1.

About 4 million samples were taken. Due to the absorption, losses in the plastic casing (2 mm thick) and shadowing, the integrated antenna has about 2 dB smaller gain than the dipole. The smallest gain difference is inside the buildings. One explanation is the more omnidirectional distribution of effective scatterers inside a building, making the average gain somewhat independent of the radiation pattern and the polarisation

### 3.3.2 Antenna configurations for reducing body loss

To obtain low absorption, all antenna current should be located as far as possible from the user's head/hand. This means controlling the current so that nearly all current is concentrated very close to/in the antenna, and placing the antenna as far from the users head/hand as possible, i.e. on the back of the handset. The radiation will then be away from the users head and not omnidirectional [46]. An omnidirectional antenna on a handset in normal speaking position, will anyway result in relatively higher radiation directed away from the users head due to losses. The size of the antenna must also be large to get a uniform current distribution over the antenna. Hereby no high current point, as the source point of a dipole, will arise.

Thus the possibility of a high SAR (specific absorption ratio) is avoided even when the handset is used in an abnormal position. Whereas it is rather easy to predict where the user will place the handset relative to the head, it can be difficult to predict where the user will place the hand. The above goal forms the new design criteria together with the fact that the antenna must be quite large but not occupy a large volume [45]. The latter, in order to control the current in a way so that the antenna can radiate by it self and minimise the coupling to the casing.

When the antenna has to be large the possibility that the user grips around or touches the antenna arises. But with careful design of the handset itself, so the user grips naturally elsewhere, this problem can be solved at 900 MHz and as frequency increases it becomes less difficult.

Present standards for handheld antennas are not only concerned about total average absorption, but also about the maximum local SAR averaged over 1g or 10g tissue. The highest SAR value measured for the FS-PIFA when the handset is used in different speaking positions is 0.19 mW/cm<sup>3</sup> averaged over 1g of tissue and 0.12 mW/cm<sup>3</sup> averaged over 10g of tissue. These figures are about 10 times lower than both the ANSI standard (1.67 mW/cm<sup>3</sup> averaged over 1g) and the German standard (2.0 mW/cm<sup>3</sup> averaged over 10g), whereas the same figures for different present-days handportable investigated by [47] all violate the criteria when used in worst case.

The FS-PIFA has demonstrated that it is possible to produce an integrated antenna with a sufficiently good match over the GSM duplex bands. The effective gain is about 2 dB less than a  $\lambda/2$  dipole, but the local absorption rate about ten times smaller than required from standards and found in existing portable antennas.

Comparing with earlier results on quarter wave monopoles on handsets [48], it is apparent from Figure 3.18 and 3.19 that the influence of the head is much smaller for

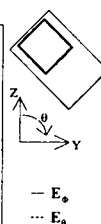
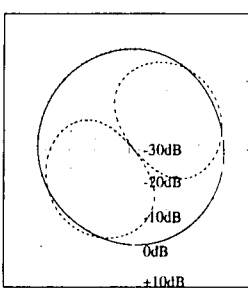
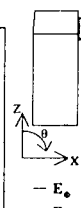
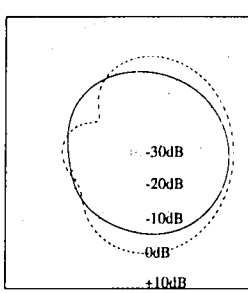
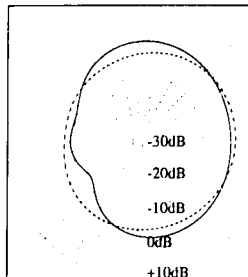


**Fig. 3.18** The radiation pattern for the handset *without* a model of the human head and hand. The handset is tilted 45°, as in "normal" speaking position a) XY-plane b) XZ-plane c) YZ-plane

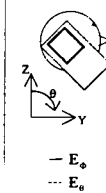
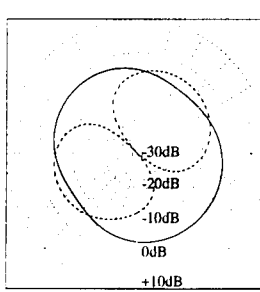
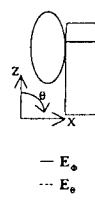
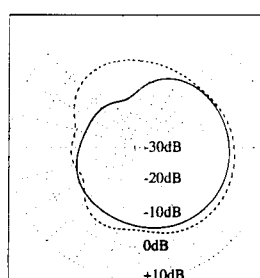
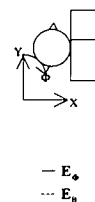
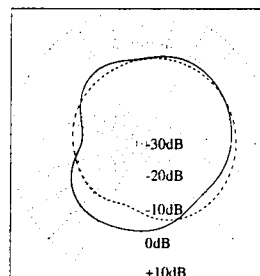


**Fig. 3.19** The radiation pattern for the handset *with* a model of the human head and hand. The handset is tilted 45°, as YZ-in "normal" speaking position a) XY-plane b) XZ-plane c) plane

the integrated antenna with reduced radiation towards the head. The integrated antenna tends to radiate more upwards and downwards. This may explain some of the relative lower effective gain. However this may be the price to pay for an integrated antenna with low local absorption.

### 3.4 Mobile and base station diversity techniques

**Silvia Ruiz Bouqe, UPC, Spain**

The local fluctuation of the signal strength, the fading, caused by propagation along multiple paths and shadowing objects between a base station an a portable unit makes it necessary to have a margin when designing the radio link budget in a system with high reliability.

This margin can be lowered by use of diversity, i.e. transmitting or receiving replicas of the information signal over decorrelated channel conditions. Diversity relies on the principle of repair by use of redundant information (several ‘copies’ of the information signal) and can thus enhance link quality or allow same quality over poorer channel conditions.

As will be seen later in section 3.5 and 3.6 the effectiveness of a diversity system depends on decorrelation of the diversity branch channel conditions. For most cases the fading envelope of radio signal is used as a measure of channel impairment. Traditionally it thus falls natural to use the envelope correlation coefficient ( $\rho$ ) between branch output fading signals, as figure of merit for the diversity system. For analogue systems or digital systems employing interleaving,  $\rho \approx 0.7$  is normally regarded as sufficient for worthwhile deployment of a diversity scheme. This section will focus on the construction of antenna system structures and their ability to decorrelate branch fading signals.

In experiments, care must be taken to assure proper quality of recorded signals on which correlation coefficients are calculated . It can be shown that the envelope correlation coefficients of Rayleigh fading signals subject to additive Gaussian noise, degrades as a second order function of the signal- to noise ratio (SNR) [49]

$$L(SNR) = \frac{\rho_{12,fading+noise}}{\rho_{12,fading}} = \frac{SNR^2}{SNR^2 + 2 \cdot SNR + 1}; \quad SNR = \frac{P(Fading)}{P(Noise)} \quad (3.4)$$

I.e. the SNR must be larger than about 20 dB for the correlation estimate to be within 2% of it's noise free value.

#### 3.4.1 Diversity domains

To achieve replicas of the information channel over decorrelated channel conditions, some discrimination or separation in one or more channel domains is needed. The art of establishing a diversity system lies in the way we can obtain and maybe combine domain separations, that lead to a desired channel state decorrelation.

The mobile radio channel domains which can be used for diversity separation purposes are:

- Space (space diversity, displacement of antenna centres)
- Antenna pattern (pattern diversity and field component)
- Antenna orientation angle (angle diversity, orientation angle)
- Polarisation (polarisation diversity)
- Temporal/frequency (delay-tap or frequency diversity)

where the first 4 domains normally are thought of as antenna diversity domains, the latter is normally system specific (i.e. through use of equaliser, interleaving, frequency hopping etc.). However decorrelation through separation in the 'antenna domains' will often also lead to decorrelation in the temporal domain.

Normally the correlation between two polarisations undergone scattering in a mobile channel, is considered virtually zero. The determining factor for a polarisation set-up is the power imbalance expressed in terms of the cross-polarisation-discrimination (XPD).

There are a few further general distinctions to be made regarding antenna diversity, that is:

- MS or BS environment
- up-link or downlink power budget
- Macro or micro scenario

The situation for the base station is different from the mobile case since the angular spread of the incoming waves is much smaller, see section 3.2. This leads to a choice of different possibilities of antenna positioning on the mast, including the use of polarisation diversity. Therefore, while the single branch radio channel link is reciprocal, the application of the combined multi branch radio link is not. Thus an antenna diversity structure will not yield the same performance (branch decorrelation) when placed at the MS or BS end of the link.

The significantly better down-link-budget for a mobile system (2W for MS and 15-20 W in BS for GSM system), makes it most advantageous to reduce the multipath fading margin on up-link by implementing base-station antenna diversity. While most diversity action is associated with short term fading (micro diversity), macroscopic diversity (i.e. having more than one base station within each cell) operates on the local mean shadow fading.

Two branches are often considered as a practical number of branches, as any further number of branches only supply little additional diversity gain.

### 3.4.2 Base station antenna diversity for outdoor environments.

#### *Space Diversity for urban macrocells*

The required spacing at the base station, is different for separation in the horizontal and vertical planes, due to the different angular spreading experienced, see section 3.2.

For **horizontal spacing** the separation depends on the angle between the line joining the antennas and the line joining the base station and the mobile (around  $20\lambda$  when the angle is  $90^\circ$  and  $80\lambda$  when the angle is  $0^\circ$ ) [50]. Both distances increase with the antenna height and decrease with the presence of local scatterers. If **vertical spacing** is considered the required separation is around  $15\lambda$  but it depends on the scattering of the area in which the mobile is located [33]. In general lower correlation coefficients can be obtained with horizontal separation than with vertical separation [51].

In [52] two different horizontal separation (0.6 and 1.4 m) have been considered with antennas at the top of buildings (10 m high). When the distance between diversity antennas is 0.6 more than half of the measured points has a correlation coefficient higher than 0.9 obtaining a poor diversity configuration. When the distance increases to 1.4 m the correlation properties improve significantly but there are still several locations with a strong cross correlation.

#### *Angle diversity for microcells*

In [53] planar-antennas from Huber&Suhner with a gain of 7.5 dBi and 3 dB beam-widths of  $80^\circ$  and  $50^\circ$  for the horizontal and vertical plane respectively were used. In one site four planar antennas were used to cover an angle of  $180^\circ$  with some overlap of the antenna patterns. In other site two pairs of directional antennas were pointing in opposite directions of the street. Horizontal spacing between antennas was arbitrary chosen to 0.4 m. For comparison both sites were also measured using dipole antennas spaced horizontally by 0.2 m. in a two branch selection diversity scheme.

Large differences in received signal for the four angular antenna sectors (received power level 5 to 15 dB lower than the power in the strongest sector) indicates that a significant improvement in CIR can be achieved by using directional antennas and time dispersion will also be reduced.

#### *Polarisation diversity*

There are few studies reported in literature about polarisation diversity. This is due to the difference in mean received power between co-polarised and cross-polarised branches when one polarisation is transmitted (cross-polarisation discrimination XPD), which is traduced in a reduction of the diversity gain. Results shown that the XPD is typically between 6-20 dB and that it is much higher in rural or sub-urban than in urban environments and it is also higher in outdoor than in indoor environ-

ments. Also the XPD increases in LOS and decreases with distance. The envelope correlation coefficient is usually higher than the value obtained when considering space diversity. Having uncorrelated polarisation's, a XPD of 10 dB corresponds to an equal branch power (space diversity) system with a  $\rho = 0.7$  [54].

Hand-holds with poor antenna polarisation purity and random orientation, will couple energy between polarisations and thus decrease the XPD. This will even further benefit polarisation diversity applications.

#### *Combined Polarisation & Space diversity in urban small and microcells*

In [55] the possibility of using polarisation together with space de-correlation at the base station is tested. Transmitter antenna is a quarter-wavelength monopole mounted on the metal roof of a car. A dual branch receiver with two identical planar array directional antennas with an azimuth and elevation 3 dB beamwidth of 60° were used. The antennas have a gain of 8 dBi and a XPD better than 30 dB. Different antenna highs (3 or 30 m above rooftops) and different antenna configurations (horizontal separation between 10-20  $\lambda$ , vertical separation, different antenna inclination) were tested. In a previous work of the same authors it was found that for large cells (10-20 km cell radius) and working at 900 MHz the XPD was in the range around 4 dB and 12 dB for urban and suburban areas respectively. For small cells and microcells the urban XPD is between 7-9 dB.

The effectiveness of compact (less than 10  $\lambda$  antenna separation) antenna configuration for urban small a microcell is shown. All configuration provide envelope cross-correlation about 0.7 or less. The individual space and polarisation effects in a combined system are independent and multiplicative [55]. Thus the combined system correlation coefficient can be expressed as

$$\rho_{combined} = \rho_{space} \cdot \rho_{polarization}(\alpha, \Gamma)$$

$$\rho_{polarization}(\alpha, \Gamma) = \frac{\Gamma + \frac{1}{\Gamma} - 2}{\Gamma + \frac{1}{\Gamma} + \frac{1}{\tan^2(\alpha)} + \tan^2(\alpha)} \quad (3.5)$$

where  $\alpha$  is the inclination angle of the antenna element with respect to the copolarisation and  $\Gamma$  is the XPD.

#### *Combination of Space and Temporal diversity for downlink operation*

There is still a low-cost possibility of reducing the multipath fading margin on the down-link by transmitting a delayed signal on a second antenna branch (uncorrelated though space diversity) in order to introduce more channel time dispersion and thus reduce the coherence bandwidth (pre-Rake transmitter). The delay is in the order of a few bit periods relative to the first branch [56]. The resulting reduction in fading

margin can be about 3-10 dB on down-link (as the GSM equaliser is better exploited) [56].

### 3.4.3 Base station diversity for indoor environments

Space diversity can also be used in a radio system to reduce the impact of sever fading within buildings. A path separation of few wavelengths is referred to as microscopic diversity (MIC), while a separation equivalent to the distance between the bases in a normal cellular configuration is called macroscopic diversity (MAC). When the separation is between 1 and 10 m intended to be used at one base station is called medium diversity (MED). Of course the system complexity is much lower with the MIC and MED schemes, since the selections can be made at each base station.

#### *Microscopic space diversity*

In [57] a space diversity technique is implemented with two quarter-wavelength monopole antennas separated a distance between  $0.25\lambda$  and  $3.5\lambda$  and a selection technique. Many measures in LOS and NLOS at 1.6 GHz were done showing that the signal at both antennas is uncorrelated (the correlation coefficient was always lower than 0.7). When de distance is equal or greater than a wavelength the correlation coefficient was always lower than 0.2.

#### *Macroscopic space diversity*

In [58] a MAC technique has been tested for indoor environments with two base station transmitters (transmitting a CW at 1700 and 1701 MHz respectively) and a mobile receiver. The distance between BS was between 50 and 120 m and LOS and NLOS cases were studied. Measures were made in the worst case, when the field strength is weakest and the receiver is equidistant from the BS. Measurements show that the signals coming from the two BS were uncorrelated (correlation coefficient lower than 0.2).

#### *Combination of macroscopic and microscopic space diversity*

If MAC is combined with MIC, then the MAC only has to reduce the long fading component and in this case the gain will not decrease so rapidly when the selection intervals are made longer. If only the long fading is considered, the minimum time between change of base stations can be as long as 0.1 s without reducing the gain of the macroscopic diversity too much (with a speed of 2m/s in an indoor environment and working at 1700 MHz band).

*Comparison between macroscopic and microscopic space diversity*

Cell-Size	Environment	$\Delta s(\lambda)$	$\rho$	COST231 TD
Pico-Cell	Indoor	0.5	0.34	(90)094
		0.75	0.32	"
		2.5	0.25	(93)014
		2.5	0.23	(93)027
	Out&Indoor	6	0.25*	(93)008
		7	0.12	(93)014
	Indoor			
Micro-Cell	Outdoor	4	0.83	(95)019
		6.5	0.18	(92)120
		8	0.54	(95)019
		9	0.48	"
		10	0.12	(92)120
Small-Cell	Outdoor	10	0.34	(92)120

**Table 3.2** Cross-correlation  $\rho$ , versus antenna separation  $\Delta s$  (\* 10 MHz BW). Last column is the corresponding COST231 document number.

In [59] measurements to test the performance of macro, medium and micro space diversity have been performed, obtaining reduction in fading margin or its equivalent the diversity gain considering the total fading (long and short term). Table 3.2 shows a summary of measured micro diversity envelope cross-correlation coefficient versus antenna separation for different cell size and different propagation environments.

#### *Polarisation diversity*

As the previously mentioned techniques, the polarisation diversity is only effective in suppressing fast fading if the signals received (co-polarised and cross-polarised) are uncorrelated.

In [60] validation of polarisation diversity technique under different conditions (LOS and NLOS) by means of the evaluation of the correlation coefficient between received signals was done. In all the measurements the correlation coefficient was lower than 0.6

#### **3.4.4 Mobile antenna diversity**

[61] considers angle at the mobile unit. The antenna consists of four corner reflectors fed by monopoles and was positioned on the roof of a van. Also an omnidirectional vertical dipole was used as a reference antenna positioned above the corner reflector antenna. The experiments show that this antenna is effective in removing deeper nulls.

### 3.4.5 Wideband Correlation

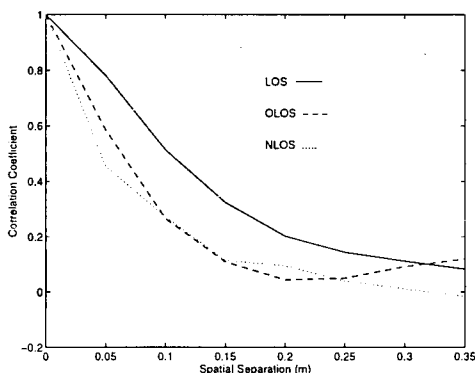


**Fig. 3.20** Average autocorrelation of the instantaneous rms delay spread versus separation in indoor environments at 1800 MHz [67].

In indoor environments the diversity improvement, related to the decrease of rms delay spread, was estimated to almost 30% by means of polarisation diversity [66].

In a wideband channel the autocorrelation of the instantaneous rms delay spread gives the spatial separation necessary to achieve significant diversity improvement. This is shown in Fig 3.20 [67] after measuring in indoor LOS, OLOS and NLOS environments. It can be seen that a separation of  $2\lambda$  gives uncorrelated delay spread values in all the investigated indoor scenarios. These results are in agreement with measurements using antenna diversity in a DECT system in indoor pico-cells[68].

## 3.5 Combining Techniques

**Peter Karlsson, Telia, Sweden**

Diversity combining techniques fall in two major groups

- Selection (switching, scanning, selection)
- Summation (equal gain, maximum ratio, optimum combining)

The first group is characterised by that only one branch signal yields active output at a time. Contrary the schemes in the second group apply weights to all the branch signals and the output signal is formed as a sum of all the branch signals. Each of the techniques is a trade-off between performance and complexity. The first group techniques apply to simple compact low-cost solution implementation, whereas the latter group techniques have better performance but require more hardware. There is a further distinction in the level of implementation

The correlation of the instantaneous rms delay spread between diversity branches gives an estimate of the ability to reduce the effects of time dispersion. It has been shown for pico-cells that a spatial separation of  $2.5\lambda$  introduces uncorrelated instantaneous delay spread values between the branches [62]. In a NLOS microcell environment the correlation of delay spread values was estimated to 0.4 [63],[65], achieving a reduction of 20% in the delay spread selecting the smallest instantaneous value of each branch. For these experiments a novel downlink base station diversity measurement technique was employed [64],[63].

- Pre-detection (RF or IF implementation)
- In-detection (equalisers, soft-detection MLSE etc.)
- Post-detection (baseband implementation)

The in-detection implementation is system specific whereas both pre- and post-detection combiners can be used in general. Post-detection requires multiple receiver branches. Pre-detection provides higher gain due to coherent summation possibilities.

It is necessary to establish the combining strategy on the appropriate criteria for a given radio system. These criteria are typically

- Carrier to noise ratio C/N (narrowband systems)
- Signal to interference ratio C/I (high capacity systems)
- Irreducible BER due to ISI (digital radio system) [62], [68].

The two first criteria are aimed for maximisation in the combining process whereas the latter is aimed for minimisation.

### 3.5.1 Gain and complexity for different combining techniques

The switched diversity combining technique offers the lowest complexity, since only one receiver is used, while switching between antenna branches. The switch diversity is mostly a pre-detection combining technique and the switching algorithm is based on a threshold level, causing the receiver to switch from one antenna to the other if the signal is below the threshold. When wideband digital radio modems are considered, it is better to base the switching algorithm on a BER threshold or a combination of BER and RSSI. Examples of combiner performance have been made using data from wideband measurements at 1800 MHz with a terminal speed of 1 m/s in micro- and pico-cell environments [69]. Analysis of the switch combiner in a DECT type of receiver shows only a marginal improvement over a single branch [70].

When true selective combining (SC) is used, the best signal of the branches is selected. This post-detection requires one receiver pr. diversity branch. In [68] a hybrid selection/switch combining technique was presented, where the RSSI selection was based on two RF-receiver parts. However, the demodulation can be performed in a single baseband receiver after fast switching between the branches. In a digital radio system it is possible to use the preamble of each frame in order to measure or monitor the RSSI level. By means of this technique it is possible to emulate the performance of selection diversity based on the RSSI level using only one [71].

Further improvement of the diversity performance can be obtained if equal-gain combining (EGC) or maximal-ratio combining (MRC) is used. By weighting the signals from the antennas according to the maximal-ratio technique, the SNR is in theory 3 dB better relative to selective combining when two independent branches are used. The combining according to SC and MRC using data measured in two

branches separated  $2.5 \lambda$ , show that the diversity improvement follows the theoretical results [72].

Equal-gain combining is not so complex to implement as MRC, since the weights are omitted. A coherent equal gain combiner is then referred to as a pre-detection scheme. As a result the diversity gain is only 1 dB lower than if MRC is used, but the EGC technique is still better than selective combining in narrowband and time-invariant channels. In a wideband system like DECT, with a frequency selective and time-variant channel, the selective combiner gives better performance than EGC [70].

### 3.5.2 Influence of the time-variant channel

The coherence time  $\Delta t_c$  of the channel determines the lower limit of the combining rate. When selection or switching combining technique is used, the best branch has to be determined at a rate higher than the channel variations in order not to deteriorate the diversity performance. Accordingly, when MRC or EGC is used the rate of the weight and/or phase adjustments must be higher than the channel variations.

In the frequency domain the channel variations are given by the Doppler spread  $B_d$ , which can be approximated with the maximum Doppler shift  $f_d$ . Thus, the radio channel is highly time-variant if the surrounding environment and/or the terminal is moving fast in relation to the carrier wave-length. An example of the diversity gain versus the combining rate for different schemes is shown in Fig. 3.21. The narrowband result is based on measurements at 1700 MHz in indoor environments [73] and the wideband results are based on simulations of switch and selection combining in a DECT system presented in [71]. Note that the combining rate  $r_c$  of the wideband characteristics in this example is an approximate estimation of the rate of the DECT system. Nevertheless, in relation to the channel variations, i.e. normalised to

the Doppler shift  $f_d$ , it is possible to make comparisons between different systems and combining techniques. The normalised combining rate  $v_{cr} = r_c / f_d$  is then equivalent to the number of possible combining adjustments per wave-length. The comparison in Fig. 3.21 indicate that the combining rate must be at least 3 times the Doppler shift when SC is used. The rate of switching combining must be up to 10 times the Doppler shift in order to take advantage of the decorrelated diversity branches.

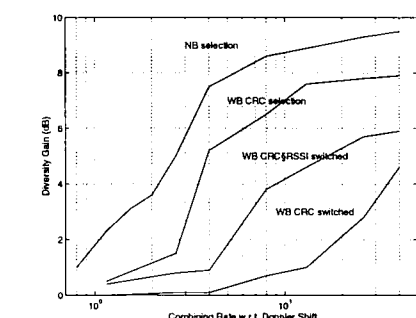


**Fig. 3.21** Diversity gain for a narrowband system with RSSI selection and for a wideband system with switch or selection combining based on RSSI and/or CRC as a function of the normalised combining rate  $v_{cr}$ .

In a system where the long-term fading is mitigated by macro diver-

sity the combining rate can be approximately one order of magnitude lower than if the short-term fading is to be reduced [73]. The spatial auto-correlation of the long-term fading component determines the necessary combining rate for different terminal speeds, in agreement with the rate for the short-term channel variations presented in Fig. 3.21.

## 3.6 Macro and Micro Diversity Gain

**Peter Karlsson, Telia, Sweden**

The probability of insufficient transmission quality over a radio channel, can be reduced by means of diversity techniques. Antenna diversity is one of the possible techniques to compensate both for the short term fading and for the long term fading and, hence, the link reliability is increased. The diversity performance is related to the decorrelation between two or more separate antennas, which are used at the mobile terminal and/or at the base stations. In the narrowband case, i.e. when frequency-flat fading is considered, the diversity gain  $G_D$  expresses the possible reduction of a given fading margin  $M$ . A wireless cellular system must have an area coverage of 99% to give the same reliability as the fixed network. Thus, the fading margin must be large enough to support the required service reliability. In many typical situations the short term fading is almost Rayleigh distributed, while the long term fading is log-normal distributed with a standard deviation  $\sigma$  of up to 10 dB. If antenna diversity with two uncorrelated branches is used in such a scenario, the 99% level fading margin  $M_{99}$  can be reduced by 10 dB considering the short-term fading when selection combining is used. Accordingly it is possible to reduce the long-term fading margin  $M_{99}$  by 10 dB in this scenario using selection combining. In the wideband case, i.e. when the fading is frequency-selective, it is also possible to reduce the effects of time dispersion by means of antenna diversity. Here, the separation between the antennas must be large enough to be able to give decorrelated power delay profiles. Thus, the diversity performance is better when the power and the time delays of the multipaths at each antenna are different.

### 3.6.1 Macro Diversity

The macroscopic diversity scheme can improve the link quality by combining the signals between the mobile or portable terminal and two or more base stations. Then the effects of the long-term fading, which is mainly caused by shadowing objects, e.g. buildings and hills in macro-cells, large vehicles and trees in micro-cells and walls and furniture in pico-cells, are reduced. In this macro diversity scenario the spatial separation  $\Delta s$  corresponds to the cell sizes, which is equivalent to the distance between the base station sites. It is obvious that macro diversity has the strongest impact on the cell boundaries, where the local mean from at least two base stations are almost the same. Thus, at the boundaries it is possible to reduce the long-term fading

margin by an appropriate combining of signals with low correlation. For outdoor macro-cells we can assume that the envelope of the long-term fading components are uncorrelated, since the propagation paths between the mobile and the base stations are totally different. An analysis of the correlation between the long-term fading at two base stations in a microcellular environment was made in [63]. The result verifies the assumption of uncorrelated long-term fading and the average power level by selecting the best branch increases. However, the measurements show that the macro diversity gain is only significant in areas where the mean levels of the attenuation between the mobile terminal and the base stations are similar. Furthermore, in some micro-cellular environments (antennas below roof-tops) the long-term fading can be partially correlated if the same shadowing object appears in both propagation paths.

Level (dB)	$\Delta s=9-17\lambda$			$\Delta s>=350\lambda$		
Environment	M99	M99	G <sub>D</sub>	M99	M99	G <sub>D</sub>
LOS	13.8	7.5	6.3	19.6	10.4	9.2
OLOS	9.2	6.0	3.2	10.2	5.5	4.7
NLOS	9.0	7.2	1.8	11.1	8.9	2.2

**Table 3.3** Fading margins and diversity gain of the long-term fading using two antenna separations in indoor environments.

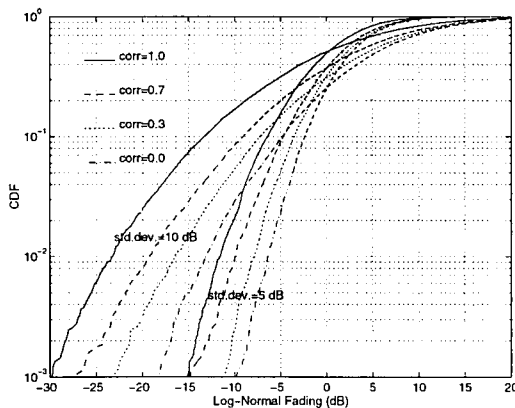


**Fig. 3.22** Cumulative distribution of the log-normal long-term fading, with standard deviations 5 and 10 dB. A selection diversity scheme with the correlation coefficients 0, 0.4, 0.7 and 1 has been used.

the range 40 m to 100 m, which corresponds to a typical base station separation. Measurements in similar environments but using the antenna separation  $17\lambda$  in LOS and  $9\lambda$  in NLOS are also included for a comparison. The correlation is

To be able to fulfil a given area coverage reliability the long-term fading margin can be reduced relative to the variations and the spatial correlation of the radio links. In theory it is possible to reduce the long-term fading margin by 10 dB if two uncorrelated branches with selection combining are used and the standard deviation of the fading is 10 dB. Of course, the gain increases with lower correlation and larger variations. Measurements at 1700 MHz in indoor environments using simultaneously sampling of the narrowband power at two receivers have been made [73]. The receiver separation was in

approximately 0.3 for the larger separation and 0.7 for shorter separation. The results concerning the possible reduction of the long-term fading are shown in Table 3.3.

The simulated macro diversity gain for two branches and selection combining are given in Table 3.4, where the 99% area coverage reliability level has been used. Note that the standard deviation of the log-normal distributed long-term fading and the spatial correlation coefficients are used as parameters. These simulated results agree closely with the diversity gain estimated from measurements in indoor environments [73]. As an example, the cumulative distribution of the log-normal fading of a single branch and when selective combining between two branches is used, are shown in Fig. 3.22.

The log-normal fading has a standard deviation of 5 and 10 dB in this example and the correlation between the branches is 0, 0.4, 0.7. Note that the distribution of a single branch is equivalent to the distribution of a diversity scheme with the correlation coefficient 1.0.

Level (dB)	$\rho=1.0$	$\rho = 0.0$		$\rho = 0.4$		$\rho = 0.7$	
$\sigma$ (dB)	M99	M99	$G_D$	M99	$G_D$	M99	$G_D$
5	11.7	9.8	4.6	10.2	3.0	12.3	1.6
8	18.6	10.2	8.5	10.7	5.4	12.2	2.8
10	23.3	13.3	10.0	6.5	6.9	6.9	4.1

**Table 3.4** Macrodiversity fading margin M99 and gain  $G_D$  for the log-normal fading component with standard deviation 5, 8 and 10 dB for three correlation levels between two branches.

### 3.6.2 Micro Diversity

The short-term power fluctuations around the local mean, i.e. when the long-term fading component is removed, can be mitigated by two antennas co-located at the same mobile terminal or base station. In this case the effects of the short-term fading can be reduced if the envelopes are uncorrelated. If the scattered waves arrive at the two antennas from all directions, a horizontal separation  $\Delta s$  of approximately  $\lambda/2$  gives a correlation coefficient of less than 0.2. This is in general the case in indoor environments and at mobile terminals in outdoor environments, where local scatterers give a uniform distribution of incoming waves. At base stations on roof tops a larger separation is necessary to combat the fading from the otherwise correlated signals [74]. Micro diversity implemented at base stations show a significant gain when two antennas are used, while it is difficult to obtain low correlation between three or more branches [25].

Level (dB)	No Div.	$\Delta s=9-17\lambda$		$\Delta s=2.5\lambda$	
		M99	G <sub>D</sub>	M99	G <sub>D</sub>
Environment	M99	M99	G <sub>D</sub>	M99	G <sub>D</sub>
LOS	12.5	4.7	7.8	5.8	6.7
OLOS	16.7	7.6	9.1	8.3	8.4
NLOS	17.4	8.8	8.6	9.2	8.2

**Table 3.5** Estimated fading margins and diversity gain by selection of strongest signal measured in two separate branches.

Measurements have been made at 1700 MHz in different propagation environments in order to quantify the correlation between the envelopes at two separated antennas and the corresponding diversity gain. The envelope correlation estimated from measurements of the narrowband signals at two antennas separated by  $2.5\lambda$  was 0.3, 0.2 and 0.3 in LOS, OLOS and NLOS indoor environments respectively [73]. The corresponding diversity gain using selection combining was estimated to 6.5, 8.3 and 8.6 dB in these LOS, OLOS and NLOS propagation scenarios. The experimental estimation of the diversity gain was also made using the horizontal antenna separation  $17\lambda$  in LOS and OLOS, while  $9\lambda$  was used in NLOS. The correlation coefficients were estimated to 0.0, 0.1 and 0.3 respectively and the corresponding diversity gain based on selection of the sampled values are presented in Table 3.5.

To be able to achieve uncorrelated branches at short antenna separations, it is efficient to use polarisation diversity. However, the diversity gain decreases if the mean levels of the branches are different ( $XPD < 0$  dB). This is specially the case in LOS. Measurements with one co-polarised and one cross-polarised antenna have been made both in LOS and NLOS indoor environments [66]. The diversity gain, related to the 99% reliability level, by using selection between the two branches was 6.3 dB. Hence, there is no significant reduction of the diversity gain due to different mean levels.

The theoretical diversity gain reaches 10 dB with selective combining in a Rayleigh fading environment, if the branches are uncorrelated. However, the gain is lower in a Ricean fading environment, since the probability of deep fades is less than in the Rayleigh fading case. In practice all the variations will be smoothed out by means of the spatial diversity and the instantaneous SNR is improved, which reduces the BER. Simulations of the Ricean distributed short fading amplitude in two different branches have been made to evaluate the diversity gain versus correlation. The simulated diversity gain for a Ricean fading channel with K-factors in the range from 0 to 4 are presented in Table 3.6. The gain corresponds to a scheme where instantaneous selection combining is assumed, i.e. selection at each sample point is allowed. Note that the channel is Rayleigh fading when  $K=0$ , which is the worst case of the short-term fading component. The channel is almost Rayleigh fading in typical NLOS environments, and here the Ricean parameter  $K=0$  or  $K=1$ . In OLOS environments typical average values for K is in the range 2-3, while the average K-factor in LOS environments is equal to 3 or 4.

The simulated diversity performance, considering the necessary fading margin for the 99%-level  $M_{99}$  and the corresponding diversity gain  $G_D$ , agree with the results from measurements presented above. The diversity gain is approximately 6 dB in LOS, 7 dB in OLOS and 9 dB in NLOS environments when the envelope correlation  $\rho = 0.3$ . This is a typical correlation level in practical antenna configurations, but the gain is still high when the branch correlation  $\rho = 0.7$ , see Table 3.6.

Level (dB)	$\rho=1.0$		$\rho=0.0$		$\rho=0.3$		$\rho=0.7$	
	K-factor	$M_{99}$	$M_{99}$	$G_D$	$M_{99}$	$G_D$	$M_{99}$	$G_D$
0		19.6	9.8	9.8	10.2	9.4	12.3	7.3
1		19.1	10.2	8.8	10.7	8.3	12.2	6.8
2		16.6	8.4	8.2	8.7	7.9	9.9	6.7
3		14.2	6.2	8.0	6.5	7.7	7.6	6.6
4		11.8	6.0	5.8	6.5	5.3	6.9	4.9

**Table 3.6** Simulated levels of fading margins and the corresponding diversity gain versus envelope correlation for the short-term fading with five different Ricean K-factors. Note that  $\rho=1.0$  is equivalent to the performance without diversity.

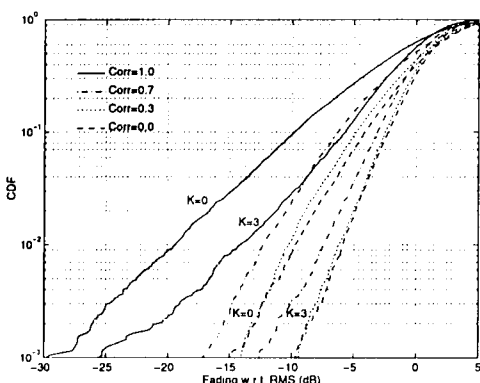


**Fig. 3.23** Cumulative distribution of the short-term fading using two-branch selection diversity with the correlation coefficients 0, 0.3, 0.7 and 1. Note that  $\rho_{env}=1$  is equivalent to the CDF without diversity, i.e. a single branch.

short-term fading is considered [67]. In pico-cells a separation of 2-3 m between the antennas give partially decorrelated branches, i.e.  $\rho \approx 0.7$ , and the total diversity gain

The simulated cumulative distributions of the short term fading when  $K=0$  and  $K=3$  are shown in Fig. 3.23. The CDF's using instantaneous selection combining between the branches with different correlation levels, are also shown. The simulated results of diversity performance agree with the experimental gain found in typical Ricean channels [73].

It is also possible to reduce the long-term fading margin with micro diversity in environments where the spatial auto-correlation of this component is "short". Hence, if the antenna separation exceeds the size of the shadowing objects, e.g. furniture, stairs and people, the diversity gain of the total fading is larger than if only

is then given by the reduction both of the long-term and short-term fading components.

### 3.6.3 Wideband Diversity Performance

If the channel is frequency selective within the given system bandwidth the problem with ISI can also be reduced by means of antenna diversity. In this case the correlation of the instantaneous rms delay spread between the diversity branches gives an estimate of the possibility to reduce the effects of time dispersion. Of course, the diversity gain increases when the time dispersion in the separate branches gets more uncorrelated.

The correlation of the delay spread values of two separate branches measured in NLOS micro-cell environments was estimated to 0.4 [63]. A 20 % reduction of the delay spread was then achieved by selection of the smallest instantaneous value of each branch. The time dispersion effects can also be reduced by means of antenna polarisation diversity, which was shown in [66]. The diversity improvement, related to the decrease of rms delay spread, was estimated to almost 30 % using the data from these measurements in indoor environments [66]. The spatial diversity makes it possible to increase the coverage area of a cell for a given system quality, since the delay spread in general increases with the cell sizes. In a system like DECT the maximum delay spread for a BER of  $10^{-3}$  can be increased from 90 ns to approximately 200 ns, when selection diversity is used [75].

## 3.7 References

- [1] E. Zollinger, *Properties of Indoor Radio Channels* (in German : *Eigenschaften von Funkübertragungsstrecken in Gebäuden*). Ph.D. ETH No. 10064, Zürich: Swiss Federal Institute of Technology Zürich, Switzerland, Nov. 1993.
- [2] A. Heilman, *Antennas I* (in German : *Antennen I*). Mannheim: Bibliographisches Institut, Hochschultaschenbücher-Verlag, 1970.
- [3] H. Meinke and F. W. Gundlach, *High-Frequency Engineering Handbook* (in German : *Taschenbuch der Hochfrequenztechnik*). Berlin: Springer, 4<sup>th</sup> ed., 1986.
- [4] R. C. Johnson and H. Jasik, *Antenna Engineering Handbook*. New York: McGraw-Hill, 2<sup>nd</sup> ed., 1984.
- [5] A. S. Duchene and J. R. A. Lakev, "The IRPA guidelines on protection against non-ionizing radiation", in *The Collected Publication of the IRPA*, chapter 5, New York: Pergamon Press, 1991, pp. 72-82.
- [6] Y.J. Guo, A. Paez, R.A. Sadeghzadeh, and S.K. Barton, "A patch antenna for HIPERLAN", to appear in *Wireless Personal Communications*, Special Issue on HIPERLAN.
- [7] Y. S. Wu and F. J. Rosenbaum, "Mode chart for microstrip ring resonators", *IEEE Trans. Microwave Theory Techn.*, vol. 21, no. 7, July 1973, pp. 487-489.
- [8] R. G. Vaughan, "Two port higher mode circular microstrip antennas", *IEEE Trans. Antennas Propagat.*, vol. 36, no. 3, March 1988, pp. 309-321.
- [9] L. C. Shen, S. A. Long, M. R. Allerding, and M. D. Walton, "Resonant frequency of a circular disc printed-circuit antenna", *IEEE Trans. Antennas Propagat.*, vol. 25, no. 5, July 1977, pp. 595-596.

- [10] P. F. M. Smulders, *Broadband Wireless LANs: A Feasibility Study*. Ph.D., Eindhoven: Technical University Eindhoven, CIP-Data Koninklijke Bibliotheek, Den Haag.
- [11] K. Uenakada and K. Yasunaga, "Horizontally polarized biconical horn antenna excited by  $TE_{11}$  mode in circular waveguide", *Trans. IECE*, vol. 54-B, Dec. 1971, pp. 125-126.
- [12] W. L. Stutzman and G. A. Thiele, *Antenna Theory and Design*. New York: John Wiley & Sons, 1981.
- [13] F. Schwering and A. A. Oliner, "Millimeter-Wave Antennas", *Antenna Handbook*. New York: Van Nostrand Reinhold Company Inc., 1988, pp. 7-1 to 7-150.
- [14] C. A. Fernandes, P. O. Francês, and A. M. Barbosa, "A dielectric lens antenna for the MBS demonstrator", RACE 2067, *RACE Mobile Telecommun. Workshop*, Amsterdam, vol. 2, May 1994, pp. 733-740.
- [15] C. A. Fernandes, P. O. Francês, and A. M. Barbosa, "Dielectric lens antenna for a mobile application at millimeterwaves", in *Proc. 17<sup>th</sup> ESA Antenna Workshop*, Noordwijk, Holland, July 1994.
- [16] C. A. Fernandes, P. O. Francês, and A. M. Barbosa, "Shaped coverage of elongated cells at millimeterwaves using a dielectric lens antenna", in *Proc. 25<sup>th</sup> Europ. Microwave Conf.*, Bologna (IT), Sept. 1995, pp. 66-70.
- [17] T. Tage and K. Tsunekawa, "A built-in antenna for 800 MHz portable radio units", in *Proc. Int. Symp. Antennas Propagat.*, Japan, Aug. 1985.
- [18] S. Seki, N. Kamimura, and A. Sasaki, "Detachable unit service in 800 MHz band cellular radiotelephone system", *IEEE Commun. Mag.*, vol. 24, no. 2, Feb. 1986, pp. 47-52.
- [19] J. Rasinger, A. L. Scholtz, W. Pichler, and E. Bonek, "A new enhanced-bandwidth internal antenna for portable communication systems", in *Proc. 40<sup>th</sup> IEEE Veh. Techn. Conf.*, VTC'90, Orlando (FL), May 6-9, 1990, pp. 7-12.
- [20] J. Rasinger, E. Bonek, K. Laukkonen, V. Santomaa, and A. L. Scholtz, "The important role of internal antennas in new personal communications", *ITU Technical Symposium, Integration, Interoperation and Interconnection: The Way to Global Services*, part 2, vol. II, Oct. 10-15, 1991, pp. 195-199.
- [21] T. Tage and K. Tsunekawa, "Performance analysis of a built-in planar inverted-F antenna for 800 MHz band portable radio units", *IEEE J. Select. Areas Commun.*, vol. 5, no. 5, June 1987, pp. 921-929.
- [22] R.H. Clarke, "A statistical Theory of Mobile-Radio Reception", *Bell Syst. Techn. J.*, 1968, pp. 957-1000.
- [23] T. Aulin, "A modified model for the fading signal at a mobile radio channel", *IEEE Trans. on Veh. Techn.*, Vol. VT-28, No. 3, 1979, pp.182-203.
- [24] A.M.D. Turkmani, J.P. Parsons, "Characterisation of mobile radio signals : base station crosscorrelation", *IEE proc.*, Vol. 138, No. 6, Dec. 1991, pp. 557-565.
- [25] W.C. Jakes (editor), *Microwave Mobile Communications*, IEEE Press classic reissue, USA 1993.
- [26] P.C.F. Eggers, "Quantitative Descriptions of Radio Environment Spreading relevant to Adaptive Antenna Arrays", *EPMCC'95 conf. proc.*, Bologna Italy, 28-30 Nov. 1995, pp.68-73
- [27] P.C.F. Eggers, "Angular Dispersive Mobile Radio Environments sensed by highly Directive Base Station Antennas", *IEEE PIMRC'95 conf. proc.*, Toronto Canada, September 1995, pp.522-526
- [28] P.C.F. Eggers, G.F. Pedersen, K. Olesen, "Multi sensor propagation", RACE II *TSUNAMI deliverable R2108/AUC/WP3.I/DS/I/046/b1*, D.3.1.1, August 1994.

- [29] A.J. Levy, J.-P. Rossi, J.-P. Barbot and J. Martin, "An improved sounding technique applied to wideband mobile 900 MHz propagation measurements", *IEEE VTC'90 conf. proc.*, May 6-9 1990, Orlando FL USA, pp. 513-519.
- [30] O. Nørklit, P.C.F. Eggers, J. Bach Andersen, "Jitter Diversity in Multipath Environments", *45th IEEE VTC conf. proc.*, Chicago, USA, July 25-28 1995, pp. 853-857.
- [31] R.W. Lorenz, "Comparison of the digital mobile radio systems in Europe (GSM) and in Japan (JDC) with special attention on the business aspects" (in German : "Vergleich der digitalen Mobilfunksysteme in Europa (GSM) und in Japan (JDC) unter besonderer Berücksichtigung der Wirtschaftlichkeitsaspekte"), *Der Fernmelde Ingenieur*, Verlag für Wissenschaft und Leben Georg Heidecker GmbH Erlangen, heft 1,2 Januar/Februar 1993.
- [32] J-P. deWeck, J. Ruprecht "Real-Time ML estimation of very frequency selective multipath channels", *IEEE Global Telecom. Conf. proc.*, San Diego, USA, 1990, pp.2045-2050.
- [33] F. Adachi, M.T.Feeney, A.G.Willianson, J.D.Parsons, "Crosscorrelation between the envelopes of 900mhz signals received at a mobile radio base station site", *IEE Proc., Pt. F*, Vol. 133, No. 6, Oct. 1986, pp.506-512.
- [34] A.F. Molisch, J. Fuhl, and E. Bonek, "Pattern distortion of mobile radio base station antennas by antenna masts and roofs", *Proc. 25th Europ. Microwave Conf.*, Bologna Italy, 1995, pp. 71-76.
- [35] H. Hollmann, "Base Station Antennas for Sector-Shaped Service Areas in Mobile Radio Communications", *Proc. of Int. Symp. on Antennas and EM theory*, URSI/CIE, 1985, pp. 712-717.
- [36] R. Rathgeber, F.M. Landstorfer, R.W. Lorenz, "Extension of the DBP field strength prediction programme to cellular mobile radio", *proc. of ICAP 91*, York UK, 15-18 April 1991, pp.164-167.
- [37] P.E. Mogensen, S. Petersen, "Antenna configuration measurements for DECT micro cells", *IEEE/ICCC proc. PIMRC'94/WCN*, The Hague, 1994, pp. 1075-1080.
- [38] T. Bull, M. Barret, R. Arnott, "Technology in Smart Antennas for Universal Advanced Mobile Infrastructure (TSUNAMI R2108) Overview", *RACE Mobile Telecom. Summit proc.*, Cascais Portugal, Nov. 22-24 1995, pp. 88-97.
- [39] Q.Garcia, F. Muncio, "Broadband Base station Arrays and Antenna Elements for Mobile Communications", *EPMCC'95 conf. proc.*, Bologna Italy, 28-30 Nov. 1995, pp.56-61
- [40] J. Wigard, P.E. Mogensen, F. Fredriksen, O. Nørklit, "Evaluation of Optimum Diversity Combining in DECT", *IEEE PIMRC'95 conf. proc.*, Toronto Canada, September 1995, pp.507-511
- [41] TSUNAMI, "Seminar and demonstration of adaptive antennas", *notes Center for PersonKommunikation*, Aalborg University, Denmark, 18th January 1996.
- [42] O. Nørklit, "Jitter Diversity Measurements", *COST231 TD(96) 21*, Belfort, France, 24-26 Jan. 1996.
- [43] R. Passerini, M. Frullone, M. Missiroli, G. Riva, "Performance of Adaptive Antenna Arrays for Wideband Indoor Communications", *Proc. of IEEE VTC'96*, Atlanta USA, 28 April - 1 May, 1996.
- [44] J. Fuhl, J-P. Rossi, E. Bonek, "Characterization of the Urban Mobile Radio Channel by 2D Direction-Of-Arrival Estimation", *COST231 TD(96) 12*, Belfort, France, 24-26 Jan. 1996.
- [45] G.F. Pedersen, J. Bach Andersen, "Integrated Antennas for Hand-held Telephones with Low Absorption", *44th IEEE VTC proc.*, Stockholm Sweden, June 8-10 1994, pp. 1537-1541

- [46] J. Fuhl, P. Nowak, E. Bonek, "Improved internal antenna for hand-help terminals", *Electronics Letters* 30 , 1994, pp.1816-1818.
- [47] N. Kuster, T. Schmid, K. Meier, "Investigations of the absorbtion in the extreme near field of transmitters" (in German : "Untersuchungen der Absorption im extremen Nahfeld von Sendern"), *ETH Zurich*, : Swiss Federal Institute of Technology Zürich, Switzerland 1993.
- [48] J. Toftgård, S.N. Hornsleth, J. Bach Andersen, "Effect on Portable Antennas by the Presence of a Person.", *IEEE Trans. Antennas and Propagation* ,vol. 41, No. 6, June 1993, pp. 739-746
- [49] P.C.F. Eggers, "Envelope Correlation Coefficients of Rayleigh fading signals corrupted by additive gaussian noise", *COST231 TD(96)02*, Belfort France 24-26 Jan. 1996. A further development is found in P.C.F. Eggers, "Diversity evaluation based on Correlation properties of Rician/Rayleigh fading signals subject to additive Gaussian noise", proc. *IEEE PIMRC'97*, Helsinki Finland, sept. 1997, pp.1064-1068.
- [50] W.C.Y.Lee "Effects of correlation between two mobile radio base station antennas" *IEEE Trans.Commun.* vol. COM-21, no.11, Nov. 1973, pp.1214-1224.
- [51] A.M.D.Turkmani, A.A.Arowojolu, P.A.Jefford and C.J.Kellett "An experimental evaluation of the performance of two-branch space and polarization diversity schemes at 1800 Mhz", *IEEE Trans. Vehic. Techn.* Vol.44, no.2, May 1995, pp. 318-326.
- [52] P.E. Mogensen, F. Fredriksen, C. Verholt, CPK Aalborg University, Denmark, "Antenna diversity measurements for fixed RLL", *COST231 TD(95)019*, Bern Switzerland, Jan. 1995.
- [53] P.E Mogensen, S Petersen, "Antenna configuration measurements for DECT micro-cells", *proc. PIMRC'94/WCN*, The Hague the Netherlands, sept. 21-23 1994, pp. 1075-1080.
- [54] R.G. Vaughan, "Polarization diversity in mobile communications", *IEEE trans. on Vech. Techn.*, Vol. 39, No. 3, Aug. 1990, pp. 177-186.
- [55] P.C.F. Eggers, J. Toftgård, A.M. Oprea, "Antenna Systems for Base Station Diversity in Urban Small and Micro Cells", *IEEE J-SAC*, Vol. 11, No.7, September 1993, pp.1046-1057.
- [56] P.E. Mogensen, "GSM Base-Station Antenna Diversity Using Soft Decision Combining on Up-link and Delayed-Signal Transmission on Down-link", proc. *IEEE VTC'93*, Secaucus NJ USA, May 18-20, pp. 611-616.
- [57] S. Ruiz-Boque, A. Baldovinos & R. Agusti, "Fading and Diversity Measurements Inside Buildings", *COST231 TD(90)094*
- [58] P. Karlsson, "Investigation of Radio Propagation and Macroscopic Diversity in Indoor Microcells at 1700 Mhz", *COST231 TD(90)052*.
- [59] P. Karlsson, "Body Effects and Diversity Performance in Indoor Radio Channels at 1700 Mhz", *COST231 TD(93)014*
- [60] S. Ruiz-Boque, "Polarization Diversity for Indoor Mobile Communications", *COST231 TD(93)7*
- [61] A. Koivumaki, "Direction Diversity Measurements at 900 Mhz", *COST231 TD(91)035*
- [62] G. Kadel, Simulation of the DECT system using wideband channel data measured in two diversity branches, *Proc. of 2nd ICUPC*, Ottawa, Canada, 1993.
- [63] G. Kadel, Measurement of wideband micro- and macro-diversity characteristics of the mobile radio channel, *IEEE Proc. of VTC'94*, Stockholm Sweden, June 8-10 1994, pp.165-169.

- [64] R.W. Lorenz, G. Kadel, "Diversity measurement technique for wideband mobile radio", proc. GLOBECOM, Houston USA, 1993, pp. 1237-41
- [65] M. Grigat, G. Kadel, "Wideband micro- and macrodiversity characteristics of the mobile radio channel," RACE Mobile Telecom. Workshop, Amsterdam Netherlands, May 1994, pp. 688-692
- [66] P.E. Mogensen, Wideband Polarization diversity measurements for wireless personal communications, *Proc. of Nordic Radio Symposium NRS'92*, Aalborg Denmark, June 1-4 1992, pp. 49-53.
- [67] P. Karlsson, "Indoor Radio Propagation for Personal Communications Services", *LUTEDX/TETE-1011/1-132(1995)*, Ph.D. Thesis, Lund University, Mar. 1995.
- [68] P.E. Mogensen and S. Petersen, Practical Considerations of Using Antenna Diversity in DECT, *IEEE Proc. of VTC'94*, Stockholm Sweden, June 8-10 1994, pp.1532-1536.
- [69] P.C.F. Eggers, J. Toftgård, "Assessment of Base Station Antenna Diversity Efficiency in Frequency Selective  $\mu$ - and pico-cell Environments", *Proc. of IEEE VTC'93.*, Secaucus NJ., USA 1993, pp.572-576.
- [70] P.C.F. Eggers, P.E. Mogensen, "Evaluation of Low Effort Dispersion-Reduction Techniques for DECT in Telepoint Environments", *Proc. of IEEE VTC94*, Stockholm, Sweden, 1994, pp.677-680
- [71] P.E. Mogensen et al., "Evaluation of an Advanced Receiver Concept for DECT", *IEEE Proc. of VTC'95*, Chicago, U.S.A., July 25-28, 1995, pp. 514-519.
- [72] G. Kadel and R.W. Lorenz, "Impact of the radio channel on the performance of digital mobile communications", *IEEE Proc. of PIMRC'95*, Toronto, Canada, Sept. 27-29, 1995, pp. 419-423.
- [73] P. Karlsson, "Measuring and Modelling of the Indoor Radio Channel at 1700 MHz", *LUTEDX/TETE-7062/1-101(1992)*, Lund University, Aug. 1992.
- [74] W.C.Y. Lee, *Mobile Communications Design Fundamentals*, John Wiley & Sons Inc., New York, 1993.
- [75] L. Lopes, "An Overview of DECT Radio Link Research in COST 231", *IEEE Proc. of PIMRC'94*, The Hague, The Netherlands, Sept. 18-22, 1994, pp. 99-104.

## Propagation Prediction Models

Dieter J. Cichon <sup>1</sup>, IBP PIETZSCH GmbH, Germany

Thomas Kürner <sup>1</sup>, E-Plus Mobilfunk GmbH, Germany

### 4.1 General Considerations

To implement a mobile radio system, wave propagation models are necessary to determine propagation characteristics for any arbitrary installation. The predictions are required for a proper coverage planning, the determination of multipath effects as well as for interference and cell calculations, which are the basis for the high-level network planning process. In a GSM/DCS-system the high-level network planning process includes, e.g., frequency assignment and the determination of the BSS (base station subsystem) parameter set. Similar planning tasks will exist also in third generation systems. The environments where these systems are intended to be installed, are stretching from in-house areas up to large rural areas. Hence wave propagation prediction methods are required covering the whole range of macro-, micro- and pico-cells including indoor scenarios and situations in special environments like tunnels and along railways. The phenomena which influence radio wave propagation can generally be described by four basic mechanisms: Reflection, penetration, diffraction, and scattering. For the practical prediction of propagation in a real environment these mechanisms must be described by approximations. This requires a three-stage modelling process: In the first step the real (analogue) terrain has to be digitised yielding digital terrain data. Therefore some interest in the COST 231 project has focused on the types, resolution and accuracy of digital terrain databases required for propagation modelling. The information includes terrain height information, land usage data, building shape and height information and building surface characteristics. Furthermore investigations have

---

<sup>1</sup> Formerly with University of Karlsruhe, IHE, Germany

been stressed on proper processing techniques to extract the relevant information in a time-efficient manner. These topics are described in Sec. 4.2. The second modelling step includes the definition of mathematical approximations for the physical propagation mechanisms. Therefore Sec. 4.3 treats basic problems as e. g. the diffraction around a non-perfectly conducting wedge, simulating a street corner and the modelling of propagation over roof-tops. Based on the solutions for the basic problems both deterministic and empirical approaches have been developed within COST 231 for the various environments, which is the third modelling step. In the different environments distinctions of the models are required both in terms of the dominant physical phenomena and the specification of the digital terrain data. In Sec. 4.4, 4.5, 4.7 and 4.8 all models dedicated for the same environment and cell type are treated in separate sections. Sec. 4.6 deals with building penetration models, which are applicable to all cell types. As the definition of cell types is not unique in the literature, the cell type definition used in this chapter is explained more detailed.

cell type	typical cell radius	typical position of base station antenna
macro-cell (large cell)	1km to 30 km	outdoor; mounted above medium roof-top level, heights of all surrounding buildings are below base station antenna height
small macro-cell	0.5 km to 3 km	outdoor; mounted above medium roof-top level, heights of some surrounding buildings are above base station antenna height
micro-cell	up to 1 km	outdoor; mounted below medium roof top level
pico-cell / in-house	up to 500 m	indoor or outdoor (mounted below roof-top level)

Tab. 4.1.1 Definition of cell types.

In "large cells" and small cells" the base station antenna is installed above roof-tops. In this case the path loss is determined mainly by diffraction and scattering at roof-tops in the vicinity of the mobile, i. e. the main rays propagate above the roof tops. In "micro-cells" the base station antennas are mounted generally below roof tops. Wave propagation is determined by diffraction and scattering around buildings, i. e., the main rays propagate in street canyons somehow like in grooved waveguides. "Pico-cells" are applied to cover mainly indoor or very small outdoor areas. In any case the base station antenna of a pico-cell is mounted inside a building or fairly below roof-top level in outdoors. The summary of the different cell types is shown in Tab. 4.1.1.

## 4.2 Geographical Information for Propagation Modelling and Simulation

Peter J. Cullen , University of Dublin, Trinity College, Ireland

The practice of the determination of radio channel characteristics in cellular UHF land mobile radio applications is dominated by surface scattering considerations. Before any propagation (scattering) computation can be performed, these surfaces must be characterised. In this brief section an outline is given of some of the basic issues relating to the use of geographical information in mobile radio communications from a propagation perspective, drawing exclusively from the experience of COST 231.

The development of propagation prediction techniques for the estimation of channel characteristics is a cyclic, three stage process: the first step is to abstract the simplest surface model which is considered to be likely to yield sufficiently accurate predictions; the second stage is concerned with finding efficient (often approximate or numerical) solutions to the scattering problems thus posed; and the third stage is to verify the choice made in the first stage. In each of these stages one must make use of geographical information.

### 4.2.1 Canonical scattering problems

Before embarking on the review, it is essential to consider the problem to be solved. Ostensibly, the characterisation of the land mobile radio channel in a particular locality is of interest. To achieve this one must tackle the physical problem of the prediction of the scattering of UHF electromagnetic radiation. It is possible to express this problem formally but aside from the obvious computational difficulties involved, it is not possible even in principle, to find exact complete solutions, since the actual scatterer can never be really specified to a sufficiently high degree of accuracy (this is not the case in any general sense for the canonical surfaces described below). Scattering is a non-linear problem, small deviations in the surface do not necessarily lead to small deviations in the fields everywhere, especially the near fields. Fortunately, one is usually not particularly interested in the very near field and, as a consequence, the modelling exercise is carried out as described in the introduction. In the main, the canonical problems that are employed are relatively simple.

*One-dimensional surfaces.*

The most familiar canonical problem in land mobile propagation is the corrugated one-dimensional perfect electrical conducting (PEC) surface. In this case, if the propagation is TMZ or TEZ the electromagnetic problem is a scalar one. Moreover, if the surface is smooth and the angle of incidence low, forward propagation will predominate. This model may be enhanced by considering the surface to be a homogeneous dielectric, further enhancements can be achieved by considering a piece-wise homogeneous dielectric. This kind of canonical model has found very wide acceptance for predicting attenuation of low angle wave propagation over irregular terrain. The primary geometrical entity to be acquired here is the surface height profile. Finite difference [1] and integral equation [2] schemes operate directly on the surface height profile. When a parabolic equation approximation is applied to the Helmholtz equation calculations can be performed using the split step method [3]. When larger steps are used this leads to a method often (inaccurately) associated with absorbing screens. Native ray-tracing approaches represent the surface by an ensemble of canonical shapes (wedges and cylinders) for which diffraction or reflection coefficients exist, in practice this approach must be rather arbitrary. Typically, the corrugated two-dimensional canonical problem is used for propagation modelling over irregular terrain. It may also arise in urban and micro-cell problems, when a two-dimensional (vertical plane) approach is followed. Over terrain, predictions are usually corrected locally through the use of clutter information which is derived from remotely sensed optical data. The height profile (array of heights) associated with this canonical problem is usually derived from the databases during the computation of the fields.

Unconnected one-dimensional surfaces arise when we consider propagation in the horizontal plane. When calculating fields around buildings, where the antenna heights are well below roof-top height and the terrain is flat (simple micro-cell case), it can be sufficient to use multiple paraxial PEC cylinders (by cylinder we mean a two-dimensional entity) to represent the buildings; where the cross-section of the cylinders is the building plan outline. This is the case for example for the most simple two-dimensional micro-cell models. Further enhancements include the use of homogeneous or piece-wise homogeneous (to allow the representation of internal and external structure) dielectric cylinders. The most natural (and increasingly popular) data structure for this type of problem is the vector (polygon) database. Each discrete cylinder is represented by one or more polygons. If appropriate, attributes (percentage of windows for example) may be attached to the faces

of the polygons to facilitate the refinement of propagation models. The vector storage data structure is well suited to ray-tracing, ray-launching and hybrid methods. The polygon structure is also capable of efficiently delivering the geometrical input requirements of other methods for handling this kind of problem including integral equation techniques, transmission line method (TLM), finite difference time domain (FDTD) etc.

### *Two-dimensional surfaces.*

An increasingly important canonical problem of interest is the two-dimensional smooth surface. This surface, like its one-dimensional counterpart, may be assumed to be homogeneous PEC, dielectric or piece-wise homogeneous dielectric. Considering the level of accuracy required in mobile propagation the most appropriate representation here is a triangular regular network (the analogue of piece-wise linear representation used in the one-dimensional case). Increased resolution may be obtained by using a triangular irregular network (TIN), or a multi-scale regular network. An outward normal is generally stored for each facet; other attributes such as roughness measures and land use classifications may be attached directly to the facets.

The most complex two-dimensional surfaces (three-dimensional databases) arise when we have to consider propagation in and around buildings located on irregular terrain. The main differences between this case and the previous one is the abrupt changes in surface height which occur at the location of building walls and in the possibility of inhomogeneity (rooms, windows etc. in buildings). This kind of data may be handled using a TIN structure if homogeneous, or more appropriately, using a vector structure. It is quite popular to consider a hybridisation of regular elevation matrix, (for the terrain) and polygon (for buildings). A fairly typical approach is described in [4], [5].

Networks are not used to characterise scattering surfaces but are important for certain propagation related tasks. Typically networks are used to efficiently locate roads, streets, railway lines etc. Some micro-cell propagation models can predict using this kind of information as a starting point. More importantly, the road networks are important areas in which to guarantee coverage.

#### 4.2.2 Acquisition of geographical data

There is little point in constructing accurate propagation methods if the geographical data which these methods rely upon is not correspondingly accurate. Traditionally, this kind of information has been obtained from paper maps. In the last decade increasing use has been made of high resolution remote sensing (aerial and satellite) for acquisition and of digital storage and distribution methods. The generation of Digital Elevation Models (DEM) and the efficient and accurate extraction of radial data from them is reviewed in [6].

Satellite remotely sensed data may be obtained from optical sources: LandSat (30m resolution), SPOT (10-20m resolution) and synthetic aperture radar (SAR) sources: ERS-1. SPOT and LandSat have been used to derive land use classes for terrain. The methodology of extraction is beyond the scope of this book. The use of SAR in propagation prediction is an open research question.

Micro-cell and indoor propagation modelling possess the heaviest reliance on high resolution geographical information. High resolution (1-2m) databases derived from aerial photography measurements are now being used by a number of organisations, particularly for cities (see also Sec. 4.5). For urban propagation, it is essential to have accurate information at least about the average height of individual buildings, when modelling larger cells or performing interference calculations and when terminals are operating close to roof-top height. It may not be so important in the case of line-of-sight links. The incorporation of information about clutter, particularly vegetation, is very important, since propagation characteristics are quite sensitive to scatterers around terminals.

Aerial stereo photography provides a means of obtaining quite accurate data on the heights and outlines (resolution of the order 1m) of building and terrain features, the location of vegetation etc. A wealth of data can, in principle, be extracted from these sources. However, the extraction of data is quite labour intensive. Sometimes such data is combined with lower resolution regular elevation matrices, in principle (but not always in practice) this should not be necessary (ground height can be accurately determined from aerial photography) this should really be avoided where possible in micro-cell work.

Information about the building cladding, windows, etc. is more difficult to obtain. It appears that accurate geographical information of this nature must

be obtained „on the ground“ as it were (using video cameras to capture data, for example). To date there appear to be few, if any, physical propagation models capable of using this kind of information (there are empirical methods). Wall properties are particularly important for estimating building penetration. For outdoor propagation, in practice we may only need this level of detail around potential BTS sites.

Considering indoor propagation [7] suggests, for the purpose of propagation modelling, that each building element should be categorised into {wall, floor, door, window, furniture,...} and specified by structure (thickness and permittivity) and finally its corner co-ordinates (twelve co-ordinates).

#### 4.2.3 Accuracy of data

Recalling that field estimates *may* be quite sensitive to surface errors, the following observations are recorded. Considering the database for the city of Munich (see Sec. 4.5), it is shown in [8] that the average difference in predictions for over-roof-top propagation estimates using a mean roof-top height and the real roof-top heights is about 4dB. The average was over an area of 2400-3400 m, the database used had a 5 m resolution and the standard deviation of the building heights was 8.56 m and that of the terrain height was 3.87 m. Considering the influence of database information on prediction accuracy it is noted in [9] that prediction errors in micro-cells of up to 15 dB were attributed to database inaccuracies arising from the omission of vegetation data and the poor resolution of terrain height data. Perturbing the scatterers (specifically: wall vector directions) in a micro-cell type problem using a two-dimensional Geometrical Theory of Diffraction (GTD) approach is shown to have a significant effect on the structure of field predictions [10]. These results are indicative of what is expected, average field estimates or field estimates very far away from a multi-scale scatterer are likely to be less sensitive to the smaller scale errors. Whereas the location of an interference null or shadow boundary may manifest a much higher sensitivity.

One rather practical point to be aware of, is that geographical information (aside from resolution limitations) is prone to contain errors. It is always advisable to visually inspect data and carry out any corrections prior to use.

#### 4.2.4 Model evaluation

In the previous section some brief consideration to the effect of database errors in field estimates is given. Probably one of the most important causes

of concern here is the effect of database inaccuracies on model evaluation. Complex models which visually correspond to the measured data often display a large error standard-deviation with respect to empirical models because of spatial offsets (see Sec. 4.5). These offsets can arise if there are small database or measurement location errors. The existence of these offsets between predictions and measurements is not necessarily an indication of a poor model. This problem is typically addressed by separately comparing the locally averaged model prediction and the statistics of the faster variations separately with the measured data.

As the micro-cell work develops and different competing solutions emerge a rigorous and standard approach is needed to compare the different models on the same data. This requires agreed simple procedures for comparing model predictions with measurements and with each other. For example, in relation to the question of the determination of the number of rays required for a ray-optical approach it is useful to consider ways of implementing the null hypothesis test that the addition of an extra ray-path does not explain any more of the data. This must be done in the light of uncertainties in the measurement location and geographical data; this would suggest a more formal probabilistic approach to model evaluation.

#### 4.2.5 Manipulation of geographical data

The reader should be aware that there is a wide range of commercial geographic information systems (GIS) which may be employed to manipulate and process geographical data; for example ARC-INFO [6], and SMALLWORLD [11]. COST 231 has not made a special study of these types of systems and it is beyond the scope of this book to make any comments as to the applicability or suitability of such commercial systems to propagation prediction. Aside from direct application in propagation modelling GIS functionality is clearly essential in preparing data for the construction of a propagation specialised database.

However, it is clear that the organisation and representation of geographical information is crucial to the provision of computationally efficient propagation estimates. Many methods used in mobile radio propagation rely on high frequency approximations and require detailed geometrical computations to be made on a basic data-set describing the environment. One such example is GTD which requires the identification of geometric ray paths. Once one has chosen to use basic GTD, methods for mobile propagation, the computational problem becomes primarily a geometric one. It is pointed out in [12] that hierarchical geometrical structures [13] can be

applied to buildings databases to aid in reducing the complexity of ray-optical approaches. To clarify the point we include the example they gave to illustrate the approach: consider a complex multifaceted building - intersections of a given ray will have to be considered for each of the facets. However, if we encapsulate the building in a simple rectangular polygon oriented parallel to the co-ordinate axes then it is a simple task to determine whether or not a ray enters this box; only if it does, we need to calculate intersections with the building facets. They add that this principle can obviously be applied not only to single buildings but also to clusters of buildings and so on. Another point is that, whilst high resolution building data is becoming increasingly widely available; from a practical point of view, one may wish to remove some of the detail (small recesses, for example) prior to using ray-optical methods, in order to keep complexity to manageable levels. Finer detail is important when one is interested in the near field and this might suggest a combination of full resolution and smoothed database for ray applications.

#### **4.2.6 Exchange of measurement and geographic information**

Radio measurement data formats have been the subject of some discussion in COST 231. Two suggestions which have been formally specified are the RACE [14]format and the universal measurement format (UMF) [15]. It appears that the DXF and regular matrix formats are adequate for the exchange of typical geographical information used by the land mobile radio propagation community.

## 4.3 Propagation Mechanisms

Jean-Frédéric Wagen , Swisscom, Switzerland

### 4.3.1 General

This section describes the radio propagation mechanisms that have been investigated within the COST 231. The propagation mechanisms are examined to help the development of propagation prediction models and to enhance the understanding of electromagnetic wave propagation phenomena involved when dealing with radio transmission in mobile and personal communications environments.

Evidently the radio propagation phenomena are by themselves not new and do not depend on the environment considered. However, considering all existing radio propagation phenomena, the most important one must be identified and investigated to improve the modelling of the mobile radio communication channel or of the prediction of radio coverage and signal quality in radio communication systems. The radio propagation phenomena to be identified as the most important depend on the environment and differ whether we consider flat terrain covered with grass, or brick houses in a suburban area, or buildings in a modern city centre etc. Propagation models are more efficient when only the most dominant phenomena are taken into account. Which radio propagation phenomena need to be taken into account and in how much detail do they need to be considered will also differ whether we are interested in modelling the average signal strength, or a fading statistic, or the delay spread, or any other characteristics.

The mobile radio environment causes some special difficulties to the investigation of propagation phenomena:

- 1) The distances between a base station and a mobile range from some metres to several kilometres,
- 2) man-made structures and natural features have size ranging from smaller to much larger than a wavelength and affect the propagation of radio waves,
- 3) the description of the environment is usually not at our disposal in very much detail.

Roughly two complementary approaches can be identified to deal with these difficulties:

- *Experimental investigations* which are closer to the reality but at the expense of weaker control on the environment, and
- *theoretical investigations* which consider only simplified model of the reality but give an excellent control of the environment.

A brief description of the possibilities, advantages and disadvantages offered by either experimental or theoretical investigations are given below to give some insights on how the propagation phenomena can be determined.

### *Experimental investigations.*

Based on measurements, the propagation mechanisms can be identified if the experiments are thoughtfully designed in a carefully chosen area or/and if numerous measurements are analysed. Several contributions to COST 231 have investigated the propagation phenomena from measurements (e.g., [16]-[18]).

Note that scaled measurements ease the control on the environment to be investigated. However, scaled measurements are scarce since they require special hardware and could be quite difficult to conduct in a worthwhile manner because of the difficulties of retaining just the right amount of complexity in the simplified scaled down model. Only a single contribution dealing with measurements in scaled tunnels has been presented to COST 231 (Section 4.8.5).

The major disadvantage of experimental investigations is the difficulties in the design of the experiments and in the interpretation of the results which usually exhibit a mix of several propagation phenomena.

### *Theoretical investigations.*

Software simulation or analytical studies of propagation phenomena have one main advantage over experimental investigations: The environment and the geometry are more easily described and modified. The major disadvantage of theoretical investigations is that the validity of the results may hold only for the particular case being simulated or investigated. Theoretical investigations should always be validated in practice. The theoretical investigations can be categorised in two approaches (see Fig. 4.3.1 and Fig. 4.3.2):

- 1)      Simulation of wave propagation, and
- 2)      ray theory.

*Simulation of wave propagation.*

Considering Maxwell's equations or the wave-equation and some boundary conditions, the electromagnetic wave propagation mechanisms can be investigated from a pure theoretical point of view and from computations based on so-called full-wave formulations. This approach is conceptually similar to performing actual measurements but the "simulated measurements" have the advantage of providing a much better control over the propagation environments. As with measurements however, extracting the various physical phenomena and their relative contributions from the simulation results requires further analysis.

*Ray theory.*

Some simplifications in solving the wave propagation problems are obtained when assuming a small wavelength which leads to view the radio wave propagation as rays similar to light rays. Under this assumption, the radio wave interacts with the propagation environment, i.e., with the atmosphere, the terrain features, buildings, walls, trees, etc., through absorption, specular reflection, diffraction and scattering. At a larger scale, several rays can be viewed as a single entity and according to this concept, guided propagation has been investigated.

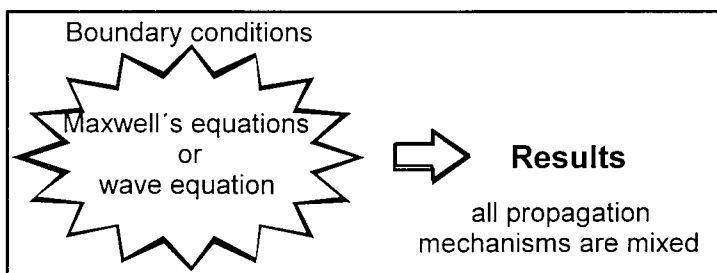


Fig. 4.3.1 Simulation of wave propagation.

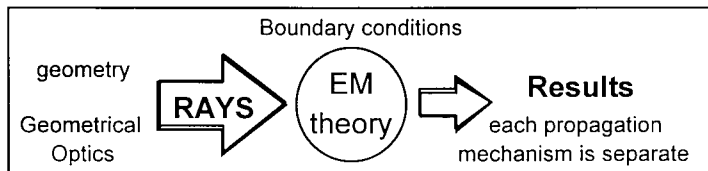


Fig. 4.3.2 Ray theory.

The ray theory approach clearly distinguishes between several propagation phenomena and give to each of them a physical and mathematical description. How clearly the ray theory propagation phenomena exist in practice depends on the frequency, on the environments and on how precisely the prediction and measurement results are analysed.

The next section reviews the propagation mechanisms relevant to the ray theory. To complement the discussion, other propagation mechanisms are mentioned in Sec. 4.3.3. The last Sect. 4.3.4 mentions the propagation mechanisms which appear to be the most important for propagation modelling and prediction in macro-cellular, micro-cellular and indoor environments.

#### 4.3.2 Propagation mechanisms in the ray theory

The main propagation mechanisms defined by the ray theory are explained below. As smaller wavelengths, i.e., higher frequencies are considered, the wave propagation becomes similar to the propagation of light rays. A radio ray is assumed to propagate along a straight line bent only by refraction, reflection, diffraction or scattering. These are the concepts of Geometrical Optics. There is no transversal dimension associated to the rays. However, the finite size of the wavelength at radio frequencies leads to hinder in some ways the assumption of infinitely thin rays. Related to the “thickness” of a radio ray is the concept of Fresnel zones. A Fresnel zone is the locus of points ( $R$ ) around the source ( $S$ ) and an observation point ( $Ob$ ) such that the phase on the path  $S-R-Ob$  equals the sum of the phase on the shortest distance  $S-Ob$  plus an additional constant (Fig. 4.3.3). When this phase difference equals  $\pi$ , the direct ray ( $S-Ob$ ) and the reflected or scattered ray ( $S-R-Ob$ ) are out of phase and the locations of points defines the so-called first Fresnel zone.

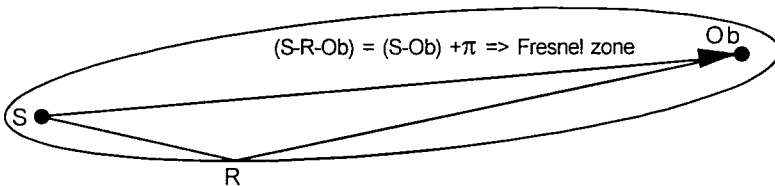


Fig. 4.3.3 The first Fresnel zone.

### *Specular reflection*

The specular reflection phenomena is the mechanism by which a ray is reflected at an angle equal to the incidence angle. The reflected wave fields are related to the incident wave fields through a reflection coefficient which is a matrix when the full polarimetric description of the wave field is taken into account. The most common expression for the reflection is the Fresnel reflection coefficient which is valid for an infinite boundary between two media, for example: air and concrete. The Fresnel reflection coefficient depends upon the polarisation and the wavelength of the incident wave field and upon the permittivity and conductivity of each medium. The application of the Fresnel reflection coefficient formulas is very popular in ray tracing software tools.

Some authors (e.g. [19]-[21]) consider constant reflection coefficients to simplify the computations. However the validity of a constant reflection coefficient is usually not investigated. Considering building penetration (Sec. 4.6.2) or indoor propagation [22], some authors showed an improved fit to measurements by using reflection and transmission coefficients varying with the incidence angle instead of constant coefficients (Sec. 4.7.2).

Specular reflections are mainly used to model reflection from the ground surface and from building walls (see Sec. 4.5 and Sec. 4.7.5). The mechanisms of specular reflections have been used to interpret measurements in some particular environments such as high rise city centre [23], micro-cells [16], indoor [17] and down in a street canyon illuminated from over the roof ("Reflections from buildings next to the mobile" [24], [25]). Whether scattering ( $1/(d_1 \times d_2)$  dependence) or truly specular reflection ( $1/(d_1+d_2)$  dependence) is the proper propagation phenomena was not mentioned and cannot be readily determined since the two phenomena are usually involved simultaneously.

It is pointed out that reflection from a finite surface is not considered in this section since it can be seen either as the sum of the two phenomena specular reflection and edge diffraction, or as a scattering process.

### *Diffraction*

The diffraction process in ray theory is the propagation phenomena which explain the transition from the lit region to the shadow regions behind the corner of a building or over the roof-tops. Diffraction by a single wedge can be solved in various ways: empirical formulas [26], [27]. Perfectly Absorbing Wedge (PAW) [28], [29], Geometrical Theory of Diffraction

(GTD) [29], [30], Uniform Theory of Diffraction (UTD) [31] or even more exact formulations [32], [33]. The advantages and disadvantages of using either one formulation is difficult to address since it may not be independent on the environments under investigations. Indeed, reasonable results are claimed for each formulations. The various expressions differs mainly from the approximations being made on the surface boundaries of the wedge considered. One major difficulty is to express and use the proper boundaries in the derivation of the diffraction formulas. Another problem is the existence of wedges in real environments: the complexity of a real building corner or of the building roofs clearly illustrates the modelling difficulties. Despite these difficulties, however, diffraction around a corner or over a roof-top are commonly modelled using the heuristic UTD formulas [34] since they are fairly easy to program, are well behaved in the lit/shadow transition region, and account for the polarisation and the wedge material.

### *Multiple diffraction*

For the case of multiple diffraction, the complexity increases dramatically. In the case of propagation over roof-top the results of Walfisch and Bertoni [24] has been used to produce the COST-Walfisch-Ikegami model (Sec. 4.4.1). The approximate procedures of Giovannelli [35] or Deygout [25], [36] have been revisited by some authors. The limitations of these approximations lead several researchers to more accurate methods: SIP/FFT [37], [38] (Sec. 4.4.3, PEM), Integral Equation (Sec. 4.4.3, MFIE), Heat Wave Parabolic Equation (Sec. 4.4.3, PEM), Reduced Integral Operator (Sec. 4.4.3, EFIE), Flat Edge Model [39], Slope Diffraction [40]. All these methods are numerical schemes to compute the multiple diffraction and apart from the last contribution they do not give a clear physical understanding of the multiple diffraction process, at least not yet.

One method frequently applied to multiple diffraction problems is UTD. The main problem with straightforward applications of the UTD is, that in many cases one edge is in the transition zones of the previous edges. Strictly speaking this forbids the application of ray techniques, but in the spirit of UTD the principle of local illumination of an edge should be valid. At least within some approximate degrees, a solution can be obtained. In [41] a solution is shown that is quite accurate in most cases of practical interest. The key point in the theory is to include slope diffraction, which is usually neglected as a higher order term in an asymptotic expansion, but in transition zone diffraction the term is of the same order as the ordinary amplitude diffraction terms [40]. Another key element in the method is automatic enforcement of continuity of amplitude and slope at each point.

For the case of diffraction over multiple screens of arbitrary heights and spacings a solution is obtained within the frame of UTD. This solution agrees to a good approximation within the known results for constant spacing and with numerical results using Vogler's solution [42]. The limitation of the method is, that it is not applicable when one spacing becomes very small relative to other spacings. Thus the method cannot predict the collapse of two screens into one.

In ITU-R 526-2 [43] equations are given to compute effects of multiple diffractions around curved cylinders. In [44], an investigation of this method revealed that a modification of the ITU equations yields good results even for multiple knife-edge diffraction. The diffraction losses for the single obstacles are replaced by the diffraction losses for single knife edges. Furthermore, the following modified correction factor  $C_N$  has to be used:

$$C_N = \frac{P_a}{P_b} \quad (4.3.1)$$

The ITU equations are simple to apply and can account for knife-edges with unequal heights and separations. In the special case of grazing incidence over a series of equal distance and equal height knife-edges, the modified ITU equations yield the correct analytical results [40]. This holds true even for very large numbers of edges. The modified ITU method is also compared to the Maciel-Bertoni-Xia-method [45]. Results with the same slope versus the number of edges are achieved. However compared to [45] the path loss is lower (higher), when the transmitter is below (above) the knife-edges.

### *Scattering*

Rough surfaces and finite surfaces scatter the incident energy in all directions with a radiation diagram which depends on the roughness and size of the surface or volume. The dispersion of energy through scattering means a decrease of the energy reflected in the specular direction. This simple view leads to account for the scattering process only by decreasing the reflection coefficient and thus, only by multiplying the reflection coefficient with a factor smaller than one which depends exponentially on the standard deviation of the surface roughness according to the Raleigh theory [46]. This description do not take into account the true dispersion of radio energy in various directions, but accounts for the reduction of energy in the specular direction due to the diffuse components scattered in all other directions.

More realistic scattering processes have been investigated within the COST 231. Most investigations (Sec. 4.4.4) deals with the application of the bistatic radar equation to account for the scattering from hills or mountain slopes. A preliminary study investigated the scattering pattern from large irregularities on a building wall [47]. The concept promoted in that study was to model the scattering by equivalent sources of scattering located at the building corners. Further investigations are required to confirm and refine this concept.

Related to both rough surface scattering and diffraction, the theoretical models mentioned above using SIP/FFT, Integral Equation, Reduced Integral Operator, etc., to account for terrain scattering indicates that the forward scattering approaches lead to reasonable results (Sec. 4.4 and Sec. 4.5.3). This indicates that the back scattering in the radial plane from a given BS antenna is usually neglected or is not taken into account in a detailed manner. The influence of individual "urban" scatterers such as lamp post, traffic light, windows, and cars has not yet been investigated within the COST 231.

#### *Penetration and absorption*

Penetration loss due to building walls have been investigated and found very dependent on the particular situation (Sec. 4.6). Absorption due to trees (Sec. 4.4.2) or the body absorption (Sec. 3.4) are also propagation mechanisms difficult to quantify with precision.

Another absorption mechanism is the one due to atmospheric effects. These effects are usually neglected in propagation models for mobile communication applications at radio frequencies but are important when higher frequencies (e.g., 60 GHz) are used as described in Sec. 8.2.

### **4.3.3 Other propagation mechanisms**

#### *Guided wave*

Wave guiding can be viewed as a particular propagation mechanism to describe the propagation in street canyon (Sec. 4.5.2 - Telekom model), in corridors or tunnels (Sec. 4.8). The wave guiding phenomena can be explained based on multiple reflections or propagation modes.

#### *Atmospheric effects*

Atmospheric effects are usually not taken into account for mobile radio applications at UHF frequencies, although empirical correction factors can

be incorporated in some coverage prediction tools to handle seasonal variations (Sec. 4.4.2).

#### 4.3.4 Main propagation mechanisms

The main propagation mechanisms usually taken into account when modelling the radio propagation in macro-cell, micro-cell and indoor environments are visualised in Fig. 4.3.4. For different propagation mechanisms the range dependence of the field strength is given in the following:

- For *specular reflection* the field is proportional to  $(d_1+d_2)^{-1}$ ,
- for *single diffraction*, the field is proportional to  $(d_1/d_2(d_1+d_2))^{-0.5}$ ,
- for *multiple diffraction* and for a source illuminating all edges, the field is proportional to  $d^{-1.9}$  [24],
- for *volume scattering* and *rough surface scattering*, the field is proportional to  $(d_1d_2)^{-1}$ ,
- for *penetration and absorption*, the field is mainly attenuated by a constant,
- for the *wave guiding* phenomena, the logarithm of the field is proportional to  $d$ .

##### *In macro-cells*

Forward propagation including multiple diffraction over terrain and buildings is used in most propagation prediction models for macro-cells (Sec. 4.4.1). Scattering or reflection from large buildings, hills, mountains are modelled to improve the prediction quality and especially to characterise the time dispersion of the radio channel (Sec. 4.4.3).

##### *In micro-cells.*

Most models rely only on specular reflection and diffraction phenomena. Some empirical formulations use guided wave (Sec. 4.5.2 - Telekom model and Uni-Karlsruhe 2D-URBAN-PICO model) or virtual source at intersections which can be viewed as a way to model the combined effects of diffraction and scattering (Sec. 4.5.2 - Ericsson model). Scattering effects from walls and trees as well as from individual scatterer such as balcony, lamp post, windows, cars, etc. remains to be carefully examined. Contributions from over-roof-top propagation are usually modelled using models similar to the ones for macro-cells (Sec. 4.5.3/ 4.5.4).

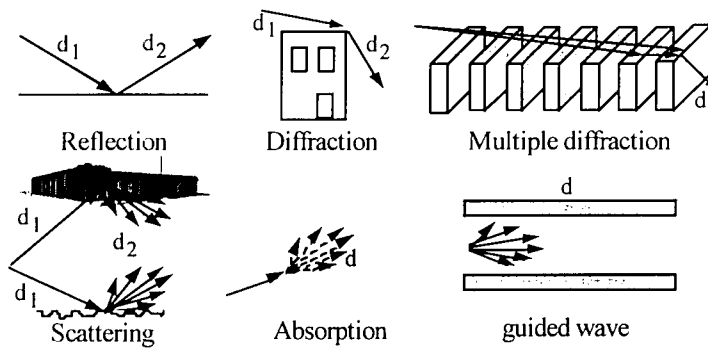


Fig. 4.3.4 Propagation phenomena.

### *Indoor*

Mainly reflection from and transmission through walls, partitions, windows, floors, and ceilings are used to predict propagation within buildings (Sec. 4.6 and Sec. 4.7). Wave guiding in corridor or in hallways are more difficult to model and thus are usually not considered. Although diffraction effects have been sometime identified (Sec. 4.7.5), diffraction at edges from walls or windows is usually not taken into account due to the difficulties related to the requirement on the input database and due to the resulting large computation time.

## 4.4 Propagation Models for Macro-Cells

Thomas Kürner , E-Plus Mobilfunk GmbH, Germany

A considerable interest has been generated in finding solutions to predict average field strengths and multipath signals in macro-cells. The predictions are based on the knowledge of topography, land usage and building height information. This section deals with five different topics - modelling in urban areas, influence of vegetation, large-scale terrain effects, multipath prediction and the combination of the different aspects yielding more general models.

### 4.4.1 Semideterministic and empirical models for urban areas

One important output of COST 231 is the development of outdoor propagation models for applications in urban areas at 900 and 1800 MHz bands. Based on extensive measurement campaigns in European cities, COST 231 has investigated different existing models and has created new propagation models. These models, valid for flat terrain, are based on the approaches of Walfisch-Bertoni [24], Ikegami [48] and Hata [49].

#### *COST 231 - Hata-Model*

Path loss estimation is performed by empirical models if land cover is known only roughly, and the parameters required for semi-deterministic models cannot be determined. Four parameters are used for estimation of the propagation loss by Hata's well-known model: frequency  $f$ , distance  $d$ , base station antenna height  $h_{\text{Base}}$  and the height of the mobile antenna  $h_{\text{Mobile}}$ . In Hata's model, which is based on Okumura's various correction functions [50], the basic transmission loss,  $L_b$ , in urban areas is:

$$L_b = 69.55 + 26.16 \cdot \log \frac{f}{\text{MHz}} - 13.82 \cdot \log \frac{h_{\text{Base}}}{\text{m}} - a(h_{\text{Mobile}}) \quad 1)$$

$$+ (44.9 - 6.55 \cdot \log \frac{h_{\text{Base}}}{\text{m}}) \cdot \log \frac{d}{\text{km}} \quad (4.4.1)$$

where:

1) "log" means " $\log_{10}$ "

$$a(h_{\text{Mobile}}) = (1.1 \cdot \log \frac{f}{\text{MHz}} - 0.7) \frac{h_{\text{Mobile}}}{m} - (1.56 \cdot \log \frac{f}{\text{MHz}} - 0.8) \quad (4.4.2)$$

The model is restricted to:

$$f: \quad 150 \dots 1000 \text{ MHz}$$

$$h_{\text{Base}}: \quad 30 \dots 200 \text{ m}$$

$$h_{\text{Mobile}}: \quad 1 \dots 10 \text{ m}$$

$$d: \quad 1 \dots 20 \text{ km}$$

COST 231 has extended Hata's model to the frequency band  $1500 \leq f(\text{MHz}) \leq 2000$  by analysing Okumura's propagation curves in the upper frequency band. This combination is called "COST-Hata-Model" [51]:

$$\begin{aligned} L_b = & 46.3 + 33.9 \log \frac{f}{\text{MHz}} - 13.82 \log \frac{h_{\text{Base}}}{m} - a(h_{\text{Mobile}}) \\ & + (44.9 - 6.55 \log \frac{h_{\text{Base}}}{m}) \log \frac{d}{\text{km}} + C_m \end{aligned} \quad (4.4.3)$$

where  $a(h_{\text{Mobile}})$  is defined in equation (4.4.2) and

$$C_m = \begin{cases} 0 \text{ dB} & \text{for medium sized city and suburban} \\ & \text{centres with medium tree density} \\ 3 \text{ dB} & \text{for metropolitan centres} \end{cases} \quad (4.4.4)$$

The COST-Hata-Model is restricted to the following range of parameters:

$$f: \quad 1500 \dots 2000 \text{ MHz}$$

$$h_{\text{Base}}: \quad 30 \dots 200 \text{ m}$$

$$h_{\text{Mobile}}: \quad 1 \dots 10 \text{ m}$$

$$d: \quad 1 \dots 20 \text{ km}$$

The application of the COST-Hata-Model is restricted to large and small macro-cells, i. e. base station antenna heights above roof-top levels adjacent to the base station. Hata's formula and its modification must not be used for micro-cells.

#### *COST 231 - Walfisch-Ikegami-Model*

Furthermore COST 231 proposed a combination of the Walfisch [24] and Ikegami [48] models. This formulation is based on different contributions from members of the "COST 231 Subgroup on Propagation Models" [51]. It

is called the COST-Walfisch-Ikegami-Model (COST-WI). The model allows for improved path-loss estimation by consideration of more data to describe the character of the urban environment, namely

- heights of buildings  $h_{Roof}$ ,
- widths of roads  $w$ ,
- building separation  $b$  and
- road orientation with respect to the direct radio path  $\varphi$ .

The parameters are defined in Figs. 4.4.1 and 4.4.2. However this model is still statistical and not deterministic because only characteristic values can be inserted and no topographical data base of the buildings is considered.

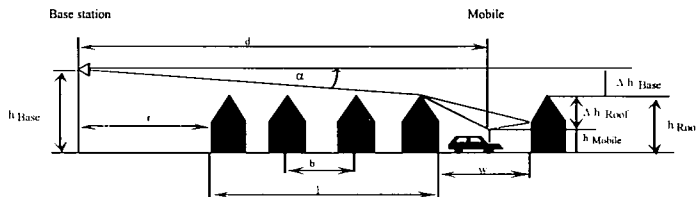


Fig 4.4.1 Typical propagation situation in urban areas and definition of the parameters used in the COST-WI model and other Walfisch-type models [24], [45], [52].

The model distinguishes between line-of-sight (LOS) and non-line-of-sight (NLOS) situations. In the LOS case -between base and mobile antennas within a street canyon - a simple propagation loss formula different from free space loss is applied. The loss is based on measurements performed in the city of Stockholm:

$$L_b(\text{dB}) = 42.6 + 26 \log(d/\text{km}) + 20 \log(f/\text{MHz}) \quad \text{for } d \geq 20 \text{ m} \quad (4.4.5)$$

where the first constant is determined in such a way that  $L_b$  is equal to free-space loss for  $d = 20$  m. In the NLOS-case the basic transmission loss is composed of the terms free space loss  $L_0$ , multiple screen diffraction loss  $L_{msd}$ , and roof-top-to-street diffraction and scatter loss  $L_{rts}$ .

$$L_b = \begin{cases} L_0 + L_{rts} + L_{msd} & \text{for } L_{rts} + L_{msd} > 0 \\ L_0 & \text{for } L_{rts} + L_{msd} \leq 0 \end{cases} \quad (4.4.6)$$

The free-space loss is given by

$$L_0(\text{dB}) = 32.4 + 20 \log(d/\text{km}) + 20 \log(f/\text{MHz}) \quad (4.4.7)$$

The term  $L_{rts}$  describes the coupling of the wave propagating along the multiple-screen path into the street where the mobile station is located. The determination of  $L_{rts}$  is mainly based on Ikegami's model. It takes into account the width of the street and its orientation. COST 231, however, has applied another street-orientation function than Ikegami:

$$L_{rts} = -16.9 - 10 \log \frac{w}{m} + 10 \log \frac{f}{\text{MHz}} + 20 \log \frac{\Delta h_{\text{Mobile}}}{m} + L_{\text{Ori}} \quad (4.4.8)$$

$$L_{\text{Ori}} = \begin{cases} -10 + 0.354 \frac{\varphi}{\text{deg}} & \text{for } 0^\circ \leq \varphi < 35^\circ \\ 2.5 + 0.075 \left( \frac{\varphi}{\text{deg}} - 35 \right) & \text{for } 35^\circ \leq \varphi < 55^\circ \text{ I)} \\ 4.0 - 0.114 \left( \frac{\varphi}{\text{deg}} - 55 \right) & \text{for } 55^\circ \leq \varphi < 90^\circ \end{cases} \quad (4.4.9)$$

$$\Delta h_{\text{Mobile}} = h_{\text{Roof}} - h_{\text{Mobile}} \quad (4.4.10)$$

$$\Delta h_{\text{Base}} = h_{\text{Base}} - h_{\text{Roof}} \quad (4.4.11)$$

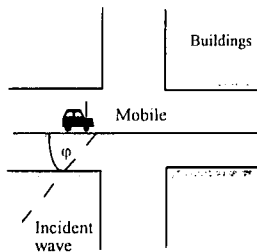


Fig 4.4.2 Definition of the street orientation angle  $\varphi$ .

Scalar electromagnetic formulation of multi-screen diffraction results in an integral for which Walfisch and Bertoni published an approximate solution in the case of base station antenna located above the roof-tops. This model is extended by COST 231 for base station antenna heights below the roof-top

1)  $L_{\text{Ori}}$  is an empirical correction factor gained from only a few measurements

levels using an empirical function based on measurements. The heights of buildings and their spatial separations along the direct radio path are modelled by absorbing screens for the determination of  $L_{msd}$ :

$$L_{msd} = L_{bsh} + k_a + k_d \log \frac{d}{\text{km}} + k_f \log \frac{f}{\text{MHz}} - 9 \log \frac{b}{\text{m}} \quad (4.4.12)$$

where

$$L_{bsh} = \begin{cases} -18 \log(1 + \frac{\Delta h_{Base}}{m}) & \text{for } h_{Base} > h_{Roof} \\ 0 & \text{for } h_{Base} \leq h_{Roof} \end{cases} \quad (4.4.13)$$

$$k_a = \begin{cases} 54 & \text{for } h_{Base} > h_{Roof} \\ 54 - 0.8 \frac{\Delta h_{Base}}{m} & \text{for } d \geq 0.5 \text{ km and } h_{Base} \leq h_{Roof} \\ 54 - 0.8 \frac{\Delta h_{Base}}{m} \frac{d / \text{km}}{0.5} & \text{for } d < 0.5 \text{ km and } h_{Base} \leq h_{Roof} \end{cases} \quad (4.4.14)$$

$$k_d = \begin{cases} 18 & \text{for } h_{Base} > h_{Roof} \\ 18 - 15 \frac{\Delta h_{base}}{h_{roof}} & \text{for } h_{Base} \leq h_{Roof} \end{cases} \quad (4.4.15)$$

$$k_f = -4 + \begin{cases} 0.7 \left( \frac{f / \text{MHz}}{925} - 1 \right) & \text{for medium sized city and suburban} \\ & \text{centres with medium tree density} \\ 1.5 \left( \frac{f / \text{MHz}}{925} - 1 \right) & \text{for metropolitan centres} \end{cases} \quad (4.4.16)$$

The term  $k_a$  represents the increase of the path loss for base station antennas below the roof tops of the adjacent buildings. The terms  $k_d$  and  $k_f$  control the dependence of the multi-screen diffraction loss versus distance and radio frequency, respectively. If the data on the structure of buildings and roads are unknown the following default values are recommended:

$$h_{Roof} = 3 \text{ m} \times \{ \text{number of floors} \} + \text{roof-height}$$

$$\text{roof - height} = \begin{cases} 3 \text{ m pitched} \\ 0 \text{ m flat} \end{cases}$$

$$b = 20 \dots 50 \text{ m}$$

$$w = b / 2$$

$$\varphi = 90^\circ$$

The COST-WI model is restricted to:

$$f : 800 \dots 2000 \text{ MHz}$$

$$h_{\text{Base}} : 4 \dots 50 \text{ m}$$

$$h_{\text{Mobile}} : 1 \dots 3 \text{ m}$$

$$d : 0.02 \dots 5 \text{ km}$$

The model has also been accepted by the ITU-R and is included into Report 567-4. The estimation of path loss agrees rather well with measurements for base station antenna heights above roof-top level. The mean error is in the range of  $\pm 3$  dB and the standard deviation 4-8 dB [53], [54]. However the prediction error becomes large for  $h_{\text{Base}} \approx h_{\text{Roof}}$  compared to situations where  $h_{\text{Base}} \gg h_{\text{Roof}}$ . Furthermore the performance of the model is poor for  $h_{\text{Base}} \ll h_{\text{Roof}}$ . The parameters  $b$ ,  $w$  and  $\varphi$  are not considered in a physically meaningful way for micro-cells. Therefore the prediction error for micro-cells may be quite large. The model does not consider multipath propagation and the reliability of pathloss estimation decreases also if terrain is not flat or the land cover is inhomogeneous.

#### *Comparison with other models*

Saunders and Bonar [52], [39] as well as Bertoni and Xia [24], [56], [45], [57] published different closed-form solutions for  $L_{\text{msd}}$  which are applicable for all values of base station antenna heights. Several papers compare the different approaches with measurements [53], [39], [54], [58], [59], [60].

The results, however, differ markedly depending on the situation, where the models are applied. This effect can be explained by the different validity limits of the different approaches. The Walfisch-Bertoni-Model supposes a high base station antenna ( $h_{\text{Base}} > h_{\text{Roof}}$ ). The COST-Walfisch-Ikegami-Model is valid for base station antenna heights below 50 m and gives reasonable agreement with measured values for  $l > d_S$  (see Fig. 4.4.1), where  $d_S$  is called the "settled-field"- distance [53], [61]:

$$d_s = \frac{\lambda d^2}{\Delta h_{\text{Base}}^2} \quad (4.4.17),$$

where  $\lambda$  is the wave length in m. The case  $l < d_s$  covers grazing incidence, where the COST-Walfisch-Ikegami-Model is poor. On the other hand Saunderson's Flat-Edge-Model covers grazing incidence as long as the condition  $r \gg l$  is fulfilled. Furthermore the COST-Walfisch-Ikegami-Model and an approach of Maciel et. al [57] include corrections for taking into account the street orientation at the mobile. In [58], [59] an adaptive combination of the different approaches is used in urban macro-cells at 1800 MHz, yielding better results than each of the single models.

#### 4.4.2 Influence of vegetation

A few papers within COST 231 investigated propagation models for wooded environments in the 900 and 1800 MHz bands. A comparative study [62] has been done in Finland applying the Okumura-Hata-Model (945 MHz), the COST-Hata-Model (1807 MHz) and the Blomquist-Ladell-Model [55] (both frequencies) to forested terrain. The Finnish experiments revealed that Hata's model can be used for path loss estimation, except for wet forests at 1800 MHz where an additional path loss of about 5 dB has to be taken into account. Middle European forests containing denser and higher trees than typical nordic woods result in larger additional attenuation. In two other papers [59], [63] forest is modelled as a dielectric layer dividing the two layers air and ground. The path loss is computed based on Tamir's lateral approach [64] yielding reasonable results at 947 MHz and 1800 MHz.

#### 4.4.3 Modelling of large-scale terrain variations

Different methods have been investigated to describe diffraction and forward-scattering processes in inhomogeneous terrain, i.e. the effect of the large-scale variation of the terrain. A rough classification of the methods is given by numerical solutions and approximations (see Tab. 4.4.1).

*Numerical solution.*

Two terrain-based propagation models for vertically polarised radio waves are described, based on the field integral equation for a smooth surface. The model developed by Aalborg University [65] is based on the Magnetic-Field-Integral-Equation (MFIE) assuming a 2D landscape with no transverse variations, no backscattering and a perfectly magnetically conducting surface (a soft surface). Under these assumptions the method is exact. The method requires only forward integration summing up the contributions

from all previous segments. No attempts have been made to reduce computation time, but the method is well suited as a reference for more approximate methods.

classification	models
numerical solutions	<b>integral equation methods (IEM):</b> - magnetic field integral equation (MFIE) [65] - electric field integral equation (EFIE) [66]  <b>parabolic equation methods (PEM):</b> - FFT multiple half-screen method [67] - parabolic differential equation method [68]
approximations (including ray-optical approaches)	<b>high-frequency asymptotic methods</b> - uniform theory of diffraction (UTD)[69]  <b>semi-empirical models</b> - forward-scattering algorithm (FSA) [70] - Hata + knife-edge diffraction [71], [72]  <b>empirical models</b> - Hata [49]  - neural network approach [73], [74]

Tab. 4.4.1 Methods to consider large-scale terrain variations.

A faster numerically exact approach based on the natural basis method applied to the Electric-Field-Integral-Equation (EFIE) is suggested by the Trinity College Dublin [66]. In this approach a moment method using a novel set of complex basis functions is used, reducing the resulting matrix by a factor of  $m^2$  and its direct solution by a factor of  $m^3$ . The basis set has been applied to undulating terrain with distances up to 10 km. For frequencies of 143.9 MHz to 1900 MHz  $m$  has ranged from 90 to 600. However, the method to reduce the computational complexity is not restricted to the EFIE but can be applied to any IE, where the unknown current density has to be calculated. Both forward and back scattering are included.

Two methods mainly based on parabolic integral equations are proposed by Berg to build new macro-cell models. The first (heuristic) method [68] is based on the parabolic heat or diffusion equation. The multiple knife-edge approach is used to determine the path loss in non-flat terrain. The equation is solved by using the simple explicit Forward-Difference method. The grid distances are 100 m in the main propagation direction and 5m in height direction in the 900 MHz band. The second method is called FFT-multiple halfscreen diffraction model [67]. The terrain profile is replaced with a number of absorbing half-screens similar to an approach described in [24]. This computational method is also very similar to the SIP procedure [37, 38,

174]. Hence the propagation is described as a multiple diffraction phenomenon where reflections are neglected. The diffracted scalar field is determined using the scalar Helmholtz parabolic integral equation. For the considered situation the Helmholtz integral can be expressed as a convolution which can be solved in a computational efficient way by application of FFT (Fast Fourier transform) techniques.

#### *Ray-optical methods and approximations*

In planning a GSM-network the empirical model by Okumura-Hata is still the most used, due to its simplicity. Therefore many variations of Okumura-Hata-based approaches have been investigated [71], [72], where Hata's path loss is combined with multiple-knife-edge diffraction models. Different methods to determine the effective base station antenna height and terrain undulation correction factors have been considered.

A new ray-optical method [69] is based on the Uniform Theory of Diffraction (UTD). For the ray path calculation with UTD, obstacles along the terrain profile have to be represented by simple geometrical objects. An approximation of the terrain profile is obtained by substituting the terrain obstacles by wedges and convex surfaces. For these objects, expressions exist to compute the UTD diffraction coefficients. For efficient computation, an algorithm for the multiple diffraction calculation is derived using a matrix formulation. Forward-scattering processes are considered heuristically [75] using a two-ray approach. This two-ray approach yields an additional path loss of 20 dB/decade if the distance between Tx and Rx exceeds a so-called breakpoint distance.

In [70] a fast forward-scattering algorithm (FSA) based on empirical propagation curves and geometrical diffraction [76] has been developed. The diffraction algorithm is able to handle up to 15 knife-edges. Measurements in the frequency range 919-1843 MHz have been used for verification. A comparison with a PEM-method [77] revealed prediction errors in the same range for the FSA and the PEM.

Another more empirical method is based on neural network training [73], [74]. The training of the network can be done either by theoretical methods like UTD or by measurements. The decisive advantage of this method is the possibility of deriving training patterns directly from measurements. This allows the system to become very flexible and adapt to arbitrary environments. The training is time consuming, but once the network is trained, the results are obtained immediately. This is supported by the highly parallel structure of the processing.

*Comparison of different models.*

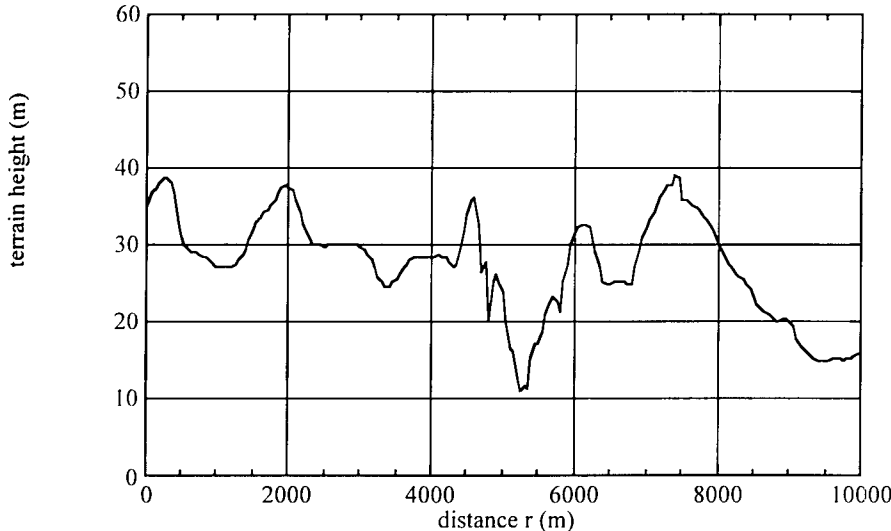


Fig 4.4.3 Terrain profile at "Hjorringvej".

The prediction models are compared to each other and with measurements [65] at different frequencies from 144.9 MHz to 1900 MHz used on five different terrain profiles in rural Denmark. The measurements have been carried out with a transmitter height of 10.4 m and the receiving antenna was 2.4 m above the profile. Polarisation was vertical for both antennas. Path lengths were of 6-11 km along roads being fairly straight over for the distance where the profiles are examined. This gives a good approximation of the 2D assumption within the above described models. The height variations are in the order of 20-50 m and only a few trees or buildings are along the profiles. Fig. 4.4.3 shows one of the profiles at "Hjorringvej".

A comparison of predictions (MFIE-method) with the measurements is depicted in Fig. 4.4.4 (970 MHz) and Fig. 4.4.5 (1900 MHz). Tab. 4.4.2 presents the numerical mean error and standard deviation for seven different models at the frequencies 970 MHz and 1900 MHz. More detailed results comparing these measurements also at other frequencies and with additional models can be found in the literature [67], [71], [75], [78]-[80].

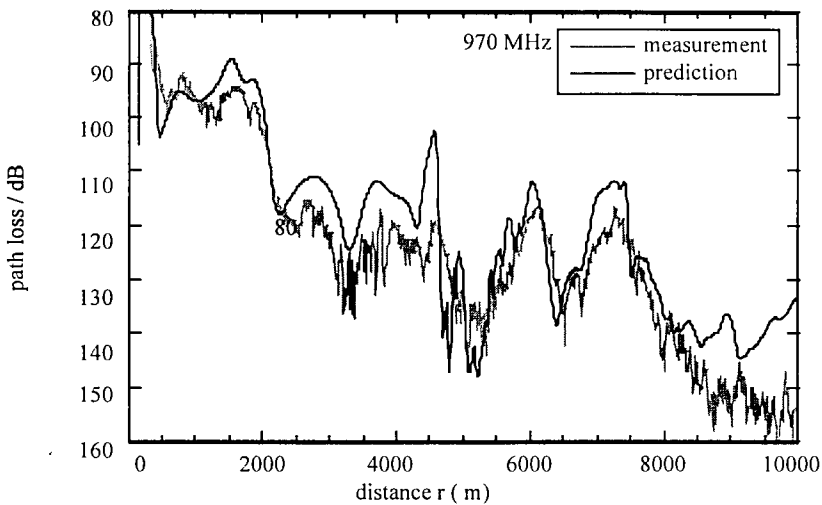


Fig 4.4.4 Measurement and prediction by the MFIE-method for the terrain profile "Hjorringvej" at 970 MHz.

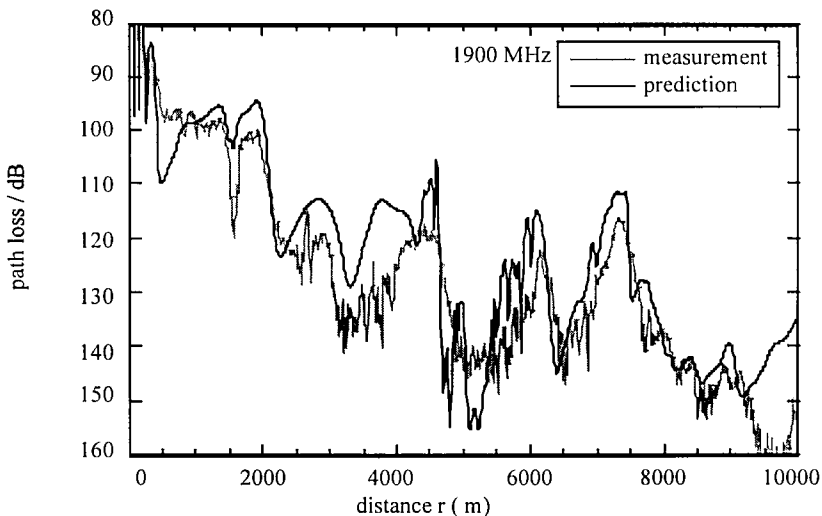


Fig 4.4.5 Measurement and prediction by the MFIE-method for the terrain profile "Hjorringvej" at 1900 MHz.

model	mean /dB 970 MHz	STD/dB 970 MHz	mean/dB 1900 MHz	STD/dB 1900 MHz
MFIE	5,5	6,3	5,1	8,7
IFIE	*)	6,5	*)	8,2
FFT-multiple half-screen	1,7	6,1	3,0	7,6
Parab. diff. FD-Method	3,0	5,4	6,7	8,3
UTD	6,2	8,9	3,4	10,2
Neural Network	2,9	5,7	*)	*)
Hata	2,8	9,0	4,0	10,3
FSA	5,0	6,0	5,3	6,8

\*) values are not available

Tab. 4.4.2 Comparison of different propagation models; numerical mean values and standard deviations derived from 5 terrain profiles (at 970 MHz from 4 profiles only).

#### 4.4.4 Estimation of time dispersion

This section addresses the prediction of multipath signals. Emphasis is placed on automatic detection of long excessive time dispersions. An overview is given over approaches and results from COST 231 participants. The task of predicting multipath signals can be subdivided into two subsequent steps. The first step consists of an algorithm to extract the relevant scattering areas. All known approaches take into account single-scattering processes only. Every potential scatter area has to fulfil the LOS-condition to both Tx and Rx. In a second step the path loss for each multipath signal has to be calculated. This calculation consists of mainly three parts:

- propagation from transmitter to the scattering surface,
- process of scattering at the surface,
- propagation from the scattering surface to the receiver,

The various models differ both in terms of the algorithms to determine the scattering areas and on the methods to determine the path loss.

The IHE-model from the University of Karlsruhe [63], [69], [75], [81] is intended to be a complete propagation simulation model for rural areas. To describe the scattering process the bistatic polarimetric scattering matrix, depending on land usage terrain classes and on the angle of incidence and both scattering angles is applied. The average bistatic cross section matrix

derived by the method of small perturbation and by the Kirchhoff method is used. Both coherent and incoherent scattering are considered in the model. The determination of the scatterer location is often a time consuming process. In [82] fast scatterer search algorithms are suggested. Large improvements are obtained saving 80-90% of computing time compared to traditional methods. A comparison between measured and predicted locations of interfering scatterers is made in [83] at a frequency of 225 MHz (Digital Audio Broadcasting). In general the agreement is satisfactory, although multiple scattering near the antennas and surroundings gave some errors.

The University of Vienna uses path tracing [84] as a practical technique for the identification of areas of heavy time dispersion based on systematic ray tracing and weighting of the paths that the power can take from transmitter to receiver. Single reflections are considered and modelled as an area element radiating isotropically to half space. Between transmitter, scatterer and receiver (quasi) free space propagation is assumed. The model is prepared and planned to be expanded to study consideration of important single scatterers.

In Davidsen's approach [85], [86] multipath propagation is modelled with single-scatter paths. Scattering is modelled as a diffuse Lambert surface. Terrain data is approximated by relatively few planes taken from maps. The planes are subdivided into area elements that are the basis of the calculation. Propagation over sea-water in fjords is studied carefully finding that scattering due to the microstructure (ripple, foam and spray) of the sea is negligible compared with line-of-sight, whereas power scattered by the macrostructure (large scale, roughly periodic waves) is significant.

The model of Deutsche Telekom [87]-[89] is based on channel sounder measurements in hilly terrain. Based upon these measured impulse responses an approach is suggested extending an existing 2D model by additional single-scatter paths. The path loss for the propagation from the transmitter to the scattering and from there to the receiver is assumed to be free space loss. Furthermore the assumption is made that the scattering area acts as a Lambert transmitter. The scattering parameter C is extracted from the measurements. It is shown that  $10 \log C = -10$  dB in the 900 MHz band ( $10 \log C = -13$  dB in the 1800 MHz band) provides a good fit to the measurements. An example for a measured and predicted scattering function is displayed in Fig. 4.4.6.

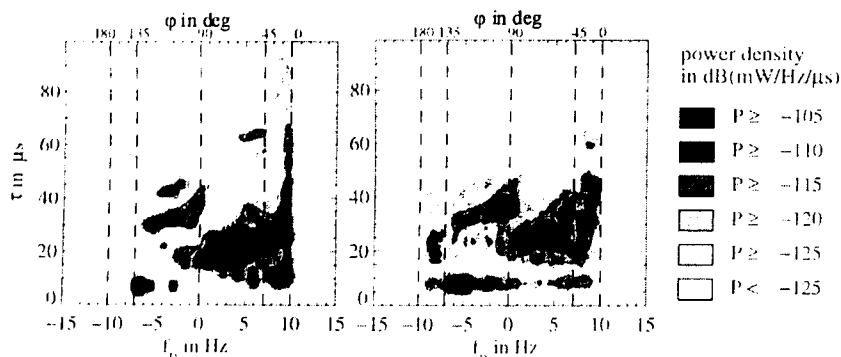


Fig 4.4.6 Measured (right) and predicted (left) scattering functions using the Telekom model.

In Fig. 4.4.6,  $\varphi$  denotes the incidence angle of the signal components with respect to the direction of the moving mobile.  $\tau$  is the time delay and  $f_D$  the Doppler-shift.

For the future channel sounder measurements will be useful to determine both empirical parameters C and bistatic scattering cross sections for different types of terrain. All the models can also be used to predict the propagation system parameters, e.g. delay spread or Q<sub>16</sub>. In [90] and [91] it is shown how the relevant parameters can be derived from a 3D prediction model.

#### 4.4.5 General models

Some new general models for estimation of path loss in macro-cells have been proposed using topographical and land usage data in resolutions from 50 m x 50 m to 250 m x 250 m.

The main idea of Vodafone's method [25], [92] is to reduce the details of path profiles to simple geometrical shapes, e. g. wedges or cylinders, and to apply additionally empirical correction factors. Losses from the free space field strength are calculated for ground reflection and diffraction, ground cover along the path and for clutter from the canopy height down to the mobile. The model is verified by an extensive measurement campaign revealing a standard deviation of about 8 dB in the 900 MHz band using a 250 m x 250 m database.

The IHE-rural-model with receiver near range extension [63], [75] incorporates typical macro situations for forested and urban areas in order to

determine additional path loss caused by land usage. In the case of an urban environment the additional path loss is determined by means of the UTD, whereas in forested areas the above described lateral wave approach is applied. The extension is also used for the multipath signals yielding reasonable agreement with both wideband and narrowband measurements in a GSM 900-network, see Fig. 4.4.7.

A hybrid propagation model for prediction of DCS 1800 macro-cells is proposed by E-Plus [58], [59]. The model is based on a "unit construction system", combining different models, e. g. COST-Walfisch-Ikegami, flat edge [52], [39] and Maciel [45] in urban areas. The prediction system consists of several modules which are selected according to practical and theoretical criteria. The switching of the modules is completely unsupervised and the computing time for the full prediction of an area of 30 km x 30 km is only 5 min on a SunSparc20 workstation. The model is verified by numerous measurements in the E-Plus-network in different landscapes in Germany, including urban, rural, flat, hilly and mountainous terrain. A typical RMS error of 6-9 dB is achieved in all areas.

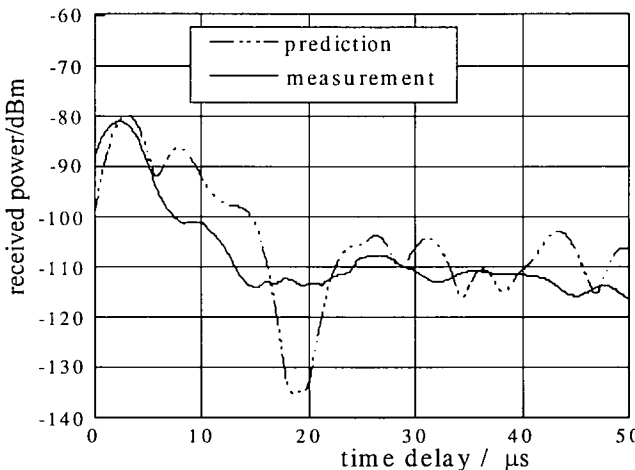


Fig 4.4.7 Measured and predicted impulse responses in a hilly terrain using the IHE-receiver-near-range model at 947 MHz. For the predicted impulse response the filter characteristic of the receiver is taken into account using the algorithms published in [90].

## 4.5 Propagation Models for Small- and Micro-Cells

Dieter J. Cichon , IBP Pietzsch KIH Group, Germany

### 4.5.1 General

The design and implementation of personal communications systems requires the prediction of wave propagation relating to signal-to-noise and signal-to-interference calculation in a cellular system [93]. Small-cell network configurations - especially micro- and pico-cell types - are of major interest for urban environments. The commonly used criteria for the definition of a micro-cell is related to the base-station height. For a typical micro-cell the base-station antenna height is below the average roof-top level of the surrounding buildings or at about the same height. Thus the resulting cell radius is in the range of about 250-500 m. However a prediction range of up to several km has to be regarded for inter-cellular interference calculations. A pico-cell base-station is usually installed inside a building providing coverage also outside around the building. A tutorial and overview on wave propagation modelling for wireless personal communications is given in [94].

The propagation models developed in COST 231 are based on theoretical and empirical approaches. Ray optical methods with either simplified analytical solutions or pure ray tracing techniques have been proposed. The availability and usage of proper urban terrain data bases, as described in Sec. 4.1, in combination with ray tracing methods (see Sec. 4.5.4) enables site-specific propagation modelling for the prediction of path loss and time spreading of the signal; the latter has a major impact on the performance of digital radio systems.

Radio transmission in urban environments is subject to strong multipath propagation. To consider these effects in a propagation model, it is necessary to gain knowledge of all dominant propagation paths. These paths depend primarily on the base station height with respect to the building heights around. A study on micro-cellular multipath propagation effects with respect to DECT-system performance is given in [95]. For simplification of propagation modelling several two-dimensional models have been developed under the assumption of infinitely high buildings (see Sec. 4.5.2). Hence these models only take into account wave propagation around buildings. As a result, computation-time efficient, analytical path loss models have been derived considering simple building geometries. In case

of low building heights, over-roof-top propagation have to be regarded, too (see Sec. 4.5.3). Analytical approaches and simple models with empirically based extensions and modifications are given in, e.g., [24], [48], [51], [45], [60].

The second group of small-cell models allow a very site-specific, three-dimensional path loss and signal spread prediction for base-station heights below as well as at about roof-top level of the buildings (see Sec. 4.5.4). Hence, not only the shape but also the height of a building has to be incorporated. Of course, due to the three-dimensional ray tracing these models require a higher computation-time than the simplified approaches mentioned above.

The micro-cell models are generally valid only for flat urban area. Investigations on the influence of terrain on micro-cell propagation are presented in, e.g. [94] and [96]. Further on the effects of urban-type vegetation (like line-up trees, parks, etc.) on radio propagation [92] are not included in these micro-cell models. Both aspects are of great interest from an engineering point of view and should be regarded in further developments of these models.

#### 4.5.2 Two-dimensional models for below roof-top propagation

##### *Uni-Lund model*

Micro-cellular path loss prediction is performed by two separate models for LOS and NLOS, respectively [97], [98]. Both models are based on the properties of free space propagation; all model parameters are empirically gained.

The LOS model describes the dual-slope behaviour [94] of the path loss, where the first part is a power function (decay index  $n \approx 2$ ) of the Tx-Rx distance  $d$ . At the break-point distance  $d_B$  the power decay increases (decay index  $n \approx 4$ ). The corresponding power decay indices  $n_1$  and  $n_2$  depend on the urban environment, thus they have to be gained by path loss measurements to be performed in the prediction area. For NLOS propagation the model is based on the observation that there is a short distance at the corner where the signal level is still of the same magnitude as in LOS. Further down the street there is a rapid increase of loss until finally the signal strength decreases with about  $n \approx 2.5\text{--}3.0$ .

### *Ericsson micro-cell model*

This model is based on a mathematical method for path loss prediction, which is recursive, reciprocal, very simple, and computation-time efficient [99]. Loss is determined along paths following the different streets, thus this method is suitable for ray tracing techniques. The approach is not restricted to perpendicular street crossings. It can handle arbitrary angle of crossing streets as well as bent streets with linear segments. The model approach is based on the well known expression for path loss between two isotropic antennas, where the physical distance is replaced by an imaginary distance, which is defined by a recursive expression as a function of the number of nodal points and corresponding street orientation angles of the path between transmitter and receiver. The dual-slope behaviour [94] of the distance dependence of the path loss is also included in the proposed model. In addition, the distance dependence of the COST-WI model is applied to consider over-roof-top propagation in case of NLOS.

### *CNET micro-cell model*

This model is based on an analytical, semi-deterministic approach for the consideration of reflected and diffracted waves [100]. Only below roof-top propagation around buildings and street crossings with four corners are regarded. The angle of crossing streets can be arbitrary. Nine reflections in a LOS case and nine reflections in a following NLOS case are included. Ground reflections and street corner diffraction between the line-of-sight and the non-line-of-sight street are regarded as well. The Uniform Theory of Diffraction is used for the street corner diffraction calculation, wherein the finite conductivity of the walls is introduced through heuristic coefficients.

### *Swiss Telecom PTT micro-cell ray tracing model*

Micro-cell environments are described by a two-dimensional layout of buildings which are given to the software program in terms of vectors defining the building walls. Arbitrary two-dimensional building geometry can be handled. Additionally, the permittivity and conductivity of each building wall can be considered if available. In operational use the electrical characteristics are usually taken to be the same for all buildings in a given area. Specular reflection and diffraction are the propagation phenomena taken into account [101]. Ground reflection, scattering and over-roof-top propagation which are expected to dominate in areas far from the transmitter are neglected so far. The software computes all reflected and diffracted rays up to some predetermined order. This is performed according to an efficient implementation of the image theory which takes advantage of the assumed

fact that rays do not traverse the buildings. To take into account the diffraction effects, virtual sources are placed on all building corners viewed by other images and virtual sources. All image and virtual point sources are generated up to a given order starting from the original source at the base-station antenna location. The image and virtual sources are then used to trace all combinations of reflected and diffracted rays. The path loss is derived by superposition of all rays at the receiver location. Alternatively the channel impulse response can be evaluated by considering the magnitude, phase and delay of each ray.

#### *Uni-Karlsruhe model 2D-URBAN-PICO*

A ray launching approach for two-dimensional prediction of wave propagation in micro-cells, including indoor coverage, is proposed in the 2D-URBAN-PICO model [4], [102], [103]. This approach takes into account multiple reflected and multiple wall-penetrated ray paths as well as combinations of multiple reflected/penetrated ray paths. The urban environment is two-dimensionally described by an arbitrary number of walls, or further windows, doors, etc., each defined by its position and type. Building walls are modelled as multi-layered media given by thickness, permittivity and tang loss factor. At the transmitter location a certain number of rays are successively launched in discrete directions, which are equally distributed over  $2\pi$  within the horizontal propagation plane. When the central ray of a ray tube intersects with an obstacle, the incident ray is decomposed into a specularly reflected and a penetrated ray. Both rays are propagating to the next intersection, where the decomposition process is repeated. This procedure is continued until a predetermined number of intersections is reached. A ray-splitting algorithm is used to restrict the maximum divergence of each ray. Reception is determined according to Fig. 4.7.3 in Sec. 4.7.5.

#### *TLM based model*

A technique similar to the so-called transmission line matrix (TLM) is applied for the propagation modelling in urban micro-cells. This method is based on a direct discretisation of the building layout onto a two-dimensional lattice. The TLM based method can be assimilated to the so-called Lattice Boltzmann Models (LBM), which describes a physical system in terms of the motion of fictitious microscopic particles on a lattice. A natural implementation of wave propagation dynamics within the framework of the LBM approach is provided by the TLM method. According to the Huygens principle, a wave front consists of a number of spherical wavelets emitted by secondary radiators. The TLM method used here is a discrete

formulation of this principle. For this purpose, space and time are represented in terms of finite, elementary units  $\Delta r$  and  $\Delta t$ . LBM are characterised by a simultaneous dynamics and a very simple numerical scheme suitable for very efficient implementations on massively parallel computers [21]. The interpretation of the dynamics in terms of flux makes the boundary conditions easy to implement. The relationships with conventional electromagnetic TLM methods remain to be examined in details.

Assuming infinite building height, the raw simulation results of the TLM based method implies a two-dimensional propagation (a cylindrical source problem). The results are converted to three-dimensional propagation consideration (point source problem) by computing a renormalisation of the predicted results according to the distance between transmitter and receiver. An additional, although simpler, re-normalisation is used to convert to the desired frequency the simulated frequency resulting from the chosen grid size of the lattice.

#### *Telekom micro-cell model*

A network of street canyons connected via the street crossings is used as standard geometrical configuration for path loss calculation. A limited set of parameters and some empirical simplifications and approximations are used. Three categories of propagation are regarded: LOS, NLOS to a perpendicular street, and NLOS to a parallel street [27]. Latter one includes also a over-roof-top propagation term according to Walfisch-Bertoni [24]. The applicability of this model is confined primarily in dense urban environments where street canyons can be assumed.

#### **4.5.3 Two-dimensional models for over-roof-top propagation**

##### *COST-Walfisch-Ikegami model*

(==> see Section 4.4)

##### *Uni-Valencia model*

The basic approach is to separate the propagation effects into "over-roof-top propagation" and "3D multipath effects in the mobile neighbourhood". A modified Walfisch-Bertoni model for description of over-roof-top propagation is applied [60]. The restriction for the incidence angle and for the "final building diffraction" angle have been eliminated [105]. Latter one has been empirically gained, however its value is very close to the theoretical solution for a 90° wedge. The empirical approach is due to the

fact that digital building maps or vector data, i.e., do not provide information about the roof-top shape, thus a theoretical expression cannot be applied, appropriately.

First and 2nd order propagation mechanisms are considered for a Tx-Rx link. It is assumed that incident rays at Rx are scattered at elements (wall, wedge, etc.) which are in LOS to Rx. These Rx-neighbourhood scatter elements are determined by application of a simple ray tracing algorithm. The incidence fields at those elements are calculated by the 2D model mentioned above [106]. Three parameters are used to describe the properties of the scatter elements as there are: Percentage of flat surface, correlation distance, standard deviation of the roughness; default values are 60 %, 3 m and 40 cm, respectively.

For applications in micro-cell environments, the ray tracing algorithm for the 3D model has to be modified to consider at least 3rd order contributions, too. In case Tx is below the mean roof-top level, a third part of the model appears, which is simply described as an additional diffraction loss (2D approach) and/or by applying the above 3D multipath model to the Tx-neighbourhood. Of course, the additional base station diffraction loss and multipath terms depend on the Rx position.

#### *Swiss Telecom PTT over-roof-top model*

A pathloss prediction software designed for flat or hilly urban areas has been developed at the Swiss TELECOM PTT. The software (called MCOR) implements multi-knife edge propagation computations over radials launched from the base station.

The propagation model is based on Deygout's approximation to compute multi-knife edge diffraction [107]. The Deygout method is modified according to the concepts presented by VODAFONE [92]. This modification mitigates the linear increase of the path loss due to multiple diffraction in the original Deygout method. The algorithm suggested by VODAFONE decreases the diffraction effects by reducing successive diffraction coefficients in dB by 1/2, 1/4 and 1/8. Inspired from this idea, this model decreases the diffraction effects on each side of the so-called main edges simply by reducing the diffraction coefficients in dB by  $(1/2)^n$ , where n is the order of the main edges in the Deygout method. For the results presented here, the maximum level is limited to 4 ( $n_{\max} = 3$ ), thus a maximum of 15 diffractions are computed. The chosen diffraction coefficient is given by the simple CCIR formula [108]. Another modification is the use of a dual slope model for the reference path loss [109]. For the results presented here, the

parameters of the dual slope model have been fitted from ten calibration points given along a particular measurement route. The buildings have been represented by a single knife-edge placed in the middle of each building, which is determined when constructing the profiles along the radials.

The MCOR computation for the results presented in Sec. 4.5.6 takes about 30 minutes on a Pentium 66 MHz under Windows NT for a prediction of 480 x 680 points with a 5 m resolution (note that the prediction data on the measured routes is then extracted from the prediction matrix over the whole region).

#### *CSELT model*

Over-roof-top propagation is regarded in this model, which is based on the Walfisch-Bertoni approach [24] extended by consideration of building heights within the vertical propagation plane. Obstacles (buildings) are treated as half-plane screens, which are perfectly absorbing, infinitely thin in propagation direction and infinitely wide across it. For base stations well above average roof-top height it is assumed that the roof-top to street diffraction at the last obstacle is the dominant loss mechanism affecting the radio link, thus Deygout's diffraction approach is applied in this model. A digital data base containing position and height of the buildings is used to obtain a site-specific two-dimensional propagation modelling approach [110].

#### **4.5.4 Three-dimensional models for arbitrary base-station heights**

The propagation models described in this section are suitable for the prediction of path loss as well as the channel impulse response under consideration of the three-dimensionally described buildings.

#### *CNET ray launching model*

The program simulates ray launching in three dimensions. Buildings are represented by polyhedrons. Multiple reflection and diffraction processes are considered in the model [111]. Building penetration, scattering at wall irregularities and diffraction at vertical wedges are neglected in the model. Reflection loss is the only physical parameter to be fitted since diffraction loss is computed from semi-empirical formulae.

#### *ASCOM-ETH micro-cell model*

To study the propagation in micro-cell, the image source method has been incorporated into a ray-tracing approach for taking into account multiple reflections from the walls and streets [16], [112]. The model used the

detailed three-dimensional description of the environment. This comprises the permittivity and conductivity of the walls and street materials. Complex impulse responses were derived from the model calculations, which were compared to the corresponding wideband measurements. A large number of different real environments have been considered to test the model. Good agreement has been found between the modelled results and the measurements. This enabled a classification into few types of environments covering the physical situations most relevant for urban micro-cells: propagation in lineal urban streets (LOS) and coupling into side streets (NLOS). The transition region between LOS and NLOS has been analysed in much detail, as the channel behaviour under such conditions is very important for wireless communication system design.

#### *Villa Griffone Lab's (VGL) model*

The field prediction program developed at the Laboratories of Villa Griffone by the researchers of the University of Bologna and of the Ugo Bordoni Foundation is based on a quasi 3D ray tracing/UTD technique [113]. It can be applied to both macro-cellular and micro-cellular systems and can provide both narrowband coverage prediction and wideband channel estimates. Each city block is represented by a prism having a polygonal base corresponding to the shape of the block and a height corresponding to the average height of the buildings in the block. To each prism the corresponding permeability and conductivity values are associated. The environment is thus described as a set of basic objects such as plane walls or lossy wedges.

A quasi 3D ray tracing procedure is performed including rays within the transverse Tx-Rx plane with multiple reflections on building walls and diffractions on corners, and in addition other significant rays experiencing reflection over terrain are considered. No predefined limit is set to the number of multiple reflections or diffractions experienced by each ray; however, a limit can be provided by the user in order to minimise computation time. The algorithm starts determining the set of objects, which have LOS to the transmitter, resulting in the first level of the "viewed objects" tree. Repeating this LOS-determination procedure under consideration of reflection and diffraction points leads to further levels in the "viewed object" tree; the receiver location is the last tree level. After completion of the tree the actual path of each ray can be determined by means of a backtracking process, and the corresponding contribution to the total received field can be computed by means of reflection and diffraction coefficients [113]. Additionally, the Saunders-Bonar model [52] is used, if

over-roof-top propagation should be regarded, too. Also the attenuation due to vegetation can be considered by means of the Foldy-Twersky method [114] when a vegetation map is available.

#### *Uni-Stuttgart 3D micro-cell model*

This is a rigorous three-dimensional modelling approach with possible path finding over the entire solid angle [115], [116]. Buildings are described by a polygon with a set of cartesian co-ordinates and a flat roof-top at constant height. Electrical building parameters can also be stored if available. A ray launching algorithm where rays are launched from a fixed point source in all relevant directions is used for path finding, a UTD approach is used for propagation calculation. At potential receiver locations the field strengths of the incident rays are summed up. Less than three diffraction but up to six reflection processes (for modelling of wave guiding effects) can be regarded in the 3D case. In case of more diffraction processes are required, a 2D prediction approach based on the Walfisch-Ikegami formula is used. Topography can be included by defining triangular surface elements which are treated as potential scatterers [117]. The basic characteristics of this approach are: fast algorithm for area prediction, simultaneous calculation for different receiver heights, and unsuitableness for point to point predictions.

#### *Uni-Karlsruhe model 3D-URBAN-MICRO*

A three-dimensional approach for propagation simulations in micro- and macro-cellular cases, where base-stations above as well as below building heights can be considered, is proposed by the 3D-URBAN-MICRO model, developed at the University of Karlsruhe [4], [81], [104], [118]. This model is able to use either grid (pixel) data or vector oriented data containing building shape and building height. For the grid data a reasonable horizontal resolution is about 5-15 m, depending on the urban micro structure and the desired approximation of the building shapes. Building heights are approximately given by the number of floors and corresponding floor height.

From numerous transmitter (Tx) to receiver (Rx) propagation paths, the most dominant ones have to be selected to obtain the total path loss. Roof-top diffracted paths are included in the vertical plane approach, while around building diffracted paths are modelled within the transverse plane approach as depicted in Fig. 4.5.1. The propagation in both the vertical and the transverse plane is two-dimensionally regarded. However, the determination of building corners in the transverse propagation plane is not necessarily performed in a horizontal plane.

Multiple wedge diffraction processes are evaluated by successively computing single wedge diffraction based on the UTD. Additional 3D propagation paths via scattering at ground and building walls are separately regarded. A modified Kirchhoff Method with scalar approximation is applied for surface scattering calculations [4]. Recently, this model has been extended for receiver locations within buildings to provide indoor coverage prediction by outdoor base stations [119].

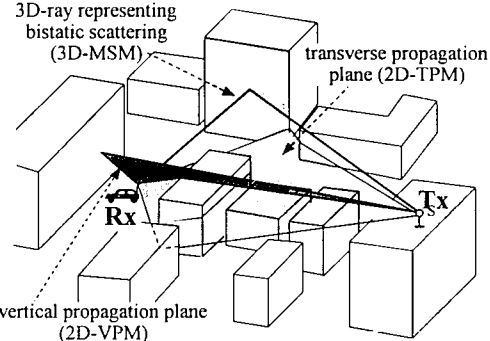


**Fig. 4.5.1** Ray tracing within a vertical and a transverse Tx-Rx plane.

#### 4.5.5 Overview over the Prediction Models

The small- and micro-cell propagation models are briefly summarised and listed in the Table 4.5.1 (CIR = channel impulse response).

#### 4.5.6 Comparison with path loss measurements at 947 MHz

A path loss measurement campaign including different base station heights at several locations have been carried out in downtown Munich by the German GSM network operator Mannesmann Mobilfunk GmbH. The performance of some of the introduced models is investigated by comparison with the measurements.

##### *Description of the measurement scenario*

Building data in vector format covering an area of about  $2.4 \times 3.4 \text{ km}^2$  in downtown Munich have been provided by Mannesmann Mobilfunk. Since the selected test site has a fairly flat ground, the topography (which has been also available) is not considered within this study of model performances. Hence, only the two-dimensional building layout with height information of each single building is used by the propagation models.

The resulting building map (based on pixel data) is shown in Fig. 4.5.2, where the absolute terrain heights are grey scale presented. Additionally, the three measurement routes METRO200 (970 points; ground height:  $512 \pm 4 \text{ m}$ ,  $s_h = 2 \text{ m}$ ), METRO201 (355 points; ground height:  $516 \pm 2 \text{ m}$ ,  $s_h = 1.3 \text{ m}$ )

and METRO202 (1031 points; ground height:  $514 \pm 5$  m,  $s_h = 1.9$  m), as well as the transmitter location (Tx) are marked in the map.

<b>prediction model</b>	<b>method</b>	<b>features/restrictions</b>	<b>terrain data</b>	<b>results</b>
Uni-Lund (S)	empirical	BS below roof-top	2D building layout	path loss
CNET micro cell model (F)	analyt. LOS + NLOS model	2D (horizontal plane) + 2D (over-roof-top)	2D building layout	path loss
RT - Swiss Telecom PTT (CH)	ray tracing	2D (horizontal plane)	2D building layout	path loss and CIR
Uni. Geneva / Swiss Telecom PTT(CH)	TLM like	2D (plane)	2D building layout	path loss
2D-URBAN-PICO Uni. Karlsruhe (D)	ray launching	2D (horizontal plane)	2D building layout	path loss and CIR
Telekom (D)	analyt. LOS +NLOS model	2D (horizontal plane) + 2D (over-roof-top)	2D building layout	path loss
Ericsson (S)	ray tracing + COST-WI	2D (horizontal plane) +2D (over-roof-top)	2D building layout	path loss
COST-231 small-cell	Walfisch-Ikegami mod.	2D (over-roof-top)	building classes	path loss
Uni. Valencia (ES)	Walfisch-Bertoni mod.	2D (vertical plane) + 3D reflections at Rx	2D building layout + building height	path loss, FS distribution
MCOR - Swiss Telecom PTT (CH)	modified Deygout	2D (over-roof-top)	2D building layout + building height	path loss
CSELT (I)	Deygout	2D (over-roof-top) BS above roof-top	3D raster data	path loss
CNET ray launching model (F)	ray launching	3D (no diffraction at vertical wedges)	3D building layout	path loss and CIR
ASCOM-ETH (CH)	Ray-tracing by image source	3D, only reflections	2D building layout + building height	path loss and CIR
Villa Griffone Lab, Bologna (I)	ray tracing; Saunders-Bonar	transverse plane + ground reflection; 2D (over-roof-top)	2D building layout + building height	path loss and CIR
Uni. Stuttgart (D)	ray launching + W/I model for 2D case =>	3D (2 diff. + 6 reflec. processes); 2D (vertical plane)	2D building layout + building height	path loss and CIR
3D-URBAN-MICRO Uni. Karlsruhe (D)	ray tracing	2D (transverse plane) 3D surface scatter	2D building layout + building height or raster data	path loss and CIR

Tab. 4.5.1 Small- and micro-cell prediction models: An overview



Fig. 4.5.2 Munich test site with measurement routes (~ 25 km) and transmitter location; terrain height is grey scaled.

by Mannesmann Mobilfunk GmbH

The measurements have been performed at 947 MHz, the transmitter and receiver height is 13 m and 1.5 m above ground, respectively. An approximately 10 m sector average of the measured signal has been converted to path loss and stored with the Rx location, which is at about the centre of the averaging sector.

### *Performance of the models*

The following institutes have participated in this study: CNET (France), CSELT (Italy), Ericsson Radio Systems (Sweden), Swiss PTT/Uni. Geneva (Switzerland), Villa Griffone Laboratories (Italy), University of Karlsruhe (Germany), and University of Valencia (Spain). For calibration purpose, all participants received the measured path loss data of 11 Rx locations selected from the METRO200 route. Except the building data in vector format and all Rx locations, no additional information have been provided to the participants, leading to an almost "blind test" of the above mentioned prediction models discussed in COST 231.

Results are presented in Fig. 4.5.3 - 4.5.5, where the model predictions and the measured path loss versus Rx locations of the 3 routes (total length of about 25 km) depicted in Fig. 4.5.2 are shown. To improve the visualisation quality of the prediction results, the original curves of the CNET, TLM, MCOR, Griffone and Uni-Karlsruhe model have been smoothed to suppress strong fluctuations and therefore to make the single curves better distinguishable. Since the transmitting antenna height  $h_t$  is at 13 m above ground, which is below roof-top of most of the buildings within the test site, almost all Rx locations are in NLOS situations, except some peaks which obviously refer to LOS propagation.

Along routes METRO200 (Fig. 4.5.3) and METRO202 (Fig. 4.5.5) the performances of the Swiss PTT MCOR model and Uni-Karlsruhe ray tracing model, both regarding over-roof-top propagation, and the Ericsson model and CNET model, both regarding around and radially over building propagation, are rather good, with a standard deviation of the prediction error in the range of 5.6-8.6 dB (see also Table 4.5.2), although different propagation paths are regarded by these models. These results indicate that the field contributions of both over-roof-top and around building propagation are in some cases of the same order of magnitude at the receiver.

The Walfisch-Bertoni type model of the University Valencia is an extension of the COST-Walfisch-Ikegami (COST-WI) model, hence regarding over-roof-top propagation. Therefore both results show similar behaviour except an offset of about 10 dB and, of course, the much better performance of the Uni-Valencia model in LOS-situations. For the COST-WI model the

parameters describing the built-up structure are estimated to be  $h_{Roof} = 20$  m,  $w = 13$  m and  $b = 26$  m, respectively. Since it is an empirical model, the model parameters should be properly adjusted to reduce the mean error of 10-17 dB; however the standard deviation of the prediction error is in the range of 6-8 dB, which is fairly good for this simple and fast prediction method. The general trend is a good agreement with the measurements obtained by the PTT ray tracing (RT) model. However, for many Rx locations no ray paths could be determined, as can be seen in Fig. 4.5.3, since the model is restricted to a maximum of 4 reflections or to a maximum of 3 reflections and 1 diffraction per ray. The application of the transmission line matrix method for propagation modelling leads to higher prediction errors compared to the other models. Since this is a very new method, the reasons have not been analysed in detail up to now. The application of the three-dimensionally working Villa Griffone and Uni-Karlsruhe models in the above scenario outperforms very well under the circumstance that these models have been developed for arbitrary base station heights; however here the transmitting antenna is placed at 13 m above ground, which is more or less below the average building height in the measurement area. This may also be the reason for the insufficient performance of the CSELT model, which is based on an over-roof-top Deygout multiple diffraction approach. The CSELT model has been proofed to perform better for higher mounted BS.

The performance of the tested models are summarised in Tab. 4.5.2, where the mean prediction errors and the corresponding standard deviations are given. An average standard deviation of the prediction error of about 7 dB up to 9 dB is achieved by the presented models, with exception of the TLM and ray tracing models of the Swiss Telecom PTT and the CSELT model, in which only 2D-horizontal contributions are taken into account.

It has to be noted that no vegetation effects are considered by any model. An interesting simulation result is that over-roof-top propagation and around-building propagation are fairly in the same order of magnitude. Differences between measurement and simulation may be due to the inaccuracies of the building data base, and of course due to the fact of disregarding further details of the real environment like cars, lamp posts, roof kind, balconies etc. However, the achieved results are very promising for both empirical-based as well as fully deterministic propagation models.

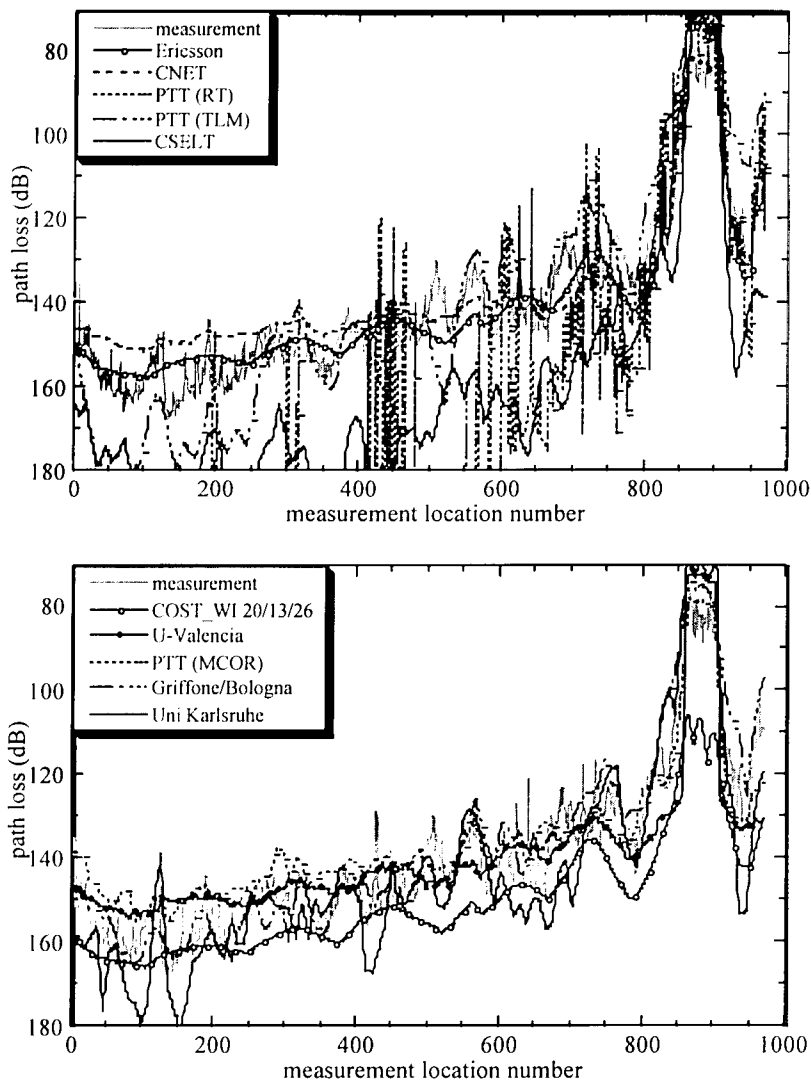


Fig. 4.5.3 Comparison between measured and predicted path loss along route METRO200 (see Fig. 4.5.2); ht = 13 m.

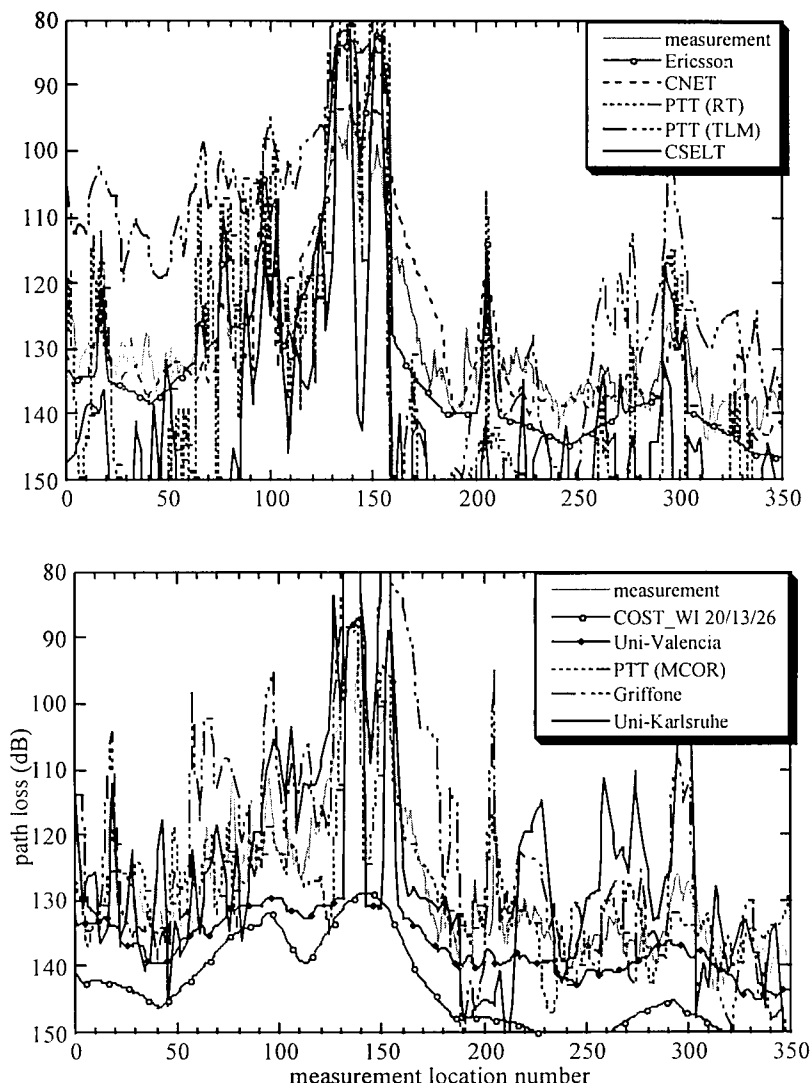


Fig. 4.5.4 Comparison between measured and predicted path loss along route METRO201 (see Fig. 4.5.2); ht = 13 m.

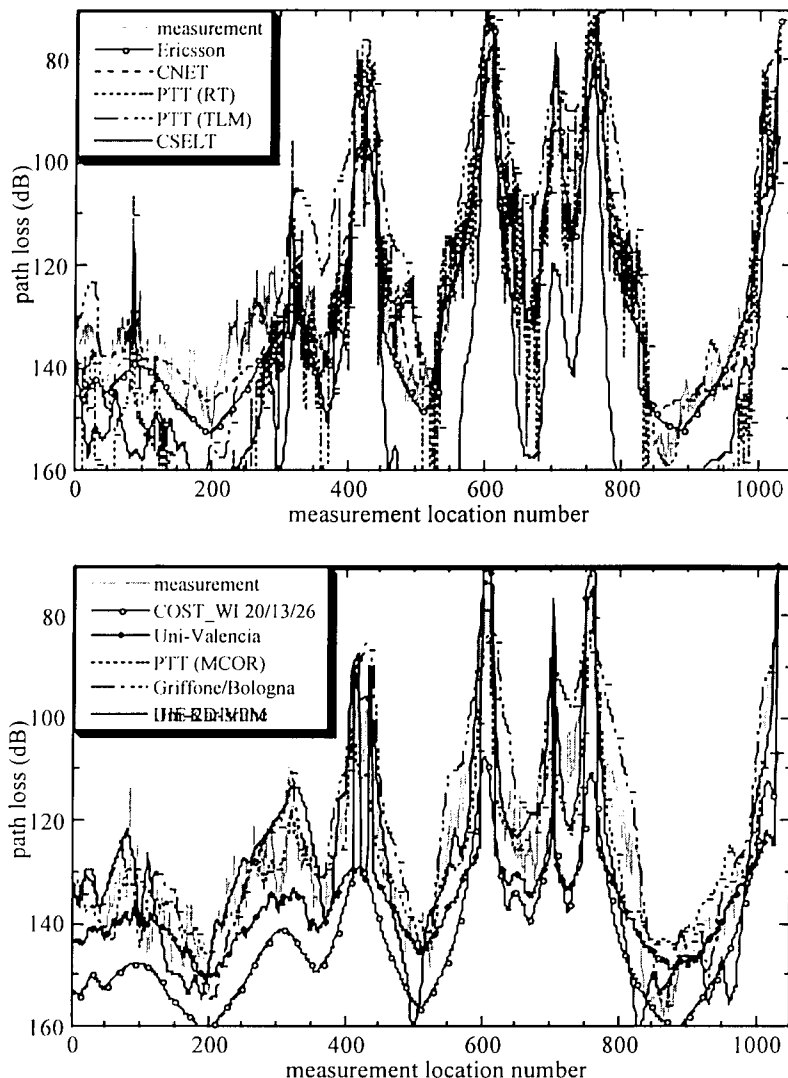


Fig. 4.5.5 Comparison between measured and predicted path loss along route METRO202 (see Fig. 4.5.2); ht = 13 m.

<b>Prediction model</b>	METRO200 (970 points)		METRO201 (355 points)		METRO202 (1031 points)		<b>average</b>
	STD (dB)	mean (dB)	STD (dB)	mean (dB)	STD (dB)	mean (dB)	
Ericsson	6.7	0.3	7.1	2.3	7.5	1.4	<b>7.1</b>
CNET	6.9	-2.1	9.5	-3.6	5.6	-0.2	<b>7.3</b>
PTT (RT)	14.6 <sup>1)</sup>	-6.1 <sup>1)</sup>	15.5 <sup>2)</sup>	-6.7 <sup>2)</sup>	12.3 <sup>3)</sup>	-1.1 <sup>3)</sup>	<b>14.1</b>
PTT (TLM)	13.8	0.8	21.7	6.7	12.9	6.5	<b>16.1</b>
COST-WI <sup>4)</sup>	7.7	10.8	5.9	15.4	7.3	16.3	<b>7.0</b>
Uni.-Valencia <sup>5)</sup>	8.7	0.2	7.0	-6.6	10.3	-7.4	<b>8.7</b>
CSELT	10.4	21.8	12.3	16.1	13.3	20.6	<b>12.0</b>
PTT (MCOR)	7.0	-3.3	6.2	-0.1	7.6	-1.1	<b>6.9</b>
Villa Griffone Lab	6.3	-1.7	10.9	-6.3	6.8	-5.5	<b>8.0</b>
Uni.-Karlsruhe	8.5 <sup>6)</sup>	-4.3 <sup>6)</sup>	9.1	2.4	8.6 <sup>6)</sup>	-1.0 <sup>6)</sup>	<b>8.7</b>

<sup>1)</sup>calculations at 425 points only; <sup>2)</sup>calculations at 264 points only; <sup>3)</sup>calculations at 774 points only; <sup>4)</sup>assumed terrain parameters: building height: 20m, street width: 13m, building separation: 26m; <sup>5)</sup>no 3D effects are considered; <sup>6)</sup>2D-vertical propagation plane only;

Tab. 4.5.2 Performance of the propagation models at 947 MHz; standard deviation and mean value (prediction - measurement).

## 4.6 Building Penetration

**Jan-Erik Berg , Ericsson Radio Systems AB, Sweden**

### 4.6.1 Introduction and definitions

A common approach in many existing planning tools is to predict the path loss outside in the proximity of the buildings and then add a constant loss in order to estimate the loss inside the building. This is a major reason why the building penetration loss usually is related to the outside levels at about 2 m height above ground.

Some concern must be taken when the median outside level is determined. If a line of sight exists between the exterior base station antenna and one or several external walls a considerable variation, tens of dB, of the path loss around the perimeter of the building may occur. Thus, the corresponding penetration loss will vary considerably depending on which reference level is used. The outside reference level must not contain both line of sight and non line of sight results!

The indoor small scale fading in an area of about 1 to 2 square metres is, for a narrowband signal in the frequency range 900-1800 MHz, usually close to a Rayleigh distribution (when the envelope variation is described in Volt). The large scale variation is obtained when this small scale fading component is removed by spatial filtering.

The penetration loss can be divided into four major categories:

- wall loss,
- room loss,
- floor loss,
- building loss,

each relative the median path loss level outside the building.

The wall loss, which is angle dependent, is the penetration loss through the wall. The true wall loss is difficult to determine when measurements are taken in a building due to multiple reflections and the furniture close to the walls.

For line of sight conditions with one dominant ray, the power of the reflected ray at the external wall can be considerable at small grazing angles, giving rise to a large penetration loss compared to perpendicular penetration.

The penetration loss of the external wall can be different at non line of sight conditions compared to a perpendicular line of sight situation. Thus, one single external wall can have considerable different penetration losses, depending on the environmental conditions.

The room loss is the median loss determined from measurements taken in the whole room about 1-2 m above the floor. In a room with an external wall, the room loss is usually greater than the corresponding external wall loss. The room loss level is practical to use when the penetration loss is displayed on a drawing describing the building. Sometimes is it practical to divide large rooms into smaller fictitious rooms.

Usually the measured room loss values are used as an input to a model which considers one or several propagating rays through the building. The difference between the model and measurements can be minimised by choosing appropriate losses for the different walls. This approach gives wall losses that can be used in the model but do not necessarily represent the actual physical wall losses. The results in this chapter are mainly based on this method.

The floor loss is the median loss in all of the rooms on the same floor in a building. The large scale variation over the floor is often log-normal distributed. The building loss is similar to the floor loss, but taken over all of the floors in the building. When this method is used, information should be given if the basement is included or not.

In some cases the penetration loss decreases with increasing floor level. This dependence is called floor height gain and given in dB/floor. Due to that the heights of the storeys vary between different buildings, it is sometimes better to describe the dependence as a function of the physical height in dB/m. The height gain effect ceases to be applicable at floor levels that are considerable above the average height of the neighbouring buildings. The sum of the outside reference loss and the height gain loss, which is negative, must not be less than the free space propagation loss.

In micro-cellular environments, where the base station antenna height is considerably lower than the surrounding building height, the penetration loss for line of sight conditions is quite independent of the floor height at larger distances. This is also valid for non line of sight conditions when the main part of the power propagates along the streets. However, in non line of sight conditions where the dominant part of the received power in the street originates from rays that due to reflections and diffraction have propagated down from the surrounding roof level, a notable floor or height gain can be

found. This is usually the case in macro-cellular environments with a base station antenna height above the height of the average building height in the area.

Median is used in the definitions above, which is preferable due to its independence of the distribution. However, the main part of result presented below, are based on averaging.

#### 4.6.2 Building penetration loss at line of sight conditions

Building penetration related papers written by COST 231 participants can be found in [120]-[134]. Results from a lot of different kind of buildings with miscellaneous distances and angles between the outdoor antennas and the surfaces of the external walls have been presented within the COST 231 project [120], [121], [123], [125], [128], [129], [131]-[134]. Different models have been proposed, each applicable for the actual measurement condition. With an attempt to describe all of the different propagation conditions in one single model, the approach described below is suggested. The parameters in the model are defined in Fig. 4.6.1.

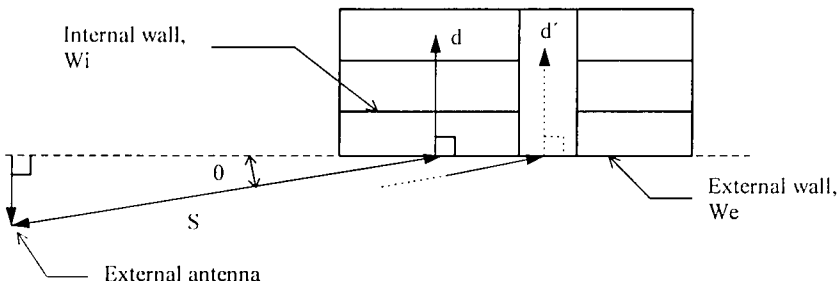


Fig. 4.6.1 Definition of grazing angle  $\theta$  and distances  $D$ ,  $S$  and  $d$ . In the building an example of a possible wall layout at one single floor is shown. The distance  $d$  is a path through internal walls and the distance  $d'$  is a path through a corridor without internal walls.

The total path loss between isotropic antennas is determined with the following expression:

$$\begin{aligned} L / \text{dB} = & 32.4 + 20 \log(f) + 20 \log(S + d) \\ & + W_e + WG_e \cdot \left( 1 - \frac{D}{S} \right)^2 + \max(\Gamma_1, \Gamma_2) \end{aligned} \quad (4.6.1)$$

$$\Gamma_1 = W_i \cdot p \quad (4.6.2)$$

$$\Gamma_2 = \alpha \cdot (d - 2) \cdot \left(1 - \frac{D}{S}\right)^2 \quad (4.6.3)$$

$D$  and  $d$  are the perpendicular distances and  $S$  is the physical distance between the external antenna and the external wall at the actual floor. All distances are in metres, frequency is in GHz. The angle is determined through the expression  $\sin(\theta) = D/S$  [134]. The only case when  $\theta = 90$  degrees is when the external antenna is located at the same height as the actual floor height and at perpendicular distance from the external wall, i.e. when  $D = S$ . Hence,  $\theta$  changes considerably with floor height at short distances  $D$ .  $W_e$  is the loss in dB in the externally illuminated wall at perpendicular penetration  $\theta = 90$  degrees.  $WG_e$  is the additional loss in dB in the external wall when  $\theta = 0$  degrees.  $W_i$  is the loss in the internal walls in dB and  $p$  is the number of penetrated internal walls ( $p = 0, 1, 2, \dots$ ). In the case that there are no internal walls, as along  $d'$  shown in Fig. 4.6.1, the existing additional loss is determined with  $a$  in dB/m. It should be noted that  $\Gamma_1$  can be replaced with  $\beta d$ , with  $\beta$  in dB/m, if the average indoor wall loss  $W_i$  and the average distance between the indoor walls are known.

The suggested model assumes free space propagation path loss between the external antenna and the illuminated wall and is not based on an outdoor reference level. This approach has been found to be valid also for line of sight conditions at small angles  $\theta$  in street micro-cells even when the path loss has been larger than free space propagation close to the surface outside the external wall. It has also been found that the model seems to generate an appropriate total loss in a street micro-cell environment, with buildings at both sides of the street, for the case when the external wall is obstructed from true line of sight conditions due to slightly shadowing neighbouring buildings [133]. In street micro-cells with buildings on both sides of the street, it could be appropriate not to use the actual distance  $D$  if it is very small. Due to reflections at the walls on the opposite side of the street, a larger value might be more suitable, e.g. half the width of the street. The model is based on measurements in the frequency range from 900-1800 MHz and at distances up to 500 m. The floor height dependence at short distances is based on very few measurements and the validity of the model for this case is vague. At short distances it might be appropriate to apply the indoor propagation models. It should be noted that the model fits the general behaviour of the path loss variation at different conditions quite well when many buildings are considered, however, there can be considerable

deviations for some explicit buildings. The following parameter values are recommended in the model:

$W_e$  : 4 - 10 dB, (concrete with normal window size 7 dB, wood 4 dB)

$W_i$  : 4 - 10 dB, (concrete walls 7 dB, wood and plaster 4 dB)

$WG_e$ : about 20 dB

$\alpha$  : about 0.6 dB/m

The wall loss is not necessarily the physical loss for a single homogeneous wall, it is the loss that gives reasonable agreement when the model is applied and it includes objects in the building, such as cupboards, shelves and other furniture. Thin wood or plaster walls can give rise to lower losses than 4 dB and concrete walls without windows 10-20 dB. Increasing window sizes decreases the loss and vice versa. Metallized window-glass or metal reinforced glass can give rise to losses considerable greater than 10 dB. An absolute value is difficult to give, due to that one must also consider the size of the window and the amount of power that penetrates through the wall around the window. A combination of metal covered walls and metallized window-glass can give rise to quite high loss levels.

Typical floor losses, 900-1800 MHz, for buildings along a street with small grazing angles  $\theta$  in an urban environment at distances  $S$  greater than 150 m is in the range of 27-37 dB and the large scale variation at one single floor is usually close to a log-normal distribution with a standard deviation from about 5-10 dB. At short distances, the floor loss can vary considerably, especially when it is related to the loss in the street at about 2 m height. This behaviour corresponds with the characteristic of the model which will give rise to a considerable variation due to its angle and distance dependence,  $\theta$  and  $d$ . Typical floor losses, 900-1800 MHz, at one single floor level vary in the range of about 4-37 dB with a standard deviation of the large scale variation, at one single floor level, of 5-15 dB. For this case, strong deviations from the log-normal distribution can occur quite often. It has been reported that the time dispersion in urban street micro-cells does only increase slightly in a building compared to the level in the street [132].

#### 4.6.3 Penetration loss at non line of sight conditions

For the scenarios shown below, the penetration loss is related to the outside loss  $L_1$  and  $L_2$  in Fig. 4.6.2, and  $L_a$  and  $L_b$  in Fig. 4.6.3, at about 2 m height above the ground.

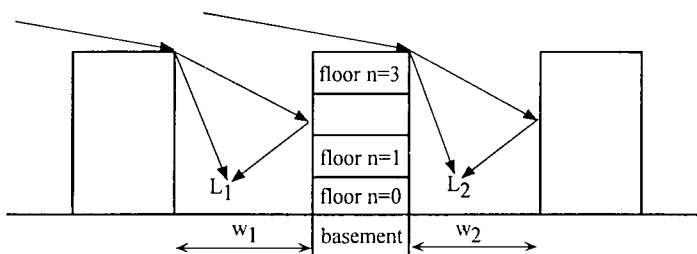


Fig. 4.6.2 Non line of sight scenario when the external antenna is located above the building height. The penetration loss is related to  $L_1$  or  $L_2$ .

The floor height gain values given below are relevant when the width  $w_1$ , see Fig. 4.6.2, in the direction towards the external antenna is about 10-50 m. When  $w_1$  increases, the floor height gain will decrease.

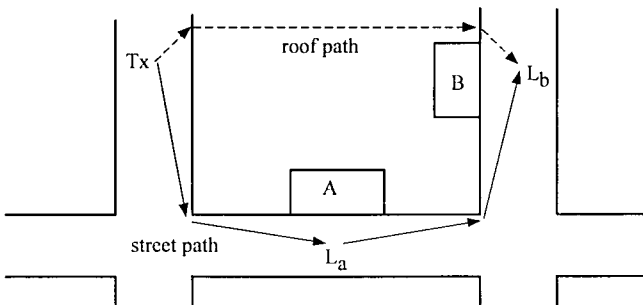


Fig. 4.6.3 Non line of sight scenario when the external antenna is located below the building height. The total area, except the streets, is assumed to be covered with buildings, though only building A and B are displayed. The penetration loss is related to  $L_a$  and  $L_b$ .

For the case when the penetration loss is related to  $L_2$ , the floor height gain will generally be less dependent of the width  $w_2$ . The total loss between isotropic antennas relative the outside reference loss,  $L_{\text{outside}}$ , is determined with the following equation [123], [124], [126], [130]-[132]:

$$L / \text{dB} = L_{\text{outside}} + W_c + W_{ge} + \max(\Gamma_1, \Gamma_3) - G_{FH} \quad (4.6.4)$$

$$\Gamma_3 = \alpha \cdot d \quad (4.6.5)$$

$$G_{FIH} = \begin{cases} n \cdot G_n \\ h \cdot G_h \end{cases} \quad (4.6.6)$$

$W_e$ ,  $\Gamma_1$ , and  $d$  are similar to the corresponding definitions in the section above, line of sight conditions. The floor number is determined by  $n$ , see Fig. 4.6.2, and  $G_n$  is the floor height gain in dB/floor while  $G_h$  is the height gain in dB/m.  $h$  is the height in metres above the outdoor reference path loss level. Reported penetration losses of the external walls differ considerably, due to different measurement methods and, of course, due to different buildings. However, there might be a physical explanation of the noticed difference, which could justify the parameter  $W_{ge}$  in the model, which is introduced in order to achieve unambiguous basic wall penetration losses.

The waves impinging on the external wall are distributed over a wide range of angles. Thus, by considering the angle dependent penetration loss, the loss will be larger compared to the case when one single wave, with equal power, penetrates perpendicularly through the wall. The difference should be more pronounced when one or several dominant waves are arriving at non perpendicular angles, which is most probable in this scenario. Another phenomenon, which could explain the increased penetration loss, is that the measured outside reference level is received from a combination of waves in the direction towards and waves reflected from the building, where the latter of course will not penetrate through the building. Similar condition is valid when perpendicular line of sight measurements are taken (with an omni antenna), but the relative power levels of the direct and the reflected wave will then be different and the direct wave will not suffer from extra angle dependent penetration loss. A value of about 3-5 dB is suggested for  $W_{ge}$  at 900 MHz. In some measurements it has been found that the floor penetration loss increases 2 dB at 1800 MHz compared to 900 MHz, thus it is suggested that  $W_{ge}(1800 \text{ MHz}) = W_{ge}(900 \text{ MHz}) + 2 \text{ dB}$ . The values on  $W_e$  and  $W_i$  given in the section above (LOS conditions) are recommended to be used. The  $a$  parameter has not been measured explicitly for this kind of scenario. Thus, at the moment, the value given in the section above (LOS conditions) is recommended, i.e.  $\alpha = 0.6 \text{ dB/m}$ . Reported values on  $G_n$  at 1800 MHz can be divided into two groups, in the range of 1.5-2 dB/floor and from 4-7 dB/floor. The latter values were taken from buildings with storey heights of about 4-5 m and it was found more appropriate to use the parameter  $G_h$  for these buildings, which varied from 1.1-1.6 dB/m at 1800 MHz. The floor height gain is lower at 900 MHz, but the difference is small. Floor

penetration loss at 1800 MHz has been found to vary between different buildings on the ground floor,  $n=0$ , from about 12-20 dB. The corresponding losses at 900 MHz were found to be about 2 dB lower. The large scale variation is log-normal, if there is no partial line of sight to the external wall, with a standard deviation of about 4-6 dB. No frequency dependence of the standard variation has been reported. The penetration loss into the basement, is about 20-30 dB, which can be either smaller or larger.

#### 4.6.4 General building penetration model

It has been found that the best method in order to estimate the received power at a fixed location within a building, is to consider all the paths through the external walls as shown in Fig. 4.6.4 [131], [132]. For each path, the received power is determined according to the methods described above and the sum of these separate power levels will then be the total received power. Those paths that are expected to give rise to loss levels far greater than the remaining paths, can of course be omitted.

The results in this chapter are based on measurements in the following towns and theoretical work performed by: Vienna, Technische Universität Wien (A), Aalborg, Aalborg University (DK), Turin, CSELT, (I), Madrid (E)/Telefónica Investigación y Desarrollo, Stockholm (S)/Telia Research and Ericsson Radio Systems, Ipswich, Liverpool, London (UK) by British Telecom Research Laboratories, The University of Liverpool, and The University of Leeds.

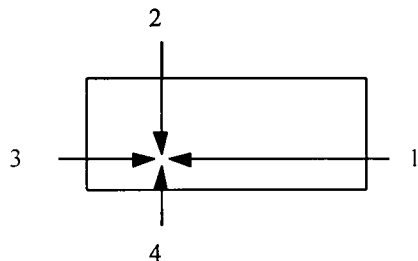


**Fig. 4.6.4** Relevant propagation paths into a building.

## 4.7 Indoor Propagation Models

**Jaakko Lähteenmäki , VTT Information Technology, Finland**

### 4.7.1 General

Predicting the propagation characteristics between two antennas inside a building is important especially for the design of cordless telephones and WLANs (Wireless local area networks). Also the design of cellular systems with indoor base stations involves the use of indoor propagation models.

The indoor propagation channel differs considerably from the outdoor one. The distance between transmitter and receiver is shorter due to high attenuation caused by the internal walls and furniture and often also because of the lower transmitter power. The short distance implies shorter delay of echoes and consequently a lower delay spread. The temporal variations of the channel are slower compared to the conditions where the mobile antenna is mounted on a car. As is the case in outdoor systems, there are several important propagation parameters to be predicted. The path loss and the statistical characteristics of the received signal envelope are most important for coverage planning applications. The wide-band and time variation characteristics are essential for evaluation of the system performance by using either hardware or software simulation.

The considered propagation models are divided into four groups: empirical narrow-band models, empirical wide-band models, models for time variations and deterministic models. Empirical narrow-band models are expressed in a form of simple mathematical equations which give the path loss as the output. The equations are obtained by fitting the model to measurement results. Empirical wide-band models are expressed in a form of a table listing average delay spread values and typical power delay profile (PDP) shapes. Models for time variations are used for example to estimate the Doppler spectrum of the received signal. Deterministic models are calculation methods which physically simulate the propagation of radio waves. These models yield both narrow-band and wide-band information of the channel.

All of the presented models are based on propagation measurements. The measurement techniques and analysis are described in Sec. 2.2 and Sec. 2.3. Propagation measurements have mostly been carried out at 1800 MHz which

is most appropriate considering the future indoor systems. Scaling of results to other frequency bands will be discussed.

#### 4.7.2 Empirical narrow-band models

Three types of empirical indoor models have been investigated.

The ***one-slope model (ISM)*** assumes a linear dependence between the path loss (dB) and the logarithmic distance

$$L = L_0 + 10n \cdot \log(d) \quad (4.7.1)$$

where

$L_0$  = the path loss at 1 meter distance,

$n$  = power decay index,

$d$  = distance between transmitter and receiver in metres.

This model is easy to use, because only the distance between transmitter and receiver appears as an input parameter. However, the dependency of these parameters on environment category (Tab. 2.3.1) has to be taken into account.

The multi-wall model [135]-[139] gives the path loss as the free space loss added with losses introduced by the walls and floors penetrated by the direct path between the transmitter and the receiver. It has been observed that the total floor loss is a non-linear function of the number of penetrated floors. This characteristic is taken into account by introducing an empirical factor  $b$  [139]. The ***multi-wall model (MWM)*** can then be expressed in form

$$L = L_{FS} + L_c + \sum_{i=1}^I k_{wi} L_{wi} + k_f \left[ \frac{k_f + 2}{k_f + 1} - b \right] L_f \quad (4.7.2)$$

where

$L_{FS}$  = free space loss between transmitter and receiver,

$L_C$  = constant loss,

$k_{wi}$  = number of penetrated walls of type  $i$ ,

$k_f$  = number of penetrated floors,

$L_{wi}$  = loss of wall type  $i$   
 $L_f$  = loss between adjacent floors,  
 $b$  = empirical parameter,  
 $I$  = number of wall types.

The constant loss in (4.7.2) is a term which results when wall losses are determined from measurement results by using the multiple linear regression. Normally it is close to zero. The third term in (4.7.2) expresses the total wall loss as a sum of the walls between transmitter and receiver. For practical reasons the number of different wall types must be kept low. Otherwise, the difference between the wall types is small and their significance in the model becomes unclear. A division into two wall types according to Tab. 4.7.1 is proposed.

It is important to notice that the loss factors in (4.7.2) are not physical wall losses but model coefficients which are optimised along with the measured path loss data. Consequently, the loss factors implicitly include the effect of furniture as well as the effect of signal paths guided through corridors.

Wall type	Description
Light wall ( $L_{w1}$ )	A wall that is not bearing load: e.g. plasterboard, particle board or thin (<10 cm), light concrete wall.
Heavy wall ( $L_{w2}$ )	A load-bearing wall or other thick (>10 cm) wall, made of e.g. concrete or brick.

Tab. 4.7.1 Wall types for the multi-wall model.

The third considered propagation model is the **linear attenuation model (LAM)**, which assumes that the excess path loss (dB) is linearly dependent on the distance (m), where  $\alpha$  (dB/m) is the attenuation coefficient:

$$L = L_{FS} + \alpha d \quad (4.7.3)$$

In some studies wall loss terms are added to the linear model which improves the performance to some extent since degrees of freedom is increased [140]. In the following the LAM is used in the simple form of (4.7.3).

#### *Optimised model coefficients*

The measurements listed in Table 2.3.2 have been used to optimise model coefficients for the three empirical models presented in the previous section.

The overall results calculated as an average of the available results from each environment category are listed in Table 4.7.2.

The multi-wall model coefficients have been optimised for the measurement category "dense". However, it can also be used in the other environments where the number of walls is small and multi-wall model yields results close to free space values.

The results given in Tab. 4.7.2. are relevant to buildings having normal type of furniture. In UPC the effect of furniture was studied. A decrease from 3.8 to 3.4 in the decay exponent was observed.

Environment	One slope model (ISM)		Multi-wall model (MWM)			Linear model (LAM)	
	$L_0$ [dB]	n	$L_{w1}$ [dB]	$L_{w2}$ [dB]	$L_f$ [dB]	b	a
Dense							
one floor	33.3 <sup>3)</sup>	4.0 <sup>3)</sup>	3.4 <sup>1)</sup>	6.9 <sup>1)</sup>	18.3 <sup>2)</sup>	0.46 <sup>9)</sup>	0.62 <sup>10)</sup>
two floors	21.9 <sup>4)</sup>	5.2 <sup>4)</sup>					
multi floor	44.9 <sup>4)</sup>	5.4					2.8 <sup>4)</sup>
Open	42.7 <sup>5)</sup>	1.9 <sup>5)</sup>	3.4 <sup>1)</sup>	6.9 <sup>1)</sup>	18.3 <sup>2)</sup>	0.46 <sup>9)</sup>	0.22 <sup>8)</sup>
Large	37.5 <sup>6)</sup>	2.0 <sup>6)</sup>	3.4 <sup>1)</sup>	6.9 <sup>1)</sup>	18.3 <sup>2)</sup>	0.46 <sup>9)</sup>	
Corridor	39.2 <sup>7)</sup>	1.4 <sup>7)</sup>	3.4 <sup>1)</sup>	6.9 <sup>1)</sup>	18.3 <sup>2)</sup>	0.46 <sup>9)</sup>	

<sup>1)</sup>Alcatel, CNET, TUW, UPC, VTT; <sup>2)</sup>Alcatel, CNET, UPC, VTT; <sup>3)</sup>UPC, TUW;  
<sup>4)</sup>VTT; <sup>5)</sup>TUW; <sup>6)</sup>VTT, UPC; <sup>7)</sup>Alcatel; <sup>8)</sup>Lund; <sup>9)</sup>VTT, Ericsson; <sup>10)</sup>TUW, Lund

Tab. 4.7.2 Results for model coefficients for path loss models at 1800 MHz. The expressions „one floor“, „two floors“ and „multi floor“ mean that Tx and Rx have been within the same floor, within two adjacent floors or within more than two floors.

#### Frequency dependency

Measurements in 5 buildings ([141], [142]) at both 900 MHz and 1800 MHz bands have been conducted. In these measurements the separation of receiver and transmitter is up to 5 floors. According to the results the path loss difference between the frequency bands is typically slightly higher than would be predicted in free space. Considering the Multi-wall model, a difference of 1.5 dB in the light wall loss and a difference of 3.5 dB in the floor loss were reported. This is in line with the results of Ericsson, which report 2.1 dB loss for plasterboard wall at 900 MHz [139]. Considering the One slope model,  $L_0$  should be reduced by 10 dB [141] in the multi floor

case. In the single floor case the appropriate reduction is 7-8 dB. For the decay index,  $n$ , same value may be applied both at 900 MHz and at 1800 MHz.

### *Fading*

The empirical propagation models presented above yield the mean path loss at a given location. In practical application of the models it is important to know also the statistics of the received signal. Two fading mechanisms can be identified: long term fading and short term fading.

In indoor environments the long term fading is understood as fluctuations of the mean value calculated over a distance of a few wavelengths. According to measurements in Lund and UPC the indoor long term fading follows log-normal distribution with  $\sigma = 2.7\text{-}5.3$  dB. Short fading has been observed to follow Rice and Rayleigh distributions. The K-value varies from negative values (Rayleigh distribution) in NLOS conditions up to 14.8 dB in clear LOS conditions.

Temporal short term fading is understood as fast fluctuations of the signal level caused by movements in the propagation environment. In environments with low level of movements or LOS condition the temporal fading has been observed to follow the Rice distribution with  $K=7\text{-}14$  dB. In an environment with NLOS condition and a lot of movements in the environment, the temporal fading follows the Rayleigh distribution [143]. In [144] the Weibull and Nakagami distributions have been found best in describing the temporal variability.

#### **4.7.3. Empirical wide-band models**

Empirical wide-band model is considered as a means for evaluation of the delay spread and average power delay profile (PDP). One of these two factors together with Doppler characteristics (see Sec. 2.1) are typically required as an input to system simulations. The overall results (i.e. results averaged over an environment category) of wide-band measurements are listed in Table 4.7.3. As expected, the delay spread has lowest values in dense environment and larger values in open and large environments. The dependency of the delay spread on the dimensions of the environment can even be utilised in prediction as shown in [136], [140], [145].

Environment	Average rms delay spread [ns]	Variability of rms delay spread [ns]	Typical profile shape
Dense: Lund	22.5	5-40 <sup>1)</sup>	power/exponential
VTT	15.3	3.4 <sup>2)</sup>	exponential
TUW	20.0	8-31 <sup>3)</sup>	-
<b>Average</b>	<b>19.3</b>		
Open: Lund	35.0	5-95 <sup>1)</sup>	power
VTT	17.7	3.1 <sup>2)</sup>	power
ETH	30.5	4.1 <sup>2)</sup>	exponential
<b>Average</b>	<b>27.7</b>		
Large: VTT	55.4	27.2 <sup>2)</sup>	exponential
ETH	79.4	4.3 <sup>2)</sup>	exponential
<b>Average</b>	<b>67.4</b>		

1)Peak-to-peak of instantaneous delay spread, 2)Standard deviation of delay spread local averages, 3)Peak-to-peak of delay spread local averages

Tab. 4.7.3 Delay spread and PDP shape in different environments.

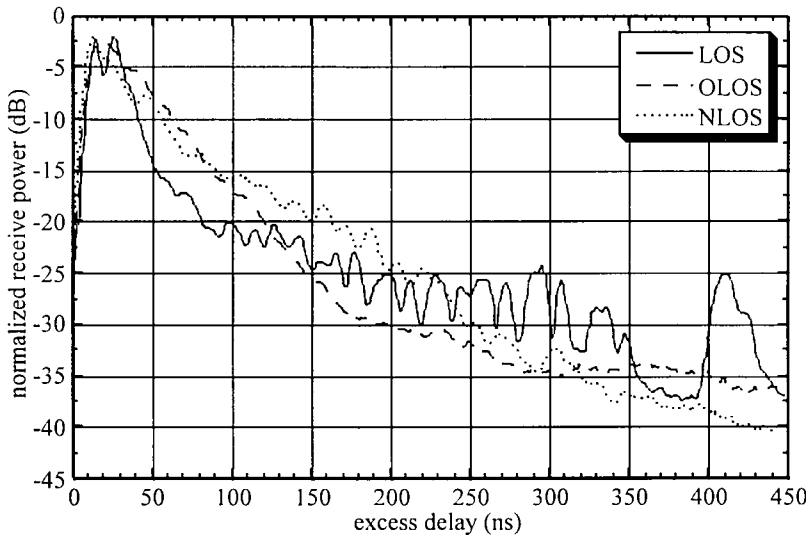


Fig. 4.7.1 Overall average power delay profiles in three configurations (Lund).

Although instantaneous values and local averages of the PDP may include a lot of environment dependent details, the overall average PDP has quite regular shape. As seen in Table 4.7.3, the PDP in dense environment has been observed to follow either power function (the decay is logarithmic in

dB scale) or exponent function (the decay is linear in dB scale). In open environment the PDP follows best the power function, because of the strong effect of the direct path. Typical averaged power delay profiles in Line-of-sight (LOS), Non-line-of-sight (NLOS) and Obstructed-line-of-sight (OLOS) conditions are shown in Fig. 4.7.1. OLOS means a condition where the direct path is blocked only by one obstacle, e.g. a piece of furniture.

#### 4.7.4 Modelling the time fluctuations of the indoor channel

**Bernard Fleury, Aalborg University, Denmark**

Time variations of the indoor radio channel essentially result from the following three mechanisms: As the location of the receiving antenna changes, the spatial fluctuations of the electric field along the receiver trajectory are translated into corresponding time variations. Time variability also arises when the orientation of the antenna changes, due to its usually non-isotropic field pattern. Finally, movements of scattering objects such as persons or furniture also contribute to make the channel system functions time-variant. Time-variations of the mobile channel have been studied earlier e.g., in [146]-[148]. Almost all attention has focused on the time-variability resulting from receiver movements with constant velocity. However, the consideration of such receiver displacements in the indoor environment is questionable since they are not realistic for describing human motion. Moreover, they force to restrict the investigations of the spatial field dependency to one specific direction determined by the receiver velocity vector. Finally, such movements do not allow to take the Doppler rate, i.e., the change of Doppler frequency, into account.

A stochastic model is proposed which reproduces a succession of realistic typical human movements performed in a random manner [149]. The model derivation relies on deterministic models which have been empirically derived from free arm movements (see references reported in [149]). The receiver trajectory is modelled as:

$$\vec{x}(t) = g(t / T) \cdot \left[ \sum_{i=1}^{\infty} \Delta \vec{x}_i \delta(t - t_i) \right] \quad (4.7.4)$$

where

$\{t_i\}$  is an homogeneous Poisson process with expected occurrence rate L,

2.  $\{\Delta \vec{x}_i\}$  is a sequence of independent random vectors with zero mean and covariance matrix  $\zeta I_3$ , with  $I_3$  being the 3-dimensional identity matrix,
3. the two sequences  $\{t_i\}$  and  $\{\Delta \vec{x}_i\}$  are independent.

The random 3-dimensional step process within the brackets describes the succession of new or corrective actions. It is convoluted with an appropriately time-scaled unit stroke function  $g(t)$  which models the smoothing due to body inertia. Under the usual assumptions on the phase of the incident waves, the time-variant channel resulting from receiver displacements according to (4.7.4) is WSSUS over the time interval  $[T, \infty)$  with a scattering function of the form:

$$P(\tau, v) = P(\tau) \cdot P_n(v) \quad (4.7.5)$$

where  $P(t)$  and  $P_n(n)$  are the power delay profile and the normalised power Doppler profile, respectively, of the channel. The normalised time correlation function of the channel, which is the inverse Fourier transform of  $P_n(n)$  has been derived in [149].

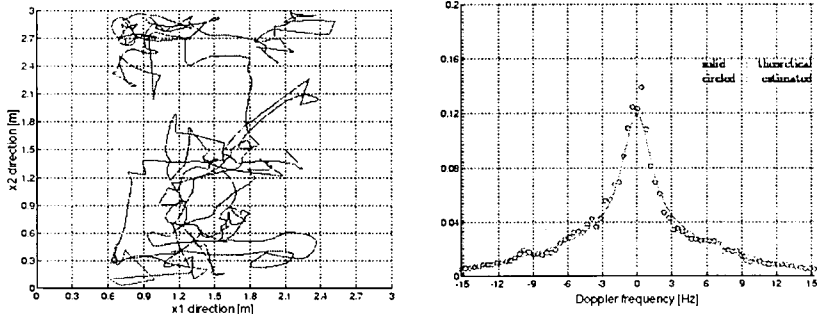


Fig. 4.7.2: a) Simulated receiver trajectory b) Estimated and theoretical normalised power Doppler profile.

A realisation of the first two components of  $\vec{x}(t)$  is depicted in Fig. 4.7.2.a. The normalised power Doppler profile has been estimated in a real environment where the receiving antenna performs random movements according to (4.7.4) with the above setting. In Fig. 4.7.2.b, the estimate of  $P_n(n)$  is compared with the curve theoretically derived from the model. For

the simulation, the parameter values and the unit stroke have been selected as follows [149]:

$$g(t) = \begin{cases} 0 & ; t < 0 \\ -t^3(15t - 6t^2 - 10) & ; 0 \leq t \leq 1 \\ 1 & ; t > 1 \end{cases} \quad (4.7.6)$$

$$T=220 \text{ ms}, \varsigma=10 \text{ cm}, \Lambda = 10 \text{ s}^{-1}$$

#### 4.7.5. Deterministic models

**Jaakko Lähtenmäki, VTT Information Technology Finland**

**Dieter J. Cichon, IBP Pietzsch, Germany**

Deterministic models are used to simulate physically the propagation of radio waves. Therefore the effect of the environment on the propagation parameters can be taken into account more accurately than in empirical models. Another advantage is that deterministic models make it possible to predict several propagation parameters. For example, the path loss, impulse response and angle-of-arrival can be predicted at the same time.

Several deterministic techniques for propagation modelling can be identified. For indoor applications, especially, the Finite Difference Time Domain (FDTD) technique and the geometrical optics (GO) technique have been studied. In COST 231 the main effort is on the geometrical optics which is more computer efficient than the FDTD. There are two basic approaches in the geometrical optics technique. The ray launching approach and the image approach. Computational complexity of ray-tracing methods is considered in [150].

##### *Ray launching model (RLM)*

The ray launching approach involves a number of rays launched at the transmit antenna in specified directions. For each ray its intersection with a wall is determined and the incident ray is divided into a wall penetrating ray and a reflected ray; each of them is traced to its next intersection and so on. A ray is terminated when its amplitude falls below a specified threshold, or a chosen maximum number of ray-wall interactions are succeeded. In, e.g., [151] a uniform angular separation of launching rays is maintained, where the spherical surface is subdivided by a geodesic polyhedron with resulting hexagonally shaped, wavefront portions, which are further approximated by

circular areas. Whether a ray reaches a receiver point or not can be accomplished by a reception sphere [152].

In Fig. 4.7.3 a two-dimensional view of the reception sphere is shown, where the unfolded total path length  $d$  and the angular separation  $\gamma$  of adjacent rays launched at Tx determine its radius  $R_{rs}$ :

$$R_{rs} = \gamma d / \sqrt{3} \quad (4.7.7)$$

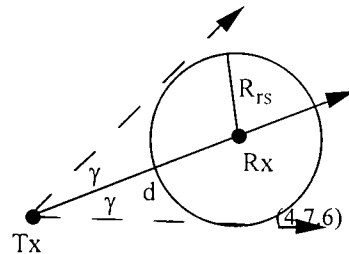


Fig. 4.7.3 2D view of the reception sphere.

However this is an approximate solution for the 3D propagation case. To achieve a complete solid angle discretisation under maintenance of unambiguous and practical reception determination, the entire solid angle  $4\pi$  is subdivided into rectangularly shaped, incremental portions of the spherical wavefront [153], [154]. In [102], [154] the propagation directions  $\theta_i$  and  $\psi_i$  of the central rays of the ray tubes and the corresponding ray tube angles  $\Delta\theta_i$  and  $\Delta\psi_i$  as depicted in Fig. 4.7.4 are determined by (4.7.8) and (4.7.9).

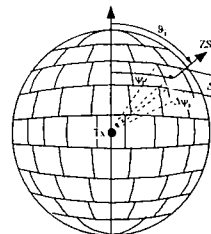


Fig. 4.7.4 Ray launching.

$$\Delta\psi_i(\theta_i) = \frac{\Delta\theta}{\sin \theta_i} \quad (4.7.8)$$

$$\theta_i = \frac{\Delta\theta}{2} + (i-1)\Delta\theta, \quad i = 1 \dots N_\theta, \quad \Delta\theta = \text{const.} \quad (4.7.9)$$

Ray launching approaches are flexible, because diffracted and scattered rays can also be handled along with the specular reflections,. To maintain a sufficient resolution the so called "ray splitting technique" can be used as given in [153] and [103].

#### *Image approach method (IAM)*

The image approach [112], [155] makes use of the images of the transmit antenna location relative to all the surfaces of the environment. The co-ordinates of all the images is calculated and then rays are traced towards these images. First and second order reflections can be calculated very fast

without sending rays to all directions. The disadvantage is that calculation time grows exponentially when the order of calculated reflections is increased. Therefore the image approach is suitable for semi-deterministic modelling, where the main signal paths, i.e. direct path and most important specularly reflected and diffracted rays are calculated in a deterministic way while more complicated phenomena are taken into account by using empirical factors. The effect of bookshelves and cupboards covering considerable parts of walls is taken into account by including an additional loss to the wall penetration loss. An additional loss of 3 dB was observed to be appropriate. This additional loss is introduced in context of walls covered by bookshelves, cupboards or other large pieces of furniture. Furthermore, it was found necessary to set an empirical limit for the wall transmission loss which otherwise becomes very high when the angle of incidence is large. The wall transmission loss is limited to twice the value (in dB) for normal incidence.

Material	Uni-Karlsruhe (ray launching)		VTT (image approach)		Typical thickness
	$\epsilon_r'$	$\epsilon_r''$	$\epsilon_r'$	$\epsilon_r''$	
concrete	9	0.9	6	0.7	25 cm
light concrete	-	-	2	0.5	10 cm
brick	-	-	4	0.1	13 cm
plasterboard	6	0.6	2.5	0.1	2 x 1.3 cm
particle board	-	-	3	0.2	2 x 1.3 cm
wood	2.5	0.03	-	-	5 cm
glass	6	0.05	6	0.05	2 x 0.3 cm
bookshelf	2.5	0.3	-	-	30 cm

Tab. 4.7.4 Material parameters [156]-[158]

#### *Building information*

Deterministic models require detailed building information, i.e. location and material parameters of walls, floors and even furniture. Usually, accurate information of materials and internal structures of walls and floors is not available and somewhat approximate values have to be adopted. The used material parameters are listed in Tab. 4.7.4. Also the typical thickness for an internal wall of each material is given.

#### 4.7.6 Comparison of the performance of the path loss models

Jaakko Lähtenmäki, VTT Information Technology Finland

**Dieter J. Cichon, IBP Pietzsch, Germany**

The performance of the propagation models was tested against three data sets. The data sets are labelled according to the organisation who has performed the measurements: Alcatel, TUW and VTT. Each building under test has normal office furniture. In one building (VTT) the base station (BS) is in different floor than most of the mobile stations. In the other buildings BS and the mobile stations are in the same floor.

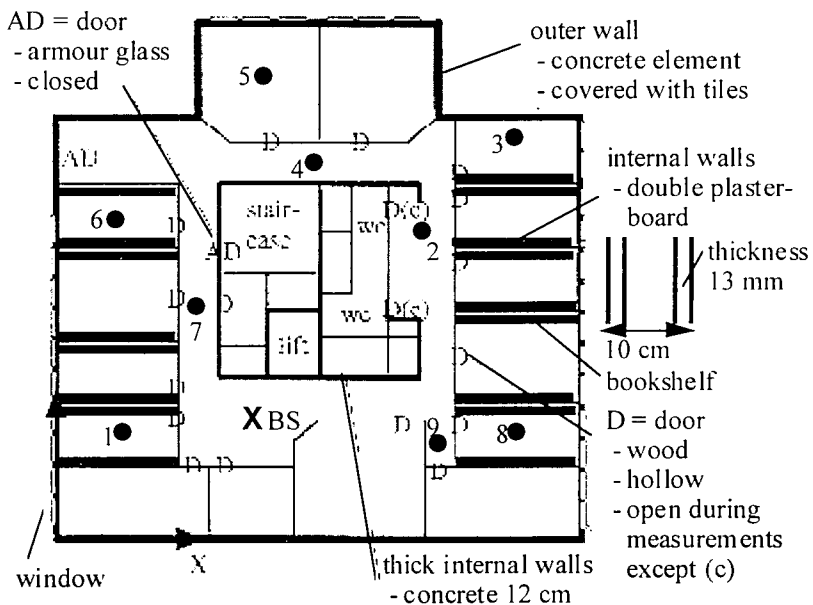


Fig. 4.7.5 Map of the 2nd floor of the office building (data set: VTT) with marked base and mobile locations (1-9).

The Alcatel data set is measured in an indoor environment with a typical office architecture: Large office rooms are located along a main corridor. Internal walls are made of thin wood panel and they are classified as "light walls". The environment category is "open" and it includes 56 measurement points. There are two base station locations: transmitter in the corridor and transmitter in one of the working rooms.

The TUW data set is measured in a "dense" indoor environment consisting of mostly small office rooms along a corridor. The walls are made of concrete and brick and they are classified as "heavy". The data set includes 40 measurement points.

The VTT data set is measured in a 7-floor building. The material of the internal walls of the working rooms is plasterboard ("light walls"). The walls in the centre of the building are concrete/light concrete ("heavy"). The data set belongs to category "dense" and it includes 9 measurement points within the same floor with the base station, which is in the second floor, and 45 measurement points are distributed in floors 3-7. For the testing of the RLM model, only the data from floors 2-5 have been used. The floor plan of the second floor is shown in Fig. 4.7.5. Other floors are essentially similar. Considering the propagation between floors, it is important to note that a similar building is located at 80 metre distance and another building having 2 floors is located at 15 metre distance.

Table 4.7.5 lists means and standard deviations (STD) of the prediction errors of the 5 models in case of single-floor propagation. The ray-launching model (RLM) takes into account up to 5 reflections and 12 transmissions per ray; the image model (IAM) is also a three-dimensional model and takes into account first and second order reflection as well as 3 most important diffraction points. The diffraction is calculated by using the Uniform Geometrical Theory of Diffraction (UTD). The empirical one-slope model and linear model are included for reference. Mean prediction errors and standard deviations in case of multi-floor propagation for mobile locations in the 3rd-4th floor and in the 3rd-5th floor, respectively, are given in Tab. 4.7.6.

	ISM		MWM		LAM		IAM		RLM	
data set / frequency	STD (dB)	mean (dB)								
Alcatel, O; 1900 MHz	5.7	-1.6	4.2	2.2	4.7	-0.8	4.3	-0.4	-	-
TUW, D; 1800 MHz	10.0	-0.7	9.5	-10.3	7.8	-7.5	7.0	-3.8	-	-
VTT, D; 2nd floor only; 856 MHz	8.6	19.2	4.4	-4.5	8.5	4.7	6.0	-11.7	4.2	3.3
	7.5	20.6	2.0	-2.7	8.4	6.5	4.1	-2.8	8.9	3.3

Tab. 4.7.5 Performance of the models for single floor propagation  
(mean error: predicted - measured path loss)

When analysing the results, it has to be noted that the three empirical models (using the coefficients given in Tab. 4.7.2) are compared to the measurement data without any fitting or adjustment. For the IAM, the furniture loss and the limit for the penetration loss were introduced after the first comparisons with the measurement data.

	1SM		MWM		LAM		IAM		RLM	
data set: VTT, D	STD (dB)	mean (dB)	STD (dB)	mean (dB)	STD (dB)	mean (dB)	STD (dB)	mean (dB)	STD (dB)	mean (dB)
3rd-4 <sup>th</sup> floor: 856 MHz 1800 MHz	10.3 12.2	-2.7 -7.3	8.3 7.1	-8.2 -11.1	10.2 11.6	-16.1 -20.3	9.0 11.3	-2.7 10.3	6.2 8.7	0.3 0.1
3rd-5 <sup>th</sup> floor: 856 MHz 1800 MHz	10.7 11.9	-7.1 -11.8	7.9 7.5	-7.2 -9.7	9.7 10.9	-19.6 -23.8	7.8 10.9	-2.6 11.7	9.1 11.8	-4.6 -5.7
3rd-7 <sup>th</sup> floor: 856 MHz 1800 MHz	9.6 10.0	-10.6 -14.1	9.4 10.2	-5.0 -5.9	8.6 9.8	-19.5 -22.7	8.4 13.5	-3.7 7.3	- -	- -

Tab. 4.7.6 Performance of the models for multi-floor propagation  
(mean error: predicted - measured path loss).

From the empirical models the Multi-wall model (MWM) gives best results although the difference to One slope model (1SM) is small. The MWM has a large mean error in TUW building where the heavy walls seem to be more lossy than in other buildings. The TUW building is relatively old (older part is built in 1910 and newer part is built in 1932) and the wall structures are thick especially between the old and new part of the building. All of the models perform well in the Alcatel building which is open and has a low number of walls. The advantage of the MWM and the deterministic models (IAM and RLM) is most clearly seen in the case when the transmitter and receiver are in different floors (VTT). The LAM yields worst results in average. One reason for this may be that the used values for attenuation coefficient are based on a small data set: Many COST 231 documents give model coefficients only for the MWM and the 1SM. Calculated and measured path loss values of the VTT data set in an office building are compared at a frequency of 856 MHz and 1800 MHz in Fig. 4.7.6 and Fig. 4.7.7, respectively. The mobile station is in the 2nd floor (points: 1-9), in the 3 rd floor (points: 10-18), in the 4th floor (points: 19-27) and in the 5th floor (points: 28-36). The general trend is that prediction accuracy is better when the vertical separation between transmitter and receiver is low. The performance of the 1SM and LAM is poor because they only take into account the distance and not the number of penetrated floors.

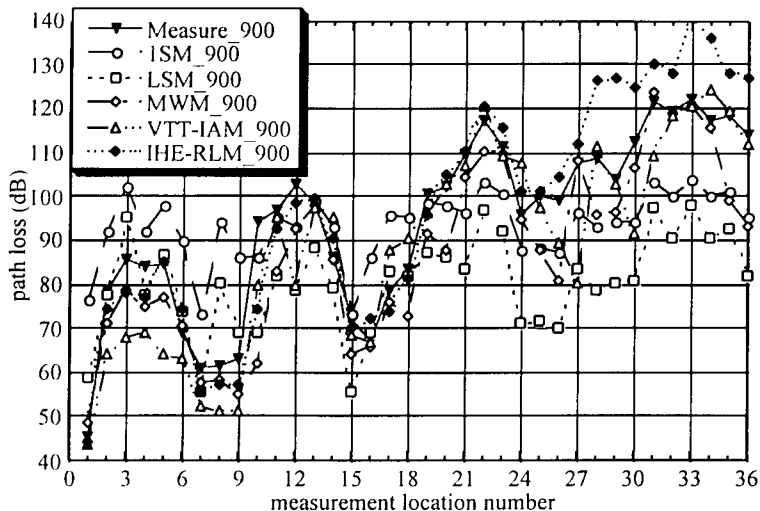


Fig. 4.7.6 Performance of empirical and ray optical propagation models at 856 MHz in 4 successive floors (base station in the 2nd floor; see Fig. 4.7.5).

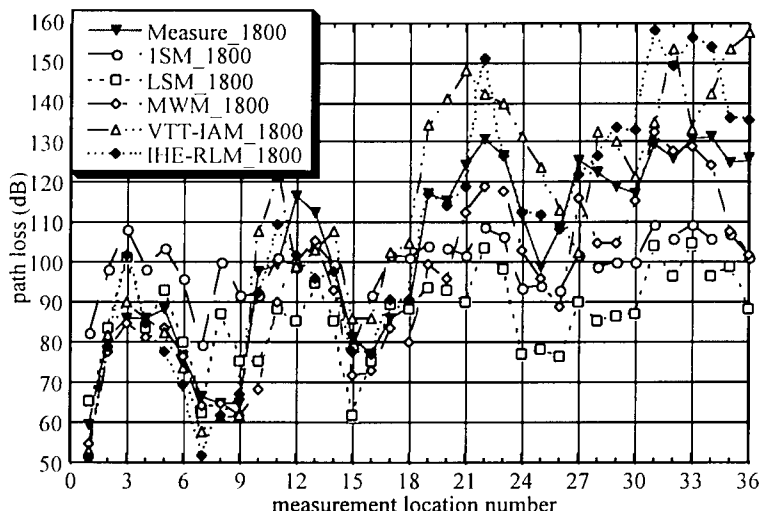


Fig. 4.7.7 Performance of empirical and ray optical propagation models at 1800 MHz in 4 successive floors (base station in the 2nd floor; see Fig. 4.7.5).

## 4.8 Tunnels, Corridors, and other Special Environments

Ernst Bonek , Technical University of Vienna, Austria

### 4.8.1 Tunnels

Wave propagation in tunnels shows different effects than in other environments due to guidance by the walls, at least at frequencies higher than 800 MHz. Even very rough tunnels driven into plain rock show good waveguiding when no installations are present [159]. The power loss observed is, in most cases, less than free space attenuation. There is a waveguiding gain, so to speak. Thus it is appropriate to consider the tunnel as an overmoded waveguide with lossy dielectric walls.

Power loss decreases with increasing frequency which is proven for frequencies up to 17 GHz by simulations and measurements, showing a slightly increasing slope of power loss up to 60 GHz [159]-[161]. Simulations of the GSM-SDCCH channel found the tunnel environment to be the least demanding case among rural or urban situations, and the lowest transmitter power is needed for a minimum  $E_b/N_0$  [162].

In tunnels, the distinction between short-term and large-scale fading is not as usual. In a smooth and straight tunnel short-term fading transforms into long and flat fades due to small phase differences between the individually reflected paths. Only close to the source short term effects caused by higher order mode excitation are observed. The source may be either an antenna inside the tunnel, the entrance aperture, or leaky feeder cables, or any secondary source, like vehicles or installations [163], [164]. If the source is distributed (leaky cable), short term fading occurs along the entire tunnel, of course. In contrast, feeding the tunnel by internal or external discrete antennas, there are usually only a small number of paths with about the same power incident at a given position. In general, heavier short term fading effects appear at higher frequencies despite the lower average loss, since the effective roughness of tunnel walls is wavelength dependent.

The small phase difference of individual paths with only few wall reflections tends to reduce the delay spread of the signal as it propagates further down the tunnel. (Paths with many reflections are subject to repeated reflection loss and die out fast.) This delay spread reduction by tunnel propagation has been experimentally proven [165]. It should be noted that corridors in buildings behave, very much like (short) tunnels, as waveguides.

Experimental proof has been given in [140] and [17]. The measured decrease in delay spread, after an expected initial rise, versus transmitter-receiver separation in a corridor is shown in Fig. 4.8.1. Multiple reflections caused by corridor ends have been measured and identified up to 8<sup>th</sup> order.

#### 4.8.2 Loss models and coverage

Different empirical models are proposed to describe propagation in tunnels as well as along corridors.

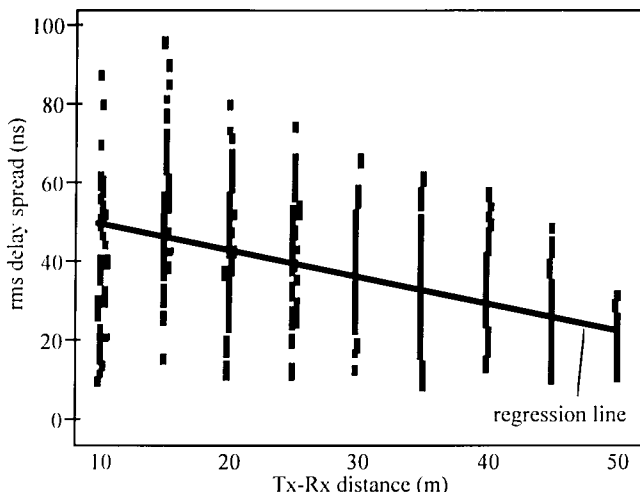


Fig. 4.8.1 Delay spread in a corridor versus Tx-Rx separation.

Commonly used are the standard model using parameter fitting (one-slope, two-slope), the waveguide model giving an attenuation in dB per unit length and the combination of both models (see also Sec. 4.7.2). Confined spaces with well-reflecting walls allow application of ray tracing approaches (see also Sec. 4.7.5). Some major effects in tunnels can be described using just a small number of rays, sometimes as few as two. As an example of the usefulness of ray tracing for tunnels, Fig. 4.8.2 compares a measurement run in a rather rough, irregularly shaped tunnel with a ray tracing simulation based on the simplifying assumption of rectangular cross section.

A slightly different point-of-view re-arranges all reflections into an array of image antennas [166]. This description leads to the hypothesis that all reference distances of propagation in tunnels or corridors should be given as multiples of the Rayleigh distance, called "critical distance",  $l_{\text{crit}}$ .

$$l_{\text{crit}} = \frac{D^2}{\lambda} \quad (4.8.1)$$

where  $D$  is the largest cross dimension of the waveguiding structure and  $\lambda$  is the free-space wavelength. At such a distance the phase differences between individual paths become smaller than a certain value (e.g.  $\lambda/2$ ). Coverage in road tunnels can be predicted by the following equation,

$$P_r = P_0 - l \cdot \alpha_0 \quad (4.8.2)$$

where  $P_r$  is the received power level in dB at a length  $l$  away from the antenna (down the tunnel),  $P_0$  is the reference level measured at  $l_0$  away from the antenna, and  $\alpha_0$  is the tunnel and frequency specific loss factor [165].

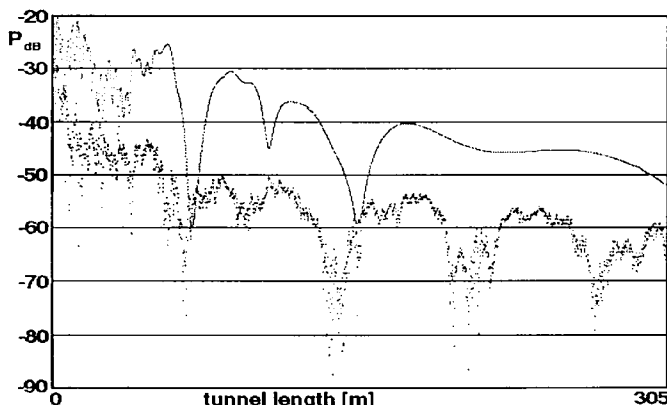


Fig. 4.8.2 Signal strength in a naturally rough tunnel at 960 MHz as compared to ray tracing (20 dB shifted).

Two reference measurements are needed to determine  $P_0$  and  $\alpha_0$  for a given type of tunnel. Averaging should be done over a length of about  $l_{\text{crit}}/10$ , which is large to smooth out fades, but small enough not to avoid waveguide attenuation effects. For a practical calculation of propagation loss or coverage distance  $l_{\text{cov}}$ , a probability margin (e.g. level difference between 50% and 99% coverage probability,  $M_{99}$ ) has to be included to get [165]

$$l_{\text{cov}} = l_{\text{crit}} + (P_0 - M_{99} - P_{\min}) / \alpha_0 \quad (4.8.3)$$

where  $P_{\min}$  is the system specific minimum received power.

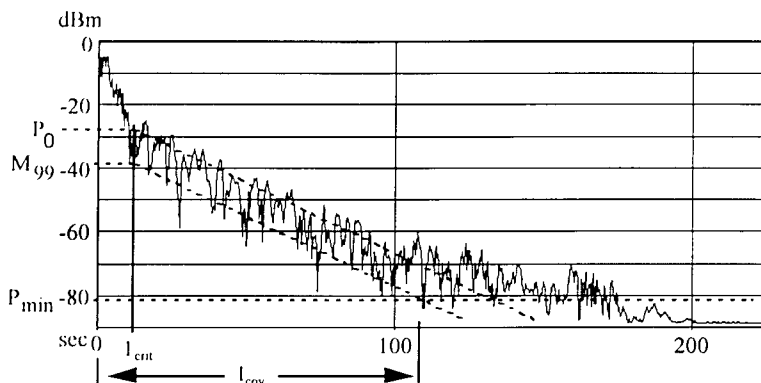


Fig. 4.8.3 Measured signal level in road tunnel and fitted model ( $f = 960$  MHz,  $v = 80$  km/h,  $100$  sec =  $1.9$  km)

Situation	$P_0$ [dBm]	$C$ [dB]	$a_0$ [dB/km]	$M_{95}$ [dB]	$M_{99}$ [dB]	$l_{cov\cdot}(95/99\%)$ [km]
960 MHz, 53dBm ERP, Tx in niche	-25	78	20	8	13	3.3 / 3 (both directions)
960 MHz, 53dBm ERP, Tx 67m outside	-23	76	18-22	8	13	~3.3 / 3
1800 MHz, 46dBm ERP, Tx in niche	-45	91	14	12	18	3 / 2.7 (both directions)
1800 MHz, 46dBm ERP, Tx 67m outside	-48	94	15	12	18	2.7 / 2.4
1800 MHz, 46dBm ERP, Tx 67m outside northern entrance	-55	101	20 (15)	12	18	1.7 / 1.4

Tab. 4.8.1 Observed power levels and coverage lengths in a Euro-standard two-lane road tunnel.

Fig. 4.8.3 shows a sample measurement and the fitted model and Table 4.8.1 gives numbers for several situations of these measurements [165].

One implicit assumption for the use of (4.8.3) is the independence of coupling loss into the tunnel and propagation loss inside the tunnel. The validity of this assumption was also proven by experiment in [165].

Interesting enough, traffic does add fades but only a few dB additional loss, if enough space over or between vehicles is left for wave propagation. Such is the case in Euro-standard road tunnels and in tunnels for high speed trains. Tunnel bends with curvature radii commonly used in such tunnels do not significantly hamper wave propagation, even if the bend is 90 degree.

#### 4.8.3 Leaky feeders

The classic solution of tunnel communication, leaky feeders, is now also available for 900 MHz. Cables designed for 900 MHz even show acceptable performance at 1800 MHz with, of course, a general decrease of received power level [167]. Compared to natural propagation leaky cables increase delay spread, but with less pronounced short-term-fading effects. Hence the Rice-parameter is lower than when using discrete antennas in the tunnel. Special cables have been manufactured that compensate for the longitudinal cable loss and the radiating loss. Mean signal level remains fairly constant over several hundred meters. Fig. 4.8.4 shows the field strength distribution along the tunnel achieved with a longitudinally compensated leaky feeder [168]. Combinations of leaky feeders terminating in a directive antenna have been shown to smoothen out signal variations and to extend coverage, but a beating phenomena between cable and antenna signals may occur. A still further alternative are so-called mode converters [168], i.e. coaxial cables with repeated radiating sections.

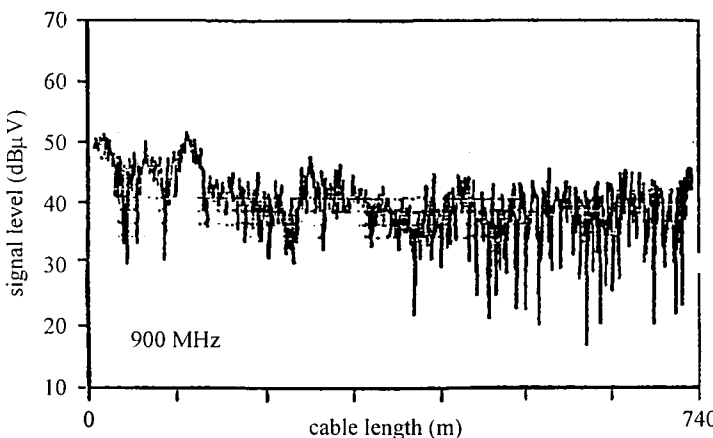


Fig. 4.8.4 Signal level in tunnel with compensated leaky feeder cable.

Between them the signal is guided as usual inside the ordinary coaxial cable.

Other approaches studied for serving GSM in confined areas by the DRIVE project ICAR include the booster concept which retransmits radio signals from the BTS to the MS and vice versa (Fig. 4.8.5). This concept is not directly tied to leaky cables and can be applied with directive antennas as well.

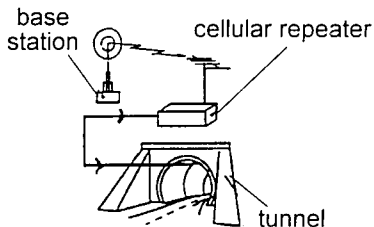


Fig. 4.8.5 Booster concept to cover confined areas.

#### 4.8.4 Railway environment and high-speed trains

The cuttings along modern railway lines can guide electromagnetic waves in quite a similar way as tunnels or street corridors. The low base station antenna and the rather high mobile antenna in addition to guiding structures like overtop wires, are responsible for flat fading effects. In general, low delay spread can be observed and Doppler spectra degenerate to a few, often a single, distinct peaks, i.e. Doppler spread is very small [169]. This has been observed as well in road tunnels with smoothly flowing traffic at constant speed [170]. An appropriate fading statistic is Ricean in connection with a rather high Rice parameter [169]. The railway environment is a favourable case for line coverage (as opposed to area coverage in ordinary mobile communications) [169], [171]. The predetermined neighbouring cell facilitates handover, and no unexpected turns will occur. A measurement campaign on high-speed trains in France and Germany [172] revealed the annoying fact that the usual tinted windows introduce an extra loss of 25-30 dB. Non-metallized, transparent windows do not cause significant added loss, unless wave incidence is grazing.

Another interesting finding was that field strength coverage alone may not be sufficient for GSM operation, because mobiles have problems in synchronising and decoding control messages at speeds around and above 250 km/h. This, however, could be a problem of the specific mobile station used. Fig. 4.8.6 shows the speed profile of the TGV Nord for a journey from Lille to Paris, the synchronisation information (number of detected neighbouring cells), and the signal strength reported by the mobile. Still, GSM is capable of meeting the requirements for radio communications for many applications foreseen for high-speed trains going up to 200 km/h [173].

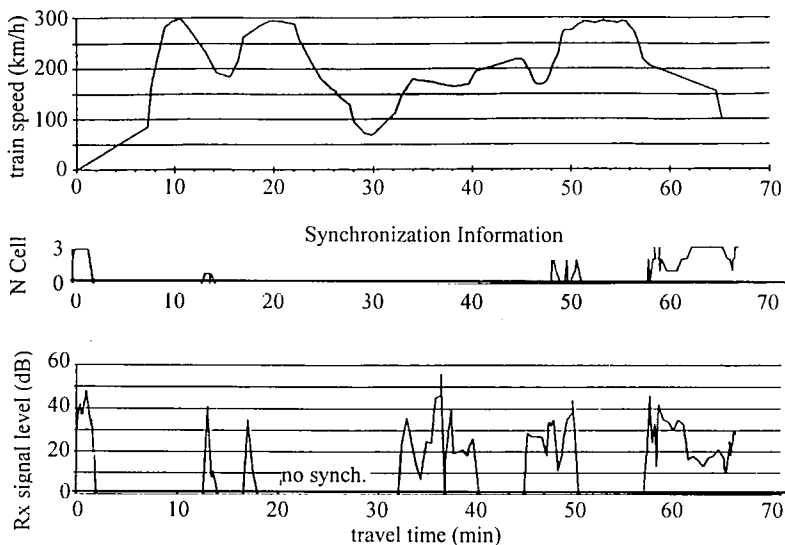


Fig. 4.8.6 Speed profile, synchronisation information and signal level along high-speed train line "TGV Lille-Paris".

Antennas mounted on the driver's cab roof bypass the mentioned problem of metallized window attenuation. For passengers using handportables either repeaters [173] - which will have to meet extremely tough dynamic-range problems - or completely novel concepts with a "moving base station" [171] have been proposed.

#### 4.8.5 Scaled-model measurements

Model-scaled measurements are a proper tool for investigations of propagation in or around tunnels, cuttings, and some indoor environments. For frequencies in the range of 2nd and 3rd generation cellular networks, scaling factors of at least 10 call for measurements above 10 GHz. Scaled measurements allow to separate individual influence parameters on wave propagation, like cross-section shape, entrance environment, antenna mounting, vehicles, and additional traffic. Many observed propagation effects are in line with measured data in real-size tunnels [164]. This pertains, e.g., for propagation differences in different lanes and the deep fade mitigation by traffic or other obstacles in the tunnel.

## 4.9 References

- [1] S. W. Marcus, "A hybrid method for computing transmission losses in an inhomogeneous atmosphere over irregular terrain," *IEEE Trans. on Antennas and Propagation*, vol. 40, no. 12, Dec. 1992, pp. 451-1458
- [2] D. T. Moroney, "Computational methods for the calculation of electromagnetic scattering from large scale perfect electrical conductors," Ph.D. Thesis, The University of Dublin Trinity College, 1995
- [3] R. H. Hardin, F. D. Tappert, "Application of the split step Fourier method to the numerical solution of non-linear and variable coefficient wave equations," *SIAM Rev.* 15(1973), p. 423
- [4] D. J. Cichon, (in German) "Strahlenoptische Modellierung der Wellenausbreitung in urbanen Mikro- und Pikofunkzellen," ("Ray optical modelling of wave propagation in urban micro- and pico-cells"), Ph.D. Thesis, University of Karlsruhe, published in *Forschungsberichte aus dem Institut für Höchstfrequenztechnik und Elektronik der Universität Karlsruhe*, vol. 8, ISSN 0942-2935, 1994
- [5] D. J. Cichon, T. C. Becker, M. Döttling, "Ray optical prediction of outdoor and indoor coverage in urban macro- and micro-cells," *Proc. IEEE Vehicular Technology Conference VTC'96*, Atlanta, USA, April 18-May 1, 1996, pp. 41-45
- [6] D. McGirl, P. C. Fannin, "Digital Elevation Modelling," *COST 231 TD(94)75*, Prague, Czech Republic, 1994
- [7] J. Lähteenmäki,, "Testing and verification of indoor propagation models," *COST 231 TD(94)111*, Sept 1994
- [8] E. Lachat, J.-F. Wagen, J. Li, "Effect of building heights on predictions in munich using multiple vertical knife-edge propagation," *COST 231 TD(96)24*, Jan 1996
- [9] B. E. Gschwendtner, "Practical investigation using ray optical prediction techniques in microcells," *COST 231 TD(94)127*, 1994
- [10] D. Grace et al., "The effects of building position tolerances on ray based urban propagation modelling," *COST 231 TD(95)16*, January 1995
- [11] R. Petersilka, "E-plus, an integrated approach using GIS in mobile communications," SMALLWORLD International Conference, Robinson College, Cambridge, October 1995
- [12] M. Perucca, B. Gschwendtner, "Aspects of ray-optical modelling in micro-cells," *COST 231 TD(95)82*, Florence, Italy, April 1995
- [13] A. Glassner (editor), *An Introduction to Ray Tracing*, Academic Press, San Diego, 1989
- [14] RACE 2084, "Definition of a data format for wide-band propagation measurements and explanation of how to use the data," *COST 231 TD(94)025*, 1994
- [15] H. Bühlér, T. Klemenschits, "UMF The Universal Measurement File-Format," *COST 231 TD(93)26*, Barcelona, Spain, January 1993

- [16] U. Dersch, E. Zollinger, "Physical characteristics of urban micro-cellular propagation," *IEEE Trans. on Antennas and Propagation*, vol. 42, no. 11, pp. 1528-1539, Nov. 1994
- [17] U. Dersch, J. Troger, E. Zollinger, "Multiple reflections of radio waves in a corridor," *IEEE Trans. on Antennas and Propagation*, vol. 42, no. 11, Nov. 1994, pp. 1571-1574
- [18] A. J. Levy, "Fine structures of the urban mobile propagation channel," *Proc. COMMSPHERE'91*, December 1991, pp. 5.1.1-5.1.6
- [19] J.-P. Rossi, A. J. Levy, "A ray model for decimetric radiowave propagation in an urban area," *Radio Science*, vol. 27, no. 6, pp. 971-979, Nov.-Dec. 1992
- [20] J.-F. Wagen, K. Rizk, "Ray tracing based prediction of impulse response in urban microcells," *44th IEEE Vehicular Technology Conference (VTC'94)*, pp. 210-214 , June 1994
- [21] B. Chopard, P. Luthi, J.-F. Wagen, "Wave propagation in urban microcells: A massively parallel approach using the TLM method," *COST 231 TD(95) 33*, Bern, Switzerland, January 1995
- [22] F. Lotse, J.-E. Berg, R. Bownds, "Indoor propagation measurements at 900 MHz," *IEEE Vehicular Technology Conf. VTC'92*, pp. 629-632, May 1992
- [23] J.-E. Berg, J. Ruprecht, J.-P. de Weck, A. Mattsson, "Specular reflections from high-rise buildings in 900 MHz cellular systems," *41st IEEE Vehicular Technology Conference VTC'91*, pp. 594-599 , May 1991
- [24] J. Walfisch, H. L. Bertoni, "A theoretical model of UHF propagation in urban environments," *IEEE Trans. on Antennas and Propagation*, vol. 36, no. 12, pp. 1788-1796, Dec. 1988
- [25] J. H. Causebrook, "Vodafone's fieldstrength prediction method," *COST 231 TD(93)1*, Barcelona, Spain, 1993
- [26] P. Kreuzgruber, T. Bründl, W. Kuran, R. Gahleitner, "Prediction of indoor radio propagation with the ray splitting model including edge diffraction and rough surfaces," *COST-231 TD(94) 50*, Prague, Czech Republic, April 1994
- [27] R. Jakoby, U. Liebenow, "Modelling of radiowave propagation in microcells," *Proc. Intern. Conference on Antennas and Propagation ICAP'95*, Eindhoven, The Netherlands, pp. 377-380
- [28] L. B. Felsen, N. Marcuvitz, *Radiation and Scattering of Waves*, Prentice-Hall Inc., Englewood Cliffs, New Jersey, Sec. 6.4 and 6.5, 1973
- [29] J.-F. Wagen, M. Keer, "Comparison of diffraction coefficients for propagation prediction in microcells," *COST-231 TD(93) 80*, Grimstad, Norway, May 1993
- [30] J. B. Keller, "Geometrical Theory of Diffraction," *J. Opt. Soc. Am.*, vol. 52, pp. 116-130, 1962
- [31] D. A. McNamara, C. W. I. Pistorius, J. A. G. Malherbe, *Introduction to the Uniform Geometrical Theory of Diffraction*, Artech House, Norwood, MA, USA, 1990, ISBN 0-89006-301-X
- [32] C. Bergljung, "Diffraction of Electromagnetic Waves by Dielectric Wedges," Ph.D. Thesis, Lund Institute of Technology, Sweden, 1994
- [33] M. Keer, (in French) "La Representation Spectrale de la Diffraction dans le Domaine Spatial," ("Spectral representation of diffraction in spatial domain"),

- Ph.D. Thesis No 1069, Swiss Federal Institute of Technology, Switzerland, 1992
- [34] R. J. Luebbers, "A heuristic UTD slope diffraction coefficient for rough lossy wedges," *IEEE Trans. on Antennas and Propagation*, vol. 37, no. 2, pp. 206-211, 1989
  - [35] J.-F. Sante, "Measurements and modelling in rural areas," *COST-231 TD(93) 121*, Limerick, Ireland, September 1993
  - [36] P. Möller, "Urban area radio propagation measurements and comparison to a new semi-deterministic model," Diplomarbeit, Universidad Politécnica de Valencia and Universität Karlsruhe, Spain and Germany, 1994
  - [37] S. Guérin, (in French) "Modélisation physique de la propagation des ondes radioélectriques en milieu urbain," ("Physical modelling of radio wave propagation in urban area"), Rapport de stage, Institut Galilée Télécommunications et CNET, 1992
  - [38] J.-F. Wagen, "SIP simulation of UHF propagation in urban microcells," *41st IEEE Vehicular Technology Conference VTC'91*, St. Louis, USA, May 1991
  - [39] S. R. Saunders, F. R. Bonar, "Explicit multiple building attenuation function for mobile radio wave propagation," *Electronics Letters*, vol. 27, no. 14, pp. 1276-1277, July 1991
  - [40] J. B. Andersen, "Transition zone diffraction by multiple edges," *IEE Proc. Microwaves, Antennas and Propagation*, vol. 141, no. 5, October 1994, pp. 382-384
  - [41] J. B. Andersen, J. Wiart, "UTD transition zone diffraction," *COST 231 TD(96)3*, Belfort, January 1996
  - [42] L. Vogler, "An attenuation function for multiple knife edge diffraction," *Radio Science*, 17, 1982, pp. 1541-1546
  - [43] ITU Recommendation ITU-R 526-2, 1994 PN Series Volume "Propagation in non-ionized media," pp. 129-149, 1994
  - [44] J. Li, J.-F. Wagen, E. Lachat, "On the ITU model for multi-knife edge diffraction", submitted to IEE, also in *COST 231 TD(96)25*, Belfort, January 1996; paper available from: Dr. J-F. Wagen, Swiss Telecom PTT, Mobile Communications, FE 421, CH-3000 Bern 29, Switzerland
  - [45] L. R. Maciel, H. L. Bertoni, H. H. Xia, "Unified approach to prediction of propagation over buildings for all ranges of base station antenna height," *IEEE Trans. on Vehicular Technology*, vol. 43, no. 1, 1993, pp. 35-41
  - [46] P. Beckmann, A. Spizzichino, *The Scattering of Electromagnetic Waves from Rough Surfaces*, MacMillan, New York, 1963
  - [47] K. Rizk, J.-F. Wagen, S. Bokhari, F. Gardiol, "Comparison between the diffraction theory and the moment method for the scattering by surface irregularities in a building wall," *Journées Internationales de Nice sur les Antennes (JINA '94)*, Nice, France, Nov. 1994
  - [48] F. Ikegami, S. Yoshida, M. Umehira, "Propagation factors controlling mean field strength on urban streets," *IEEE Trans. on Antennas and Propagation*, vol. 32, no. 8, August 1984, pp. 822-829

- [49] M. Hata, "Empirical formula for propagation loss in land mobile radio services," *IEEE Trans. on Vehicular Technology*, vol. 29, pp. 317-325, 1980
- [50] Y. Okumura, E. Ohmori, T. Kawano, K. Fukuda, "Field strength and its variability in VHF and UHF land-mobile service," *Review of the Electrical Communication Laboratory*, vol. 16, no. 9-10, 1968, pp. 825-873
- [51] COST 231, "Urban transmission loss models for mobile radio in the 900- and 1,800 MHz bands (Revision 2)," *COST 231 TD(90)119 Rev. 2*, The Hague, The Netherlands, September 1991
- [52] S. R. Saunders, F. R. Bonar, "Prediction of mobile radio wave propagation over buildings of irregular heights and spacings," *IEEE Trans. on Antennas and Propagation*, vol. 42, no. 2, pp. 137-144, 1994
- [53] K. Löw, "Comparison of CW-measurements performed in Darmstadt with the flat edge model," *COST 231 TD(92)8*, Vienna, January 1992
- [54] K. Löw, "Comparison of urban propagation models with CW-measurements," *Proc. Vehicular Technology Conference VTC'92*, pp. 936-942, 1992
- [55] L. Ladell, "Transmission loss predictions in wooded terrain," *Proc. Nordic Radio Symposium NRS'86*, Sweden, 1986, pp. 41-50, ISBN 91-7056-072-2
- [56] H. H. Xia, H. L. Bertoni, "Diffraction of cylindrical and plane waves by an array of absorbing half-screens," *IEEE Trans. on Antennas and Propagation*, vol. 40, no. 2, 1992, pp. 170-177
- [57] L. R. Maciel, H. L. Bertoni, H. H. Xia, "Propagation over buildings for paths oblique to the street grid," *Proc. PIMRC'92*, Boston, USA, pp. 75-79
- [58] Th. Kürner, (in German) "Ein modulares Konzept zur Feldstärkeprädiktion urbaner DCS-1800 Makrozellen," ("A modular concept for fieldstrength prediction of urban DCS 1800 macro cells"), *ITG-Fachbericht 135, Proceedings ITG-Fachtagung Mobile Kommunikation*, Neu-Ulm, September 1995, pp. 35-42
- [59] Th. Kürner, R. Fauß, A. Wäsch, "A hybrid propagation modelling approach for DCS1800 macro cells," *Proc. IEEE VTC'96*, Atlanta, Georgia, USA, April 28-May 1, 1996, pp. 1628-1632
- [60] N. Cardona, P. Möller, F. Alonso, "Applicability of Walfisch-type urban propagation models," *Electronics Letters*, vol. 31, no. 23, November 1995
- [61] P. Eggers, "Note on the usage of Walfisch-type urban path loss prediction models," *COST 231 TD(91)87*, The Hague, September 1991
- [62] R. Leppänen, J. Lähteenmäki, S. Tallqvist, "Radiowave propagation at 900 and 1800 MHz bands in wooded environments," *COST 231 TD(92)112*, Helsinki, 1992
- [63] Th. Kürner, D. J. Cichon, W. Wiesbeck, "The influence of land usage on UHF wave propagation in the receiver near range," *IEEE Transactions on Vehicular Technology*, vol. 46, no. 3, August 1997, pp. 739-747
- [64] T. Tamir, "Radio wave propagation along mixed paths in forest environments," *IEEE Trans. on Antennas and Propagation*, vol. 25, no. 4, 1977, pp. 471-477
- [65] J. T. Hviid, J. B. Andersen, J. Toftgard, J. Bojer, "Terrain-based propagation model for rural areas - an integral equation approach," *IEEE Trans. on Antennas and Propagation*, vol. 43, no. 1, January 1995, pp. 41-46

- [66] D. Moroney, P. J. Cullen, "A fast integral equation approach to UHF coverage estimation," *Proc. of the Joint COST 227/231 Workshop*, Florence/Italy, April 1995, published in *Mobile and Personal Communications*, edited by E. del Re, Elsevier 1995, pp. 343-350
- [67] J. E. Berg, H. Holmquist, "An FFT multiple half-screen diffraction model," *Proc. IEEE VTC'94*, Stockholm, Sweden, pp. 195-199, 1994
- [68] J. E. Berg, "A macrocell model based on the parabolic differential equation," *Proc. Virginia Tech's Fourth Symposium on Wireless Personal Communications*, pp. 9.1-9.10, June 1-3, 1994
- [69] M. Lebherz, W. Wiesbeck, W. Krank, "A versatile wave propagation model for the VHF/UHF range considering three dimensional terrain," *IEEE Trans. on Antennas and Propagation*, vol. 40, no. 10, October 1992, pp. 1121-1131
- [70] P. Kuhlmann, "A forward-scattering algorithm for prediction of the direct-link in a three-dimensional model," *COST 231 TD(95)137*, Poznan, September 1995
- [71] Th. Kürner, R. Fauß, (in German) "Untersuchungen zur Feldstärkeprädiktion im 1800 MHz-Bereich," ("Investigation of path loss algorithms at 1800 MHz"), *Nachrichtentechnik Elektronik, ne-Science*, vol. 45 (1995), no. 2, pp. 18-23
- [72] M. Badsberg, J. B. Andersen, P. Mogensen, "Exploitation of the terrain profile in the Hata model," *COST 231 TD(95)9*, Bern, January 1995
- [73] K. E. Stocker, F. M. Landstorfer, "Empirical prediction of radiowave propagation by neural network simulator," *Electronics Letters*, vol. 28, no. 8, April 1992, pp. 724-726
- [74] K. E. Stocker, B. E. Gschwendtner, F. M. Landstorfer, "An application of neural networks to prediction of terrestrial wave propagation for mobile radio," *IEE Proceedings-H*, vol. 140, no. 4, August 1993, pp. 315-320
- [75] Th. Kürner, (in German) "Charakterisierung digitaler Funksysteme mit einem breitbandigen Wellenausbreitungsmodell," ("Characterisation of digital radio systems using a wideband propagation model"), Ph.D. Thesis, University of Karlsruhe, published in *Forschungsberichte aus dem Institut für Höchstfrequenztechnik und Elektronik*, vol. 3, ISSN 0942-2935, 1993
- [76] G. A. Dechamps, "High frequency diffraction by wedges," *IEEE Trans. on Antennas and Propagation*, vol. 33, no. 4, April 1985, pp. 357-368
- [77] P. Kuhlmann, (in German) "Schätzung der Funkfelddämpfung mit einem theoretischen Vorwärtsstreuomodell," ("Path loss estimation using a theoretical forward scattering model"), *Proceedings Kleinheubacher Berichte 38*, 1995, pp. 175-184
- [78] J. Bach Andersen, J. Hviid, J. Toftgard, "Comparison between different path loss prediction models," *COST 231 TD(93)6*, Barcelona, January 1993
- [79] N. Geng, W. Wiesbeck, "Parabolic equation method simulations compared to measurements," *IEE International Conference on Antennas and Propagation ICAP'95*, Eindhoven, The Netherlands, April 1995, pp. 359-362
- [80] D. Moroney, P. Cullen, " An integral equation approach to UHF coverage estimation," *IEE ICAP'95*, April 1995, pp. 367-372

- [81] Th. Kürner, D.J. Cichon, W. Wiesbeck, "Concepts and results for 3D digital terrain based wave propagation models - an overview," *IEEE Journal on Selected Areas in Communications*, vol. 11, no. 7, pp. 1002-1012, 1993
- [82] T. C. Becker, Th. Kürner, D. J. Cichon, "Fast scatterer search algorithms for 3D wave propagation modeling," *COST 231 TD(95)10*, Bern, 1995
- [83] Th. Kürner, T. C. Becker, W. Wiesbeck, "Comparison of measured and predicted locations of interfering scatterers," *Proc. IEE ICAP'95*, Eindhoven, The Netherlands, April 1995, pp. 363-366
- [84] H. Bübler, E. Bonek, B. Nemsic, "Estimation of heavy time dispersion for mobile radio channels using a path tracing concept," *Proc. IEEE VTC'93*, Secaucus, New Jersey, USA, pp. 257-260, 1993
- [85] K. Davidsen, M. Danielsen, "Predicting impulse responses in mountainous areas," *Proc. PIMRC'94*, The Hague, The Netherlands, pp. 25-27
- [86] P. Eggers, C. Jensen, A. Oprea, K. Davidsen, M. Danielsen, "Assessment of GSM-link quality dependence on radio dispersion in rural environments," *Proc. IEEE VTC'92*, Denver, May 1992, pp. 532-535
- [87] U. Liebenow, P. Kuhlmann, "Theoretical investigations and wideband measurements on wave propagation in hilly terrain," *Proc. IEEE VTC'94*, Stockholm, Sweden, pp. 1803-1806
- [88] U. Liebenow, (in German) "Ein dreidimensionales Ausbreitungsmodell im Vergleich mit Messungen," ("A three-dimensional propagation model compared to measurements"), *ITG-Fachbericht 135*, *Proc. ITG Mobile Kommunikation*, Neu-Ulm, 1995, pp. 43-50
- [89] U. Liebenow, P. Kuhlmann, "A three-dimensional wave propagation model for macrocellular mobile communication networks in comparison with measurements," *Proc. IEEE VTC'96*, Atlanta, USA, April 28-May 1, 1996, pp. 1623-1627
- [90] Th. Kürner, D. J. Cichon, W. Wiesbeck, "Evaluation and verification of the VHF/UHF propagation channel based on a 3D-wave propagation model," *IEEE Trans. on Antennas and Propagation*, vol. 44, no. 3, March 1996, pp. 393-404
- [91] D. J. Cichon, T. Kürner, W. Wiesbeck, "Polarimetric aspects in antenna related superposition of multipath signals," *IEE Proc. Eighth Intern. Conf. on Antennas and Propagation ICAP'93*, pp. 80-83, Edinburgh, United Kingdom, March 30 - April 2, 1993
- [92] J. H. Causebrook, "Signal attenuation by buildings and trees," *COST 231 TD(90)106*, Darmstadt, 1990
- [93] J. Bach Andersen, "Issues and challenges of propagation studies for mobile networks," in *Proc. Personal, Indoor and Mobile Radio Conference PIMRC'94*, pp. 1285-1291, The Hague, The Netherlands, September 1994
- [94] H. L. Bertoni, W. Honcharenko, L. R. Maciel, H. H. Xia, "UHF propagation prediction for wireless personal communications," *Proceedings of the IEEE*, vol. 82, no. 9, pp. 1333-1359, 1994

- [95] U. Kauschke, "Propagation and system performance simulations for the short range DECT system in microcellular urban roads," *IEEE Trans. on Vehicular Technology*, vol. 44, no. 2, pp. 253-260, November 1994
- [96] J. Wiart, P. Metton, "Terrain influence on line of sight microcellular propagation," *COST 231 TD(95)78*, Florence, Italy, April 1995
- [97] H. Börjeson, C. Bergljung, P. Karlsson, L. O. Olsson, S.-O. Öhrvik, "Using a novel model for predicting propagation path loss," *COST 231 TD(93) 86*, Grimstad, Norway, May 1993
- [98] H. Börjeson, C. Bergljung, L.G. Olsson, "Outdoor microcell measurements at 1700 MHz," *Proc. 41th IEEE Vehicular Technology Conference*, 1992
- [99] J.-E. Berg, "A recursive method for street microcell path loss calculations," *6th PIMRC'95*, Toronto, Canada, September 1995, pp. 140-143
- [100]J. Wiart, "Microcell modelling when base station is below roof tops," *Proc. 44th IEEE Vehicular Technology Conference VTC'94*, Stockholm, Sweden, May 25-28, 1994, pp. 200-204
- [101]K. Rizk, J.-F. Wagen, F. Gardiol, "Ray tracing based path loss prediction in two microcellular environments," in *Proc. Personal, Indoor and Mobile Radio Conference PIMRC'94*, pp. 384-388, The Hague, The Netherlands, 18-23 September, 1994
- [102]D. J. Cichon, T. C. Becker, W. Wiesbeck, "A ray launching approach for indoor and outdoor applications," *COST 231 TD(94)32*, Lisbon, Portugal, January 1994
- [103]D. J. Cichon, W. Wiesbeck, "Indoor and outdoor propagation modeling in pico cells," in *Proc. Personal, Indoor and Mobile Radio Conference PIMRC'94*, pp. 491-495, The Hague, The Netherlands, September 1994
- [104]D. J. Cichon, T. Kürner, W. Wiesbeck, (in German) "Modellierung der Wellenausbreitung in urbanem Gelände," ("Wave propagation modelling in urban area"), *FREQUENZ*, vol. 47, no. 1-2, pp. 2-11, 1993
- [105]N. Cardona, F. Navarro, P. Möller, "Applicability of Walfisch-type urban propagation models," *COST 231 TD(94)134*, Darmstadt, Germany, September 1994
- [106]P. Möller, N. Cardona, D. J. Cichon, "Investigations in a new developed urban propagation model," *COST 231 TD(94)135*, Darmstadt, Germany, September 1994
- [107]J. Deygout, "Multiple knife-edge diffraction of microwaves," *IEEE Trans. on Antennas and Propagation*, vol. 14, no. 4, pp 480-489, 1966
- [108]CCIR, vol. V Report 567-4, "Propagation data and prediction methods for the terrestrial land mobile service using the frequency range 30 MHz to 3 GHz"
- [109]T. Kürner, D. J. Cichon: "Comments on TD (93) 6: Comparison between different path loss prediction models", *COST 231 TD(93)81*, Grimstad, Norway, May 1993
- [110]M. Perucca, "Small cells characterization using 3-D database and Deygout diffraction approach," *COST 231 TD(94)54*, Prague, Czech Republic, April 1994

- [111]J. P. Rossi, J. C. Bic, A. J. Lévy, "A ray launching model in urban area," *COST 231 TD(90)78*, Paris, France, October 1990
- [112]U. Dersch, E. Zollinger, "Propagation mechanisms in microcell and indoor environments," *IEEE Trans. on Vehicular Technology*, vol. 43, no. 4, pp. 1058-1066, November 1994
- [113]P. Daniele, V. Degli-Esposti, G. Falciasecca, G. Riva, "Field prediction tools for wireless communications in outdoor and indoor environments," *Proc. IEEE MTT-Symp. European Topical Congress "Technologies for Wireless Applications"*, Turin, Italy, November 1994
- [114]A. Ishimaru, *Wave propagation and scattering in random media*, vols. I and II, Academic, New York, 1978
- [115]B. E. Gschwendtner, (in German) "Adaptive Wellenausbreitungsmodele für die Funknetzplanung," ("Adaptive propagation models for radio network planning"), Ph.D. Thesis, University of Stuttgart, ISBN 3-8265-1318-5, 1995
- [116]B. E. Gschwendtner, G. Wölflé, B. Burk, F. M. Landstorfer, "Ray tracing vs. ray launching in 3-D microcell modelling," *Proc. European Personal and Mobile Communications Conference EPMCC'95*, Bologna, Italy, November 24-26, 1995, pp. 74-79
- [117]B. E. Gschwendtner, F. M. Landstorfer, "3-D propagation modelling in microcells including terrain effects," *Proc. IEEE Intern. Personal, Indoor and Mobile Radio Conference PIMRC'95*, USA, 1995, pp. 532-536
- [118]D. J. Cichon, W. Wiesbeck, "Comprehensive ray optical propagation models for indoor and outdoor environments: Theory and applications," *Proc. COMMSPHERE'95*, Eilat, Israel, January 22-27, 1995, pp. 201-208
- [119]D. J. Cichon, T. C. Becker, M. Döttling, "Ray optical prediction of outdoor and indoor coverage in urban macro- and micro-cells," *Proc. IEEE Vehicular Technology Conference VTC'96*, Atlanta, USA, April 18-May 1, 1996, pp. 41-45
- [120]J. Jakobsen, "Radio Propagation Measurements in Two Office Buildings," *COST-231 TD(90)28*, Copenhagen, Denmark, May 1990
- [121]I. T. Johnson, W. Johnston, F. J. Kelly, "CW and Digital Propagation Behaviour from Outdoor Public Cells Measured in Customer Premises Cells," *COST-231 TD(90)82*, Paris, France, October 1990
- [122]T. A. Wilkinson, "A Review of Radio Propagation into and Within Buildings," *COST-231 TD (90) 85*, Paris, France, October 1990
- [123]"Propagation Models" subgroup, "Building penetration losses," *COST-231 TD(90)116 Rev.1*, Florence, Italy, January 1991
- [124]A. M. D. Turkmani, J. D. Parsons, A. F. de Toledo, "Radio Propagation into Buildings at 1.8 GHz," *COST-231 TD(90)117*, Darmstadt, Germany, December 1990
- [125]P. Backman, S. Lidbrink, T. Ljunggren, "Building penetration loss measurements at 1.7 GHz in micro cellular environments," *COST 231 TD(90)121*, Darmstadt, Germany, December 1990
- [126]M. Sandén, "Building penetration loss measurements in the small cell environment," *COST-231 TD(90)122*, Darmstadt, Germany, December 1990

- [127]E. Zollinger, "Dielectric Properties of Building Materials and Biological Tissues: A short Bibliographic Overview," *COST 231 TD(91)4*, Florence, Italy, January 1991
- [128]CSELT, "Microcellular propagation: Measurements with low Base Station Antennas," *COST 231 TD(91)82*, Leidschendam, Netherlands, Sep. 1991
- [129]J.-E. Berg, "Building Penetration Loss at 1700 MHz Along Line of Sight Street Microcells," *3rd PIMRC'92*, Boston, USA, October 1992, pp. 86-87
- [130]J. Jimenez Delgado & J. Gavilan, "Indoors Penetration Results," *COST-231 TD(93)118*, Barcelona, Spain, Jan. 1993
- [131]R. Gahleitner, "Wave Propagation into Urban Buildings at 900 and 1800 MHz," *COST-231 TD(93)92*, Grimstad, Norway, May 1993
- [132]R. Gahleitner, "Radio Wave Propagation In and Into Urban Buildings," Ph.D. Thesis, Technical University of Vienna, 1994
- [133]J.-E. Berg, "Comments on methods to assess penetration losses to be used in microcell models," *COST-231 TD(95)108*, Poznan, Poland, September 1995
- [134]J.-E. Berg, "Angle-dependent building penetration loss along LOS street microcells," *COST-231 TD(96)6*, Belfort, France, January 1996
- [135]J. M. Keenan, A. J. Motley, "Radio coverage in buildings," *British Telecom Technology Journal*, vol. 8, no. 1, Jan. 1990, pp. 19-24
- [136]J. Lähteenmäki, "Radiowave propagation in office buildings and underground halls," *Proc. of European Microwave Conference*, Espoo 1992, pp. 377-382
- [137]P. Bartolomé, "Indoor propagation models validation," *COST 231 TD(93)51*, Barcelona, 1993
- [138]S. Ruiz-Boqué, M Ballart, C. Clúa, R Agusti, "Propagation models for indoor mobile communications," *COST 231 TD(91)14*, Florence, Italy, 1991
- [139]C. Törnevik, J.-E. Berg, F Lotse, "900 MHz propagation measurements and path loss models for different indoor environments," *Proc. IEEE VTC'93*, New Jersey, USA, 1993
- [140]P. Karlsson, "Indoor radio propagation for personal communications services," Ph.D. Thesis, University of Lund, 1995
- [141]J. Lähteenmäki, "Indoor propagation between floors at 855 MHz and 1.8 GHz," *COST 231 TD(94)37*, Lisbon, Portugal, 1994
- [142]S. Ruiz-Boque, R. Agusti, J. Perez, "Indoor wideband channel characterization (900 and 1800 MHz) by means of a network analyzer," *COST 231 TD(91)71*, Barcelona, Spain, 1991
- [143]S. Ruiz-Boqué, R Agusti, "Polarization diversity for indoor mobile communications," *COST 231 TD(93)7*, Barcelona, Spain, 1993
- [144]H. Hashemi, "A study of temporal and spatial variations of the indoor radio propagation channel," *Proc. PIMRC'94*, pp. 127-134, 1994
- [145]P. Karlsson, H. Börjeson, T. Maseng, "A statistical multipath propagation model confirmed by measurements and simulations in indoor environments at 1800 MHz," *Proc. PIMRC'94*, pp. 486-490, 1994
- [146]R. P. Bultitude, "Measurement, characterization and modeling of indoor 800/900 MHz radio channels for digital communications," *IEEE Communications Mag.*, vol. 25, no. 6, pp. 5-12, June 1987

- [147]D. Molkdar, "Review on radio propagation into and within buildings," *IEE Proc.-H*, vol. 138, no. 1, pp. 61-73, February 1991
- [148]D. Cox, "Antenna diversity performance in mitigating the effects of portable radiotelephone orientation and multipath propagation," *IEEE Trans. on Comm.*, vol. 31, no. 5, pp. 620-628, 1983
- [149]B. Fleury, D. Dahlhaus, "Investigations on the time variations of the wide-band radio channel for random receiver movements," *Proc. IEEE Int. Symp. on Spread Spectrum Techniques and Applications ISSSTA'94*, vol. 2, pp. 631-636, Oulu, Finland, 1994
- [150]T. Huschka, "Ray-tracing models for indoor environments and their computational complexity," *Proc. PIMRC'94*, pp. 486-490, 1994
- [151]W. Honcharenko, H. L. Bertoni, J. L. Dailing, J. Qian, H. D. Yee, "Mechanisms governing UHF propagation on single floors in modern office buildings," *IEEE Trans. on Vehicular Technology*, vol. 41, no. 4, pp. 496-504, 1992
- [152]K. R. Schaubach, N. J. Davis, T. S. Rappaport, "A ray tracing method for predicting path loss and delay spread in microcellular environments," *Proc. IEEE VTC'92*, pp. 932-935, Denver, 1992
- [153]P. Kreuzgruber, P. Unterberger, R. Gahleitner, "A ray splitting model for indoor radio propagation associated with complex geometries," *Proc. IEEE VTC'93*, NJ, USA, 1993, pp. 227-230
- [154]D. J. Cichon, T. Zwick, J. Lähteenmäki, "Ray optical indoor modeling in multi-floored buildings: Simulations and measurements," *Proc. IEEE Intern. Antennas and Propagation Symposium AP-S'95*, Newport Beach, USA, 1995, pp. 522-525
- [155]J. Lähteenmäki, "Testing and verification of indoor propagation models," *COST 231 TD(94)111*, Darmstadt, Germany, 1994
- [156]M. Lebherz, W. Wiesbeck, (in German) "Beurteilung des Reflexions- und Schirmungsverhaltens von Baustoffen," ("Estimation of reflectivity and electromagnetic shielding properties of building materials"), *Bauphysik*, no. 12, 1990
- [157]J. B. Hasted, M. A. Shah, "Microwave absorption by water in building materials," *Brit. Journal of Applied Physics*, vol. 15, 1964, pp. 825-835
- [158]E. Zollinger, "Eigenschaften von Funkübertragungsstrecken in Gebäuden," ("Properties of indoor radio transmission"), Ph.D. Thesis, no. 10064, Swiss Federal Institute of Technology Zürich (ETH), Zürich, Nov. 1993, pp. 20-28
- [159]T. Klemenschits, "Mobile Communications in Tunnels," Ph.D. Thesis, Technical University of Vienna, Austria, 1993
- [160]K. Gunmar, "Broadband technique for car to car communication at 60 GHz," *COST-231 TD(91)41*, Lund, Sweden, 1991
- [161]Z. Ghebretnsae, "Simulations of beacon-vehicle communications for DRIVE applications," *COST-231 TD(92)53*, Leeds, United Kingdom, 1992
- [162]K. Gunmar, "Simulation of the GSM-SDCCH-channel for LOS microcell communication for DRIVE applications," *COST-231 TD(92)87*, Helsinki, Finland, 1992

- [163]J. Wickman, "Measurements and simulations of wave propagation in a corridor at 1800 MHz," *COST 231 TD(90)124*, Darmstadt, Germany, 1990
- [164]T. Klemenschits, A. L. Scholtz, E. Bonek, "Microwave Measurements in Scaled Road Tunnels Modelling 900 MHz Propagation," *Proc. 43rd IEEE Vehicular Technology Conf.*, May 1993, Secaucus, NJ, USA, pp. 70 - 72
- [165]T. Klemenschits, E. Bonek, "Radio Coverage of Road Tunnels at 900 and 1800 MHz by Discrete Antennas," *Proc. of the 5th Intern. Symposium on Personal, Indoor and Mobile Radio Communications*, 411 - 415, The Hague, The Netherlands , 1994
- [166]T. Klemenschits, "Wave propagation in road tunnels - The method of image antennas," *COST-231 TD(91)33*, Lund, Sweden, 1991
- [167]CSELT-SIRTI (Italy), "Propagation measurements inside tunnels," *COST-231 TD(91)83*, Leidschendam, 1991
- [168]DRIVE Consortium V2014-ICAR, "System and radiating elements analysis for the transmission of the GSM signals in tunnels," *COST-231 TD(93)59*, Grimstad, Norway, 1993
- [169]M. Göller, K. D. Masur, (in German) "Ergebnisse von Funkkanalmessungen im 900-MHz-Bereich auf Neubaustrecken der Deutschen Bundesbahn," ("Results of radio channel measurements at 900 MHz along German high-speed railway lines"), Teil 1 u. 2, *Nachrichtentechnik Elektronik* 42, pp. 143 ff, 1992
- [170]R. Gahleitner, T. Klemenschits, R. Stepanek, "First results of a direct-conversion channel sounder (DCCS-1800) recorded in a road tunnel," *COST-231 TD(93)88*, Grimstad, Norway, 1993
- [171]M. Uhlirz, "Concept of a GSM-based Communication System for High-Speed Trains," *Proc. IEEE VTC'94*, Stockholm, Sweden, pp. 1130 - 1134
- [172]M. Uhlirz, "Adapting GSM for Use in High-Speed Railway Networks," Ph.D. Thesis, Technical University of Vienna, Austria, 1995
- [173]R. H. Rækken, M. Sneltvedt, "Using an autonomous measurement system to evaluate GSM coverage along railways", in *Proc. Nordic Radio Symposium 1995 (NRS'96)*, Saltsjöbaden, Sweden, April 1995, pp. 201-206
- [174]G.G. Cook, A.P. Anderson, A.S. Turnbull, "Spectral Incremental Propagation (SIP) procedure for fast calculation of scattered fields from conducting bodies", *IEE Proc.*, Vol. 136, Pt. H, No.1, Feb. 1989, pp. 34-38



## **Research into Performance and Enhancements of Second Generation Systems: GSM and DECT**

**Luis Lopes, University of Leeds, UK**

**Andreas F. Molisch, T.U. Wien, A**

### **5.1 Introduction**

**Luis Lopes (University of Leeds, UK)**

This chapter reports on some of the work carried out in COST-231 with relation to second generation personal communication systems, and specifically GSM and DECT. The performance of basic versions of such systems is relatively well known, and the focus of the work was therefore on advanced features and possible limitations. These topics are of importance not only in relation to the full exploitation of the potential of the systems, but also in terms of possible evolutionary transitions towards the third generation via progressive enhancements of the radio and network performance.

GSM is first considered in the chapter, with full discussion of features such as novel diversity schemes and different frequency hopping strategies, and their effects on radio link performance and system capacity. This is followed by a treatment of DECT which tends to focus on emerging DECT outdoor applications. Among the covered topics are a study of DECT receiver performance, propagation measurements for DECT, new proposals for link enhancement, a report on a field trial, and discussion of DECT network capacity in WPBX and RLL applications.

## 5.2 On Antenna and Frequency Diversity in GSM

Preben E. Mogensen, Jeroen Wigard (CPK, Denmark)

Antenna diversity is a well-known method to mitigate the effect of multipath fading (refer to Chapter 3 for a general discussion of diversity techniques). Analytical expressions for antenna diversity gains in the presence of Rayleigh fading can be found, for example, in [13,15]. Such analytical results are not directly applicable to the GSM system for several reasons: firstly, the GSM signal has a bandwidth of 200 kHz and for some propagation environments frequency selective fading is introduced. Secondly, the channel coding and interleaving processes reduce the impact of signal fading and furthermore the diversity gain becomes speed dependent for a non-frequency hopping transmission link.

The GSM transmission link can gain from frequency diversity in two ways: the required channel Equaliser [9] can exploit frequency selective fading within the channel bandwidth, and Frequency Hopping (FH) [5] can provide decorrelated fading for successive received bursts. Thanks to the channel coding and interleaving, this fading decorrelation can be converted into a frequency diversity gain for slow moving users.

### 5.2.1 The GSM Test Profiles

The GSM recommendation specifies test power delay profiles for validation of GSM mobile terminals [9]. The profiles are: Typical Urban (TU), Rural Area (RA), and Hilly Terrain (HT), as shown in Figure 5.1. The profiles were modeled from wideband propagation measurements and are representative of various mobile communication environments [2]. The numerical value  $x$  after the profile abbreviation determines the simulation speed in km/h, e.g., TU3.

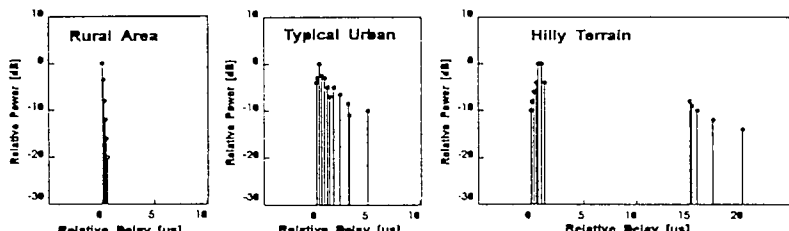


Figure 5.1: GSM specified power delay profiles: Rural Area (RA), Typical Urban (TU) and Hilly Terrain (HT).

The signal strength distribution of the GSM signal exposed to the various test profiles is shown in Figure 5.2. In the GSM context, the RA profile is a narrow-band model, and the small deviation from a Rayleigh distribution is mainly due to a coherent term in the model, which introduces Ricean fading. The TU profile includes considerable time dispersion resulting in frequency selective fading within the GSM bandwidth. The signal strength distribution is therefore significantly improved compared to the Rayleigh distribution. Finally, the time dispersion of the HT profile exceeds the 18.5  $\mu$ s equalizing window of a typical GSM demodulator<sup>1</sup>. The long time delays mitigate the fading probability, but unfortunately also introduce non-equalisable Inter Symbol Interference (ISI). The signal-strength distribution for the HT profile is therefore not directly related to the received signal quality.

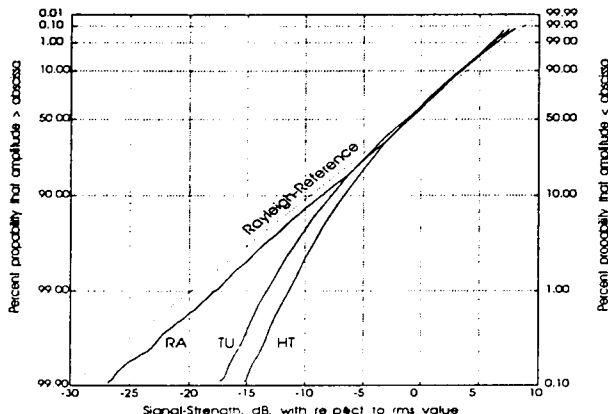


Figure 5.2: Normalized signal-strength distribution for the three GSM specified profiles: Rural Area, Typical Urban, and Hilly Terrain.

It should be noted that these power delay profiles are not suitable for system bandwidths beyond approximately 1-2 MHz, and are therefore inappropriate for simulating non-ideal frequency hopping in GSM. Ideal frequency hopping will be applied in the analysis of FH, i.e., uncorrelated fading between hopping radio channels. This assumption requires in practice a channel separation of approx. 400-600 kHz for urban environments [3].

<sup>1</sup> A 16 state Viterbi algorithm can cope with time dispersion up to approx. 18.5  $\mu$ s

### 5.2.2 The GSM TCH/FS Transmission Mode

GSM specifies a variety of transmission modes on the Traffic Channel (TCH). These modes are :

- TCH/FS, TCH/F9.6, TCH/F4.8, TCH/F2.4 are the transmission modes over a TCH/F (Traffic CHannel/Full rate), respectively for full rate speech, 9.6 kbit/s, 4.8 kbit/s, and 2.4 kbit/s data rates.
- TCH/HS, TCH/H4.8, TCH/H2.4 are the transmission modes over a TCH/H (Traffic CHannel/half rate), respectively for half rate speech, 4.8 kbit/s, and 2.4 kbit/s data rates.

The various transmission modes differ in the details of error correction and error detection (coding and interleaving) schemes [5,6]. Additionally, the control and common channels again use other channel encoding schemes. The performance of the transmission link and the obtainable frequency and antenna diversity gain are dependent on the actual transmission mode. *Only the GSM transmission mode for full rate speech, TCH/FS will be considered in the analysis.* A diagram of the GSM transmission and receiving path for the TCH/FS mode is given in Figure 5.3.

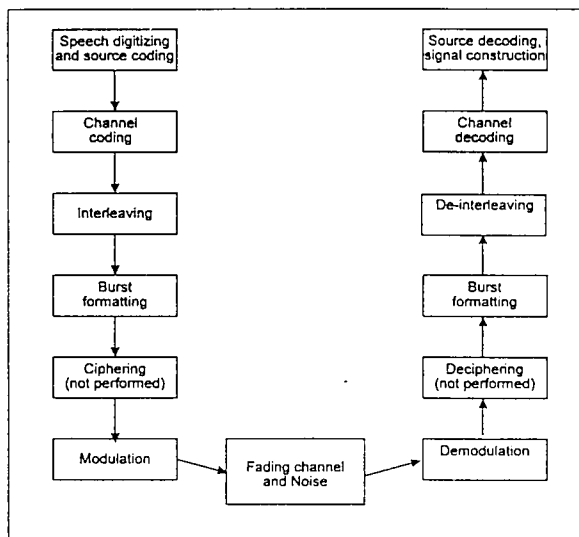


Figure 5.3: Schematic flow diagram of the TCH/FS transmission and receiving path.

The full rate *speech encoder* delivers a data block of 260 bits for every 20 ms (i.e. a net bit rate of 13 kbit/s). The bits produced by the speech encoder

are divided into classes according to importance (Classes 1a, 1b, and 2, in order of decreasing importance). The Class 2 bits have only a small impact on the received speech quality, and are often disregarded in signal quality analysis.

The process of *channel encoding* increases the bit rate by introducing redundancy into the transmission flow. For the TCH/FS mode, a 3 bit CRC is firstly applied to the 50 Class 1a bits. This field is used for frame erasure detection at the receive end. Secondly, all class 1 bits are convolutionally encoded (Code rate = 1/2, Constraint length = 5), whilst class 2 bits remain unprotected. The channel encoding produces a data-block of 456 bits, which corresponds to a gross bit rate of 22.8 kbit/s. The *reordering and interleaving* process mixes the 456 encoded bits and sub-groups them into 8 half-bursts of 57 bits, which are transmitted on 8 successive bursts, i.e. an interleaving depth of 8 [6].

The errored bits tend to appear in “faded” bursts, but convolutional codes perform better when errors are randomly positioned. The reordering and interleaving in the GSM signal transmission flow randomize the error events, provided the 8 successive bursts carrying an encoded data block are exposed to decorrelated fading. This requirement can be ensured by either a spatial movement of the mobile station or a change in frequency (i.e. frequency hopping).

### 5.2.3 GSM Link Tests

Patrick C.F. Eggers (CPK, Denmark)

In the pre-operational phase of GSM, reliable link performance test equipment was not available. Furthermore, statistically based hardware simulators cannot cater for the specific propagation conditions experienced in the field. For this reason, measurements were carried out by various groups together with software modem implementation (stored channel simulation) [7,8,55]. In [8,55] the GSM transmission was simulated whereas in [7] a GSM superframe generator was used to transmit ‘live’ GSM data over the network.

As expected, GSM link performance was found to be better correlated with the delay window based W9 and Q16 parameters (see chapter 2) than with delay spread, due to the finite equalisation capability of real GSM receivers. For each modem implementation, a signature surface (link performance level) can be spanned by CNR and Q16 (or W9) [7,55]. This provides a

simple means to gain a basic GSM link performance estimate directly from radio channel parameters, and in addition it enables reuse of radio channel measurements, avoiding time consuming simulations.

As an example of results obtained, it was concluded in [7] that GSM coverage could not be provided in areas surrounding fjords by using mountains as passive reflectors (as is done with NMT900). This implies that approximately twice the number of base stations would be required for GSM in mountainous terrain.

With the expansion of fully operational GSM networks, interest has turned to performance enhancement techniques (covered in the remainder of this chapter), and to its use in special environments and applications (e.g. high speed trains - see section 4.8.4).

#### 5.2.4 Frequency Diversity

The activation of slow Frequency Hopping (FH) in GSM offers two advantages:

- *Frequency diversity*: Improved burst decorrelation for slow moving users.
- *Interference diversity*: Interference averaging in the network

Only the improvement from frequency diversity is considered here; interference diversity will be discussed later in the chapter.

**Power Envelope Correlation.** A power envelope correlation coefficient below 0.7 is often used as a criterion for diversity applications [13]. Assuming that this coefficient is given by  $J_0^{-2}(\beta v t)$  [13], then it can be found that the speed of a mobile station must exceed approximately 35 km/h in order to meet the above criterion between two successive received bursts. The frequency diversity gain from FH is thus most essential for mobile station speeds much lower than 35 km/h, i.e. pedestrian speed. The frequency diversity gain from FH will be marginal for high speed mobile stations, because the required decorrelation is obtained through spatial movement.

**GSM Hopping Sequences.** Distinct *cyclic* and *random* modes of frequency hopping are specified in GSM [5]. The random mode provides both frequency and interference diversity, whereas sequential hopping can only provide frequency diversity. The maximum number of frequencies,  $N_{max}$ , that can be used in the hopping sequence is 63 [5]. However, in practice, the number of hopping frequencies  $N$  will be much lower because of the limited allocated spectrum and the necessary frequency reuse scheme of a cellular

network. For GSM BTS equipment which does not support synthesized frequency hopping, the frequency hopping is performed at baseband, and thus  $N$  will be limited to the number of installed TRX's.

In cyclic mode, the maximum frequency diversity gain is achieved for  $N \geq 8$  (determined by the interleaving depth). For small values of  $N$ , cyclic hopping provides a noticeably higher frequency diversity gain than random hopping. This is because, for the random hopping case, the probability of using a radio frequency channel more often than  $8/N$  times within the interleaving depth of 8 is high, and thus the fading decorrelation within a speech-frame is not optimal.

**Frequency Hopping Results.** The performance of both random and cyclic frequency hopping has been simulated for a range of values of  $N$ , from 1 (no hopping) up to 12 [16].

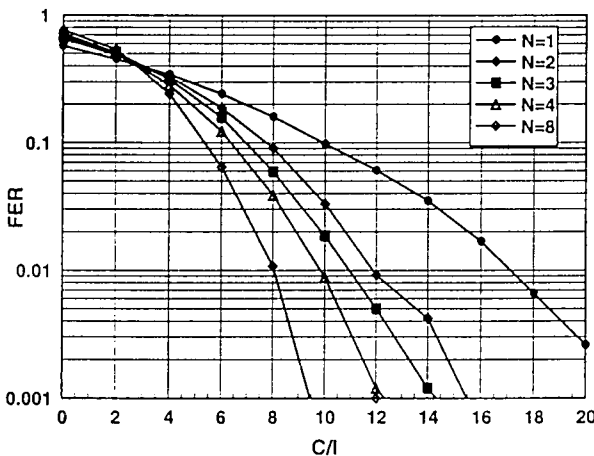


Fig. 5.4: FER (Frame Erasure Rate) as a function of C/I for Cyclic Frequency Hopping, ( $N$  is the number of frequencies in the hopping sequence)

Fig. 5.4 shows the results for the case of cyclic hopping and the TU3 test condition. It can be observed that the frequency diversity gain is considerable (about 8 dB for  $N = 8$  at a FER of 2 %). Even for a low number of hopping frequencies ( $N \geq 2$ ), the gain from FH is significant for this test condition. Random hopping gives approx. 1-2 dB lower gain than cyclic hopping for low values of  $N$  [16]. However, random hopping may still

provide the best overall network performance once the improvement from interference diversity is taken into account [30,12].

In Table 5.1, the results for cyclic frequency hopping for the case of co-channel interference are given for both TU3 and TU50. As expected, the frequency diversity gain from FH is modest for the TU50 test condition; the gain is only of the order of 1-2 dB. From the Table, it can be observed that the absolute performances for the TU3 and TU50 test conditions are almost identical, once ideal frequency hopping is applied ( $N = 8$ ).

No of hopping frequencies	TU50: C/I at FER= 2 %		TU3: C/I at FER= 2 %	
	Absolute level [dB]	Relative gain [dB]	Absolute level [dB]	Relative gain [dB]
1	10.0	0.0	15.5	0.0
2	9.0	1.0	11.0	4.5
3	9.0	1.0	10.0	5.5
4	8.5	1.5	9.0	6.5
8	8.0	2.0	7.3	8.2

Table 5.1: Simulation results for Cyclic Frequency Hopping with  $N = 8$  under co-channel interference [9].

### 5.2.5 Antenna Diversity

The radio link power budget in GSM typically favours the up-link. For cell range extension (and in order to reduce the power budget imbalance), it is desirable to install antenna diversity at the base stations for up-link reception. Downlink antenna diversity may also be required for capacity enhancement, and may be implemented as either Tx diversity (installed at the BTS) or Rx diversity (installed at the Mobile Station). Alternative implementations of antenna diversity in GSM have been studied [17,19,21,22] (see also Chapter 3 for a broader discussion of diversity techniques).

***Up-link Diversity Schemes for GSM.*** The additional cost of antenna diversity at the base station is not critical (both in terms of equipment and power consumption). However classical combining techniques are not suitable due to the frequency selective nature of the channel. Two possible schemes for diversity combining at the base station are described below.

**Matched Filter Combining** is a pre-detection scheme [17], which is a simple implementation of *Wideband Maximal-Ratio combining*. The GSM demodulator unit estimates the radio channels' impulse responses from the training sequence, and the received signals are matched filtered before

detection. Individual matched filtering of each diversity branch co-phases the diversity signals. After the matched filters, the signals can be directly combined and passed to the data-detector, see Fig. 5.5. The combining operation can use weighting coefficients derived from knowledge of the channel conditions (see e.g. [20]).

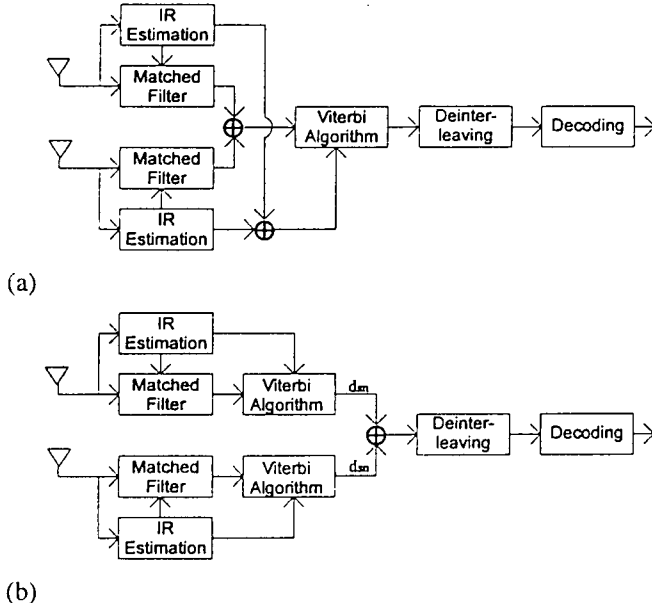


Fig. 5.5: Block diagram of: (a) matched filter combining and (b) soft decision combining.

Soft Decision Combining is a post-detection implementation of Maximal-Ratio combining. An independent data detection is performed for each diversity branch, and the soft decision outputs are combined and passed to the channel decoding unit [17].

The two proposed combining schemes for GSM have nearly equal performance, and the choice will depend on implementation issues. Matched Filter combining gives about 0.3 dB gain over Soft Decision combining under noise conditions, whereas Soft Decision has an advantage of about 0.3 dB in the case of co-channel interference [23].

**Downlink Antenna Diversity Schemes.** The above combining schemes are not suitable for a mobile station because they demand two parallel RF

receiving chains. Two sub-optimal but simple diversity schemes for downlink antenna diversity have been proposed:

- Rx Diversity: Pre-Selection diversity
- Tx Diversity: Delayed signal combining

### Pre-Selection Diversity

Switching and Pre-Selection [13,15] is a simple diversity algorithm which is in general applicable to low cost TDMA radio equipment because it requires one RF receiver chain only. Such a scheme may be based on power measurements of the previous received burst(s) or the previous burst in the TDMA frame structure. However, this requires a high degree of envelope power correlation, and this condition will not be fulfilled in GSM for a fast moving MS or in a Frequency Hopping GSM network<sup>2</sup>. This issue excludes also the feedback type of diversity implementations [13,15].

For Pre-Selection diversity implementation in GSM, the signal strength can be measured during the leading part of each received burst. Unfortunately, the GSM burst structure does not contain an initial preamble field prior to the data bits (as in DECT), which might have been used for measuring signal strength. However, it has been found that the corruption of the first few bits in each burst only introduces a degradation of the order of 0.5-1 dB [22]. These bits may therefore be used for signal strength monitoring, since the degradation is much smaller than the diversity gain of “true” Selection diversity.

Such a “destructive” pre-selection diversity scheme has been proposed and analyzed in [22]. The optimum period  $k$  for signal-strength estimation has been found to be 3-5 bit periods, and the switching and receiver settling time  $m$  has been assumed to be 3 bit periods (see Fig. 5.6).

When the first observed diversity antenna is selected  $2*(k+m)$  bits are corrupted, whereas only  $(k+m)$  bits are corrupted if the last observed antenna branch is selected.

---

<sup>2</sup>With the exception of mobiles on the BCCH carrier, where the previous timeslot in the TDMA-frame can be used for diversity measurements.

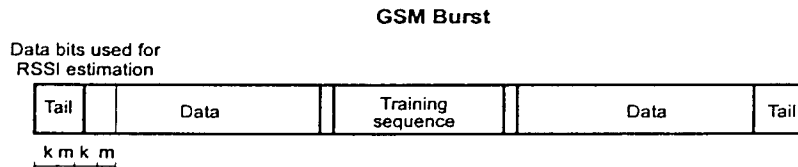


Fig. 5.6: A GSM normal burst with indication of the signal-strength measurement period  $k$  and the switching time  $m$

### Delayed Signal Transmission

Antenna diversity has not been implemented in GSM mobile stations until now. However, a Delayed Signal transmission scheme for the down-link path is possible, with simultaneous transmission from a second antenna branch at the base station, and where the relative transmission delay of the second branch is of the order of 2 bit periods [17,18]. The received signal at the mobile station comprises two decorrelated signals with a time delay offset (see Fig. 5.7). These signals are coherently combined by the equaliser, thus reducing the fading probability.

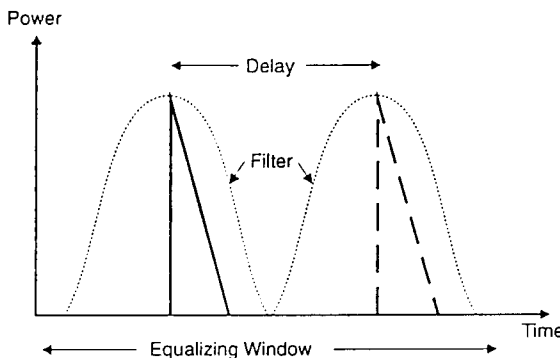


Fig. 5.7: Delayed signal combining of GSM signals

#### 5.2.6 Antenna Diversity Performance Results

Fig. 5.8 and Fig. 5.9 show simulation results for the different antenna diversity implementations in terms of Frame Erasure Rate (FER) and raw (class 2) BER, respectively.

It can be seen from these that the potential gain from two branch antenna diversity in GSM is very high under the conditions given. The figures also illustrate the complexity of antenna diversity evaluation for GSM: the raw performance of Pre-Selection diversity is worse than that of a single antenna

at high C/I levels (Fig. 5.9), but its FER performance approaches that of “true” Selection diversity (Fig. 5.8). The distribution of bit errors before channel decoding strongly affects the FER performance, and thus the raw BER is not a good measure of the received signal quality. This is analogous to the case of frequency diversity and FH (FH does not improve the raw BER but nevertheless significantly reduces the FER).

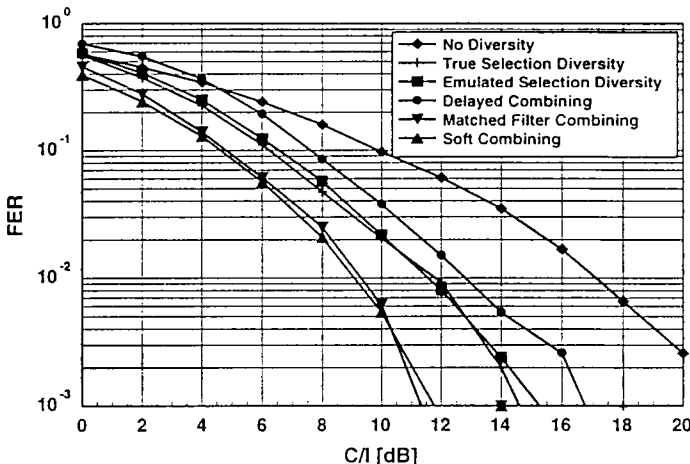


Fig. 5.8: Simulated antenna diversity gain for various diversity algorithms (TU3, no FH, and co-channel interference) [23]

The antenna diversity gain is shown in Table 5.2 for both ideal FH and no hopping. In the latter case, all diversity schemes provide gains (4-7 dB). When ideal FH is used, the antenna diversity gains are reduced by 3-3.5 dB, and only the Maximal-Ratio type of combining schemes (MF and Soft-Decision combining) show a diversity gain exceeding 3 dB.

	TU3 (No FH)		TU3 (Ideal FH)	
No Diversity	15.5	(0.0)	7.3	(0.0)
Delayed Combining	11.3	(4.2)	6.8	(0.5)
Emulated Selection	10.2	(5.3)	6.2	(1.1)
True Selection	10.0	(5.5)	5.2	(2.1)
MF Combining	8.3	(7.2)	4.0	(3.3)
Soft Combining	8.0	(7.5)	3.2	(4.1)

Table 5.2: Required C/I [dB] for a FER of 2 percent for different antenna diversity techniques. The antenna diversity gain [dB] is shown in brackets [23].

Table 5.3 shows antenna diversity performance in noise conditions for TU3, RA250 and HT100. The diversity gain is high for the case of TU3 and no FH, but is lower than 3-4 dB for all other test conditions.

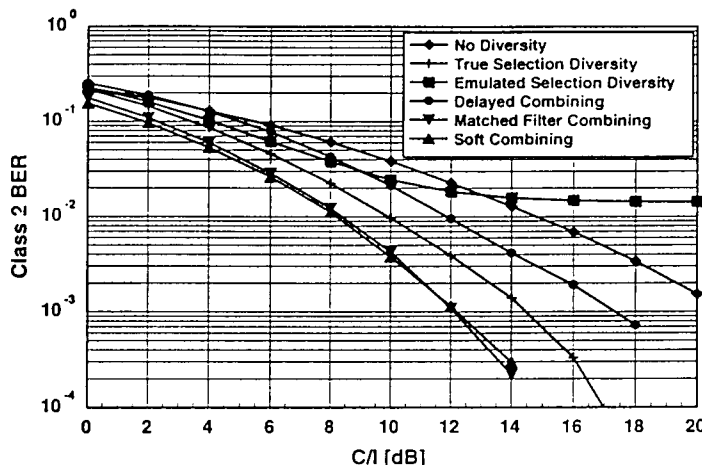


Fig. 5.9: Simulated antenna diversity gain for various diversity algorithms (TU3, no FH, and co-channel interference) [23]

	TU3 (No FH)		TU3 (Ideal FH)		RA250 (No FH)		HT100 (No FH)	
No Diversity	12.5	(0.0)	5.5	(0.0)	5.9	(0.0)	6.9	(0.0)
Delayed Combining	9.4	(3.1)	5.2	(0.3)	5.3	(0.6)	8.2	(-1.3)
Emulated Selection	8.2	(4.3)	3.6	(1.9)	4.0	(1.9)	5.0	(1.9)
True Selection	7.2	(5.3)	2.5	(3.0)	3.2	(2.7)	3.5	(3.4)
MF Combining	5.8	(6.7)	1.6	(3.9)	1.1	(4.8)	2.1	(4.8)
Soft Combining	5.9	(6.6)	1.8	(3.7)	1.1	(4.8)	2.1	(4.8)

Table 5.3: Required Eb/No [dB] for a FER of 2 percent for different antenna diversity techniques. The antenna diversity gain [dB] is shown in brackets [23].

### 5.3 Capacity Study of a Frequency Hopping GSM Network

Preben E. Mogensen, Jeroen Wigard (CPK, Denmark)

This section discusses capacity improvement in a GSM network through the use of random FH combined with fractional network loading. In general, two strategies can be used for increasing the capacity of such a network:

- Increased capacity per cell
- Reduced cell size (deploying additional base stations)

These two strategies do not exclude each other. Cell size reduction on its own can be very effective since the GSM cell area can vary from more than  $100 \text{ km}^2$  to under a tenth of a  $\text{km}^2$ . No other capacity enhancing methods can provide such a range of more than 3 decades. However, the introduction of micro-cells has some drawbacks in terms of network cost and management.

On the other hand, the combination of Frequency Hopping with RF power control and DTX can provide an increased capacity per cell. When further combined with adaptive antennas, the potential for increased capacity becomes very significant, as will be seen later.

#### 5.3.1 Conventional Fixed Frequency Reuse Schemes

The frequency re-use factor  $K$  is given by  $K = k / n$ , where  $k$  is the ideal cluster size (number of base sites), and  $n$  is the number of frequency sets used in a cluster, e.g., for  $k = 3$ ,  $K = 3/3$  and  $K = 3/9$  respectively represent omni-directional and  $120^\circ$  sectorised BTS configurations.

*The BCCH Carrier.* The frequency reuse for the BCCH carrier (the beacon frequency) is relatively poor, since the BTS must transmit continuously in all timeslots without RF power control. The most efficient reuse has been found to be when  $K = 4/12$  (for 10 % outage at a CIR threshold of 9 dB) [14]. However, this result is based on a ‘regular’ network layout and a simple pathloss model, and may therefore be slightly optimistic. However, for a sectorised BTS, there is a large step between the cluster size 4/12 and the next value of 7/21 (requiring 75 % more frequency channels). A more flexible frequency reuse method is based on the so called *co-channel interference matrix*, whereby the actual BTS location and configuration are taken into account. A reuse scheme using a pool of 14-18 frequencies for the BCCH carriers is often employed in conjunction with the co-channel interference matrix method [27].

*The Traffic Carriers.* With non-hopping Traffic (TCH) carriers, the frequency reuse is very similar to that of the BCCH carrier. Even when the

GSM capacity enhancing features (DTX and RF power control) are activated, the capacity improvement is modest without random FH. The frequency reuse for the TCH carrier requires typically a pool of 12-14 channel sets [14,27]. It should be noted that the co-channel interference matrix method allows joint frequency assignment for both BCCH and TCH carriers from a common frequency pool.

### 5.3.2 Frequency Reuse on Hopping TCH Carriers

When random frequency hopping is activated, a conventional frequency reuse scheme based on a worst case interference situation (i.e. 100 % load) is spectrally inefficient [1,29]. Congestion (hard-blocking) limits the capacity of the network well before the CIR values (soft-blocking) become crucial, since random FH provides both frequency and interference diversity. For the case of full rate speech (TCH/FS), the interference varies<sup>3</sup> over the interleaving period of 8 bursts. The mean co-channel interference level in the network can be adjusted by two parameters:

- The frequency reuse factor,  $K$
- The mean fractional loading,  $F$

*Fractional loading* is the percentage  $F$  of the available channels in the network that may be in use simultaneously (e.g. a fractional loading of 25 % reduces the mean interference level by 6 dB). It is apparent that the two parameters  $K$  and  $F$  interact closely: the higher reuse factor  $K$ , the higher the fractional loading  $F$  and vice-versa. The advantages of random FH combined with fractional loading can be seen from the following:

- Interference diversity (averaging): all users will be heard nearly equally as interference and therefore a higher mean interference level in the network will be accepted.
- Therefore a low frequency reuse scheme can be combined with fractional loading. The increased number of channels per cell reduces the hard-blocking probability significantly.

---

<sup>3</sup>The interference is not truly averaged as in DS-CDMA

### 5.3.3 Impact of Allocated Frequency Spectrum

Many GSM network operators have been allocated a narrow frequency band. In Table 5.4 the number of available traffic carriers (TCH) is shown for various frequency bandwidth allocations. It can be observed that the first 2.6 MHz of spectrum (including a guard-band channel) only covers the basic BCCH carrier requirement. For a conventional non-hopping GSM network, the TCH carriers also require 12 frequency channels for a sectorised configuration [1,14]. The number of TCH carriers per cell is thus modest for narrow spectrum allocations, see Table 5.4.

Allocated Spectrum	5.0 MHz	9.8 MHz	17.0 MHz
No of RF carriers	24	48	84
No of BCCH carriers	12	12	12
No of TCH carriers	12	36	72
TCH carrier per cell:			
K = 1/1	12	36	72
K = 1/3	4	12	24
K = 3/9	1.3	4	8
K = 4/12	1	3	6

Table 5.4: The number of available TCH carriers per cell for various spectrum allocations and frequency reuse factors

Table 5.5 shows the maximum relative load of a cell due to blocking, for various numbers of carriers per cell. It can be seen that 4-6 carriers per cell are required in order to achieve a high spectral efficiency. Additional TCH carriers only give a marginal improvement in spectral efficiency (e.g. Erlang/MHz). From Table 5.4 and Table 5.5 it can be concluded that from a hard-blocking perspective, the best frequency reuse schemes are  $K = 1/1$  or  $1/3$ , especially when the allocated spectrum is less than 10 MHz, whereas for large bandwidth not much can be gained by increasing  $K$  beyond  $3/9$ . The penalty of a low frequency reuse scheme is obviously higher co-channel interference, which must be compensated for by having the network fractionally loaded.

The optimum solution to the two divergent limitation factors of hard blocking (dismissed calls) and soft blocking (low CIR) can be found by simultaneously optimizing the frequency reuse,  $K$ , and the fractional loading,  $F$ . This has been examined via computer simulations [1,14].

Carriers	TCH/F Channels	Erlang B (2 % blocking)	Relative mean load of TCH	Spectral Efficiency
1+1	8+6	8.2	59 %	51 %
2+1	16+6	14.9	68 %	62 %
3+1	24+6	21.9	73 %	68 %
4+1	32+5	27.3	74 %	68 %
6+1	48+5	43.1	81 %	77 %
8+1	72+4	64.9	85 %	81 %
12+1	96+4	88.0	88 %	85 %

Table 5.5: Maximum relative load of a GSM cell at a 2 % hard-blocking level

### 5.3.4 Results From GSM Network Simulations

Network level simulations of a GSM system have been made in order to investigate DTX, RF power control, random FH, frequency reuse, and fractional loading. The impact of the propagation parameters such as path-loss slope, standard deviation of shadow fading, radiation pattern of the base station antenna and back scattering have also been investigated [14].

Table 5.6 summarizes some of the essential parameters used in the capacity study (for more details see [14,29]). It can be seen that one of the two network performance criteria is the call dismissal probability of 2 % (hard-blocking). The second criterion is based on the fact that 90 percent coverage probability is usually accepted in a GSM network [1]. Hence, if co-channel interference is the dominant quality limitation, it is expected that the network quality will be acceptable if no more than 10 percent of the CIR values are below 9 dB. It should be noted that both the selected threshold values have a strong influence on the achieved capacity.

Path loss	$L_p = 35 \log d$
Log-normal fading standard deviation	6 dB
Correlation distance	1/e at 110 m
Call mean hold time	100 s
Mobile velocity	50 km/h
Cell radius	2 km
Antennas	90° sectorised
Allocated spectrum	9.8 MHz
Frequency hopping algorithm	random hopping
DTX factor	0.5
CIR threshold	9 dB with a 90 % probability
Blocking	Erlang B, 2 %

Table 5.6: The parameters of the GSM network simulation

**Random Frequency Hopping.** Random frequency hopping leads to an averaging of the interfering signals. For illustration, Fig. 5.10 shows the CIR of two mobiles using random and no hopping (both without DTX). It can be observed that, without random FH, the signal quality (CIR) is only affected by the shadow fading, which is updated every 0.48 s within the simulation.

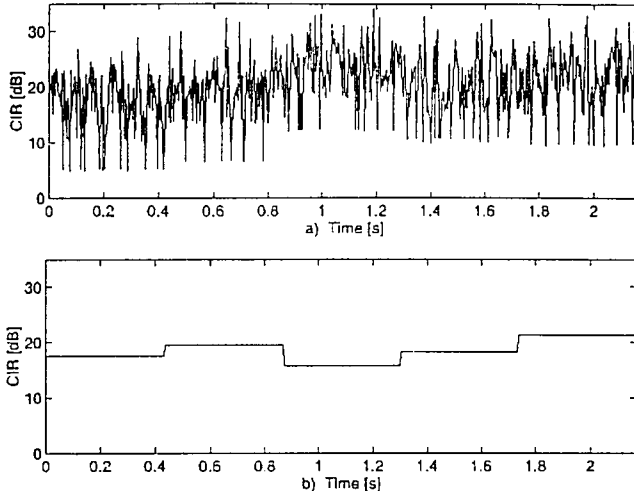


Fig. 5.10: The instantaneous CIR of two mobiles during a period of 520 bursts: a) is with random frequency hopping and b) is without frequency hopping [29]

The interference level on each individual channel changes very slowly and depends effectively on whether a strong interfering signal is present or not on the specific channel. Conversely, when random frequency hopping is activated, the interfering conditions change for each burst. Under such conditions, the average received CIR becomes critical, rather than the worst case situation. The interference reduction from RF-power control and DTX can then be directly translated into a capacity increase, since the improvement is averaged among all mobiles in the network. Without random FH the improvement in mean CIR will not directly translate into a capacity increase since the Mobile Stations will benefit differently.

**Impact of DTX and Fractional Loading.** The results from the simulation of DTX showed a linear proportionality between the DTX factor and the CIR improvement (i.e., decreasing the DTX factor to 0.5 leads to an interference reduction of 3 dB). The same proportionality holds for the fractional load  $F$ : a reduction in traffic load by a factor of 2 reduces the mean interference level by 3 dB. These results are as expected and confirm that DTX and

fractional loading are very powerful means to reduce the mean interference level in a random hopping GSM network.

**Relation Between Reuse Factor and Fractional Loading.** From a hard-blocking perspective a low reuse factor  $K$  is optimal, but the drawback is the higher potential interference level, which demands a low fractional loading  $F$ . Table 5.7 shows the maximum fractional loading for various reuse factors. The lowest reuse factor that allows full loading is  $K = 3/9$ . The maximum fractional loading of 25-30 % for  $K = 1/3$  implies a need for interference reduction of 5-6 dB relative to a fully loaded network.

Reuse factor K	1/1	1/3	3/9	4/12
Maximum load due to interference	6-7 %	25-30 %	100 %	100 %

Table 5.7: The maximum load of a FH GSM network limited by co-channel interference ( $C/I > 9$  dB with 90 % probability)

**Maximum Capacity.** Various reuse factors and fractional loading values have been simulated in order to determine an optimal network configuration. Maximum capacity has been defined as the smallest load for which one of the blocking criteria is reached. The hard blocking limit depends on the allocated frequency spectrum, and therefore a configuration with 36 TCH carriers (9.8 MHz) is used as an example. Table 5.8 provides the resulting maximum capacity figures.

Random Frequency Hopping			
Reuse	Erlang/cell	Erlang/site	Blocking
1/1	20.2	20.2	Soft
3/3	61.4	61.4	Soft
4/4	60.5	60.5	Hard
1/3	28.8	86.4	Soft
3/9	23.7	71.0	Hard
4/12	16.6	49.7	Hard

Static (no interference diversity)			
Reuse	Erlang/cell	Erlang/site	Blocking
4/12	16.6	49.7	Hard

Table 5.8: Maximum capacity of various reuse factors for a network with 36 TCH carriers (at 2% call congestion and 9 dB C/I with 90 % probability). Note that capacity from the BCCH TCH timeslots is ignored [29].

These results are also illustrated in Fig. 5.11.

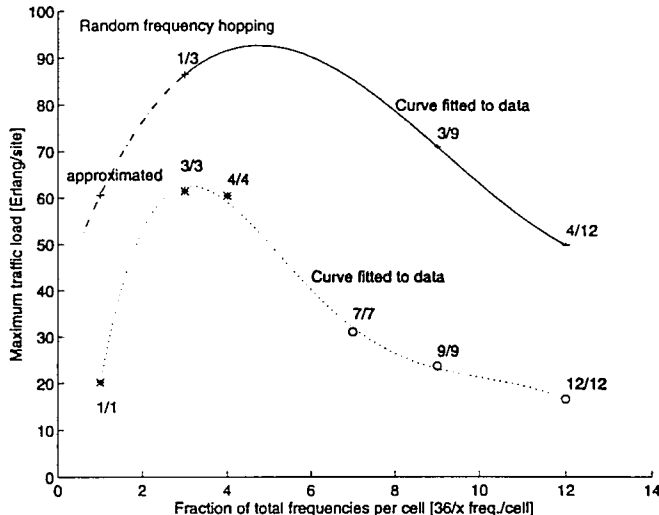


Fig. 5.11: Maximum capacity per site as a function of frequency reuse factor  $K$  for a network with 36 TCH carriers (excluding BCCH carrier traffic). The upper curve is for sectorised BS sites and the lower one is for omni-directional sites.

The maximum capacity per site is obtained for a sectorised base station and a frequency reuse factor  $K = 1/3$ . This result has also been found in [1]. The capacity increase of a random FH network using a frequency reuse scheme of  $K = 1/3$  is approx. 74 % compared to a non FH network with a frequency reuse scheme of  $K = 4/12$ . (but in general the capacity increase depends on the spectrum allocation).

In practice, use of the  $K = 1/3$  scheme would make frequency planning trivial. However, a large number of TRXs is required in each site (in the case of baseband hopping), and intelligent radio resource management software must be included in the Base Station Controller for control of fractional network loading.

### 5.3.5 Interference Gain from Fractional Loading

The capacity study of a random FH GSM network [14] was based on a 9 dB mean CIR threshold. The CIR threshold of 9 dB is determined by link simulations with a continuous co-channel interfering signal according to the test specifications in [9].

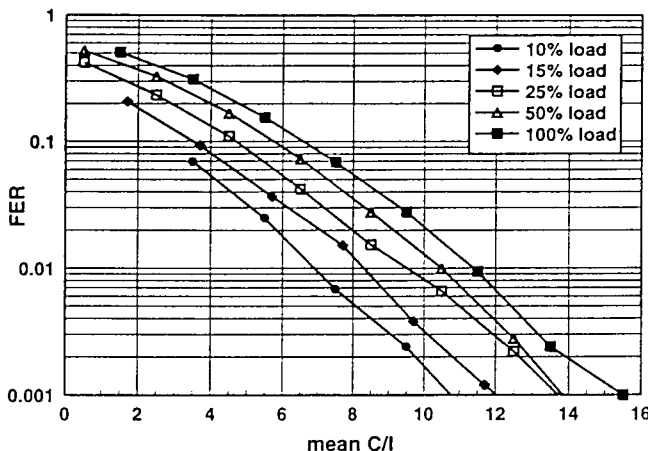


Fig. 5.12: FER as a function of mean CIR for a fractionally loaded network. The load values given are a combination of DTX and fractional network loading [30]<sup>4</sup>.

However, when using random FH combined with DTX and fractional loading, the co-channel interference pattern will not be continuous, but instead change significantly from burst to burst. Thus, some bursts will be heavily interfered whilst other bursts will be received virtually without any interference. Results from link simulations with such an interference behaviour have shown a significantly reduced Frame Erasure Rate [12,30], compared to the test interference situation specified in GSM 05.05 [16]. For an ideal reuse cluster there will be, on average, 6 equally strong interfering signals [13]. Due to shadow fading, the 6 interferers will have distinct instantaneous levels. In [11] and [30], it has been shown that only one or two of the interferers are usually dominant at a time, and thus the on/off pattern created by DTX and fractional network loading will be reflected in the interference pattern. In Fig. 5.12, the FER is shown as a function of mean CIR for several values of fractional loading. At 15 % load (i.e., 30 % fractional loading and a DTX factor of 0.5), the quality improvement corresponds to about 2-3 dB gain in CIR. However this interference gain from fractional loading cannot be linearly converted into an additional capacity improvement, because the higher fractional loading will decrease the interference gain.

---

<sup>4</sup>Log-normal fading has been added to the interfering signal.

**Base Station Synchronization.** The results shown above assume an ideally synchronized network. In real life the BTSs in a GSM network are not synchronized, and the relative time alignment of interfering bursts will be random and uniformly distributed. The impact of this has been analyzed in [30]. For the case of 30 % fractional loading and a DTX factor of 0.5, the relative degradation from an unsynchronized network is below 0.5 dB compared to the ideal synchronized case shown above (where the propagation delay is also ignored).

### 5.3.6 Potential Capacity Gain from Smart Antenna Systems in a K = 1/3 Random FH GSM Network

Recently, interest in smart antenna systems (either adaptive steerable or switched beam antenna arrays) has increased due to their potential for capacity and range enhancement of mobile communications systems.

For a random FH GSM network the frequency reuse factor,  $K$  can be changed from  $K = 4/12$  to  $1/3$ , which gives the maximum capacity per site. The capacity limitation for the  $K = 1/3$  reuse scheme is CIR outage (soft blocking), and the fractional loading of the network must be kept below 25-30 % (see Table 5.7). By using adaptive antenna arrays to suppress interference, the fractional loading can in theory be increased to the hard-blocking limit. The CIR gain of the antenna array needs to be of the order of 5-6 dB if the system is to reach the load set by hard-blocking.

Frequency reuse Scheme	K = 1/3	K = 4/12
<b>GSM network without adaptive antenna array</b>		
Load limit from Soft-blocking	30 %	100 %
Load limit from Hard-blocking	87 %	69 %
Capacity per site [Erlang]	86.4	49.7
<b>GSM network with ideal adaptive antenna array</b>		
Relative potential capacity gain	2.9	1.0
Capacity per site [Erlang]	250.6	49.7
Capacity increase relative to K=4/12	400 %	0 %

Table 5.9: Potential capacity increase of a random FH GSM network using  $K=1/3$  frequency reuse and adaptive antenna arrays. The hard blocking limit is calculated for 36 TCH carriers (9.8 MHz).

In [32] the antenna array geometry has been analysed. Simulations which include the effect of angular spreading from the environment indicate that an 8 element (horizontal) linear array meets the CIR requirements. Table 5.9 gives the potential capacity increase of a random FH GSM network using adaptive antennas, assuming that the required CIR gain of about 5-6 dB is achieved.

## 5.4 The DECT Standard

**Andreas F. Molisch, Heinz Novak, Josef Fuhl (TU Wien, Austria)**

### 5.4.1 General

The pan-European DECT (Digital Enhanced Cordless Telecommunications) Standard [33,34] enables the deployment of a new generation of cordless telephones and indoor personal communication equipment. DECT specifies the wireless connection set-up and release between fixed base stations and mobile terminals. The mobiles can be cordless telephones or other terminals in a short range private or business indoor environment.

From the user's point of view the most striking change from existing cordless telephones is that one base station can serve multiple mobiles simultaneously. Additionally, in business networks the user is not related to one particular base station, which results in higher accessibility.

The DECT mobile can perform handovers between different base stations of a wireless network as in cellular mobile communication. The difference is that location, coverage range and frequency reuse of the base stations need not be preplanned by a system operator because the system is self organising in its use of spectral resources.

To reduce hardware costs in the base stations accessing multiple mobiles and to minimise management efforts, the DECT standard embodies a change from today's conceptually simple, analogue FDD/FDMA (Frequency Division Duplex / Frequency Division Multiple Access) to the more complex FDM/TDD/TDMA (Frequency Division Multiplex / Time Division Duplex / Time Division Multiple Access) with digital speech transmission. This means that a number of freely accessible frequency channels are shared by multiple users for both transmission directions.

### 5.4.2 The DECT Standard and its Challenges

In the DECT standard, the FDM dimension allows access to 10 different frequency channels in the range 1.88 to 1.90 GHz. The TDD format means that each frequency channel has a repetitive frame structure, with each frame having up-link and downlink sections (as shown in Fig. 5.13). In addition, DECT provides 24 slots in each frame, enabling up to 12 users to share a frequency channel in time division multiple access mode. The slots are separated by guard times to ensure that consecutive time slots are not overlapping, for channel switching and TDMA power ramping. A total of 120 logical channels would therefore be available at a single base station if

there were no reuse constraints. In practice, a standard DECT base station has a single transceiver and can access only 12 of these simultaneously, so that more than one base station can service a particular area without collision problems. This allows a dense packing of base stations, without defined cell boundaries, resulting in large traffic capacities [35].

As seen in Fig. 5.13, a DECT slot begins with a 16 bit preamble and a 16 bit packet synchronisation word (the 32 bit S-field). This is followed by 64 bits of signalling (A-field), which include a robust Cyclic Redundancy Check (CRC) for the detection of packet reception failures. Finally, the B-field contains 324 bits of data, enabling the transmission of 32 kBit/s ADPCM coded speech using a single slot. The transmission data rate is 1.152 Mbit/s.

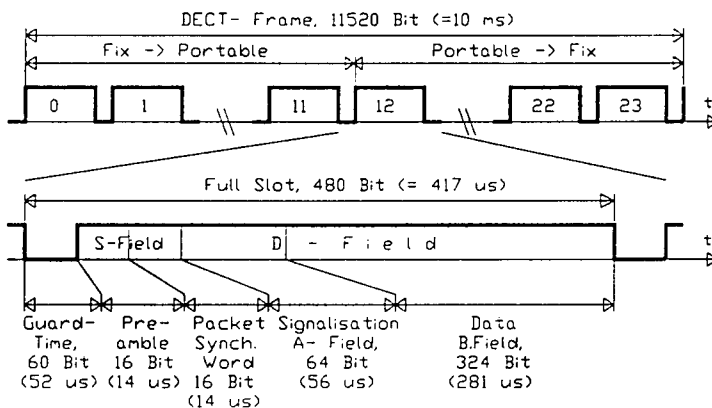


Fig. 5.13: DECT frame and DECT slot structures

DECT uses the well known modulation format GFSK with the moderate BT product of 0.5, which provides a compromise between emitted spectrum and intersymbol interference [36]. The resulting RF-channel bandwidth is about 1.33 R or 1.559 MHz (for a 99% power criterion). With the specified channel spacing of 1.728 MHz (1.5 R), a very significant adjacent channel emission of -40 dBc occurs (in analogue systems this value is normally below -80 dBc). For successful operation of a wireless DECT speech connection, bit error rates below  $10^{-3}$  and slot error rates below  $10^{-2}$  are required. Table 5.10 shows a summary of important DECT parameters.

Transmission Format:	FDM/TDD/TDMA
Frequency Band:	1880 - 19000 MHz
Centre Frequency for Channel N (0..9)	1 897 344 - N * 1 728 kHz
Number of Frequency Channels	10
Channel Spacing:	1.728 MHz
Frame Length (24 Slots):	10 ms
Data Rate:	1.152 Mbit/s
Modulation Method:	GFSK, BT = 0.5
Tolerated Bit Error Rate (*):	< 10 <sup>-3</sup>
Tolerated Slot Error Rate:	< 10 <sup>-2</sup>

Table 5.10: Important parameters of the DECT standard

(\*) for speech service only

The DECT standard does introduce some new technical challenges when compared to classical analogue systems, as listed below [37,38]:

- The dynamic range between consecutive slots can be up to 100 dB due to the absence of power control.
- Due to transmission delays, channel variations, and synchronisation errors, the incoming slots can be asynchronous at bit, slot, and frame level.
- High adjacent channel- and co- channel interference cause conflict situations, leading to a requirement for intracell handover .
- Distributed slot and channel allocation requires intelligent terminals with field strength and signal quality measurement capabilities to estimate, avoid and handle transmission collisions.
- Even in indoor applications, the DECT RF channel suffers from significant dispersion (delay spread).
- The absence of channel coding for error protection (and interleaving) means that terminals must be able to handle error bursts and missing slots.
- FDM/TDMA requires extremely fast switching of synthesisers.
- Additional outdoor and indoor/outdoor applications are envisaged (e.g. public access, radio in the local loop) which may pose further challenges.

## 5.5 A Physical and Medium Access Layer DECT Testbed

Andreas F. Molisch, Heinz Novak, Josef Fuhl (TU Wien, Austria)

Several testbeds were developed by participating organisations in COST in order to evaluate the performance of transmission according to the DECT standards. In the following some of the features of these are described.

### 5.5.1 Modelling of a DECT Wireless Link

The design of a DECT testbed requires the analysis of a realistic DECT wireless link. The slots are transmitted over a fading channel, and both up-link and downlink are interfered by various adjacent- and co-channel signals. The incoming signal at the receiver's antenna is the sum of these signals after convolution with each individual, time variant channel impulse response, as well as white gaussian noise. Disregarding some differences at higher layers of the standard, the DECT link is on average (but not instantaneously) symmetrical, and in practice there is usually one dominant interferer. Therefore it follows that a single transmission direction can be considered, and it is possible to replace the set of interferers by one well defined adjacent- or co-channel transmitter without losing much generality.

Further, a single dispersive fading RF channel is required (for the desired signal). In the case of the interfering signal, it is expected that the small indoor delay spreads will not modify the interfering signal behaviour significantly, and it will be sufficient to implement flat Rayleigh fading.

### 5.5.2 The DECT Testbed

The basic arrangement of the DECT testbed of [39] is shown in Fig. 5.14. It consists of a unidirectional DECT RF link scenario, including one desired transmitter (TX1), one interfering transmitter (TX2), the receiver (DRX) and an optional channel simulator (CAN). The return link is performed by a wired low data rate signalling connection from the receiver via a controlling personal computer (DTC) back to the desired transmitter (TX1). Transmitted data (D<sub>TX</sub>), received data (D<sub>RX</sub>) and slot synchronisation information (DV<sub>TX</sub>, DV<sub>RX</sub>) is transported by a wired high data rate connection to an error counter (ERC).

The error counter has as inputs the delayed data and data-valid signals from the desired transmitter TX1, and the equivalent signals from the DRX. Three statistical parameters are used to quantify the transmission quality in burst

mode: the bit error rate (BER), the synchronisation error rate (SER), and the average bit error rate (ABER) [39].

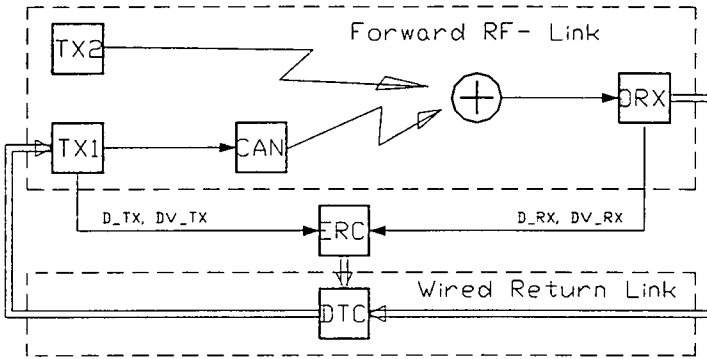


Fig. 5.14: Basic arrangement of the DECT testbed

The channel emulator (CAN) used with this testbed is realised by a tapped delay line with repeater amplifiers which can supply antennas at delays of 0 to 450 ns in steps of 50 ns. The output power of each tap is adjustable in order to select desired power delay profiles, thereby synthesising a particular radio environment. The time variant instantaneous delay profile then results from the natural Rayleigh fading of every discrete delayed path in a low dispersion environment. To provide statistically independent signal paths, the antennas are separated by a distance much greater than the coherence distance of the spatial fading pattern.

Conversely, the DECT testbed of [40,42] has no wired connections, enabling applications and Tx-Rx separations in excess of what is practically possible with a wired approach. It is therefore particularly suitable for outdoor operation and direct testing in dispersive environments. This testbed includes a dual receiver, allowing for live diversity tests. The transmitter and receiver radio parts are built from standard integrated components, and the modems are implemented via DSPs following ADC/DAC at a suitable IF.

## 5.6 Propagation studies for DECT environments

**Andreas F. Molisch, Heinz Novak, Josef Fuhl (TU Wien, Austria)**

The performance of DECT strongly depends on the propagation characteristics observed within the deployment area. Channel characteristics experienced under typical operation conditions are therefore of great interest. As discussed later, for satisfactory performance the rms delay spread should not exceed 100ns (without antenna diversity) and could go up to maxima of 250ns and 450ns with, respectively, RSSI and ideal BER driven diversity [47].

The environments may be categorised according to the three different types of DECT system operation [48]:

- 1) Indoor propagation channel: residential and business cordless telephones applications
- 2) Indoor/outdoor propagation channel: radio extension of public and private networks
- 3) Outdoor propagation channel: Telepoint system applications

### 5.6.1 Measurement Results

Narrowband and wideband measurements have been performed in order to assess the performance of a DECT link for the different classes of environments. The main focus was on wideband measurements [49,50,51,53,57,59,58] and specifically on determining delay spread and fading statistics. The results vary in scope due to the different types of environments under consideration.

Reference [48] reported typical values for the delay spread of 11-147ns for environments of category 1, 43-270ns for environments of category 2, and 57-231ns for environments of category 3. When Ricean fading was observed in the measurements the K-factor was usually low ( $K < 2$ ).

Propagation measurements for environments of category 3 (two streets and two city squares of downtown Oslo) were given in [59]. In streets, the mean delay is less than 75ns and the delay spread is less than 63ns at 90% of the measurement locations. However, for squares (whose dimensions are larger), these figures rise to 157ns and 148ns, and the delay spread is less than 100ns in only 55% of the locations.

Tests were carried out in outdoor and indoor Telepoint environments [53] in Aalborg (in a railway station and hardware store respectively). These showed delay spreads up to around 300 ns and corresponding frequency domain magnitude variations  $V_m$  [58] around 20 dB (see also chapter 2 regarding this parameter), using antenna BS heights of 4 m. The corresponding average dispersion figures were around 100 ns and 10 dB.

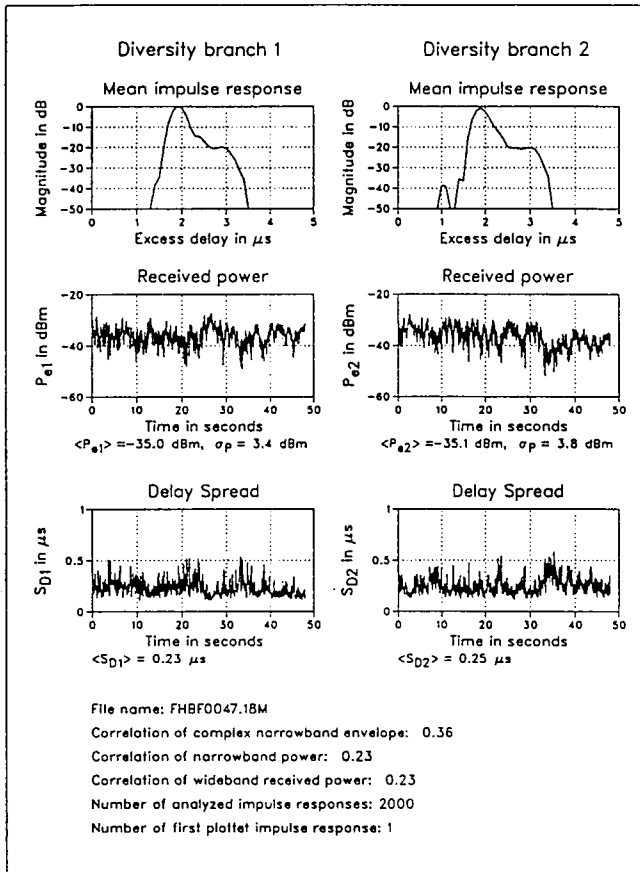


Fig. 5.15: Measured impulse responses, wideband received power and delay spread in the two diversity branches [57].

Wideband propagation measurements were carried out at the Frankfurt railway station using two diversity branches [57,58,77]. Most of the observed power delay profiles show an exponential decrease, suggesting that the scatterers are located all around the receiver. Maximum excess delays of 3μs and delay spreads up to 200 - 300ns have been observed. The delay

spreads are reduced if the base station antennas employ shaped elevation patterns. Fig. 5.15 shows the mean impulse responses, the received power levels and the delay spreads for one such diversity measurement [57]. The power levels and delay spreads of the two branches have the same statistics, but their instantaneous values are distinct.

For two monopole antennas mounted 20cm ( $1.2\lambda$ ) away, the correlation coefficient of the wideband received power was less than 0.25, i.e. the two branches can be considered to be uncorrelated.

Finally, measurements reported in [49,50,52] concentrated on street canyons. It was observed that the path loss is reduced with respect to free space loss by a wave guiding gain factor, and that the delay spread tended to be below 90 ns when the transmitter is placed well below rooftop. However, paths with larger delays are observed in roundabouts and street crossings, and, similarly, the delay spread also increases dramatically if the transmitter antenna is placed above rooftop. It was also shown that the dominant propagation paths are the direct LOS path, reflections from the wall of canyons and back reflections from building fronts at the end of the canyon. Besides these deterministic rays which may be derived using ray tracing, additional scattered components were found arising from obstacles which may vary from day to day, and which require a statistical characterisation.

Measurements performed in a typical office area [51] showed that, under indoor LOS conditions, the delay spreads are very small (typically about 25 ns). However, the delay spreads increase by a factor of four when the transmitter is placed in the central court yard and in addition the path loss can increase beyond the DECT limits due to e.g. fire protecting walls.

The measurements quoted suggest that time dispersion could impact system performance for environments types 2 and 3. However, even in these cases, the delay spread values are within a range where diversity and/or equalisation techniques [47] can be successfully employed.

### 5.6.2 Channel Models

From the measurement results obtained, channel models have been derived for simulation and performance assessment. An example is the set of models in [60], which are all single exponentials with delay spread and maximum excess delay dependent on the type of environment. For type 1 environments, the suggested typical and worst case values are: delay spread 100ns and 200ns, and maximum excess delay 691ns and 1382ns. For types 2 and 3, the delay spread range is 150ns/300ns and the maximum excess delay

range is 1036ns/2072ns. The profile taps are Rayleigh fading with a fading rate of 2 Hz for all environments. The most common channel model, however, is the two path channel with equal power in the two paths, although this model is rather simplified [49,60]. Typically, both paths will be Rayleigh-fading. A more appropriate model is a 2-delay exponential decay profile. A simple method for controlling the delay spread for this model in a test site was presented in [61].

## 5.7 Basic Performance of DECT

**Andreas F. Molisch, Heinz Novak, Josef Fuhl (TU Wien, Austria)**

In contrast to GSM, DECT does not use an elaborate channel coding scheme, and the speech coding is much simpler (enabling lower production and development costs). As a result, good speech quality can only be achieved with BERs below  $10^{-3}$ . This is therefore the performance threshold that should be achieved by a DECT system in most circumstances. An alternative criterion is a Burst Failure Rate (due to code check failure or lack of synchronisation) below 1%.

As any mobile communications system, the BER in DECT is determined mainly by 5 factors: (i) thermal noise (additive white Gaussian noise AWGN), (ii) co-channel interference (CCI), (iii) adjacent channel interference (ACI), (iv) intersymbol interference (ISI), and (v) random FM. However, the relative importance of these factors differs from usual (cellular) systems. Firstly, DECT is intended to operate mostly under conditions of large SNR, particularly in high traffic density areas where base station coverage will overlap, so that SNRs in excess of 30dB can be expected. For GMSK modulation, this implies a BER due to noise smaller than  $0.5 \times 10^{-3}$  (even for a flat Rayleigh fading channel), so that reasonable speech quality can be anticipated in such an environment. Error rates due to co-and adjacent channel interference are also typically small, because of the flexibility in channel assignment, avoiding interfered channels (this may not be the case in an office building where various DECT systems are installed or in cordless PABXs). The random FM is completely negligible because of the high data rate.

A physical process that may strongly constrain the available quality is the time dispersion (frequency selectivity) of the radio channel, which causes intersymbol interference. The resulting errors cannot be decreased by simply increasing the transmitter power, and are thus often called "error floor" or "irreducible errors" (although in a later subsection we will see how these errors can be reduced by diversity or equalisers). In contrast to GSM, the specifications for DECT do not foresee an equaliser (since performance in dispersive channels is not specified), so that DECT may be quite sensitive to time dispersion. Any echo with a delay larger than one bit length will clearly appear as co-channel interference, but even much smaller delays can lead to considerable BERs. This subject has been at the core of much of the DECT research in COST 231, and has led to new insights into the error mechanisms.

The simplest *model* for a DECT system consists of a pure MSK modulator, a GWSSUS channel, and a simple differential detector. Sampling is done either on the first arriving path or on the average mean delay. This system formed the basis of most of the earlier investigations of the error floor, performed using Monte Carlo simulations, measurements, or analytical computations.

- (i) Monte Carlo simulations [49,58,60,63] are essentially a straightforward computer implementation of the system, where the statistically changing parameters, such as the channel transfer function, noise samples, etc., are chosen from the appropriate statistical distributions. They are very flexible, and many detailed effects can be implemented and studied.
- (ii) Measurements were performed on the DECT testbeds described in the previous section [40,42,64].
- (iii) Analytical investigations were carried out using the group-delay method [65]: the errors are caused by phase distortions, which are in turn related to changes in the group delay occurring in the fading dips. Similar results were also obtained through the *echo* method, and the *correlation matrix* method (more details can be found in Chapter 6).
- (iv) Another interpretation of the errors can be given by considering the phasors of the channel impulse response [66]. This method is especially suited for the two-delay channel model, where the impulse response is

$$h(t, \tau) = a_1(t) \times \exp(j\varphi_1) \times \delta(\tau - \tau_1) + a_2(t) \times \exp(j\varphi_2) \times \delta(\tau - \tau_2) \quad (5.1)$$

where  $a_1$  and  $a_2$  are the statistically distributed amplitudes (e.g. with independent Rayleigh distributions) and  $\varphi_1$  and  $\varphi_2$  are the uniformly distributed phase shifts;  $\tau_1$  and  $\tau_2$  are the delays of the two paths. For such a channel, errors occur if the normalised total phasor  $1 + \exp[j(\varphi_2 - \varphi_1)] \cdot a_2/a_1$  falls into certain "error regions" in the complex plane. These error regions are circles, whose centre co-ordinates and radii depend on  $\tau_2 - \tau_1$  and the bit combination. The error regions are close to the origin; in other words, errors occur mainly in deep fades (the same result as obtained by the group delay method). The average BER is then the probability that the total phasor falls into the error region, averaged over the statistics of the impulse response. For small delay spreads, a two-delay Rayleigh channel, and sampling at  $T_s = (\tau_2 - \tau_1)/2$  (i.e. the optimum fixed sampling time), we get the exact result

$$\text{BER} = (1/2) \times (\pi/4)^2 \times (S/T)^2 \quad (5.2)$$

The main conclusion from these investigations was that the average BER is approximately  $0.5 \times (S/T)^2$ , where  $S$  is the delay spread of the channel, and  $T$  the bit length, and that the shape of the delay power profile has very little

influence on the BER (less than a factor of 2). The maximum delay spread that still gives tolerable speech quality is of the order of 40-100ns, corresponding to path length differences between 20 and 50m. This can occur easily in larger office buildings, and in outdoor environments. The latter has become of special importance recently, because of increasing interest in the use of DECT for radio in the local loop (RLL) applications [54,59], and for PCS systems.

The errors are also bursty: if the mobile is in a fading dip, then the BER is extremely high (of the order of 25%), otherwise no errors are observed. Such error bursts can be quite long, due to the slow speeds typical of cordless systems, and the fact that the environment in homes and offices is often quite static.

**Performance with Adaptive Sampling :** The BER can, however, be much improved if burst adaptive sampling is used in the model [67]. The ISI often distorts the eye pattern in such a way that, whilst there is a residual opening, the position of this opening changes with the instantaneous channel constellation. With adaptive sampling, it is possible to follow the most *open* position of the eye, while for fixed sampling, the sampling instant may lie inside an eye closure region.

For the case of pure MSK without receiver filtering, adaptive sampling leads to a complete elimination of the error floor. Depending on the channel constellation, the optimum sampling time is at the mean excess delay plus/minus one half the bit length (where the eye will be open). In an actual DECT system, however, the data sequence is filtered to make the spectrum narrower (i.e. GMSK is used), and the received signal is filtered in order to reduce noise. These filtering processes lead to a *smearing* of the bit transitions, and to further closure of the eye. In this case, complete elimination of the error floor is not possible, and the BER (due to ISI) is of the form  $k*(S/T)^2$ , where  $k$  is a constant which depends on the filter width [68]. BER computations can be done efficiently for a two-path model, by using a generalised definition of the *error region concept*: these comprise all channel constellations that lead to errors regardless of the sampling time.

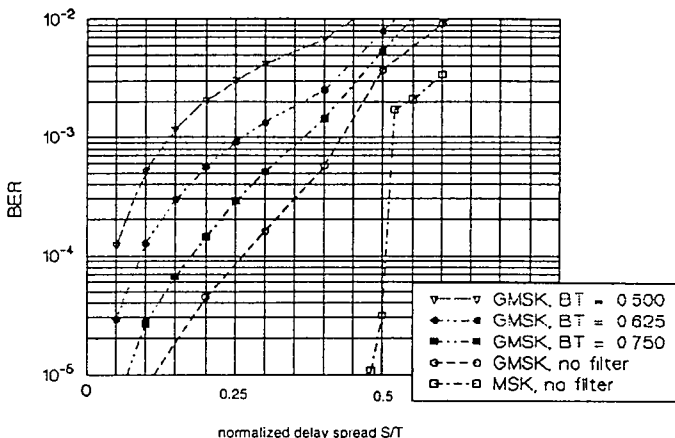


Fig. 5.16: Error floor with adaptive sampling

Fig. 5.16 shows the computed BER floor using near-optimum adaptive sampling (exhaustive search of sampling point using 16 times oversampling). Most striking about the figure is the dependency of the results (e.g. delay spread for BER of  $10^{-3}$ ) on the modulation scheme and receiver filter bandwidth. For example, increasing the single sided bandwidth by 50% more than doubles the delay spread range. In terms of absolute performance, the figure predicts that delay spreads of 0.14-0.26 T (i.e. 120-225 ns) could theoretically be achieved whilst using the range of IF filter bandwidths typical of DECT. However this assumes perfect synchronisation to sometimes negligibly small eye openings, no phase distortion in the receiver filter, perfect frequency synchronisation, and an ideal differential phase detector. In practice a limit of around 100 ns is more realistic.

The determination of the optimum (adaptive) sampling time is thus a matter of considerable importance for performance optimisation of DECT in dispersive channels. One possible method is to use a metric based on the size and length of the eye opening [69]: if the eye is open in several regions, then the middle of the region with the longest opening is chosen as the sampling time. Another possibility is the explicit use of the DECT preamble,

which is known to the receiver. It is possible to make an N-fold oversampling of the received signal, correlating it with the transmitted sequence, and search for the maximum correlation point. The optimum sampling time can only be found if noise is negligible, and infinitely high oversampling used. However, numerical computations have shown that  $N=4$  or  $N=8$  give results that hardly differ from very large oversampling.

## 5.8 DECT Radio Performance Enhancement

Luis Lopes (University of Leeds, UK)

The above discussion has concluded that there are some environments (particularly some of type 2 and 3) where the performance of the *basic DECT receiver* (i.e. standard limiter discriminator or phase detector without diversity) will be degraded by time dispersion. DECT however is a flexible standard enabling the integration of additional performance enhancement features as a function of cost and performance requirements. Specifically, it is possible for manufacturers to deploy a large variety of different spatial diversity techniques or channel equalisation - but none of these is demanded or constrained by the standard. In the following, a number of novel proposals developed during the course of the project will be discussed.

### 5.8.1 Standard Spatial Diversity: Switch and Selection Techniques

In general, it is envisaged that some form of diversity should be provided at the base station only, most commonly by using two antennas. Antenna combining has been only briefly considered [53,70], and most proposed arrangements use some form of switch or selection, as illustrated in Fig. 5.17.

In *switch diversity*, a metric is computed at the base station on reception of each burst; this metric could be simply the RSSI or the CRC check, or another parameter. Using this metric, a decision is made as to which antenna to use for transmission, as well as for the next reception. In *selection diversity*, two parallel receiver chains are provided such that two metrics can be computed. Typically, antenna selection on the up-link would be made *after detection*, on observation of the CRC check and RSSI, and the chosen antenna retained for the downlink.

The implementation variables are therefore the quality metric and the configuration. If the channel is static (no movement of either environment or portables) and the only impairment is low signal level, then there will be minimal performance differences resulting from these variables. This situation is however untypical of real cordless environments which can display both continuous and bursty channel variations, and suffer from interference (and in some cases from time dispersion).

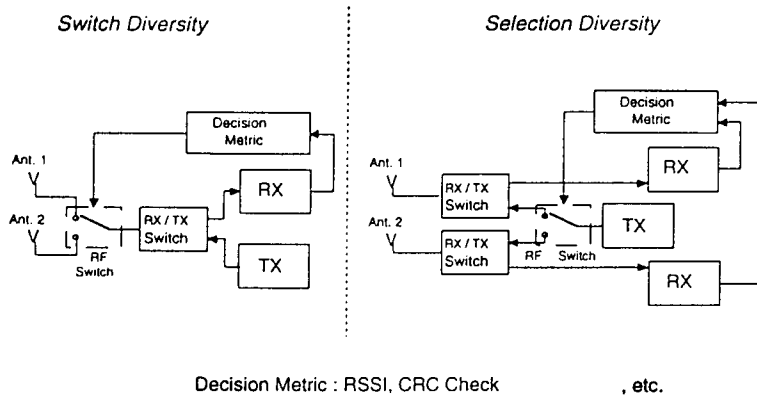


Fig. 5.17: Switch and selection diversity configurations

The best theoretical performance from a dual antenna arrangement is achieved when knowledge of errors at both antennas is available. Under both noise and interference conditions, a gain of about 10 dB is then obtained under Rayleigh fading at the target BER or BFR (Burst Failure Rate). For time dispersive conditions, the error region method previously discussed can also be used to compute this performance limit. In this case, errors occur if the total phasors of both diversity branches fall into an error region, and it is found that the error floor is much smaller for low delay spreads but increases with  $(S/T)^4$ . The theoretical maximum delay spread would again be a function of the IF filter, but is typically in excess of 400 ns.

Typical BFR performances of selection diversity schemes based on CRC and RSSI are shown in Fig. 5.18, for a delay spread of 200ns [40]. As expected, the performance of a standard detector is not acceptable even at high values of  $E_b/N_0$ . RSSI selection diversity provides some gain but still has a very marginal performance; and finally CRC selection is clearly superior (although it still loses a few dB with respect to a flat fading channel). Similar results have been obtained by other studies [60,62,63]; for example, in the context of the Frankfurt railway station measurements discussed in Section 5.6.1 [57, 58], it was concluded that only error rate (CRC) driven selection diversity could deliver a satisfactory performance.

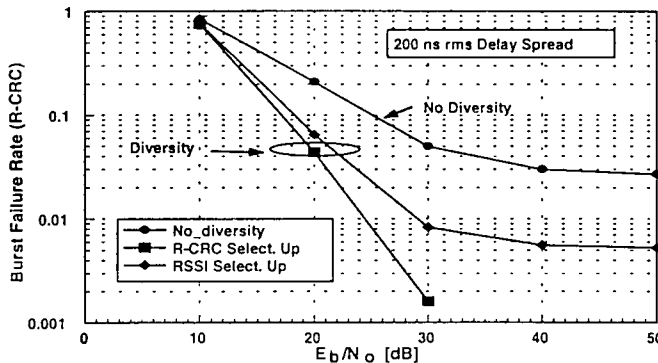


Fig. 5.18: Burst Failure Rate for a two path Rayleigh fading channel with delay spread of 200 ns

However, the use of two receiver chains at the base station (required for selection diversity) is not very practical, so implementations tend to use a switch arrangement. This means that the up-link antenna is chosen on the basis of the quality of the previous burst (a delay of 10 ms); in addition, for both selection and switch diversity, the downlink antenna is chosen on the basis of the previous up-link (a delay of 5 ms). In realistic channel conditions, it is quite possible that the channel characteristics will have changed enough during such delays for the antenna selection to be incorrect. In the extreme, the choice of antenna would not be correlated to real channel conditions, and all diversity gain will be lost [41,62].

This important limitation is illustrated in Fig. 5.19 [41], which shows that virtually all diversity gain is lost at portable speeds of 1 m/s and above when a switch configuration is used. Up-link selection diversity provides a gain of about 10 dB, independent of speed, while the downlink still degrades considerably less than in switch mode (since both diversity branches are sensed simultaneously in the uplink, providing additional information). In summary, diversity is a very powerful means to improve DECT performance under a wide range of impairments but its effectiveness can be seriously reduced under mildly dynamic conditions if the more efficient switch configuration is employed (see also chapter 3 for a more general discussion of diversity techniques).

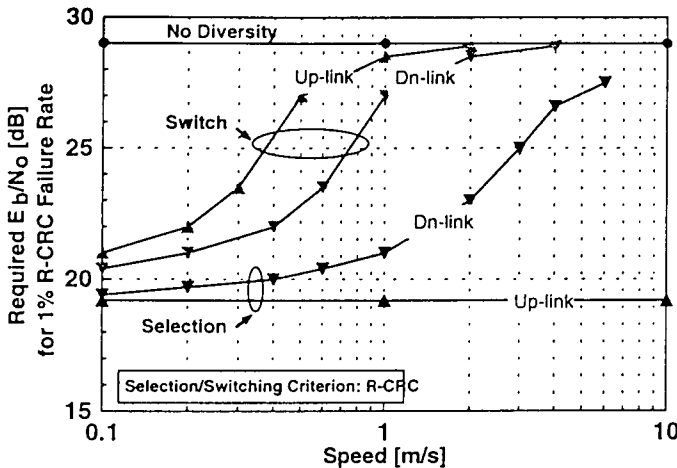


Fig. 5.19: Performance of different diversity arrangements on up-link and downlink directions as a function of portable speed

### 5.8.2 Diversity Techniques in Dynamic Channels

Various algorithms to reduce speed dependence and generally improve diversity performance have been proposed during the course of the project.

**Combined RSSI and CRC criterion for switch diversity** [43]. In this algorithm, the up-link RSSI is averaged using a sliding window. Then an antenna switch is performed if either there is a CRC failure (as before) or the RSSI falls below a threshold (e.g. 10 dB below the current average). Both the threshold and the width of the window can be adjusted for best performance. This scheme effectively provides *soft* information in addition to the hard CRC check, which may prevent the occurrence of some CRC failures. Under Rayleigh flat fading conditions and at 1 m/s, the scheme gains about 2 dB with respect to a CRC controlled switch, but still falls well short of selection diversity (see Fig. 5.19).

**RSSI prediction for downlink antenna selection** [44]. This algorithm is primarily connected with selection diversity schemes and aims at improving the performance of the downlink (which still suffers from a 5 ms delay). If both antennas have an identical CRC check result (either correct or failed), then a decision on which antenna to use is made by predicting the RSSI level at the instant of the downlink, and choosing that which gives the highest value. This algorithm gives a relatively small improvement to the downlink

performance, but this is obtained at virtually no cost in complexity since all metrics used are already computed anyway, and the prediction method can be very simple.

**Emulation of RSSI selection diversity** [45,78]. This scheme attempts to emulate ideal selection diversity whilst using one antenna only. Considering the DECT burst structure shown in Fig. 5.13, it can be seen that overall, the preamble and packet synchronisation word carry a total of 32 bits which makes clock and frame synchronisation possible for simple receivers on a burst-by-burst basis. However, more sophisticated receivers may only require a portion of this 32 bit field to achieve synchronisation, and in particular a scheme was proposed by Kadel [77] which achieves this goal.

In this case, a significant portion of the initial preamble (typically 14 bits) becomes redundant and may be used for other purposes, such as pre-detection RSSI measurements.

The principle of operation of this scheme is shown in Fig. 5.20..As can be seen, the receiver makes fast RSSI measurements on the two antennas, finally settling on the highest RSSI antenna for reception of the burst. As such, it will emulate ideal RSSI selection diversity in the up-link whilst operating only a single receiver. It will also improve the downlink performance since it provides knowledge of the current RSSI of both antennas.

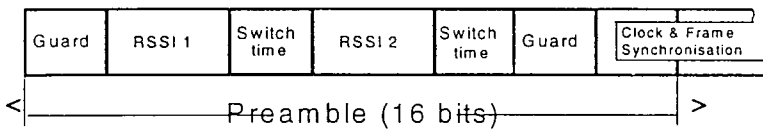


Fig. 5.20: Timing diagram for RSSI measurements on two antennas during the preamble

Practical questions of importance with this scheme are to what extent switching intervals are sufficient for switching and settling of the receiver, and the required interval for RSSI measurement. Typically, only 3-4 bit periods may be available for each antenna; however the signal is periodic during the preamble and so is the envelope. Hence signal level averaging should settle reasonably quickly. In addition, the absolute accuracy of the measurements is relatively unimportant, since only a comparative measure of the antennas is required. This scheme shows good promise for base station diversity, as well as possibly for portable diversity, since it requires

one receiver only. It must operate in conjunction with a synchronisation algorithm similar to that used for equaliser initialisation, and for this reason studies of its performance when combined with equalisation have been carried out, and are discussed later.

*Optimum diversity combining* [46,70]. Finally, optimum diversity combining has also been evaluated for DECT. In this scheme, it has been assumed that 31 bit Gold sequences are added to each DECT burst (providing in principle different mobiles with different sequences so as to identify co-channel interferers). This is then used on reception to estimate optimum combining weights for an antenna array. It is shown that, in the up-link direction, it is possible for the base station receiver to differentiate between the wanted signal and co-channel interferers, as well as to reduce the sensitivity to delay spread.

It will be difficult to realise such gains in practice since, for example, the antenna phases would need to change during the burst to track carrier frequency offsets and in addition actual DECT synchronisation words are identical for all portables. The downlink case is more problematic as the combining weights for transmission will be incorrect due to channel variations (and the interfering environment is not identical in the up-link and downlink directions).

*Antenna pattern diversity* [53]. All the above schemes use standard antenna spatial diversity. In [53], the diversity branches correspond to different patterns resulting from combining with different relative phases. This concept can provide orthogonal patterns with strong and wide nulls, and the resulting spatial filtering may provide less dispersion than omnidirectional space diversity.

### 5.8.3 Equalisation Techniques for DECT

In future PCS applications of DECT, both time dispersion and portable movement may be significant and simple switch diversity will not provide sufficient quality. Even the advanced diversity algorithms discussed above have limitations since they are either based on RSSI measurements or only deliver up-link gain (or both). Equalisation can therefore be considered as a possibility.

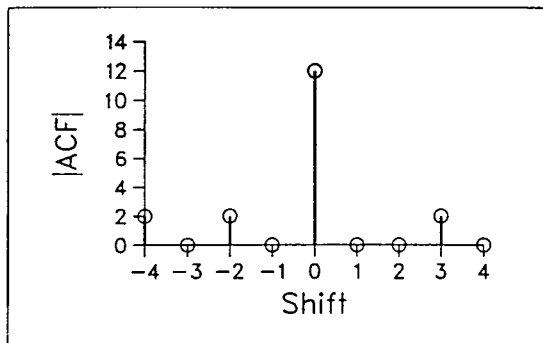


Fig. 5.21: Magnitude of the autocorrelation of the S-field subsequence starting at bit 17 with length 11 [77]

Since the design did not envisage the use of equalisation, no training sequence was provided in the DECT burst for channel estimation and synchronisation. However, there is a sub-sequence of the S-field with very useful autocorrelation properties [77], as shown in Fig. 5.21. This sequence starts at bit 17 of the S-field and has a length of 11 bits (a total of 12 modulated samples). As can be seen from the figure, this sequence would allow channel estimation for a short length channel, or even for longer lengths with relatively small error.

This sequence was used in [77] to estimate the channel, modelled by only two taps, and hence set up the table for a simple 2-state Viterbi equaliser. It was shown by simulations that such an equaliser can extend the delay spread range (in very high SNR) to at least 600 ns. Additionally, using the measurements from the Frankfurt railway station [57,58], it was found that the equaliser could deliver reasonable performance in areas where previously error driven diversity would have been required. Further, the combination of such diversity with an equaliser was found to remove completely the high SNR error floor.

A study using a Decision Feedback Equaliser was also carried out [71]. Both these structures, however, suffer from a residual lack of compatibility with the standard, since DECT units have high degree of tolerance in respect of operating carrier frequency and frequency deviation. Both equaliser structures mentioned will not operate in conditions where the relative frequency offset between the two ends of the link is greater than about 0.2–0.3% of the bit rate (about 300 Hz) [77].

A non-coherent equaliser receiver has been proposed as a means to overcome these drawbacks [72,73,74]. A basic proposal for this simply

consists of a differential operation (multiplying the signal by its delayed complex conjugate) followed by a Viterbi equaliser.

It is found that the samples of the output can still be expressed as a linear combination of the original data bits plus some non-linear terms, enabling the operation of a MLSE algorithm. Further modifications to this structure have been introduced in order to extend the dispersion range and increased tolerance to frequency offset [74,78]. Fig. 5.22 shows the performance that can be obtained, with a maximum delay spread of over 400 ns at an  $E_b/N_0$  of 30 dB. In addition, it can support offsets close to 10% of the bit rate, which should be adequate in the DECT context.

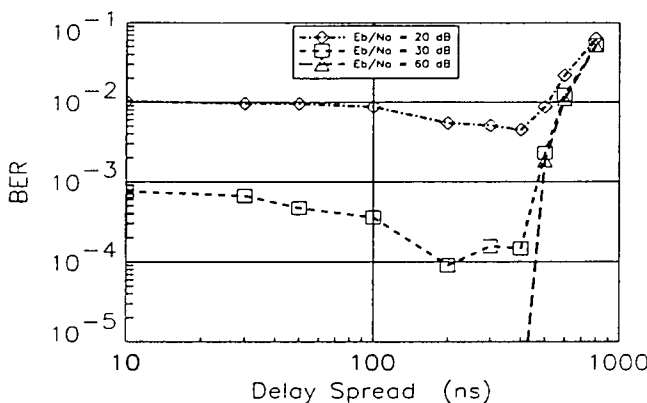


Fig. 5.22: Delay spread performance of the non-coherent equaliser [74]

#### 5.8.4 An Advanced DECT Receiver Concept

This structure is the natural development of some of the ideas discussed in the previous sections. Since the algorithm for emulation of RSSI diversity requires only some of the S-field, and does not overlap with the equaliser training sequence, it becomes possible to combine diversity emulation and equalisation in a single receiver. Such a structure provides excellent all round performance, as found in the various evaluations carried out [78,79,80]. It can be applied to base stations as well as portables since it requires a single receiver chain (but a double antenna arrangement must be provided, as well as additional signal processing).

Table 5.11 shows an overall comparison of some of the most important receiver types discussed in this section, taking the basic (standard) receiver as a reference. Shaded boxes highlight aspects that do not quite meet performance or complexity requirements. The Table confirms that the advanced concept briefly described above (last row of the Table) provides a very robust overall performance. In fact, it has been shown by practical measurements to outperform CRC driven selection diversity, even though this makes use of two parallel receiver chains [79].

Receiver Structure	Diversity	Dispersion	Speed	Complexity	
	Gain	Limit	Dependency	Implementation	Signal Proc.
Standard Receiver (LD or DD)	0 dB	80-100 ns	LOW	Single RX	LOW
RSSI-driven Diversity (Switch)	» 10 dB	170-200 ns	HIGH	Single RX	LOW
CRC-driven Diversity (Switch)	» 10 dB	350-400 ns	HIGH	Single RX	LOW
CRC-driven Diversity (Selection)	» 10 dB	350-400 ns	LOW	Double RX	LOW
Emulated RSSI-driven Diversity (Preamble-based)	» 10 dB	150-200 ns	LOW	Single RX	LOW
Non-coherent Equaliser	» 0 dB	450-530 ns	LOW	Single RX	HIGH
Preamble-based Diversity & Non-coherent Equaliser	» 10 dB	480-560 ns	LOW	Single RX	HIGH

Table 5.11: Comparative performance of DECT receivers

## 5.9 A DECT Field Trial in a Multipath Environment

Magne Pettersen, Rune Harald Rækken, Bjørn Erik Eskedal (Telenor R&D, Norway),  
Joar Løvsletten, Jan Tore Deilkås (Telenor Mobile AS, Norway)

This section describes briefly some performance studies using a DECT field trial network set up by Telenor of Norway in order to gain experience and evaluate the subscribers' interest in mobility at the local level [75,76]. Other such trials have been reported (e.g. [54]), but this is used here as an illustrative example. Førde, the location of the trial, has 9000 inhabitants and is located in a mountainous area creating challenging radio propagation scenarios. The main reason for choosing Førde for the field trial was that the distances between residential and business/industrial areas are relatively short. If roaming is allowed between different environments, coverage can be provided within the entire local community.

The DECT trial system at Førde was delivered by Ericsson, and consists of 240 handsets (portable parts - PP), 160 radio base stations (RBS) and a central control fixed part. In all, the system can carry 40 simultaneous calls. Environment characteristics and system planning aspects of the field trial are shown in Table 5.12.

Space diversity is employed on the RBSs: a simple switching diversity algorithm based on the cyclic redundancy check (CRC) of the previous frame is used to switch between antennas. Average distance between RBSs equipped with omnidirectional antennas and customers residences is approximately 50 meters. When the base stations are equipped with directional antennas the average distance to the customers is increased to 80-90 meters. The maximum cell radius in the system is 400 meters.

**Services offered.** Approximately 50 households and 55 business/industry companies participate in the trial. The number of handsets used in a family varies typically between 1 and 3. By allowing in some cases several family members to have their own handset with a dedicated telephone number, a personal service is offered to the customers. The number of handsets offered to a company varies between 1 and 11. Calls can be made and received within the entire covered area (2.0-2.5 sq. km) and seamless handover is performed between all 160 base stations. Some trial customers both live and work within the coverage area, benefiting from the possibility to use the same handset both at work and at home. During the test period private customers pay the same tariff as for fixed telephone. The same offer is given

to business users. In addition, all normal PBX functions are provided allowing business users for instance to make free internal calls within the covered area.

***Experiences from the trial.*** Most existing DECT products have been designed and targeted for indoor applications. However keeping in mind the potential of DECT in an outdoor environment both as a technology providing local mobility and as a fixed radio access solution (replacing copper), one of the main technical goals was to understand the strengths /weaknesses and improvements needed on current versions of the DECT system in order to operate in both indoor and outdoor environments.

	Residential area	Downtown area	Business/Ind. area	Recreation area
Area characteristics	0.9 km <sup>2</sup> 700 residences both hilly and flat areas with some vegetation	0.4 km <sup>2</sup> shops, public buildings (3-6 floors) flat area	0.4 km <sup>2</sup> massive buildings with thick concrete walls flat area	0.5 km <sup>2</sup> fields, open green areas, sporting areas
Planned coverage	outdoor indoor in most rooms except basements	outdoor indoor in public areas and for all business customers partly in shops	outdoor indoor in areas of importance for the trial customers	outdoor indoor in public areas
Installed base stations	64, all outdoor	15 outdoor 40 indoor	11 outdoor 19 indoor	3 outdoor 6 indoor
Subscribers	52 families	27 business customers	16 business customers	4 business customers
Number of handsets	90 handsets	74 handsets	58 handsets	10 handsets

Table 5.12: Environment characteristics and system planning aspects of the DECT field trial at Førde [76]

Regarding indoor coverage, several aspects were found that can minimise the number of base stations whilst still achieving high speech quality. These include accurate positioning of the base stations, 3-dimensional planning strategy, knowledge of the interior constructions and types of reflecting objects and materials of ceiling, walls and floors attenuating the signal strength. Experience from the trial has given valuable information about the expected cell range in a variety of different indoor environments ranging from more than 50 metres in open hall areas to less than 15 metres in heavily reinforced areas. As a result of the limited cell radius careful site planning can reduce the number of indoor base stations by more than 30 %.

In outdoor areas, many subjective tests have been performed giving valuable information on the system performance. On the positive side, it has been found that the speech quality is in general good (e.g. better than GSM) as long as there exists a free line of sight path between the base station and the terminal, and no major reflecting objects are in close vicinity. Good speech quality has been obtained more than 400 m from the closest BS (without directive antennas) and approximately 1 km from base stations using directive antennas. Finally, tests show that it is possible to communicate and perform handovers whilst driving even though the system was not developed for use in cars. However a certain degradation in quality is experienced.

On the other hand, it has also been found that the link quality is highly dependent on whether line-of-sight (LOS) is available, and that the speech quality is variable in open square areas (typically surrounded by reflecting buildings) even when there exists a LOS path between the BS and the terminal and the average received signal strength is high. The link quality is also dependent on whether the user moves or stands still, and is affected by the user's orientation and positioning of the handset relative to the base station.

However, the overall impression from customer surveys indicates that most of the customers are satisfied with the DECT QoS within the planned coverage area. In the following, the focus will be on outdoor problem areas, pointing out possible solutions to aid in the system planning.

### 5.9.1 The Measurement Equipment

Telenor R&D's channel sounder [59] is based on a frequency sweep technique, and has a maximum measurement bandwidth (BW) of 200 MHz. Only instantaneous impulse responses (IRs) are treated; based on these, the cumulative distributions of the Delay Spread and the Delay Window are obtained [59] (see chapter 2 for definitions of these).

The channel sounder can be used to derive parameters indicating performance of DECT in a multipath environment. The delay spread gives an indication of radio system performance for a standard DECT receiver, while the delay window is well suited to indicate the performance of a receiver that employs a channel equaliser. Simultaneously, the Symbionics DECT Propagation Tester provides measurements of a number of parameters, including signal level (RSSI) and BER. Handsets are included to allow subjective evaluation of speech quality.

Microcellular city street and city square measurements have been performed in the Oslo area, as reported in [59]. In city streets delay spread values are usually small, and multipath propagation does not limit DECT performance. In city squares with larger dimensions, multipath propagation would often cause severe problems to DECT communications, raising the need for some means to combat the influence of frequency selective fading. To verify DECT vulnerability to multipath propagation, laboratory measurements were performed with a fading simulator between the TX and the RX of the Symbionics DECT propagation tester. The BER shows a strong dependence on delay spread, and the DECT performance limit of  $BER = 10^{-3}$  [77] is reached at delay spread values of about 100 ns.

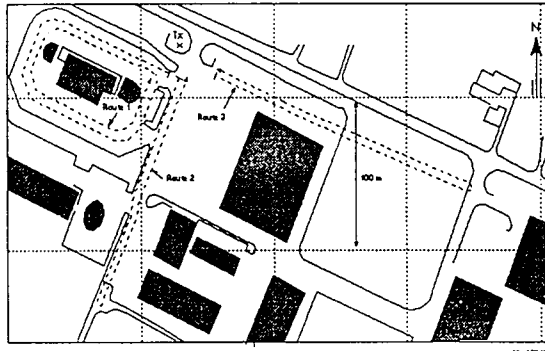


Fig. 5.23: Førde, measurement routes 1-3. Shaded areas represent buildings

### 5.9.2 Førde Measurements

**Measurement scenarios.** Measurements were performed at different locations within the coverage area of the DECT trial system, particularly in regions where QoS was reported to be unsatisfactory despite sufficient signal level [75]. In all measurements, the RX antenna was omnidirectional with 2.1 dBi gain positioned on a 2 m high pole fastened to the car. All measurements were made at a speed of about 20 km/h (approximately 30 cm between IRs). Fig. 5.23 shows routes 1 to 3.

In routes 1, 2 and 3 the TX antenna was omnidirectional, elevated to 3.5 meters, and positioned as shown in the figure. Outside the map, to the south, there is a steep hill rising about 300 meters above the measurement area. Along route 3 the direct path was sometimes blocked by moving cars. Most of the buildings in this area were brick or stone houses of two or three floors. In route 4, an omnidirectional TX antenna elevated to 5 meters was

used. There was a metal shed between the TX and RX antennas, blocking the direct path in most of the route.

Measurement routes 5 and 6 are shown in Fig. 5.24. In both routes, the TX antennas were directional pointing south, parallel to the road. TX antenna heights were 4 meters. In route 5 the TX antenna gain was 7.1 dBi, and 14.1 dBi in route 6. There was a line-of-sight path from the TX to the road of route 6, but the LOS was sometimes blocked by residential wooden houses.

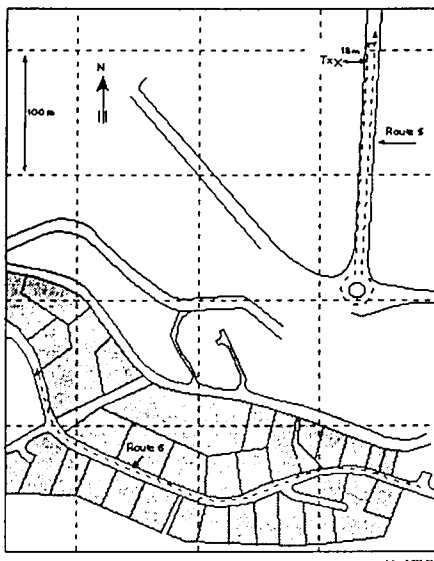


Fig. 5.24: Førde, measurement routes 5-6. Shaded areas represent lots with residential houses

**Measurement results [75].** The delay spread and window parameters were measured using the channel sounder, and their cumulative distributions were calculated. In addition, the DECT propagation tester was used to measure BER and RSSI. and the 50 and 90 percentiles of the delay spread and 90% delay window parameters are shown in Table 5.13.

From the DS measurements, only route 3 would be expected to have propagation conditions that the basic DECT receiver could handle [77]. The others have many locations with delay spreads exceeding 10% of the DECT bit interval. In route 4 the DS is almost all the time above 100 ns, indicating that DECT communication without diversity or channel equalisation would be impossible. Both routes 4 and 6 have delay spread values which exceed

those reported to be possible to handle by using diversity techniques. It should be kept in mind, however, that the routes are chosen from areas where QoS problems have been reported. Some of the time dispersion could easily have been removed with different RBS location. In routes 3 and 6 the maximum distance between RX and TX exceeds the normal cell radius used in the Førde system.

Route	Delay Spread (ns)		Delay Window (ns)	
	50%	90%	50%	90%
1	76.6	218.9	40	440
2	75.3	141.1	60	260
3	41.1	96.7	40	60
4	272.0	316.9	640	700
5	60.5	132.7	40	120
6	106.6	415.1	100	1040

Table 5.13: Measurements from Førde

The time dispersion is severe on both routes 5 and 6, showing that the use of directive antennas to extend the coverage area of the RBS may cause problems due to time dispersion when the receiver is not located within the main lobe of the TX antenna pattern. This is because strong reflections from the most strongly illuminated areas can reach the receiver with considerable excess delay due to the larger dimensions of the cell. It is also noted that, in general, the delay spread has its largest values in positions where there is no LOS path from the transmitter to the receiver.

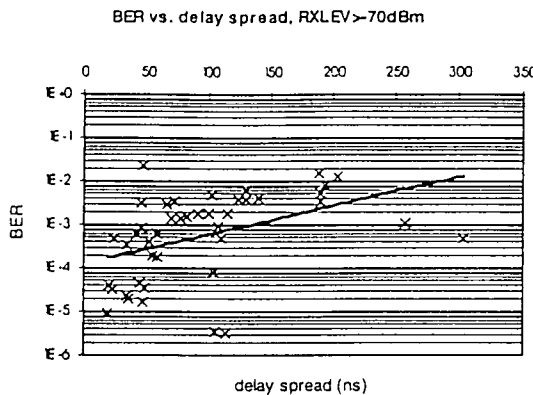


Fig. 5.25: BER versus delay spread from Førde

It was expected that the high delay spreads found among these measurement routes cause high BER values. To verify this, averages of the delay spread taken over the same distance as the BER were calculated. Fig. 5.25 shows BER as a function of delay spread for all the measurements made at Førde. The RX level was rarely below -70 dBm, and the points for which the RX level was below this level have been removed (so as to focus on the effect of time dispersion). The plot also shows the regression line, which crosses the BER of  $10^{-3}$  at approximately 120 ns.

### 5.9.3 Conclusions from Field Trial and Measurements

The experience in the trial shows that the DECT technology is a strong candidate for providing speech services and mobility in indoor domestic/business/industrial environments. However, for providing outdoor local mobility the technology is relatively immature and too sensitive to radio propagation conditions [75,76].

For this reason, wideband multipath measurements at 1950 MHz and DECT performance tests have been performed in a number of environments in the DECT field trial area where unacceptable QoS was reported. There was severe time dispersion in many of the routes, and in some of the cases the delay spread exceeded values reported to be handled by DECT employing simple diversity schemes. The use of directive antennas can extend the range of the cell, but the multipath situation can worsen if the receiver is not

located within the main lobe of the TX antenna radiation pattern. The dispersion also increases considerably if the LOS path is obstructed.

Some of the time dispersion affecting DECT QoS could easily have been reduced by a different choice of RBS location, demonstrating the importance of proper base station planning. DECT performance would in any case improve significantly if advanced diversity techniques or a channel equaliser are introduced to cope with multipath propagation [78,79]. This should be born in mind when planning outdoor DECT implementations for public use.

With an improved air interface, the high capacity of DECT, the variety of services supported by the standard and its simple/flexible network structure makes it a very interesting candidate both as a pure copper replacement connecting subscribers to the fixed network and as a public radio access solution providing local mobility.

## 5.10 Traffic Capacity for the DECT system

Valerio Palestini (CSELT, Italy)

This section deals with DECT capacity for service provision. DECT enables both voice and data services at bit rates suitable, for example, for ISDN connection, high capacity and a dynamic channel selection mechanism which avoids the need for frequency planning. DECT is in fact an access system to networks such as PSTN, ISDN, GSM, etc.

One DECT transceiver [83] can manage up to 12 bi-directional voice channels, due to the frame architecture shown in Fig. 5.26. A bi-directional voice conversation uses a so-called "duplex bearer", comprising two time-slots separated by 5 ms on the same carrier.

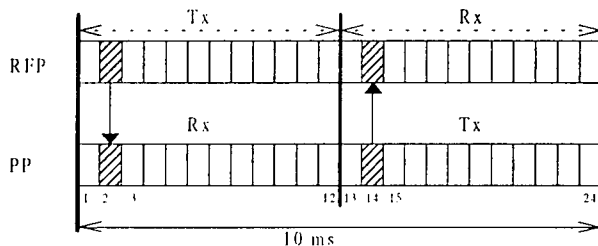


Fig. 5.26: Frame architecture for one DECT duplex bearer

Capacity results are provided for two of the most commonly mentioned applications of DECT - the WPBX (Wireless Private Branch eXchange) and RLL (Radio Local Loop). DECT was in fact originally designed with WPBXs in mind, but many other possibilities proved to be very interesting, and particularly the replacement of the last part of copper wires connecting a subscriber to the fixed network by a radio path (usually referred to as RLL). In both cases, the capacity results are obtained by simulations, using the ad-hoc scenarios described.

### 5.10.1 WPBX application

**Voice service.** Terminals are randomly positioned (with uniform distribution) within a reference three-storey building 100 metres x 100 metres x 9 metres, in which 16 base stations are regularly spaced in each storey (Fig. 5.27). Terminals are considered to be static during the call; each terminal generates 0.2 Erlang of traffic and the mean duration of a call is 120 seconds. The radio propagation model assumes a propagation decay equal to 3.5, an attenuation

between floors of 15 dB, an additional factor in the range +/- 10 dB to account for shadow fading, and a Rayleigh fade margin of 10 dB, if antenna diversity is applied, or 20 dB, without antenna diversity.

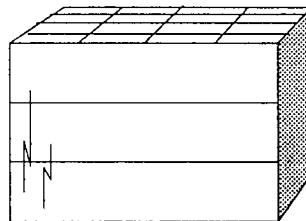


Fig. 5.27: Reference building

The system spectrum allocation, the radio parameters (transmitted power, receiver noise floor, adjacent channel rejection factors, etc.), and the call procedures (set-up and handover for both single and multi-bearer channel allocation models), are in accordance with the DECT specifications [83]. The aim of this work is to evaluate, for each type of terminal, the grade of service (GOS) versus the number of bases per floor:

$$\text{GOS} = \frac{\text{Number of blocked calls} + 10 \cdot \text{Number of interrupted calls}}{\text{Number of total calls}} \quad (5.3)$$

In works dealing with DECT simulation performance [84], the maximum acceptable GOS is 1%. Different scenarios are taken into account:

- a single system in the building;
- three different systems (one per floor) synchronised or unsynchronised.

As a first assumption, systems are considered unsynchronised if frames are not aligned; in addition, the shift between the first timeslot of the frames of each system is taken to be not greater than one timeslot as shown in Fig. 5.28.

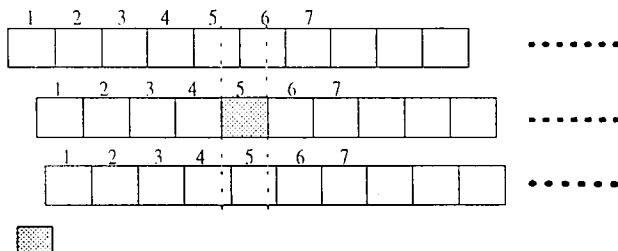


Fig. 5.28: Three unsynchronised systems in the building

When a single WPBX system is introduced in the building with a floor attenuation of 15 dB, the maximum capacity of the system in terms of Erlang per RFP reached with a GOS equal to 1% is about 5.6 Erlang, corresponding to 9000 Erlang/km<sup>2</sup>/floor; if a higher separation between floors is introduced (i.e. Af=20 dB), this value becomes 6 Erlang (9600 Erlang/km<sup>2</sup>/floor).

In the second scenario, a different WPBX system is positioned on each floor of the building; terminals can only set up a call and make handovers with base stations of their system, that is of their floor. The cases of all systems synchronised and all unsynchronised are taken into account. The comparison between the three scenarios is shown in Fig. 5.29.

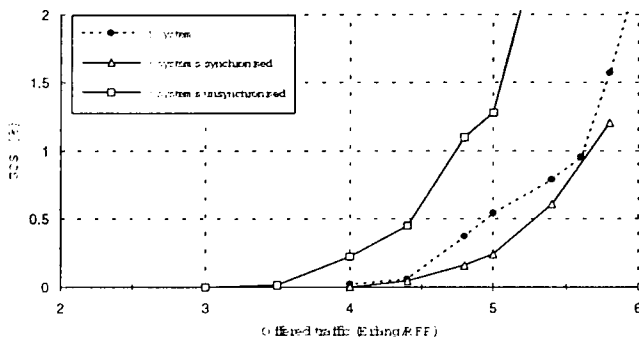


Fig. 5.29: Offered traffic per RFP with three systems in the building (synchronised and unsynchronised)

The results obtained by simulations show that coexistence of different WPBX systems, also unsynchronised, is possible with a loss in capacity, in the worst case, of less than 20%; in fact the total capacity obtained is about 7400 Erlang/km<sup>2</sup>/floor, instead of about 9000 Erlang/km<sup>2</sup>/floor for the reference case of 1 system in the building with Af=15 dB.

	Af (dB)	Erlang/RFP	Erlang/km <sup>2</sup> /floor
1 system	15	5.6	9000
	20	6	9600
3 systems synchronised	15	5.7	9100
3 systems unsynchronised	15	4.6	7400
	20	5.8	9300

Table 5.14: Traffic capacity for different system scenarios.

Better performance is obtained when the physical separation between different systems is higher, that is when the floor attenuation considered is 20 dB. In fact, in that case, the loss in capacity when 1 system in the building is substituted by 3 unsynchronised systems is almost negligible: the total capacity decreases from 9600 Erlang/km<sup>2</sup>/floor to 9300 Erlang/km<sup>2</sup>/floor. Results are summarised in Table 5.14.

**Mixed voice-data scenario.** The results reported hereafter on the performance of DECT in a mixed voice-data scenario have been obtained under conditions similar to the case of voice service only; the differences are in the dimensions of the reference building, (now 60 m x 60 m x 9 m) and the traffic per terminal (0.15 Erlang instead of 0.2 Erlang).

Terminals are considered to be static during a call, so that only intra-cell handover can occur. The total number of terminals (belonging to the same DECT system) in the building is 540 (so that, on average, there is one per 20 square metres of floor). The results are presented in the cases of either 100% voice terminals or 80% (i.e. 432) voice terminals, 10% (i.e. 54) ISDN terminals and 10% fax terminals. It is assumed that a voice terminal requires one duplex channel, an ISDN terminal requires one normal duplex channel for signalling plus one or more duplex channels (multi-bearer symmetric connection), and a fax terminal requires one normal duplex channel for signalling plus one or more double simplex channels (multi-bearer asymmetric connection). In the two latter cases, a multi-bearer connection is defined by the minimum number of bearers ( $B_m$ ) that the connection can accept and the target number of bearers ( $B_t$ ) needed by the connection. These bearers, in general, could be obtained from different base stations, but here it is assumed that they are obtained from the same base.

The mean traffic at the base is calculated as the average number of slots used at the base. For each type of terminal the average number of active connections per base is also computed. As in the case of voice service the reference value of GOS is set to 1%.

The performance results, presented in Fig. 5.30 and Fig. 5.31, show five curves in each graph; one for the reference case of 100% voice terminals and four for the case of 80% voice, 10% ISDN and 10% fax terminals, distinguishing, for the latter case of an asymmetric connection, between the up-link (terminal-to-base station) and the down-link (base station-to-terminal).

In all cases it can be seen that for fax terminals the up-link is more critical than the down-link, as base stations are affected by interference from other base stations transmitting in the same time slot (particularly those vertically aligned on different floors); the same happens in the down-link for voice or data terminals, but as they are randomly positioned this effect is less significant. A possible action to improve performance can be to install base stations in such a way as not to be aligned on adjacent floors.

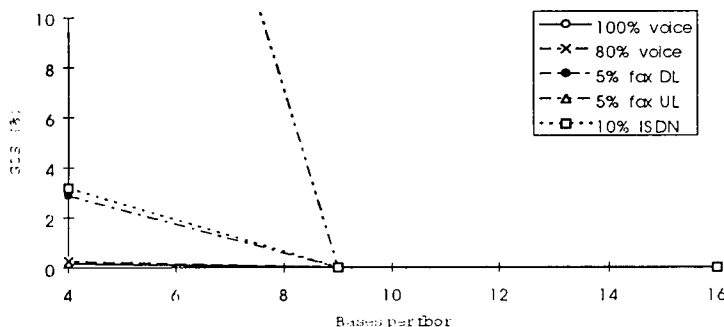


Fig. 5.30: Performance with diversity in a mixed voice-data scenario. The minimum ( $B_m$ ) and target ( $B_t$ ) numbers of bearers are as follows:

$$B_m = B_t = 3, \text{ for ISDN terminals}$$

$$B_m = 2, B_t = 3, \text{ for fax terminals}$$

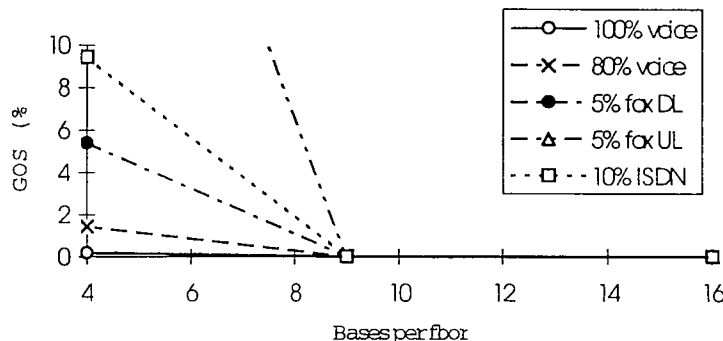


Fig. 5.31: Performance with diversity in a mixed voice-data scenario. The minimum ( $B_m$ ) and target ( $B_t$ ) numbers of bearers are as follows:

$B_m=2$ ,  $B_t=4$ , for ISDN terminals

$B_m=B_t=2$ , for fax terminals

Bases per floor	Diversity	Number of connections per base				Mean traffic per base	
		Voice	ISDN	fax uplink	fax downlink	Mixed voice-data	voice only
4	with	5.44	0.23	0.1062	0.12	6.7	6.9
	without	2.42	0.10	0.06	0.05	3.0	3.1

Table 5.15: Traffic evaluation in a mixed voice-data scenario. For fax terminals the minimum ( $B_m$ ) and target ( $B_t$ ) number of bearers are  $B_m=2$ ,  $B_t=3$ ; for ISDN terminals  $B_m=B_t=3$ . This table shows the average number of connections per base for each type of terminal and the mean traffic per base in terms of average number of used slots.

The voice service does not seem to be much impaired in the mixed voice-data scenario with respect to the case of voice only; in the case of 9 bases/floor and diversity, for all the examined kinds of terminals the GOS is below 1%.

Table 5.15 and Table 5.16 show the mean traffic for each kind of terminal, in terms of average number of active connections/base, and the total mean traffic, in terms of average number of slots/base. It is worth noting that for

voice only and 4 bases/floor with diversity (a case in which the GOS is less than 1%) the traffic is 6.9 Erlang/base, which corresponds to about 7700 Erlang/km<sup>2</sup>/floor. For mixed voice-data services, the necessary number of bases/floor to have GOS less than 1% is 9 (if diversity is applied), for all kinds of terminals; the tables indicate that in all the examined cases the mean traffic is in the range 3-3.3 Erlang/base, corresponding to 7500-8200 Erlang/km<sup>2</sup>/floor.

		Number of connections per base					Mean traffic per base	
Bases per floor	Diversity	Voice	ISDN	fax uplink	fax downlink	Mixed voice-data	voice only	
4	with	5.37	0.18	0.15	0.17	6.7	6.9	
	without	2.61	0.08	0.09	0.08	3.3	3.1	

Table 5.16: Traffic evaluation in a mixed voice-data scenario. For ISDN terminals the minimum ( $B_m$ ) and target ( $B_t$ ) number of bearers are  $B_m=2$ ,  $B_t=4$ ; for fax terminals  $B_m=B_t=2$ . This table shows the average number of connections per base for each type of terminal and the mean traffic per base in terms of average number of used slots.

**Conclusions.** Computer simulations of the DECT wireless PBX application have shown that in the case of voice service only, with one DECT system in the reference building, the capacity is around 9000 Erlang/km<sup>2</sup>/floor. This value is not impaired if three different systems (one per floor) coexist in the same building, provided that they are synchronised; if this is not the case, a capacity loss of under 20% may be expected. If DECT terminals are present that require multi-bearer connections (e.g. ISDN and fax terminals), traffic densities of the same order may still be achieved at the same GOS, but at the expense of roughly doubling the number of base stations per reference area unit.

### 5.10.2 RLL Application

This section focuses on the possibility of replacing the last part of copper wires connecting a subscriber to the fixed network by a radio path; this application is usually referred to as the Radio Local Loop (RLL). The interest

in RLL applications is growing with the opening of new markets in Eastern Europe and in other developing countries.

Many existing and proprietary standards have been analysed [86], but, as yet, none has emerged as the clear favourite for this type of application (all systems considered show pros and cons depending on factors such as the environment that is assumed).

Two possible scenarios are shown in Fig. 5.32; in a), a base station that allows local mobility to the user, both inside and outside buildings, with the support of repeater units, and in b) the case of the provision of the basic telephony to a few isolated houses is considered (in this case it is also possible to extend the range of the base station by means of a repeater).

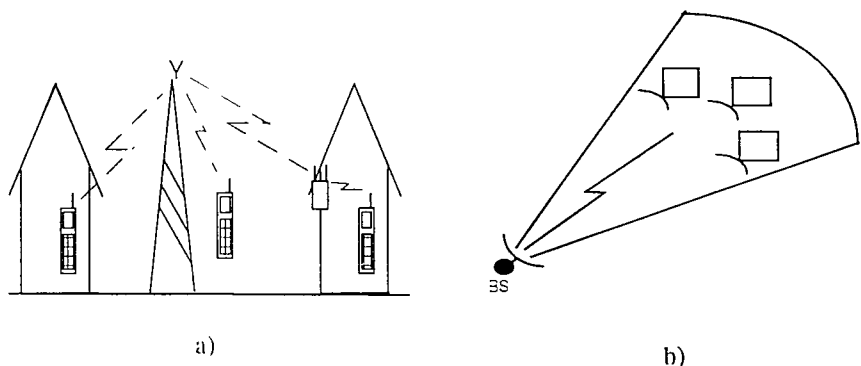


Fig. 5.32: Some typical scenarios for the RLL application

DECT is one of the standards being considered: in fact, a profile for this kind of application is being standardised [87] in the sub-technical committee ETSI RES3.

***Impact of the Wireless Relay Station on the System Capacity.*** A scenario in which the service allows local mobility to the user, both inside and outside buildings, implies facing the propagation problems due to additional wall attenuation. To offer a suitable indoor coverage, the relay function seems to be a viable solution. For this purpose, an additional unit, here called Wireless Relay Station (WRS), is needed.

Two different architectures have been proposed during ETSI meetings and an Interim ETS [81] including both proposals has been written. The main difference between the two solutions, called respectively CRFP and REP, is the occurrence of the retransmission of the slot at the WRS.

The CRFP may receive and transmit, during any slot of a frame a duplex bearer to either the PP and the RFP, supported by a combination of a CRFP Rx and Tx slot separated by one half frame (a typical frame multiplexing structure is shown in Fig. 5.33).

The REP unit receives a slot in one frame and retransmits it in the same frame (Fig. 5.34); in addition the REP, in order to maintain the symmetry of the bearers, sets up a new kind of bearer towards the RFP: the Double duplex bearer.

As an example, in the next section the performance of the REP unit will be evaluated by means of some computer simulations in which the system grade of service (GOS) is calculated as described above.

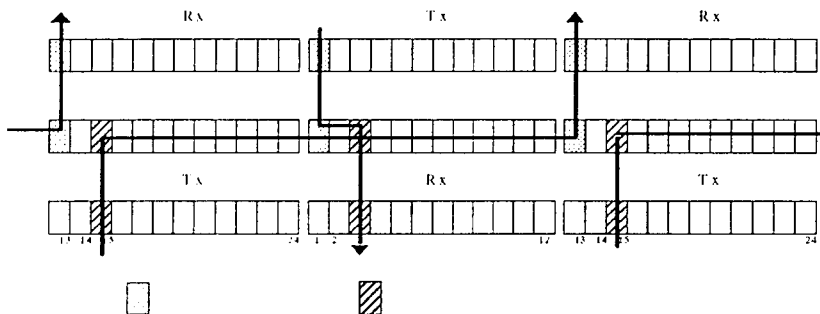


Fig. 5.33: Typical frame architecture of the CRFP unit

**REP unit.** The REP unit can use a simplified RFP hardware and an adapted software with some modifications in the MAC (Medium Access Control) layer. It has two antennas: one, usually directional, points to the strongest RFP that supports the RFP-RFP outdoor link, and an omnidirectional one for the REP-PP (Portable Part) indoor link.

The basic working idea is to make the REP switch continuously from transmit to receive mode on a slot by slot basis (after the initial synchronisation to the strongest RFP). It duplicates and re-transmits the received burst on the other slots, within the same half frame. This previous solution proposed in [82] has been modified, because the speech service was not supported using a duplex bearer as specified.

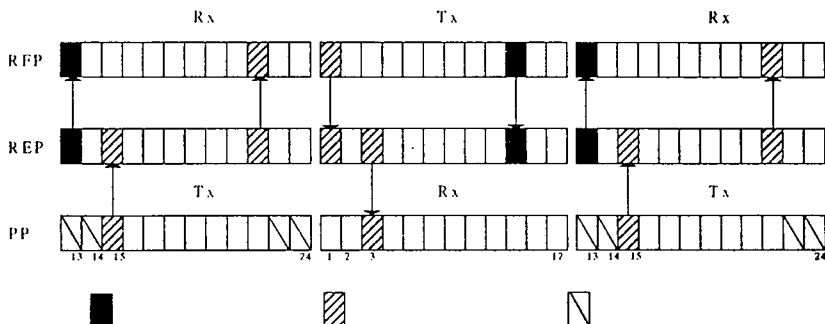


Fig. 5.34: Typical frame architecture of the REP unit

In order to consider as duplex the two channels involved in the same connection between RFP and REP, a new bearer is introduced, containing identity messages ( $N_I$ ). This allows a good exploitation of DECT Dynamic Channel Selection Algorithm, as the position of the two mentioned channels does not have to be static. As shown in Fig. 5.34, after an initial set-up on the PP-REP link, the repeater chooses two other physical channels to close the connection with the RFP. This new type of bearer is called "*double duplex bearer*", and is composed of a pair of duplex bearers referring to the same connection at MAC level; the duplex bearers share their simplex bearers for the information flow [83].

The REP unit can reduce the required channel allocation by sharing the bearers between connections. As shown in Fig. 5.35, two Portable Parts use the same link from REP to RFP (Shared link) in order to maintain symmetry at the RFP for both connections. This process is called "*interlacing*".

**REP performance.** The REP performance is evaluated by simulation, taking into account the interlacing procedure during the set-up of the "double duplex bearers" (the two duplex slots for the REP-RFP link). Two very simple cases are taken into account, in order to estimate the capacity of the system using a REP repeater; in the first case, 1 RFP and 1 house with a REP are considered (Fig. 5.36a), whilst the second comprises 1 RFP and 2 houses with one REP each (Fig. 5.36b).

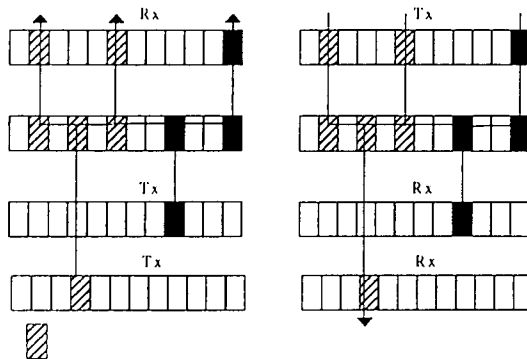


Fig. 5.35: Example of the interlacing procedure

Some tests made for RLL applications [85] have shown that communication quality rapidly decreases for distance values of more than 70 m without a WRS. In the two scenarios a distance between REP and RFP of 90 m has been chosen in order to analyse almost only connections between PP and RFP through REP.

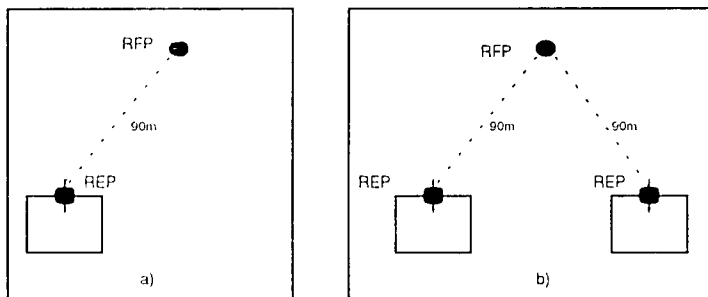


Fig. 5.36: The two simulation scenarios considered

A variable number of users with a traffic of 70 mErlang each are positioned inside the houses. The propagation law taken into account in the simulation is:

$$\text{Attenuation} = 53 + 20\log(\text{distance}) + \text{shadowing} + \text{wall attenuation (15 dB)}$$

For both cases the capacity of the system is evaluated with and without the interlacing procedure described above.

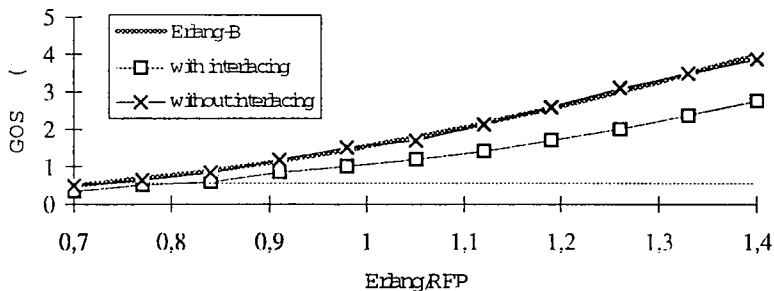


Fig. 5.37: GOS versus the Erlang/RFP in case of 1 RFP and 1 REP

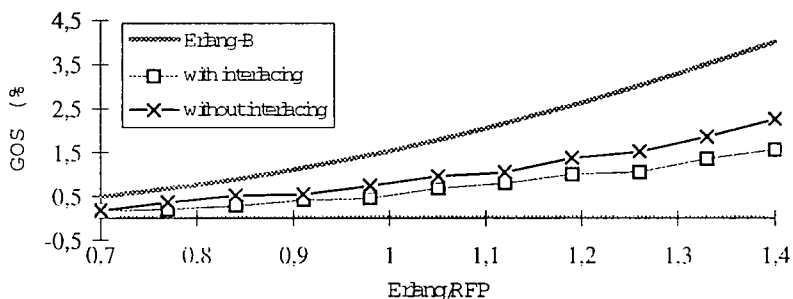


Fig. 5.38: GOS versus the Erlang/RFP in case of 1 RFP and two REPs

Both Fig. 5.37 and Fig. 5.38 show an improvement when using the interlacing procedure, since this decreases the occupation of the timeslots at the base station, allowing other direct connections or calls through the repeater.

In fact, as shown in Fig. 5.35, without the interlacing procedure the maximum number of connections to an RFP through the REP is 4, because each connection needs two links to the RFP: that means a traffic per RFP equal to 0.7 Erlang (i.e., 10 users) with a GOS of 0.5% and equal to 0.84 Erlang (12 users) with 1%. The curve is very close to the traffic at an RFP with only 4 available channels obtained with the Erlang-B formula. However, with the

interlacing procedure and a GOS of 0.5%, the traffic per RFP becomes 0.84 Erlang (12 users), whilst at 1% about 1.1 Erlang (15 users) can be supported.

Interlacing also improves capacity in the second scenario, but less so than in the first. Users are now distributed between two houses, and therefore the number of connections through each REP decreases and so does the possibility of interlacing two different connections.

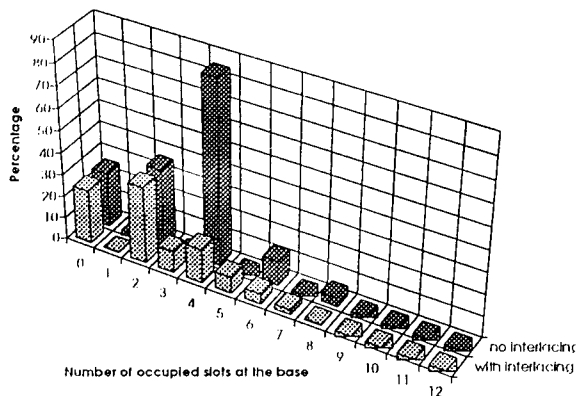


Fig. 5.39: Distribution of occupied slots at the RFP

As an example, Fig. 5.39 shows the distribution of occupied slots at the RFP, with reference to the first scenario. It can be seen that without interlacing only the even slots are used, while with interlacing the distribution is better spread over the slots, ensuring a better exploitation of the resources.

**Conclusion.** A Wireless Relay Station can be profitably introduced in a RLL application based on the DECT system, in order to guarantee a better quality and coverage of the area and a bigger range of the system. It does introduce a capacity limitation, since it has been verified that, using a REP, the mean traffic per RFP is less than 1E for a GOS of 0.5%.

This capacity limit seems to be acceptable in a RLL application where the user density and the mean traffic per user are both expected to be much lower than in a business environment. This means that in the case of a low density area, a WRS can be a more attractive and economic solution than an RFP.

### 5.11 References

- [1] Carneheim, C, Jonsson, S-O, Ljungberg, M, Madsfors, M and Näslund, J, "FH-GSM Frequency Hopping GSM", Proc. VTC'94, Stockholm, June 1994, pp. 1155-1159.
- [2] COST 207 , "Digital land mobile radio communications", Final report 1989,
- [3] Cox, D C., "Correlation Bandwidth and Delay Spread Multipath Propagation Statistics for 910-MHz Urban Mobile Radio Channels, IEEE Trans. Commun., vol. COM-23, pp. 1271-1280, Nov. 1975.
- [4] Crossley, D, Stevens, P, Owens, D, Skinner, D, and Haines, C, "Frequency Hopping Results from Live DCS1800 Network", Proc. EPMCC '95, Bologna, Nov. 1995, pp. 103-106.
- [5] ETSI TC-SMG, GSM 05.02: "European digital cellular telecommunication system (Phase 2): Multiplexing and multiple access on the radio path", Sep. 1994.
- [6] ETSI TC-SMG, GSM 05.03: "European digital cellular telecommunication system: Channel Coding", Feb. 1992.
- [7] Eggers, P, Jensen, C, Oprea, A, Davidsen, K and Danielsen, M, "Assessment of GSM link quality dependence on radio dispersion in rural environments", Proc VTC92, Denver, May 1992, pp.532-535.
- [8] Ibbetson, L J, Lopes, L B, Bic, J C and Levy, A, "An assessment of cell size versus receiver complexity using measured propagation data", Proc VTC94, Stockholm, June 1994, pp.1824-1828.
- [9] ETSI TC-SMG, GSM 05.05: "European digital cellular telecommunication system (Phase 2); Radio transmission and reception", March. 1995.

- [10] Forssén, U, Karlsson, J, Johannesson, B, Almgren, M, Lotse, F, and Kronestedt, F, "Adaptive Antenna Arrays for GSM900/DCS1800", Proc VTC'94, Stockholm, June 1994, pp. 605-609.
- [11] Hagerman, B, "On Downlink Co-Channel Interference in Cellular Radio systems", Proc. Nordic Radio Symposium 1995, Salsjöbaden, Sweden, pp. 61-66.
- [12] Olofsson, H, Näslund, J and Sköld, J, "Interference Diversity Gain in Frequency Hopping GSM", Proc VTC'95, Chicago, July 1995, pp. 102-106
- [13] Jakes, W., "Microwave Mobile Communications", John Wiley & Sons, 1974.
- [14] Johansen, J and Vejlgaard, B, "Capacity Analysis of a Frequency Hopping GSM System", Master Thesis Report, Aalborg University, June 1995 (in English)
- [15] Lee, W.: "Mobile Communications Engineering", McGraw-Hill, Inc., 1976.
- [16] Mogensen, P E., Wigard, J and Frederiksen, F, "Performance of slow frequency hopping in GSM (Link level)", COST 231 TD(95)-121, Poznan, Sep. 1995.
- [17] Mogensen, P E., "GSM Base-Station Antenna Diversity Using Soft Decision Combining on Up-link and Delayed-Signal Transmission on Down-link", Proc. VTC'93, pp. 611-616.
- [18] Lopes, L, "A combined space/time diversity technique for narrowband TDMA mobile radio systems", Electronics Letters, vol.25, no.15, pp.1001-1002, July 1989.
- [19] D'Avella, R, Montano, R, Moreno, L and Sant'Agostino, M, "Evaluation of diversity schemes in TDMA mobile radio", COST231 TD(90)97.

- [20] D'Avella, R, Montano, R, Moreno, L and Sant'Agostino, M, "A diversity receiver for the pan-european mobile digital system", COST231 TD(90)97.
- [21] Ibbetson, L J and Lopes, L B, "Performance comparison of alternative diversity schemes using a GSM radio link simulation", Proc 7th IEE European Conference on Mobile Personal Communications, Brighton, December 1993, pp.11-15.
- [22] Mogensen, P E., Wigard, J and Frederiksen, F, " A Pre-selection Antenna Diversity algorithm for GSM", (Internal AUC document and patent , to be published).
- [23] Mogensen, P E. and Wigard, J., " On Antenna and Frequency Diversity in GSM Related Systems (GSM-900, DCS-1800, and PCS1900)", Proc. IEEE PIMRC'96, Taipei, Oct. 1996, pp. 1272-1276.
- [24] Mouly, M and Pautet, M-B, "The GSM System for Mobile Communications",
- [25] Møller, H K and Toft, M, "Synchronization and optimization of GSM Baseband Receiver", Master thesis report, AUC 1995 (in English)
- [26] Olofsson, H, Näslund, J, Ritzén, B, and Sköld, J, "Interference diversity as means for increased capacity in GSM", Proc. EPMCC '95, Bologna, Nov. 1995, pp. 97-102
- [27] Scheinert, S. "Is frequency planning obsolete?", Mobile Europe, September 1995, pp. 19-24.
- [28] Steele, R, "Mobile Radio Communications", Chap. 7, Pentech Press 1992, London
- [29] Vejlgaard, B, Johansen, J, Mogensen, P E, and Wigard, J, "Capacity analysis of a Frequency Hopping GSM System", COST 231 TD(95)-122, Poznan, Sep. 1995

- [30] Wigard, J and Mogensen, P E, Johansen, J., and Vejlgaard, B., "Capacity of a GSM network with fractional loading and random frequency hopping", Proc. IEEE PIMRC'96, Taipei, Oct. 1996, pp. 723-727.
- [31] Wigard, J, "Link simulation tool for the GSM TCH/FS", Version 2.0, Internal report, Aalborg University, Jan. 1996
- [32] Zetterberg, P, "Some signal processing aspects on base station antenna array structures for cellular systems", (Aalborg University, Nov. 1995)
- [33] ETSI, "Radio Equipment and Systems Digital European Cordless Telecommunications Common Interface", DECT Specification, Part 1 to 3, Ver 02.01, May 17, 1991.
- [34] Tuttlebee, W.H.W. (ed), "Cordless Communication in Europe", Berlin, Heidelberg, New York: Springer Verlag, 1990.
- [35] Akerberg, D, "Properties of a TDMA Pico Cellular Office Communication System". Proceedings of the 39th IEEE Vehicular Technology Conference. (1989), VOL I, pp. 186. 36
- [36] Murota, K and Hirade, K, "GMSK Modulation for Digital Mobile Radio Telephony". IEEE Transactions on Communications. (1981) VOL. COM.-29, No. 7, pp. 1044
- [37] Schultes, G. Bonek, E, Weger, P, and Herzog, W, "Basic Performance of a Direct Conversion DECT- Receiver". Electronics Letters, Vol.26, No.21, 11th October 1990, pp 1746-1748.
- [38] Schultes, G: Bonek, E; Scholtz A L.; Kreuzgruber, P, "Low- Cost Direct- Conversion Receiver Structures for TDMA Mobile Communications". Proceedings of 6th IEE Conference Mobile Radio and Personal Communications, University of Warwick, December 9-12, 1991, pp 143 - 150.
- [39] Schultes, G. Simbürger, W, Novak, H and Hapl, M, "Physical and Medium Layer DECT Testbed", COST231 TD(92)28.

- [40] Mogensen, P E and Petersen, S, "Practical Considerations of using Antenna Diversity in DECT", Proc VTC'94, Stockholm, June 1994, pp.1084-1088.
- [41] Mogensen, P E, "Practical Considerations of using Antenna Diversity in DECT", COST231 TD(93)122.
- [42] Mogensen, P E and Petersen, S, "Antenna Configuration Measurements for DECT Microcells", Proc PIMRC'94 /WCN, The Hague, September 1994, pp.1075-1080.
- [43] Mogensen, P E, Thomsen, P K and Frederiksen, F, "A new Switching Diversity Scheme for DECT driven by a Combined RSSI and Error Criterion", COST231 TD(94)121.
- [44] Mogensen, P E, Frederiksen, F and Wigard, J, "A Linear Power Prediction Algorithm for TX Selection Diversity in DECT", COST231 TD(95)120.
- [45] Mogensen, P E, Frederiksen, F and Thomsen, P K, "A Preamble Based Switching Diversity Algorithm for DECT", COST231 TD(94)122.
- [46] Wigard, J, Mogensen, P E and Frederiksen, F, "Evaluation of Optimum Diversity Combining in DECT", COST231 TD(95)59.
- [47] Lopes, L, "An Overview of DECT Radio Link Research in COST 231", Proceedings of PIMRC '94, The Hague. September 18-22, 1994, Vol. 1, pp. 99-104.
- [48] Wilkinson, T A, "Radio Propagation Channel Modeling for the DECT Test Bed", COST 231 TD(91)48, Lund. June 4-7, 1991.
- [49] Kauschke, U, "Propagation and System Performance Simulations for the Short Range DECT System in Microcellular Urban Roads", IEEE Transactions on Vehicular Technology, 44, no.2, May 1995, pp. 253-260.
- [50] Kauschke, U, "Propagation measurement with RUSK SX and Simulations for a Typical DECT Scenario in Urban Streets", Proceedings of

the 2nd Joint COST 227/231 Workshop on Mobile and Personal Communications, Florence, April, 20-21, 1995.

[51] Kauschke, U, "Wideband Indoor Channel Measurements for DECT Receiver positioned inside and outside an Office Building", Proc. PIMRC'94 and WCN, The Hague, Sep 1994, Vol IV, pp. 1070-1074.

[52] Kauschke, U, in: ne Science (series on COST231 results and reprints), Berlin, 45(1995)3, pp.39-44 (in German).

[53] Eggers, P C F, Mogensen, P E, "Evaluation of Low Effort Dispersion Reduction Techniques for DECT in Telepoint Environments", Proc VTC'94, Stockholm, June 1994, pp.677-680.

[54] Mogensen, P E and Verholdt, C, "Measurement Results from using DECT in a RLL Application", Proc VTC'94, Stockholm, June 1994, pp.1065-1068.

[55] Kadel, G, "Determination of the GSM system performance from wideband propagation measurements", Proc 42nd IEEE Vehicular Technology Conference, Denver, USA, pp.540-545.

[56] Kadel, G, and Lorenz, R W, "Impact of the radio channel on the performance of digital mobile communication systems", Proceedings of the Sixth International Symposium on Personal, Indoor and Mobile Communications (PIMRC), Toronto, September 1995, pp.419-423.

[57] Kadel, G, "Simulation of the DECT System using wideband channel data measured in two diversity branches", Proceedings of the 2nd International Conference on Universal Personal Communications (ICUPC), Ottawa, Canada, 1993, pp. 546-550.

[58] Kadel, G, "Simulation of the DECT system using Wideband Diversity Measurements for Channel Description", COST231 TD(93)27.

[59] Rækken, R H and Eskedal, B E, "DECT performance in multipath environments", Nordic Radio Symposium, Saltsjöbaden, April 1995.

- [60] Wilkinson, T A, "Channel Modeling and Link Simulation Studies for the DECT Test Bed Program", Proceedings of the 6th IEE International Conference on Mobile Radio and Personal Communications, University of Warwick, UK, December 9-12, 1991, pp. 293-299.
- [61] Crohn, I, Schultes, Gahleitner, G, and Bonek, E, "Irreducible error performance of a digital portable communication system in a controlled time-dispersion indoor channel", IEEE J. Select. Areas Comm. vol. SAC-11, 1024-1033 (1993).
- [62] Lopes, L B and Heath, M R, "The Performance of DECT in the Outdoor 1.8 Ghz Radio Channel", Proc IEE Mobile Radio and Personal Communications Conference, Warwick, December 1991, pp.300-307.
- [63] Lopes, L B, "Performance of the DECT system in fading dispersive channels", Electronics Letters 26, 1416-1417 (1990).
- [64] Schultes, G and Crohn, I, "Measured performance of DECT transmission in low dispersive indoor radio channel", Electronics Letters 28, 1625-1627 (1992).
- [65] Crohn, I and Schultes, G, "Error performance of differentially detected MSK in small delay-spread Rayleigh channel", Electronics Letters 28, 300-301 (1992).
- [66] Molisch, A F, Fuhl, J, and Proksch, P, "Error floor of MSK modulation in a mobile-radio channel with two independently-fading paths", *IEEE Trans. Vehicular Techn.*, 45, pp. 303-309 (1996).
- [67] Lopes, L B and Safavi, S, "Relationship between performance and timing recovery mechanisms for a DECT link in dispersive channels", Electronics Letters 29, 2173-2174 (1993).
- [68] Lopes, L B, Molisch, A F, Paier, M, and Fuhl, J, "On the error floor in DECT-like systems", Proc. Europ. Personal and Mobile Comm. Conf. Bologna 1995, 170-175.
- [69] Brandao, A L, Lopes, L B, and McLernon, D C, "Method for timing recovery in presence of multipath delay and cochannel interference", Electronics Letters 30, 1028-1029 (1994).

- [70] Wigard, J. Mogensen, P E, Frederiksen, F and Nørklit, O, "Evaluation of Optimum Combining Diversity in DECT", Proc PIMRC'95, Toronto, September 1995, pp.507-511.
- [71] Fuhl, J and Schultes, G, "Adaptive Equalisation for DECT Systems operating in Low Time Dispersion Channels", Electronics Letters, vol.29, no.24, Nov 1993, pp.2076-2077.
- [72] Safavi, S and Lopes, L B, "Simple Non-Coherent Equaliser for the DECT System", Electronics Letters, vol.30, no.10, May 1994, pp.756-757.
- [73] Safavi, S and Lopes, L B, "A Non-Coherent Equaliser Receiver Structure for DECT-type Systems", Proc VTC'94, Stockholm, June 1994, pp.1084-1088.
- [74] Safavi, S and Lopes, L B, "An Approach to Performance Enhancement of Non-Coherent Equaliser Receivers", Proc PIMRC'94, The Hague, September 1994, pp.214-218.
- [75] Petersen, M, and Rækken, R H, "DECT offering mobility on the local level - experiences from a field trial in a multipath environment", Proc IEEE VTC96, Atlanta, May 1996, pp.829-833.
- [76] Eskedal, B E, Løvsletten, J, and Deilkäs, J T, "DECT field trial at Førde" Telektronikk no. 4, 1995
- [77] Kadel, G, "Performance of the DECT system with a 2-state-Viterbi equaliser", COST 231 TD(93)78, 1993
- [78] Safavi, S, Lopes, L B, Mogensen, P E and Frederiksen, F, "An Advanced Base Station Receiver Concept for DECT", Proc VTC'95, Chicago, July 1995, pp.150-154.
- [79] Mogensen, P E, Frederiksen, F, Thomsen, P K, Safavi, S and Lopes, L B, "Testbed Evaluation and Measurements of an Advanced Receiver Concept for DECT", Proc VTC'95, Chicago, July 1995, pp.514-519.

- [80] Safavi, S, Lopes, L B, Mogensen, P E and Frederiksen, F, "A Hierarchy of Receiver Options for DECT Systems", Proc PIMRC'95, Toronto, September 1995, pp.1351-1356.
- [81] ETSI-ETS 300 700, "Wireless Relay Stations", February 1996
- [82] Bonzano, L, De Benedittis, R, Palestini, V, Rosina, G, "A new radio access strategy using a repeater in the DECT Radio Local Loop application", ICUPC'94
- [83] ETSI-ETS 300 175(1-9) Second Edition, "DECT: Common Interface (CI)", July 1996
- [84] ETSI-ETR 42, "Guide to features that influence traffic capacity"
- [85] Scientific Generics Ltd, Report of DECT standard in Public Access Applications, Results and Demonstration, 21/4/1994, Budapest Marriott Hotel
- [86] ETSI-ETR 139, "ETR on Radio Local Loop", ETSI-ETR 139, November 1994
- [87] Draft ETSI-ETS, "Radio Local Loop Access Profile", January 1996

## Advanced Radio Interface Techniques and Performance

**H. Rohling, Technical University of Braunschweig, Germany**

This chapter summarises the results of the technical activities performed mainly by the Working Group 1 (WG 1) members of COST 231. WG 1 focused on general radio system aspects but in this chapter the description of transmission techniques and their performance is given priority. A large number of technical documents and reports were written in recent years by the WG 1 members giving detailed information and analysis of radio interface techniques for 3rd generation mobile radio systems. These reports which are available in the open literature are referenced in this chapter. The different technical subjects in which WG 1 members were involved are covered in separate subsections and the names of all authors responsible for each subsection are given at the beginning of that subsection. Readers are invited to contact individual authors.

Chapter 6 is organized as follows: The first subsection deals with linear (QAM, PSK) and nonlinear (MSK, GMSK, QMSK, MAQMSK, multi-h CPM) modulation techniques which are analysed and optimised for various radio propagation conditions. Furthermore, transmitter linearisation methods are discussed in conjunction with linear modulation techniques.

Subsection 2 deals with advanced equalisation techniques and equalisation in combination with diversity. In addition, the convergence properties of the classical algorithms to perform adaptive equalisation are described.

Subsection 3 discusses the capacity of a cellular TDMA system which can be greatly increased if enhanced techniques such as adaptive modulation, adaptive coding or dynamic channel allocation are applied. The performance of such an enhanced TDMA system is compared with different CDMA systems in terms of spectral efficiency and capacity.

The fourth subsection in this chapter deals with CDMA which was extensively studied in WG 1. Results relating to the performance of DS-CDMA, FH-CDMA and hybrid systems are presented.

Subsection 5 describes a special data detection method in CDMA systems called Multiuser-Detection, which uses the a-priori knowledge about the code sequences of other users in conjunction with the channel state information. Three different detection algorithms were analysed: Joint Detection CDMA, Joint Parameter Estimation with Data Detection and Interference Cancellation.

A further enhancement of the system capacity can be obtained by combining the advantages of both TDMA and CDMA and such Hybrid TDMA/CDMA systems are discussed in subsection 6.

Multicarrier systems are analysed in subsection 7 which concentrates on OFDM and combinations of OFDM with CDMA in the frequency and time domains. The final subsection deals with MAC protocols for radio data transmission.

## 6.1 Modulation and Channel Coding

**L. Delaunay-Ledter, France Telecom/CNET, France (6.1.1, 6.1.4)**  
**E. Casadevall, UPC, Spain (6.1.1)**  
**A. Rodrigues, Instituto Superior Técnico Lisboa, Portugal (6.1.2)**  
**A.F. Molisch, TU Wien, Austria (6.1.3)**  
**J. Fuhl, TU Wien, Austria (6.1.3)**

### 6.1.1 Linear Modulation

#### M-PSK and M-QAM Modulations

To provide high data rates required in third generation mobile systems, the use of bandwidth efficient linear modulation could become necessary even if linear amplifier or linearisation techniques have to be added.

The performance of binary phase shift keying (BPSK) with convolutional coding and antenna diversity was analysed. It was shown that partial interleaving strongly degrades the performance in a Rayleigh channel with low Doppler shift in comparison with ideal interleaving, assuming perfect decorrelation of the fading. As an illustration, the ITU-T recommendation G.173 [1] has limited the mean one-way propagation time of public land mobile networks (PLMN) to 40 ms and as a consequence of this, the interleaving depth might be reduced to 10 ms. Coding gains obtained for a rate 1/2 convolutional code of constraint length 5 with a 10 ms partial block interleaver and differential BPSK are given in Tab. 6.1.

	no diversity	2nd-order diversity	4th-order diversity
$f_d \cdot T_s = 10^{-4}$	no	no	no
$f_d \cdot T_s = 10^{-3}$	no	0.8 dB	no
$f_d \cdot T_s = 10^{-2}$	12 dB	6.8 dB	3.2 dB
(ideal interleaver)	(17 dB)	(8.2 dB)	(3.8 dB)

Table 6.1: Coding gains for rate 1/2 convolutional coding with 10 ms partial block interleaving in dependence on different normalised Doppler frequencies  $f_d \cdot T_s$  and diversity-orders; transmission rate  $R_b = 32$  kbit/s (BPSK); carrier frequency 1.8 GHz

Simulations were also carried out with slow frequency hopping using a 1/3 rate Reed Solomon (6,2) code or a repetition code with interleaving and coherent demodulation in an indoor channel environment, (the power delay profile is modelled as a double Poisson process, [2]). In hopping over 6 frequencies, a normalised frequency separation  $S_f \tau_{rms}$  ( $\tau_{rms}$  for root-mean-square delay spread) larger than 0.1 and 0.2 for the

Reed Solomon code and the repetition code respectively does not improve the performance significantly. On the other hand, for  $S_f \tau_{rms}$  larger than 0.05, Reed Solomon codes are more efficient than repetition codes.

Moreover, the cellular mobile radio impairments, (multi-path fading, shadowing, large-scale path loss, [3], and interferer signals), have been considered with a coherent BPSK receiver. For micro (Ricean channel), and macro (Rayleigh) cellular networks, it was shown that at high signal-to-interference ratios ( $C/I > 20$  dB), shadowing affects the bit error rate (BER) less than the Ricean factor within the usual range of these parameters (less than 12 dB of shadowing and Ricean factor between 0 and 1000). The average bit error rate is given in [4].

Assuming a small frequency selectivity, the approximate irreducible bit error rate for multi-level PSK modulation was analysed in [5] with the result that 4-PSK is most robust in Rayleigh channels. In addition, the performance of multi-level quadratur amplitude modulation (M-QAM) in an indoor environment was studied based on a channel model that was determined by a ray-tracing technique. A rectangular pulse shape of length twice the bit period was used, independent of the modulation level. Considering a normalised signal-to-noise (SNR) ratio of 21 dB (irreducible error floor of  $10^{-8}$ ), the data rate may be increased from about 10 Mbit/s for 4-QAM, to 23 Mbit/s for 16-QAM, and 29 Mbit/s for 64-QAM with the same bandwidth being occupied.

Further work was done on  $\pi/4$ -QPSK which is a trade-off between linear and constant envelope modulation.

## Transmitter Linearisation

In order to decrease the power spectrum spreading of a linear modulation passed through a class AB, B or C power amplifier, several classical linearising techniques for power amplifiers have been proposed in the literature categorized as: feedforward, feedback, predistortion and LINC (Linear Amplification with Nonlinear Components) transmitter. Among them, the two most promising have been analysed: the predistortion and the LINC transmitters.

In the predistortion technique, the original baseband signal is first predistorted to compensate the amplifier nonlinearity by using a look-up table which could be updated by feedback information. One way to configure the look-up table is to map both inphase and quadrature into an output signal vector. It is also possible to use only one dimensional tables since the distortion in the power amplifier is essentially caused by input amplitude variations. The predistortion using one dimensional look-up tables has appeared more suitable for low data rate systems because of its faster convergence.

The basic principle of the LINC transmitter is to represent any arbitrary bandpass signal, which may have both amplitude and phase variation, by means of two signals which are of constant amplitude and only have phase variations [6]. These two angle modulated signals can be amplified separately by using class C,D,E or S amplifiers that provide enough power. Finally, the amplified signals are passively combined to

produce an amplitude modulated signal.

Even using the highly non-linear classes C, D, E or S power amplifiers, if perfect balance between both RF branches is assumed, the system is able to obtain a performance as good as that obtained with an ideal linear amplifier. However, in a practical LINC transmitter there are several mechanisms that degrade the overall performance, e.g. the power gain and delay (or phase) imbalances between the two RF paths that cause imperfect generation of the constant amplitude phase modulated signal component. Some theoretical [6] and practical [7] works have been addressed to characterise the impact of these circuit malfunctions on the system performance and so an upper bound on the adjacent channel rejection  $U_r$  (ratio between the power in the useful channel with respect to the power in the adjacent channel) has been derived from the gain imbalance  $\Delta G$  (in dB), the phase imbalance  $\Delta f$  (in degrees), and the normalised guard band between adjacent channels ( $\Delta B_g T$ ), see Tab. 6.2

4-QAM	$U_r[\text{dB}] \geq 32.5 - 19.2 \log_{10}(\Delta G) + 5(\Delta B_g T)$ $U_r[\text{dB}] \geq 48.0 - 20.5 \log_{10}(\Delta f) + 5(\Delta B_g T)$
16-QAM	$U_r[\text{dB}] \geq 32.0 - 19.0 \log_{10}(\Delta G) + 7(\Delta B_g T)$ $U_r[\text{dB}] \geq 45.4 - 20.75 \log_{10}(\Delta f) + 7(\Delta B_g T)$
64-QAM	$U_r[\text{dB}] \geq 28.5 - 19.0 \log_{10}(\Delta G) + 7(\Delta B_g T)$ $U_r[\text{dB}] \geq 44.5 - 21.2 \log_{10}(\Delta f) + 7(\Delta B_g T)$

Table 6.2: Upper bound of the channel rejection with a maximum error of 3dB

The effects of these imbalances on the bit error probability have been analysed, too. In order to emphasise the influence of the imbalances, a system free of intersymbol interference has been assumed. Whereas 4-QAM and 16-QAM modulations remain more or less insensitive to imbalance effects, the 64-QAM and higher order modulations are very sensitive and careful implementations of the RF part are requested when real LINC transmitters are assumed.

In order to evaluate the degradation in terms of BER induced by gain and phase imbalances in a realistic system, the dependence of the BER on the signal-to-noise ratio is shown in Fig. 6.1 and 6.2 for a typical urban environment using a class AB amplifier. A bit rate of 500 kbit/s and a 16-QAM modulation scheme have been considered. As shown in Fig. 6.1, the gain imbalance has to be lower than 0.5 dB to assure no significant performance degradation.

Therefore, although the application of the LINC transmitter is very promising when linear power amplification is required, an imperfect implementation causes an important degradation of the system performance that can completely invalidate the system design, and correction techniques have to be added.

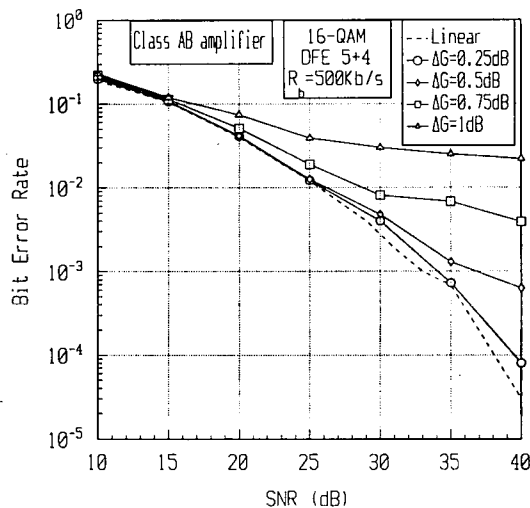


Figure 6.1: Effect of gain imbalances

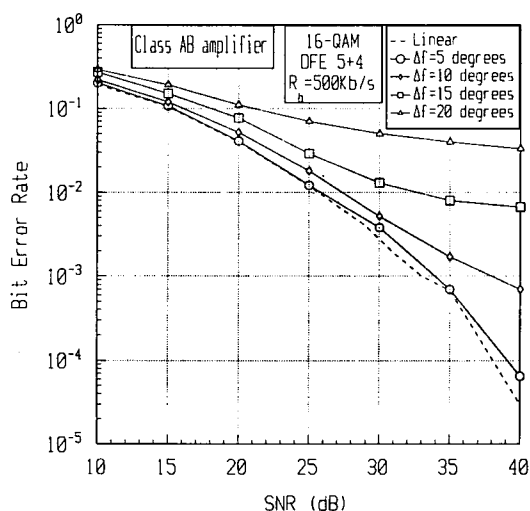


Figure 6.2: Effect of phase imbalances

### 6.1.2 Continuous Phase Modulation

#### MSK and GMSK

Constant envelope phase modulations are currently chosen in mobile radio systems for their ability to support non-linearities in the propagation channel as well as for their good spectral efficiencies and error performances.

The Gaussian minimum-shift keying (GMSK) signal can be efficiently received using a simple MSK-type linear coherent receiver with an appropriate phase detector for the adaptation of a decision directed phase-locked loop. Simulations were performed for different values of phase offset (0 to 15 degrees) and showed that the performance of coherent GMSK with a time-bandwidth product  $BT = 0.5$  is almost identical (less than 1 dB degradation) to that of coherent MSK in an additive white Gaussian noise (AWGN) channel [8].

Although the index value 0.5 is needed for coherent demodulation, this choice is not optimum for a limiter discriminator detection. A joint optimisation of modulation index, filters and carrier spacing was done in the AWGN and the minimum bit error rate was achieved for a modulation index of the order of 0.6, with corresponding optimised filters for a C/I ratio equal to 25 dB. Performance in a flat Rayleigh fading channel with or without interference was also evaluated for the modulation index 0.5 and a normalised Gaussian filter bandwidth of 0.3 and 0.5. Using a pre-discriminator filter in the receiver, the required C/I ratio at  $BER=10^{-3}$  is 27 dB for  $BT = 0.5$  and 27.5 dB for  $BT = 0.3$ , respectively.

The study of rate 1/2 convolutionally encoded tamed frequency modulation (TFM) [9] with RSSE (Reduced State Sequence Estimation [10]) reception was performed in [11] assuming an AWGN channel. The system optimisation problem was reformulated in order to include the hardware complexity of the receiver, introducing the concept of the “optimum transmitter” under a given receiver complexity constraint. The result show that with an appropriately selected suboptimal receiver an additional coding gain in the order of 0.6-1.2 dB can be achieved compared to uncoded TFM detection.

#### QMSK and MAQMSK

In order to obtain a better spectral compactness than that obtained with MSK and GMSK, quadratur minimum-shift keying (QMSK) modulation [14] can be used. In comparison with MSK this scheme increases the signal dimensions by a factor of 4 which allows a better spectral efficiency especially if the scheme is combined with multi-amplitude input signals. These multi-amplitude signals are called MAMSK and MAQMSK respectively and their phase diagrams are depicted in Fig. 6.3.

A simple method of calculating the power spectral density permits the comparison of different modulation schemes. Among the different modulation schemes considered, MSK is shown to have better spectral performance than QPSK or QMSK which performed alike. When considering multi-amplitude schemes MAMSK has the most compact performance in comparison with MAQMSK and MSK schemes [15].

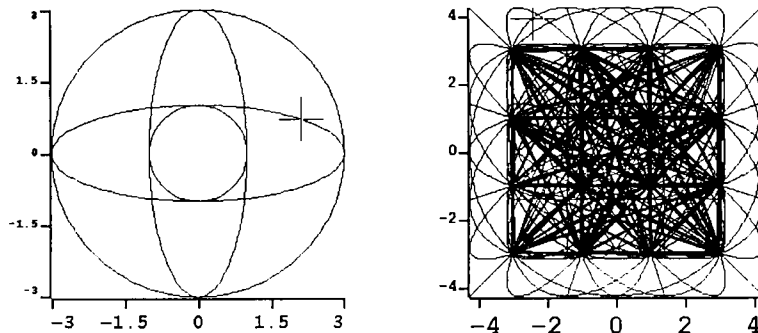


Figure 6.3: MAMSK and MAQMSK signal constellation diagrams

The performance of the QMSK signal was investigated in additive white Gaussian noise and in fast Rayleigh fading channels also considering Doppler frequency shifts and co-channel interference but without considering the existence of multipath. In a AWGN channel and in Rayleigh fading channels with co-channel interference QMSK performs better than GMSK and  $\pi/4$ -QPSK showing that it is a more resistant scheme in a co-channel interference limited environment (see Fig. 6.4).

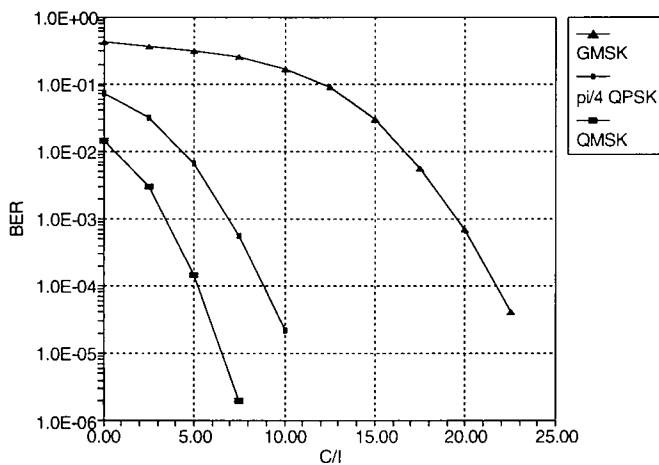


Figure 6.4: Performance of QMSK, GMSK and  $\pi/4$ -QPSK signal in Rayleigh fading channel with cochannel interference

However, when Doppler shifts are considered the QMSK scheme shows a greater sensitivity to these shifts than GMSK or  $\pi/4$ -QPSK [15].

### Multi-h CPM

As an alternative to the use of single modulation index schemes like MSK or GMSK, multi modulation index schemes (multi-h) [16] were also considered. For a two-path channel model (static two-path) with AWGN, the signature areas of a 2-h CPM scheme were computed as a function of the relative delay of the second path and these were compared with that obtained for 16-, 64- and 256-QAM modulation. Results presented in Fig. 6.5 show the CPM scheme to be less sensitive to interference than the QAM schemes for the same source bit rate and for constant channel bandwidth even when the different bandwidth efficiencies of the CPM and QAM schemes are considered. All the schemes present a maximum of sensitivity for a value of the relative delay between 0.05 and 0.6 times the symbol period [17].

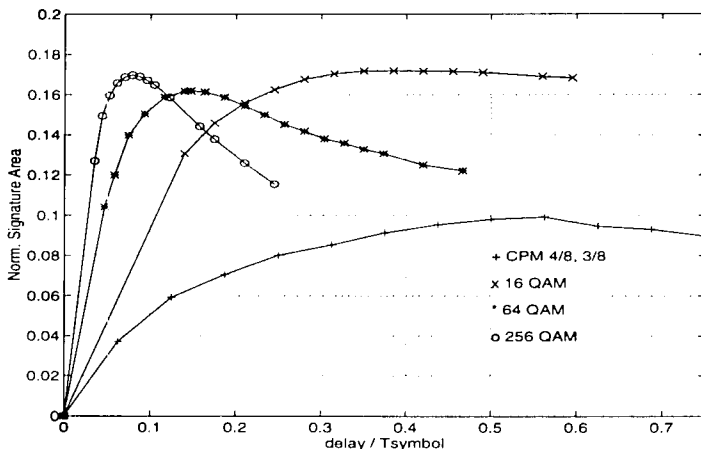


Figure 6.5: Comparison of the signature areas for constant bandwidth as a function of  $\tau/T_{symbol}$  compensated for the different bandwidth efficiencies

Multi-h CPM modulation schemes are more spectral efficient than GMSK. An analysis of the performance of 2-h CPM was performed for both typical urban and hilly terrain COST 207 channel models [18]. The use of a post-detection diversity (PD) scheme implemented by means of two Viterbi receivers was also considered allowing further performance improvements.

Also a combination of a multi-h CPM modulation with a direct sequence spread spectrum system and its performance in several indoor environments was investigated.

Three different channels were analysed: line-of-sight, non line-of-sight and large buildings with maximum delay spreads of 100, 200 and 400 ns, respectively [19]. Results are given for two different multi-h codes considering a coherent receiver structure and two types of diversity: selection diversity (SD) and post-detection diversity. Results in Fig. 6.6 indicate that multi-h spread spectrum systems can achieve good performances in indoor environments for relatively high data rates (1 Mchip/s) but the use of diversity is essential to achieve an acceptable BER with realistic  $E_b/N_0$ , specially in large buildings [20, 21].

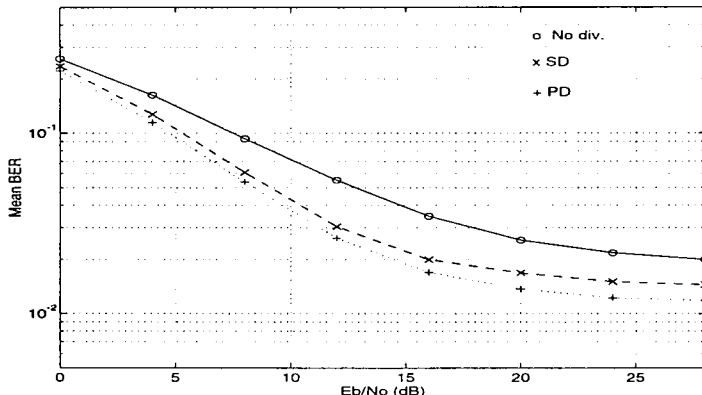


Figure 6.6: Error performance of coherent multi-h CPM ( $h_1 = 2/4; h_2 = 3/4$ ) in a an urban area (large buildings) without diversity, with selection div. (SD) and post-detection div. (PD)

A comparison between multi-h CPM and CPFSK (continuous phase frequency shift keying) was also made for AWGN channels using the concept of equivalent minimum distance for non-coherent detection. Multi-h signals maintain their superiority over CPFSK in the case of non-coherent detection with gains up to 2.28 dB. The performance of the non-coherent receiver can be as good as the coherent one for certain values of the modulation index and for long observation intervals in the receiver (greater than 100 symbol periods) [22].

### 6.1.3 Performance of MSK in time dispersive channels

The time dispersion of the mobile radio channel causes intersymbol interference (ISI) that results in an irreducible BER usually called error floor. The error floor constitutes the performance limit for a given channel and a modulation/detection scheme (without

equalisation). For cordless phones, the cost and system complexity must be kept low so they usually have no equalisers. Furthermore, the SNR in indoor scenarios is high, so the error floor is a quite good performance measure. In Chapter 5 (DECT), the results and practical applications are described. In this section, we concentrate on the basic mathematical methods. For the case of differentially detected pure MSK with fixed sampling and delay spreads that are small compared to the bit length, various computation methods have been developed:

**The group delay method** [23, 24] — The differential detector decides that a “1” was transmitted if the phase difference between two adjacent samples lies between 0 and  $\pi$ , and a “-1” was transmitted if the phase difference lies between  $\pi$  and  $2\pi$ . Without time dispersion, the phase difference is  $\pi/2$  or  $3\pi/2$ , respectively. The differential detector thus makes an error if the phase error introduced by the (instantaneous) group delay lies between  $\pi/2$  and  $3\pi/2$ . Averaging over the statistics of the group delay [25] we get an approximate equation for the BER:  $\text{BER} = (1/2)(S/T)^2$ . Here,  $S$  is the mean delay spread and  $T$  is the bit length. Closer inspection of the error mechanisms show that group delay bursts occur when the amplitude of the received signal becomes very small, i.e. in deep fades.

**The error region method** [26, 27] — This method is described in Chapter 5, since it is also suitable for adaptive sampling, and thus can be readily applied to DECT systems.

**The echo method** [28] — For the echo method, we interpret the (general) impulse response, as a sequence of echoes, where each echo has its amplitude  $A_i$  and phase  $\phi_i$ . Using the Gaussian WSSUS model and the assumption of a slowly varying channel, the  $A_i$  are (known) constants, while the  $\phi_i$  are uniformly distributed statistical variables. We can then compute the total phase for a certain input sequence and determine for which  $\phi_i$  errors occur. Averaging over the statistics of the  $\phi_i$ , we finally arrive at the error probability.

All three methods have some restrictions: the group delay method gives only approximate results and is only applicable if the delay spread is much smaller than the symbol length, sampling is done on the average mean delay, and we have no LOS component. The error region method is essentially restricted to the two-delay channel but works also for LOS, larger delay spreads, and arbitrary sampling time. The echo method requires that we have no LOS components and that  $S \ll T$ , but works for general impulse responses and arbitrary sampling times. In none of these methods noise is included.

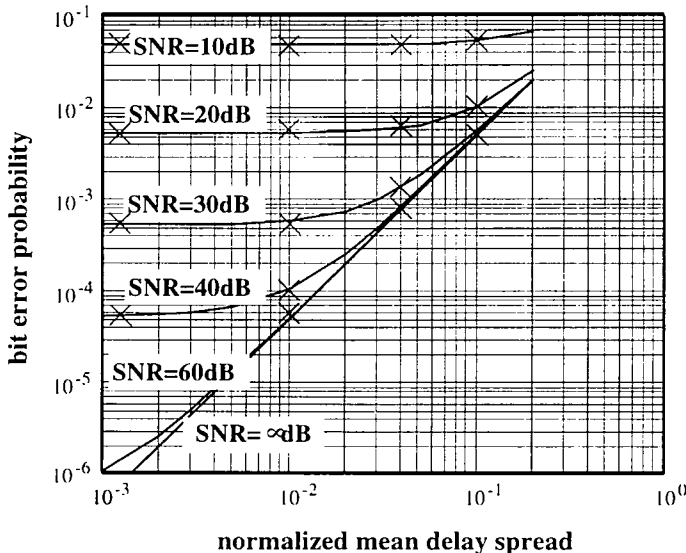


Figure 6.7: Error probability of MSK in a 10-path fading channel

**The correlation matrix method** [29] — A fourth method, the so-called “correlation matrix method”, lifts these restrictions. It can be shown that the real and imaginary parts of the received signal at two subsequent samples are Gaussian variables, whose correlation matrix can be determined from the average channel parameters and the modulation format. The BER is then the probability that a certain combination of these samples fulfills an error condition. Several methods for the evaluation of this probability exist: direct numerical evaluation, approximation methods for small error probabilities, and construction of an “equivalent” two-path model that has the same correlation matrix, and thus the same error probability.

The second case of interest are outdoor scenarios, especially in the context with GSM (see Chapter 5). For typical delay power profiles, the duration of the impulse response is larger than the bit length. In that case, the approximate BER can be computed for sampling at the shortest excess delay. The mean power of the current bit is  $P_b = \int_0^T P(t) dt$  and the power of the interfering bits is  $P_h = \int_T^\infty P(t) dt$ . It was shown [30] that the average BER is approximately  $\text{BER} = [2(1 + 2P_r)]^{-1}$ , where  $P_r = P_b/P_h$ . This equation is also valid in indoor scenarios for very high data rates. Such high data rates are possible if a strong LOS component is present; e.g. for a 10 dB LOS and 2-PSK, 20 Mbit/s are possible. For non-LOS, the BER with fixed sampling and 100 ns delay spread is in the order of  $10^{-2}$  for bit rates of 1 Mbit/s.

### 6.1.4 Trellis Coded Modulation (TCM)

TCM represents an attractive solution to improve performance for mobile radio transmission without extra bandwidth requirements. Two different concepts of TCM exist, one based on the Ungerboeck method [31] with one convolutional code, other based on the Imai method [32] where the partition levels are encoded with several binary codes.

A new criterion for designing the Imai code for a Rayleigh channel was proposed, derived from the Sundberg's approach, [33]. The main difference was to use sub-codes with unequal Hamming distances, chosen to optimise the coding gain at a specific bit error rate. The optimised solutions for a  $10^{-3}$  bit error rate in a Rayleigh channel are given in Tab. 6.3, [34].

rate (bit/symbol)	Modulation	code	required $E_b/N_0$ (dB)
0.5	4-PSK	1/4	3.5
		1/2	5.1
		3/4	9.2
1	8-PSK	3/8,3/4,7/8	11.5
1.5	16-PSK	1/4,2/3,5/6,11/12	13.1
2	16-PSK	1/2,4/5,11/12,11/12	16.7
2.667			
3.167			

Table 6.3: Summary of code rates and required  $E_b/N_0$  for  $\text{BER}=10^{-3}$  (Rayleigh fading channel)

However, whatever the access technique may be, partial interleaving has an influence on coding efficiency and therefore on TCM performance. A modified Chernoff bound taking into account the effect of correlated fadings can be found in [35]. This point has been illustrated for coded 8-PSK with code rate 2/3. The simulation results reported in Tab. 6.4 refer to a 64 kbit/s data rate in a Rayleigh channel considering pedestrian and vehicle speed by a 10 ms interleaver delay.

BER	perfect interleaving	v=190km/h	v=40km/h	v=4km/h
$10^{-2}$	6 dB	4.6 dB	2.1 dB	0.5 dB
$10^{-3}$	12.5 dB	10.6 dB	7.3 dB	4.6 dB

Table 6.4: Coding gains of trellis coded 8-PSK compared to uncoded QPSK;  $R_h=64$  kbit/s;  $32 \times 10$  block interleaver;  $f_0=1800$  MHz

Frequency hopping techniques can provide the way to make the interleaving process

more effective. In particular, the effect of frequency hopping was analysed for eight-states trellis coded 8-DPSK taking into account the correlation among the different frequency channels involved. In each channel flat fading was assumed with a maximum Doppler frequency of 5 Hz. The correlation of the complex channel transfer function  $H_c(f, t)$  versus the frequency separation  $S_f$  was assumed to be

$$E[H_c^*(f, t)H_c(f + S_f, t)] = \frac{1}{1 + j2\pi S_f \tau_{rms}}$$

resulting from an exponentially decreasing power delay profile with rms delay spread  $\tau_{rms}$ . A block interleaver of order  $N_L \times N_C$  was considered, and the  $N_L$  formed slots were modulated according to  $N_L$  assigned hopping frequencies. As shown in Fig. 6.8 for  $S_f \tau_{rms}$  smaller than 0.15, the degradation of performance with respect to the uncorrelated case becomes significant. The uncorrelated results can be found in [9].

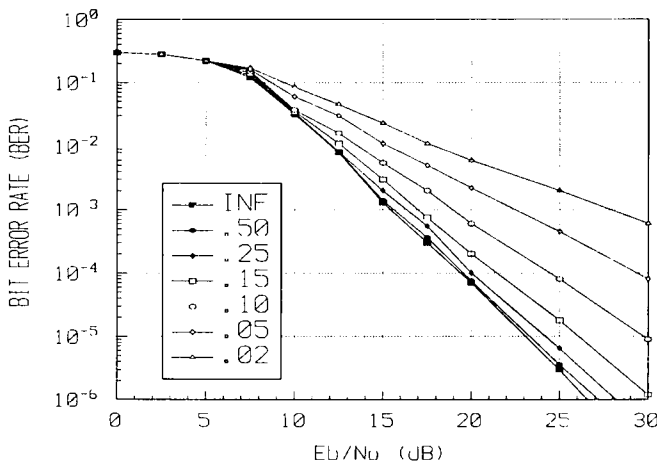


Figure 6.8: Bit error rate for FH-TCM-8DPSK with normalised frequency hopping separation as parameter

The two-branch post-detection diversity solution to combat the Rayleigh fading has been also investigated with perfect interleaving assumption. At a BER of  $10^{-3}$ , post-detection selection, equal gain combining (EGC) and maximal ratio combining (MRC) diversity techniques have offered a relative coding gain over the eight-states trellis coded 8-DPSK (rate 2/3) without diversity of approximately 5.9, 6.2 and 6.6 dB respectively. Additional results have also pointed out that TCM with diversity is more robust than TCM without diversity regarding the effects of co-channel interference.

The primary interest of TCM for a mobile system is its bandwidth efficiency. As described in [36], the spectrum efficiency  $\eta$  of a cellular mobile system depends on the C/I ratio, on modulation parameters, and on propagation characteristics as cell radius and propagation loss factor  $\alpha$ . As shown in Tab. 6.5, the system efficiency in a macro cellular environment can be greatly improved by using a coded 16-QAM modulation (16 states 2/4 code built from two one-dimensional TCM schemes) instead of uncoded 4-QAM.

	$\alpha = 4$	$\alpha = 6$	$\alpha = 8$
$\frac{\eta(\text{TCM})}{\eta(\text{4-QAM})}$	5.61	3.15	2.37
$\frac{\eta(\text{TCM})}{\eta(\text{16-QAM})}$	6.3	2.7	1.77

Table 6.5: Spectrum efficiency in a cellular network

## 6.2 Equalization

**G. Kandus, Institute Jozef Stefan, Slovenia (6.2.1)**  
**L. Delaunay-Ledter, France Telecom/CNET, France (6.2.2)**  
**E. Casadevall, UPC, Spain (6.2.3)**

Equalisation techniques with or without an adaptive component can be added to combat the degrading effects of multipath propagation on wideband single carrier transmission systems.

### 6.2.1 Convergence of classical adaptive algorithms

The convergence properties of adaptive algorithms such as the gradient, conjugate gradient (CG), least mean square (LMS) and recursive least square (RLS), and the conditions for their stability have been studied. It was shown that both the gradient algorithms and the LMS algorithm converge slowly, requiring many iterations. The RLS algorithm gives a better performance than the LMS algorithm at the cost of increased computational complexity. The RLS algorithm requires  $N^3$  iterations ( $N$ =number of filter coefficients) or  $N^2$  in a modified form whereas the CG algorithm requires only  $N$  iterations. None of these first order methods could compare with the optimum Kalman filtering method. Finally, the implementation of parallel algorithms was suggested to improve the rate of convergence.

The fast adaptive, zero order conjugate algorithm, used to find the optimal weights for an adaptive filtering process by minimising the sum of squares of non-linear functions, has also been studied in detail. The method could be applied to personal mobile systems if the number of adaptive filter coefficients is less than 12.

### 6.2.2 Advanced Equaliser Techniques

The first investigations on equaliser techniques concentrated on reducing the complexity of the well known Viterbi equaliser. The sub-optimal decision-feedback sequence estimation (DFSE) algorithm allows a higher transmission rate with only a small performance degradation [37]. In most cases, prefiltering prior to the DFSE leads to an additional performance gain [38]. Numerical results with COST207 multipath channels are given in subsection 6.2.3 [39].

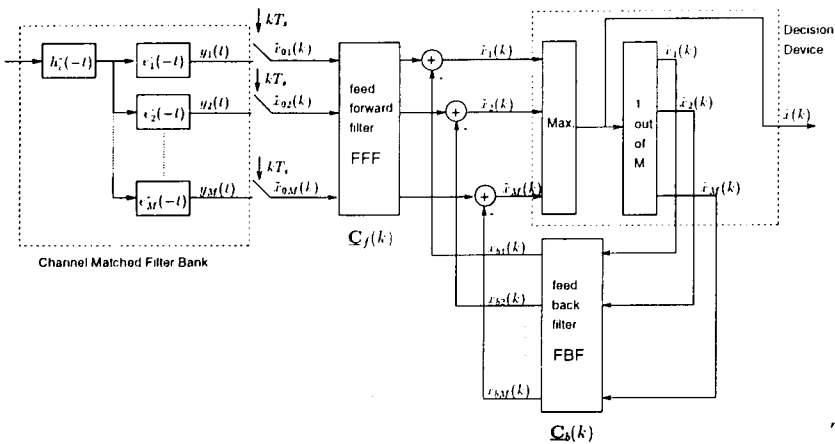


Figure 6.9: Structure of a vector decision-feedback equaliser for M-ary orthogonal signals

When transmitting over fast fading channels, the information symbols are usually arranged in blocks separated by known symbols as in the GSM system. The zero-forcing decision-feedback equaliser (ZF-DFE) has been adapted to such a scheme leading to the zero-forcing block-decision-feedback equaliser (ZF-BDFE).

In addition, the vector decision-feedback equaliser (VDFE) known from multi-user detection techniques has been applied to a single user system with M-ary orthogonal modulation, [40], see Fig. 6.9. Compared to a conventional receiver for orthogonal modulation, the selection device has been replaced by the VDFE where the input and output signals are vectors. Consequently, the feedforward and feedback filters are matrix FIR filters. As shown in Fig. 6.10, in a two-path channel significant performance gains have been obtained using the VDFE. Although the VDFE has been designed for a single user system with M-ary orthogonal modulation, it can be used as a first stage of a multi-stage multi-user detector, each user using a different codeset, e.g. Walsh-Hadamard codes like in the Qualcomm CDMA system (IS-95).

Finally, the neural network equaliser concept has been evaluated for an indoor radio channel and compared to the traditional linear transversal equaliser structure. The performance has been evaluated for the Multilayer Perceptron (MLP) with 2- and 4-PSK modulation. But the performance gain obtained by the MLP is too small to justify its additional complexity.

### 6.2.3 Joint diversity and equalisation Techniques

The diversity concept can be included in the equalisation procedure to improve the system performance. Two major equalisation techniques have been studied. Maximum

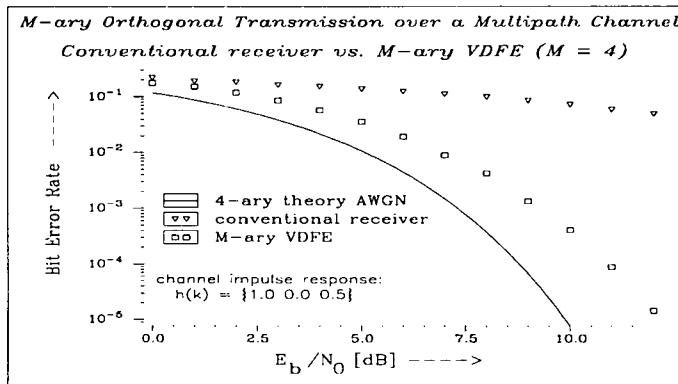


Figure 6.10: Performance of vector decision-feedback equalisation using a two path channel model

Likelihood Sequence Estimation (MLSE) and Decision Feedback Estimation (DFE).

### Maximum Likelihood Sequence Estimation

Two solutions applied to the DFSE algorithm have been suggested: combining/selection at sample level, i.e. the signals received in different diversity channels have to be combined before equalisation and combining/selection at the metric level, i.e. the metrics used in the Viterbi algorithm have to be modified (in the combining technique, the partial metric on the Viterbi algorithm trellis is calculated as the sum of metrics from each diversity channel, and in the selection technique, the channel with the higher power level is selected).

Fig. 6.11 shows the simulation results obtained for various receiver structures for a transmission over the HT50 COST207 channel. GMSK modulation and a 4-state trellis with metrics evaluated as proposed in [41], [42] were used.

Of the receivers tested, the DFSE operating with combining at the metric level provides the best performance. However, the structure with selection at the sample level seems to be more suitable because of its lower complexity for only 2dB loss.

### Decision Feedback Equaliser

The performance of the joint diversity and DFE equalisation techniques was analysed for the 4-QAM modulation and the variation of the BER with the normalised delay spread  $\tau_{rms}R_b$ , where  $R_b$  denotes the bit rate, was considered. As shown in Fig. 6.12, the BER values with diversity can be decreased by an order of magnitude if the channel introduces low distortion. When equalisation is added to cope with the ISI, the system

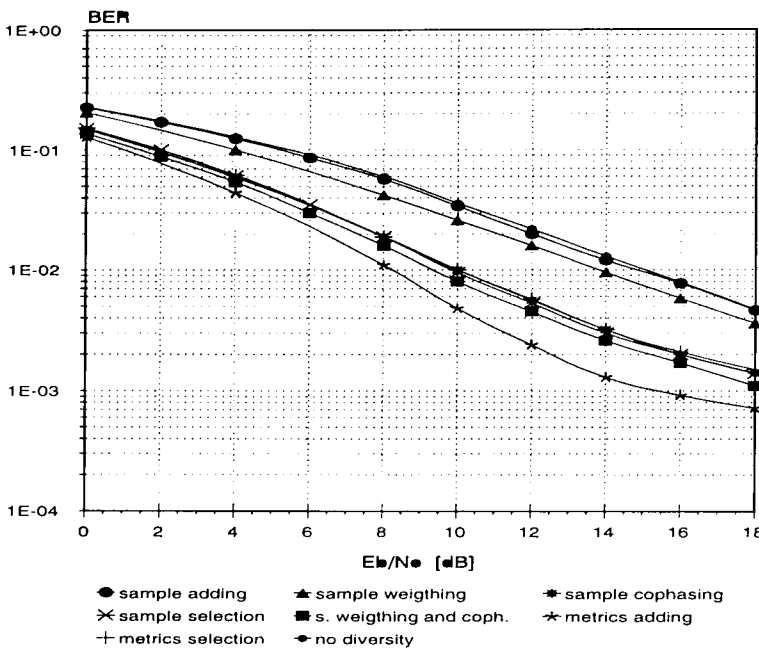


Figure 6.11: Performance of DFSE with diversity in the HT50 channel

is able to maintain a similar performance for high values of  $\tau_{rms}R_b$  when compared to the performance obtained in frequency-non-selective channel. On the other hand, with joint diversity and equalisation techniques, the system performance improves approximately by two orders of magnitude when compared to the use of equalisation alone. No advantage in terms of maximum transmit data rate has been found with 16-QAM modulation [43].

The influence of the impulse response correlation between both diversity branches was analysed, too. If the correlation between these two branches in a Rayleigh channel with normalised delay spread  $\tau_{rms}R_b = 1$  is lower than 0.5 the system performance shows no more improvements.

Finally, the use of a micro-diversity technique for the mobile and portable set could substantially improve the system performance with no prohibitive increase in complexity.

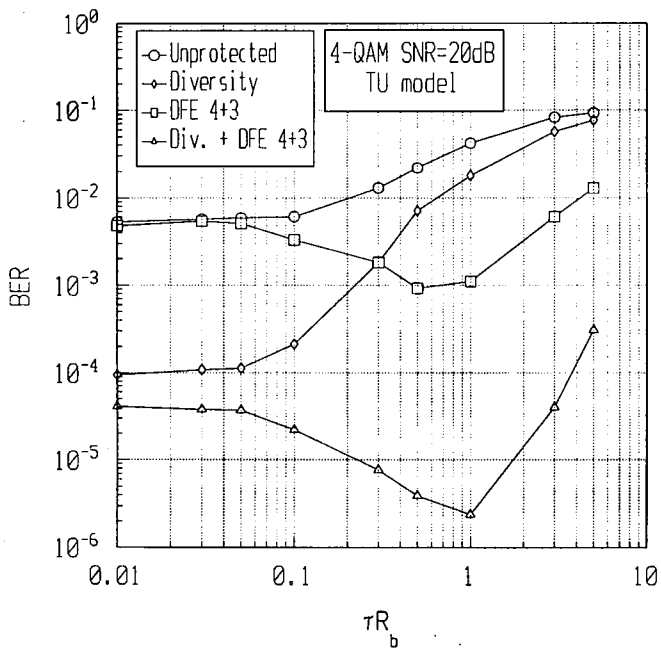


Figure 6.12: Performance of joint diversity and DFE equalisation as a function of the normalized delay spread

## 6.3 Enhanced TDMA

A. Burr, University of York, United Kingdom

### 6.3.1 TDMA enhancements

Consideration of possible enhancements to TDMA systems necessarily involves a number of concepts that are dealt with in much more detail elsewhere in this report. The object of this section is to describe how these concepts may enhance the performance of TDMA systems. Therefore to avoid excessive overlap we will cover here only the influence of these areas on TDMA performance specifically.

#### Coding and coded modulation

The development of enhanced coding and coded modulation techniques and their application to mobile and personal communication systems has been considered in section 6. However, it has been shown that the application of FEC coding and coded modulation can enhance the capacity of a cellular system significantly. In TDMA systems, it allows much reduced re-use distances, and hence increased re-use factors. Second generation digital systems such as GSM and IS-54 in general make use of coding only for special purposes, such as to protect class I speech bits. Hence there are enhancements possible in an advanced third generation TDMA system by this means.

Both FEC coding and coded modulation are used in the ATDMA adaptive transport architecture. A “toolkit” consisting of a range of both modulation and coding techniques, including a coded modulation scheme [44], is available for use where channel conditions and service requirements warrant it. More details are given in chapter 7. The improvement from the use of coded modulation has been evaluated at about 4 dB, when used in conjunction with DFE on a Hilly Terrain channel model with ideal interleaving. This may allow a reduction in cluster size.

A range of FEC codes are also available in the coding “toolkit”. These are concatenated codes based on a 1/2 rate convolutional inner code and an extended Reed-Solomon outer code, which may be punctured to increase its rate. A range of rates between 3/4 and 1/4 is available by this means. Again, more details are given in chapter 7. Special care is required for speech services to remain within the delay budget. For these services interleaving depth is restricted to 4.

It has been shown by means of simulation that in general the use of FEC can increase capacity by a factor of nearly two on an AWGN channel, and by more than four on a Rayleigh fading channel. It also allows 100% re-use, even in TDMA systems, which both increases capacity and removes the need for frequency planning. The spectral efficiencies of these schemes are compared in Table 6.6.

### Adaptive modulation and coding

Adaptivity has been identified as the most effective means of enhancing a TDMA system for the third generation [45, 46, 47]. There are two reasons for this: firstly, a third generation system must accommodate a very wide range of services and channel types, from pico- to macrocellular, and for data rates up to 2 Mbit/s. It is clear that no one air interface can be optimal for all these conditions. Secondly, it has been shown that such adaptivity can increase the average capacity of a cellular system by several times. Conventional TDMA cellular systems must be designed for the worst case, which will lead in most cases to an air interface which is substantially over-specified. Allowing adaptation to the actual channel conditions can result in much more efficient use of resources on average.

The system may adapt to a range of factors related to both the channel and service. On the most fundamental level a different air interface is likely to be required in different cell types, and for different services (whether speech or data, data rate, BER and delay requirements). In addition, it may take into account the current characteristics of the channel, such as fading conditions, delay spread, and co-channel interference. For example, the delay spread is likely to limit the maximum symbol rate used. Adaptation may apply to the modulation scheme and signalling constellation and to the FEC coding scheme, among other system features.

Adaptive modulation and coding is a major feature of the ATDMA system. Fig. 6.13. shows the architecture of the ATDMA adaptive transport interface, showing the features that can be adapted and the range of measurements on which the adaptation is based.

In addition, the effect of adapting the modulation/coding to co-channel interference in a non-fading channel has been considered. Fig. 6.14 shows how this gives rise to an improvement. In a conventional TDMA system, the coding must be chosen so that communication at a sufficient quality is provided for the proportion of cases specified by the availability requirement (as shown). This constrains the choice of code and hence the spectral efficiency. In an adaptive system, however, the code can be chosen according to the actual signal-to-interference ratio encountered. Note, too, that because the spectral efficiency of the codes increases more rapidly than linearly with signal to noise ratio, the efficiency of the adaptive scheme is greater than that of a CDMA scheme, which because of interferer diversity operates at near the average signal to interference ratio.

### PRMA

A form of statistical multiplexing is available in speech transmission systems by taking advantage of the voice activity factor, defined as the proportion of the time a link in a full duplex speech connection is actually occupied by a speech signal, and is usually taken as about 0.4. This effect is widely quoted as an advantage of CDMA over TDMA, since in a CDMA system advantage can be taken of it in a particularly simple way by means of voice activation. However, a similar advantage can be obtained

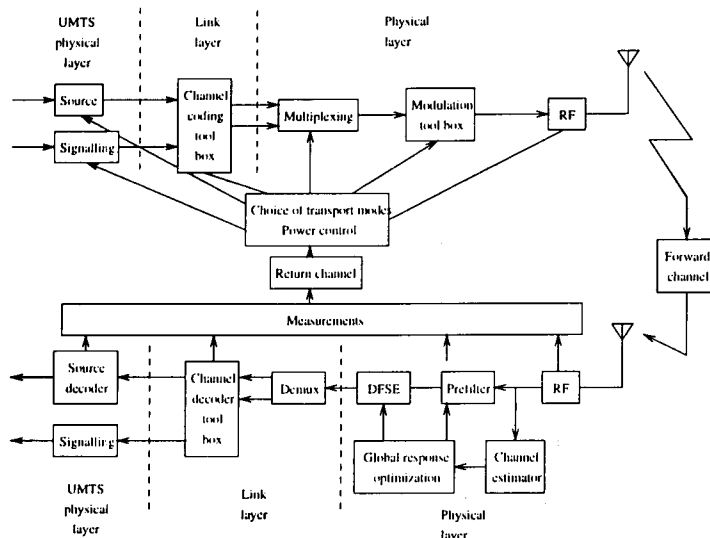


Figure 6.13: Architecture of ATDMA adaptive transport interface

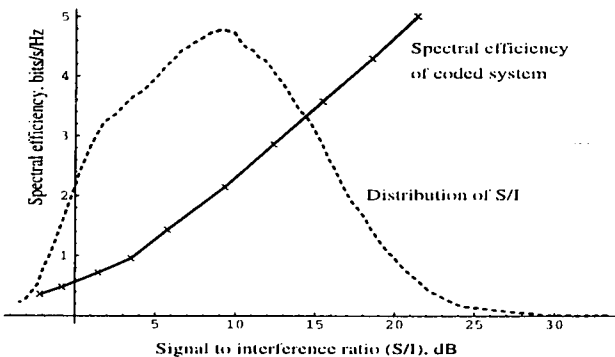


Figure 6.14: Spectral efficiency of adaptive TDMA

in TDMA, albeit with higher complexity, using reservation schemes such as Packet Reservation Multiple Access (PRMA).

The capacity of a PRMA system has been evaluated using a Markov model of the channel assignment process [48]. It is assumed that one speech packet may be buffered while waiting for a successful reservation without causing excessive delay. Packets delayed any further than this are dropped. For a TDMA system containing 20 slots, with probability of successful reservation 0.4, it was found that 37 users may be accommodated for a packet dropping probability of less than 1%. Given the voice activity factor of 0.43 assumed in this work, this corresponds to a throughput of 79%.

A more detailed simulation study [49] has evaluated PRMA in a cellular system, taking into account a number of system design options. A distinction is made between packets dropped due to delays arising from unsuccessful contention for a reservation, and due to interference from neighbouring cells. Packet dropping from both sources is to be kept below 1%. The system options considered are as follows:

- Use of additional error protection in packet headers, so that reservation may be held even if information cannot be received (described as “Option 1”);
- Use of power control;
- Speech model capable of taking into account “minigaps” in speech activity (described as “fast” as opposed to “slow”)
- Cluster size

The results show that “Option 1” does not increase capacity, since normally the packet loss is dominated by interference effects. It is better to allow a reservation to be lost and try again. Power control does help because of the reduction in interference, although it prevents the capture effect in contention. The “fast” speech model in fact degrades capacity because it increases contention, and thus also interference. As expected, capacity per cell increases with increasing cluster size, but overall spectrum efficiency is in fact highest with a cluster size of unity. For cluster size 3 and required C/I threshold of 8 dB a capacity of 32 users/cell is attainable (in an urban area), corresponding to a throughput of 67%. However, the maximum efficiency in users/cell/carrier is 12, for cluster size unity.

A more theoretical analysis of the use of PRMA within an adaptive TDMA system gives a throughput increase of 64% when voice activity is taken into account. The overall throughput is then 66%, but this takes into account also the variation in system capacity due to the use of adaptive coding. Also this assumes only 30 users/cell: larger numbers would allow greater throughput by increasing the statistical multiplexing effect.

A variant of PRMA called PRMA++ is used in the ATDMA system [50], as described in chapter 7. In all cases the base station is in control of the process. A set of random-access channels is used for mobile stations (MS) to request resources. Note that, as in the analysis described in the previous paragraph, the PRMA++ system is also used

with link adaptation, to allocate new resources whenever a change in channel conditions requires new resources. Likewise repeat requests are treated as a new demand for resources.

### Dynamic channel allocation

Dynamic channel allocation (DCA) has been described as one of the most important means by which capacity can be increased in third generation TDMA systems, allowing them to compete with CDMA. Dynamic channel assignment schemes allow channels to be allocated to cells according to actual traffic load, rather than according to a fixed re-use plan (described as Fixed Channel Assignment – FCA).

Some DCA schemes of this sort have been compared with FCA. Several schemes are described, the simplest assigning any available channel in the cell and its immediate surrounding cells. More sophisticated schemes assign the channel re-used in the nearest cell site outside the surrounding cells. The results suggest that DCA is superior to FCA, especially when the traffic is non-uniform either in time or space, but for uniform traffic the difference is not large.

A PRMA scheme has been described which also effectively functions as a DCA scheme [49]. Here a channel is assigned to a packet stream on the basis of the interference detected in that channel. Thus channel assignment depends on channel usage at the time of assignment. It has been shown that the greatest capacity is obtained in this system with a cluster size of 1 (i.e. 100% re-use), in which case the scheme is equivalent to full DCA.

Note that adaptation to co-channel interference levels, mentioned in section 6.3.1. above, also has a similar function to dynamic channel assignment, since it can similarly take into account the actual usage of channels in the vicinity of a cell. Further, consideration of coded TDMA suggests that the optimum capacity in coded TDMA systems may be obtained with 100% frequency re-use, thus avoiding frequency-planning altogether.

### 6.3.2 Capacity comparisons

A great deal of research has compared the performance (in terms, mainly, of capacity per unit bandwidth per cell) of TDMA and CDMA. A wide variety of approaches have been used in this work, from fundamental theoretical bounds to detailed consideration of specific systems, and a wide range of conclusions are reached. The comparison of specific systems will be left to chapter 7. Here we are concerned more with any inherent difference between the multiple access techniques.

An analysis of information-theoretic capacity of TDMA and CDMA systems within a single cell has been performed [51]. The results are given in Fig. 6.15. This shows that on the conventional assumption that other users are treated as noise, binary TDMA capacity ( $C_{Bin}, K = 1$ ) exceeds CDMA capacity ( $C_{ON}$ ). If, however, other users are not treated as noise, presupposing some form of interference cancellation or joint detection, then CDMA capacity ( $C_{Bin}, K = 10$ ) exceeds binary TDMA. If both TDMA and

CDMA signals have a Gaussian distribution, (and CDMA is jointly-detected), then capacity is equal ( $C_{Gauss}$ ). For CDMA this indicates that joint detection is desirable; for TDMA that the availability of non-binary modulation schemes is important.

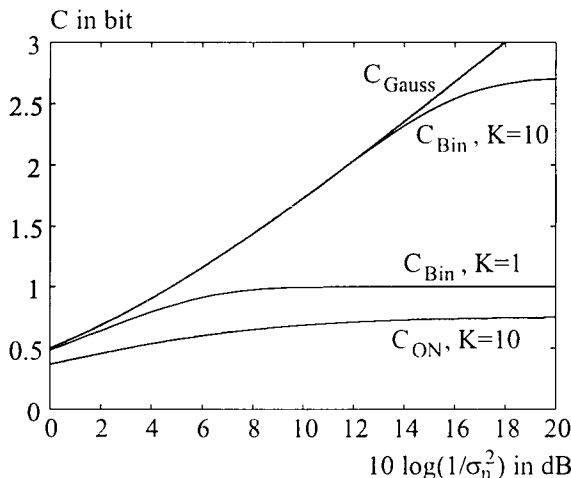


Figure 6.15: Information theoretic capacity of single-cell systems

A generic approach for multicellular systems has been developed [52, 45]. Here an attempt has been made to compare TDMA and CDMA on a equitable basis, assuming that wherever possible features of a CDMA system are also taken into account for the TDMA system. Thus interferer diversity may be included using SFH (see section 6.6.1); power control and voice activation are both included in the TDMA systems; and suitable FEC codes and coded modulation schemes are included, of equivalent power in both systems. Worst-case and average-case analyses have been obtained, but capacities have also been calculated for 95% and 99% availability. The results are given in Table 6.6 , in the form of spectral efficiency in bits/s/Hz/cell-site. In this table “orthogonal CDMA” refers to CDMA schemes in which true orthogonality is achieved, for example frequency-hopping with orthogonal patterns, or decorrelation receivers. “Ideal cancellation” assumes perfect cancellation of all intra-cell interference. The results show that conventional DS-CDMA outperforms TDMA, even with coding. However, it should be noted that PRMA is not used here, and might increase TDMA capacity. Orthogonal CDMA gives a smaller advantage than might be expected, mainly because low rate codes cannot be used in the same way as in DS-CDMA. It will, however, be largely immune to the near-far effect. CDMA with ideal interference cancellation gives the best results, but is not necessarily achievable, even with maximum-likelihood multiuser detection. Adaptive TDMA, however,

Scheme Availability	AWGN		Fast fading	
	95%	99%	95%	99%
Uncoded TDMA	0.34	0.19	0.11	0.06
Coded TDMA (cluster size 3)	0.39	0.24	0.28	0.20
Coded TDMA (cluster size 1)	0.60	0.46	0.49	0.39
DS-CDMA	0.72	0.67	0.67	0.62
Orthogonal CDMA	1.19	1.10	0.54	0.49
CDMA with ideal cancellation	1.72	1.51	1.57	1.38
A-TDMA	1.94		1.05	

Table 6.6: Spectral efficiencies (bits/s/Hz/cell) of various multiple access schemes

is very close to it.

### 6.3.3 Summary

We conclude by noting that there are two main approaches to enhancing the capacity of a TDMA system, which are to a large extent incompatible, as well as a wide range of other techniques that can be used to enhance any system.

The first approach is to invoke the interferer diversity effect, by adding an element of spectrum spreading. This is exemplified by the hybrid systems, considered in section 6.6: TDMA/SFH, JD-CDMA, and CTDMA. These systems also make use of a TDMA element and/or advanced signal processing to eliminate the intra-cell or self-interference which degrades the capacity of conventional CDMA systems. The effect is that each user encounters interference due to a large number of users in co-channel cells, leading to an averaging effect. Thus all users encounter co-channel interference close to the average, and system design can be for the average case, rather than the worst-case interference. Note that this approach also readily benefits from the use of voice activation.

The second approach, exemplified by the ATDMA system, is to adapt to the co-channel interference encountered. Thus more spectrally-efficient modulation/coding can be used when the C/I ratio is high, using fewer resources, with less spectrally-efficient modulation and more powerful coding when the interference level requires it. Thus a larger average capacity is achieved. In principle this may yield a larger capacity than the interferer diversity approach, since a graph of spectral efficiency against C/I is non-linear (Fig. 6.14), such that the average capacity for variable C/I exceeds the capacity achieved at average C/I. However in practice it may be more difficult to implement the more spectrally-efficient modulation schemes required. The approach also lends itself well to the use of PRMA, which also allows voice activity to be taken advantage of quite readily. This approach may be considered as theoretically and potentially more efficient, but also technically more difficult.

## 6.4 CDMA

### P. Hulbert, Roke Manor Research Ltd., United Kingdom

This section covers direct sequence (DS) and frequency hopped (FH) CDMA as well as some work on packet radio technology based on hybrid DS–FH CDMA.

#### 6.4.1 DS-CDMA

A considerable amount of research was conducted on this topic under COST 231, reflecting the high level of international interest. This sub-section has been further sub-divided into six parts. The first four cover design aspects which critically affect capacity or spectral efficiency. The fifth covers detailed evaluations of the resulting capacity. The sixth part covers a key element relating to efficient implementation.

#### Diversity Receiver Performance in Multipath Conditions

The subsection covers research to evaluate the performance of several Rake receiver architectures with particular modulation schemes and various channel models. One example of antenna diversity evaluation is also included. For each of the evaluations, the radio channel model was based on a tapped delay line with discrete multipath components with random phase and amplitude. The relative levels of the mean tap energies and the progression of the levels and phases with time differed according to the research team.

The work reported by Y. Tanik et al. of METU, Ankara, Turkey related to spread spectrum pulse shaped BPSK modulation. The channel model was based on the work of Hashemi [53], combining experimental data taken at 1280 MHz with 100 ns resolution and spatial resolution of 1 m.

In the Rake receiver the matched-filtered input signal was quadrature-demodulated and sampled at the chip rate. This complex valued sequence was then passed through a tapped delay line whose outputs were de-spread and weighted by the estimated multipath gains of the channel to form a maximal ratio combiner. The path estimates were obtained through a decision feedback mechanism: The despread outputs were multiplied by the detected bits and low-pass filtered. The cutoff frequency of the lowpass filter (LPF) was assumed to pass Doppler components of the multipath processes.

The BER performance was evaluated both analytically and by simulation producing detailed results. In both cases a Gaussian approximation was made for other user interference. A typical result was a BER of 0.02 for  $E_b/N_0 = 6.7$  dB, for a spreading factor of 100. The filtering method of channel estimation was found to produce negligible increase in BER.

Another significant result was that the number of taps could be reduced below that necessary to cover the complete delay spread of the channel without significant performance penalty. In fact coverage of as little as  $3 - 4 \mu\text{s}$  was found to give acceptable performance. But although the input SNR was assumed to be a constant (through

power control) the average BER was observed to vary in a range up to a decade due to fading.

The team at CSELT, Torino, Italy (Palestini, Levi, et al) examined filtered (Root Raised Cosine) spread spectrum DBPSK modulation processed by a Rake receiver which maximal ratio combined the multipath components after differential decoding. The Rake fingers were aligned on a 1 chip "grid". The channel model was based on the COST 207 typical urban channel. The BER performance was evaluated as a function of the number of Rake fingers for 1 and for 5 Mcips/s. It was shown that the optimum number of Rake fingers rose from 6 to 10 in moving to the higher chip rate as more multipath components were resolved.

The same team also extended the evaluation to cover antenna diversity. Essentially, the above model was extended to multiple antennas with various types of combining of the Rake receiver (one for each antenna) outputs. Equal gain combining gave the best performance.

The diversity gain is significantly notable; for example, by considering uncorrelated fading and no channel coding in the one user scenario, at  $\text{BER}=10^{-3}$  a 6 dB gain was obtained with second order diversity and a further 2.5 dB gain was achieved by adding a third antenna. When channel coding and interleaving were simulated, the gain became 3.5 and 5 dB with 2 and 3 antennas, respectively.

With correlated fading, a certain degradation was introduced, but in comparison to the case where no antenna diversity is applied, a gain was still present due to uncorrelated thermal noise.

The last two topics presented considered different aspects of the performance of the IS-95 uplink and downlink respectively.

Benthin et al. from the University of Hamburg-Harburg, Germany, evaluated a chip time aligned Rake receiver for modulation similar to the IS-95 uplink. The channel model was based on the COST 207 bad urban model with Rayleigh fading. A comparison between coherent maximal ratio combining and non coherent combining of the multipath components was presented. For the latter case, two strategies were adopted for limiting the number of paths selected: either restrict to 5 or threshold at 20% of the largest. Both of these strategies gave similar performance but the difference between performance for the coherent and the non coherent receiver was very significant, corresponding to a capacity ratio of about 2.5:1 at 4% BER.

Finally, Beck et al (University of Ulm, Germany) presented simulation results for modulation similar to the downlink of IS-95. The COST 207 typical urban channel along with measurements in Frankfurt and Darmstadt was used in the evaluation. The motivation of this work was to examine the effects of increasing multipath diversity which, on the one hand increases immunity to multipath fading but, on the other hand, destroys the inherent orthogonality of the Walsh function based signal. The most interesting results are shown in Fig. 6.16:

The "1 User" results indicate the performance without reference to CDMA orthogonality. Here Channel 1 is much better than Channel 2. However, with multiple users, the higher intra-user interference for Channel 1 resulted in performance significantly

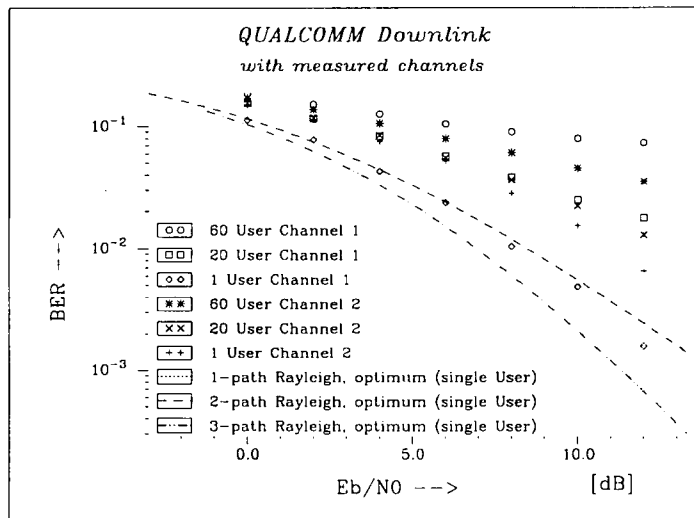


Figure 6.16: Simulation Results for IS-95 Downlink with Channel 1 (Frankfurt measurements) and Channel 2 (Darmstadt measurements)

worse than for Channel 2 under the same conditions.

### Power Control

The uplink of a CDMA mobile radio system was shown to be heavily influenced by the near far effect unless power control is applied. Further work, by R. Prasad et al (Delft University of Technology, Delft, Netherlands) explored the influence on capacity of power control imperfections, expressed in terms of numbers of users versus power control error standard deviation. Fig. 6.17 shows the results. It should be observed that the protection ratio figure of 7 dB used in the analysis was obtained from [54]. This reference obtained the protection ratio figure in the presence of power control imperfections due to fading. Thus the power control variation specified in Fig. 6.17 would be due to some additional phenomenon.

In evaluating the downlink of such a system, a sharp distinction is made between single and multiple cell systems. It was shown that power control is unnecessary (from the viewpoint of capacity) for a single cell systems since all users receive the interference over the same path as the signal and therefore at the same relative level. However, for the multiple cell case, it was shown that mobiles near the edge of the cell receive significantly more interference from other base stations. By controlling C/I at each of the mobiles a significant improvement in capacity was shown.

Two research groups examined the overall power control strategy and its effect on

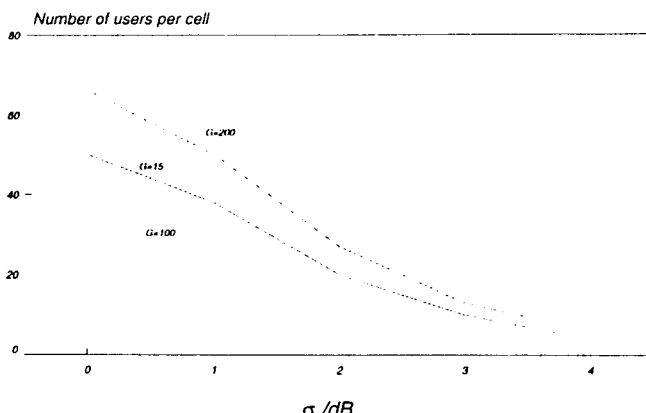


Figure 6.17: Uplink capacity as function of power control imperfection for three values of the processing gain  $G$ , outage probability=0.01 and voice activity  $\alpha = 0.375$

capacity. Nadal et al (Barcelona, Spain) compared two power control strategies: a simple approach in which the SIR values are equalised within each cell but not from cell to cell and a centralised approach in which the SIR values are equalised over the entire deployment. It was shown that the latter approach led to significantly higher capacities than the former, particularly in the case of a non uniform distribution of mobiles.

At 1% blocking with  $\alpha = 4$  (power law) the capacity increase is of the order of 20% in the uniform traffic case. In the specific case of non uniform traffic evaluated, the increase was about 25%. These results were corroborated by G. Falciasecca et al (Universita di Bologna, Italy) who used a similar approach and also showed a capacity increase of around 20%, this time at 5% blocking.

### Modulation and Bandwidth Limitation for CDMA Transmission

This subsection considers the issue of modulation and bandwidth limitation for CDMA transmissions and relates to work performed by Aldis & Barton (University of Bradford, UK). The first work reported was a simulation of Butterworth filtered QPSK received using a fully matched correlator (oversampled with filtered correlator sequence). The simulation result was the effective processing gain based on interference consisting of like-modulated users, both synchronised and unsynchronised to the target signal. It was shown, for synchronised interferers that the effective processing gain rose linearly with filter bandwidth up to the point where the (double sided) filter bandwidth was equal to the chip rate (Fig. 6.18).

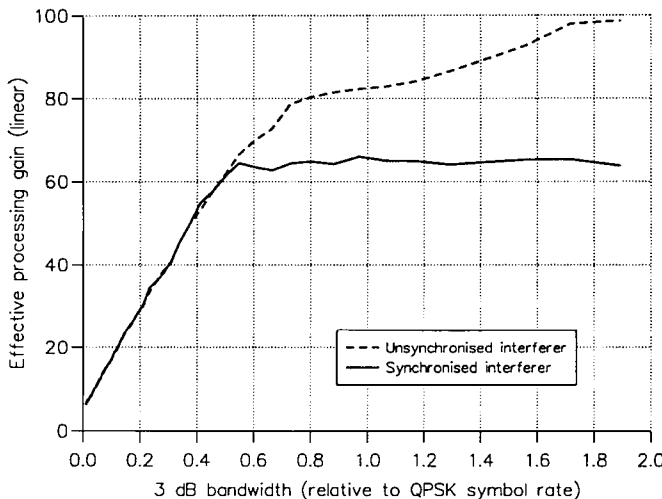


Figure 6.18: Performance of Low Pass Filtered DS-CDMA, 64 chips per bit

If the spreading factor were defined as the ratio of the signal bandwidth (as defined by the filter bandwidth) to the data symbol rate, then we would see that the processing gain is approximately equal to this spreading factor for all filter bandwidths up to the chip rate. Beyond this point, the relative processing gain falls. Thus the optimum bandwidth is equal to the chip rate. For unsynchronised signals, the processing gain continues to rise with increasing filter bandwidth but in spite of this, the relative processing gain falls since the filter bandwidth rises more rapidly than the processing gain.

The second activity examined the use of GMSK for spreading modulation and explored the processing gain as a function of the bandwidth of the pre-modulation Gaussian filter. Again, the interference was like modulated signals rather than AWGN. In this case, two receiver types were evaluated, one (complex) based on the full matched filter, the other (simple) involving multiplication by the same pseudo random bit sequence as that used in the transmit filter at the instants of maximum "eye opening". The results are shown in Fig. 6.19. The curves are plotted against the time-bandwidth product of the Gaussian filter.

When the time bandwidth product is small, the simple receiver is inferior to the complex receiver as expected because of the high ISI under these conditions. Synchronous and asynchronous interference behaves similarly. At high bandwidths unsynchronised interferers lead to significantly larger processing gains. Surprisingly, the simple receiver significantly outperforms the complex receiver under this condition.

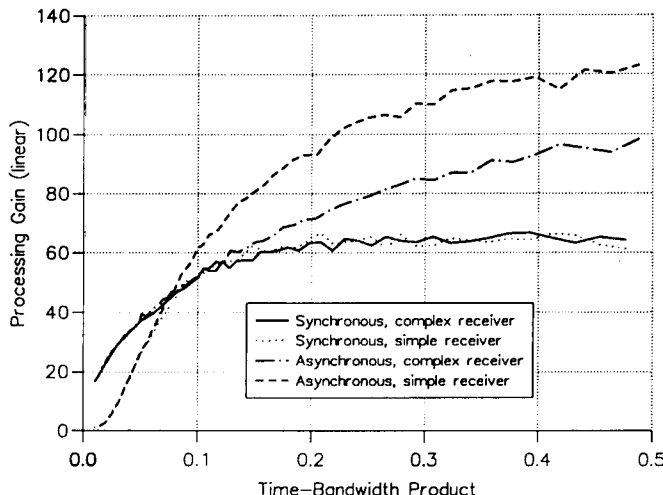


Figure 6.19: Effective Processing Gain of DS-CDMA systems using GMSK

The overall conclusion is that GMSK leads to slightly poorer performance than filtered QPSK when the actual occupied bandwidths are used to define the spreading factors although the difference will depend upon the definition of occupied bandwidth.

### Code Set Selection for Synchronous CDMA (S-CDMA)

This section covers work done by Tanik et al. (Electric. Electron. Eng. Dept, METU, Ankara, Turkey) to find optimum code sets for CDMA system in which all spreading sequences are synchronised to a fraction of a chip (intra cell and inter cell, both uplink and downlink). This is referred to as Synchronous CDMA (S-CDMA).

The system investigated had  $N$  ( $N=31$  or  $32$ ) mobile users per cell, a spreading ratio of  $N_p$  ( $N_p = N$ ) and a code reuse pattern of 4. The base stations and the mobile units transmitted TDD bursts synchronously. Since the system was designed mainly for indoor use the cellular structure employs picocells and thus the communication medium could be a flat fading Rayleigh channel. Consequently, time delays due to propagation remained in one chip interval. Power control was employed in the uplink path within a cell, so all signals from the users of the same cell were received with equal power by the base station. However, the signal coming from any mobile of the neighbouring cells experienced a path loss factor denoted by  $\alpha$ , a random variable depending on the communication medium and the relative position of the mobile with respect to the base station of concern. In the analytical study, an average  $\alpha$  was used for all mobile users of neighbouring cells. Communication was maintained via two orthogonal chan-

nels (inphase and quadrature) and convolutional FEC of rate 1/2 was used to provide a BER of  $10^{-3}$  which is sufficient for reliable communications. Spreading was performed on a single coded bit in each channel. For the uplink, the total multiple access interference affecting any user is directly proportional to the mutual cross-correlations between that user and the other users of the system. Thus spreading codes with low correlation parameters are required. Conventionally, maximal-length shift register sequences (m-sequences) have been used because of their appealing correlation properties. However, m-sequences are still above the theoretical Welch bound. The study aimed to find spreading code sequences with better performance than m-sequences. The problem of designing a low correlation codebook which contains  $4N$  bipolar sequences of length  $N$  was formulated as a constrained optimisation problem. The codewords were arranged as rows of a  $4N \times N$  codebook matrix. The optimisation criteria was to minimise the maximum of the total interference encountered by all the users of the system.

Two stochastic global optimisation techniques were applied: Genetic Algorithms and Simulated Annealing, but the results obtained are not promising. This was believed to be because of the high dimensionality and the discrete nature of the problem. Given this, more computing power would be required.

The additional problem of distributing a given code set among cells was also addressed. When the code set of concern is the set of m-sequences, it was proved that the optimum distribution is the conventional one where all phases of an m-sequence are assigned to a cell. When the code is the large class of Gold Sequences, the problem of selecting codes must also be solved together with the problem of distributing them. The exhaustive solution of this combined problem requires heavy computation. Therefore, another Genetic Algorithm was implemented to solve it and an improvement over m-sequences was obtained.

Finally, an iterative search technique, which performed small perturbations on the existing codebook such as swap/toggle two bits or set to  $\pm 1$ , was applied. The initial codebook was obtained by placing the  $32 \times 32$  perfectly orthogonal Hadamard set in all the cells. It was observed that the performance criteria became considerably worse when the slightest perturbation was made on the Hadamard codebook. Furthermore, the Hademard codebook was found to have slightly better performance than the m-sequences. Although it would not be practical to use the Hadamard set in all the cells of the system, it could be effectively used if the codes of the users were dynamically assigned according to their relative positions. This problem of dynamically assigning codes is a new topic for further study.

## System Capacity

This subsection covers overall system capacity evaluations. Hulbert et al (Roke Manor Research, Romsey, UK) performed an overall evaluation of CDMA based on the IS-95 Uplink. This evaluation covered simulation of re-use efficiency, and voice activity detection taking account of statistical fluctuations and using the 99 percentile in both

cases, leading to very conservative figures. In this evaluation, an absolute worst case re-use efficiency of 0.48 was derived. This was based on log normal shadowing at 8 dB standard deviation and a graded range law, becoming fourth law beyond the cell boundary. The voice activity factor of the IS-95 variable bit rate coder operation, derived using a Markov model, was 63% at the 99 percentile (the mean figure was 45%). The uplink  $E_b/N_0$  requirement for  $10^{-3}$  BER was derived by simulation as 5.1 and 6.5 dB for 10 and 30 mph respectively. A comparison with half rate GSM indicated higher spectral efficiency for CDMA when both systems used sectored antennas.

An Italian collaboration among the University of Bologna, Fondazione U. Bordoni and CSELT performed a detailed theoretical study of the effect of propagation characteristics on spectral efficiency. As propagation model a path loss proportional to  $r^\gamma \cdot 10^{\xi/10}$  was assumed, where  $r$  is the transmitter-to-receiver distance,  $\gamma$  is the propagation factor and  $\xi$  is a random, normally distributed variable, simulating the shadow fading and characterised by zero mean and standard deviation  $\sigma$  (in dB). Ordinarily, analytic evaluations of CDMA with shadowing are precluded because of the need, on occasions, to alter the mobile affiliation according to the shadow depth. This work analytically generated an upper bound on re-use efficiency by limiting, for every interferer, the ratio of shadow depth to the nearest cell to the shadow depth to the cell of interest whenever the cell of interest would otherwise become the preferred cell for affiliation. Fig. 6.20 illustrates the performance results for a particular case. It shows, for example that, with 8 dB shadow standard deviation, the capacity increases by about 57% when the range law changes from 3 to 5.

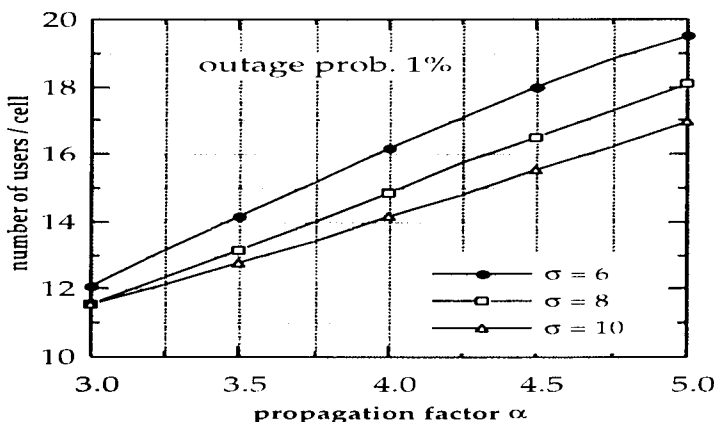


Figure 6.20: Number of Users against propagation factor,  $\alpha$  with outage probability 1% and various propagation standard deviation factors,  $\sigma$

Gaiani & Palestini (CSELT, Torino, Italy) have evaluated system capacity in a multicell system with at least two tiers of interfering cells around the reference one and a uniform distribution of static users within the overall area. The same propagation model as described above was used. The most important differences between the two links are related to the power control methodology: In the uplink a sort of ideal open loop (based on the path loss estimation on the base-to-mobile link) was applied, while in the downlink a C/I driven control was adopted.

Fig. 6.21 shows that the application of a C/I-driven power control improves the C/I ratio by about 4 dB in the downlink, at an outage probability of 10%, with respect to the case of no power control. The performance is similar, although slightly lower, to that obtained for the uplink using ideal open loop control. The performance difference in the two directions was due to the fact that, in the simulated model, the external interference was slightly greater than in the uplink in the average of the cases. However, it was verified that, at an outage probability of 1%, the uplink is more critical.

In both links the performance is better for an urban area (here simulated through a propagation factor  $\gamma=5$  and a standard deviation of the shadowing  $\sigma=10$  dB) than for a rural area ( $\gamma=3$ ,  $\sigma=6$  dB) by a factor equal to 54% in terms of capacity, (see Fig. 6.22) if  $E_b/N_0$  ratio equal to 7 dB and a processing gain  $G = 128$  are assumed (for instance 16, 17 users/site in urban area and 10, 11 users/site in rural area).

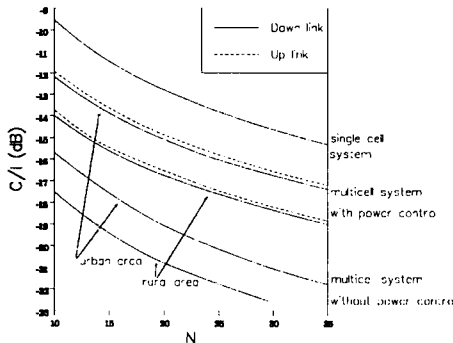


Figure 6.21: C/I ratio vs the number of user per cell computed (for both links) at an outage probability of 10%, for both a single and a multicell system with the base stations equipped with omnidirectional antennas, in a rural area and in an urban area, when power control is applied and when it is not applied.

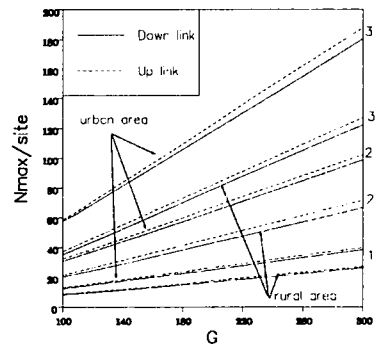


Figure 6.22: Maximum number of users per site vs the processing gain computed (for both links) for a multicell system equipped with omnidirectional antennas (curves 1), 120-degree (curves 2) and 60 degree (curves 3) sector antennas, in a rural area and in an urban area, when power control is applied

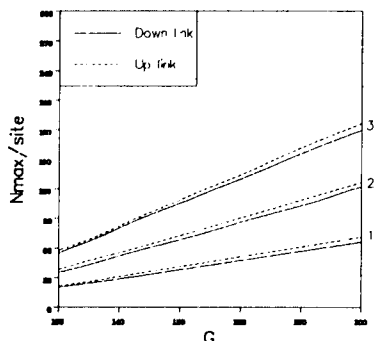


Figure 6.23: Maximum number of users per site vs the processing gain computed (for both links) for a multicell system equipped with 120-degree sector antennas in a rural area with power control and without application of VAD (curves 1), and with VAD under the hypothesis that the transmission rate is equal to 0.29 times the normal rate (curves 2) or equal to 0 (curves 3) if there is no speech.

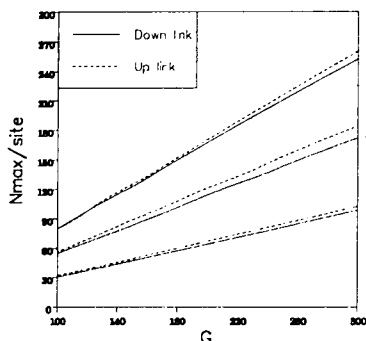


Figure 6.24: Maximum number of users per site vs the processing gain computed (for both links) for a multicell system equipped with 120-degree sector antennas in an urban area with power control and without application of VAD (curves 1), and with VAD under the hypothesis that the transmission rate is equal to 0.29 times the normal rate (curves 2) or equal to 0 (curves 3) if there is no speech.

If the base stations are equipped with directional antennas the capacity gain factor due to cell sectorization is about 2.6 in the case of 120-degree sectorization and about 4.6 in the case of 60-degree sector antennas. These values have been found for both links and for both urban and rural area.

The application of VAD (voice activity detection) was shown to cause an improvement of the capacity (in both directions, for both rural and urban areas) of about 1.8, if, in the case of no speech, the signal is assumed to be transmitted at a reduced rate equal to 0.29 times the normal rate. The results are shown in Fig. 6.23 and 6.24 for rural and urban areas respectively.

The VAD gain becomes about 2.6 if no signal is transmitted when there is no speech. Therefore it was concluded that a DS-CDMA system could increase its capacity by a factor roughly equal to 4.5 if, for instance, three-cell sectorization and VAD are applied. Under these conditions, the number of users/site was equal to 50 for a rural area and 75 for an urban area. The above described gains were found to be independent of the processing gain, at least in the range up to 300.

A simulation of hot spot conditions was performed, for which the result were found to be similar for both directions. For example, with a fixed number of users in the whole simulated area, if the number of users in the hot spot doubled, while maintain-

ing a uniform distribution of terminals in the other cells, the degradation of C/I ratio evaluated in the hot spot cell at an outage probability of 10% was about 1.5 dB in a rural area and about 2 dB in an urban area, as a consequence of the increased internal interference which has a greater effect than the reduction of the external contributions.

### Acquisition of DS Code Phase

Before any of the DS-CDMA systems described earlier in this section can operate, a local version of the spreading code clock in the receiver must be synchronised to the received code. Synchronisation is achieved by correlating all possible phases of the local code against the received signal until a particular phase leads to a correlation output conclusively indicating correct de-spreading of the signal. The different phases may be handled serially, in parallel or any combination of the two. Moreover, a number of successive correlations on the same search phase (dwells) may be performed, to advantage, as part of the search strategy.

A simple serial synchroniser would despread the signal once for each code phase in turn, comparing the resultant energy against a threshold. This threshold would need to be set high enough almost to eliminate false alarms (to avoid considerable increase of synchronisation time due to false synchronisation). This high threshold would in turn lead to a low probability of detection, requiring many search cycles to detect the signal. In a multiple dwell strategy, a low threshold is set for the initial dwell on each code phase (resulting in significant initial detection rates). Various strategies of subsequent dwells are then used to determine whether the current phase is the correct one.

Professor Simsa et al (Inst of Radio Eng & Electronics, Academy of Sciences of the Czech Republic, Praha) examined multiple dwell serial search strategies for signals with low signal-to-noise ratio (typically -6 dB) following de-spreading. Operating at these low signal-to-noise ratios permits short integration periods, thereby allowing synchronisation in the presence of significant frequency uncertainty.

Many different multiple dwell algorithms could be considered. Two of those evaluated were the "up-down counter" (UDC) and the "two step rejection" (TSR) algorithms. Both involved an initial correlation followed by a sequence of  $I$  verification correlations. In the case of the UDC, a failure at the  $i$ -th correlation leads to a repeat at the  $(i-1)$ -th stage (except for the 1st stage which leads to an immediate reject). In the case of TSR, a failure at any stage is followed by a second observation. Failure here leads to immediate rejection. Success resets the verification back to the beginning.

Some of the results generated by a detailed theoretical analysis of the AWGN case are illustrated in Fig. 6.25 and 6.26. Where:  $T_a$  is the acquisition time in bits;  $L$  is the code length;  $q$  is number of search cells ( $\leq$  twice code length for 1/2 chip steps);  $\vartheta$  is the penalty (in bits) of false detection;  $\delta_1$  and  $\delta_2$  are the threshold during initial and verification correlations respectively;  $I$  is the number of verification steps;  $M_1$  and  $M_2$  are the initial and verification correlation times in bits respectively.  $\delta_2$  is optimised individually for each value of  $I$ . It is seen that the UCD performs significantly better

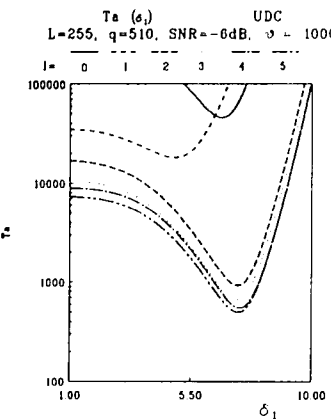


Figure 6.25:  $T_a$  versus  $\delta_1$  for UDC with  $M_1 = 1, M_2 = 5$

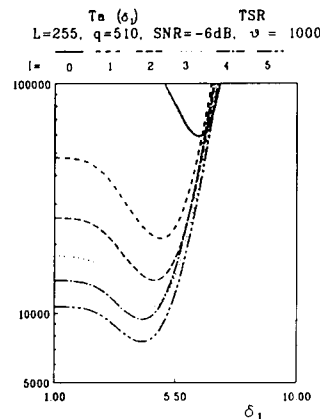


Figure 6.26:  $T_a$  versus  $\delta_1$  for TSR with  $M_1 = 1, M_2 = 5$

than the TSR.

Yuan Wu at CNET, also analysed serial and parallel search strategies with matched filter detection. Fig. 6.27 illustrates the correlation signal detection part of the system. The input signals are digital samples at complex baseband. Like most acquisition systems, the system (examined with serial or parallel search strategy) works in either search mode ( $S_{mode}$ ) or verification mode ( $V_{mode}$ ). It starts in the  $S_{mode}$  and may go into the  $V_{mode}$ . In  $S_{mode}$ , each sample of the correlation signal  $C_s$  represents one of the possible cells (PN-sequence alignments). In  $V_{mode}$ , all the samples of  $C_s$  correspond to one specific cell. The PN-sequence generating device gives the local PN-sequence and ensures that the switching of the operation modes is done as rapidly as possible.

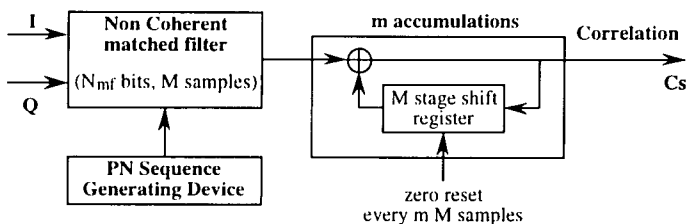


Figure 6.27: The correlation signal detection scheme

For the serial search strategy, the  $S_{\text{mode}}$  consists in the comparison of the samples of  $C_s$  with a threshold  $\beta$  until the system finds a sample greater than  $\beta$ , then at the corresponding cell, the  $V_{\text{mode}}$  tests  $A$  independent samples: if there are at least  $B$  samples greater than  $\beta$ , the acquisition is declared, if not, the system goes back into  $S_{\text{mode}}$ . The parallel search strategy works as the serial except in the  $S_{\text{mode}}$  where it searches the maximum  $C_s$  sample among all the samples of the possible cells and switches the system in  $V_{\text{mode}}$  for the corresponding cell.

The system performance, given by the mean acquisition time,  $T_a$ , would normally be calculated using the probability density function (pdf) of the correlation signal  $C_s$ . Because determination of the exact pdf expression would take considerable computer time, a simplified pdf expression was generated, based on the following model: the auto-correlation noise was artificially divided into two zero mean, independent and equal variance noise components, one in-phase with the auto-correlation signal; the other in quadrature. The sum of their variances was made equal to that of the auto-correlation noise. The numerical results showed that the approximate values of  $T_a$  obtained by use of the simplified pdf expression was very close to the exact value, for both search strategies.

The Nyquist pulse shape was found to be better than the rectangular pulse shape because it gives a small sensitivity to the offset of the local chip clock when the number of samples per chip is more than one. Two samples per chip were found to be sufficient to give acceptable degradation in  $T_a$ .

The two search strategies were compared in different situations. In general, it was concluded that it is better to use the parallel strategy when the  $N_{mf}$  is large and  $m$  small. In the case of  $N_{mf}$  small and  $m$  large, the serial strategy appeared more interesting. When the PN-sequence length is small, the parallel strategy is better; but when it is larger, the serial strategy becomes the better. The influence of a non optimum threshold was also studied and the parallel strategy appeared more robust than the serial strategy.

### Tracking of DS Code Phase

In a CDMA system a DLL (Delay Locked Loop) can be used to keep fine tracking of the received code phase. In a narrow-band system, where the receiver can not resolve the different propagation paths, deep signal fadings are likely to happen due to multipath. As the DLL parameters (closed loop gain, noise bandwidth, etc) depend on the received signal power, its performance can be severely degraded with respect to the static channel situation [55]. In this situation the DLL will frequently lose lock due to noise. In order to measure the DLL performance, one key parameter is the mean time between two consecutive losses of lock (MTLL). Assuming a wide-band transmission system, the receiver may have enough bandwidth to resolve more than one propagation path. In this case we can make use of the fact that the signals arriving from different paths have been independently faded and use a modified DLL scheme that, like a diversity system, takes advantage of multipath. Fig. 6.28 is a block diagram of the proposed DLL assuming that we can resolve a second propagation path with a delay

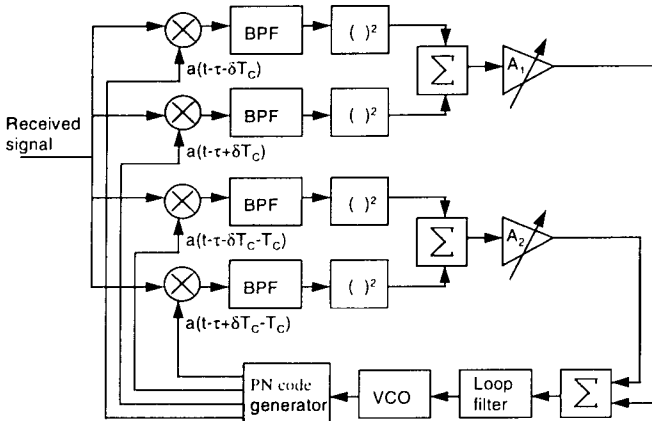


Figure 6.28: Block diagram of the proposed DLL

of  $T_C$  seconds (one chip interval) with respect to the first one. In Fig. 6.28 we can see how the error signal of the loop is obtained by adding the weighted contributions of two independent delay detectors working with local PN code sequences that are phase shifted by  $T_C$  seconds. As shown in [55], the weights  $A_1$  and  $A_2$  should be proportional to the signal to noise ratio in each path.

In order to assess the performance of the proposed scheme, computer simulations have been carried out. The results show a remarkable improvement with respect to the conventional (single delay detector) DLL. Tab. 6.7 shows the logarithm of the obtained MTLL normalized to  $B$ , the bandwidth of the data signal. The product  $MTLL \cdot B$  can be interpreted as the MTLL expressed in bit periods. In Tab. 6.7  $\sigma$  is the doppler spread of the channel and  $\gamma_2$  is the mean signal to noise ratio in the second path.

$\gamma_2$ (dB)	$\sigma/B = 0.001$ $\log(MTLL \cdot B)$	$\sigma/B = 0.01$ $\log(MTLL \cdot B)$
-15	4.55	4.48
-10	4.66	4.58
-5	5.27	5.34
0	6.3	6.45
5	7.33	7.5

Table 6.7: Mean time between two consecutive losses of lock (MTLL) under different channel conditions using the DLL shown in Fig. 6.28

The signal to noise ratio in the first path is constant and equal to 5 dB. The situation  $\gamma_2 = -15$  dB is almost equivalent to a narrow band system, since the weight of the second path is very small. It can be verified that two paths with the same signal to noise ratio (5 dB) give a MTLL = 48 minutes with 100 Hz of doppler spread and  $B = 104$  Hz.

A different approach to the above DLL based schemes has been also considered to improve the performance of a tracking scheme of DS code phase. In particular, these schemes are optimum for a AWGN channel but not for operation in frequency-selective fading channels, like those encountered in mobile communications.

A first attempt to introduce specific synchronizers for operation in those environments was presented in [56], where an Extended Kalman Filter structure was proposed to jointly estimate the PN code delay in tracking and the channel impulse response. Nevertheless, this approach fails in the presence of high-interference environments, usual in mobile communication systems. Pilar Díaz and Ramón Agustí from UPC proposed and analysed a scheme based on the EKF approach, but conveniently modified in order to improve its performance in terms of MTLL (Mean Time to Lose Lock) and the mean root square estimation (jitter) error when operating under realistic conditions (i.e., signal-to-interference input ratios from -20 dB to 0 dB). The performance of this scheme was assessed by means of computer simulations for band-limited Nyquist-filtering receivers (see [57]).

In [56] it is shown that the EKF is capable of estimating the channel delay in the tracking phase from the received samples and maintaining synchronization between the received code and the local code. However, this delay estimator only works with large signal-to-interfering ratios at the receiver input. Since this is not the usual condition in a CDMA cellular system, some signal processing before estimation is required. For the sake of improving this signal-to-interfering power ratio, the proposed delay estimator consists of two blocks: a first block known as "pre-filter", responsible for processing the received signal and improving the signal-to-interfering power ratio, and a second block, which is the EKF, now capable of estimating the channel delay in a CDMA environment.

As an example of the estimator performance, Fig. 6.29 shows the normalised jitter for rectangular and Nyquist pulses. The values obtained show that the rms jitter is lower than the 10% of the chip interval,  $T_c$ , even for  $SIR = -20$  dB.

## 6.4.2 FH-CDMA

Conventionally, CDMA systems use direct sequence spread spectrum (DSSS). However, frequency hopping (FH) is equally applicable. Slow FH has the advantage of allowing orthogonal transmission for both the downlink and the uplink, whilst preserving the benefits of multipath and interferer diversity. A combination of TDMA with slow frequency hopping is covered in Section 6.6. It is also possible to use slow frequency hopping without a TDMA element and re-use the same contiguous frequency band in all cells in the same way as for DS-CDMA.

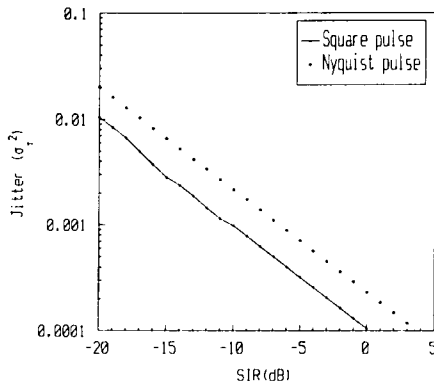


Figure 6.29: Normalised jitter for rectangular and Nyquist pulses in terms of  $SIR$

Livneh, Ritz, Silbershatz (Rafael) & Meidan (Motorola) evaluated a slow frequency hopping solution with the following parameters: 500 hops per second over 12.5 MHz; intra cell hopping orthogonal - with accurate uplink synchronisation; intercell - minimal cross correlation; interleaving over 20 hops (for multipath and interferer diversity); frequency spacing of 16 kHz; modulation  $\pi/4$ -QPSK; data rate 12 kbit/s overall with 8 kbit/s dedicated to coded voice; half rate convolutional coding – constraint length 9; voice activity detection and modest performance power control applied.

Simulation results projected 2295 active users per 3 sectored cell, corresponding to a capacity 35 times greater than AMPS. The one way interleaver delay was 40 ms.

#### 6.4.3 Hybrid DS/SFH CDMA

This subsection presents work performed by R. Prasad (Delft University of Technology, Delft, Netherlands) on throughput and delay analysis of a packet-switched CDMA network. The performance of the network was investigated with three CDMA techniques, viz. Direct Sequence (DS), Slow Frequency Hopping (SFH) and hybrid DS/SFH, where both an analytical channel model and measured channel characteristics were used. Furthermore the effects of modulation techniques, selection diversity and Forward Error Correction (FEC) codes on the performance were evaluated.

##### Network description

The network, which consisted of  $C$  users all communicating with the same basestation, had the following characteristics: i) Data transmitted in packets of  $N_p$  bits; ii) Slotted; iii) Time slot equal to packet duration; iv) Positive acknowledgement scheme. In order to be able to give some close expressions for the throughput, the following five

assumptions were made: i) all users identical from a statistical point of view, the same holding for the transceivers at the base station, ii) the averaged received power at the base station common to all users, iii) acknowledgements almost cost free from a capacity point of view, fully reliable and instantaneous, iv) channel memoryless and v) system in a stable state.

### **Analytical and measured channel models**

In case of the analytical channel the following assumptions were made concerning the channel parameters: i) Rician distributed path gains,  $\beta_{kl}$ ; ii) delays,  $\tau_{kl}$ , uniformly distributed random variables over  $[0, T]$ ; iii) phases,  $\gamma_{kl}$ , uniformly distributed over  $[0, 2\pi]$ . The channel was assumed to be slow fading, leading to random variables which did not change considerably for the duration of one packet. The Rice parameter  $R$  is defined as the ratio of the power associated with the specular signal component  $A^2/2$  and the power associated with the scattered components  $\sigma$  [53, 58]. This parameter incorporates the radio characteristics of the environment. In the measured pico cellular channel model the true measured values of the path gains were used for the calculations [59].

### **Throughput and delay analysis**

The throughput  $S$  is defined here as the expected number of successfully received packets per time slot, given by [58]:

$$S = \sum_{k=1}^C k \cdot p_k \cdot P'_k(k)$$

where  $p_k$  is the probability density function of the composite arrivals in a given time slot. For identical, independent and a finite number of users, this PDF was shown to be a binomial distribution given by:

$$p_k = \binom{C}{k} \cdot \left(\frac{G}{C}\right)^k \cdot \left(1 - \frac{G}{C}\right)^{C-k}$$

where the offered traffic  $G$  is defined as the average number of transmissions (new plus retransmitted packets) per time slot by  $C$  users.  $P$  is the packet success probability, which incorporates the effects of fading, modulation, FEC coding and diversity. The average normalised delay  $D$  of the system is defined as the average number of time slots between the generation and the successful reception of a packet. According to [4] the normalised delay is given by:

$$D = 1.5 + \left(\frac{G}{S} - 1\right) \cdot (\lfloor \delta + 1 \rfloor + 1)$$

where  $(G/S - 1)$  represents the average number of retransmissions needed for a packet to be received successfully and  $\delta$  denotes the mean of the retransmission delay. The

round trip propagation delay can be neglected in a pico cellular environment. Tab. 6.8 presents the throughput  $S$  normalised on the offered traffic  $G$  for Q-, B- and DPSK modulation with the order of selection diversity  $M$  as a parameter, where  $L$  is the number of resolvable paths and  $N_d$  and  $N_b$  are the spreading code lengths for D- and BPSK respectively and  $q$  is the number of hopping frequencies. QPSK yields relatively the largest throughput and DPSK relatively the poorest. Selection diversity enhances the performance in comparison with nondiversity ( $M = 1$ ).

Order of diversity	$S$ for QPSK	$S$ for BPSK	$S$ for DPSK
$M = 1$	51,8 %	48,1 %	32,9 %
$M = 2$	63,8 %	60,0 %	44,1 %
$M = 3$	69,0 %	65,9 %	50,0 %

Table 6.8: Comparison of the maximum throughput  $S$  normalised on the offered traffic  $G$  of the hybrid DS/SFH system with Q-, B- and D-PSK for  $M = 1, 2$  and  $3$ .  $N_q = 255$ ;  $N_b = N_d = 127$ ;  $q = 10$ ;  $L = 3$  at fixed bandwidth.

In Fig. 6.30 the throughput of hybrid DS/SFH is compared with the throughput of pure DS and SFH for B- and Q-PSK modulation using FEC coding on the analytical channel model and for a fixed bandwidth. The comparison is done according to [60] where  $N_q = 2N_b$ .

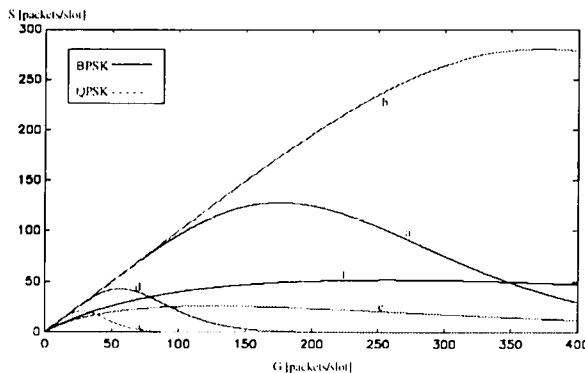


Figure 6.30: Hybrid DS/SFH, DS and SFH with (23,12) Golay coding. a) hybrid:  $L = 3$ ,  $q = 10$ ,  $N = 63$  b) hybrid:  $L = 3$ ,  $q = 10$ ,  $N = 127$  c) DS:  $L = 21$ ,  $N = 630$  d) DS:  $L = 21$ ,  $N = 1270$  e) SFH:  $q = 630$ ,  $L = 1$  f) SFH:  $q = 1270$ ,  $L = 1$

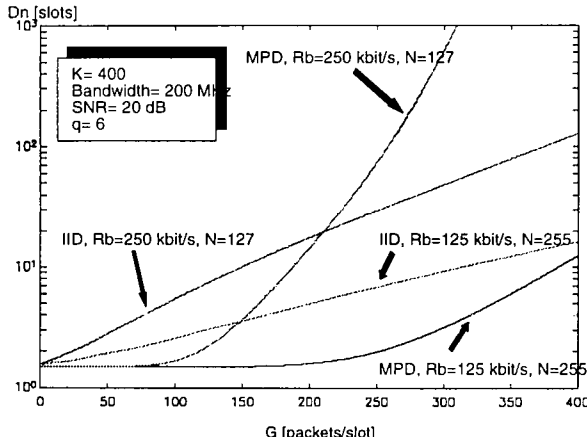


Figure 6.31: Delay performance of hybrid DS/SFH with BPSK modulation, using a measured and analytical channel model

It is seen that the hybrid DS/SFH technique has the highest throughput. Moreover, the maximum throughput values for both SFH and DS are almost equal, although the throughput for SFH doesn't vary much over the large range of  $G$ . In Fig. 6.31 the delay of hybrid DS/SFH, using the measured channel model has been compared with the performance using the analytical model. The rms delay spread is taken equal to 10 ns.

It is seen that the delay obtained using the MPD channel model is lower than in case of the analytical IID channel model. For higher bit rates the delay is higher than for lower bit rates.

## 6.5 CDMA with multi-user detection

P.W. Baier, University of Kaiserslautern, Germany (6.5.1)

A. Klein, University of Kaiserslautern, Germany (6.5.1)

D. Dahlhaus, Swiss Federal Inst. of Technology, Switzerland (6.5.2)

A. Radović, Swiss Federal Inst. of Technology, Switzerland (6.5.2)

G. Romano, CSELT, Italy (6.5.3)

T. Frey, University of Ulm, Germany (6.5.3)

### 6.5.1 Joint detection CDMA

In CDMA mobile radio systems, a number  $K$  of independent users are simultaneously active in the same frequency band, only discernible by different user-specific spreading codes. Each data symbol of the data symbol sequence  $d^{(k)}$  transmitted by user  $k$  is multiplied by the user-specific spreading code. The resulting signal of user  $k$  is transmitted over the time-variant multipath mobile radio channel. In the uplink, the mobile radio channels of all  $K$  users are in general different. At the receiver of the base station, the superposition of the contributions of all  $K$  users appears. At the receiver, transmission over the time-variant multipath mobile radio channels results in both intersymbol interference (ISI) between the data symbols of one and the same user and multiple access interference (MAI) between data symbols of different users. MAI is also termed inter-user interference (IUI). The superposition signal is also disturbed by a sequence  $n$  representing intercell interference and thermal noise. The received sequence  $e$  containing samples at the chip rate has to be processed at the receiver by a data detection algorithm to determine estimates  $\hat{d}^{(k)}$  of the data symbol sequences  $d^{(k)}$ ,  $k=1 \dots K$ , of all  $K$  users.

The conventional suboptimum single-user receiver is implemented as a bank of  $K$  matched filters or  $K$  RAKE receivers, which consider each user as if it were the only one present. This is inefficient since MAI is treated as noise. In mobile radio systems using single-user receivers, measures as accurate power control combating fast fading, voice activity monitoring, antenna sectorisation and soft handover are necessary to obtain an acceptable performance. These measures as well as synchronisation at the chip level can be avoided when applying multi-user receivers, which exploit a-priori knowledge about both ISI and MAI. In addition, however, when applying multi-user receivers, the above-mentioned measures can be beneficially employed. The optimum multi-user receiver is too complex to be implemented in third generation mobile radio systems. Therefore, suboptimum multi-user receiver techniques were proposed and investigated in COST 231. Concerning JD techniques, the four equalisers

- zero forcing block linear equaliser (ZF-BLE),
- minimum mean square error block linear equaliser (MMSE-BLE),
- zero forcing block decision feedback equaliser (ZF-BDFE),
- minimum mean square error block decision feedback equaliser (MMSE-BDFE)

were developed and extensively investigated. These four equalisers, which perform JD, are designed for

- multipath channels and
- burst transmission.

The transmission can be described mathematically by the matrix–vector–expression

$$e = A d + n \quad (6.1)$$

with the received vector  $e$ , which is a function of the combined data vector  $d$ , the system matrix  $A$ , and the interference and noise vector  $n$ . The combined data vector  $d$  contains all transmitted data symbol sequences  $d^{(k)}$ ,  $k=1\dots K$ , of all  $K$  users. The system matrix  $A$  is determined by the spreading codes of all  $K$  users and the mobile radio channel impulse responses of all  $K$  users. The mathematical description (6.1) is valid for the uplink as well as for the downlink, and for the case of one receiver antenna as well as for the case of more than one receiver antenna. The derivation of (6.1) and the exact definitions of  $e$ ,  $A$ ,  $d$  and  $n$  can be found in [61, 62] for the case of one receiver antenna and in [63] for the case of more than one receiver antenna.

(6.1) represents a system of linear equations. At the receiver, this system, which is time–variant, has to be solved in order to determine an estimate  $\hat{d}$  of  $d$ . For solving this system of linear equations, it is assumed that, besides the received vector  $e$ , the spreading codes of all  $K$  users and the mobile radio channel impulse responses of all  $K$  users and thus the system matrix  $A$  are known at the receiver. When using training sequences, the  $K$  mobile radio channel impulse responses can be estimated at the receiver by an algorithm for joint channel estimation which was developed within COST 231. A detailed description of this algorithm can be found in [64]. The system of linear equations (6.1) can be solved according to the criteria zero forcing (ZF) or minimum mean square error (MMSE), which lead to two different approaches for jointly determining an estimate  $\hat{d}$  of  $d$ . Assuming additive white Gaussian noise of variance  $\sigma^2$  and uncorrelated data, the ZF–BLE yields the estimate

$$\hat{d}_{\text{ZF}} = (A^{\dagger T} A)^{-1} A^{\dagger T} e \quad (6.2)$$

and the MMSE–BLE gives the estimate

$$\hat{d}_{\text{MMSE}} = (A^{\dagger T} A + \sigma^2 \mathbf{I})^{-1} A^{\dagger T} e. \quad (6.3)$$

The symbol  $(\cdot)^{\dagger T}$  denotes complex conjugation and transposition and  $\mathbf{I}$  is the identity matrix. Equations (6.2) and (6.3) have the same structure. In the case of the MMSE–BLE, the variance  $\sigma^2$  of the noise is taken into account, which requires that  $\sigma^2$  is estimated at the receiver. The ZF–BLE for JD leading to (6.2) is a generalization of the single–user ZF equaliser presented in section 6.2. Also in the case of more than one receiver antenna and coherent receiver antenna diversity (CRAD), (6.2) and (6.3) remain valid, as is explained in [63]. Instead of the inversion of the matrices

$(A^T A)$  and  $(A^T A + \sigma^2 I)$  in (6.2) and (6.3), respectively, Cholesky decomposition of these matrices can be applied, which considerably reduces computational complexity. Furthermore, when applying Cholesky decomposition, decision feedback (DF) can be introduced to improve performance without increasing the computational complexity. Introducing DF in (6.2) and (6.3) leads to the ZF-BDFE or the MMSE-BDFE, respectively. To avoid the impairing effect of error propagation when using DF, a method termed channel sorting has been proposed. Details on the applications of Cholesky decomposition, DF including channel sorting and the extension of the equalisers to the case of non-white noise are given in [65] and [63] for the cases of one or more receiver antennas, respectively.

Concerning the computational complexity of the ZF-BLE, MMSE-BLE, ZF-BDFE and MMSE-BDFE for JD, the most important results are:

- All four equalisers require essentially the same computational complexity.
- The computational complexity required is independent of the size of the data symbol alphabet.

The computational complexity required for JD is larger than that required by conventional suboptimum single-user detectors. However, considering the potential of modern microelectronics, the computational complexity required for JD is feasible already today. Especially in systems as proposed in section 7.4, which include a TDMA component leading to a reduction of the number  $K$  of simultaneously active users, the computational complexity required for JD seems to be affordable.

The ZF-BLE, MMSE-BLE, ZF-BDFE and MMSE-BDFE have been applied to the JD-CDMA system proposal described in section 7.4. The performance in terms of simulated bit error rate (BER)  $P_b$  versus signal-to-noise ratio  $E_b/N_0$  per bit of the ZF-BLE, MMSE-BLE, ZF-BDFE and MMSE-BDFE for one and for two antenna receivers in the uplink is given in Fig. 6.32. Convolutional forward error correction coding (FEC) with rate 1/2 and constraint length 5 is considered. The system parameters used in the simulations are given in section 7.4. The Rayleigh fading multipath mobile radio channels have been modelled according to the COST 207 model bad urban (BU) area channel with a mobile speed of 30 km/h. 8 mobile stations are assumed to be active simultaneously. To obtain the results in Fig. 6.32, channels have been estimated according to [64], so that the effect of imperfect channel estimation is included. More details about the simulations and simulation results can be found for the cases without FEC in [66] and with FEC in [67]. Details about the achievable cellular spectrum efficiency can be found in [68]. The most important results are:

- The two equalisers ZF-BDFE and MMSE-BDFE with DF show a better performance than the two equalisers ZF-BLE and MMSE-BLE without DF.
- The two MMSE equalisers MMSE-BLE and MMSE-BDFE perform slightly better than the two ZF equalisers ZF-BLE and ZF-BDFE, respectively.
- Coherent receiver antenna diversity with two receiver antennas allows  $E_b/N_0$  to be reduced by about 6 dB to 11 dB depending on the type of terrain as compared

with the case of one receiver antenna. 3 dB of this improvement is due to an energy gain, the additional improvement is due to diversity.

- When applying coherent receiver antenna diversity with two receiver antennas, the performance difference of the four equalisers is smaller than in the case of one receiver antenna.
- When applying FEC, the performance difference of the four equalisers is smaller than in the case where no FEC is applied.
- The achievable cellular spectrum efficiency is of the order of 0.2 bit/(s·Hz) per base station in the uplink [68] and 0.39 bit/(s·Hz) per base station in the down-link [69].

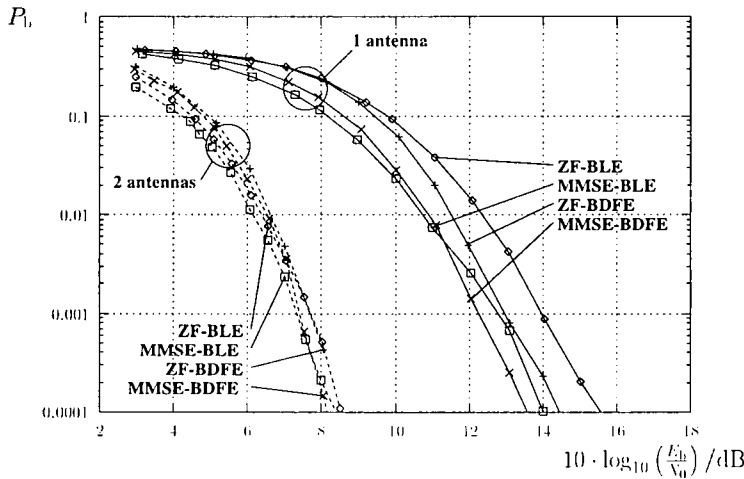


Figure 6.32: BER performance of the ZF-BLE, MMSE-BLE, ZF-BDFE and MMSE-BDFE

### 6.5.2 Joint Parameter Estimation and Data Detection

The uplink of a CDMA system is considered where  $K$  users simultaneously transmit data packets over  $K$  multipath time-invariant channels using binary phase-shift keying direct sequence spread spectrum (BPSK/DSSS) modulation. The baseband complex impulse response of the  $k$ -th user channel is assumed to consist of  $L$  paths, each of which is characterised by a complex coefficient  $g_{k\ell}$  and a delay  $\tau_{k\ell}$ . These channel parameters together with the transmitted energies of all users are arranged in a parameter vector  $\Theta$  which is assumed to be unknown at the receiver. The transmitted symbols of all users in a certain data packet are represented by the matrix  $\mathcal{B}$ . With the above definitions, the received signal  $y(t)$  can be written as  $y(t) = \mathcal{S}(t; \mathcal{B}, \Theta) + n(t)$ .

where  $S(t; \mathcal{B}, \Theta)$  is the superposition of  $K \cdot L$  signals contributed by the incident waves and corrupted by zero-mean additive white complex Gaussian channel noise  $n(t)$  with  $E[n(t + t_0) n^*(t)] = N_0 \delta(t_0)$ . An algorithm has been proposed which *jointly estimates the channel parameters and the data bits of all users* [70]. Maximum likelihood (ML) solutions of the problem are given by values  $(\mathcal{B}, \Theta)$  which maximise the log-likelihood function  $\Lambda(\mathcal{B}, \Theta; y(t)) = 2 \int_0^T \operatorname{Re} \{y(t) S^*(t; \mathcal{B}, \Theta)\} dt - \int_0^T |S(t; \mathcal{B}, \Theta)|^2 dt$ . Since the maximisation of  $\Lambda(\mathcal{B}, \Theta; y(t))$  is computationally too intensive, we rely on iterative algorithms to separate the task into several separate optimisation problems. The expectation maximisation (EM) algorithm is used to estimate  $\Theta$  while the data symbols are detected by means of a multistage detection (MS) algorithm. Both algorithms are combined within a Gauss-Seidel scheme. Monte-Carlo simulations have been carried out, where the symbol energies  $\mathcal{E}_k$  of all users at the receiver remain constant during different simulation runs, although the delays and amplitudes vary in a random manner. Fig. 6.33 depicts the uncoded bit error probability  $P_{b,1}$  of the first user in a system with  $K = 6$  and  $L = 3$ . In comparison to the RAKE receiver with perfect estimates of the channel parameters, the proposed iterative scheme achieves a substantial improvement in performance. The resulting bit error probability is very close to that of a single-user detector, as denoted by the dotted line (BPSK). Fig. 6.34 shows the bit error probability  $P_{b,1}$  for a constant  $\gamma_1 = 8$  dB as a function of symbol energies  $\mathcal{E}_k$ ,  $k = 2 \dots 6$ , of the interfering users relative to  $\mathcal{E}_1$ . Additional simulation results [70] of a two-user system with a data rate of 128 kbit/s using macrocellular channel measurements at carrier frequency 1980 MHz show the capability of the proposed scheme to eliminate the near-far effect even in realistic environments.

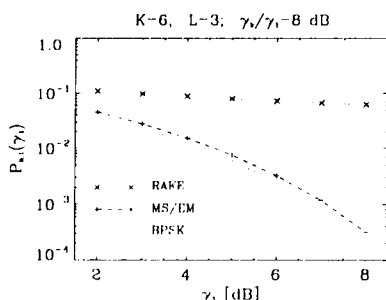


Figure 6.33: Bit error probability  $P_{b,1}(\gamma_1)$  of user 1 as a function of the signal-to-noise ratio  $\gamma_1 = \mathcal{E}_1/N_0$  in the presence of 5 interfering users with  $\gamma_k = \mathcal{E}_k/N_0$ ,  $k = 2 \dots 6$

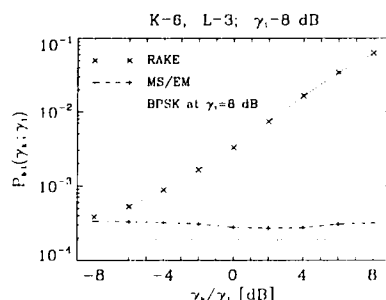


Figure 6.34: Bit error probability  $P_{b,1}(\gamma_1)$  of user 1 for constant  $\gamma_1 = 8$  dB and various interference levels  $\gamma_k = \mathcal{E}_k/N_0$ ,  $k = 2 \dots 6$

### 6.5.3 CDMA with Interference Cancellation

Performance in terms of BER for the uplink of a DS-CDMA communications system using the Interference Cancellation (IC) technique [71, 72] and non coherent reception has been presented in Ricean fading environments. These investigations have been carried out by L. Levi and G. Romano from CSELT, Torino, Italy. The considered propagation channel is affected by Ricean fading, characterised by a ratio  $\rho$  between the line of sight and the multipath components; the fading phenomena are assumed independent for the different users. For sake of simplicity, synchronous reception was assumed in the simulations, although the technique can be used also in the asynchronous case [71]. The IC technique considered is based on orthogonal modulation (i.e. Walsh–Hadamard encoding) and on the signal demodulation from the strongest to the weakest one according to a power list. User assigned pseudo noise (PN) sequences are used to distinguish the different signals but do not introduce any spreading. In this way the first signal to be demodulated is the one that presents the highest signal to interference ratio ( $C/I$ ) and thus it is less impaired by interference. The signal is then cancelled and so the overall  $C/I$  ratio increases and also the weaker signals can reach the  $C/I$  needed for the required performance. Considering that the base station has to demodulate all the received signals and that it knows all the user-assigned PN codes, it starts the demodulation of the strongest signal on the basis of the received signal power list. The base station performs the descrambling of the received signal with the PN code associated with the strongest user and then the Hadamard decoding by applying a Walsh–Hadamard Transform (WHT) to both the inphase and quadrature signal components. The chosen code word, which is the one with largest modulo value after WHT, is cancelled and the resulting signal is subject to inverse WHT and scrambled with the same PN sequence. The procedure is then iterated with the second signal in the power list. The power list can be obtained in an adaptive way at time  $T_i$  by analysing the demodulated signals at time  $T_{i-1}$ , where  $T$  is the time duration of each Hadamard code word. The signal power is related to its maximal co-ordinates after WHT, thus the power list can be obtained by ordering the maximal co-ordinates of all the demodulated signals. The initial conditions can be achieved either by the power control algorithm or by random initialisation.

A scenario in which 10 active users are simulated has been considered. Each user's signal is encoded with a Hadamard block code  $H(128, 7)$ , scrambled with the user-assigned PN code and then BPSK modulated; the overall processing gain is  $P_g = 128/7$  (12.62dB). The transmitted signals, affected by independent Ricean fading, are summed up at the receiver side to obtain the overall received signal. From the simulated results, it was found that the IC technique allows a greater capacity than the of conventional CDMA, even with a relatively low processing gain. Increasing the number of cancelled interferers improves performance but, on the other hand, the receiver is more complex, and a trade off between complexity and performance has to be found. Performance depends on the Ricean factor  $\rho$ , which characterises the propagation channel, and, especially for low factors, the curves with all the inter-

ferers cancelled approach the one user case. The best performance is obtained with  $\rho = 10$  dB, while with  $\rho = 100$  dB the algorithm cannot work at its best for the first signals to be demodulated and cancelled because the received signals present almost the same power and thus it is not possible to find the strongest one. For  $\rho = -100$ , 0 and 100 dB, simulations with the computed power list give performances which approach that obtained with the ideal list, while for  $\rho = 10$  dB (where errors in the demodulation order are not negligible with respect to the effects of fading) there is a loss of about 1.5 dB in the  $E_b/N_0$  ratio at BER =  $10^{-2}$ . Simulation results also show that the adopted interference cancellation technique is less sensitive than conventional CDMA to non perfect power control and chip synchronisation.

A special kind of IC technique, suitable for the synchronous downlink of CDMA systems, has been developed by M. Bossert and T. Frey, University of Ulm, Ulm, Germany. A less complex receiver implementation is achieved by exploiting the restriction of synchronism with suitable spreading codes.

The conventional approaches in JD and IC deal with the general case of a mobile radio link. The asynchronous uplink has different channel impulse responses for each user. The downlink is treated as a special case having some simplifications (because of synchronism and a common impulse response) but is nevertheless a computationally expensive task, especially considering that it has to be performed in the mobile with restrictions on size and power consumptions. For the JD/IC algorithm there are no principal restrictions to the spreading sequences used and quasiorthogonal Gold codes are widely used because of their good correlation properties at a sufficient large code set size.

The inherent synchronism of the downlink allows the use of orthogonal spreading codes. An example is the Qualcomm-System which uses spreading sequences based on scrambled Hadamard codes. These sequences deliver an ideal user separation in AWGN channels because the orthogonality avoids inter-user interference (IUI). With increasing time dispersion of the channel the orthogonality diminishes and turns into a quasiorthogonality, which results in the occurrence of IUI.

The IUI is proportional to the interference parameter

$$I_h := \sum_{k \neq 0} |\phi_{hh}(k)|^2 \quad (6.4)$$

of the time discrete equivalent channel  $h(k)$ .

The main idea of this IC technique is to restore the lost orthogonality due to the multi-path propagation by applying an equaliser working on the input signal (on chip level) before despreading. Due to the fact, that the equaliser has no knowledge of the de-spreading data, only a linear type equaliser is applicable. Although the MMSE criterion is used for coefficient calculation, the resulting noise enhancement limits the performance of IC. Applying a time-invariant (no fading) channel with 3 paths of equal power on a fully loaded system (number of users = spreading length) the loss is about 4dB at a bit error rate of  $10^{-3}$  compared to the single user bound (ideal BPSK). In

terms of the interference parameter  $I_h$ , which determines the link performance, the 3-path channel used is worse ( $I_h = 0.667$ ) than the COST207 channel models, where  $I_h = 0.28$  is derived from the delay power profile of the typical urban channel.

In order to overcome the penalty of noise enhancement this method was combined with interference estimation and subtracting, cf. Fig. 6.35. The input signal is now

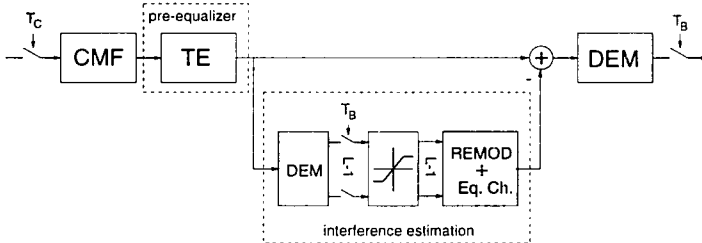


Figure 6.35: Receiver structure

only weakly equalised in order to keep the noise enhancement small. Then the signals of the other users were predemodulated, decided, remodulated and convolved with the equivalent channel, which delivers an estimate for the IUI. In order to keep the effect of error propagation small, the reliability of each decision is considered by a nonlinear characteristic. The estimation of the IUI is subtracted from the input signal. For further details see [73]. This scheme shows that even in the fully loaded case only a slight degradation of approximately 1 dB compared to the optimum single user bound (cf. Fig. 6.36) and thus promises a good performance on mobile radio channels.

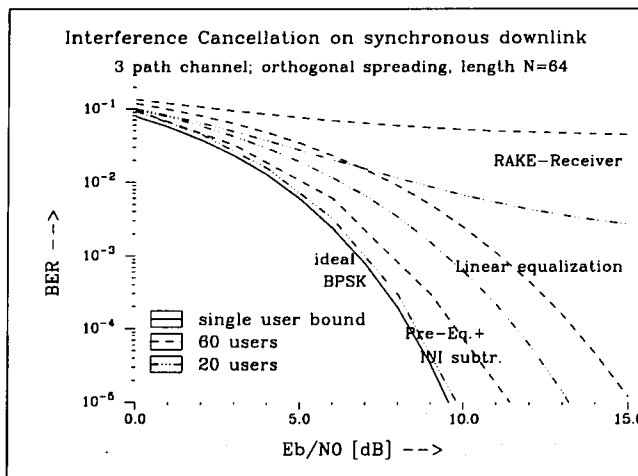


Figure 6.36: Performance comparison of the different receiver types

## 6.6 Hybrid TDMA/CDMA

### A. Burr, University of York, United Kingdom

A number of schemes have been proposed which are hybrids of TDMA and CDMA. The objective of these is to avoid the shortcomings of both TDMA and CDMA, and thus to obtain enhanced capacity. Some of the schemes are also considered in more detail elsewhere in this chapter: the objective here is to show how the inclusion of elements of one scheme may enhance the capacity (or other performance objective) of the other.

#### 6.6.1 TDMA/SFH

The use of slow frequency-hopping has been considered together with coded modulation. The effect of SFH in this context is to enhance the effect of the diversity of the code without requiring long delays due to interleaving. To avoid self-interference, zero-coincidence hopping patterns synchronised among all users would have to be employed in a cellular system. The effect of correlation between the frequency channels is considered, and it is shown that for a separation between hopping frequencies greater than  $0.15/\text{(delay spread)}$ , the degradation of the system is negligible. It is also shown that performance within 1 dB of ideal is achieved with no more than 5 hopping frequencies.

#### 6.6.2 JD-CDMA

A TDMA element (as well as FDMA) is included in the Joint Detection (JD-CDMA) system developed at the University of Kaiserslautern [74], in a system which is based on DS-CDMA. This system is reviewed in more detail in section 6.5 and in chapter 7. Here we will consider the extent to which the inclusion of FDMA and CDMA elements provide advantages over a pure TDMA or CDMA system.

Firstly, the availability of all three forms of multiple access provides flexibility, since the system is able to switch between them. This is important in a third generation system, since it allows operation in a range of operating environments, for a variety of service types, and supports a range of terminal types. It would also provide interoperability between mobiles and base stations using different types of air interface.

Secondly, it allows the system to take advantage of a wide range of different forms of diversity. Diversity has been identified as essential in overcoming the degrading effects of the mobile radio channel, by reducing the random variation of the signal to interference ratio due to fading, etc. Fig. 6.37 summarises the types of diversity available in any mobile radio system. All these forms are available in the JD-CDMA system because of the availability of CDMA and TDMA. For example, frequency diversity is provided by the CDMA spreading, time diversity by coding and interleaving on a TDMA basis, and interferer diversity through CDMA (which implies that a number of users share the same channel). Various forms of antenna diversity have also been investigated, and offer further improvements.

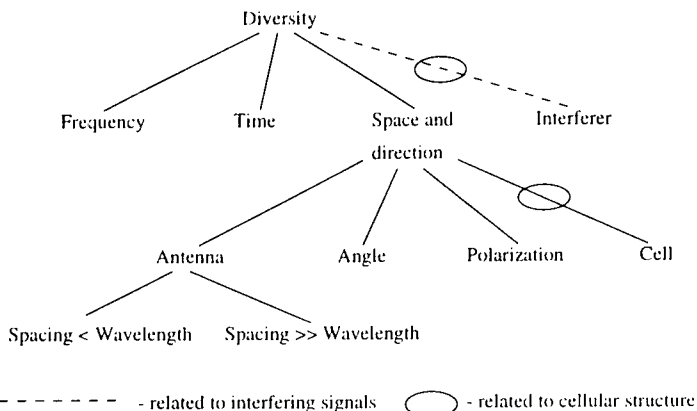


Figure 6.37: Diversity approaches in cellular systems

### 6.6.3 CTDMA

Coded Time-Division Multiple Access (CTDMA) is also proposed [75]. This is based on TDMA, but the signal is spread in the frequency domain using a pseudo-random code, as in CDMA. The principle is described in chapter 7. Each user's signal is converted to a symbol-by-symbol TDMA waveform. This is convolved with a pseudo-random sequence common to all users within a single cell. At the receiver the signal is passed through the aperiodic inverse filter of the spreading sequence, which in effect reverses the convolution and regenerates the TDMA signal. Hence the users may be perfectly separated. Since the aperiodic inverse filter is not a matched filter the performance is degraded relative to matched filter reception. However, it has been shown that spreading sequences exist for which this degradation is very small,  $\approx 0.4$  dB. These sequences are binary with chip values  $\pm 1$ , so that the resulting signal is constant envelope.

The above description neglects the effect of multipath, which will cause interference between users occupying adjacent slots. This can be overcome in two ways. For small delay-spreads a guard time may be introduced between users. For delay-spreads significantly greater than the chip period (greater than  $5 \mu s$ ), this would excessively degrade the spectral efficiency. Hence an equaliser must be used in the receiver. It is proposed to use the *Maximum-a-posteriori* (MAP) equaliser, which has optimum performance, and whose complexity is kept within bounds because only a few users will overlap at any one time.

In a cellular system CTDMA would use a different spreading sequence in each of one cluster of cells. In this case inter-cellular interference would appear as uncorrelated noise, as it does in a CDMA system, and therefore 100% frequency re-use is possible

due to the interferer diversity effect. It has been shown that multiple sequences with good interference rejection properties exist.

The advantages of CTDMA over a conventional TDMA system can be summarised as follows:

- The peak-to-mean power ratio of the signal is reduced to unity, giving electromagnetic compatibility (EMC) advantages
- In a cellular system 100% frequency reuse is possible, as in CDMA systems
- The inherent frequency diversity of DS-CDMA is also available to CTDMA
- Inter-cellular interference reduction techniques such as voice activity detection apply equally to CTDMA as to CDMA
- Since the receiver after the inverse filter is TDMA, the system has a high degree of compatibility with TDMA.

The main disadvantage is the additional complexity of a linear filter of length  $N$  in the transmitter, and another of length  $3N$  in the receiver.

## 6.7 Multicarrier techniques

**L. Vandendorpe, Universite Catholique de Louvain, Belgium**

Multicarrier techniques have been recently considered for transmission over fading channels. These techniques use more than one carrier to transmit the information associated with a particular user. OFDM (Orthogonal frequency division multiplexing) which is a particular case of multicarrier modulation is currently used in the DAB (Digital audio broadcasting) system and is a serious candidate for DVB (Digital video broadcasting) over terrestrial networks. Also OFDM has been seriously investigated for high bit rate transmission over telephone lines. OFDM can be seen as a parallel transmission: the input symbol stream is divided into parallel streams which are used to modulate carriers which are orthogonal on the symbol duration. Hence the symbol duration is increased and the signal should be more resistant to large delay spreads. To state it in the frequency domain the number of carriers should be such that the bandwidth of each of these carriers becomes sufficiently narrow to consider the channel as frequency non-selective. Using this modulation technique the time discrete transmission signal can be calculated in a cost effective way by an IFFT (inverse fast Fourier transform), and an FFT can be used in the receiver. OFDM transmitter and receiver are depicted in Fig. 6.38.

### 6.7.1 OFDM with guard time

A very elegant way to remove the problem of ISI is to use the technique of guard interval of length  $T_g$ . If the channel impulse response is about  $T_g$  the OFDM symbols of length  $T_u$  can be periodically extended to build a symbol of length  $T_g + T_u$ . After transmission the first  $T_g$  seconds of each OFDM symbol will be corrupted because of the channel impulse response. If the detector uses the last  $T_u$  seconds of each symbol this part is not corrupted by the previous OFDM symbol and the subcarriers keep their orthogonality. The signal at the  $q$ th output of the FFT device and associated with

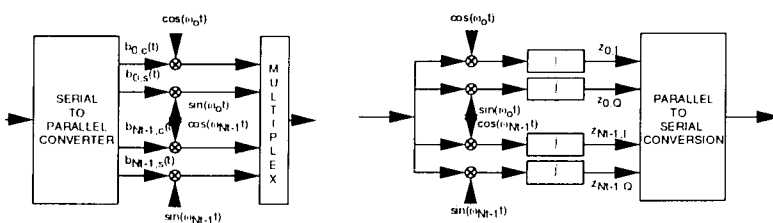


Figure 6.38: OFDM transmitter and receiver

symbol  $n$  ( $I_q^n$ ) is given by

$$y_{g,q}^n = \sqrt{\frac{2P}{N_t}} I_q^n C(2\pi q/T) T + v_{g,q}^n \quad (6.5)$$

where  $C(2\pi q/T)$  is the Fourier transformation of the channel impulse response  $c(t)$  for frequency  $2\pi q/T$  and  $v_{g,q}^n$  is the effect of the additive Gaussian noise. Orthogonality between the tones is maintained and ISI is avoided. However the symbol affecting the  $i$ -th carrier in the OFDM multiplex is affected by the value of the channel transmittance at that frequency. Assuming that complex gain can be estimated the symbol can be corrected by the receiver. The price to be paid to use guard times is a loss of  $T_g/T_k + T_u$  in useful power or an equivalent increase of the bandwidth. How absolute and differential (de)modulations could be performed with OFDM has also been investigated [76]. Differential detection is very attractive, because when the channel can be considered as constant between two successive symbols, its affect is compensated for by the differential detector. Fig. 6.39 shows the sensitivity of OFDM to time variations of the channel. The channel was the Bad Urban defined in COST 207.

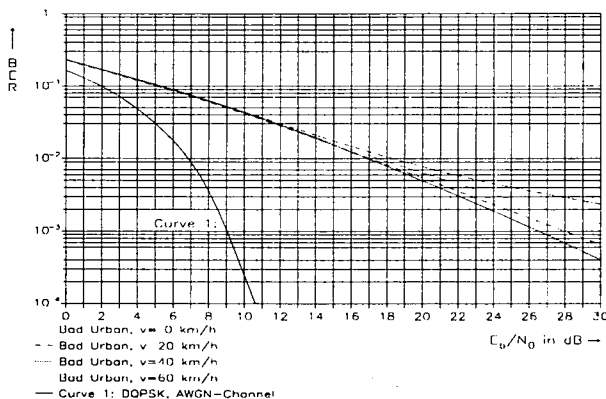


Figure 6.39: Performance of OFDM in the Bad Urban channel for various speeds

OFDM might be used also in an FH (frequency hopping) scenario. In order to avoid a user being allocated to a fading frequency, its frequency is modified according to a specific pattern. The frequencies in the hopping set may be selected such that they are orthogonal and hence this scheme is implemented very easily by means of (I)FFTs. OFDM was also investigated for a radio link at 34 Mbits/s in a bandwidth of 8 MHz. Absolute and differential modulation schemes were compared for AWGN and multipath propagation [77]. A drawback of OFDM signals is the non constant envelope which has a large dynamic. Therefore a power loss has to be accepted in the presence

of a nonlinear device such as a high power amplifier. These aspects were analytically investigated as well.

### 6.7.2 OFDM without guard time

If OFDM without guard time is used, the system is affected by ISI. Moreover the orthogonality between tones is lost and hence cross-carrier interference (CCI) appears. The efficiency of OFDM transmission over a specular multipath fading channel has been analytically computed in [78]. For a given delay range and assuming Rician distributions of the path gains, it is shown that when the number of tones goes up the system performance improves. However the limiting effect is this scenario would be the channel variations. It is expected that an optimum number of tones could be found. Also it was assumed that the filters in the receiver were matched to the symbol shape only.

### 6.7.3 OFDM-CDMA

In order to provide the system with a multiple access capability CDMA can be mixed with OFDM. There are two ways to combine OFDM with CDMA.

#### Method 1

A first possible combination was investigated in [79] for a multiple access and multipath scenario. The transmitted signal is first OFDM modulated and then spreading is put on top of it. Basically this scheme resembles a CDMA system; the main difference is that the spread signal is a multitone signal. This combination benefits from the properties of CDMA as well as from its drawbacks. In [78], the total interference was modelled as Gaussian distributed. To keep the bandwidth constant the chip duration has to be constant and hence longer pseudo-noise codes can be used with larger numbers of tones. Consequently more users can be accommodated in the same bandwidth. Diversity reception was investigated and the computational results show the advantage associated with larger numbers of tones in combatting both the multipath effect and the multiple access interference. For this type of combination the technique of guard interval is no longer relevant. Hence Multiple Input-Multiple Output (MIMO) equalisation structures were investigated for OFDM-CDMA in [80, 81, 82]. The equalisation structures were derived for filters matched to both the channel and the symbol shape. The steady-state behaviour of linear [81] and decision feedback [82] equalisers was investigated. Adaptive versions [80] have also been proposed. Adaptive RLS (recursive least square) structures were derived and presented in the form of a Kalman algorithm. Simulation results obtained for a time-varying channel modeled by means of a tapped delay line show the effectiveness of the equalisation.

For such a system, Joint Detection (JD) was investigated as well. The device processes the outputs of filters matched to the channel and the symbol shape. It turns out that the matched filter outputs suffer from ISI (inter Symbol Interference), IBI

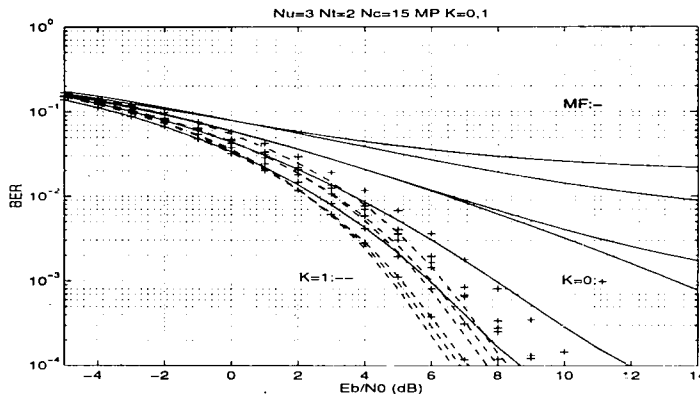


Figure 6.40: BER for  $N_c/N_t = 15/2$ ,  $N_u = 3$  users, and channels with 2 paths (equal amplitudes) per user and matched filtering only (MF), interference cancellation only (1 tap filters,  $K = 0$ ), and JEIC with (3 taps filters,  $K = 1$ ).

(Inter Band Interference) and MAI (Multiple Access Interference). The maximum-likelihood sequence estimator was derived for such a system, but is very complex. Therefore suboptimum detectors based on the processing of matched filter outputs were investigated. The receiver contains  $N_u \times N_t$  matched filters where  $N_u$  and  $N_t$  are the number of users and tones respectively. It was first assumed that the channel information was available and hence channel matched-filtering was performed. Then a solution was proposed to perform symbol shape matched filtering only.

When designing joint detection devices the main challenge is to obtain structures whose complexity is only linear with the number of users and which are near-far resistant. That makes it possible to avoid a fine power-control strategy. Different types of joint detection devices were investigated for multipath channels. They do not assume block transmission. These structures are

1. The linear joint detector [83] (T-JEIC, meaning transversal joint equaliser and interference canceller), see Fig. 6.40. The MMSE MIMO joint detector uses coefficients such that the expectation of the error between the true symbols and their prediction built from the sampled matched filter outputs is minimum.
2. The decision feedback detector [84] (DF-JEIC), see Fig. 6.41. Actually two types of DF joint devices have been investigated. In the first one (DF-JEIC-1), the estimates are built from current matched filter outputs, a few future ones and previous decisions. For mathematical tractability it was assumed that the decisions are always correct. In the second device (DF-JEIC-2), the users are

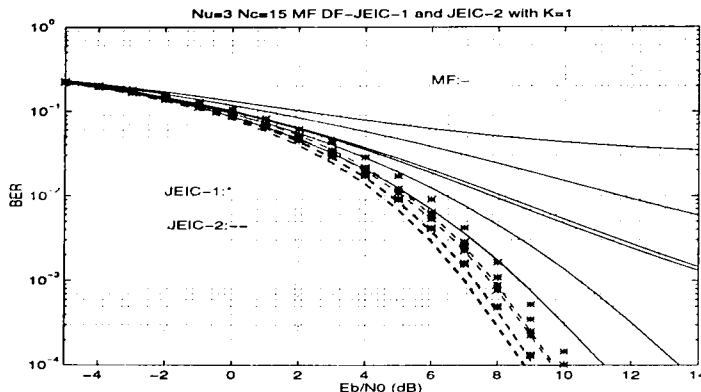


Figure 6.41: Bit error rate as a function of  $E_b/N_0$  for  $N_c/N_t = 15/2$  and  $N_u = 3$  over one-path asynchronous channels. The solid curves are for matched filtering only (MF), the stars are for DF-JEIC-1 with 3 tap filters and the dotted curves are for DF-JEIC-2 with 3 tap filters.

ordered in decreasing order of power. The most powerful user is detected with the first DF strategy. Then, for the second most powerful user, the estimates are built similarly except for the current decision of the strongest user which is used instead of the matched filter output, and so on for the other users.

3. The fractionally spaced linear joint detector (FSJD). When the channel is time varying, both the channel matched filter and the joint detector have to be adaptive. Rather than performing channel matched filtering, symbol shape matched filtering can be performed but in order to be able to render the effect of the channel in the adaptive device the sampling rate at the output of the matched filters has to be increased. The receiver is then only supposed to know the pseudo-noise codes of the users.

All these detectors have been designed for an MMSE criterion. A zero-forcing design would correspond to an MMSE design at infinite  $E_b/N_0$  ratio. For all these structures, it has been shown how to obtain the coefficients of the equalisers in close form and how to adapt them by LMS or RLS techniques. Moreover, from the decision variables obtained after joint detection, assuming BPSK modulation it has been shown how to obtain a close form expression of the BER.

The steady-state performance of all these joint detectors has been investigated in asynchronous scenarios with one-path or two-paths per user. Also the resistance against a near-far effect for the same channels has been demonstrated, see Fig. 6.42. The re-

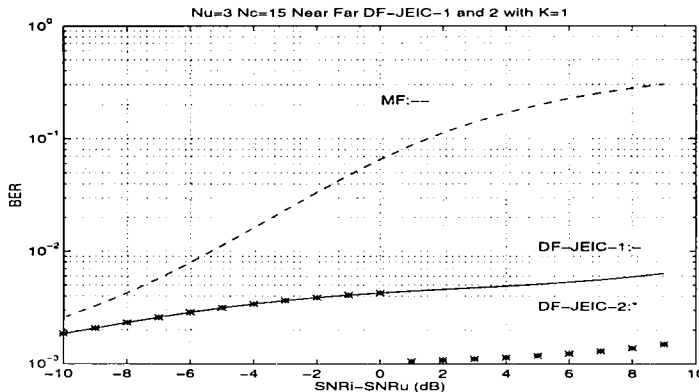


Figure 6.42: Illustration of the near-far resistance for  $N_c/N_t = 15/2$  and  $N_u = 3$  over one-paths asynchronous channels.  $E_b/N_0 = 7 \text{ dB}$ . Matched filter detection (MF), DF-JEIC-1 (solid line) and DF-JEIC-2 (stars) both with 3 taps ( $K = 1$ ).

sults are that, assuming channel matched filtering, and for a constant complexity, DF-JEIC-2 is best, then comes DF-JEIC-1 and then T-JEIC. Decision feedback fractionally spaced joint detection has not yet been studied, but is certainly the most promising candidate.

## Method 2

A second method to combine OFDM with CDMA was analysed in [85] for the down-link. Here, spreading is performed on the information symbol level prior to multi-tone modulation. If  $N_t$  subcarriers are available every information symbol of a single OFDM symbol is spread over one subset of  $M_t$  subcarriers using  $M_t$ -dimensional orthogonal codes. Originally this technique was regarded as a multiple access technique but it can also be regarded as a diversity technique. To obtain a maximum diversity gain,  $N_t/M_t$  ( $M_t < N_t$ ) code sets were used in every OFDM symbol which were arranged like a comb thus minimising the correlation among the subcarriers allocated by a single code set. Since the orthogonality of the codes is destroyed by the channel equalisation is necessary in the receiver. Three different equalisation algorithms were investigated in [85]: Restoring the orthogonality by multiplying the received signal vector with the inverse channel transfer function (ORC) shows poor behaviour in Rayleigh-Fading channels because weak subcarriers cause a high noise amplification. Better results were obtained if only those subcarriers are restored whose power lies above a certain threshold (TORC). The best performance was achieved by an iterative procedure evaluating the Likelihood function of all symbol sequences of code length

$M_t$  with only one bit difference to a starting symbol sequence which was obtained by TORC. The most probable sequence was then used as the starting sequence for the next iteration step. Four iteration steps were sufficient to get an  $E_b/N_0$  gain of more than 8dB at a BER of  $10^{-3}$  in comparsion to a conventional OFDM system (see Fig. 6.43).

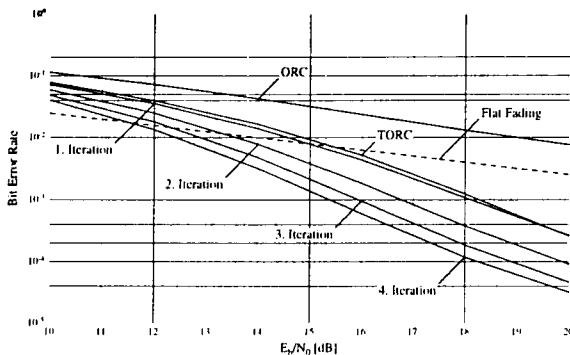


Figure 6.43: BER as function of the average  $E_b/N_0$  for different OFDM-CDMA equalisation algorithms under Rayleigh-Fading conditions. (4-QAM, uncorrelated fading, noisy channel state information  $\sigma^2 = 0.1N$ ,  $M_t = 32$ )

The idea of OFDM-CDMA has also been investigated in [86] for a DECT-like system. Here, spreading was performed on bit level using orthogonal Walsh codes. With Walsh codes of length four a differential detection structure can be maintained and no channel estimation has to be performed at the receiver.

## 6.8 MAC Protocols

C.J. Burkley, University of Limerick, Ireland

The Medium Access Control (MAC) sub layer is located between the Data Link Control (DLC) layer and the Physical layer in the OSI Model. Functionally it is a sub layer of the DLC layer and its purpose is to allocate the multi-access medium among several nodes.

A radio medium is generally a broadcast transmission medium unless a special effort is made to focus the transmission in one direction. The radio interface is therefore analogous to a broadcast system rather than to a dedicated line for an individual connection. Thus, a mechanism is required to ensure that users gain access to the medium in a fair manner and also that efficient use is made of the medium.

The two main categories of random access are ALOHA and carrier sense multiple access (CSMA). In CSMA, which is one of the most common accessing techniques in use today, a node wishing to transmit a packet, first listens to the channel to determine whether another user is currently accessing the channel. CSMA is less prone to instability problems than ALOHA and its efficiency can be further improved by using collision detection (CD) so that colliding sources cease to transmit when a collision has been detected rather than waiting until the end of a packet. However CSMA/CD is difficult to implement in a radio environment as it may be difficult for sources to detect a collision in the presence of severe fading. CSMA/CD is also unsuitable for voice traffic because of its unbounded packet delay. Other possible multiple-access techniques are the token ring and token bus, but these schemes are more difficult to manage in the fading radio environment.

There is therefore, a need for a multiple access protocol, which would perform efficiently in the hostile radio environment and which would be suitable for integrating both voice and data traffic.

Packet access mechanisms for cellular radio were considered in the RACE Mobile Telecommunications Project 1043 [87]. The primary advantage of packet transmission is that bandwidth may be allocated on a demand basis. Four different techniques were examined, TM-BCMA/CD (time-multiplexed base-controlled multiple access with collision detection), PRMA (packet reservation multiplex access), HPS-DB (hybrid packet system with dynamic boundary) and HPS-FB (hybrid packet system with fixed boundary) and it was concluded that the PRMA protocol is an attractive candidate for mixed services over a range of cell sizes as it can accommodate fixed channel access, reserved channel access and random channel access.

In the PRMA protocol [88], the channel is divided into slots, which are grouped in frames. Within a frame each slot is recognised as available or reserved on the basis of a feedback packet broadcast in the previous frame from the base station to all the terminals. As in slotted ALOHA, terminals with new information contend for access to available slots. At the end of each slot the base station broadcasts a packet that reports the results of the transmission. A terminal that succeeds in sending a packet to the base station obtains an implicit reservation for exclusive use of the corresponding

time slot in subsequent frames. PRMA requires all terminals to listen to acknowledgements in all slots. Frame reservation multiple access (FRMA) [89], is a variant of this scheme in which the base station broadcasts the acknowledgement for all the slots in a frame at the end of the frame. This results in reduced receiver activity and the system can be further enhanced by using an adaptive permission probability scheme, where the permission probability is chosen depending on the number of reserved slots at the beginning of the frame.

In order to support synchronous and isochronous services, while guaranteeing acceptable grade-of-service some kind of isochronous circuit allocation capability has to be provided by the MAC sublayer and a Space Division Multiple Access (SDMA) protocol with reservation demand assignments (DA) discipline to provide hybrid packet and circuit switching services has been proposed [90]. The channel timing format is a slotted channel, each time slot corresponding to the packet size of the lower bit rate service provided by the network. Packets corresponding to different services are integer multiples of slots. Slots are grouped onto fixed frames and the number of slots in a frame is calculated so that the delay between two consecutive voice packets does not affect the quality of speech. Slots are divided into reservation slots and data transmission slots and the number of slots for each class can be modified as a function of the collision rate or the number of re transmissions.

Polling can also be used as a technique for controlling access to the medium and a number of different multiple access techniques including full polling, partial polling and a contention protocol within a polling structure have been proposed and investigated [91] for their suitability for an integrated voice/data indoor radio system. Results showed that 2.5 Mbits/s user data throughput can be supported with the partial polling or contention schemes with a 20 ms frame length and with acceptable voice delays.

A new transmission/resource sharing scheme which uses a pure RTS (Request to Send)/CTS (Clear to Send) protocol has been proposed [92] as a resource sharing scheme for radio LANs. In this scheme the available bandwidth is divided into sub-bands and when a base station has a message to send it sends an RTS over an primary sub-band that was not busy to the destination station which was also not busy. The source station then listens to that set of sub-bands for a CTS from the destination. If the RTS is received intact at the destination a CTS is sent to the source over the set of sub-bands. On receiving the CTS, the source station sends the data over the set of sub-bands. On receiving the data the destination sends an acknowledgement back over the sub-bands.

Since the deployment of new personal telecommunications networks is likely to occur simultaneously with that of new broad band networks the MAC protocol data unit structure should be compatible with the ATM cell structure, which is based on a fixed packet size including a virtual circuit identifier. The need for an additional header (for synchronisation addressing) in the air interface has been identified [90] as well as the need to handle error control for the radio channel. ATM will offer a flexible transfer capability to all services supported by the radio network.

An important feature of the system, related to its spectrum efficiency and its quality

of service, is the channel assignment policy. For non-uniform traffic conditions, dynamic channel allocation (DCA) schemes, in which channels are assigned on demand, out performed fixed channel allocation (FCA) schemes. Hybrid channel allocation (HCA) schemes, in which only some of the available channels are assigned permanently and the remainder are shared dynamically may be simpler to implement and their performance would be somewhere in-between DCA and FCA.

A MAC protocol for ATM-based Indoor Radio Networks has been proposed [93] which uses a request/permit mechanism to control the access to the shared medium. Each remote station declares its required capacity by sending requests to the access control located in the base station. The available capacity is allocated by means of a strategy which approximates a global FIFO queue in such a way that the peak bit rate is enforced and fair access is achieved. The remote stations are informed about the obtained capacity by means of permits, which authorise the remote station to send a cell. The MAC protocol is thus cell based, meaning that an issued permit initiates the transmission in a single cell.

To meet the requirements of future systems in the fading mobile environment an efficient channel management system is needed. The system should include a flexible multiple access technique and dynamic channel assignment. To be compatible with future B-ISDN, the application of ATM is an obvious choice. However, even though some media access systems have been suggested further work needs to be done before a universal system can be proposed.

## 6.9 References

- [1] ITU-T: Transmission Planning Aspects of the Speech Service in Digital Public Land Mobile Networks. Recomendation G.173, March 1993
- [2] A.A.M. Saleh, R.A. Valenzuela: A statistical model for indoor multipath propagation. IEEE SAC, February 1987
- [3] J.G. Proakis: Digital Communications, Second Edition. McGrawHill Inc, New York, 1983
- [4] J.P.M.G. Linnartz, A.J.'t Jong: Average bit error rate for coherent detection in micro and macro cellula. Proc. 6th IEE Int. Conf. on Mobile Radio and Personal Communications, Warwick, UK, 9-12 December 1991
- [5] J.B. Anderson: Propagation parameters and bit errors for a fading channel. COMMSPHERE 91, Herzlia, Israel, December 1991, paper 8.2
- [6] F.J. Casadevall, A. Valdovinos: Performance analysis of M-QAM modulations applied to the LINC transmitter. IEEE Trans. on Vehicular Technology, Vol. 42, No. 4, November 1993, pp. 399-406
- [7] S.A. Hetzel, A. Bateman, J.P. McGeehan: A LINK transmitter. Proceedings 41st, IEEE Vehicular Technolmogy Society Conference, St Louis, USA, pp. 133-137
- [8] G. Kaleh: Simple coherent receiver for partial response continuous phase modulation. IEEE JSAC, Vol. 7, No. 9, December 1989, pp. 1427-1436
- [9] E. de Jager, C. B. Dekker: Tamed frequency modulation, a novel method to achieve spectrum economy in digital transmission. IEEE Trans. on Commun., Vol. COM-26, May 1978, pp. 534-542
- [10] M. V. Eyuboglu, S. Qureshi: Reduced-state sequence estimation with set partitioning and decision feedback. IEEE Trans. on Commun., Vol. COM-36, January 1988, pp. 13-20
- [11] F. Morales - Moreno, W. Holubowicz, S. Pasupathy: Optimization of trellis coded TFM via matched codes. IEEE Trans. on Commun., Vol. COM-42, February-April 1994, pp. 1586-1594
- [12] L. B. Lopes: Relationship between performance and timing recovery mechanisms for a DECT link in dispersive channels. Elect. Letters, 1993, pp. 2173-2174
- [13] I. Crohn: Short term modelling of the land mobile radio channel. Doct. Thesis, TU Wien, 1991

- [14] D. Saha, T. G. Bridsall: Quadrature - quadrature phase-shift keying. IEEE Trans. on Commun., Vol. COM-37, No. 5, May 1989, pp. 437-448
- [15] T. Javornik, G. Kandus: QMSK modulation technique in mobile radio channel environment. IEEE 2nd Symposium on Commun. and Vehicular Tech. in the Benelux, Louvain-la-Neuve, Belgium, November 1994, pp.20-27
- [16] J. B. Andersson, T. Aulin, C. Sundberg: Digital phase modulation. Plenum Press, New York, 1986
- [17] A. Rodrigues, A. Albuquerque: Digital signatures of M-QAM and CPM systems in a static two-path channel. Internal report, Inst. Superior Técnico, Lisbon, Portugal, January 95
- [18] COST 207 - Digital land mobile radio communications. Final report, CEC, 1989
- [19] U. Dersch, J. Delgado: CODIT model for propagation. RACE Mobile Telecommun. Workshop, Metz, France, June 1993, pp. 373-377
- [20] A. Rodrigues, L. Vandendorpe, A. Albuquerque: Performance of direct-sequence spread spectrum multi-h CPM in indoor mobile radio systems. 44th IEEE Vehicular Tech. Conf. (VTC'94), Stockholm, Sweden, June 1994, pp. 578-581
- [21] A. Rodrigues, L. Vandendorpe, A. Albuquerque: Diversity techniques in indoor mobile radio with DS-CDMA multi-h CPM. IEEE 5th Int. Symposium on Personal, Indoor and Mobile Radio Communications (PIMRC'94), The Hague, The Netherlands, Sept. 1994, pp. 1383-1387
- [22] R. Podemski, W. Holubowicz: Influence of average number of the nearest neighbours on the optimum choice of CPM signals. RR-30/1993, Franco-Polish School of New Information and Communication Technologies, Poznan, Poland, August 1993
- [23] I. Crohn, G. Schultes, R. Gahleitner, and E. Bonek: Irreducible error performance of a digital portable communication system in a controlled time-dispersion indoor channel. IEEE J. Select. Areas Comm. vol. SAC-11, 1993, pp. 1024-1033
- [24] I. Crohn., G. Schultes, R. Gahleitner, and E. Bonek: Error floor mechanisms in indoor digital portable communications. Proc. 3rd IEEE Internat. Symp. on Personal, Indoor and Mobile Radio Comm., Boston (MA), Okt 1992, pp. 320-328.
- [25] J. B. Andersen, S. L. Lauritzen, and C. Thommesen: Distribution of phase derivatives in mobile communications, Proc. IEE Part H, vol. 137, 1990, pp. 197-204

- [26] G. Schultes and J. Fuhl: Phasor explanation of error mechanisms for MSK Transmission over a slightly dispersive radio channel. Proc. Melecon 94, Antalya, 38–42 (1994).
- [27] A.F. Molisch, J. Fuhl, and P. Proksch: Error floor of MSK modulation in a mobile–radio channel with two independently–fading paths. IEEE Trans. Vehicular Techn., in press.
- [28] V. Lipovac and A.F. Molisch: On the performance of MSK signal transmission over a multipath channel with small time dispersion. IEEE Vehicular Technology Conf. 1995, Chicago 1995, 1995, pp. 25–29
- [29] A.F. Molisch and J. Fuhl: Bit error probability of differentially detected (G)MSK in indoor mobile radio channels. 46th IEEE Vehicular Techn. Conf., Atlanta 96, in press (1996).
- [30] I. Crohn, and E. Bonek: Modeling of intersymbol–interference in a Rayleigh fast–fading channel with typical delay power profiles. IEEE Trans. on Vehicular Technology 41, 1992, pp. 438–447.
- [31] G. Ungerboeck: Channel coding with multi-level/phase signals. IEEE Trans. inform. Theory, Vol. 28, January 1982, pp. 55–67
- [32] H. Imai, S. Hirakawa: A New multilevel coding technique using error correcting codes. IEEE Trans. Inform. Theory, Vol. IT-23, No. 3, May 1977, pp. 371–377
- [33] N. Seshadri, C.E.W Sundberg: Multilevel coded modulation for fading channels. Proc. 5th Int. Tirrenia workshop, Elsevier, 1992, pp. 305–316
- [34] A.G. Burr: Optimised multistage coded modulation design for Rayleigh fading channels. IEEE Int. Symp. on Information Theory, Vancouver, Canada, September 1995
- [35] K. Boulle-Leeuwink, J.C. Belfiore, G. Kawas-Kalch: Chernoff bound of trellis coded modulation over correlated fadings channels. IEEE Trans. on Comm., Vol. 42, No. 8, August 1994, pp. 2506–2512
- [36] K. Boulle, G. Femenias, R. Agusti: An overview of trellis coded modulation research in COST231. PIMRC'94 conference, pp. 105–109
- [37] C. Mourot: A high bit rate transmission technique in mobile radio cellular environment. IEEE VTC conference, Denver, May 1992, pp. 740–743
- [38] A. Wautier, C. Mourot, J.L. Dany: Phase correcting filters for sub–optimum equalizers. International Zurich Symposium on Digital Communication, 1994
- [39] K. Wesolowski, R. Krenz, K. Das: Efficient receiver structure for GSM mobile radio. International Journal of Wireless Information Networks, Plenum Press, 1995

- [40] M. Reinhardt, J. Lindner: Vector Decision Feedback Equalization for M-ary orthogonal transmission over multipath channels. 3rd International Symposium on communication theory and applications, Charlotte Mason College, Ambleside, Lake District, UK, July 1995, pp. 166-173
- [41] G. Ungerboeck: Adaptive maximum likelihood receiver for carrier modulated data transmission systems. IEEE Trans. on Comm., Vol. 32, 1984, pp. 624-636
- [42] R. Krenz, K. Wesolowski: Comparison of several space diversity techniques for MLSE receivers in mobile communications. Proc. Personal, Indoor and Mobile Communications (PIMRC 94), den Haag, September 94
- [43] A. Valdovinos, F.J. Casadevall: Equalization and space diversity techniques in mobile environments. IEEE Network, Vol. 8, No. 2, March-April 1994, pp. 36-42
- [44] M.L. Moher, J.H. Lodge: TCMP - a modulation and coding strategy for Rician fading channels. IEEE Journal of selected Areas in Communications, Vol. 7, No. 9, December 1989
- [45] A.G. Burr: Bounds and estimates of the uplink capacity of cellular systems. Proc. IEEE 44th Vehicle Technology Conference, Stockholm, VTC'94, pp. 1480-1484
- [46] A.G. Burr, T.C. Tozer, S.J. Baines: Capacity of an adaptive TDMA cellular system: comparison with conventional access schemes. IEEE Conference on Personal, Indoor and Mobile Radio Communications, PIMRC'94, The Hague, Netherlands, 1994
- [47] M. Streeton, A. Uriel: System model for adaptive cellular mobile systems. Proceedings of International Conference on Universal Personal Communications, ICUPC'93, 1993
- [48] C. van den Broeck, D. Sparreboom, R. Prasad: Performance evaluation of Packet Reservation Multiple Access protocol using steady-state analysis of a Markov chain model. Proc. Joint COST 231/227 Workshop, Limerick, Ireland, pp. 454-462 (Publ. University of Limerick)
- [49] M. Mastroforti: Uplink capacity evaluation of a PRMA based system in a terrestrial radio mobile environment. Proc. Joint COST 231/227 Workshop, Firenze, Italy, 1993 (Publ. Kluwer)
- [50] J.M. de Vile: A reservation-based multiple access scheme for future universal mobile telecommunications system. Proc. European Conference on Mobile and personal Communications, 1993 (Publ. IEE, U.K.)
- [51] A. Klein, P. W. Baier: On the capacity of discrete-time synchronous Gaussian CDMA and TDMA channels. International Journal of Electronics and Communications, Vol. 48, January 1994, pp. 28-33

- [52] A.G. Burr: Bounds on spectral efficiency of coded CDMA and FDMA/TDMA. Colloquium on spread spectrum techniques for radio communication systems, London, 27th April 1993 (Publ. IEE)
- [53] H. Hashemi: Simulation of the urban radio propagation channel. IEEE Trans. Veh. Technology, Vol. VT-28, August 1979, pp. 213-224
- [54] K.S. Gilhousen, L.M. Jacobs, R. Padovani, A. Viterbi, L.A. Weaver Jr, C.E. Wheatley III: On the capacity of a cellular CDMA system. IEEE Trans. Veh. Technology, Vol. VT-40, May 1991, pp. 303-312
- [55] J.J.Olmos, R.Agustí: Performance Analysis of a Second Order Delay-Lock Loop with Application to a CDMA System with Multipath Propagation. In 1st International Conference on Universal Personal Communications (ICUPC'92), Dallas (Texas), September 1992
- [56] R. A. Iltis: Joint Estimation of PN Code Delay and Multipath Using the Extended Kalman Filter. IEEE Trans. on Comm., Vol. 38, No. 10, October 1990
- [57] P. Díaz, R. Agustí: A PN Code Delay Estimator Based on the Extended Kalman Filter for a DS/CDMA Cellular System. Proceedings of the 4th International Symposium on PIMRC, September 1993
- [58] C.A.F.J. Wijffels, H.S. Misser, R. Prasad: A Micro-cellular CDMA System over Slow and Fast Rician Fading Radio Channels with Forward Error Correction Coding and Diversity. IEEE Transactions Vehicular Technology, Vol. 42, November 1993, pp. 570-580
- [59] G.J.M. Janssen, R. Prasad: Propagation measurements in an indoor radio environment at 2.4 GHz, 4.75 GHz and 11.5 GHz. Vehicular Technology Society 42nd VTS conference frontiers of Technology, Denver, Colorado, 10-13 May 1992, pp. 617-620
- [60] L.Vandendorpe, R.Prasad, R.G.A. Rooimans: Hybrid Slow Frequency Hopping/Direct Sequence Spread Spectrum Communications systems with B- and Q-PSK Modulation in an Indoor Wireless Environment. Proceedings of the Fourth International Symposium on Personal, Indoor and Mobile Radio Communications, Yokohama, Japan, September 9-11 1993, pp. 498-502
- [61] A. Klein, P.W. Baier: Simultaneous cancellation of cross interference and ISI in CDMA mobile radio communications. Proc. IEEE International Symposium on Personal, Indoor and Mobile Radio Communications (PIMRC '92), Boston, USA, 1992, pp. 118-122
- [62] A. Klein, P.W. Baier: Linear unbiased data estimation in mobile radio systems applying CDMA. IEEE Journal on Selected Areas in Communications, Vol. 11, 1993, pp. 1056-1066.

- [63] P. Jung, J. Blanz, P.W. Baier: Coherent receiver antenna diversity for CDMA mobile radio systems using joint detection. Proc. IEEE International Symposium on Personal, Indoor and Mobile Radio Communications (PIMRC '93), Yokohama, 1993, pp. 488-492
- [64] B. Steiner, P.W. Baier: Low cost channel estimation in the uplink receiver of CDMA mobile radio systems. Frequenz 47, 1993, pp. 292-298
- [65] A. Klein, G.K. Kaleh, P.W. Baier: Equalisers for multi-user detection in code division multiple access mobile radio systems. Proc. IEEE International Conference on Vehicular Technology (VTC '94), Stockholm, 1994, pp. 762-766
- [66] P. Jung, J. Blanz, M. Naßhan, P.W. Baier: Simulation of the uplink of JD-CDMA mobile radio systems with coherent receiver antenna diversity. Wireless Personal Communications, Vol. 1, 1994, pp. 61-89
- [67] M. Naßhan, P. Jung: New results on the application of antenna diversity and Turbo-Codes in a JD-CDMA mobile radio system. Proc. IEEE International Symposium on Personal, Indoor and Mobile Radio Communications (PIMRC '94), The Hague, Netherlands, 1994, pp. 524-528
- [68] J. Blanz, A. Klein, M. Naßhan, A. Steil: Performance of a cellular hybrid C/TDMA mobile radio system applying joint detection and coherent receiver antenna diversity. IEEE Journal on Selected Areas in Communications, Vol. 12, 1994, pp. 568-579
- [69] M. Naßhan, A. Steil, A. Klein, P. Jung: Downlink cellular radio capacity of a joint detection CDMA mobile radio system. Proc. IEEE International Conference on Vehicular Technology (VTC '95), Chicago, 1995
- [70] D. Dahlhaus, A. Radović, B.H. Fleury: Joint Parameter Estimation and Data Detection for DS/SSMA Systems Operating in Time-Dispersive Channels. ITG-Fachtagung "Mobile Kommunikation", Neu-Ulm, Germany, 1995
- [71] P. Dent, B. Gudmundson, M. Ewerbring: CDMA-IC: a novel code division multiple access scheme based on interference cancellation. Proc. IEEE International Symposium on Personal, Indoor and Mobile Radio Communications (PIMRC '92), Boston, 1992
- [72] L. Levi, F. Muratore, G. Romano: Simulation results for a CDMA interference cancellation technique in a Rayleigh fading channel. International Zurich Seminar on Digital Communications, Zurich, March 1994.
- [73] M. Bossert, T. Frey, T: Interference cancellation in the synchronous downlink of CDMA-systems. ITG-Fachtagung "Mobile Kommunikation", Neu-Ulm, Germany, 1995

- [74] P. Jung, J. Blanz, M. Nasshan, P.W. Baier: Simulation of the uplink of JD-CDMA mobile radio systems with coherent receiver antenna diversity. *Wireless Personal Communications*, Vol. 1, 1994, pp 61-89
- [75] J. Ruprecht, F.D. Neeser, M. Hufschmid: Code time division multiple access: An indoor cellular system. Proc. of the 42nd IEEE Vehicular Technology Conference, Denver, 1992
- [76] C. Reiners, H. Rohling: Multicarrier transmission technique in cellular mobile communications systems. Proc. IEEE Vehicular Technology Conference (VTC'94), Stockholm, 1994, pp. 1645-1649
- [77] V. Engels, H. Rohling: Differential modulation techniques for a 34 Mbit/s radio channel using orthogonal frequency division multiplexing. Accepted for publication in *Wireless Personal Communications - Special Issue on Multi-Carrier Communications*, Kluwer Academic Publishers, to be published 3rd quarter 1995
- [78] L. Vandendorpe: Multitone system in an unlimited bandwidth multipath Rician fading environment. Proc. IEE Conference on Mobile and Personal Communications (MPC'93), Brighton, 1993, pp. 114-119
- [79] L. Vandendorpe: Multitone Spread Spectrum Communications Systems in a Multipath Rician Fading channel. *IEEE Transactions on Vehicular Technology*, Vol. 44, No. 2, 1995, pp. 327-337
- [80] O. van de Wiel, L. Vandendorpe: Adaptive equalization structures for multitone CDMA systems. Proc. Fifth IEEE International Symposium on Personal, Indoor and Mobile Radio Communications (PIMRC'94). The Hague, Netherlands, 1994, pp. 253-257
- [81] L. Vandendorpe, O. van de Wiel: Performance analysis of linear MIMO equalizers for multitone DS/SS systems in multipath channels. Accepted for publication in *Wireless Personal Communications - Special Issue on Multi-Carrier Communications*. Kluwer Academic Publishers, to be published 3rd quarter 1995
- [82] L. Vandendorpe, O. van de Wiel: Performance analysis of MIMO DFE equalisation of multitone SS signals. *IEEE Vehicular Technology Conference (VTC'95)*, Chicago, 1995, pp. 394-398
- [83] L. Vandendorpe, O. van de Wiel: Performance analysis of linear joint equalization and interference cancellation for multitone CDMA. Accepted for publication in *Wireless Personal Communications*, August 1995.
- [84] L. Vandendorpe, O. van de Wiel: Decision-feedback joint detection for multitone CDMA. Paper invited for the *Seventh Tyrrhenian International Workshop on Digital Communications*, Viareggio, 1995.

- [85] T. Müller, H. Rohling, R. Grünheid: Comparison of different detection algorithms for OFDM-CDMA in broadband Rayleigh fading, IEEE Vehicular Technology Conference (VTC'95), Chicago, 1995, pp. 835-838
- [86] O'Neil, L. B. Lopes: A simple OFDM transmission scheme for small dispersion environments. To appear at the European and Mobile Communications Conference, Bologna, 1995
- [87] J. Dunlop: Packet access mechanisms for cellular radio. Electronics and Communication Eng Jnl., Vol. 5, June 1993, pp. 173-179
- [88] D.J. Goodman et al.: Packet reservation multiple access for local wireless communications. IEEE Trans. COM-37, August 1989, pp. 885-890
- [89] P. Narasimhan, R. Yates and D.J. Goodman: Performance analysis of frame reservation multiple access. 3rd International Conference on Universal Personal Communications Record, San Diego, September 1994, pp. 26-30
- [90] I. Berberana, J. Jimenez, F.J. Gavilan: A packet media access protocol for mobile networks. Ann. Telecommun (France) Vol. 47, pp. 235-42, May-June 1992
- [91] C.J. Burkley and M.P. Moroney: Two new hybrid multiple access protocols for indoor wireless communications. Proc. 1992 URSI ISSSE, Paris, France, September 1992, pp. 701-703
- [92] S.A. Black, M. Smith, T.A. Wilkinson: Analysis of a wireless LAN MAC protocol. ETSI RES 10R 92/35, November 1992
- [93] C. Blondia, O. Casals, J. Garcia: Performance analysis of a MAC protocol for a broad band network access facility. Symp. on Teletraff. Anal. of ATM Systems '93, Eindhoven 1993

## Potential Radio Interface Subsystems

**Edited by R. J. Goodwin, Siemens Roke Manor Research, U.K., and Alister G. Burr, University of York, U.K.**

### 7.1 Advanced TDMA Mobile Access (ATDMA)

**M. Streeton, Siemens Roke Manor Research, U.K.**

This section provides a brief description of the advanced TDMA system which has been developed by the RACE ATDMA project.

This description is based on a submission made to COST231 by the RACE project consortium, which consists of the following companies; Siemens AG, Roke Manor Research, Alcatel Mobile Communication France, Alcatel Standard Eléctrica S.A. Universidad Politécnica de Cataluna, Télécom Paris, France Télécom CNET, ESG Elektronik-System-Gesellschaft GmbH, Fondazione Ugo Bordoni, The University of Strathclyde, DeTeMobil, Nokia Mobile Phones and Nokia Research Centre.

Further details of this system may be found in the published papers such as [1], and those at the RACE workshops [2, 3].

The submission to COST231 was made before the end of the project, and hence can not fully represent the final system design. For this the system description produced at the end of the project [4] should be consulted, which also describes the evaluation results obtained using the testbeds developed by the project.

#### 7.1.1 Design Rationale

At the start of the project a set of design requirements were set. Where possible these followed the evolving vision of what UMTS and FPLMTS were in the respective standards bodies.

The ATDMA system is designed to provided:

- A wider range of services in a wide range of environments.
- Better quality and reliability.
- Higher capacity.
- Easier network planning & deployment.

To support all services it is thought that only a small set of bearers are needed. Based on this approach the following radio bearer services have been selected :

- Voice (high and normal quality)
- Data service with low delay (9.6 kb/s - 2 Mb/s at < 30 ms)
- Data services with long delay (9.6 kb/s - 2 Mb/s at < 300 ms)
- Data services with unconstrained delay (8 and 53 Byte cells)

The operating environments also place different constraints and requirements on the radio access system design, and so a single set of air interface parameters will undoubtedly not be optimal in all the situations. This consideration has lead to the project's concept of an adaptive air interface. Using this the system can be both more reliable, and more efficient.

The main forms of adaptation are:

*Adaptation to Cell Types and associated propagation conditions*

The different propagation conditions can not be optimally met with one radio interface with a fixed carrier spacing and so three basic cell types are required : pico, micro and macro cells. Each cell type is supported with a variant of the physical layer.

*Adaptation to Interference*

The error protection overheads and carrier slot assignments are dynamically varied to match the current conditions.

*Adaptation to Source Activity*

Physical channels are dynamically assigned to match the current requirements of each service.

### 7.1.2 Radio Access System Model

To correctly understand and capture the inter-relationships between these adaptation techniques and other radio access processes such as handover and admission control, the project has adopted a functional modelling approach [5].

The key features of the model are :

- i a formal division between those functionalities involving the Transport of user and control messages over the air interface (modulation, error coding, etc.) where OSI layered techniques are appropriate, from those involving the Control of these transport functionalities (power control, packet access, handover, etc.) where functional modeling methods are more useful.
- ii an abstract network architecture consisting of only three system elements: Mobile stations (MS), Base stations (BS) and the fixed Network.. This allows the radio access system to be specified independently of the final fixed network architecture.

The system is then modelled using the following logical groups:

*Transport (TP)*. All radio and terrestrial transmission functions.

*Link Controller (LC)*. Direct control of the transport group and co-ordination of the collection and pre-processing of all transport chain measurements.

*radio Resource Allocator (RA)*. Responsible for the allocation of radio resource between different radio links and base stations.

*Routing Controller (RC)*. Controlling the routing for the connection to the MS.

*Traffic Controller (TC)*. Responsible for all call control functionalities.

*Location Manager (LM)*. Responsible for the location management (registration, paging, etc.) of all attached mobile stations

Each of these Logical Groups will be distributed over some or all of the three basic network elements (see Figure 7.1.1).

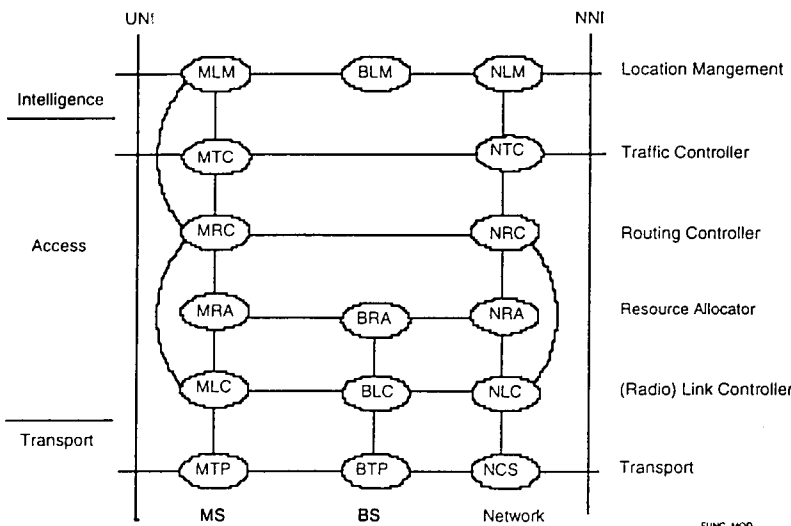


Figure 7.1.1 ATDMA Functional Model

In accordance with the OSI model the radio interfaces within the Transport group is defined by a three layer structure, with the upper network layer split into User and Control Planes :

*Radio Physical layer (RPL)*. Transport of TDMA bursts.

*Radio Link Layer (RLL)*. Transport of logical channels.

*UMTS adaptation layer (UAL)*. User plane of Network Layer. Adaptation of user traffic onto ATDMA radio bearer types

*Signalling Network Layer (SNL)*. Control plane of Network Layer. Adaptation of Signalling messages (segmentation, rate adaptation) onto the ATDMA radio bearer types and support for content based routing to various locations in the fixed network. This layer is in parallel with the

UAL,

Figure 7.1.2 shows the layers within transport expanded, with other logical groups lumped together as the control applications.

This model is used in the following sections as the basis for describing the system.

### 7.1.3 Transport Technique

The transport chain for the air interface has been designed based on speech requirements and the desire to support an ISDN-B channel on a single carrier in macrocells.

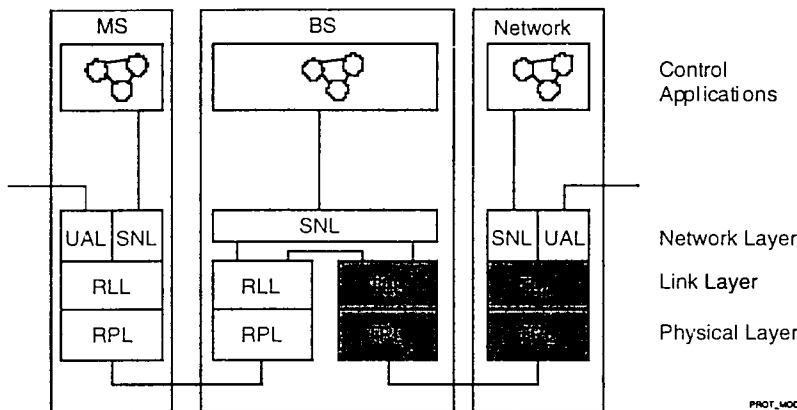


Figure 7.1.2 ATDMA Protocol Model

To support adaptation a set of modes are defined, each characterised by a certain configuration of the set {modulation, error control code, amount of radio resources} which guarantees a given performance for a given level of signal-to-noise + interference. The mode used will be selected by the link adaptation process which is described in the following section.

This overall radio transport chain is shown in figure 7.1.3 for a typical downlink traffic channel with the physical, link and UMTS adaptation layers indicated.

#### 7.1.3.1 Radio Physical Layer

The physical layer provides the transport over the air interface of TDMA bursts (modulation, equalisation, frequency hopping, etc.). Key specifications for the ATDMA physical layer are given in table 7.1.1. Note that all channel spacings, carrier bitrates, slot duration periods can be generated from a common reference oscillator of 14.4 MHz.

##### *Burst structure*

The principle influences behind the design of the burst and frames

structures are the range and characteristics of the services to be supported, the constraints imposed by physical limitations and natural phenomena, and of the current state of the art of transport techniques and hardware implementation.

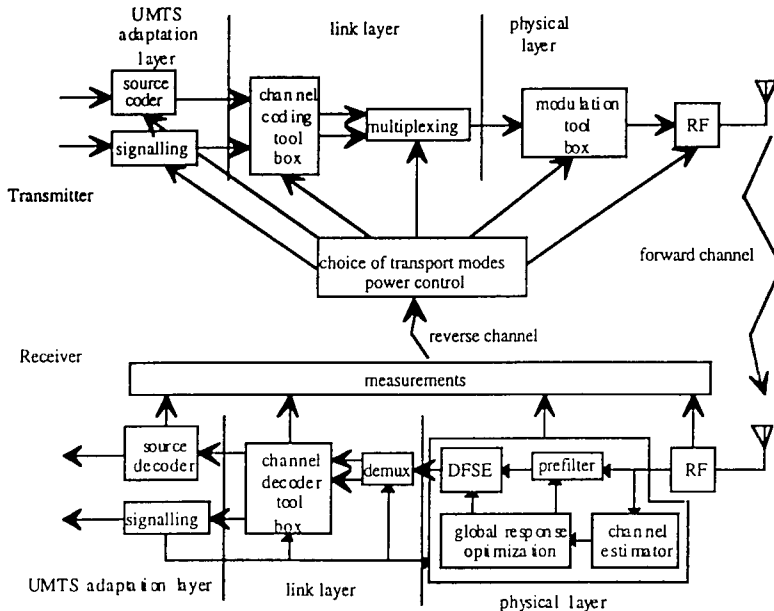


Figure 7.1.3 Example of an Adaptive transport chain for a downlink traffic channel

The format for the generic transmission burst is shown in figure 7.1.4.

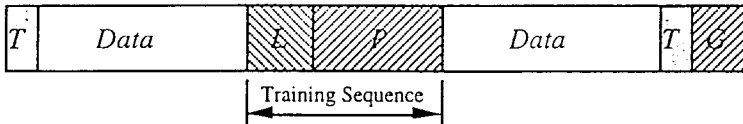


Figure 7.1.4 Generic burst structure

In addition when more than one burst per TDMA frame is assigned to the same bearer, e.g. for high data rate services, then these individual bursts can be concatenated into one and their contents redistributed to improve the use of radio resources.

#### Modulation

Binary offset QAM has been selected as the common basic modulation scheme for most cell types because of its spectrum efficiency, and because it is more robust to power amplifier non-linearities than straight QAM. Higher level quaternary offset QAM is used to increase the carrier bit rate. In addition to these linear schemes, the GMSK

modulation scheme is used to extended the maximum range of macrocells.

Cell type	<i>long-</i> Macro	<i>short</i> Macro	Micro	Pico
Modulation	GMSK	Binary Offset QAM		
Carrier Symbol Rates (kbaud)	360	450	1800	
Carrier Separation (kHz)	276.92		1107.69 = 4 x 276.92	
Slot Length (symbol)	120	125		
Training Sequence (symbol)	23	29 or 33		15
Payload (symbol)	76	72 or 76		96
Tail Bits (symbol)	8		6	
Guard Time (symbol)	13	12		8
Frame Duration (ms)	5			
Slots per Frame	15	18	72	
Frames per multiframe	128			

Table 7.1.1 : Transport parameters for static adaptation

The complex envelope of Offset QAM may in general be expressed as:

$$u(t) = \sum_k [a_{2k}h(t - 2kT) + ja_{2k-1}h(t - (2k-1)T)]$$

where  $1/T$  is the symbol rate, and  $a_k$  is the  $k$ th data symbol taking on values of  $\pm 1$  for Binary Offset QAM and  $\pm 1$  or  $\pm 3$  for Quaternary Offset QAM.

In order to make Binary Offset QAM fully compatible with differential encoded GMSK (as in GSM), the data bits  $a_{2k}$  and  $a_{2k-1}$  are multiplied by  $(-1)^k$  thus having alternate signs in both in-phase and quadrature components of the signal.

The shaping filter  $h(t)$  is a filter having square root raised cosine spectrum :

$$|H(f)| = \begin{cases} 1 & 0 \leq |f| < (1-\alpha)/4T \\ \cos[2\pi f / 4T] & (1-\alpha)/4T \leq |f| < (1+\alpha)/4T \\ 0 & (1+\alpha)/4T \leq |f| \end{cases}$$

### *Equalisation*

It was decided in the ATDMA project not to undertake any theoretical studies on equalization but rather to exploit available results, particularly from RACE 1043. This resulted in two alternative equalization methods being selected, namely Decision Feedback Equalization (DFE) and Decision Feedback Sequence Estimation (DFSE) see [9].

#### **7.1.3.2 Radio Link Layer**

This layer is responsible for the transmission and reception of individual blocks over the air interface. The link layer is service type dependent with separate specifications for speech, low and long constrained delay data, delay constrained control channels and the short and large block unconstrained delay data bearer types.

The link layer for each of these bearer types when using binary offset QAM or GMSK modulation in the physical layer is defined below. When quaternary offset QAM modulation is used the base channel codes can be maintained however the number of interleaved bursts will be halved and the spectral efficiency doubled.

##### *Speech*

Speech coding has not been studied in detail inside the ATDMA project and so its associated error protection scheme has only been considered at a generic level.

It is assumed that the speech source coded blocks will use a conventional structure of FEC with inner convolutional coding and outer block coding.

A 13 kb/s gross rate is used which supports possible net bit rates ranging from 6.4 to 9.6 kb/s with different levels of redundancy added. Also a more robust mode, having a gross bit rate of 26 kb/s, is provided. These figures correspond well with the emerging standard for 8 kb/s speech coding in the ITU [10].

##### *Constrained Delay Data*

The low delay data service requires a delay < 30 ms and a  $10^{-6}$  BER integrity in all cell types. For the long delay service the delay constraint is relaxed to 300ms (although increases over 200ms were found not to give further efficiency improvements).

A concatenated coding scheme has been chosen with a fixed 1/2 rate, constraint length 7, convolutional inner code and a variable rate outer Reed-Solomon code to provide a set of operation mode for link adaptation. Additional tail bits are appended to every input block to the encoder to fill up its memory and allow the corresponding trellis to end in a known state.

Codes have been defined for a range of different service bit rates. For example for the 64 kb/s service a set of 3 operating modes have been defined. These are shown in tables 7.1.2 and 7.1.3.

Mode number	Inner code rate	Outer code rate	Global rate	Bits per coded block	Half-bursts per interleaving period
1	1/2	1	1/2	1320	40
2	1/2	2/3	1/3	1980	60
3	1/2	1/2	1/4	2640	80

Table 7.1.2 : Summary of mode characteristics for 64 kb/s low delay Service.

Mode	Inner code rate	Outer code rate	Global rate	Bits per coded block	Data segments in interleaving period
1	1/2	1	1/2	3960	360
2	1/2	3/4	3/8	5544	504
3	1/2	1/2	1/4	7920	720

Table 7.1.3 : Summary of mode characteristics for 64 kb/s long delay Service

#### *Short Block Unconstrained Delay Data*

This bearer type is used for bi-directional signalling channels where the control applications can not directly support error detection but can tolerate a variable throughput. This is the assumed bearer for most fixed network-mobile signalling : call set-up, location registration, handover, etc.

The transmission scheme is based on a hybrid FEC/ARQ mechanism with a concatenated inner (4 ; 3) parity code and outer RS (8 ; 4 ; 5) code over GF(2<sup>3</sup>). A Service Data Unit (SDU) is transmitted over four bursts, hence containing 16x3x2 = 96 information bits. A field of 6 control bits protected by 6 CRC bits and 4 additional error correction bits to avoid false decoding is included. This leaves 80 bits for use by the Signalling Network Layer with the possibility to include a segmentation process to support longer messages.

#### *Large Block Unconstrained Delay Data*

A SDU of the size of an ATM (Asynchronous Transfer Mode) cell is used, i.e. 53 bytes. An extra byte is then added to this for carrying block numbering which has extra error protection.

A coding scheme has been selected which uses an inner (7,6,2) parity code and an outer RS (45,36) code. A cell is then mapped into two code words and carried by 10 burst. These can be transmitted over 10 TDMA frames, or sent more quickly when multiple slots are assigned.

When a cell is incorrectly received it will be re-transmitted by the control process. The receiver will then combine the two copies to allow a greater error correction capability. This allows a hybrid scheme to be implemented, but without the need for separate repeat numbering.

### 7.1.4 ATDMA Control System

While the design of the transport chain will contribute to the UMTS objective of improved spectrum efficiency and the support of a wide range of environments and services, most of the gain is achieved through the use of an active control system that continuously adapts the air interface to match the current conditions.

The following algorithms have been developed:

#### *Quality based power control*

Control of transmit power is used on both up and down links. The control algorithm uses link quality measurements on the link being controlled for longer term control, and measurements on the reverse link (as an estimate of path loss) for short term control. The range of short term power control is adjusted depending on the correlation between path loss in the two directions.

For services with multiple-slot allocations, each traffic slot is separately controlled.

#### *Dynamic Link Adaptation*

The operating mode of transport (coding, modulation, interleaving, etc.) for each of the delay constrained bearer services (speech and low and long constrained delay data) is adaptive to meet changing conditions. The link adaptation process selects the operating mode based on the need to ensure that service quality is being maintained with the minimum of assigned radio resources.

Two different link adaptation algorithms have been defined :

- i    *Short term link adaptation.* This process operates with an update period of between 0.5 and 5 seconds and bases its decision on the observed average channel quality of the assigned radio resource.
- ii    *Long term link adaptation.* This process is based on the observation that the distribution of C/I is dependent on the distance from the base station and so the transport operating mode is selected accordingly[8].

#### *Large Block Unconstrained Delay Data*

ARQ is used for traffic which require a high integrity, but can tolerate a variable delay (see section 1.1.3.2). The protocol used to control this uses both Positive and Negative Acknowledgments with a Positive Acknowledgment (ACK) for a particular block number representing an acknowledgment for all previous blocks (issued when the receiver successfully decodes a block that is in-sequence) while a Negative Acknowledgment (NAK) generates repeat transmissions of the selected blocks (issued when the receiver successfully decodes a block that is out of sequence - which implies that some blocks are missing). The use of a mixed acknowledgment type provide resilience to corrupted signaling.

The throughput and input buffer length are monitored and used to

dynamically change the allocated resources to the service, likewise during periods of congestion the allocated resources can be reduced and reassigned to higher priority services.

#### *Dynamic channel assignment*

A priority list based scheme is used to assign carriers and time slots. This is used each time a channel is assigned which could be at the start of a call, or for speech on every talk spurt.

This algorithm avoids the need for frequency planning, and provides some adaptation to current traffic distribution, but avoids the need for the base stations to communicate directly.

#### *Handover and macro diversity*

Since propagation conditions in some UMTS environments may be changing too rapidly for the mobile station to report measurements to the network and then wait for a handover decision, all normal handover trigger decisions are taken by the mobile and then signalled via either the old or new basestations.

Four separate handover criteria are included in the handover trigger stage: Link quality, Path loss, Range, and Power budget. This is necessary to give reliable handover in a system where slot allocation may be quickly changing, affecting interference, and link adaptation may maintain the bearer quality even when the mobile is in a non optimum cell.

Following handover trigger, the mobile selects the best candidate new base station. This step includes consideration of the new base station's current load (this is broadcast on the BCCH), path loss criteria and a desire to remain in the same cell type. This final criteria is designed to encourage slow moving mobiles to stay in microcells while keeping faster mobiles in macrocells.

An independent, demand assigned, Dedicated Control Channel (DCCH) is established to carry handover signaling. The existing traffic channels are not interrupted and so a true "seamless" handover is possible. An added advantage of the ATDMA handover process is that the release of the old traffic channels can be delayed until after the establishment of new traffic channels, and so a period of macro-diversity can be included.

#### *Packet access*

The previous sections may give the impression that each techniques has been designed separately. This is not the case, as many interaction must be considered to developed an overall system. Packet access is a technique which is utilised by several control algorithms to quickly assigned physical channels for TCH and DCCHs. It is described here in some detail to serve as an example of how the system model has been used to model the algorithms.

Capacity is allocated on demand using a technique called PRMA++ [6]. Like the original scheme proposed by Goodman [7], the PRMA++

protocol avoids wasting capacity during breaks in traffic source activity (during silence period in speech or for highly bursty data services), or the need to permanently allocate capacity for the maximum bit rate a call may need. It is also used to assign control channels for handover.

The main features of PRMA++ are:

- Time-slot allocation under BS control
- Separate physical channels for access control
- Physical channels allocated when requested, and kept until released (separate request not needed for each block sent)
- Common technique used for all traffic and dedicated control channels.

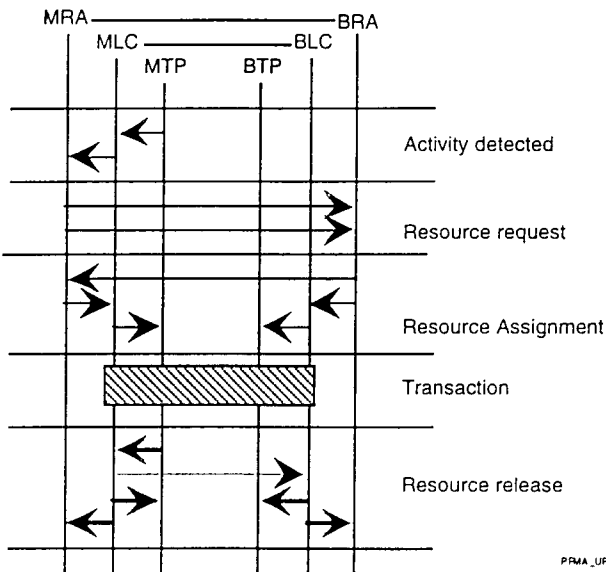


Figure 7.1.5 PRMA++ Uplink

The process for gaining access for uplink traffic is described below, and illustrated in figure 7.1.5.

- 1 Activity is detected by transport and the MLC informed. The MLC then asks the MRA to allocate capacity for the channel. Alternatively the request could originate in the MLC, for example, from the ARQ control algorithm.
- 2 The MRA will then make a request to the BRA for capacity using a random access control channel known as the R-slot with a message that states the Mobile Station and Logical channel Identifiers. The BRA will return the allocation on a paired acknowledgment channel, the "A-slot", with a message that states the Mobile Station

and Logical channel Identifiers and the allocated resources (in terms of carrier and slot numbers). This message also includes an Acknowledgment type flag which serves to indicate if the resource allocation has been queued (in case of congestion) or if the allocation message has been split over two or more bursts. If collisions occur on the R-slot then, following a time-out, the request from the Mobile is repeated.

- 3 The MRA and BRA will inform the LCs of the allocation
- 4 The traffic bearer becomes active and traffic is sent.
- 5 MTP detects the last item of data and the LCs then inform the RAs that the allocation can be released.

The process for the downlink is the same apart from the initial access procedure where contention access is not required, and the BS simply sends fast paging messages to allocate slots.

#### 7.1.4.1 Resource Allocation

A key element in the ATDMA system which is used by all control techniques is the resource allocator. This base station centered entity is the key arbitrator in the ATDMA system and has the task of distributing the limited radio resources between various competing traffic sources (within the same MS and BS link), between different mobile stations (within the same cell) and between different base stations (within the same cluster and/or between cell types located in the same region).

The resource allocation functions can be divided into two broad classes : assignment of physical time-slots on a short term basis (channel assignment) and acceptance of a call into an individual cell (admission control).

#### 7.1.5 Logical Channels

The ATDMA control channel structure is based on the CCITT classification [11], with refinements to accommodate the mixed use of both packet and circuit switched channels.

The control channels defined are:

##### *Packet access common control channels (CCCHs)*

A set of fast channels using single burst messages to provide the specialized common channels for PRMA++ access.

##### *Leash Control Channel (LCCH)*

A permanent control channel is used to keep control of each mobile that has set up a connection, even when no traffic is being carried. It supports a "watchdog" process (hence its name) and offers a low but guaranteed bandwidth. In a TDMA packet access scheme this channel is essential since it maintains time advance for Request slot bursts even after a long period of in-activity from the mobile.

### *Associated Control Channels (ACCH)*

These control channels are strictly associated with each unidirectional bearer. A separate pair (forward and return) exists with each unidirectional component of a TCH or DCCH. The forward ACCH (ACCHf) is used for commands such as downlink mode changes. The return ACCH (ACCHr) carries mainly measurement information. This association with each unidirectional bearer allow flexibility in supporting unbalanced or unidirectional traffic.

This association is illustrated in figure 7.1.6.

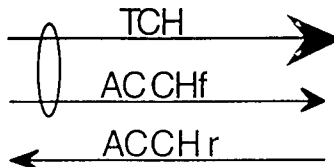


Figure 7.1.6 : Relationship between Traffic and Associated channels

### **7.1.6 Evaluation and Recommendations**

The ATDMA system described has been extensively evaluated. This has provided results on the operation of each technique and the overall system, and led to a set of recommendations on the design of UMTS.

#### *System Evaluation*

The performance of the system has been evaluated by analysis, and using the projects simulation testbeds. The results are recorded in a publicly available deliverable [12].

The main conclusion is that the system fully meets the requirements which were set, and is hence a suitable candidate for the UMTS air interface. In particular it supports all the required service, does not require frequency planning, and can provide a high quality of service.

The evaluation of capacity is not easy to summarise, as the results depend greatly on the scenarios used for each test. For example link adaptation gives the largest improvements where higher coverage is required. However results generally show a significant improvement over existing system. [12] should be consulted for details.

#### *Recommendations on UMTS Design*

Based on the experience of ATDMA, recommendations for the design of UMTS have been made. The adoption of these would ensure that the lessons learned can be applied, even if UMTS is finally quite different from the ATDMA proposal. These recommendations are described in [4], and have also been submitted to ETSI [13]. These cover most aspects of UMTS including services, access network and air interface design.

## 7.2 A CDMA Air-interface for Mobile Access

### M. A. Beach, University of Bristol, U.K

#### 7.2.1 Project Rationale

A three year project funded through the U.K. DTI/EPSRC LINK Personal Communications Programme (PC019) was established in 1992 in order to carry out a rigorous evaluation of CDMA for third generation mobile radio systems, culminating with a field trial demonstration of the selected DS-CDMA architecture. Members of the consortium included AT&T NS UK Ltd, Hewlett Packard Laboratories (Bristol) and the Universities of Bradford and Bristol, with approximately 25 man years of funded effort spread throughout the partners. The key objectives of the project were as follows:

- Study of UMTS requirements - teleservices and bearers.
- Comparative study of frequency hopping (FH) and direct sequence (DS) CDMA for UMTS service provision.
- Design and development of a DS-CDMA field trial system.
- Demonstration of a working DS-CDMA radio link, with a subset of the proposed UMTS services.

#### 7.2.2 Service Requirements for UMTS

The Universal Mobile Telecommunications System (UMTS) was taken as the target European Personal Communication System for this project. The diverse range of teleservices and environments envisaged for UMTS were studied by the consortium, and number of key teleservice attributes were identified. In particular, bit throughput, error rate, connection duration, delay, and occupancy was evaluated [14, 15] for a wide range of teleservices encompassing both low and high bit rate voice and audio, as well as, data transfer, graphics and video services, in order to ascertain the radio bearer requirements. To satisfy these requirements, the bearer classifications within the IBC Common Functional Specification D730 was adopted by the consortium. Here there are essentially two types of bearer service - circuit mode and packet mode. The former provides a predetermined amount of transmission capacity on an exclusive basis for the duration of the call. Packet mode provides a variable bit throughput by the use of packets and connections by routing. This activity thus provided the baseline specification for the project, as well as highlighting the need for a completely new air interface specification in order to fully support the UMTS Vision [16].

#### 7.2.3 Assessment of DS and FH CDMA for UMTS

In order to assess the most appropriate spreading technique for a CDMA based UMTS implementation, the capacity, hardware complexity, network

management issues and overall quality of service (QoS) aspects of both DS and FH CDMA were appraised. The architecture of the LINK CDMA test bed was then based on the outcome of these studies.

### 7.2.3.1 Traffic Capacity

The results reported in literature indicate that both DS and FH can potentially support high traffic loads for voice only communications, although the figures given differ widely. The results of both DS and FH capacity simulation carried out as part of this study [17,18] indicated that the traffic capacity that could be supported by slow FH was equivalent to, or better than, a DS system. This result is summarised in graphical form in figure 3.1 where it can be seen that the FH scheme could offer 24 users/MHz/cell compared to 21 users/MHz/cell with DS. However, given the error bounds of this type of approach, the result does not indicate a significant advantage either way.

The sensitivity of these capacity figures to variations in system parameters was the focus of much of the simulation work. The results indicated that DS is extremely sensitive to, for example, variations in the propagation environment and power control errors. This is clearly a difficult issue for any future DS-CDMA system and should be given careful consideration if a DS solution is selected for UMTS.

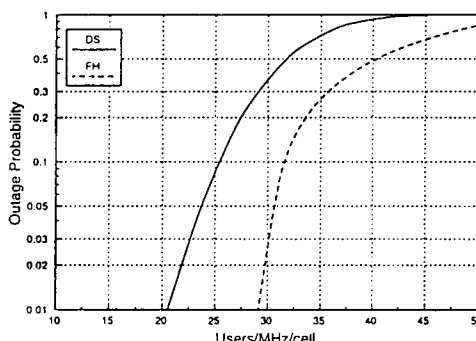


Figure 7.2.1: Performance Comparison of DS and FH CDMA

- Total number of base-stations: 37
- Path loss exponent: 4
- Log-normal shadowing std. dev.: 8dB
- Power control: Shadowing & path loss.
- Power control error (std. dev.): 0 dB
- Handover margin: 0 dB

- Voice activity factor: 0.5
- Cell sectorisation: None
- Antenna diversity: Dual
- Spreading/hopping bandwidth: 1 MHz

### 7.2.3.2 Hardware

The choice of CDMA scheme, specifically direct sequence, or fast or slow frequency hopping, will influence heavily the design and implementation of both mobile station and base station transceiver hardware. The power consumption, size and cost constraints of present state-of-the-art integrated circuit (IC) technology were taken as the starting points from which to base predictions for the potential UMTS hardware [17]. These can be briefly summarised as follows:

#### DS-CDMA

- DS chip sets are readily available providing a very flexible solution.
- The need for a Rake receiver increases complexity significantly.
- Power consumption and cost increase significantly with bandwidth.

#### FH-CDMA

- Limitations of RF synthesiser technology restrict FH to less than 1khop/sec, i.e. slow frequency hopping.
- A digital solution is possible (exploiting commonality with DS) enabling the hop rate to increase.

Given that the system performances of DS and FH are found to be basically equivalent, or at least complementary for certain scenarios, then it was expected ultimately that the hardware considerations of cost, size and power consumption will be evenly matched for both DS and FH.

### 7.2.3.3 Network Infrastructure Management

CDMA potentially offers complete frequency reuse within each sector or cell, thereby considerably easing the task of network planners, but the network topology may impose other restrictions. These problems were considered in the context of a mixed cell environment with both handover and signalling overheads. The following conclusions were drawn from this activity:

- The need to support a comprehensive set of UMTS teleservices will require a large bandwidth to be allocated to each operator within a given geographic area.
- A mixed cell architecture will require CDMA to operate with different frequency bands unless alternative near-far resistant techniques are considered.
- Multiple operators and the need for a contiguous bandwidth could limit the maximum allocation for DS-CDMA to as little as 5MHz.
- Initial studies show that the signalling overhead for the seamless, or soft handover, offered with Qualcomm's DS-CDMA system is no greater than with the hard handover procedures of GSM. However, the network traffic would be increased in proportion to the number of base-stations involved.
- The tight power control requirements for DS-CDMA increase the signalling overhead.

#### 7.2.3.4 Quality of Service

The definition of 'Quality of Service' (QoS) adopted followed established CCITT practices, although this was extended to include such parameters as spectral efficiency. The project output [19] was a set of QoS parameters, together with target values. These ranged from specifying a maximum BER of 10<sup>-3</sup> for speech to a handover success rate of greater than 99.95%. Of particular interest was how these parameters could be traded off with each other, e.g. spectral efficiency or system capacity versus SNR. The extent and ease of this process was itself considered an important quality aspect of system implementation.

#### 7.2.3.5 Selection of Spreading Technique for LINK CDMA Demonstrator

Although many of the issues associated with the selection of either a DS or FH air interface for UMTS remain unanswered, the results summarised above indicated that there would appear to be nothing to choose between the two techniques in terms of available traffic capacity and hardware implementation. Thus, on balance it was decided that DS would offer the better, lower risk solution at this point in time. This argument was based upon the amount of background work already carried out with DS, i.e. Qualcomm and CoDiT, and the level of support for this technique from hardware manufacturers, i.e. chip-sets aimed specifically at DS applications. This is not to say that there is no future with FH CDMA [20].

### 7.2.4 Test Bed Specification & Design Issues

Key parameters defining the channel structure and air interface specifications of the 8.2Mchip/s of the LINK CDMA test bed are given in figure 7.2.2 and table 7.2.1 respectively.

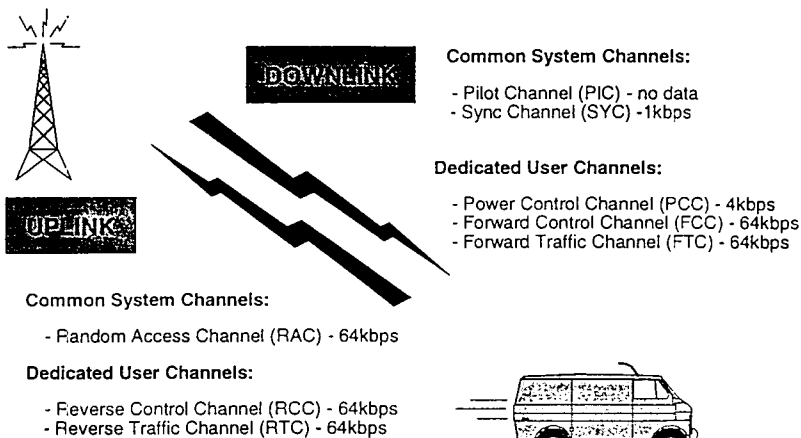


Figure 7.2.2 LINK CDMA Channel Structure

Original plans included the production of two base station (BS) and two mobile station (MS) units connected together through the fixed network via a Mobility Manager (MM). However, in order to obtain meaningful test bed results within the time period and with the resource limitations, the configuration was restricted to a single base station and mobile station as shown in figure 7.2.3. Although much of the software was written and tested to support an ISDN interface, there was insufficient time to complete the system integration, and hence the fixed terminal interface was reduced to an analogue telephone or 64 kbps data interface. Since the aim of this assessment was principally to evaluate the radio link performance, the loss of the ISDN call set-up facility in no way devalues the results obtained.

#### 7.2.4.1 Downlink Design

Here the BS digital modulators produce the encoded, interleaved, spread and filtered signals which are combined in analogue form at baseband before being upconverted in quadrature directly to RF and transmitted. The received signal at the MS is mixed down to a first IF at 70MHz where AGC is carried out, prior to the final downconversion process to quadrature

	Downlink	Uplink
<b>Channel Structure:</b>	All defined as separate physical channels with a unique PN code assignment.	
System	<b>PIC</b> - Pilot PN sequence with no data. <b>SYC</b> - 1kbps continuous data channel carrying essential system information, e.g. system timing reference.	<b>RAC</b> - Random access channel for call set-up. Non-continuous with a burst transmission rate of 64kbps.
User	<b>PCC</b> - Variable rate ( $\leq$ 4kbps) to control MS Tx power during a call. <b>FCC</b> - Carries all signalling and control messages to MS including paging. Non-continuous at 64kbps. <b>FTC</b> - Supports continuous user traffic with Bearer A or B.	<b>RCC</b> - Carries all signalling and control messages to BS. Non-continuous at 64kbps. <b>RTC</b> - Supports continuous user traffic with Bearer A or B.
<b>PN Code Assignment:</b>	All codes synchronised to timing reference at MM.	
System	Augmented m-sequence with each BS assigned a fixed phase offset. Length = $2^{17}$ chips (16msec period).	As for user channels below.
User	Long m-sequence with each user assigned a unique phase offset based on user ID. Each channel is then given a further fixed offset. Length = $2^{29}-1$ chips (65.5 sec period).	
Error Control Coding	$\frac{1}{2}$ rate, constraint length 7 convolutional code (industry standard) on all channels except PIC and PCC.	
Block Interleaving	12msec frame for Bearer A (speech) and 36msec frames for Bearer B (data).	
Modulation & Spreading	QPSK with a preferred pair of PN sequences.	BPSK with RAC/RCC in phase quadrature with the RTC.
Pulse Shaping	33 Tap digital FIR filter (3dB signal BW 8MHz)	
Chipping Rate	8.192MHz	
RF Carrier Frequency	1823MHz	1727.5MHz

Table 7.2.1: Air interface parameters.

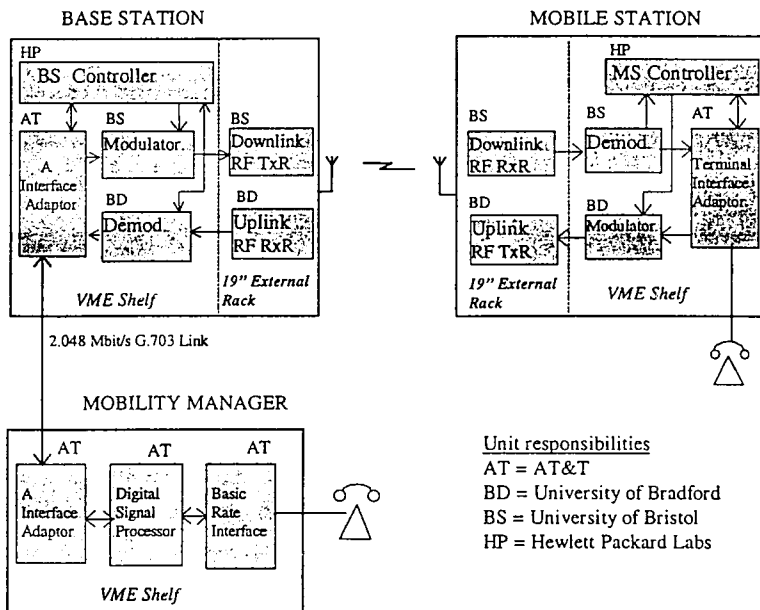


Figure 7.2.3 Partitioning of LINK CDMA Test Bed

baseband and subsequent analogue-to-digital conversion. Thereafter follows the process of extracting the user data from the spread signal, the key modules of which are illustrated in figure 4.3.

Crucial to this whole process is the acquisition and tracking of the Pilot signal. This synchronisation task is on a number of levels and can be broken down as follows:

1. Acquire the Pilot PN code from the strongest BS signal (coarse acquisition).
2. Acquire and track carrier and provide necessary AFC for the 70MHz local oscillator.
3. Recover and track clocks, synchronising with the downlink data.
4. Generate estimates of the channel coefficients (amplitude, phase and time) for coherent Rake reception.
5. Demodulate SYC to extract system timing and align long PN code generators as well as establish frame synchronisation.

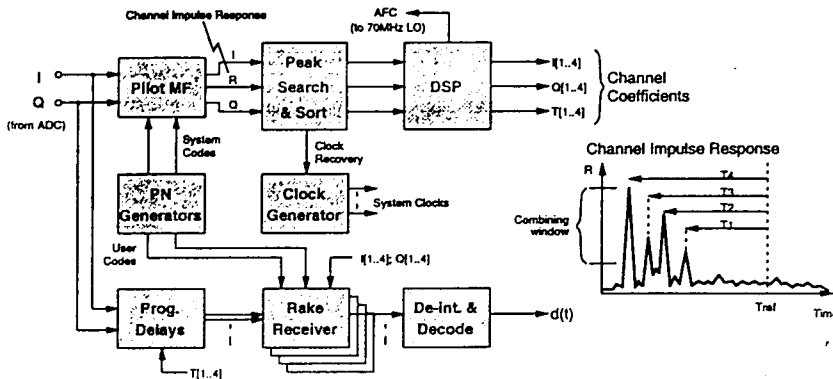


Figure 7.2.4 MS demodulator.

Central to this is the Pilot Matched Filter (PMF) which generates the complex impulse response from the received Pilot signal. This employs an FIR filter structure with the locally generated Pilot PN sequence forming the filter coefficients. The filter is 128 spreading chips long giving an impulse response of 15.6msec which is sufficient to enable all significant multipath activity to be detected and utilised. This is carried out by the Peak Search and Sort process which extracts the strongest multipath components (up to a maximum of four) and passes the channel coefficient data to an embedded DSP which programs the Rake receivers. Each of the Rake receivers comprises up to four paths, or tines, each consisting of a programmable delay block, serial despreader and complex coefficient multiply. The time-aligned outputs are then combined in a maximal ratio sense before the final demodulation process extracts the data. During handover, a second Pilot Matched Filter detects and tracks another BS. The DSP simply treats the outputs as additional multipath which are combined in the Rake receiver in the same manner.

In order to maximise the resolution of the multipath signals, the PMF outputs are averaged over a number of integration cycles. The choice for the number of cycles is a compromise between providing sufficient dynamic range in the filter to detect the signals and being fast enough to follow the rapidly changing phase. To allow further investigation, the integration period can be varied between 1, 0.5 and 0.25msec, providing coefficient update rates of 1, 2 and 4kHz respectively.

#### 7.2.4.2 Uplink Design

The uplink air interface and receiver design are very similar to those for the downlink. The principal differences are that no pilot channel is available and that BPSK rather than QPSK modulation is used. In addition, the uplink

requires accurate power control in order to take into account the distance of the MS transmitter from the BS.

The uplink receiver is a coherent rake structure with four tines, as illustrated in figure 4.4. The signal received at the base station is down-converted from 1727.5 MHz to baseband via a 70 MHz IF. It is then converted to digital as a complex baseband signal, sampled at 24.576 MHz. As in the downlink receiver, a parallel estimate of the channel impulse response is formed from the averaged outputs of a filter matched to the incoming PN sequence. Because no pilot sequence is transmitted the filter must obtain its taps from the traffic channel PN sequence. A decision feedback loop is therefore required, to remove the effect of the traffic channel data. The matched filter used is half the length of that used in the downlink, providing a 7.8 microsecond window on the channel impulse response.

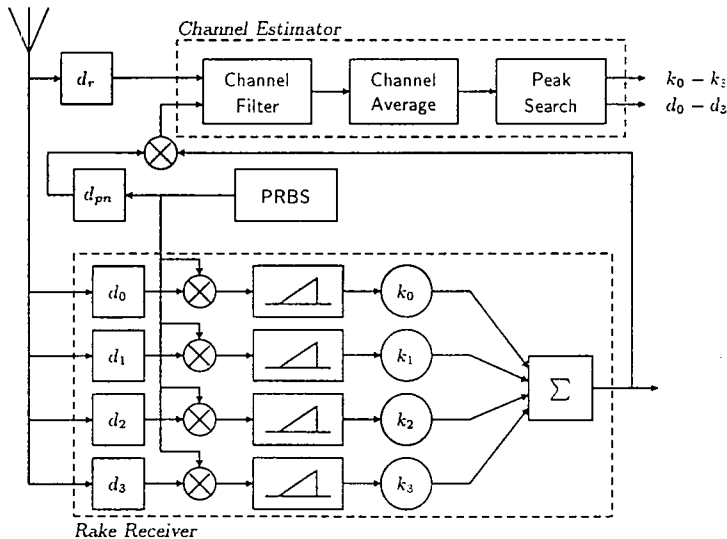


Figure 7.2.5 Coherent Rake Receiver for Uplink

Since there is no pilot channel on the uplink, there is a 180 degree ambiguity in the phase of the recovered channel estimate. This must be resolved before de-interleaving and decoding in order that the symbols from different base stations may be combined during handover. The phase ambiguity is resolved through the transmission of regular polarity symbols, using the (code separated) reverse control channel. The overhead required to transmit these symbols is small (<0.2 dB performance degradation). In addition, no carrier frequency recovery is done in the base station receiver. Instead the system relies upon a frequency extraction and re-transmission loop in the mobile station. Because of this, the frequency offset at the base station receiver is guaranteed to be no greater than twice the Doppler frequency plus the

inherent frequency tolerance of the oscillator (<1ppm). This greatly simplifies the design of the coherent uplink.

The base station receiver uses a reduced search algorithm for acquisition of the mobile. This is possible because the phase of the PN sequence in the mobile is set using system timing information recovered from the downlink SYC channel. This phase and that of the PN sequence in the base station should therefore be the same, to within the round-trip delay over the radio link. Once the PN sequence has been acquired, carrier phase is tracked by means of the matched filter channel estimate, as described above for the downlink. There is also a simple loop which tracks any clock offset by adjusting the receiver PN sequence timing so that the largest peak of the channel estimate is forced to a fixed position in the channel estimate vector.

In order that system capacity is maximised, the transmissions from a mobile station are power controlled by a fast accurate closed loop. The loop uses the downlink PCC channel to send a stream of power control commands. Each command is a single bit, indicating that the mobile should either "turn up" or "turn down" its power. The bit rate may be set to one of a range of values, the greatest being 4 kbps. These bits are generated in the base station receiver, by comparing an estimate of the post-despreading signal-to-noise ratio with a preset threshold. The power control step in the mobile may be set to either 1 or 2 dB. The mobile station has an 80 dB range in its output power.

#### 7.2.4.3 Mobility Manager Design

The mobility manager provides the interface (control and user) between the fixed ISDN terminal equipment and the base station(s) via 2.048 Mb/s G.704 links. In particular, the MM converts the speech/data to a format that is acceptable to interface with the radios, i.e. convolutional encoding/Viterbi decoding for all control/traffic channels and the interleaving/de-interleaving function. In addition, it can support the diversity handover function as the mobile station passes from one base station operational region to another.

#### 7.2.5 Validation and Test Bed Performance

Testing was broken down into four phases:

- Phase 1 - Basic error rate measurements performed on the bench with the multipath simulator. These were carried out at the unencoded rate of 128kbps.
- Phase 2 - As with Phase 1 but at 64kbps with coding and interleaving.
- Phase 3 - Radiating tests in the laboratory.

- Phase 4 - Repeat of Phase 3 test but fully mobile in various outdoor environments.

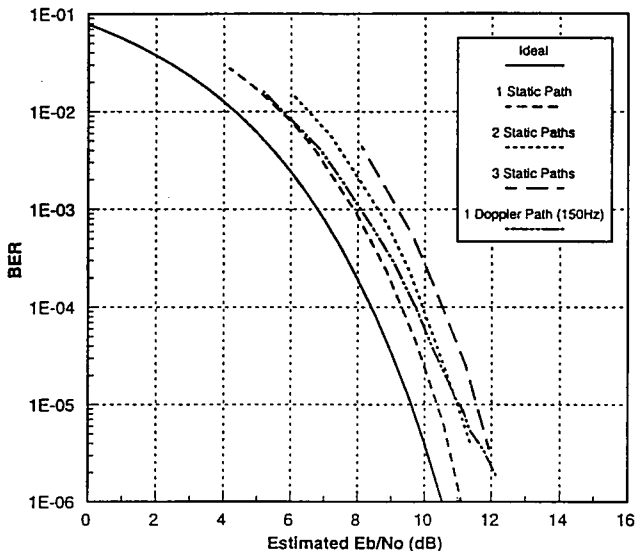


Figure 7.2.6 Uplink BER measurements with the channel simulator.

At the time of writing, only Phase 1 and 2 have been completed to any extent, with radiating tests limited to the laboratory environment [21]. One of the many basic sets of BER measurements is given in figure 7.2.6 for the uplink using a multipath channel simulator developed by the consortium. This provides up to 9 parallel paths, each having its attenuation controlled either manually or via a PC. Instantaneous bandwidth in excess of 10MHz is provided together with delays in the range 5ns to 1000ns; Doppler can also be added to one of the paths.

The different curves shown in figure 7.2.6 represent four simulated channels. Note that no power control is employed and that the averaging process in the channel estimator is over 32 channel filter outputs. This corresponds to a period of 0.25msec or an update rate of 4kHz. The static channel employed increasing numbers of fixed, equal amplitude paths with offsets from the undelayed path (single path) of 250nsec and 500nsec respectively. This ensures that no paths are within a single chip period. The single path offers an additive white Gaussian noise (AWGN) channel. Using equal amplitude paths in the multiple path channels provides a "worst case" scenario. The Doppler path is a single path with a fixed amplitude and a 150Hz offset.

The system performs best with the single static path channel, as expected. There is an implementation loss (relative to the theoretical performance of a perfect coherent receiver on an AWGN channel, also shown on the graph) of

between 1 and 2dB. This implementation loss is slightly worse for high BERs than for low ones, being around 1.5dB at a BER of 10<sup>-2</sup>, a possible operating point for the coded system.

The BER over a static two path channel is only slightly worse than for a single path channel. This proves the rake receiver to be giving a multipath gain. Without the rake a degradation of at least 3dB would be inevitable. A further and more severe degradation is apparent when the channel moves to three static paths. The degradation is about 1dB. When a 150Hz frequency offset between mobile and base station is included, the performance for a single path is slightly worse. This is because the channel estimation loop is too slow to track the changing carrier phase accurately. There is however no cycle slipping and no irreducible BER.

### 7.2.6 Conclusions

The results obtained to date by the consortium illustrate that a DS-CDMA radio link based on a single mobile, base station and mobility manager for a sub-set of the UMTS teleservices is viable. The system supports two common channels (pilot and synchronisation) and three channels per user (power control, forward control and forward traffic) on the downlink. On the uplink it supports a common random access channel and two channels per user (reverse control and reverse traffic). All channels on the same link are code separated with a common chipping rate of 8.192 Mchip/s. The mobility manager architecture can support several base stations, handling ISDN control signals, converting between line and radio signal formats including coding and interleaving, and supporting diversity handover.

A range of special test equipment and assessment tools was developed to support the design of future generation CDMA systems, and employed here to facilitate bit error rate testing over a multipath simulator with and without coding and interleaving. This clearly demonstrating the need for these functions, and the trade off between channel estimator averaging time and Doppler tracking capability. Further, the diversity gain of the Rake receiver was clearly demonstrated. In addition, the robustness of the synchronisation process and the effects of varying the power control loop update rate were also demonstrated.

Many potential follow-on activities have been identified, both for exploiting the test-bed as a facility and building on the spirit of collaboration which has been built up among the partners.

## 7.3 Code Time Division Multiple Access

by Jürg Ruprecht (Swiss Telecom PTT), Urs Loher, Gerhard Krämer  
 (ETH Zentrum, Switzerland)

### 7.3.1 Designs Rationale

The most popular multiple accessing techniques for cellular systems, Time Division Multiple Access (TDMA) and Code Division Multiple Access (CDMA), have their own advantages, but also some disadvantages. In TDMA, there is no intracell interuser interference but the high peak-to-average power and the necessary frequency planning or dynamic channel allocation between adjacent cells detract from the utility of this scheme. On the other hand, CDMA excels in just these areas: a constant-envelope signal is transmitted and a cluster size of one can be used. However, a limiting factor in CDMA is intracell interuser interference. To combine the advantages of CDMA and TDMA, Massey (unpublished) proposed a wideband communications system for *indoor* cellular applications called *Code Time Division Multiple Access (CTDMA)* [31]. In particular, CTDMA can yield a peak-to-average power ratio of one and a cluster size of one. Moreover, interuser interference is resolved using the same techniques as the resolving of intersymbol interference in TDMA.

### 7.3.2 System Description

*Code Time Division Multiple Access (CTDMA)* incorporates both CDMA and TDMA aspects: whereas the signal sent over the air interface is spread in a CDMA fashion, the processing at the receiver is similar to that of a TDMA receiver. Hereafter, we describe its discrete-time baseband representation (cf. Figures 1 and 2) that will be used throughout this section.

The binary information sequence  $b_k[\cdot]$  of user  $k$ ,  $0 \leq k < K$ , is encoded and mapped to the complex sequence  $x_k[\cdot]$  which has a symbol rate  $R_X$ . The sequence  $x_k[\cdot]$  is oversampled (or “expanded”) and delayed by  $\Theta_k$  chips to yield a symbol-level TDMA sequence  $d_k[\cdot]$ . The sequence  $d_k[\cdot]$  is then sent through a linear filter  $s[\cdot]$  of length  $L$  which is common to all users in one cell. Thus, in effect,  $d_k[\cdot]$  has been “spread in time” by  $s[\cdot]$ , or alternatively  $x_k[\cdot]$  has been spread in a DS-CDMA fashion by a spreading sequence  $s[\cdot]$  and then delayed by  $\Theta_k$  chips. The spread sequence  $q_k[\cdot]$  passes through a user-specific multipath channel with impulse response  $h_k[\cdot]$  and is distorted by additive white Gaussian noise with zero mean and variance  $\sigma_z^2 = \mathcal{N}_0$ , where  $\mathcal{N}_0$  is the noise power density. The receiver then sees the sequence  $r_k[\cdot]$ .

In order to separate the users, the receiver of user  $k$  passes the incoming sequence  $r_k[\cdot]$  through the *aperiodic inverse filter*  $v[\cdot]$  [30] of the spreading se-

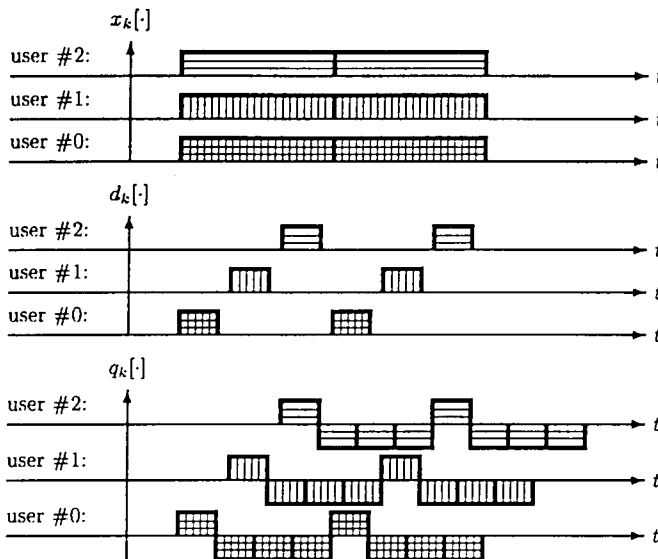


Figure 1: CTDMA example for  $K = 3$  users: The modulated/mapped information sequences  $x_k[\cdot]$  (for clarity, we have only used “+1”-symbols), TDMA separation on a symbol level ( $d_k[\cdot]$ ) and spreading in time by the common spreading sequence  $(+1, -1, -1, -1)$  of length  $L = 4$  ( $q_k[\cdot]$ ).

quence  $s[\cdot]$ . A perfect implementation of the inverse filter  $v[\cdot]$  completely reverses the spreading and, if the durations of the impulse responses  $h_k[\cdot]$  of the multipath channels do not exceed the TDMA guard time, perfectly separates the users such that there is no intracell interuser interference that usually appears in CDMA.

To assure a constant-envelope transmitted signal for each user, we shall hereafter assume that  $|x_k[i]| = 1$  (all  $i$ ) and  $|s[n]| = 1$  (all  $0 \leq n < L$ ), which yields a peak-to-average power ratio of one in the transmitted sequences  $q_k[\cdot]$ . The TDMA guard time is defined by the *relative user offsets*  $\Delta_k$ , which are the transmission time differences (in chips) of the two adjacent users  $k$  and  $k-1$ , and which may be dynamically allocated. The *absolute user offsets* are then given by  $\Theta_k = \sum_{i=0}^k \Delta_i$  (in chips).

The *aperiodic inverse filter*  $v[\cdot]$  is defined by

$$(v * s)[n] = \sum_{l=-\infty}^{\infty} v[l] s[n-l] = \sum_{l=0}^{L-1} v[n-l] s[l] = \begin{cases} 1 & \text{if } n=0 \\ 0 & \text{otherwise,} \end{cases} \quad (1)$$

where we have used the fact that  $s[n] = 0$  for  $n < 0$  and  $n \geq L$ . In theory, the

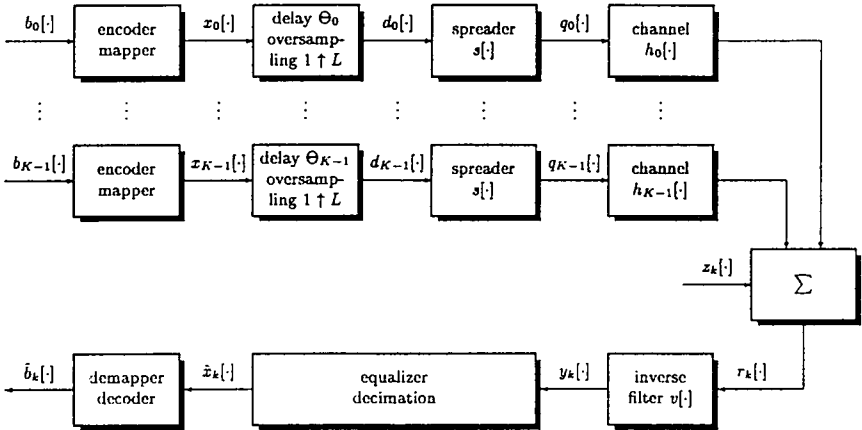


Figure 2: Block diagram of a CTDMA system.

inverse filter completely eliminates the sidelobes that appear in matched filter processing and that is the reason why the matched filter is not recommended in a CTDMA receiver. The drawback of the inverse filter is its poorer noise performance when compared to the matched filter, which is known to maximize the signal-to-noise ratio  $SNR$  at the filter output. However, there exist suitable binary  $(\pm 1)$ -sequences where the loss in  $SNR$  compared to the matched filter is less than  $0.5 dB$  [30, 31, 33]. This loss is referred to as the inverse filter noise enhancement factor  $\varepsilon^{(vs)}$ , which in turn defines the inverse filter processing gain  $G^{(vs)} = L/\varepsilon^{(vs)}$ . Another drawback of the aperiodic inverse filter is that it has non-zero coefficients  $v[n]$  in the entire range  $-\infty < n < \infty$  [30]. Therefore, it must be implemented by a finite length approximation  $v_N[\cdot]$  [30]. Usually, a length of  $N = 3L$  in  $v_N[\cdot]$  suppresses the sidelobes in  $s[\cdot] * v_N[\cdot]$  well below  $40 dB$ , which is sufficient for practical applications.

## CTDMA Receiver Design

In a multipath environment, the transmitted signal propagates via a multipath channel with impulse response  $h(t)$ , an example of which is illustrated in Figure 3. In environments for which the excess delay is small, i.e., within a few chips,  $\Delta_k$  may be made large enough to eliminate interuser-interference. More precisely, there is no interuser-interference in a multipath environment if

$$\Delta_k \geq \frac{\max(\tau_E)}{T_c},$$

where  $T_c$  is the chip duration. Since one may use the same frequency band in all cells, allowing a small increase in  $\Delta_k$  causes no capacity degradation with respect to the classical schemes FDMA and TDMA that use different frequency bands in adjacent cells. E.g.,  $\Delta_k = 7$  provides the same capacity as a classical scheme with a cluster size of 7.

As soon as the excess delay exceeds the relative user-shift, however, such as in hilly terrain where  $\tau_E$  is typically larger than  $5\mu s$ , interuser-interference occurs, e.g., for chip rates of  $1.25 M\text{Chips}/s$  and  $\Delta_k = 6 \text{ chips}$ .

To combat this interference, one could simply shift the users further apart. At some point, however, the spectral efficiency would be too severely diminished so that we must allow some interuser interference in the received signal, i.e., an equalizer is needed. For example, one may want to use a Viterbi Algorithm to resolve the interference, but then one is throwing out “soft” information which is useful for the decoder [26]. A better choice for the equalizer is the Forward-Backward Algorithm [29], or some variant of this algorithm (see, e.g., [23] or the more recent [24]). A disadvantage of this maximum *a posteriori* equalizer is certainly that its complexity grows exponentially with the number of overlapping users, but because of the relative user shifts, the number of overlapping users in a CTDMA system is relatively small even for long multipath channels. For instance, in an outdoor environment, where a maximum excess delay of  $\tau_E = 20\mu s$  is not unusual, and a relative user-shift of  $\Delta = 4.8\mu s$  is used (which corresponds to 6 chips at  $1.25 MHz$ ) there are only four overlapping users, which is still manageable. Moreover, this receiver concept is applicable to both the downlink and the uplink.

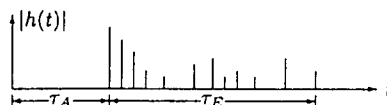


Figure 3: Example of a multipath channel impulse response  $h(t)$  with absolute delay  $\tau_A$  and excess delay  $\tau_E$ .

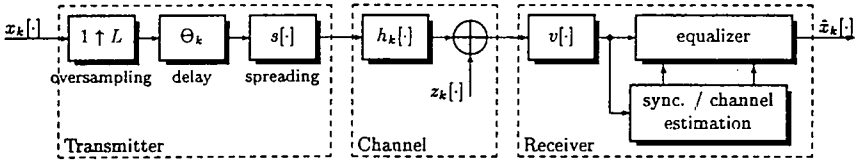


Figure 4: CTDMA transmitter, noisy multipath channel and CTDMA receiver.

Figure 4 shows the corresponding CTDMA transmitter, noisy multipath channel and receiver: the encoded and mapped data sequence  $x_k[\cdot]$  of user  $k$  is oversampled with a factor of  $L$ , shifted by  $\Theta_k$  chips and spread with  $s[\cdot]$  in a CDMA fashion. The multipath channel  $h_k[\cdot]$  and the additive white Gaussian noise sequence  $z_k[\cdot]$  distort this transmitted signal. The receiver despreading the signal with the inverse filter  $v[\cdot]$  of  $s[\cdot]$ , passes it through the equalizer and decimates this sequence by a factor of  $L$  in order to get the soft decision estimate  $\hat{x}_k[\cdot]$  for  $x_k[\cdot]$ .

The necessary synchronization and channel estimation information can be obtained in an easy manner by using a pilot signal in both the downlink and the uplink. In the downlink one of the user slots is reserved for a symbol rate pilot, and in the uplink a pilot symbol is sent intermittently.

### Cellular CTDMA

The considerations above are valid for a CTDMA system with *one* cell. An extension to several cells within the same frequency band is possible by using different spreading sequences and allowing intercell interuser interference.

For good system performance, we must require that all spreading sequences have a low inverse filter noise enhancement factor  $\epsilon^{(vs)}$  (which limits the noise influence), that the spreading factor  $L$  is large enough for the signal bandwidth to be at least in the order of the coherence bandwidth (yielding a diversity gain) and that any particular cell's sequence causes as little interference as possible at the outputs of the inverse filters of all the other cells.

Given the basic binary spreading sequence  $s[\cdot]$  of length  $L$  with inverse filter noise enhancement factor  $\epsilon^{(vs)}$  and corresponding inverse filter processing gain  $G^{(vs)}$ , the “frequency-shifted” sequences

$$s^{(m)}[n] = s[n] e^{j \frac{2\pi m n}{L}}, \quad m = 0, 1, \dots, M-1, \text{ all } n, \quad (2)$$

where  $M$  is the *sequence cluster size*, are all constant envelop complex sequences with the same parameters  $L$ ,  $\epsilon^{(vs)}$ , and  $G^{(vs)}$ . The “frequency” offset guarantees fairly good crosscorrelation properties between  $s^{(m)}[\cdot]$  and  $v^{(n)}[\cdot]$  for  $m \neq n$ , where  $v^{(n)}[\cdot]$  is the inverse filter for the  $n$ -th sequence  $s^{(n)}[\cdot]$ . For

realization,  $s^{(m)}[\cdot]$  can be implemented as  $s[\cdot]$  with a carrier frequency offset  $mf_o$ , where

$$f_o = \frac{1}{L \cdot T_C} = \frac{1}{T_B}$$

(where  $T_C$  and  $T_B$  denote the chip and bit durations, respectively), i.e.,

$$s^{(m)}[n] = s[n] e^{j2\pi mn f_o T_C},$$

such that only one sequence generator and one inverse filter implementation are needed for all cells. Note that, in [22], this approach has been proposed for intracell user separation in Code Frequency Division Multiple Access (CFDMA).

### 7.3.3 System Performance

As the basic  $\pm 1$  spreading sequence, we shall use the length-32 sequence with a hex representation of 00F2D533 that provides the smallest noise enhancement of all sequences of the same length [32, 33]. Its inverse filter noise enhancement factor is only  $\epsilon^{(vs)} = 0.74 \text{ dB}$ , and it yields an inverse filter processing gain of  $G^{(vs)} = 14.3 \text{ dB}$ .

Instead of the true inverse filter  $v[\cdot]$ , which is of infinite length, a truncated version  $v_N[\cdot]$  of length  $N = 134$  chips is used, which has a *peak/off-peak ratio (POP-ratio)*

$$\rho_N^{(vs)} = \frac{|(v_N * s)[0]|}{\max_{m \neq 0} |(v_N * s)[m]|}$$

of  $\rho_{134}^{(vs)} = 40 \text{ dB}$ .

Simulation results for this CTDMA system in a fading environment are shown in Figure 5. These simulations were performed for a single cell in which there were 8 users ( $\Delta_k = 4$ ) sending their data at  $40 \text{ kSymb/s}$ , which results in a chip rate of  $1.28 \text{ MChips/s}$  and in a gross symbol rate of  $320 \text{ kSymb/s}$ . Thus, the efficiency is only 25% ( $= 1/\Delta_k = 1/4$ ) for this *single* cell. We note, however, that the efficiency will improve if one considers the *cellular* environment with frequency reuse, or if one makes  $\Delta_k$  smaller.

The channel model used in the simulations was the COST-207 Rural Area model at a carrier frequency of  $900 \text{ MHz}$  and a velocity of  $100 \text{ km/h}$ . We put 4th-order Butterworth filters with baseband bandwidths of  $625 \text{ kHz}$  at the output and input of the transmitter and receiver, respectively. The channel response was estimated using a symbol rate pilot for the downlink and a pilot sent every four symbols for the uplink (note that this implies that the information rate for the uplink is reduced by 25%). As the channel response length was short, a matched filter with 3 fingers was used to provide the decoder with soft

inputs. The code used was the maximum  $d_{free}$  rate-1/2 binary convolutional code with constraint length 6 [25] decoded with the Viterbi Algorithm, and a  $4 \times 2.5\text{ ms}$  interleaver was used to mitigate the effects of fading. Perfect chip synchronization was assumed for all simulations. In Figure 5, the reference curve labelled "AWGN" is the error performance for an uncoded signal sent over the additive white Gaussian noise channel.

The simulations indicate that one loses about 1 to 2 dB on the uplink due to poorer channel estimation. This loss could be reduced, of course, by sending a pilot symbol more often.

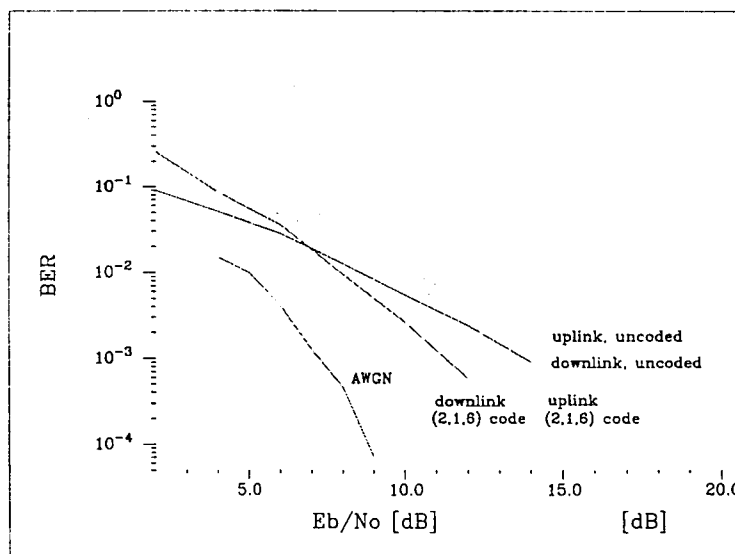


Figure 5: CTDMA error performance for the COST-207 RA100 channel model.

### 7.3.4 Service Provision

In this section we consider the implementation of several services: By means of orthogonal Walsh-Hadamard layers, orthogonal user families with symbol rather than chip level inter-family synchronization requirements are introduced. This approach is then applied to accommodate multiple and variable bit rates, and to separate connection-oriented and connectionless, as well as, in a different cell separation scenario, to provide a dynamic mixed-cell architecture. Note that, for sake of simplicity, no additional protocol information is considered in the described scenarios; these have to be added and the corresponding rates have to be changed accordingly for a real-world system.

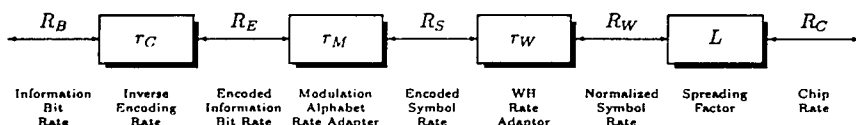


Figure 6: Rates overview of a generalized CTDMA system.

### Rates Overview

Figure 6 shows the various rates in a generalized CTDMA system. The rate adapters are used to generate a large variety of data rates. The CTDMA encoder converts the information bit rate  $R_B$  into the encoded information bit rate  $R_E = r_C R_B$ , where  $r_C$  is the inverse encoding rate of a rate- $\frac{1}{r_C}$  error correcting code. The adaption to the encoded symbol rate  $R_S = r_M R_E$  is done via the modulation alphabet rate adaptor with factor  $r_M$ , where  $r_M = 1/\log_2(A)$  and where  $A$  is the modulation alphabet size (in the case of BPSK,  $A = 2$  and  $r_M = 1$ , and for QPSK,  $A = 4$  and  $r_M = 1/2$ ). We shall see below that these factors  $r_C$  and  $r_M$  have to be designed such that the requirements on  $R_S$  are met. These requirements are that only discrete values of  $R_S$  are allowed, namely  $R_S = R_C/L$ ,  $R_S = kR_C/L$ , or  $R_S = 2^{-k}R_C/L$  ( $k = 1, 2, 3, \dots$ ).

This rate  $R_S$  is then adapted to the (fixed) normalized symbol rate  $R_W$  by means of a Walsh-Hadamard (WH) rate adaptor: If  $R_S = R_W$  then there is no rate adaption necessary and  $r_W = 1$ . If  $R_S > R_W$ , multiple time slots are used for the transmission of this signal and  $r_W = k$  ( $k=1,2,3, \dots$ ). If  $R_S < R_W$ , a Walsh-Hadamard coding technique (cf. Section "Orthogonal Walsh-Hadamard Layers") increases the rate by factors of  $2^k$ , and we get  $r_W = 2^k$ . In this latter case,  $2^k$  such users can sometimes be assigned the same time slot.

This rate  $R_W$  is then multiplied by the spreading factor  $L$  in order to obtain the chip rate  $R_C = LR_W$ .

### Orthogonal Walsh-Hadamard Layers

Given the basic CTDMA system with chip rate  $R_C$ , spreading factor  $L$  and encoded symbol rate  $R_S = R_C/L$ , several orthogonal Walsh-Hadamard (WH) layers can be implemented in CTDMA: Given a set of  $Q = 2^k$  orthogonal WH sequences  $w_q[\cdot]$  ( $q = 0 \dots Q-1$ ) of length  $Q$ , the encoded symbols of the basic CTDMA system can be further encoded with these sequences  $w_q[\cdot]$ . We then get  $Q$  orthogonal user families, each providing basic symbol rates of  $R_S/Q$ . Note that there is a need of an inter-family synchronization within  $Q$  symbol duration  $QT_S$  (which is the duration of  $Q$  WH symbols) corresponding to chip numbers 0 to  $QL - 1$ : All chip numbers  $n$  in the range  $0 \leq n < L - 1$  can be used to allocate time slots, but not the ones in  $L \leq n < QL - 1$ .

As examples, we hereafter depict the WH codes of lengths  $Q = 2$  and  $Q = 4$ :

$$\begin{array}{ll} N = 2 : & w_0[\cdot] = [+1, +1] \\ & w_1[\cdot] = [+1, -1] \\ N = 4 : & w_0[\cdot] = [+1, +1, +1, +1] \\ & w_1[\cdot] = [+1, -1, +1, -1] \\ & w_2[\cdot] = [+1, +1, -1, -1] \\ & w_3[\cdot] = [+1, -1, -1, +1] \end{array}$$

We will see that this technique of layering signals is very convenient for both multiple and variable bit rates as well as, in some cases, for the design of dynamic mixed-cell architectures.

### Multiple Bit Rates

Multiple information bit rates, i.e., different user bit rates, can be accommodated via appropriate design of the parameters  $r_C$ ,  $r_M$  and  $r_W$ . Some examples are given in Table 7. If  $r_W > 1$ , more than one user can be allocated to the same time slot (as stated in “Rates Overview” and in “Orthogonal Walsh-Hadamard Layers”).

### Variable Bit Rates

Variable information bit rates, i.e., information bit rates of one specific user that vary during transmission, can be accommodated the same way as above with multiple bit rates. Here, due to the statistical nature of the information bit rate change, no additional users can usually be allocated to the same time slot; the overall system however still benefits by a decreased intercell interference.

### Connection-Oriented and Connectionless Service

We propose to use the WH codes of length  $Q = 2$ , i.e.,  $w_0[\cdot] = [+1, +1]$  and  $w_1[\cdot] = [+1, -1]$  to separate connection-oriented and connectionless services.

The codes  $w_0[\cdot]$  and  $w_1[\cdot]$  can then be assigned to the connection-oriented and the connectionless services, respectively (or vice versa). As long as the inter-family synchronization requirements mentioned in the Section “Orthogonal Walsh-Hadamard Layers” are fulfilled and ideal inverse filtering is applied, both services do not interfere with each other. A practical inverse filter realization will however cause very little interference between the two service types.

### Mixed-Cell Architecture

In “Cellular CTDMA” of Section 7.3.2, CFDMA was proposed to separate adjacent cells. Different cell types in a hierarchical mixed-cell architecture (where e.g. umbrella cells cover several underlying micro cells) can then be separated only by FDMA, i.e., by allocating non-overlapping frequency bands to different cell hierarchies. However, the cell separation within the same hierarchy can still be done by CFDMA. This is a rather rigid solution since the corresponding capacities cannot be shared between the layers.

Another promising, yet not deeply investigated cell separation technique, is to allocate the same spreading sequences and center frequencies to all cells and to adopt a *dynamic channel allocation (DCA)* technique (as is done for instance in DECT by applying a TDMA/TDD scheme) to maintain the required link quality. If the transmission of a user is distorted by strong interference, e.g., when the same time-slot in an adjacent cell is occupied by a very close user, one of this two users has to change the time-slot allocation. Since in this scenario, either none or only a few users are involved into mutual interference, an implementable *interferer separation (IS)* technique could be applied for capacity enhancements. This would be a more dynamic solution since capacities can softly be allocated to both hierarchies.

#### 7.3.5 Chip Rates, Spreading Factors, Symbol Rates and Bit Rates

For given chip rates of 0.2, 1, 5 and 20M $\text{Chips}/\text{s}$ , we have evaluated the corresponding symbol rates for the case of no WH code application ( $Q = 1$ ), the case of length-2 WH code application ( $Q = 2$ ) and the case of length-4 WH code application ( $Q = 4$ ) and listed the results in Table 8. These results emphasize that a spreading factor of  $L = 2^5 = 32$  rather than the previously considered case of  $L = 169$  might be a good choice; Table 9 therefore summarizes the corresponding results for  $L = 32$ .

Table 7 then gives examples for possible rate scenarios for  $L = 32$  and  $R_C$  in the order of 0.2, 1, 5 and 20M $\text{Chips}/\text{s}$ . The following assumptions were made in this table:

Info Bit Rate $R_B$ [kBits/s]	Inverse Encoding Rate $r_C$	Encoded Information Bit Rate $R_E$ [kBits/s]	Modulation Alphabet Rate Adaptor $r_M$	Encoded Symbol Rate $R_S$ [kSymb/s]	WII Rate Adaptor $r_W$	Normalized Symbol Rate $R_W$ [kSymb/s]	Spreading Factor $L$	Chip Rate $R_C$ [MChips/s]
16	5/2	40	1/2	20	1/4	5	32	0.16
16	5/4	20	1/2	10	1/2	5	32	0.16
12	5/3	20	1/2	10	1/2	5	32	0.16
8	5/2	20	1/2	10	1/2	5	32	0.16
8	5/4	10	1/2	5	1	5	32	0.16
128	5/2	320	1/2	160	1/4	40	32	1.28
128	5/4	160	1/2	80	1/2	40	32	1.28
64	5/2	160	1/2	80	1/2	40	32	1.28
64	5/4	80	1/2	40	1	40	32	1.28
32	5/2	80	1/2	40	1	40	32	1.28
32	5/4	40	1/2	20	2	40	32	1.28
16	5/2	40	1/2	20	2	40	32	1.28
16	5/4	20	1/2	10	4	40	32	1.28
12	5/3	20	1/2	10	4	40	32	1.28
8	5/2	20	1/2	10	4	40	32	1.28
8	5/4	10	1/2	5	8	40	32	1.28
512	5/2	1280	1/2	640	1/4	160	32	5.12
512	5/4	640	1/2	320	1/2	160	32	5.12
256	5/2	640	1/2	320	1/2	160	32	5.12
256	5/4	320	1/2	160	1	160	32	5.12
128	5/2	320	1/2	160	1	160	32	5.12
128	5/4	160	1/2	80	2	160	32	5.12
64	5/2	160	1/2	80	2	160	32	5.12
64	5/4	80	1/2	40	4	160	32	5.12
32	5/2	80	1/2	40	4	160	32	5.12
32	5/4	40	1/2	20	8	160	32	5.12
16	5/2	40	1/2	20	8	160	32	5.12
16	5/4	20	1/2	10	16	160	32	5.12
12	5/3	20	1/2	10	16	160	32	5.12
8	5/2	20	1/2	10	16	160	32	5.12
8	5/4	10	1/2	5	32	160	32	5.12
2048	5/2	5120	1/2	2560	1/4	640	32	20.48
2048	5/4	2560	1/2	1280	1/2	640	32	20.48
1024	5/2	2560	1/2	1280	1/2	640	32	20.48
1024	5/4	1280	1/2	640	1	640	32	20.48
512	5/2	1280	1/2	640	1	640	32	20.48
512	5/4	640	1/2	320	2	640	32	20.48
256	5/2	640	1/2	320	2	640	32	20.48
256	5/4	320	1/2	160	4	640	32	20.48
128	5/2	320	1/2	160	4	640	32	20.48
128	5/4	160	1/2	80	8	640	32	20.48
64	5/2	160	1/2	80	8	640	32	20.48
64	5/4	80	1/2	40	16	640	32	20.48
32	5/2	80	1/2	40	16	640	32	20.48
32	5/4	40	1/2	20	32	640	32	20.48
16	5/2	40	1/2	20	32	640	32	20.48
16	5/4	20	1/2	10	64	640	32	20.48
12	5/3	20	1/2	10	64	640	32	20.48
8	5/2	20	1/2	10	64	640	32	20.48
8	5/4	10	1/2	5	128	640	32	20.48

Figure 7: Rates examples of a generalized CTDMA system (protocol overhead neglected).

Chip Rate $R_C$ [MChips/s]	Spreading Factor $L$	Encoded Symbol Rate $R_S$ [kSymb/s]		
		for $Q = 1$	$Q = 2$	$Q = 4$
0.2	16	12.50	6.25	3.13
0.2	20	10.00	5.00	2.50
0.2	24	8.33	4.17	2.08
0.2	28	7.14	3.57	1.79
0.2	32	6.25	3.13	1.56
0.2	36	5.56	2.78	1.39
0.2	40	5.00	2.50	1.25
0.2	44	4.55	2.27	1.14
0.2	48	4.17	2.08	1.04
0.2	52	3.85	1.92	0.96
0.2	56	3.57	1.79	0.89
0.2	60	3.33	1.67	0.83
0.2	64	3.13	1.56	0.78
1.0	16	62.50	31.25	15.63
1.0	20	50.00	25.00	12.50
1.0	24	41.67	20.83	10.42
1.0	28	35.71	17.86	8.93
1.0	32	31.25	15.63	7.81
1.0	36	27.78	13.89	6.94
1.0	40	25.00	12.50	6.25
1.0	44	22.73	11.36	5.68
1.0	48	20.83	10.42	5.21
1.0	52	19.23	9.62	4.81
1.0	56	17.86	8.93	4.46
1.0	60	16.67	8.33	4.17
1.0	64	15.63	7.81	3.91
5.0	16	312.50	156.25	78.13
5.0	20	250.00	125.00	62.50
5.0	24	208.33	104.17	52.08
5.0	28	178.57	89.29	44.64
5.0	32	156.25	78.13	39.06
5.0	36	138.89	69.44	34.72
5.0	40	125.00	62.50	31.25
5.0	44	113.61	56.82	28.41
5.0	48	104.17	52.08	26.04
5.0	52	96.15	48.08	24.04
5.0	56	89.29	44.64	22.32
5.0	60	83.33	41.67	20.83
5.0	64	78.13	39.06	19.53
20.0	16	1250.00	625.00	312.50
20.0	20	1000.00	500.00	250.00
20.0	24	833.33	416.67	208.33
20.0	28	714.29	357.14	178.57
20.0	32	625.00	312.50	156.25
20.0	36	555.56	277.78	138.89
20.0	40	500.00	250.00	125.00
20.0	44	454.55	227.27	113.64
20.0	48	416.67	208.33	104.17
20.0	52	384.62	192.31	96.15
20.0	56	357.11	178.57	89.29
20.0	60	333.33	166.67	83.33
20.0	64	312.50	156.25	78.13

Figure 8: CTDMA chip rates  $R_C$ , spreading factors  $L$  and encoded symbol rates  $R_S$  for  $Q = 1, 2$  and  $4$  orthogonal WH families (protocol overhead neglected).

Chip Rate $R_C$ [MChips/s]	Spreading Factor $L$	Symbol Rate $R_S$ [kSymb/s] for $Q$ orthogonal WH families:		
		$Q = 1$	$Q = 2$	$Q = 4$
0.2	32	6.25	3.13	1.56
1.0	32	31.25	15.63	7.81
5.0	32	156.25	78.13	39.06
20.0	32	625.00	312.50	156.25

Figure 9: CTDMA chip rates  $R_C$  and encoded symbol rates  $R_S$  for a fixed spreading factor  $L = 32$  and  $Q = 1, 2$  and  $4$  orthogonal WH families (protocol overhead neglected).

- The chip rates corresponding to the bandwidths 0.2, 1, 5 and 20 MChips/s are assumed to be 0.16, 1.28, 5.12 and 20.48 MChips/s. This approach is very convenient since there are only factors of  $2^k$  between these rates, i.e.,  $1.28 = 8 \times 0.16$ ,  $5.12 = 4 \times 0.16$ ,  $20.48 = 4 \times 0.16$ .
- We assume a fixed modulation alphabet of  $A = 4$  (QPSK modulation) resulting in a modulation alphabet rate adaptor of  $r_M = 1/2$ . Of course,  $r_M = 1/\log_2(A)$  could also be varied, which could add even more flexibility to the system.
- We further assume that there is only one service type offered, i.e., there is no additional Walsh-Hadamard layer implemented to distinguish connection-oriented and connectionless services or to split into several cell-hierarchies as is the case in a mixed-cell architecture of the above mentioned DCA cell separation scenario. In these other cases the rates have to be changed accordingly.

The following observations can then be made from Table 7:

- The function of the inverse encoding rate  $r_C$  is, beside its main task to protect the data against errors, to translate the information rate  $R_B$  in some discrete realizations of  $R_E$ , since the CTDMA-chip rate is fixed. Since the corresponding values of  $R_S$  must be  $R_S = R_C/L$ ,  $R_S = kR_C/L$ , or  $R_S = 2^{-k}R_C/L$  ( $k = 1, 2, 3, \dots$ ) and  $r_M$  is assumed to be 1/2,  $R_E$  must then take on values  $R_E = R_S/r_M$ , i.e.,  $R_E = R_C/(Lr_M)$ ,  $R_E = kR_C/(Lr_M)$ , or  $R_E = 2^{-k}R_C/(Lr_M)$  ( $k = 1, 2, 3, \dots$ ).
- The required service quality can, within the required values, still decide what order of inverse encoding rate  $r_C$  shall be implemented. In Table 7, it is usually either 5/2 or 5/4 (except, for  $R_B = 12$  kBits/s,  $r_C = 5/3$ ). It could, however, also take on any value described by  $5/4 \times 2^k$  ( $k = 0, 1, 2, \dots$ ).

Note again that these figures do not account for protocol overhead.

### 7.3.6 Compatibility with GSM

GSM is basically a TDMA system offering 8 users to transmit at approximately  $24\text{kBits/s}$  each with an overlayed FDMA channel spacing of  $200\text{kHz}$ . In order to reduce intercell interference to an acceptable level, a (frequency) cluster size of around 12 must be implemented.

A CTDMA system with  $200k\text{Chips}$  could be installed within these  $200\text{kHz}$ -channels. If a relatively short sequence is used as a spreading sequence (e.g.,  $L = 32$ ), a symbol rate close to  $12k\text{Symbols/s}$  corresponding to  $24\text{kBits/s}$  (due to QPSK modulation in CTDMA) can be provided to each user. With appropriate time shifts, a pilot and at least one (but less than 8) users can be allocated to the same frequency in a specific cell. A frequency cluster size of about 1 then improves the overall Erlang capacity at least to the one of GSM.

After the cluster size is fixed, multiple adjacent channels can be combined in order to offer larger channel spacings and higher bit rates (wherever necessary).

## 7.4 Joint Detection CDMA

by P.W. Baier, J.J. Blanz, P. Jung, A. Klein, M.M. Naßhan, A. Steil and B. Steiner, Research Group for RF Communications, University of Kaiserslautern, Kaiserslautern, Germany

### 7.4.1 Designs rationale

A key issue in the development of a new mobile radio system concept, evolving from second generation mobile radio, is the organization of the multiple access (MA). In a new mobile radio system concept, the MA can be based on the well-known basic MA principles [35, 36] code division multiple access (CDMA), frequency division multiple access (FDMA) and time division multiple access (TDMA). It is vital for the successful development of a new mobile radio system concept to thoroughly understand the key issues and hence the advantages and disadvantages of these three basic MA principles.

All of the second generation mobile radio systems are based on hybrid MA schemes. The most common hybrid MA scheme is F/TDMA already applied in GSM [37] and also proposed for the RACE II concept ATDMA [38]. Hence, it is reasonable to assume that third generation mobile radio systems such as UMTS (Universal Mobile Telecommunication System) and FPLMTS (Future Public Land Mobile Telecommunications System), which is also termed IMT-2000 (International Mobile Telecommunications 2000), are also going to use hybrid MA schemes. In this section, the designs rationale, i.e. the selection of the hybrid MA scheme, for a joint detection CDMA (JD-CDMA) mobile radio system concept developed within COST 231 shall be explained.

It is beyond question that UMTS and FPLMTS, providing global coverage, must use FDMA, consequently enabling frequency planning and reuse, flexible frequency allocation as well as intercell interference control [36]. Furthermore, the implementation of overlay concepts is eased by using FDMA. Now, it is the question whether FDMA shall be combined with only CDMA such as described in [39], only TDMA such as in [38] or a combination of both CDMA and TDMA, cf. e.g. [40]. The pros of TDMA are capacity advantage over CDMA, because intracell interference is avoided, and high degree of acceptance, because the most successful second generation mobile radio system GSM [37] uses TDMA. The main disadvantages of TDMA are increased intersymbol interference therefore requiring the application of adaptive equalizers, high momentary peak transmission powers leading to EMC problems, mutual synchronization of the users and lack of flexibility [36]. The pros of CDMA are frequency diversity, interferer diversity and a flexibility advantage over TDMA because user signals can be switched on and off independently and data rates can be chosen individually [36, 39]. The cons of CDMA are oc-

currence of intracell interference and its novelty to mobile radio and therefore lack of acceptance [36, 39].

Since none of the MA schemes CDMA and TDMA seems to incorporate the ultimate advantage, it is a tempting idea to inherit the capacity advantage of TDMA on the one hand and the flexibility advantage of CDMA on the other hand to a hybrid MA scheme, comprising a proper combination of FDMA, TDMA and CDMA and therefore termed F/T/CDMA. F/T/CDMA may enjoy broad acceptance by being based on known standards and is therefore a promising candidate for UMTS and FPLMTS.

The benefits of F/T/CDMA shall be discussed in this paragraph. Figure 10 shows two hybrid MA schemes. A total of 24 users is considered in the examples of Figure 10. In Figure 10a the conventional hybrid MA scheme F/TDMA, e.g. being used in GSM [37] where the time slots have duration  $\Delta t$  equal to 576.9  $\mu$ s and the frequency slots have width  $\Delta f$  equal to 200 kHz, and in AT-DMA [38] with  $\Delta t$  equal to e.g. 277.8  $\mu$ s and  $\Delta f$  equal to 276.9 kHz, is depicted. Each of the rectangles in Figure 10a represents one user burst. An optional CDMA component is introduced into the F/TDMA MA scheme of Figure 10a, by pooling the narrow frequency slots, having width  $\Delta f$ , of spectrally adjacent users, e.g. of users five to eight in the first time slot to a wider frequency slot, and by occupying this wider frequency slot commonly by user signals five to eight in such a way that these user signals are spectrally spread by user specific CDMA codes to this wider frequency slot. This approach is schematically depicted in Figure 10b. The larger the number of pooled frequency slots, the more distinct the CDMA component. In the second time slot of Figure 10b, eight original narrow frequency slots of width  $\Delta f$  are pooled and in the third time slot of Figure 10b no pooling at all occurs and, consequently, no CDMA component is applied in this third time slot. As demonstrated in Figure 10b a CDMA component can be introduced very flexibly whenever it pays with respect to both capacity and flexibility. A dynamically reconfigurable hybrid MA and channel allocation scheme is thus obtained.

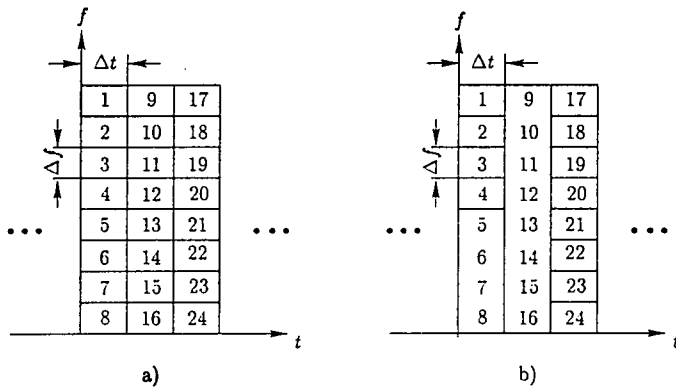


Figure 10: Hybrid multiple access schemes

- a) F/TDMA multiple access scheme used in GSM [37] and ATDMA [38]
- b) adaptive flexible multiple access scheme combining FDMA and TDMA with CDMA

#### 7.4.2 System description

##### Uplink

In this section, the more elaborate uplink of the JD-CDMA mobile radio system concept shall be described in detail [40, 41]. Figure 11 shows the uplink frame structure which is, as mentioned above, similar to GSM [37] and ATDMA [38]. Table 1 contains an overview over the main system parameters [40, 41]. A maximum of  $K$  equal to 8 mobiles are simultaneously transmitting signals of bandwidth  $B$  equal to 1.6 MHz in the same frequency band of width  $B$  equal to 1.6 MHz. The above-mentioned user signals can be distinguished by their different user specific CDMA codes. The transmission occurs by using a single transmitter antenna per mobile. In the considered JD-CDMA mobile radio system, the user signals are received over  $K_a$  equal to one or two receiver antennas at the base stations. Thus, either no or dual receiver antenna diversity are considered [41, 42].

The structure of the bursts transmitted by each of the 8 mobiles is depicted in Figure 12. Each burst has duration  $T_{bu}$  equal to 500  $\mu$ s. The radio channel can be regarded as time invariant during that time period  $T_{bu}$  which is favourable with respect to the receiver complexity. According to Figure 12 each burst consists of two data blocks containing  $N$  equal to 24 quaternary data symbols, each block having a duration of 168  $\mu$ s, a user specific midamble of duration

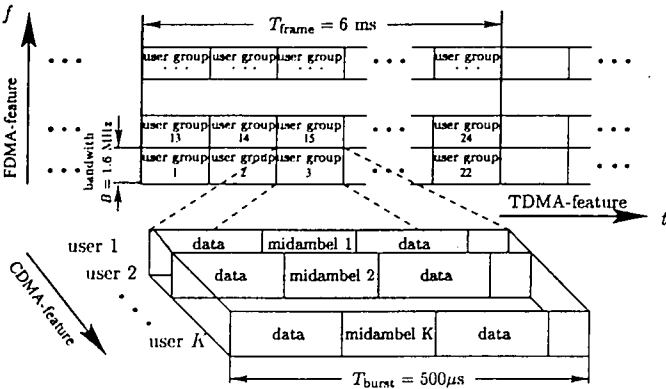


Figure 11: Uplink frame structure of the JD-CDMA mobile radio system concept

$134 \mu s$  containing  $L_m$  equal to 268 binary midamble chips of duration  $T_c$  equal to  $0.5 \mu s$  which is used for channel estimation [43], and a guard interval of duration  $T_g$  equal to  $30 \mu s$ . Each quaternary data symbol has a period  $T_s$  equal to  $7 \mu s$  and is spread by a user specific CDMA code of  $Q$  equal to 14 chips with a chip duration  $T_c$  equal to  $0.5 \mu s$ . With respect to the TDMA component of the JD-CDMA mobile radio system, the eight different mobiles simultaneously transmit bursts in a time slot of duration  $T_{bu}$  equal to  $500 \mu s$ . Twelve such time slots make up one TDMA frame of duration  $D_{bu}$  equal to 6 ms. Taking into account both CDMA and TDMA components, respectively, 96 different mobile users can be accommodated per frequency band of bandwidth  $B$  equal to 1.6 MHz [40]. By allocating more than one time slot as well as more than one user specific CDMA code to a particular mobile, services with different gross bit rates between 16 kbit/s and 1536 kbit/s can be provided. Due to the use of channel coding with code rate  $R_c$  equal to  $1/2$ , the user bit rate can be varied between 8 kbit/s and 768 kbit/s depending on the required service.

The block structure of an uplink transmitter is shown in Figure 7.4.2. This uplink transmitter [40, 41] consists of

- a data source,
- a channel encoder, which is either a conventional convolutional encoder with code rate  $R_c$  equal to  $1/2$ , constraint length 5 and octal generators 23, 35, or the Turbo-Code TC-BL of [44],
- a  $4 \times 96$  block interleaver,

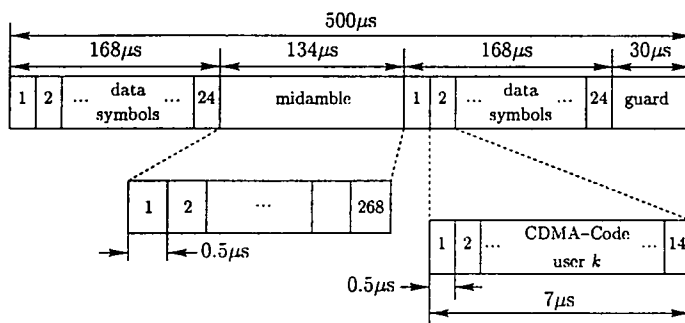


Figure 12: Uplink burst structure of the JD-CDMA mobile radio system concept

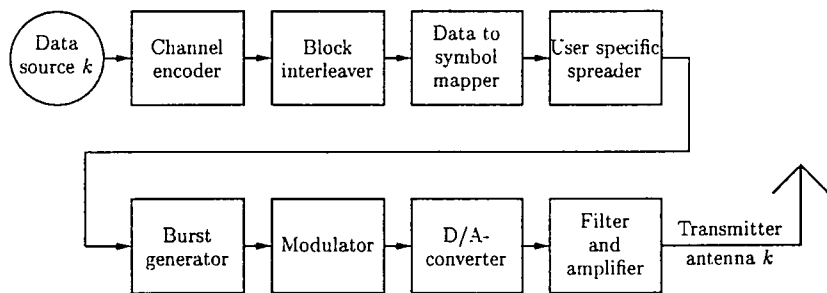


Figure 13: Block structure of an uplink transmitter of the JD-CDMA mobile radio system concept

<b>general:</b>	$K_a = 1, 2$ $B = 1.6 \text{ MHz}$ $D_{bu} = 6 \text{ ms}$  $12$  $K = 8$ $8 \text{ kbit/s} \leq R \leq 768 \text{ kbit/s}$ ZF-BLE, MMSE-BLE, ZF-BDFE, MMSE-BDFE
<b>filters:</b>	analogue transmitter filter Butterworth filter, order 4, cutoff frequency 1.6 MHz analogue receiver filter Butterworth filter, order 10, cutoff frequency 1.2 MHz digital receiver filter ≈ ideal low pass filter, cutoff frequency 1MHz
<b>burst structure:</b>	burst duration $T_{bu} = 0.5 \text{ ms}$ midamble chips $L_m = 268$ guard interval $T_g = 30 \mu\text{s}$ data symbols per data block $N = 24$ symbol duration $T_s = 7 \mu\text{s}$ data modulation scheme 4PSK chips per symbol $Q = 14$ chip duration $T_c = 0.5 \mu\text{s}$ spreading modulation scheme linearized GMSK, time-bandwidth-product 0.3
<b>channel encoder:</b>	NSC constraint length $K_c = 5$ rate $R_c = 1/2$ generators in octal 23, 35 RSC for Turbo-Code TC-BL constraint length $K_c = 5$ rate $R_c = 1/2$ generators in octal 37, 21
<b>block interleaver:</b>	interleaving matrix $4 \times 96$ interleaving depth $I_D = 4 \text{ bursts}$

Table 1: Important system parameters of the uplink

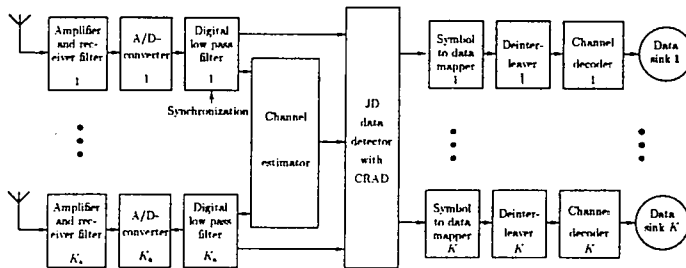


Figure 14: Base station receiver of the JD-CDMA mobile radio system concept

- a data to symbol mapper,
- a user specific spreader,
- a burst generator,
- a digital modulator,
- a D/A converter,
- a transmitter filter and an amplifier as well as
- a transmitter antenna.

The data source generates speech frames containing 192 bits. Each speech frame is encoded by the channel encoder. The 384 coded data bits are then interleaved by applying a block interleaver with an interleaver matrix of 4 rows an 96 columns. The 384 coded and interleaved data bits are then mapped onto 192 4PSK data symbols. Each 4PSK data symbol is spread by the user specific CDMA code allocated to mobile  $k$ . Then,  $I_D$  equal to 4 bursts as shown in Figure 12 are generated based on the 192 spread 4PSK data symbols and the user specific midambles [43, 41]. After linear modulation by using a linearized version of Gaussian minimum shift keying (GMSK) with time-bandwidth-product 0.3 and D/A conversion, the signal is passed through a Butterworth low pass filter of order 4 and cutoff frequency 1.6 MHz. Finally, this signal is amplified [41].

Figure 7.4.2 shows the block structure of the base station receiver. In the base station receiver, coherent receiver antenna diversity (CRAD) [42] is applied. This base station receiver [40, 41] consists of

- $K_a$  receiver antennas,
- $K_a$  amplifiers and receiver filters,
- $K_a$  A/D converters,
- $K_a$  digital low pass filters,
- $K_a$  channel estimators,
- a JD data detector with CRAD, cf. Sect 6.6 and [41, 42],
- $K$  symbol to data mappers,
- $K$   $96 \times 4$  block deinterleavers,
- $K$  channel decoders and
- $K$  data sinks.

The amplified signal received at each receiver antenna  $k_a$ ,  $k_a = 1 \dots K_a$ , is the sum of additive stationary noise and the 8 user signals, associated with the eight simultaneously active mobiles, which are distorted with the  $8 \cdot K_a$  time varying and frequency selective mobile radio channels. After low pass filtering this amplified signal by using a Butterworth low pass filter of order 10 and cutoff frequency 1.2 MHz, A/D conversion takes place at a sampling rate of  $2/T_c$  [41]. A synchronization unit at the receiver compensates for slightly different delay times of the  $K_a$  received signals. The set of samples is then digitally low pass filtered in order to allow decimation of the sampling rate to  $1/T_c$ . The particular parts of the received sequence stemming from the user specific midamble are processed by the  $K_a$  channel estimators. The JD data detector with CRAD which uses predetection maximal-ratio combining then determines continuous valued estimates for the  $2 \cdot K \cdot N$  equal to 384 data symbols. The four suboptimum JD techniques ZF-BLE, MMSE-BLE, ZF-BDFE and MMSE-BDFE are available at the JD data detector with CRAD, cf. Sect. 6.6 and [41, 42]. The  $2 \cdot N$  equal to 48 complex and continuous valued estimates of the data symbols transmitted by each mobile  $k$ ,  $k = 1 \dots K$ , are then mapped onto a real valued data stream of 96 samples. After four bursts were processed, the 384 real valued samples are deinterleaved and convolutionally decoded by a soft input decoder. The  $K$  decoded data sequences are then transferred to the  $K$  data sinks.

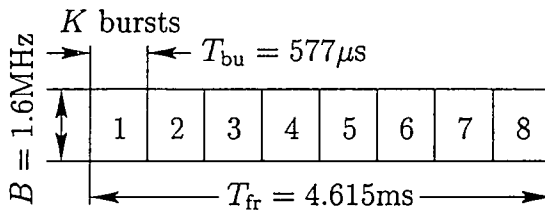


Figure 15: Downlink frame structure of the JD-CDMA mobile radio system concept

### Downlink

In this section, the downlink of the JD-CDMA mobile radio system concept is briefly introduced [45]. We only refer to both the frame and burst structures, respectively. Due to their close relationship to the uplink transmitters and receivers, the downlink transmitters and receivers shall not be described here.

Figure 7.4.2 shows the downlink frame structure of the JD-CDMA mobile radio system concept. It is obvious from Figure 7.4.2 that the downlink is fully compatible with GSM [37]. Nevertheless, compatibility to ATDMA [38] can easily be achieved. Like in the uplink,  $K$  equal to 8 users are simultaneously active in the same frequency band of bandwidth  $B$  equal to 1.6 MHz and in the same time slot of duration  $T_{\text{bu}}$  equal to  $577\mu\text{s}$ . Eight such time slots form one TDMA frame of duration  $T_{\text{fr}}$  equal to 4.615 ms. The transmission occurs by using a single transmitter antenna per base station. In the considered JD-CDMA mobile radio system concept, antenna diversity can be implemented in the downlink receivers in a similar fashion to the Japanese Personal Digital Cellular [46].

The minimum net data rate per user is set to be 13 kbit/s in the downlink. As it is the case in the uplink the data rate can be varied with respect to the desired service by assigning more than one time slot as well as more than one user specific CDMA code to a particular user. The maximum net bit rate is thus equal to 832 kbit/s. It is easy to see that in the downlink only a single radio channel must be estimated at the receiver in order to enable coherent reception. Therefore, the midamble used in the downlink is shorter, taking only  $T_m$  equal to  $64.5\mu\text{s}$ , than the midamble required for the uplink channel estimation which is  $134\mu\text{s}$  long. The chip period in the downlink is the same as in the uplink, namely  $T_c$  equal to  $0.5\mu\text{s}$ . However, the number of elements contained in a user specific CDMA code is 16 in the downlink. In contrast to the up-

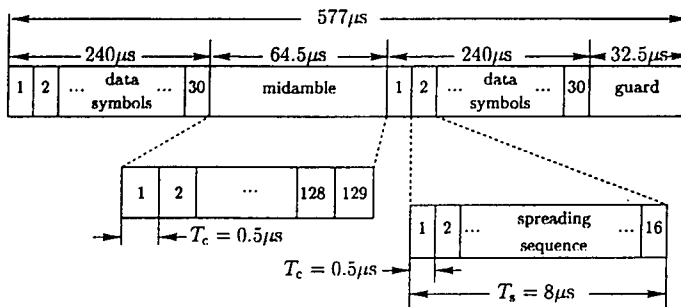


Figure 16: Downlink burst structure of the JD-CDMA mobile radio system concept

link, orthogonal binary user specific CDMA codes are applied in the downlink which enables a better performance than in the case of using nonorthogonal user specific CDMA codes, e.g. randomly chosen user specific CDMA codes.

### Performance

The performance of the JD-CDMA mobile radio system concept was studied e.g. in Sect. 6.6 and [41, 42, 43].

### Acknowledgements

The editors are grateful to Mr D. Grace of the University of York for his assistance in preparing this chapter.

## 7.5 References

- [1] M. Streeton, A. Urie and C. Mourot. "An Advanced TDMA Mobile Access System for UMTS," *IEEE Personal Communications*, February 1995.
- [2] *RACE Mobile Telecommunications Workshop*, Amsterdam, May 17-19, 1994.
- [3] *RACE Mobile Telecommunications Summit*, Cascais Portugal, 22nd-24th November 1995.
- [4] "ATDMA System Definition, Issue 4," *R2084/AMCF/PM2/DS/P/056/b1*, March 1995.
- [5] A. Urie and M. Streeton, "System model for adaptive cellular mobile systems," *Proceedings of 2nd International Conference on Universal Personal Communications*, 12-15 October 1993, Ottawa.
- [6] J. DeVile, "A reservation multiple access scheme for an adaptive TDMA air interface," *4th WINLAB workshop*, 19 Nov. 1993
- [7] D. J. Goodman, "Cellular Packet Communications," *IEEE Trans. Comms.*, Vol. 38, pp 1272-1280, August 1990.
- [8] E. Le Strat and A. Wautier, "Distance based dynamic adaptation of the air interface in TDMA," *Proceedings of the IEEE 2nd Symposium on communications and Vehicular Technologies in the Benelux*, Nov. 2-3 1994, Louvain-la-Neuve, Belgium.
- [9] C. Mourot, "A High bitrate transmission technique in mobile radio cellular environment," *Proceedings of the 42nd IEEE Veh. Tech. Conf., Denver, CO*, May 1992, pp 740-743.
- [10] "Ad hoc 8 kb/s speech coding Group," *ITU-TS SG15*,
- [11] "Digital PLMN channel structures and access capabilities at the radio interface (Um reference point)," *Q.1063, CCITT, Blue book 1988*,
- [12] "Report of System Performance," *R2084/DTM/SP4/DS/P/045/b1*, March 1995.
- [13] Alcatel France and Siemens, "Recommendations to SMG5 from RACE 2084 ATDMA Project," *Temporary doc. SMG5 TD (95) 386*, Presented at ETSI SMG5 #15, Dresden, 11-15/12/95

- [14] "LINK CDMA Consortium, "Workpackage 1000: Service Requirements," *Project Deliverable*, Version 2.0, Feb. 1993.
- [15] "Framework and Services to be Supported by UMTS," *ETR/SMG-050201*, Annex C.
- [16] R.S. Swain, "UMTS & MBS System Requirements," *Race Communications Summit*, Cascais, Portugal, 22-24th November, 1995.
- [17] S.C. Swales, T. Busby, D.J. Purle and M.A. Beach, "A Comparison of CDMA Techniques for Third Generation Mobile Radio Systems," *43rd IEEE Vehicular Technology Conference*, New Jersey, USA, May 1993, pp.424-427.
- [18] "LINK CDMA Consortium, "Workpackage 2100: Summary of CDMA Traffic Capacity Analysis"," *Project Deliverable*, Version 1.2, Sept. 1993.
- [19] F. De Ferrari, C.I'Anson, M.Vocale and J.Waters, "Assessment Methods for a CDMA Trial System," *IEEE COMSOC'93*, Tokyo, Dec 1993.
- [20] N. Livneh, R. Meidan, M.Ritz and G. Silbershatz, "Frequency Hopping CDMA for future cellular Radio," *IEEE 42nd VTC*, pp404-404, May 1992.
- [21] S.C.Swales, J.P.Aldis, T.Busby, S.K.Barton and M.A.Beach, "A DS-CDMA Air Interface for UMTS," *ibid [16]*.
- [22] Günther, C.G., Ruprecht, J., Habermann, J., Rüegg, R., Jung, P., "Code frequency division multiple access: A downlink multiplexing in support of effective multi-user equalization," *Proceedings of the 2nd International Conference on Universal Personnel Communications ICUPC'93*, Ottawa, pp. 39-43, October 1993.
- [23] Hagenauer, J., Hoeher, P., "A Viterbi Algorithm with soft-decision outputs and its applications," *Proc. Globecom '89*, vol.3, pp. 47.1.1-47.1.7, Nov. 1989.
- [24] Li, Y., Vucetic, B., Sato, Y., "Optimum Soft-Output Detection for Channels with Intersymbol Interference," *IEEE Trans. Inform. Theory*, vol. IT-41, no. 3, pp. 704-713, May 1995.
- [25] Lin, S., Costello, D.J., *Error Control Coding: Fundamentals and Applications*, Prentice-Hall, Englewood Cliffs, N.J., 1983.

- [26] Massey, J.L., "Coding and Modulation in Digital Communications," *Proc. IEEE Int. Zurich Sem. Digital Comm.*, pp. E2(1)-(4), 1974.
- [27] Massey, J.L., *Code Time Division Multiple Access*, private correspondence (unpublished), 1989.
- [28] Proakis, J.G., *Digital Communications*, Singapore: McGraw-Hill, 1989.
- [29] Rabiner, R.L., "A Tutorial on Hidden Markov Models and Selected Applications in Speech Recognition," *Proc. IEEE*, vol. 77, no. 2, pp. 257-286, Feb. 1989.
- [30] Ruprecht, J., *Maximum-Likelihood Estimation of Multipath Channels*, ISBN 3-89191-270-6, Hartung Gorre Verlag, Konstanz, Germany, 1989.
- [31] Ruprecht, J., Neeser, F.D., Hufschmid, M., "Code time division multiple access: An indoor cellular system," in *Proceedings of the 42nd IEEE Vehicular Technology Conference*, Denver, 1992.
- [32] Ruprecht, J., Rupf, M., "On the search and construction of good invertible binary sequences", *Proceedings of the 1994 IEEE International Symposium on Information Theory ISIT'94*, Trondheim, Norway, 1994.
- [33] Ruprecht, J., Rupf, M., "On the design of aperiodic binary invertible sequences," to be published in *IEEE Trans. Info. Th.*, 1996/97.
- [34] Salmasi, A., Gilhausen, K.S., "On the system design of code division multiple access (CDMA) applied to digital and personal communication networks," *Proceedings of the 41th IEEE Vehicular Technology Conference*, St. Louis, 1991, pp. 57-62.
- [35] Simon, M. K.; Omura, J. K.; Scholtz, R. A.; Levitt, B. K.: Spread spectrum communications. Vol. III, Rockville: Computer Science Press, 1985.
- [36] Baier, P. W.: CDMA or TDMA? CDMA for GSM? Invited paper. *Proceedings of the 5th International Symposium on Personal, Indoor, and Mobile Radio Communications (PIMRC '94)*, The Hague, pp. 1280-1284, 1994.
- [37] Mouly, M.; Pautet, M.-B.: The GSM system for mobile communications. Published by the authors, ISBN 2-9507190-0-7, 1992.

- [38] Cygan, D.; David, F.; Eul, H. J.; Hofmann, J.; Metzner, N.; Mohr, W.: RACE-II advanced TDMA mobile access project – an approach for UMTS. Proceedings of the 1994 International Zürich Seminar on Digital Communications, pp. 428-439, 1994.
- [39] Baier, A.; Fiebig, U.-C. G.; Granzow, W.; Koch, W.; Teder, P.; Thielecke, J.: Design study for a CDMA-based third-generation mobile radio system. IEEE Journal on Selected Areas in Communications, vol.12, pp. 733-743, 1994.
- [40] Blanz, J. J.; Klein, A.; Naßhan, M. M.; Steil, A.: Performance of a cellular hybrid C/TDMA mobile radio system applying joint detection and coherent receiver antenna diversity. IEEE Journal on Selected Areas in Communications, vol. 12, pp. 568-579, 1994.
- [41] Jung, P.; Blanz, J. J.; Naßhan, M. M.; Baier, P. W.: Simulation of the up-link of JD-CDMA mobile radio systems with coherent receiver antenna diversity. Wireless Personal Communications – An International Journal (Kluwer Academic Publishers), vol. 1, pp. 61-89, 1994.
- [42] Jung, P.; Blanz, J. J.: Joint detection with coherent receiver antenna diversity in CDMA mobile radio systems. IEEE Transactions on Vehicular Technology, vol. 42, 1995.
- [43] Steiner, B.; Jung, P.: Optimum and suboptimum channel estimation for the uplink of CDMA mobile radio systems with joint detection. European Transactions on Telecommunications and Related Technologies (ETT), special issue on “Multiple Access in Radio Communication Networks”, vol. 5, pp. 39-50, 1994.
- [44] Jung, P.; Naßhan, M. M.: Dependence of the error performance of Turbo-Codes on the interleaver structure in short frame transmission systems. Electronics Letters, vol. 30, pp. 287-288, 1994.
- [45] Naßhan, M. M.; Steil, A.; Klein, A.; Jung, P.: Downlink cellular radio capacity of a joint detection CDMA mobile radio system. To be presented at IEEE 45th Vehicular Technology Conference (VTC-1995), session on “Joint Detection for CDMA”, Chicago, 1995.
- [46] Lorenz, R. W.: Comparison of digital mobile radio systems in Europe (GSM) and in Japan (JDC) with special consideration of commercial aspects (in German). Der Fernmelde-Ingenieur, vol. 47, no. 1 & 2/93, 1993.



## Broadband Systems

**Stephen Barton, University of Leeds, UK**

### 8.1 Introduction

This chapter is concerned with wireless communication to mobile, or at least portable, equipment at very high data rates, defined for this purpose as greater than 2 Mbit/s, so as to ensure that there is no overlap with UMTS. Such systems are generally referred to as Wireless Local Area Networks (WLANs). Such fourth generation systems have been addressed by a small group within COST231 (Working Group 3, Broadband Systems) between 1989 and 1996. Such systems will form an increasingly important focus of the proposed follow-on project. Systems operating at data rates up to 155 Mbit/s have been proposed and studied by simulation.

Initially, operating frequencies in the Millimetre Wave (mmw) bands or at Infra Red (IR) were considered the only viable ranges offering sufficiently large contiguous blocks of spectrum not already allocated to other services. IR was eliminated quite early because of considerations of eye safety, and most of the propagation work concentrated on the mmw bands. Subsequently however, spectrum at 5.2 and 17.2 GHz has been allocated by CEPT to HIPERLAN, a system with a transmission rate of 23.5 Mbit/s, and material about broadband transmission in HIPERLAN is included in the later sections.

Material originating in RACE project 2067, Mobile Broadband System (MBS), and ESPRIT project 7359, Local Area network User Radio Access (LAURA), together with many independently funded projects contributing to COST 231 WG3 is also included.

Initial applications of WLANs will be in wired LAN replacement. This is because in large organisations typically 30% of computer networks are relocated or reorganised every year, and this can account for over 80% of the lifetime cost of a LAN. A system providing the last 50 m connection from the end user to the backbone fibre optic network over the air would save most of this. WLANs can also be installed rapidly, often by the users themselves, and may also provide an opportunity to try out the services available before committing to the investment in a full-scale fibre-based network. Access to the services provided by private wired computer networks such as Ethernet and FDDI, or the future ATM based B-ISDN public network will be via centrally controlled access points at data rates high enough to maintain the quality of service. Once such radios are installed in portable equipment, however, there will be a desire to operate in other locations

remote from the central base station. This leads to the requirement to support distributed architecture ad-hoc networks.

The chapter is organised as follows: in section 8.1.1 the reasons for rejecting IR are briefly reviewed. Section 8.1.2 covers safety and technology aspects of mmw, leading to the decision to concentrate on these bands. Sections 8.2, 8.3 and 8.4 deal with various aspects of radio propagation at 60 GHz. 8.2 covers the characterisation of building materials in terms of their reflection and scattering properties, and methods of estimating these from measurements of dielectric constant and loss tangent on samples of brick, concrete, plaster, wood, glass, etc. 8.3 deals with narrow-band and wide-band measurements of the indoor radio channel, and compares these with statistical and deterministic models derived from the material properties. 8.4 makes the corresponding comparisons for the outdoor radio channel. Section 8.5 deals with the performance of digital modulation systems over the point-to-point radio channels characterised in the last two sections. Section 8.6 deals with network architectures, both centralised and distributed, and Medium Access Control (MAC) protocols designed to provide efficient and fair sharing of the radio channel among users. Finally, section 8.7 summarises the chapter.

### 8.1.1 Infra-Red Safety

IR has an abundance of bandwidth free from regulation, and IR components are small and inexpensive. It is already used at very low data rates, eg TV remote control, car keys etc, and at rates up to a few hundred kbit/s for linking palmtop computers. IR penetrates glass, but not walls, allowing neighbouring cells to co-exist without interference. However, the received power levels required by IR systems are much higher than those of radio systems. This is because the photodetector is exposed to ambient noise sources such as sunlight, incandescent and fluorescent lamps, and heaters. An optical filter has been proposed to minimise this effect, but this then becomes a key cost driver. In order to provide full mobility, diffuse links relying on scattering from the local environment are essential, and this leads to transmit power requirements that are beyond the current state of the art.

It is possible to support a 50 Mbit/s transmission rate over distances up to 30 m provided a lens is used to direct the transmitted beam towards the intended receiver. However, stringent limitations on power densities a few cm from the transmitter are imposed by eye safety considerations. The human eye focuses the incident light on to the retina increasing the energy density by factors of 100,000 or more. The Maximum Possible Exposure (MPE) levels are therefore quite small. The cornea, the outer layer of the eye, filters out all wavelengths except those in the visible and near infrared range. The eye thus forms a window for infrared light. Exposure to high levels of IR radiation may damage the eye leading to cataract-like disorders. Various standards organizations worldwide have specified MPEs for IR. They are nearly in consensus on a  $1.6 \text{ mW/cm}^2$  limit. The power limits on infrared

transmitters imposed by safety considerations eliminate the possibility to use IR for reliable broadband communications in cells with radii in excess of about a few metres. A detailed analysis of these considerations is given in reference [1].

### 8.1.2 Millimetre wave Safety and Technology

Mmw radiation is relatively harmless compared with the conventional mobile UHF frequency bands. The reason is the much smaller electromagnetic skin depth of biological tissues at these frequencies. This is reflected in the existing safety limits of transmitted power. For many European countries, these limits are laid down in the Recommendations of the International Non-Ionizing Committee, a working group of the International Radiation Protection Association (IRPA/INIRC).

The maximum power density for continuous exposure for the general public is 1 mW/cm<sup>2</sup> for mmw. Assuming that this limit is set at 6 cm from an antenna with 9 dBi directivity, the transmitted power is limited to about 50 mW. Limiting transmit power levels to some tens of mW is not only a safety requirement, but also a measure to limit the coverage range in order to improve the frequency reuse capabilities, with the objective of gaining network capacity.

The safety limit of 50 mW transmitted power is about equal to the power level that is feasible with state-of-the-art technology at 60 GHz. A preliminary feasibility study [2] showed that 50 mW might be sufficient for reliable broadband communication in a typical office environment. This may be realizable by taking advantage of advances in Microwave and Millimetre wave Monolithic ICs (M<sup>3</sup>ICs), which will supply the signals to the Very High Speed Integrated Circuit (VHSIC) chips at a rate that is compatible with the high processing speeds. The maturity of these technologies has already been demonstrated, although the initial costs of producing such systems can be quite high. However, with large-volume manufacturing of individual circuit functions, the costs can be competitive when compared with installing new copper or fibre networks.

Low-power transmission at mmw frequencies enables improved portability of hand-held equipment because low power implies light and small-sized batteries and mmw radio-frequency components and antennas are small, with dimensions in the order of only a few centimetres. However, it is important to realize that radio receivers for high bit rate signals have to perform complex signal processing order to combat radio channel imperfections to meet the performance requirements. These requirements are much more stringent than requirements for low speed data and coded speech as supported by the present radio networks. Although the intensive signal processing may be performed by sophisticated VHSIC technology it may be expected that the required complexity will contribute significantly to the size and weight of initial broadband radio equipment.

In view of the safety limitations of IR and the apparent lack of suitable blocks of free spectrum below the mmw bands, the next three sections will concentrate

exclusively on short range propagation effects at mmw. Sections 8.5 and 8.6 contain material which is also relevant to 5.2 and 17.2 GHz operation.

## 8.2 Material Characterisation

Luis Correia, IST, Portugal

Propagation phenomena at the mmw band can be modeled simply on the basis of Geometrical Optics (GO) since diffraction is usually negligible. The use of GO models requires knowledge of the reflection coefficients of the surfaces, which depend on the electrical properties of the materials. Thus, besides the characterization of the surface roughness, it is essential to know the values of the relative dielectric constant,  $\epsilon_r$ , and the loss tangent,  $\tan(\delta)$  of the building materials used in both indoor and outdoor environments. The lack of values for these parameters in the literature, in particular at mmw, has motivated the work on materials characterization.

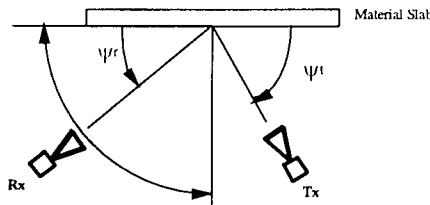
Additionally, the isolation and transmission properties of materials have been calculated, in order to evaluate both indoor coverage in different rooms and co-channel interference not only between indoor and outdoor systems but also among indoor systems.

### 8.2.1 Measurement Methods

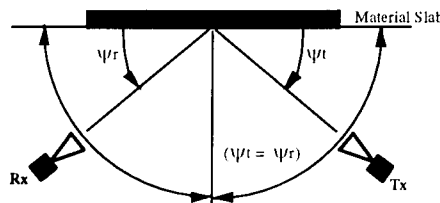
The electromagnetic characteristics, such as  $\epsilon_r$  and  $\tan(\delta)$ , of materials cannot be measured directly in most cases. This implies that other quantities must be measured, from which these parameters can be estimated. The two usual procedures are: 1) to insert a sample of material within a waveguide and perform standing wave measurements, and 2) to illuminate a slab of material in an anechoic chamber, and perform reflected and transmitted power measurements. The first is very difficult to use at the mmw frequencies, since waveguides have dimensions of a few mm and this would imply samples of bricks or plaster, for example, with such dimensions, which is impractical. Therefore, all the measurements were done using the second procedure.

In general, three types of measurements have been conducted, as shown in Fig. 8.2.1(a), (b), and (c). The scattering patterns (a) allow the surface roughness to be investigated. The bistatic reflection (b) corresponds to the measurement of the specular reflection coefficient, from which the parameters can be estimated. The transmission pattern (c) includes the measurement of the actual transmission coefficient, also enabling the estimation of parameters. Measures of reflectivity,  $R$ , and transmissivity,  $T$ , are special cases. The first corresponds to the bistatic reflection with  $\psi_t = \psi_r = \pi/2$  and the second is the transmission with  $\psi_t = \pi/2$ . In all cases, power is measured relative to a reference: received power from free space

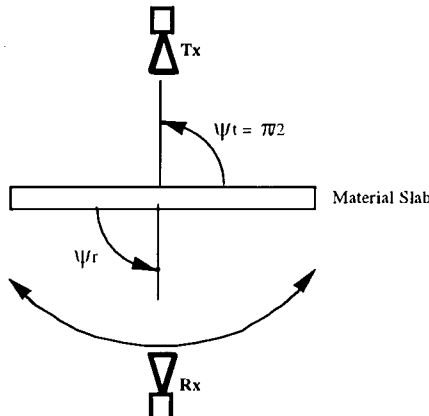
propagation for the transmission case; received power from reflection on a perfectly conducting plane for the reflection case.



(a) scattering pattern: for several  $\psi_t$ ,  $\psi_r$  varies over range



(b) bistatic reflection:  $\psi_t = \psi_r$  over range



(c) transmission pattern:  $\psi_t$  fixed,  $\psi_r$  varies over range

Fig. 8.2.1 Measurement setups for power measurements

### 8.2.2 Measurement Results and Parameter Estimation

Several groups within WG3 were involved in materials characterization in the 60 GHz band, using one of the measurement procedures described above. Initially reflectivity [3] and transmissivity [4] measurements were conducted. However, these results did not allow the estimation of the electromagnetic parameters, and a literature survey [5] has shown that values for  $\epsilon_r$  and  $\tan(\delta)$  were known only for glass and wood. Thus, measurements allowing the estimation of parameters were conducted: transmissivity for different slab thicknesses [6]; scattering and transmission patterns, and bistatic reflection measurements [7], [8]. Since it is not possible to extract the values of  $\epsilon_r$  and  $\tan(\delta)$  directly from the measurements, a model is needed.

The phenomenon of reflection of a plane wave by a perfectly flat infinite surface separating two indefinite media is well known, and can be described by a pair of reflection coefficients, according to the wave polarization. The reflection coefficients  $\Gamma$  can be found in many text books (e.g. [9]); they are a function of the incident angle (to the surface plane)  $\psi$ , and of the refraction coefficient of the medium  $n$ , which can be expressed by  $n^2 = \epsilon_r - j \epsilon_r \tan(\delta)$ . When the material thickness is large (compared to the wavelength) and/or the material losses are high, the reflection of a plane wave on a dielectric slab can be approximated by the reflection coefficient referred to above. However, when these conditions are not satisfied, this simple model can lead to significant errors, and a better model is necessary. The model that leads to a better approximation, and yet is not too complicated, is the one based on successive reflections of plane waves, as indicated in Fig. 8.2.2. With this model, the reflected field can be expressed by a generalized reflection coefficient,  $\Gamma_g$ , given as the addition of the simple reflection coefficient (from the first reflection) with the sum of a geometric progression corresponding to the reflections and transmissions inside the slab

$$\Gamma_g = \Gamma(1 - (1 - \Gamma^2) e^{-j2ks} e^{-2\alpha s} e^{jk_0 d} \cos(\psi)) / \Delta \quad (8.2.1)$$

and a generalized transmission coefficient,  $\tau_g$ , can then be obtained as well

$$\tau_g = (1 - \Gamma^2) e^{-jks} e^{-\alpha s} / \Delta \quad (8.2.2)$$

where:

$k = 2\pi\sqrt{\epsilon_r}/\lambda$  is the propagation constant inside the slab;

$\alpha = \omega \tan(\delta) \sqrt{\mu_0 \epsilon_r \epsilon_0} / 2$  is the attenuation coefficient, also inside the slab;

$k_0 = 2\pi/\lambda$  is the free space propagation constant,

and the denominator,  $\Delta = 1 - \Gamma^2 e^{-j2ks} e^{-2\alpha s} e^{jk_0 d} \cos(\psi)$ .

The path length inside the slab between the two surfaces is:

$$s = \ell / \sqrt{1 - (\cos^2(\psi) / \epsilon_r)}.$$

The path length difference on the slab of two consecutive departing reflections or transmissions is  $d = 2 \ell / \sqrt{(\epsilon_r / \cos^2(\psi)) - 1}$ .

With this model, reflected and transmitted powers from the dielectric slab will then be given simply by

$$P^r = |\Gamma_g|^2 P^i \text{ and } P^t = |\tau_g|^2 P^i,$$

$P^i$  being the power of the incident wave; since it is assumed that the material is lossy, one has  $P^r + P^t < P^i$ . Although this model assumes that the slab is infinite, it can be expected that the results will be acceptable if the material sample is wide enough (compared with the intersection of Fresnel's first ellipsoid). Also it will contribute to a better approximation of this model to the physical reality if the losses are not very low, in order to make negligible the power carried by the waves that should propagate outside the real slab material, compared to the ideal slab.

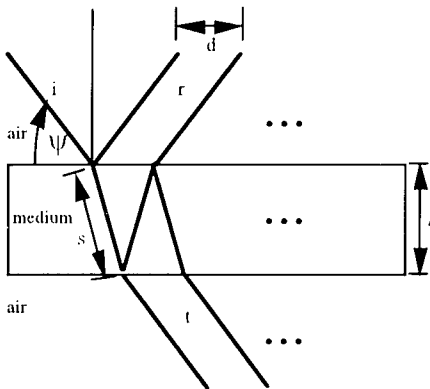


Fig. 8.2.2 Multiple reflections within a slab

The approach taken in [8] was to derive the parameters from the generalized reflection and transmission coefficients. These can be expressed as functions of the type  $\Gamma(\psi, f, \epsilon_r, \tan(\delta))$ ,  $\Gamma_g(\psi, f, \epsilon_r, \tan(\delta), \ell)$  and  $\tau_g(\psi, f, \epsilon_r, \tan(\delta), \ell)$ . Measurements are taken at as many different values of  $\psi$  as desired. The problem of deriving  $\epsilon_r$  and  $\tan(\delta)$  then reduces to the resolution of a non-linear overdetermined equation system. There is no exact solution for this kind of problem. One approach is to use a least-squares method [10] in which several implementations can be used, all based on an iterative procedure. Some of them, although offering a faster convergence, require the evaluation of derivatives, which makes them very heavy from the computational point of view. Thus, a simple

algorithm was used, increasing or decreasing alternately the value of  $\epsilon_r$  or  $\tan(\delta)$ , until the root mean square error between the measured and modeled values is minimised.

A different approach was taken in [6]. Transmissivity measurements were performed for a structure involving two slabs. The transmission coefficient of the double slab structure, as a function of the distance between the slabs ( $d_s$ ) is approximated as

$$\tau = |\Gamma_g| [ 1 - |\Gamma_g|^2/2 + |\Gamma_g|^2 \cos(2kd_s + 2\arg(\Gamma_g)) ] \quad (8.2.3)$$

It is clear from this approximation that when the distance ranges in a given interval the transmissivity will oscillate between two values. From this, the values of  $\epsilon_r$  and  $\alpha$  were estimated by fitting the measured results to the expression. The results of all these measurements and estimations are summarized in Table 8.2.1. It should be noted that: ranges of variation are given each time more than one value has been obtained, either because different polarizations were used, or because they correspond to the results of different groups. The values presented here show a good agreement with others presented in the literature, e.g. [11].

Material	$\epsilon_r$	$\tan(\delta)$	$\alpha$ [dB/cm]	R [dB]	T [dB]
Stone	6.72/8.55	0.005/0.066	0.67/9.39	-7.1/-6.0	-25.8/-2.8
Marble	11.56	0.007	1.25/5.00	-5.0	-4.8
Concrete	6.14	0.049	6.67	-8.2/-5.6	-35.0
Brick	--	--	4.00	-9.5/-5.1	-28.0
Aerated concrete	2.26	0.045	3.70	-14.0	-18.9
Tiles	4.01/8.58	0.023/0.091	3.70/9.94	-12.4/-3.8	-6.2/-5.7
Glass	4.70/6.13	0.033/0.082	4.05/9.97	-15.2/-1.4	-4.7/-2.1
Acrylic glass	2.52	0.012	1.03	-7.4	-0.9
Plasterboard	2.60/3.08	0.014/0.018	1.30/2.00	-16.7/-2.0	-3.9/-1.4
Wood	1.50/1.64	0.060/0.068	4.52/5.99	-16.1/-8.2	-13.0/-6.6
Chipboard	2.78/3.15	0.049/0.057	4.50/6.00	-15.2/-10.1	-13.9/-5.3

Table 8.2.1 Characteristics of building materials at mmw

Parameters  $\epsilon_r$ ,  $\tan(\delta)$  and  $\alpha$  are independent of the slab thickness, and have been estimated from measurements. Both R and T correspond to direct measured values and have a very strong dependence on the slab thickness, the values given here being for the usual thicknesses of materials in real buildings, to give an idea of their order of magnitude. This is not a complete list, and many more materials (especially composite cases) can be found in the references [11-14].

Later on, direction of arrival measurements were performed [12], [13]. In this case, the receiver antenna (with a very narrow horizontal beam width) is rotated through  $2\pi$ , resulting in a "receiver radiation pattern" with lobes associated with incoming rays reflected from walls. By comparing the magnitudes of the incoming rays with their path loss, estimates of reflection coefficients for the real room walls were obtained. From these, values for  $\epsilon_r$  and  $\tan(\delta)$  were calculated, which agree with those presented in the table.

### 8.2.3 Isolation and Transmission of Building Materials

Applications for the 60 GHz band are foreseen for both indoor and outdoor environments, which may pose interference problems. This suggests that the isolation as well as transmission properties of building materials should be evaluated, to facilitate coverage and interference calculations.

The attenuation suffered by a plane wave when going through a wall can be expressed as:  $A_W = -20 \log |\Gamma_g|$ . Three terms can be identified:

- 1)  $\alpha s$  comes from the attenuation of a wave propagating in the slab,
- 2)  $-20 \log |\Gamma - \Gamma^2|$  is related to the transmission coefficients of both surfaces, and
- 3)  $-20 \log |\Gamma - \Gamma^2 e^{-j2ks} e^{-2\alpha s} e^{jk_0 d} \cos(\psi)|$  is associated with the internal reflection phenomenon. The relative weight of these terms is not the same, and in particular it is interesting to obtain the conditions in which the last term can be neglected, that is to say, when it is not necessary to consider the internal reflection phenomenon, the attenuation then being given by

$$A_W [\text{dB}] = \alpha s - 20 \log |\Gamma - \Gamma^2| \quad (8.2.4)$$

Correia and Francês [14] have estimated the material thicknesses that enable the use of this approximate expression, for the average values of  $\epsilon_r$  and  $\tan(\delta)$  presented in table 8.2.1. It can be used for almost all the materials with their usual thickness, the exceptions being glass, plasterboard and acrylic glass, for which thicknesses much larger than the usual values are needed.

For cell planning and interference purposes the isolation (ie the minimum value of attenuation, independent of polarization or incidence angle) provided by building materials is required. For this reason, it is important to establish a criterion and to

calculate minimum thicknesses for given values of isolation. The relative weight of the two terms of the approximate expression for the attenuation depends on the polarization of the incident wave, the incidence angle  $\psi$  and the wall thickness  $\ell$ . The first term,  $\alpha s$ , does not depend very much on  $\psi$  ( $s/\ell \in [1, \sqrt{\epsilon_r}/(\epsilon_r - 1)]$  when  $\psi [0, \pi/2]$ ), but is proportional to  $\ell$ . On the other hand the second term,  $-20 \log |\Pi - \Gamma^2|$ , does not depend on  $\ell$ , but shows a strong dependence on  $\psi$  (approximately  $\in [0, \infty]$  for parallel polarization and  $\in [-20 \log (4\sqrt{\epsilon_r}/(\sqrt{\epsilon_r} + 1)^2), \infty]$  for perpendicular polarization). Thus, the isolation may be expressed [14] as

$$I_w [\text{dB}] = \alpha \ell \quad (8.2.5)$$

which takes into consideration that the second term can be 0, as well as the fact that  $s$  is of the order of  $\ell$  (the maximum value of  $\sqrt{\epsilon_r}/(\epsilon_r - 1)$  is 1.732 for the materials considered here).

Type of material	$\ell_I [\text{cm}]$		
	10 dB	20 dB	40 dB
Stone	1.75	3.49	6.98
Marble	8.00	16.00	32.00
Concrete	1.50	3.00	6.00
Aerated concrete	2.70	5.41	10.81
Tiles	1.28	2.56	5.12
Glass	1.65	3.31	6.61
Acrylic glass	9.71	19.42	38.83
Plasterboard	6.62	13.25	26.49
Wood	2.37	4.74	9.48
Chipboard	1.94	3.88	7.77

Table 8.2.2 Wall thicknesses for specific values of isolation

The values of wall thickness,  $\ell_I$ , that ensure 10, 20 and 40 dB isolation are presented in Table 8.2.2. For an isolation of 10 dB one can already use the approximate expression for the attenuation for the cases referred to before. Again one can see that, with the exception of glass, acrylic glass and plasterboard, all the other materials will isolate at least 20 dB when they have the usual thicknesses in building walls and floors.

One may conclude that for indoor systems the same frequency can be used in all rooms, assuming that there will be no glass or plasterboard walls to separate them, in which case different frequencies will be needed. Co-channel interference between indoor and outdoor systems will always be a problem, since glass is generally used in buildings (at least for windows), and the usual thickness of this material is not enough to isolate the two environments.

### 8.3 Indoor Radio Channel

**Peter Smulders, EUT, Netherlands and Stephan Guérin, CNET, France**

Indoor propagation measurements have been reported to WG3 by Technical University of Eindhoven (NL) [15], [16], VTT (Finland) [12], Deutsche Telekom [17] and France Telecom [13], and simulation results by the universities of Eindhoven, Ulm (D) and Aveiro (P). The bulk of this section is based on [16], which represents by far the largest contribution.

#### 8.3.1 Narrowband Measurements

Narrowband measurements are not able to discriminate the multipath dispersion in the time domain, and are therefore limited to path loss and direction of arrival measurements. Path-loss measurements at 60 GHz have been performed with a CW source and spectrum analyser. The radiation pattern of the measurement antennas was narrow in the vertical plane ( $3 \text{ dB beamwidth} = 5^\circ$ ) and broad in the horizontal plane ( $3 \text{ dB beamwidth} = 90^\circ$ ). This kind of configuration is appropriate for a wireless LAN concept.

Results in an office building are shown in Fig. 8.3.1. Results from the same environment and the same distance range at 1.7 GHz have been included to highlight the differences between the two frequency bands. All the measurements are performed with base station (BS) and remote station (RS) on the same floor. The direct path is typically blocked by furniture or a light internal wall. A clear line-of-sight path is present only in few of the measurements.

In Fig. 8.3.1 it can be seen that the path loss is considerably higher at mmw. One reason for this is the antenna radiation pattern which introduces excess attenuation at short distances. Even at higher distances (15 m) where the excess attenuation is small, the difference between the two frequencies is rather high: 45 dB. Free space difference (31 dB) explains this result partly. The rest of the difference, 14 dB, is due to higher penetration loss of materials as well as higher reflection and diffraction loss at mmw. It can also be seen in Fig. 8.3.1 that the variance of data is proportional to frequency. The rms error at mmw is 11 dB while at 1.7 GHz it is only 6.3 dB. This is due to more severe shadowing effects at mmw.

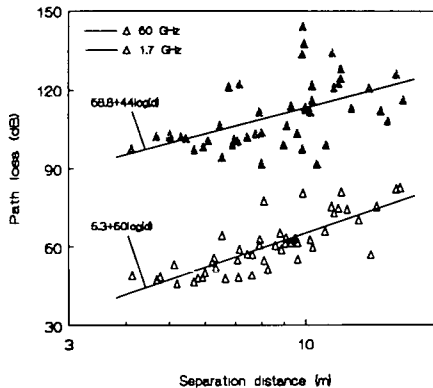


Fig. 8.3.1 Path-loss versus distance at 1.7 and 60 GHz.

Direction-of-arrival (DOA) measurements have been performed by TUE, VTT, and CNET using the same type of measurement system, but with a different antenna at the RS. This antenna has a narrow beamwidth ( $5^\circ$ ) in both vertical and horizontal planes. The antenna is rotated through  $360^\circ$  while path loss between the RS and BS is measured. Deutsche Telekom, on the other hand, used a synthetic aperture approach with an omni-directional antenna moving along an accurately defined track [17]. The DOA data can be used to investigate individual signal paths and to assess the advantage that can be achieved by using the steered high-gain antenna. If the DOA pattern shows distinctive peaks it is clear that the path loss can be reduced by steering a high gain antenna towards the maximum peak.

Typical measured DOA distributions in a room of size  $11 \times 13 \times 3 \text{ m}^3$  in a laboratory room are shown in Fig 8.3.2. in the room there are open shelves with metallic supporting structures and cupboards entirely made of wood. The DOA plots consist of two lines. The thin line corresponds to a measurement in which the RS antenna is rotated in the azimuth plane. The thick line refers to a measurement in which the RS antenna is slightly elevated so that it is pointed directly at the BS antenna. Sliding average has been applied to remove fast fading.

At the point RS1 the direct path is blocked by a cupboard which introduces an additional loss of about 20 dB to the signal. It can be seen that the signal consists of several paths of the same order of magnitude. It is interesting to note that the signal level in any direction is very sensitive to the vertical orientation of the antenna. Therefore, manual or automatic steering of the antenna in both vertical and horizontal planes is useful in a real system implementation.

At the point RS2 there is a direct line-of-sight between the antennas. In this case only two dominant signal paths can be identified: the direct path and the wall reflected path. The reflected path is in this case very strong because the wall contains metallic plates.

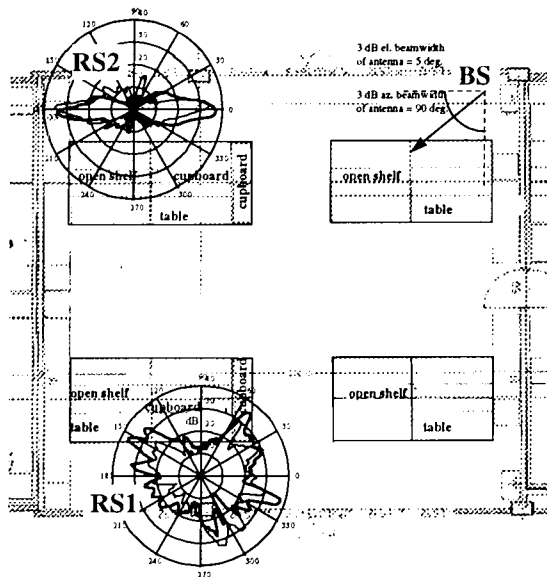


Fig. 8.3.2 Measured DOA distributions in a laboratory.

The level of link improvement achievable by using antenna steering in the azimuth plane can be estimated by calculating the DOA pattern gain. The gain is calculated by dividing the maximum peak of the pattern by the average received power.

According to 27 measured DOA patterns the gain is better than 8.4 dB for a probability level of 90%.

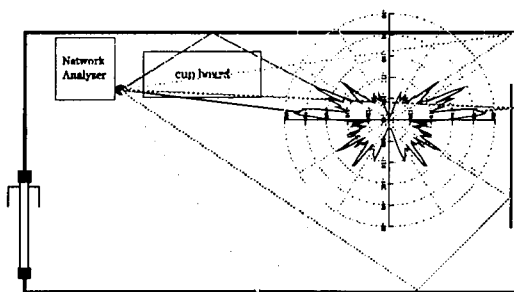


Fig. 8.3.3 Direction of arrival from Doppler Spectrum

Figure 8.3.3 shows results derived from the Doppler spectrum technique of Deutsche Telekom. Note that the pattern is symmetrical about the path taken by the antenna, but only one of each pair of lobes represents a real path. This is because the technique can only measure the angle from this line and therefore the direction can lie anywhere on a cone.

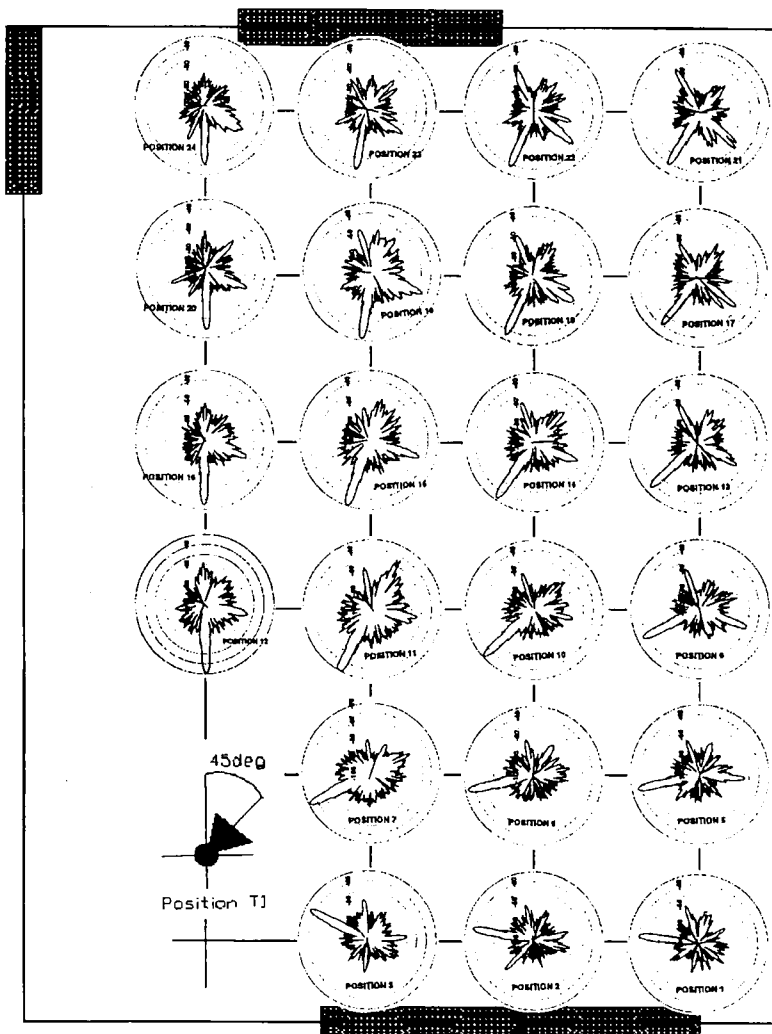


Fig. 8.3.4      Measured DOA distributions, 10dB/circle (CNET).

Measurements at 60.5 GHz have been performed by France Telecom CNET [13] at 22 positions on a 1 m grid in an empty room with dimensions  $6 \times 4.7 \times 3$  m<sup>3</sup>, see figure 8.3.4. Using a narrow beam antenna and a rotating positioning system at the receiver, DOA results and wall reflection coefficients were found. For all measurements, the height of the transmit and receive antennas was 1.5 m. A wide beam antenna, having a 3 dB aperture around 70°, was used at the transmitter. At the receiver a narrow beam antenna with 3 dB aperture close to 4.4° on a 2D rotating system was used. Measurements were made at 1° intervals so that every DOA could be found.

The direct ray is clearly dominant for each receiving position in the room. The number of significant rays depends on the receiving position. For positions in the middle of the room, the number of significant received rays is important. For these cases, contributions arrived from each wall in the room with about the same path lengths. In addition, because of the larger beam transmit antenna, each wall received direct contributions coming from the transmitter. Hence the situation is ideal for multipath propagation.

At other positions the number of significant rays is less. Where the receiver was close to walls, only the first order reflection is significant. The path length of second and third order reflections are specially large for these positions. Finally, for positions where the transmitter was not sighted directly towards the closer walls and the path lengths of all reflected rays are very long, second and third order reflections can be significant.

### 8.3.2 Wideband Measurements

The main purpose of wideband measurements is to characterise the dispersive nature of the radio channel, in order to dimension the equalisers that will be needed to overcome these effects. It is also useful, however, for taking signal strength measurements which are not subject to deep Rayleigh fading. Many techniques exist for wideband measurements, but for the indoor application, where distances are small and the channel can be made static, swept frequency measurements are invariably used. This permits much wider bandwidth, and hence finer delay resolution, than any other technique.

The system for performing the wideband measurements was built up around the HP 8510C vector network analyzer, which performs the frequency-domain measurements of the complex channel transfer function. The network analyzer controls an RF source which steps through the frequency range from 57 GHz to 59 GHz in 801 equally spaced steps. The resulting alias-free range in the time-domain is therefore  $(801-1)/(2 \text{ GHz}) = 400$  ns. A schematic diagram of the setup is depicted in Fig. 8.3.5. With the applied Kaiser window a time-domain resolution of 1 ns was achieved.

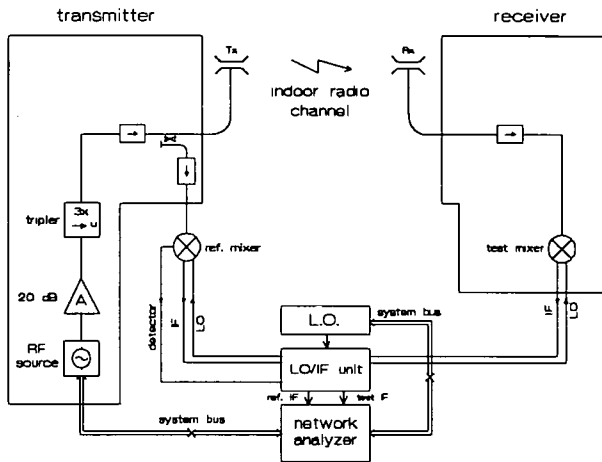


Fig. 8.3.5 Setup for wide-band measurements

The impulse response of an indoor radio channel is greatly influenced by the type of antennas used. These should be regarded as part of the indoor channel. For the experiments two identical biconical horn antennas were constructed, based on a design described in [18]. These antennas exhibit an omnidirectional radiation pattern in the azimuth plane and a toroidal beam in the elevation plane. The 3 dB elevation beamwidth was 9°, and the directivity 9 dB.

Room	Dimensions (m)	Shape	Comments
A	24.3×11.2×4.5	Cuboid	Empty, 1 glass wall, others wood
B	30.0×21.0×6.0	Amphitheatre	Cushioned chairs
C	43.0×41.0×7.0	Complex	Plastered concrete walls, ceiling
D	33.5×32.2×3.1	Complex	Metal computer cases
E	44.7×2.4×3.1	Corridor	Metal walls, empty
F	9.9×8.7×3.1	Cuboid	One side glass, others metal
G	12.9×8.9×4.0	Cuboid	One side glass, others wood
H	11.3×7.3×3.1	Cuboid	One side glass, others plaster

Table 8.3.1 Wideband Measurement Environments

The wideband measurements were carried out in eight different indoor environments at the Eindhoven University of Technology, denoted A to H, see table 8.3.1. Each consists of a single room, corridor, or hall, because millimetre waves are severely attenuated by most inner walls. In each room at least one series of measurements at 57-59 GHz was conducted at randomly chosen positions of the RS throughout the room. The RS transmitting antenna height was 1.4 m above the floor. The BS receiving antenna height was 3 m. The BS was placed in the centre of the room. Both antennas were levelled horizontally at every measurement position. The impulse responses were measured at about 20 positions of the RS, with the BS fixed, in each environment.

Owing to the difference in height between the RS and BS antennas, the path loss is partially compensated by the antenna radiation pattern in elevation. Hence; the received power does not depend significantly on the horizontal position of the RS.

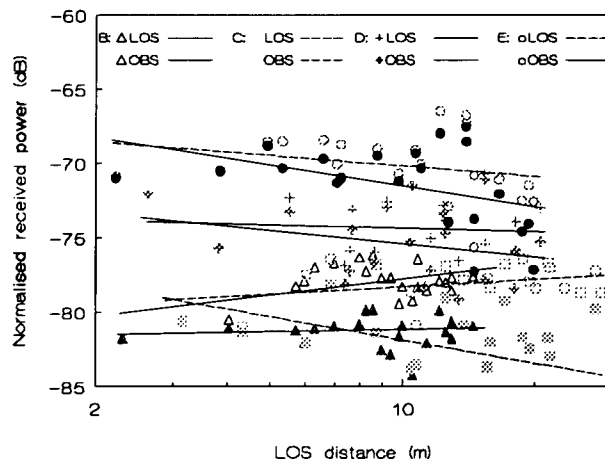


Fig. 8.3.6 NRP in the large rooms, hall and corridor.

Fig. 8.3.6 shows scatter plots of the normalized received power (NRP) versus separation distance for both line-of-sight (LOS) and obstructed (OBS) situations in the large rooms, hall and corridor. The values for OBS are derived from the time-domain data base under LOS conditions by mathematical removal of the direct ray. This method is justified by the experience that blockage of the direct ray by a person or cabinet caused a total drop of the LOS ray. The lines are linear fits based on the minimum mean square error. High values are found for environments with highly reflective (metal) objects and metal walls, while relatively low values are found in environments with only low reflective materials like wood. The fact that differences in received power between LOS and OBS-situations are only small (a few dBs at maximum) indicates that coverage is maintained under the circumstance that the direct LOS-ray is blocked. Measured values of the power-distance

decay rate exponent were typically much smaller ( $<0.5$ ) than those reported for indoor UHF radio channels. This is because this parameter is not only determined by the LOS-distance, but by the antenna-gain function in elevation as well [18].

Fig. 8.3.7 shows the cumulative distribution functions of rms delay spread (RDS) values for both LOS and OBS-situations. Rms delay spread values tend to increase with the increasing reflectivity of the walls. Rms delay spread values in the small Environment F with metal walls (0 dB return loss) are even larger than in the large environment B with concrete walls (2 dB return loss).

Furthermore it is clear from Fig. 8.3.7, that the rms delay spread is fairly independent of the separation distance within each environment. Blocking of the direct path does not necessarily imply that rms delay spread has to increase; slightly higher and lower values for OBS-situations are observed in Fig. 8.3.7. Values between 10 ns and 100 ns have been found.

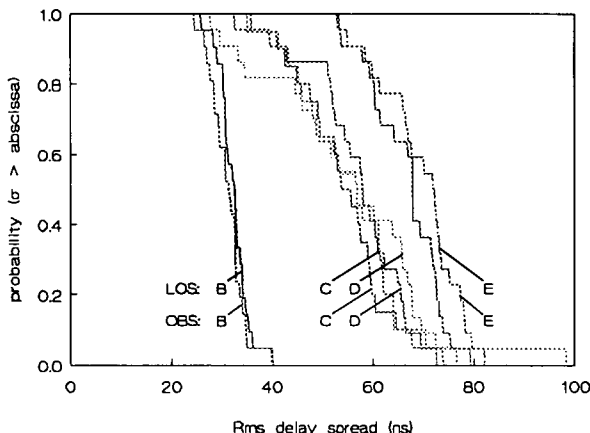


Fig. 8.3.7 Cumulative distributions of RDS in large rooms, hall and corridor.

### 8.3.3 Statistical Modeling

The measurement results can be used to describe the indoor radio characteristics in terms of statistical distributions and moments of the details of the complex equivalent low-pass impulse response. In Fig. 8.3.8 an example of an observed low-pass impulse response is shown (magnitude only). Individual rays could be detected by blocking the associated ray by an absorbing mat, while other rays were not noticeably influenced. This shows that a millimetre wave indoor radio channel is essentially a multipath channel. Hence, millimetre waves are sufficiently small to be modelled as rays following discrete paths.

The complex equivalent lowpass impulse response of a millimetre wave indoor radio channel can therefore be considered as discrete.

It is assumed that the amplitude statistics of reflected rays follow a Rayleigh distribution. This assumption was verified with a goodness-of-fit test, conditioned on the event that a ray exists. LOS rays were excluded. Data values that are not recognized as reflected rays are not taken into account and each detected ray is represented as a single point having a particular amplitude and excess delay in the impulse response. With this approach a meaningful amplitude distribution for each measurement subset is obtained since each resulting sample set contains only "non zero" ray amplitudes. Hence the test can be utilized to model the ray amplitude generation process independent from the ray arrival process.

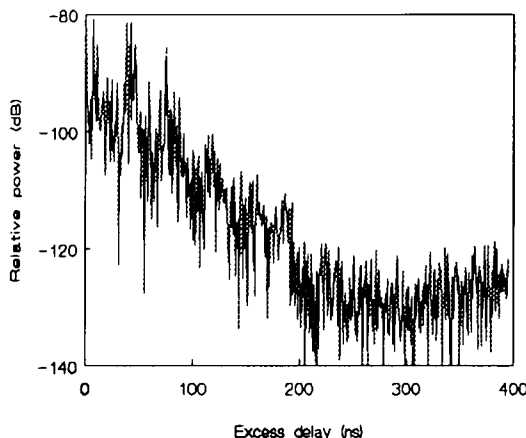


Fig. 8.3.8 Example of measured impulse response.

A reasonable assumption for the ray phases is that they are mutually independent random variables which are uniformly distributed over  $[-180^\circ, 180^\circ]$ . This follows from the fact that the ray phase is critically sensitive to the path length, changing by  $360^\circ$  as the path length changes by a wavelength, or only a few mm. The assumption of uniformly distributed ray phases was checked for all measurement subsets and found to be true.

The interarrival time pdf's were subjected to a MMSE test. (A chi-squared goodness-of-fit test failed to yield significant results because of the limited number of interarrival time classes). Good correlation coefficients between exponential fit and empirical frequency distributions were found. The mean interarrival time is most reliably characterised as being 1 to 3 ns with the proviso that those rays are

excluded that have amplitude values more than -20 dB below the highest ray amplitude.

In calculating the average power delay profile (PDP), each individual PDP is weighted by its normalized received power value. This is done because a single PDP should not dominate in the average PDP. Three examples of average PDPs are shown in Fig. 8.3.9. These profiles have been obtained in the environments F, G and H. They are typical for all measurement subsets obtained. A typical PDP can be modelled by a LOS ray followed by a constant-level part up to  $\tau = 60$  ns which in turn is followed by a linear decrease (of dB value) down to the noise floor.

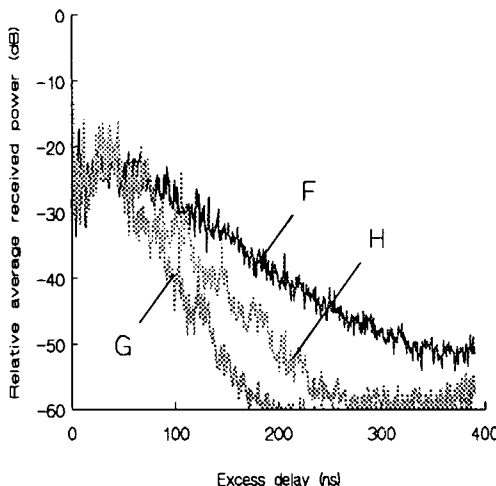


Fig. 8.3.9 Example of an average PDP.

The normalized received power of the LOS component can be calculated using the radio equation. OBS situations can be modelled by completely omitting the LOS component. The constant level part is caused by the elevation dependence of the antenna radiation patterns and the height difference between the transmit antenna and receive antenna. The pulses in a response that immediately follow the first pulse (LOS pulse) are likely to come from single reflected rays. This suggests that the difference between the height of the first LOS pulse and the height of the constant-level part is determined by the average return loss of the dominant wall partitions.

### 8.3.4 Deterministic modeling

Ray-tracing programmes are used extensively for the examination of radio propagation characteristics. In order to investigate the propagation characteristics in an indoor environment various algorithms were developed taking into account the effect of transmission through walls and polarization. More sophisticated techniques have also been developed incorporating the effects of diffraction.

For simulation of the indoor propagation of mmw, the simulation package PROpagation SIMulation (PROSIM) has been developed at the Telecommunications Division of the EUT. The basic algorithms and procedures underlying the simulation package are based on Geometrical Optics (GO). This means that the ray-tracing algorithm applied traces possible rays between transmit and receive antenna according to Snell's reflection law.

Calculation of mmw propagation on the basis of GO yields a good compromise between accuracy and complexity [19]. Using GO means that ray paths are calculated along which electromagnetic power travels from transmitter to receiver. Fresnel reflection coefficients are applied, electromagnetic field polarization states considered and rays weighted with the radiation patterns of the transmit and receive antennas. PROSIM only considers the reflectivity of walls and objects (eg. furniture) but not the transmissivity. The walls (and windows) of the room are assumed infinitely thick and the objects within the room do not allow an electromagnetic wave to travel through them. The room and the objects within are represented by smooth faces. Objects are assumed to stand on the floor and can be arbitrarily orientated with respect to the horizontal plane.

Antenna directivity functions can be entered in formula form or stored in a look-up table. The latter enables the use of measured data without data reduction. Two types of aperture antennas are considered: 1) sectoral horn antennas and 2) biconical horn antennas. Radiation patterns of both these antennas are stored.

With the biconical horn antennas the accuracy of the applied GO model has been examined by comparing simulation results with measurement results, and good agreement found [19]. The use of PROSIM was continued for a more thorough examination of the influence of the environment and antenna characteristics on NRP and RDS.

The relation between NRP and RDS and the shape and orientation of antenna radiation beams has been evaluated under both LOS and OBS conditions. To examine the influence of wall reflectivity two rooms are considered having dimensions similar to those of Environment A. One room has low reflective walls (10 dB return loss at perpendicular incidence) whereas the second room has walls with high reflectivity (1.5 dB). In both rooms the BS receive antenna is located at 3 m height in the middle of the room and the RS transmit antenna is placed at 1.4 metres height at 24 randomly chosen positions throughout the room (as with the measurements). For every position of the RS antenna the impulse response was calculated. The NRP and RDS were derived from each obtained profile.

The antennas implemented in PROSIM are smooth walled sectoral horn antennas and biconical horn antennas. In contrast with the omnidirectionally radiating biconical horns, sectoral horns produce highly directive radiation beams. To examine the influence of directivity antennas are implemented with various values. The directivity of the biconical horns was in the range 6.9 to 12.7 dBi whereas the directivity of the sectoral horns ranged from 9.1 to 25.2 dBi.

Simulations were performed for the three different antenna setups depicted in Fig. 8.3.10. Fig. 8.3.10a shows the antenna setup with a sectoral horn at both the RS and BS, denoted as “sec-sec”. Fig. 8.3.10b depicts the “sec-bic” setup with a sectoral horn at the RS and a biconical horn at the BS. Fig. 8.3.10c shows the “bic-bic” setup with biconical horns at both the RS and BS.

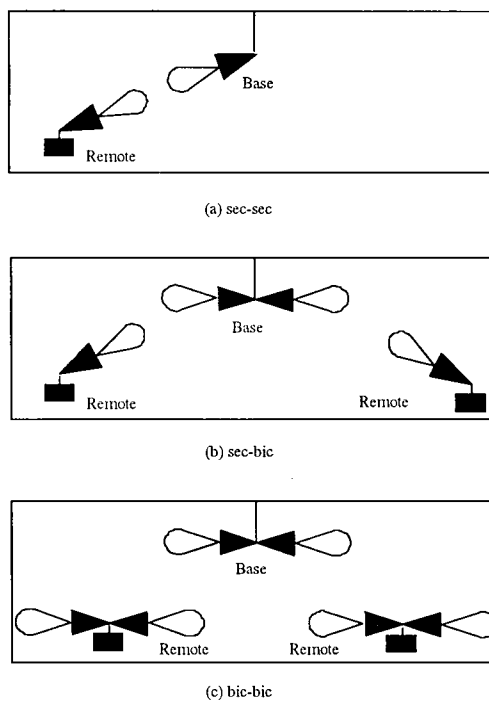


Fig. 8.3.10 Simulated antenna setups.

The sectoral horns in Fig. 8.3.10a are pointing towards each other, eventually with a certain amount of mispointing in order to examine the effects of pointing errors. The orientation of the error angles at the RS and the BS are mutually independent and randomly chosen. In the sec-bic setup the sectoral horn at the RS is pointing towards the biconical horn. Here, pointing errors are only introduced in the

radiation beam of the sectoral horn at the RS. In the bic-bic setup both biconical horn antennas are radiating in the horizontal direction.

With respect to the sec-sec setup it could be observed that 25.1 dBi sectoral horns at both ends yield the lowest RDS values and the highest NRP values when compared with the other configurations, provided that there is no obstruction of the LOS path and the antenna beams are exactly pointing towards each other. The sec-sec setup is however highly sensitive to LOS obstruction and mispointing. This is illustrated in Fig. 8.3.11 and Fig. 8.3.12, respectively, which show the NRP versus RDS for every position of the remote station. The combination of LOS obstruction and 5° mispointing results in a fairly uniform spread in RDS and NRP. A higher reflectivity of the walls results in higher NRP values as well as higher RDS values.

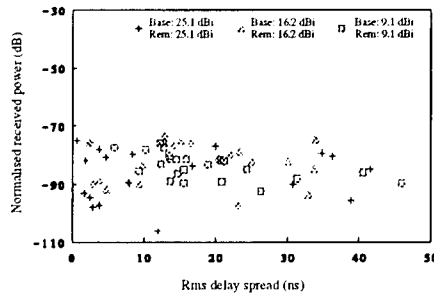


Fig. 8.3.11 Results for the low reflective environment with "sec-sec" setup and obstructed LOS.

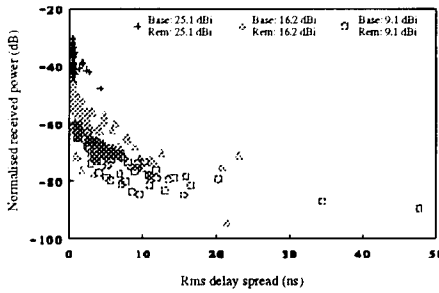


Fig. 8.3.12 Results for the low reflective environment with "sec-sec" setup and 5° pointing error.

As with the sec-sec setup the bic-sec setup is sensitive to obstruction of the direct ray and mispointing. The difference with the sec-sec results is however that the minimum and

maximum values for NRP and RDS for the sec-bic setup are not so extreme. The spread in NRP values is significantly lower.

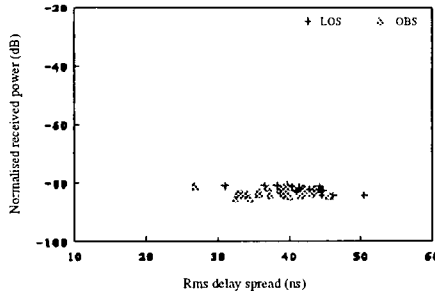


Fig. 8.3.13 Results for the low reflective room with bic-bic setup under LOS and OBS conditions.

With respect to the bic-bic setup, in contrast with the sec-sec and sec-bic setup, an increase in antenna directivity yields an increase of the RDS values. Fig. 8.3.13 depicts the results obtained with a 9 dBi biconical horn at each end for both LOS and OBS. The differences in NRP values between those two cases are only a few dB. This indicates that the bic-bic setup is highly insensitive to LOS obstruction. Furthermore the low spread in NRP values is striking. It demonstrates that with the application of properly dimensioned biconical horn antennas, an almost uniform coverage within the boundaries of an indoor cell can be achieved.

This phenomenon is explained by the fact that for larger separation distance, the corresponding larger free-space loss is compensated by the elevation dependence of the radiation patterns [18]. The similarity between LOS and OBS and uniformity in coverage is also found for the highly reflective room with slightly higher worst-case values of about 55 ns RDS and -72 dB NRP.

## 8.4 Outdoor Radio Channel

**Luis Correia, IST, Portugal, and Per Lehne, Telenor, Norway**

The use of the mmw band in an outdoor environment has been proposed for mobile applications, eg. car to car and fixed roadside cell to car communications, and communication between TV cameras and a central control room [20]. Particular interest has been devoted to the oxygen absorption band, [57,63] GHz, where the specific attenuation is greater than 11 dB/km, thus limiting the cell radius to a few hundreds of meters, and enabling efficient frequency re-use. The work carried out on propagation modelling concerns two different topics: path loss modelling, for the estimation of cell radius and carrier-to-interference ratio, and impulse response modelling, for evaluation of the wideband radio channel characteristics.

Measurements play an important role in propagation modelling at all frequencies, being of extreme importance at the mmw band since there are not many results in the literature, and the relative importance of many phenomena need to be clarified by an experimental procedure. Therefore, measurement campaigns were undertaken in different outdoor scenarios (streets, open squares, highways, tunnels, airports, etc.).

#### 8.4.1 Path Loss Modeling

Estimation of power for coverage or interference calculations is essential in every mobile system. At the UHF band several types of models have been developed, using different approaches, from which two categories can be considered: 1) decay of the average power with distance, depending on several parameters of the system and environment (like base station antenna height or street width), and 2) ray-tracing on 3D models of the scenarios under analysis, demanding a very accurate knowledge of the characteristics. These approaches have also been used at the mmw band.

Both narrow and wideband measurements have been conducted in several outdoor scenarios in the mmw band. Initially, narrowband measurements of power versus distance were performed [21], [22] in scenarios chosen so that very different cases were considered: airport field, urban street and city tunnel. In all cases, results show an interference pattern, typical of those associated with the sum of several rays, suggesting that ray-tracing techniques can be used to model the propagation phenomena. Results were compared with ray-tracing tools.

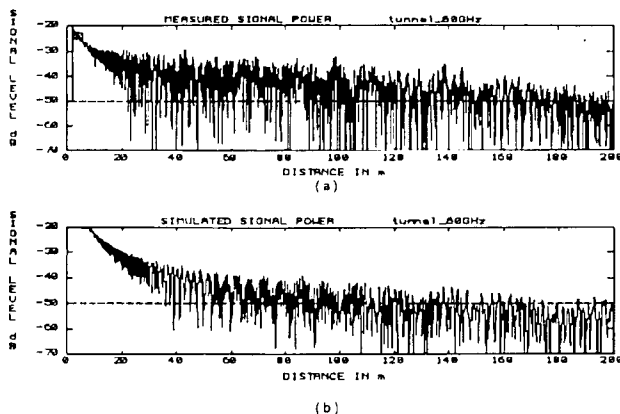


Figure 8.4.1 Comparison between measured (a) and simulated (b) power in a city tunnel at 60 GHz.

Simple ray-tracing tools have been developed [21], [22], accounting only for direct and reflected (up to the second order) rays; scenarios were considered to be as simple as possible, neglecting any objects (for instance streets are considered as dielectric canyons). Comparisons of measured and simulated results, of which Fig. 8.4.1 is a good example, show good agreement indicating that reflections of third order, or higher, and diffraction can be neglected, as far as modeling the variation of power versus distance is concerned.

According to simulations, frequency or space diversities mitigate fading effects, decreasing the fade depths by several dB. Selective combining of two or more frequencies (with a separation of the order of 1 GHz) shows that diversity is more effective for lower frequencies (10 GHz compared to 60 GHz). Selective combining of signals from two antennas separated by 1 m (much more than the correlation length at mmw) show similar improvements.

The models used at UHF for the decay of power with distance usually have the slope dependent on the environment and on break-point distances. They are very simple models based on the interference of a direct and a ground reflected ray, leading to a simple dependence of the power on distance  $d$ , of the type  $10 \alpha \log(d)$ ,  $\alpha$  being the decay slope. It is well known [9] that a two ray model leads, under conditions that are usually verified, to a fourth power law, rather than the square law found in free space. One of the conditions to be satisfied is that the path length difference between direct and reflected rays is less than  $\lambda/2$ , which defines the break-point distance,  $d_{bp} = 4 h_t h_r / \lambda$  ( $h_t$ ,  $h_r$  being the receiver and transmitter antenna heights) beyond which the fourth power law can be used. Such a model for the mmw band requires the evaluation of the break-point distance, and an environment classification according to the different values of  $\alpha$ . Assuming a frequency range [60, 66] GHz, and  $h_r = 1.8$  m,  $h_t \in [5, 50]$  m,  $d_{bp} \in [7.2, 79.2]$  km, which is far beyond the expected maximum range for the cell radius (up to 0.5 or 1 km). This means that it is not expected to have the fourth power law at mmw band, and that  $\alpha$  will be close to that of free space ( $\alpha = 2$ ), which is confirmed by the few results from measurements available in the literature, see Table 8.4.1.

The value of  $\alpha$  does not seem to depend only on the scenario, since a value of 2.3 is found in an open space as well as a street. The range in which  $\alpha$  varies is not very large [2, 2.5]. The antenna height seems to influence the value of  $\alpha$  (but note also the influence of the radiation pattern, when the antenna is very high). The value of  $\alpha$  will, of course, be of greater importance for larger distances, since larger values of  $\alpha$  contribute to a faster decay of the power.

The model developed for the mmw band (60 - 66 GHz) [25] includes two additional terms, compared to the UHF band, besides the usual term related to the slope of the power decay with distance: one to account for oxygen absorption and the other for rain attenuation. These terms are negligible in the UHF band, but cannot be neglected for higher frequencies. Moreover, oxygen absorption is the main reason

for choosing the 60 GHz band. Other factors can affect wave propagation, but they are not considered here: water vapour absorption can be neglected, since its attenuation coefficient is of the order of 0.1 dB/km; fog, hail, snow, sand, etc. are not very well studied, but their influence can also be neglected, either because the attenuation coefficient is very low, or because they occur with very low probability.

Scenario	Gain [dBi]		Height [m]		d [m]	$\alpha$
	Tx	Rx	Tx	Rx		
Open area (grass) [23]	20	6	1.5	1.5	200	2.3
Open area (asphalt) [22]	17	15	5.	1.5	200	2.0*
Open area [21]						2.2*
Urban Street [22]	17	15	5.	1.5	120	2.2*
Campus street [24]	6	20	1.5	2.	120	2.1
				5.5	120	2.3
Tunnel [22]	17	15	1.5	1.5	200	2.5*

Table 8.4.1 Power-distance decay rate at mmw in outdoor scenarios  
(\* -- estimated from figure)

An expression for the oxygen absorption has been developed, based on [26]

$$\gamma_0(f) = \begin{cases} (15.10 - 0.104(f - 60))^{3.26} & (60 \leq f \leq 63) \\ (11.35 + (f - 63)^{2.25} - 5.33(f - 63)^{1.27}) & (63 \leq f \leq 66) \end{cases} \quad (8.4.1)$$

Where  $f$  is the frequency in GHz. This specific attenuation due to oxygen,  $\gamma_0$  (dB/km) can take relatively high values at 60 GHz (around 15 dB/km), but it decreases an order of magnitude when the frequency is near 66 GHz. This decrease must be taken into account when the frequencies are chosen for the up and down links, especially if the distances are greater than 1 km.

Rain attenuation can also be of some importance at the mmw band, depending on the rate,  $R$  (mm/hr). The model given by ITU-R [27] is used,

$$\gamma_r(f, R) = k(f) R a(f) \quad (8.4.2)$$

where  $\gamma_r$  (dB/km) is the specific attenuation due to rain,  $k(f)$  and  $a(f)$  are approximated by:

$$k(f) = 10^{1.203 \log(f) - 2.290} \quad (8.4.3)$$

$$a(f) = 1.703 - 0.493 \log(f) \quad (8.4.4)$$

Rain can play an important role in cell coverage reduction, since its attenuation can reach values larger than those of oxygen, depending on the rain rate (18 dB/km for 50 mm/h). Oxygen and rain attenuations cannot be neglected if large distances (~1 km) are to be considered, but for calculations within cells (with ranges less than 200m), they may not be of great importance.

The average received power can be estimated by combining the expressions of almost free space received power with the attenuation by oxygen and rain. Thus the total received power is given by:

$$P_r = P_t + G_t + G_r - 32.4 - 10\alpha \log(d) - 30\alpha - 20 \log(f) - \gamma_{rd} - \gamma_{od} \quad (8.4.5)$$

where  $P_t$  is the transmitted power (dBm),  $G_t$ ,  $G_r$  are the transmitter and receiver antenna gains (dBi), and  $d$  is the distance (km). The value for  $\alpha$  has to be chosen with some care, depending on the specific application intended for the model. This expression cannot be used for very small distances where the antenna radiation patterns will have a great influence. This model agrees very well with the data from [23], giving a maximum 2 dB error in the estimation of the received power. Comparison with the data from [24] also leads to good results. However, note that the measurements in Table 8.4.1 have a maximum range of 200 m. There is a need for more measurements over a larger range, to check the model for distances up to 2 or 3 km (necessary at least for interference calculations).

#### 8.4.2 Wideband Characterisation

When designing the air interface, reliable information about the propagation conditions is of vital importance. Since little work had previously been published on propagation measurements in the mmw band, measurement campaigns with a 60 GHz channel sounder were performed by Telenor R&D. A channel sounder based on correlation, transmitting a digitally generated frequency sweep, was assembled [28]. The received signal is digitized and stored, and then correlated with a Taylor weighted version of the transmitted sweep. Diversity measurements are possible, since the input from two antennas can be synchronously sampled. Several hundred impulse responses per second may be transferred to the PC, or the receiver may calculate delay-Doppler spectra based on successive responses and transfer these spectra to the PC. The RF center frequency is 59.0 GHz, with a maximum bandwidth of 200 MHz, corresponding to a best resolution of 5 ns. The output transmit power is 500 mW.

The basic wideband measurement is the channel impulse response (CIR) which is a time function of the received signal, showing the arrival times of the different radio paths. This type of measurement is very well suited to describe multipath phenomena. From the CIR measurements several parameters may be extracted, and they may have different significance when describing the channel or for the design of a mobile system. Mean delay (MD), delay spread (DS), delay interval (DI), and delay window (DW) are defined in [9]. A new delay window parameter, the sliding delay window (SDW) was introduced, defined as the length of the

shortest portion of the CIR containing a certain percentage of the total energy, which is believed to be a better measure than DW, e.g. when judging equalizer performance.

R t e.	S c e	E n v.	W	C	MD [ns]		DS [ns]		9 dB DI [ns]		90% DW [ns]		90% SDW [ns]	
					50%	90%	50%	90%	50%	90%	50%	90%	50%	90%
A1	ST	s	36	s	10.2	13.7	7.6	16.5	10	25	20	35	10	25
B1	ST	s	23	s	7.8	10.5	4.2	6.5	5	20	10	20	10	20
C	ST	n	20	f	9.3	16.1	8.4	13.1	15	35	20	40	15	30
D	ST	f	19	m	9.0	14.2	6.8	11.8	15	30	20	35	15	30
E	ST	f	14	m	5.7	11.1	3.6	12.6	5	20	10	35	10	20
F	ST	m	13	m	6.5	20.6	3.6	48.3	10	35	10	80	10	40
G	ST	m	27	m	6.2	11.4	4.6	16.0	5	20	10	50	10	20
H1	SQ	f	100	f	22.5	65.5	31.9	55.2	25	130	95	155	55	125
H2	SQ	f	100	f	11.5	39.1	20.1	60.2	5	135	10	160	10	140
I	SQ	f	70	f	17.3	62.2	28.1	76.6	10	150	55	195	15	150
J1	SQ	s	100	s	17.4	49.2	40.8	92.2	5	150	45	270	10	135
J2	SQ	s	100	s	19.5	57.0	37.8	83.7	10	200	90	220	15	160
K1	T	m	15	m	10.9	17.1	6.8	11.5	15	30	20	35	15	30
N	G	n	67	n	37.0	74.6	38.4	61.2	40	160	115	175	55	145

Table 8.4.2 Main figures from the wideband measurements (Scenario: ST = street, SQ = square, T = tunnel, G = garage; Env.: W = width of street or tunnel, or largest dimension of city square or parking garage, C = moving cars; n = none, f = only a few, s = some, m = many).

The measurement campaigns that started early 1994 include wideband channel soundings and wideband path loss measurements in city streets and squares in downtown Oslo, a road tunnel and a parking garage, [29], [30]. A 90° horn was used as transmitter antenna in all measurements, and a biconical horn was the

receiver antenna, all vertically polarized with vertical half power beamwidth of  $20^{\circ}$ . The height of the receiver antenna in all outdoor measurements was 2.2 m, and the transmitter antenna height was generally around 4 m.

Results from these measurements are summarized in Table 8.4.2. 50% and 90% values from cumulative distributions of the channel parameters are tabulated. In Figure 8.4.2, 'street A' scenario is shown together with a sample of an impulse response.

For outdoor scenarios the main conclusion is that city streets do not normally represent a severe multipath situation, values of DS and 90 % SDW being typically lower than 20 ns and 50 ns respectively. The dimensions of a city square, typically being larger than the city streets, result in a much larger dispersion. In this case, the 90 % SDW may be 150 ns or more. A road tunnel represents a very homogenous situation and has many similarities to the city street environment. A parking garage represents a bad multipath situation because of the large dimensions and the relatively smooth surfaces creating strong reflections.

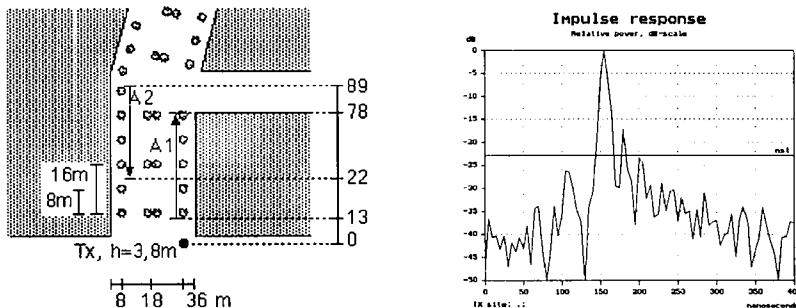


Figure 8.4.2 Street plan and sample CIR for 'street A' (circles represent trees; arrows A1 and A2 represent mobile movement; shadowed areas are buildings)

Besides the model for the average received power, a model for characterization of the signal in terms of fading depths and duration and of wideband parameters (MD, DS, etc.) is needed. A ray-tracing tool was developed [31], with the following main features: it accounts for direct and reflected rays (up to the third order), neglecting diffuse reflections and diffractions; rays are interrupted by non-reflecting objects like trees (measurements have shown that diffuse reflection from trees is negligible).

The scenario is described as a dielectric canyon, having rough surfaces. Polarization and radiation patterns of both transmitting and receiving antennas are taken into consideration. This tool, more complex than the previous ones, is intended to simulate signal behaviour in outdoor scenarios, more specifically in urban streets, allowing the estimation of both narrow and wideband channel characteristics.

Results (CIR) from this tool were checked against measurements [30] showing that this approach is correct. Fig. 8.4.3 shows a comparison of results for one of the streets, street 'A' which has trees both in the middle and on the sidewalks. In general good agreement is observed, with the exception of the 90% SDW. This can be understood as this parameter is very sensitive to reflected rays with low amplitude, therefore presenting large differences between model and reality.

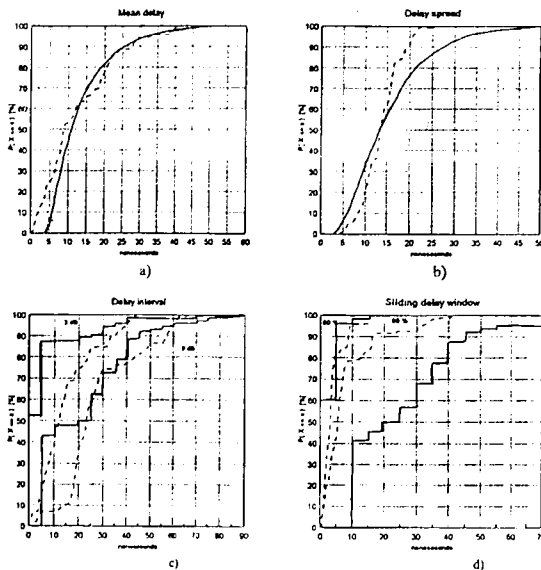


Figure 8.4.3 Comparison between ray-tracing and measurements, of statistical parameters (— measurements; - - - simulations)

One of the main conclusions is that simple ray-tracing can be used to estimate channel characteristics, both for narrow and wideband systems. Several improvements are being considered for further study, such as the inclusion of motor traffic.

## 8.5 Transmission Performance Evaluation

**Witold Holubowicz, EFP, Poland, Peter Smulders, EUT, Netherlands and Ramjee Prasad, DUT, Netherlands**

The most important characteristic of the radio channel for high speed data transmission is the RDS. Multipath dispersion produces an irreducible BER which is independent of the signal to noise ratio and increases with increasing RDS. Where no countermeasures are taken, as a rule of thumb, an irreducible BER of  $10^{-3}$  results from a normalised RDS of 0.1. This means that the maximum useable transmission rate is 0.1/RDS. For 100 ns RDS, this is only 1 Mbit/s. There are four main countermeasures that may be considered: Direct Sequence Spread Spectrum (DSSS) with a RAKE receiver, multi-carrier techniques such as Orthogonal Frequency Division Multiplex (OFDM), Antenna Diversity, and Adaptive Equalisation. All of these techniques have been considered in WG3, both singly and in various combinations, but equalisation has received most attention. This section addresses each of these techniques in turn, leading to further elaboration of the equaliser approach in the context of the HIPERLAN standard. It ends with some material on synchronisation and channel coding for wideband systems.

### 8.5.1. Early Performance Predictions

In [32], the design of a wireless indoor transmission chain with 10 Mbps bit rate at about 30 GHz is described. Different techniques are discussed that allow such high rates to be achieved within buildings: proper choice of multiple access method, use of higher level modulation, adaptive equalisation, antenna diversity, and frequency diversity. First, a comparison between CDMA and narrow-band transmission is carried out. It is shown that for the spreading factor of at least 250 and 20 users each transmitting at 10 Mb/s, the transmitted signal would have too large spectrum and the spread spectrum approach was therefore not further pursued. A more promising approach, according to the authors, was a single-channel-per-carrier (SCPC) FDMA system for the uplink and multicarrier FDM for the downlink. Apart from the mobile-to-base and base-to-mobile connections, another layer of radio links is also assumed: between the base stations and one central station in the company. Different solutions for communication in that layer, based on demand-assignment SCPC/FDMA are also proposed. According to the authors the system proposed is a good compromise between spectral efficiency and relatively low cost.

In [33] the authors present results of simulation and analyses concerning indoor signal transmission in the presence of co-channel interference from the adjacent room in the one cell per room scenario. The performance of MPSK, narrowband GFSK ( $\beta = 0.5$ ) and wideband GFSK ( $\beta = 2.0$ ) is considered. Error performance is calculated for exponential PDP models in the presence of co-channel interference modelled as AWGN. Amongst the modulation systems considered wideband GFSK

with the modulation index of  $\beta = 2.0$  seems to offer the best performance. The results show that, with a significant line-of-sight path present (LOS  $\geq 10$  dB), the performance of the 8-ary GFSK system subject to 15 dB signal-to-co-channel interference (S/CCI) ratio and with 13 dB SNR can achieve bit rates up to 100 Mbps in large rooms, with as much as 90 ns rms delay spread, without the use of adaptive techniques. The general conclusion is therefore that for systems with a line-of-sight present (or one dominant reflected component) bit rates of 100 Mbps can be achieved in quite large rooms by using suitable modulation techniques (especially wideband GFSK), without the need for diversity or adaptive equalisation.

In [34] wideband measurements in eight indoor locations are described. The objective was to examine the propagation characteristics of mmw indoor radio channels. In each area, measurements were performed for 20 randomly chosen positions of the remote antenna. Gray-coded QPSK modulation was used, without any equalisation. The normalised bit rate (maximum bit rate, averaged over 20 locations, and multiplied by the rms delay spread) was calculated for the threshold value of  $\text{BER} = 10^{-6}$ . Finally, it was noted that the normalised bit rate values do not depend significantly on the considered indoor area and the type of antennas.

### 8.5.2 Spread spectrum

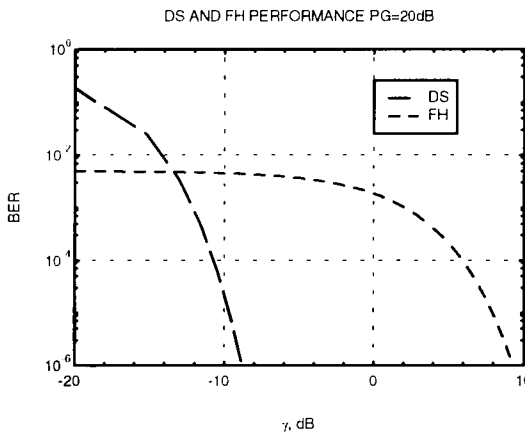


Fig. 8.5.1 DS and SFH performance, 20 dB processing gain;  $\gamma$ : signal to interference ratio.

Early Wireless LAN products operated at about 1 Mbit/s in the Industrial Scientific and Medical (ISM) bands around 902 - 928 MHz and 2.400 - 2.4835 GHz and used spread spectrum to avoid interference. It was therefore logical to investigate whether these techniques could support higher data rates. In [35] the two major

classes of spread spectrum used in WLAN, Direct Sequence (DS) and Slow Frequency Hopping (SFH), are compared. The modulation scheme considered is differential BPSK. The interferer is considered as narrowband white noise source (narrowband in the sense that the interferer bandwidth is less than the signal before spreading or after de-spreading). The network topology considered is mesh (no base stations and therefore no power control). SFH is found to be more robust than DS in the presence of narrowband interference, see fig. 8.5.1, but only DS offers any advantage against multipath dispersion.

A DS system with a RAKE receiver is considered in [36]. The channel model used is a discrete exponential power delay profile truncated at 30 dB power decay with components at chip delay intervals. BPSK modulation is used with two demodulation schemes, differential and quasi-coherent, and three different methods of combining the RAKE branch outputs (signal strength selection, equal gain combining and maximal ratio combining).

An irreducible BER of  $10^{-3}$  is achieved with normalised RDS up to 0.3, 0.7 and 0.9 for selection, equal gain and maximal ratio combining respectively, see fig. 8.5.2. This means that for 100 ns RDS, data rates of 3, 7, and 9 Mbit/s can be achieved. DS WLANs use the lowest possible processing gain in order to maximise the instantaneous data rate for the active terminal, typically using 11-chip Barker codes as spreading sequences. The bandwidth requirements for the systems above would thus increase to at least 33, 77, and 99 MHz. This processing gain is insufficient to withstand interference from other users, so CDMA is not possible, and the MAC protocol is required to control access to the channel.

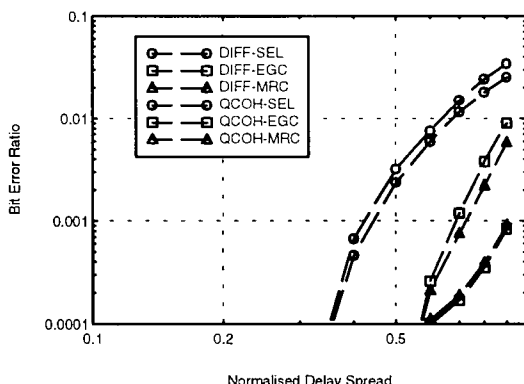


Fig. 8.5.2 Irreducible BER vs. NDS. DIFF: differential demodulation; QCOH: quasi-coherent demodulation; SEL: signal strength selection; EGC: equal gain combining; MRC: maximal ratio combining.

### 8.5.3. Multicarrier modulation

Several multicarrier schemes were proposed to ETSI RES-10 as candidates for the HIPERLAN standard, and are summarised in [37]. The main reasons for rejecting multicarrier schemes were connected with the high peak to mean power ratio. The spectrum was allocated by the regulators under the constraint of a maximum isotropically radiated peak envelope power of 1 W. This means that the average power is limited to 1W divided by the number of carriers unless the peak is limited, eg. by clipping, which leads to out-of band radiation. As HIPERLAN is intended for battery powered portable computers, it was desirable to use efficient Class-C power amplifiers and this effectively precluded multicarrier schemes.

A hybrid system incorporating multitone, DS and equalisation is studied in [38]. A bidimensional RLS (Recursive Least Square) linear equaliser is described. At high data rates, multipath propagation leads to ISI on individual carriers, and also cross-carrier interference (CCI). The equaliser is therefore a multiple input, multiple output bidimensional device. The structure can be simplified to a block diagonal matrix. Simulation results are presented for a system operating at 10 Mbaud in the 5.2 GHz band, using 1, 2, 3, 8 or 16 carriers in a channel with 50 ns rms delay spread, see fig. 8.5.3. A 7-bit m-sequence is used as a spreading code for the single tone system, with longer sequences for the higher number of carriers.

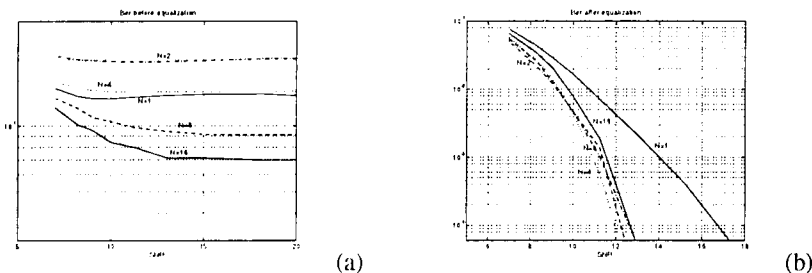


Fig. 8.5.3 BER for DS-multitone without (a) and with (b) equalisation for different numbers of tones.

The positive effect of increasing the numbers of tones is demonstrated, especially when no equalisation is used. It is noted that the multitone effect is reduced by the equaliser and that convergence problems may arise when the number of tones is more than two.

### 8.5.4. Antenna Diversity

A well known way of antenna signal combining is maximal-ratio combining. This however, is a narrowband technique which is optimal for the flat fading channel and does not take into account intersymbol-interference (ISI). Maximal-ratio

combining requires a priori knowledge of the complex impulse response of the channel for each antenna element. A better result is achieved by Minimum Mean Square Error (MMSE) signal combining, however here also a priori knowledge of the channel's complex impulse response is required.

A way of combining multiple antenna signals which does not require a priori knowledge of the complex channel impulse responses for the different antenna elements was presented in [39]. The technique is based on quasi-coherent (QC) combining of the dominant path of the signals received by M different closely spaced antenna elements. Because of the small array dimensions, the channel PDP is nearly equal for all antennas. The M antenna signals are phase shifted so that the phases of the dominant path become nearly equal. Summation of these signals results in coherent addition of paths which arrive from the same direction as the dominant path. Signals which arrive from other directions will add incoherently. Therefore, the dominant path is strongly enhanced compared to other paths, and the resulting PDP shows less delay spread and consequently has a more equalised frequency response. Coherent combining, which is the optimum case for this scheme, requires exact knowledge of the phase of the dominant paths. However in a practical situation these phases are unknown and have to be estimated. Therefore, the term quasi-coherent combining is used.

The scheme of a coherent BPSK receiver with QC-combining of multiple antenna signals is shown in Fig. 8.5.4. Remodulation is applied for carrier phase recovery, by multiplying the delayed input signal by the estimated data. A delay time  $T_b$  is added to take into account the time required for optimum detection of  $d(t)$ . In case no errors are made, remodulation fully removes the modulation, and the result is a clean carrier signal from which the reference phase is determined. In case of errors, the fraction  $(1-2P_e)^2$  of the total signal power is concentrated in the recovered carrier [40].

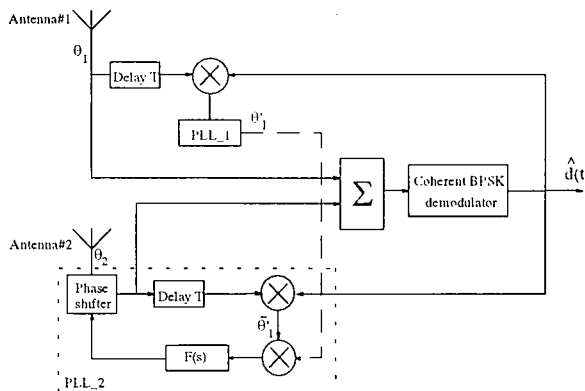


Fig. 8.5.4 Scheme of proposed BPSK receiver with quasi-coherent signal combining.

It was found that QC-combining shows superior performance enhancement compared to unity gain combining. A significant improvement of performance is achieved by QC-combining of a relatively small number of antenna signals, and small array dimensions. A four element antenna array requires a circle with radius of about  $\lambda/2$ , which is a relatively small area at high frequency. Its performance is nearly equal to maximal-ratio combining with a slight decrease in performance for low bit rates, however without the requirement of a priori knowledge of the channel impulse profiles.

### 8.5.5 Adaptive Equalisation

In [2] a preliminary evaluation of the capacity limitations on broadband indoor networks was carried out for a single carrier indoor radio link within a typical office environment ( $40 \times 60 \times 4$ ) m<sup>3</sup> and reflectivity of each wall equal to 0.2. Within this room, mobile stations are communicating using antennas located a few decimetres above a table, whereas the base station antenna is located in the middle of the room just beneath the ceiling. All antennas have omnidirectional radiation patterns in the horizontal plane. The availability of the LOS path between the transmitter and the receiver was assumed. For this configuration the radio channel information capacity was calculated. Evaluation of indoor radio channel characteristics was based on power delay profile, i.e., magnitude squared of the complex impulse response of the channel. The target throughput of 30 Mbps (corresponding to a coded moving picture) was assumed. Under the assumption of the required bit error rate of  $10^{-6}$ , 8 Mbps is achievable without an equaliser, 30 Mbps transmission is feasible with a 3-tap DFE equaliser, or even 70 Mbps transmission if a 7-tap DFE equaliser is used.

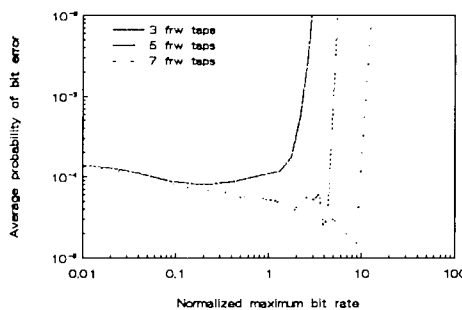


Fig. 8.5.5 Average probability of bit error versus normalised maximum bit rate for various number of forward taps.  
Room A.

In [41] a decision feedback equaliser (DFE) is considered and it is shown that the number of forward taps has a profound influence on the maximum normalised bit rate; an increase from 3 to 7 forward taps results in a maximum rate increase of about a factor of 5, as shown in fig. 8.5.5.

It could also be noted that a significant improvement of the maximum normalised bit rate (maximum bit rate multiplied by the rms delay spread) can be obtained by applying a high gain circular horn antenna at the base station or remote station instead of a biconical horn antenna. The best results are achieved if the remote is equipped with a circular horn.

### 8.5.6 HIPERLAN

In [42] the constraints on the choice of modulation scheme for HIPERLAN are described. First, requirements for the modulation scheme are discussed, such as: robustness to interference, low hardware complexity, constant envelope and amenability to low-complexity DFE structures. Some of these requirements arise from the peak envelope power restriction and the requirement for uncoordinated ad-hoc mesh networks. A steep spectral roll-off is required to accommodate four channels in 100 MHz bandwidth, and constant or near-constant envelope to avoid the need for highly linear amplifiers. Based on these criteria, two modulation schemes are selected:  $\pi/4$  DQPSK and GMSK. It is concluded that the linearity requirements of  $\pi/4$  DQPSK are too stringent for HIPERLAN, so continuous phase FSK is retained for further examination. Finally, GMSK modulation is shown to be a good compromise in terms of spectral roll-off and ISI.

In [43] the performance of the linear transversal equaliser (LTE) and the DFE is compared with the matched filter bound in a wide band tapped delay line that characterises the multipath fading in the indoor radio environment. Results show that the matched filter bound improves as the rms delay spread increases, and is virtually independent of roll-off factor. DFE is typically 2 dB and LTE 5 dB worse than the matched filter bound for the three delay spreads (50, 100 and 150 ns) considered by HIPERLAN. The performance of equalisation techniques for QPSK modulation with square root raised cosine filtering was evaluated using Monte Carlo simulations for the indoor channel. The channel impulse response consists of 128 independent taps with a uniform tap spacing of 7.8 ns. The ensemble average power delay profile is assumed to be exponential. Taking into account LTE, DFE and matched filter bound, the DFE closely follows the matched filter bound, and outperforms the LTE.

In [44] the effects of a finite equaliser span on the performance of a radio link in a delay spread channel are analysed. The equaliser is assumed to remove all ISI over a limited equaliser range of delays (its span). The residual ISI after the equaliser is combined with co-channel interference to produce a probability of outage, defined as the probability that the signal to interference ratio (SIR) falls below 10 dB. The

analysis shows that there is an irreducible outage probability which depends on the ratio of the rms delay spread to the equaliser span, see fig. 8.5.6.

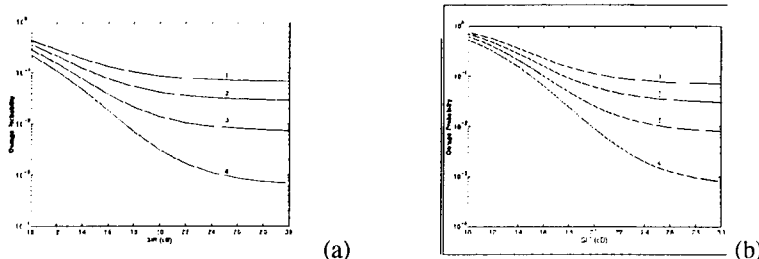


Fig. 8.5.6 Outage probability vs. SIR, simplified channel model, (a) single interferer, (b) two identical, independent interferers, RDS values: 1: 70 ns, 2: 60 ns, 3: 50 ns, 4: 40 ns.

Proposed modulation schemes for ESPRIT project 7359, LAURA, emphasising the synchronisation and training/acquisition properties are described in [45]. Three different sequences are embedded in the data to indicate "start of burst", "end of burst" and at regular intervals for measurement of phase rotation rate (frequency offset).

Simulations of the performance of synchronisation codes optimised for recovering frame synchronisation in an asynchronous mesh network are described in [46]. Because HIPERLAN is intended to operate without a central control station, synchronisation must be recovered on a packet by packet basis, using synchronisation sequences. The packet loss rate is a function of the false acceptance and false rejection rates, which depend on the correlator output threshold. The steepness of the curves indicates that the threshold level, set by the automatic gain control (AGC), must be very accurate. A sequence length of at least 80 bits is required to achieve a packet loss probability of 0.5%.

Because a large part of the research presented within the WG3 activities was related to the HIPERLAN standardisation activities, several papers were also presented at COST-231 where either the HIPERLAN system proposed was presented in general, or where the implementational aspects of HIPERLAN were discussed. In [47] the signal processing hardware in the LAURA project is described, see fig. 8.5.7. The transmission rate is 15 Mbps. The GMSK modulator, synchronisation circuits, equaliser and FEC decoder are described.

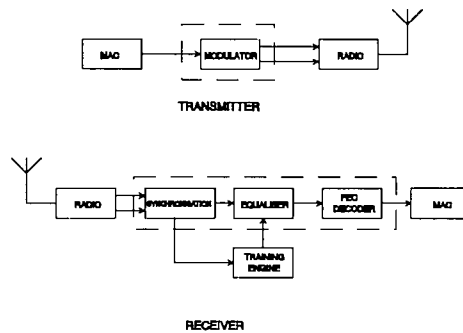
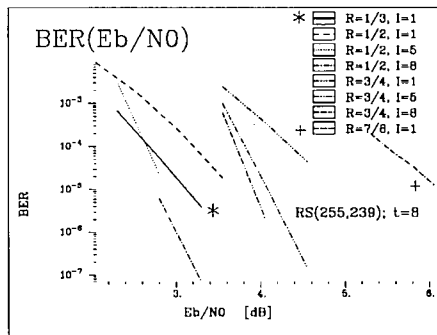


Fig. 8.5.7 System block diagram.

### 8.5.7 Channel coding

Ref. [48] discusses the requirements for error control in ATM-based indoor radio LANs. The maximum acceptable cell-loss rate varies from  $10^{-5}$  to  $10^{-9}$  according to the type of traffic. ATM is designed for fibre networks with very low BER and therefore has only end to end error control. Radio links require error control on a link by link basis to achieve the same cell loss rates. BCH codes capable of correcting one or two errors in a 511 bit block are considered, with and without a single re-transmission strategy (when uncorrectable errors are detected). It was found that dual antenna diversity was essential for all schemes to achieve the required transmission rates.

Fig. 8.5.8 The BER performance vs.  $E_b/N_0$  for concatenated and multiplexed coding schemes (soft decision). R — the rate of convolutional code; I — interleaving depth.

Ref. [49] addresses an issue of Viterbi decoding of convolutional codes in the situation where the speed of a single decoder chip is too low and multiplexed decoders have to be used. In the paper, two methods of multiplexing low speed Viterbi decoders are compared. In the first, multiple encoders are used and the data

multiplexed between them. In the second, a single encoder is used and the decoders operate on overlapping sections of the received data stream.

The required length of overlap depends on the code rate,  $E_b/N_0$ , and decision depth, and varied from a few bits to about 200. This was found not to be a major overhead as the block lengths could be up to 20,000 bits. Results of shortening the outer RS code, and RS symbol interleaving are also reported. The sufficient depth of interleaving is around 5–8 RS symbols, see fig. 8.5.8. Finally, no significant additional coding gain is expected from the decreased coding rate of a shortened RS code.

## 8.6 Network Performance Evaluation

**Peter Smulders, EUT, Netherlands, Ramjee Prasad, DUT, Netherlands  
and Stephen Barton, University of Leeds, UK**

A number of different network architectures and types of traffic have been considered within WG3. Access networks to a fibre backbone, which use radio only for the last 50m, will typically have a centrally controlled star architecture, with overlapping cell coverage areas accommodated by a frequency reuse pattern. In such networks all communication is between RS and BS, and either frequency (FDD) or time division duplex (TDD) can be used to separate the up- and down-link traffic. As with fixed networks, Medium Access Control (MAC) protocols based on demand assignment are better for networks with small numbers of nodes generating roughly constant traffic, while random access protocols are better for large numbers generating sporadic traffic. Ad-hoc networks, on the other hand, are essentially distributed in nature and therefore cannot accommodate any central control function, so random access protocols must be used. In this section a demand assignment protocol for access to the public switched B-ISDN network, a random access protocol for access to private computer networks such as FDDI, and some distributed protocols for ad-hoc networks are discussed.

### 8.6.1 Centralised control based on polling

Most efficient traffic throughput is provided by systems in which access to the medium is allocated centrally, provided the signalling overhead is not too great. Fairness is achieved by maintaining a unified queueing system in the central controller. A protocol based on access units matched to the standard 53-octet ATM cell, and proposed by Smulders and Blondia [50],[16] is described in this section.

It operates according to a request/permit mechanism as follows; each RS declares its capacity requirements by means of requests, which are sent to the master of the protocol located in the BS. Using these requests, together with parameters agreed at

call set-up, the protocol dynamically allocates the available upstream capacity. The RSs are then informed about the allocated capacity by means of permits.

Requests contain information about the number of ATM cells awaiting transmission in the local queue at the RS. Two types of requests are available:

- 1) Requests coupled to the upstream ATM cells. An RS which already has a permit to transmit a cell may attach a request to it.
- 2) Requests contained in dedicated request blocks. An RS which does not have a permit to transmit a cell must wait for the BS to declare a dedicated request block, and for its turn in the sequence to use these blocks.

Without the second type of request, an RS which had been inactive for a short time could never rejoin the system. The request blocks are the same length as an upstream cell, and contain<sup>1</sup> short request packets originating from a number of consecutive RSs.

Fig. 8.6.1 shows the upstream information structure. In this figure, a Physical Layer Packet Data Units (PL PDU) consists of a PL preamble including a request field and an ATM PDU, i.e., a standard ATM cell. The PL preamble may also include a field for error control, see [51],[16].

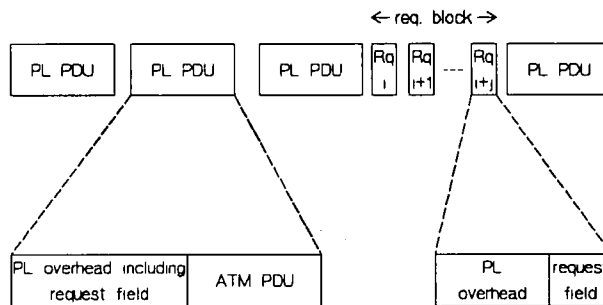


Fig. 8.6.1     Upstream information structure.

The protocol allocates the available capacity among the RSs by means of permits broadcast on the down-link. Permits are attached to downstream cells, which need not be addressed to the same RS as the permit. There are two types of permits, distinguished by a permit class bit, CL:

---

<sup>1</sup> A request block also contains a dedicated time slot in which a new station can send a request for registration. A randomised retransmission strategy is used to avoid persistent collisions and large retransmission delays. When the BS receives a request for registration it initiates a registration procedure and allocates an address to the new RS.

1) Permits for ATM cells. These ( $CL = 1$ ) contain the address of one RS, indicating that it is allowed to send one ATM cell.

2) Permits for request blocks. These ( $CL = 0$ ) contain the address of the next RS in the list. The permit entitles this RS, and the next five on the list, to send a short request packet.

The BS issues permits for request blocks whenever it has no permits for ATM cells to send. Therefore, the idle periods of the upstream traffic are used for transmitting request blocks. In this way, the spare upstream capacity is exploited to increase the reaction speed of the protocol to changing traffic situations. Fig. 8.6.2 shows the downstream traffic structure, both for permits for ATM cells and permits for request blocks.

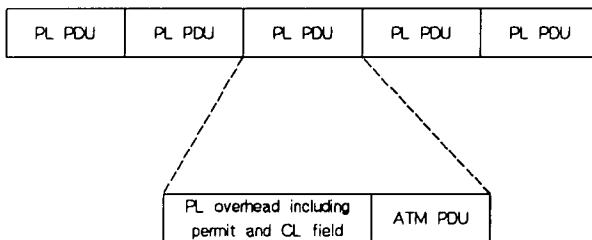


Fig. 8.6.2 Downstream information structure.

The main characteristics of the permit distribution algorithm are: 1) the peak bit rate per RS is enforced by spacing the cells, 2) a global FIFO discipline is used (over all RSs) to minimize cell delay variation and to achieve fair access, and 3) cells awaiting transmission are buffered in the RSs (distributed buffering).

To control the maximum allowed peak bit rate for each RS( $i$ ), the protocol enforces a minimum time spacing,  $t(i)$  between consecutive cells, inversely proportional to the peak bit rate agreed in an initial negotiation procedure between RS and BS. The number of new cell arrivals is deduced from the requests and the necessary permits are assigned to the RS. These permits are put into a FIFO queue together with permits for the other RSs with the constraint of minimum time spacing between two consecutive permits for the same RS. In this way, the actual queuing takes place in the RSs, while the central control in the BS maintains a permit FIFO queue, by which the transmission instants and the order in which the different RSs are emptied are governed.

The central controller maintains two counters per RS, one indicating the number of requests which have not yet been allocated a permit, and one indicating the time which must elapse before another permit can be granted to RS( $i$ ). The requests declare the number of cells currently waiting in the RS queue. From this is

subtracted the number of permits for RS(*i*) currently waiting in the BS permit queue. In this way the possibility of a cell remaining permanently in the RS because either request or permit is incorrectly received is avoided. Each time a new permit is added to the queue the timer is reset to  $t(i)$ . This is then decreased by one every timeslot until it reaches zero, when a new permit for RS(*i*) can be added to the queue. In this way the maximum rate for RS(*i*) is maintained at one cell per  $t(i)$  timeslots.

### 8.6.2 Centralized control based on random access

This section presents the throughput analysis of a random access protocol: nonpersistent inhibit sense multiple access (ISMA) in the mmw band for indoor communications. In random access protocols any RS may transmit whenever it believes the medium to be free, assisted by any side-information provided by the system. In a radio network a RS may not be able to detect the activity of another RS, even if its transmit and receive frequencies are the same. This “hidden node” problem means that Carrier Sense Multiple Access, with or without Collision Detection (CSMA/CD) becomes unreliable. On the other hand, differences in received signal levels at the BS from different RSs leads to a capture effect, in which collisions do not necessarily cause the loss of both colliding packets. Providing the signal to interference (plus inter-symbol-interference plus noise) ratio exceeds the “capture ratio”, denoted  $z_0$ , the stronger signal will be successfully received

In ISMA, the BS transmits inhibit bits on the down-link, indicating that the up-link is busy. The RS must wait until the inhibit bit is reset before it may transmit. This does not completely prevent collisions as two waiting RSs may start to transmit at the same time. This problem is mitigated to some extent by the nonpersistent random back-off algorithm. As with other contention based protocols, performance is further improved by a time slotting structure.

The performance of both slotted and unslotted non-persistent ISMA over an idealised mmw radio channel based on the results in section 8.3 above, and for various values of normalised RDS and  $z_0$  is presented in [52],[53]. An example of the results is shown in figure 8.6.3. This shows the throughput of slotted np-ISMA over the LOS channel with Ricean K-factor of 0 dB on both up- and down-links, and RDS = 0.5, for five different values of  $z_0$ .

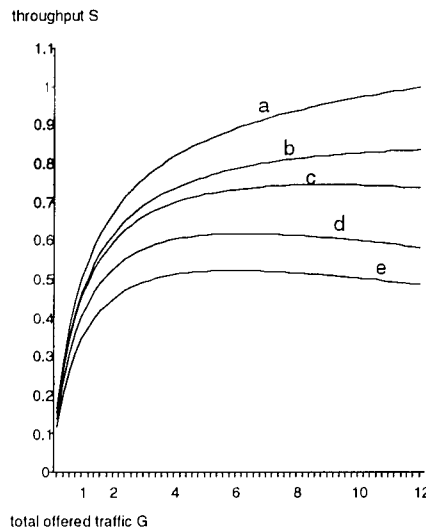


Fig.8.6.3 Throughput of slotted non-persistent ISMA, capture ratio = a: 0 dB, b: 2 dB, c: 4 dB, d: 6 dB, e: 8 dB.

### 8.6.3 Distributed Networks

In Ad-hoc networks there is no BS with overall control of access to the transmission medium. A node which happens to give access to the fibre backbone network is treated the same as any other. Communication is on a peer-to-peer basis and the network topology is Mesh. The lack of a central base station also means that there is no separation between up-link and down-link channels, so that a single channel is used for all traffic. This is no bad thing because typical LAN traffic is far from symmetrical, so that a fixed division of resources between up- and down-link traffic would be inefficient. It does introduce another problem for radio LANs, however, because a node cannot receive signals at -70 dBm from a distant transmitter at the same time as it is transmitting up to +30 dBm on the same

frequency. Thus collision detection is not available, so alternative means of avoiding collisions must be found. Three approaches, referred to as the COMB-scheme, Elimination Yield Non-Pre-emptive Priority Multiple Access (EY-NPMA), and Request to Send/Clear to Send (RTS/CTS) are discussed below.

The COMB scheme [37] is based on collision resolution rather than detection. Each node precedes its transmission by a signalling period in which it switches between transmitting and receiving according to some random pattern of bits known as the comb, see Fig. 8.6.4. All users contending for access to the channel synchronize to the end of the previous transmission, and transmit during the first 'tooth' of the comb. Where two users both transmit or both receive in the same tooth, they will not detect one another. As soon as one transmits when the other is receiving, the receiving one detects the other and defers. In this way, given sufficient teeth in the comb, the number of contending users is reduced to one, which can then transmit its data.

The COMB scheme is claimed to be more efficient than CSMA/CD because collisions are resolved, allowing one node to transmit successfully, whereas in CSMA/CD both contending nodes cease transmission. However, it does rely on all nodes being able to receive one another, i.e. it does not accommodate hidden nodes. The requirement to switch rapidly between transmit and receive mode is also difficult for the radios to meet.

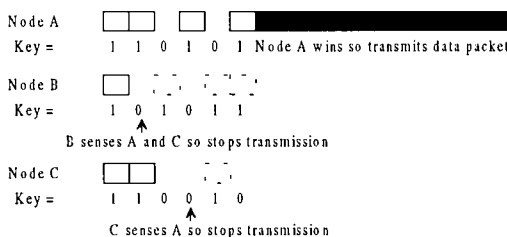


Fig. 8.6.4 COMB Scheme

The protocol which has been adopted for HIPERLAN, EY-NPMA [54] is a further development of the COMB scheme, requiring only a single signalling pulse to be transmitted before the data, and thus reducing the need for rapid switching of the radio between transmit and receive modes, see Fig. 8.6.5.

All contending nodes are again synchronised to the end of the previous burst. The access cycle is divided into four phases: prioritisation, elimination, yield and transmission. In the prioritisation phase, nodes listen to the channel for a number of 10 µs slots depending on the priority of the packet awaiting transmission. Top priority packets wait 10 µs, lower priority packets 20 µs etc. If no node of higher priority asserts the channel during its listening period, a node may transmit the priority assertion pulse. Otherwise it must defer until the next access cycle. Thus,

if the highest priority packet awaiting transmission is priority 3, all nodes with priority 3 packets transmit at the same time, i.e. after 30  $\mu$ s.

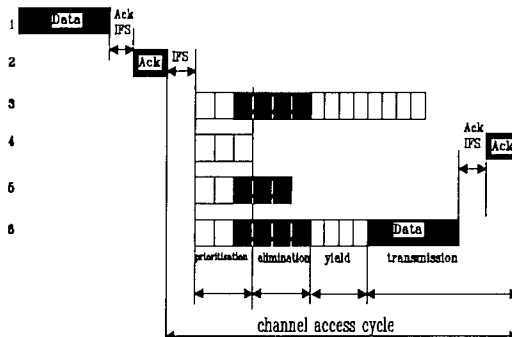


Fig. 8.6.5 EY-NPMA

In the elimination phase, all surviving nodes choose a random number of slots to transmit their elimination burst. At the end of its elimination burst a node must listen to check whether another node is still transmitting, in which case it defers until the next access cycle. The nodes which have chosen the longest elimination burst now move into the yield phase. Each surviving node now listens for a random number of slots. When the node which has chosen the smallest number of yield slots starts to transmit its data, any remaining survivors hear it and yield until the next access cycle.

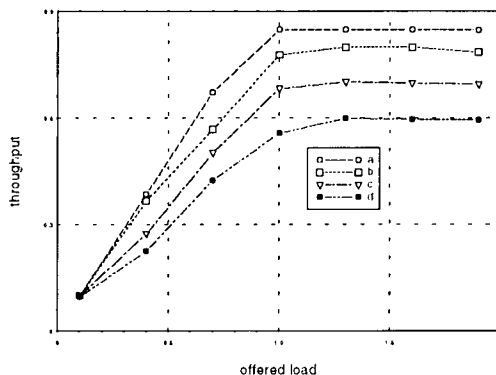


Fig. 8.6.6 Throughput with Hidden Nodes: a: fully connected, b: 1, c: 3, d: 5 pair of hidden nodes.

Fig. 8.6.6 shows the throughput of a network of ten nodes with different numbers of hidden nodes. There are  $10 \times (10 - 1)/2 = 45$  different possible connections [54]. The throughput rises to 0.85 for the fully connected network and remains at this level in the congested region. However, with increasing numbers of hidden node pairs the throughput is reduced. The main reason is that a node which is hidden from the current transmitter believes the channel to be free, and can therefore transmit asynchronously causing a collision at the receiver which can hear both.

The basic problem with these collision resolution protocols is that they rely on sensing the channel at the transmitter, whereas collisions occur at the receiver. One protocol has been proposed which does not suffer from this problem.

In the RTS/CTS protocol [54] data transmission is preceded by an exchange of short packets between source and destination nodes, see Fig. 8.6.7. The RTS and CTS packets contain source and destination addresses, and the length of the data packet which is to follow. Other nodes which hear either RTS or CTS defer for the length of the data packet. Any node which is might interfere with the data reception at the destination hears the CTS and defers, even if it is hidden from the source and cannot hear the RTS or the data. Unfortunately, the RTS/CTS protocol does not readily accommodate multicast or broadcast traffic. It is therefore included only as an option in the draft IEEE P802.11 standard.

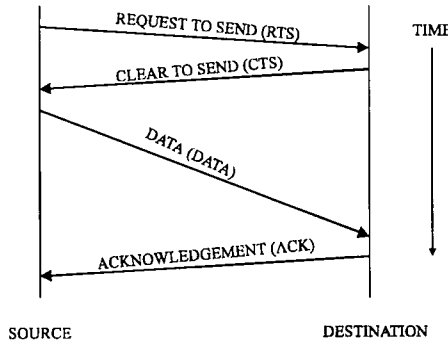


Fig. 8.6.7 RTS/CTS protocol

## 8.7 Summary

**Stephen Barton, University of Leeds, UK**

After eliminating IR as a candidate transmission medium on grounds of eye safety in section 8.1.1, and finding mmw technology relatively mature and safe in section 8.1.2, the next three sections concentrated on mmw channel characterisation. In section 8.2 methods of characterising building materials at mmw based on scattering, bistatic reflection and transmission were described and the main electrical parameters of many common building materials tabulated. Also tabulated were the minimum thicknesses required for various degrees of isolation between rooms to control interference. Walls made from all materials except glass and plasterboard will provide sufficient isolation to enable re-use of the same frequency in every room.

Section 8.3 described narrow and wideband measurements, statistical and deterministic modeling of the mmw indoor radio channel. The narrowband measurements concern mainly DOA, which can be used to investigate individual signal paths. The results indicate that a gain of 8.4 dB can be achieved by using an adaptively steered antenna at the remote station. Wideband measurements in a variety of indoor areas with different shapes, dimensions and wall material were described. From the resulting time-domain data base, cell coverage and RDS under LOS and OBS conditions were derived. Values varied between 10 and 100 ns.

A statistical model for the power delay profile of the indoor mmw channel has been derived from the measurements. It consists of an LOS ray followed by a constant level part up to 60 ns, followed by a linear decrease (in dB). A deterministic model of mmw indoor radio propagation based on GO was also described. Computer simulations with various combinations of antenna characteristics showed that a setup with biconical horns at both ends yields NRP and RDS which are insensitive to LOS blocking and distance.

Section 8.4 described narrow and wideband measurements, statistical and deterministic modeling of the outdoor mmw channel. Here the Oxygen absorbtion is expected to limit cell radii to less than 1 km. The break point between inverse square law and fourth power law propagation is found to be at least 7 km, so that in all realistic situations a path loss exponent between 2 and 2.5 can be assumed. Wideband measurements and a ray-tracing model indicated that DS in city streets and tunnels would be in the 10 - 50 ns range while in open areas such as squares it could reach 100 ns or more.

Section 8.5 reviews the main types of transmission techniques which may be used to overcome the limitations of the wideband multipath dispersive channel. These are DSSS with a RAKE receiver, multicarrier or OFDM modulation, antenna diversity and adaptive equalisation. Studies of equaliser performance in the

HIPERLAN application are also considered. The section also includes material on synchronisation in HIPERLAN and channel coding for wideband radio systems.

In section 8.6 MAC protocols for ATM access to the public B-ISDN, for random access to a wired backbone network, and for ad-hoc networks are described. The first uses a request/permit mechanism to control the access to the shared medium. The available capacity is allocated by means of a global FIFO queue in so that the peak bit rate is enforced. In the second, the uplink is declared busy or free by inhibit bits transmitted on the downlink. This enables RSs to avoid collisions. In the ad-hoc networks there is no BS to control access to the channel so a distributed protocol must be used. Two contention resolution protocols based on sensing the channel at the transmitter and one based on a handshake procedure are described.

## 8.8 References

- [1] J. J. G. Fernandes, P. A. Watson and J. C. Neves, "Wireless LANs: Physical Properties of Infrared Systems vs Mmw Systems", IEEE Communications Magazine, August, 1994
- [2] P. F. M. Smulders, "Feasibility Considerations of Broadband Indoor Networks", Proc. of the Int. Symp. on Subscriber Loops and Services '91, April 1991, pp. 76-80.
- [3] P. Blakeborough, "Reflection Coefficients in the Range 8 to 50 GHz for Typical Indoor Building Materials", COST 231 TD(92)050, Leeds, Apr. 1992
- [4] S. Meyer, J. C. Leost, J. Guena, E. Penard and M. Goloubkoff, "Experimental Characterization of a 60 GHz Communication Channel Inside a Building", International Symposium on Personal, Indoor and Mobile Radio Communications, Yokohama, Sep. 8-11, 1993
- [5] L.M. Correia and P.O. Francês, "Materials Characteristics in the Millimetre Waveband", COST 231 TD(93)065, Barcelona, May 1993
- [6] J. Lähteenmäki and T. Karttaavi, "Transmission Coefficient Measurements of Building Structures at 60 GHz", COST 231 TD(93)115, Limerick, Sep. 1993
- [7] B. Langen, G. Lober and W. Herzog, "Reflection and Transmission Behaviour of Building Materials at 60 GHz", International Symposium on Personal, Indoor and Mobile Radio Communications, The Hague, Sep. 21-23, 1994
- [8] L. M. Correia and P. O. Francês, "Estimation of Materials Characteristics from Power Measurements at 60 GHz", International Symposium on Personal, Indoor and Mobile Radio Communications, The Hague, Sep. 21-23, 1994
- [9] J. D. Parsons, "The Mobile Radio Propagation Channel", Pentech Press, London, 1992

- [10] G. Dahlquist and A. Björck, "Numerical Methods", Prentice-Hall, Englewood Cliffs, N.J., 1974
- [11] K. Sato, T. Manabe, I. Ihara, Y. Kasashima, and K. Yamaki, "Measurement of Reflectivities of Interior Construction Materials at 60 GHz" (in Japanese), Tech. Report of IEICE Japan, AP 93-36, June 1993
- [12] J. Lähteenmäki, "Modelling of the Indoor Short Range Propagation Channel", 24th European Microwave Conference, Workshop on short range radio communications, Cannes, Sep. 1994, pp 167 - 172.
- [13] S. Guérin, "Indoor Wideband and Narrowband Propagation Measurements around 60.5 GHz in Empty and Furnished Room", VTC'96, April 28 - May 1, Atlanta, GA.
- [14] L. M. Correia and P. O. Francès, "Transmission and Isolation of Signals in Buildings at 60 GHz", International Symposium on Personal, Indoor and Mobile Radio Communications, Toronto, Sep. 27-29, 1995.
- [15] P. F. M. Smulders, A. G. Wagemans, "Wideband measurements of mm-wave indoor radio channels", Proc. of the IEEE 3th Int. Symp. on Personal, Indoor and Mobile Radio Commun, Oct 1992., pp. 329-333.
- [16] P. F. M. Smulders, "Broadband Wireless LANs: A Feasibility Study", Ph.D. thesis, ISBN: 90-386-0100-X, 1995.
- [17] G. Kadel, "Doppler analysis of wide-band propagation measurements", Nachrichtentechnik & Elektronik, Berlin 42 (1662), pp 13 (in German).
- [18] P. F. M. Smulders, A.G. Wagemans, "Biconical Horn Antennas for Uniform Coverage in Indoor Areas at Mm-Wave Frequencies", IEEE Trans. Veh. Technol., Vol. VT-43, no. 4, pp. 897-901, Nov. 1994.
- [19] P. F. M. Smulders, "Geometrical optics model for millimetre-wave indoor radio propagation", Electr. Lett., Vol. 29, pp. 1174-1176, June 1993.
- [20] P. A. Watson, "Modelling radio propagation at millimetre wavelengths for communications and remote sensing", 7th International Conference on Antennas and Propagation, Apr. 1991.
- [21] K. Gunmar, "Broadband Technique for Car to Car Communication at 60 GHz", COST 231 TD(91)041, Lund, Sweden, June 1991.
- [22] Z. Ghebretensae, "Simulation of Beacon-Vehicle Communications for Drive Applications", COST 231 TD(92)053, Leeds, U.K., Apr. 1992.
- [23] A. R. Tharek and J. P. McGeehan, "Outdoor Propagation Measurements in the Millimetre Wave Band at 60 GHz", Military Microwaves'88, July 1988.

- [24] N. D. Hawkins, R. Steele, D.C. Rickard and C.R. Shepherd, "Path Loss Characteristics of 60 GHz Transmissions", Electron. Lett., Vol. 21, No. 22, pp. 1054-1055, 24th Oct. 1985.
- [25] L. M. Correia and P. O. Francês, "A Propagation Model for the Estimation of the Average Power in an Outdoor Environment in the millimetre waveband", IEEE 44th Vehicular Technology Conference, Stockholm, Sweden, June 1994.
- [26] ITU-R Rep. 719-2, Recommendations and Reports of the CCIR, Vol. V, ITU, Geneva, 1986.
- [27] ITU-R Rep. 721-2, Recommendations and Reports of the CCIR, Vol. V, ITU, Geneva, 1986.
- [28] G. Løvnes, S. E. Paulsen and R. H. Rækken, "A Versatile Channel Sounder for Millimetre Wave Measurements", 4th IEEE International Symposium on Personal, Indoor and Mobile Radio Communications, Yokohama, Japan, Sep. 8-11, 1993
- [29] G. Løvnes, J. J. Reis and R. H. Rækken, "Channel Sounding Measurements at 59 GHz in City Streets", 5th IEEE International Symposium on Personal, Indoor and Mobile Radio Communications, The Hague, The Netherlands, Sep. 21-23, 1994.
- [30] E. Antonsen, G. Løvnes, J. J. Reis and R. H. Rækken, "59 GHz Wideband Propagation Measurements", Telenor R&D Report TF R 36/94, Kjeller, Norway, 1994.
- [31] J. J. Reis and L. M. Correia, "A Propagation Model for Outdoor Mobile Communications at the Millimetre Waveband in Urban Scenarios", COST231 TD(95)002, Bern, Jan. 1995.
- [32] H. Aghvami, I. D. Robertson, and S. A. Mohamed, "High Bit-Rate Indoor Radio Communications", 3rd IEE Conference on Telecommunications, March 1991, pp. 101-106.
- [33] H. Amca and P. A. Watson, "Simulation of MPSK and Wideband FM in Multipath LOS Channels Subject to Co-Channel Interference", COST231 TD (92) 109, Helsinki, Sep. 1992.
- [34] P. F. M. Smulders and H. T. Müskens, "Bit Rate Performance of Millimetre-Wave Indoor Radio Systems", Electron. Lett., Vol. 28, No 23, Nov. 1992, pp. 2152-2153.
- [35] T. A. Wilkinson and S. K. Barton, "Spread Spectrum for Radio Local Area Networks", URSI International Symposium on Signals, Systems and Electronics, Paris, 1-4 September 1992, pp. 60-63.
- [36] T. A. H. Wilkinson, I. R. Johnson, and S. K. Barton, "Performance of Direct Sequence Spread Spectrum ISM-Band Radio LANs in a Multipath Time

Dispersive Channel”, Electronics Letters Vol. 29, No. 24, 25th November 1993, pp. 2048-2085.

[37] T. A. H. Wilkinson, T. G. C. Phipps and S. K. Barton, “A report on HIPERLAN Standardisation”, International Journal on Wireless Information Networks, Vol 2, No 2, 1995, pp. 99-119.

[38] L. Vandendorpe and O. van de Wiel, “Performance Analysis of Linear MIMO Equalisers for Multitone DS/SS Systems in Multipath Channels”, Wireless Personal Communications, Special Issue on Multicarrier Techniques, Vol. 2, No 1-2, 1995, pp. 145-165.

[39] G. J. M. Janssen, L. Maranatha, and R. Prasad, “Evaluation of BER Performance for Measured Indoor Microwave Channels Using Quasi-Coherent Combining of Multiple Antenna Signals”, pp.239-253 in Mobile and Personal Communications, Proc. 2nd Joint COST 227/231 Workshop, Firenze, 20-21 April 1995, ed. E del Re, Elsevier, Amsterdam, 1995.

[40] G. J. M. Janssen, “Dual-Signal Receiver Structures for Simultaneous Reception of Two BPSK Modulated Co-Channel Signals Using Signal Cancellation”, Wireless Personal Communications, vol. 1, no. 1, 1994, pp. 43-59.

[41] P. F. M. Smulders and H. T. Müskens, “Performance of Decision Feedback Equalisation in mm-Wave Indoor Radio Systems”, IEEE 2nd Int. Symp. on Univ. Personal Commun., Ottawa, Oct. 1993, pp. 890-893.

[42] M. Li, A. Nix, J. Marvill, M. A. Beach, T. A. H. Wilkinson, I. R. Johnson, and S.K. Barton, “Radio LANs Air Interface Technique Using Equalisation”, WCN'94, The Hague, 21-23rd September 1994, pp. 964-968.

[43] C. Tellambura, Y. J. Guo, and S. K. Barton, “Equaliser Performance for HIPERLAN in Indoor Channels”, Wireless Personal Communications special issue on HIPERLAN, Vol. 3, No. 4, 1996, pp 397 - 410.

[44] C. Tellambura, Y. J. Guo, and S. K. Barton, “Co-channel and Self Interference Analysis for Indoor Wireless Channels”, Wireless Personal Communications special issue on HIPERLAN, Vol. 3, No. 4, 1996, pp 411 - 419.

[45] I. R. Johnson, T. A. H. Wilkinson, A. E. Jones, S. K. Barton, M. Li, A. Nix, J. Marvill, and M. A. Beach, “On Suitable Codes for Frame Synchronisation in Packet Radio LANs”, 44th Vehicular Technology Conference, Stockholm, 7-11th June 1994, pp. 1421-1424.

[46] D. A. G. Gillies, Y. J. Guo, and S. K. Barton, “Synchronisation Techniques for HIPERLAN”, Wireless Personal Communications special issue on HIPERLAN, Vol. 4, No. 1, 1997, pp 1 - 10.

- [47] I. R. Johnson and S. K. Barton, "Signal Processing Hardware in a Radio LAN Demonstrator", Wireless Personal Communications special issue on HIPERLAN, Vol. 3, No. 4, 1996, pp 429 - 443.
- [48] P. F. M. Smulders, "Error Control in ATM-Based Indoor Radio LANs", IEEE 5th Int. Symp. on Personal, Indoor and Mobile Radio Comm., The Hague, Sept. 1994, pp. 237-241.
- [49] P. Matuszczak, W. Holubowicz, and M. Moeneclaey, "Satellite Modems Using Multiplexed and Concatenated Codes", 3rd International Symposium on Communication Theory and Applications, Ambleside 1995, pp. 347-354.
- [50] P. F. M. Smulders and C. Blondia, "Application of the Asynchronous Transfer Mode in Indoor Radio Networks", WCN'94, The Hague, pp. 839-843, Sept. 1994.
- [51] P. F. M. Smulders, "Error Control in ATM-Based Indoor Radio LANs", Proc. of the IEEE 5th Int. Symp. on Personal, Indoor and Mobile Radio Comm., The Hague, pp. 237-241, Sept. 1994.
- [52] R. Prasad, "Performance analysis of mobile packet radio networks in real channels with inhibit sense multiple access", IEE Proc-I, Vol 138, No.5, October 1991.
- [53] R. Prasad and C. Y. Liu, "Throughput analysis of some mobile packet radio protocols in Rician fading channels", IEE Proc-I, Vol 139, No.3, June 1992.
- [54] K. Fu, Y. J. Guo and S. K. Barton, "Performance of the EY-NPMA Protocol with Hidden Nodes", Wireless Personal Communications special issue on HIPERLAN, Vol. 4, No. 1, 1997, pp 41 - 50.

# Annex I

---

## List of Participating Entities

Aalborg University, Denmark  
Alcatel Mobile Communications, France  
Alcatel SEL, Germany  
Alcatel Sesa, Spain  
ASCOM - Autophon, Austria  
Austrian PTT, Austria  
Bosch Communication Research Institute, Germany  
British Telecom Laboratories, United Kingdom  
Brunel University, United Kingdom  
CNET - France Telecom, France  
Creative Mobile Consultants, France  
CSELT, Italy  
DETECON, Germany  
DeTeMobil, Germany  
Deutsche Aerospace, Germany  
Deutsche Telekom, Germany  
EPFL, Switzerland  
École Nationale Supérieure de Télécommunications, France  
Electronica ENSA, Spain  
Elektroniksystem und Logistik, Germany  
E-Plus Mobilfunk, Germany  
Ericsson Radio Systems, Sweden  
Ericsson Business Mobile Networks, The Netherlands  
ESA/ESTEC, The Netherlands  
ETHZ, Switzerland  
Fundazione Ugo Bordoni, Italy  
France Telecom Mobiles, France  
Franco-Polish School of Poznam, Poland  
General Directorate of Post and Telecom, Finland  
Helsinki Telephone Company, Finland  
Hutchison Microtel, United Kingdom  
King's College, United Kingdom  
IMST, Germany  
Institut Jozef Stefan, Slovenia  
Instituto Superior Técnico, Portugal  
IREE - Academy of Sciences, Czech Republic  
Iskra Ljubljana, Slovenia  
Istituto Superiore PT, Italy

Italtel, Italy  
KPN Research, The Netherlands  
Mannesman Mobilfunk, Germany  
Matra Communication, France  
Mercury Personal Communications, United Kingdom  
Nokia Telecommunications, Finland  
Philips Drake Electronics, United Kingdom  
Politecnico di Milano, Italy  
Poznam University of Technology, Poland  
Radiocommunications Agency, United Kingdom  
Roke Manor Research, United Kingdom  
Siemens, Germany  
SFR/GIE Cofira, France  
Swisscom, Switzerland  
Technical University of Athens, Greece  
Technical University of Delft, The Netherlands  
Technical University of Eindhoven, The Netherlands  
Technical University of Middle East, Turkey  
Technische Universität Braunschweig, Germany  
Technische Universität Dresden, Germany  
Technische Universität Hamburg-Harburg, Germany  
Technische Universität München, Germany  
Technische Universität Wien, Austria  
Technology Development Centre of Finland, Finland  
Telecom Denmark Mobil, Denmark  
Telecom Finland, Finland  
Telecom Italia, Italy  
Telefonica I+D, Spain  
Telefunken Systems, Germany  
Telenor R&D, Norway  
Telettra Espana, Spain  
Telia Research, Sweden  
Thomson-CSF, France  
TRT, France  
Universidad de Cantabria, Spain  
Universidad Politecnica de Catalunya, Spain  
Universidad Politecnica de Madrid, Spain  
Universidad Politecnica de Valencia, Spain  
Universita di Bologna, Italy  
Universität Erlangen, Germany  
Universität Kaiserslautern, Germany  
Universität Karlsruhe, Germany  
Universität Siegen, Germany  
Universität Stuttgart, Germany  
Universität Ulm, Germany  
Université Catholique de Louvain, Belgium

University of Aveiro, Portugal  
University of Bradford, United Kingdom  
University of Bristol, United Kingdom  
University College of Swansea, United Kingdom  
University of Dublin, Ireland  
University of Faroe Islands, Faroe Islands  
University of Leeds, United Kingdom  
University of Limerick, Ireland  
University of Lund, Sweden  
University of York, United Kingdom  
Vodafone, United Kingdom  
VTT Information Technology, Finland  
Yorkshire Television, United Kingdom



# Annex II

---

## List of Editors/Contributors

- J. Bach Andersen, Aalborg University, Denmark  
P.W. Baier, Universität Kaiserslautern, Germany  
S.K. Barton, University of Bradford, United Kingdom  
M.A. Beach, University of Bristol, United Kingdom  
J.-E. Berg, Ericsson Radio Systems, Sweden  
J.-C. Bic, CNET - France Telecom, France  
J.J. Blanz, Universität Kaiserslautern, Germany  
E. Bonek, Technische Universität Wien, Austria  
C.J. Burkley, University of Limerick, Ireland  
A. Burr, University of York, United Kingdom  
F. Casadevall, Universidad Politecnica de Catalunya, Spain  
D.J. Cichon, Universität Karlsruhe, Germany  
L.M. Correia, Instituto Superior Técnico, Portugal  
P.J. Cullen, University of Dublin, Ireland  
D. Dahlhaus, ETHZ, Switzerland  
E. Damosso, CSELT, Italy  
J.T. Deilkås, Telenor Mobile, Norway  
L. Delaunay-Ledter, CNET - France Telecom, France  
P. Eggers, Aalborg University, Denmark  
B.E. Eskedal, Telenor R&D, Norway  
B. Fleury, ETHZ, Switzerland  
T. Frey, Universität Ulm, Germany  
J. Fuhl, Technische Universität Wien, Austria  
R.J. Goodwin, Roke Manor Research, United Kingdom  
S. Guérin, CNET - France Telecom, France  
W. Holubowicz, Franco-Polish School of Poznam, Poland  
P. Hulbert, Roke Manor Research, United Kingdom  
J. Jimenez, Telefonica I+D, Spain  
P. Jung, Universität Kaiserslautern, Germany  
G. Kadel, Deutsche Telekom, Germany  
G. Kandus, Institut Jozef Stefan, Slovenia  
P. Karlsson, Telia Research, Sweden  
A. Klein, Universität Kaiserslautern, Germany  
G. Krämer, ETHZ, Switzerland  
T. Kürner, E-Plus Mobilfunk, Germany  
J. Lähteenmäki, VTT Information Technology, Finland  
P.H. Lehne, Telenor R&D, Norway  
U. Loher, ETHZ, Switzerland

L. Lopes, University of Leeds, United Kingdom  
J. Løvsletten, Telenor Mobile, Norway  
P.E. Mogensen, Aalborg University, Denmark  
A.F. Molish, Technische Universität Wien, Austria  
M.M. Naßhan, Universität Kaiserslautern, Germany  
H. Novak, Technische Universität Wien, Austria  
V. Palestini, CSELT, Italy  
G.F. Pedersen, Aalborg University, Denmark  
V. Perez, Telefonica I+D, Spain  
M. Pettersen, Telenor R&D,Norway  
R. Prasad, Technical University of Delft, The Netherlands  
R.H. Rækken, Telenor R&D,Norway  
A. Radovic, ETHZ, Switzerland  
A. Rodrigues, Instituto Superior Técnico, Portugal  
H. Rohling, Technische Universität Braunschweig, Germany  
G. Romano, CSELT, Italy  
S. Ruiz Bouqe, Universidad Politecnica de Catalunya, Spain  
J. Rupprech, Swisscom, Switzerland  
P. Smulders, Technical University of Eindhoven, The Netherlands  
A. Steil, Universität Kaiserslautern, Germany  
B. Steiner, Universität Kaiserslautern, Germany  
M. Streeton, Roke Manor Research, United Kingdom  
L. Vandendorpe, Université Catholique de Louvain, Belgium  
J.-F. Wagen, Swisscom, Switzerland  
J. Wigard, Aalborg University, Denmark  
E. Zollinger, IMST, Germany

European Commission

**EUR 18957 — COST Action 231**

**Digital mobile radio towards future generation systems —  
Final report**

Luxembourg: Office for Official Publications of the European Communities

1999 — xxxiv, 474 pp. — 14.8 x 21 cm

ISBN 92-828-5416-7



**Venta • Salg • Verkauf • Πωλήσεις • Sales • Vente • Vendita • Verkoop • Venda • Myynti • Försäljning**

<b>BELGIQUE/BELGIË</b>	<b>ÖSTERREICH</b>	<b>HRVATSKA</b>	<b>ISRAËL</b>
<p>Jean De Lannoy Avenue du Roi 202/Koningslaan 202 B-1190 Bruxelles/Brussel Tel. (32-2) 536 43 00 Fax (32-2) 536 08 61 E-mail: <a href="mailto:jean-de-lannoy@infoboard.be">jean-de-lannoy@infoboard.be</a> URL: <a href="http://www.jean-de-lannoy.be">http://www.jean-de-lannoy.be</a></p> <p>La librairie européenne/ De Europeesche Boekhandel Rue de la Loi 244/Wetstraat 244 B-1040 Bruxelles/Brussel Tel. (32-2) 295 26 39 Fax (32-2) 326 00 60 E-mail: <a href="mailto:mail@libeurop.be">mail@libeurop.be</a> URL: <a href="http://www.libeurop.be">http://www.libeurop.be</a></p> <p>Monteur belge/Belgisch Staatsbed Rue de la Loi 424/Wetstraat 42 B-1040 Bruxelles/Brussel Tel. (32-2) 532 22 11 Fax (32-2) 511 01 84</p>	<p>Manz'sche Verlags- und Universitätsbuchhandlung GmbH Kohlmarkt 16 A-1010 Wien Tel. (43-1) 53 16 11 00 Fax (43-1) 53 16 11 07 E-mail: <a href="mailto:bestellen@manz.co.at">bestellen@manz.co.at</a> URL: <a href="http://www.manz.at/index.htm">http://www.manz.at/index.htm</a></p>	<p>Mediatrade Ltd Pavila Hatzka 1 HR-10000 Zagreb Tel. (385-1) 481 94 11 Fax (385-1) 481 94 11</p>	<p>ROY International 41, Mishmar Hayarden Street PO Box 13056 61150 Ramat Gan Tel. 972-3 649 94 69 Fax 972-3 648 60 39 E-mail: <a href="mailto:roy@nevision.net.il">roy@nevision.net.il</a> URL: <a href="http://www.royint.co.il">http://www.royint.co.il</a></p>
<b>DANMARK</b>	<b>PORTUGAL</b>	<b>Sub-agent for the Palestinian Authority: Index Information Services</b>	
<p>J. H. Schultz Information A/S Herstedvæng 10-12 DK-2620 Albertslund Tel. (45) 43 63 23 00 Fax (45) 43 83 68 69 E-mail: <a href="mailto:schultz@schultz.dk">schultz@schultz.dk</a> URL: <a href="http://www.schultz.dk">http://www.schultz.dk</a></p>	<p>Distribuidora de Livros Bertrand Ltd.<sup>*</sup> Gruppo Bertrand, SA Av. das Necessidades, 4-A Apartado 60037 P-2700 Amadora Tel. (351-1) 495 90 50 Fax (351-1) 496 02 55</p>	<p>EuroInfo Services Éuropa Ház Margitsziget PO Box 475 H-1475 Budapest 62 Tel. (36-1) 350 90 25 Fax (36-1) 350 90 32 E-mail: <a href="mailto:euroinfo@mail.metav.hu">euroinfo@mail.metav.hu</a> URL: <a href="http://www.euroinfo.hu/index.htm">http://www.euroinfo.hu/index.htm</a></p>	<p>Sub-agent for the Palestinian Authority: Index Information Services PO Box 19502 Jerusalem Tel. 972-2 627 16 34 Fax 972-2 627 12 19</p>
<b>DEUTSCHLAND</b>	<b>SUOMI/FINLAND</b>	<b>JAPAN</b>	
<p>Bundesanzeiger Verlag GmbH Vertriebsabteilung Amsterdamer Straße 192 D-50735 Köln Tel. (49-221) 97 68 80 Fax (49-221) 97 68 70 E-mail: <a href="mailto:vertrieb@bundesanzeiger.de">vertrieb@bundesanzeiger.de</a> URL: <a href="http://www.bundesanzeiger.de">http://www.bundesanzeiger.de</a></p>	<p>Imprensa Nacional-Casa da Moeda, EP Rua Marquês Sá de Bandeira, 16-A Tel. (351-21) 507 99 99 Fax (351-1) 533 02 94 E-mail: <a href="mailto:decim@intra.pt">decim@intra.pt</a> URL: <a href="http://www.intra.pt">http://www.intra.pt</a></p>	<p>PSI-Japan Asahi Sanbancho Plaza #206 7-1 Sanbancho, Chiyoda-ku Tokyo 102 Tel. 81-3 32 34 69 21 Fax 81-3 32 34 69 15 E-mail: <a href="mailto:books@psi-japan.co.jp">books@psi-japan.co.jp</a> URL: <a href="http://www.psi-japan.com">http://www.psi-japan.com</a></p>	
<b>ΕΛΛΑΣ/GREECE</b>	<b>SVERIGE</b>	<b>MALAYSIA</b>	
<p>G. C. Elterhoudeklis SA International Bookstore Faneroplistis 10 GR-10554 Athens Tel. (30-1) 331 41 80/2/3/4/5 Fax (30-1) 323 98 21 E-mail: <a href="mailto:eltebooks@elcor.gr">eltebooks@elcor.gr</a></p>	<p>Akateeminen Kirjakauppa/ Akateemische Buchhandlung Keskustori 1/Centralringstrasse 1 PL/PB 128 FIN-00101 Helsinki/Helsingfors P-addr. <a href="mailto:helsinki@akateeminen.com">helsinki@akateeminen.com</a> URL: <a href="http://www.akateeminen.com">http://www.akateeminen.com</a></p>	<p>MILLER DISTRIBUTORS LTD Millers International Airport PO Box 25 Luqa LO 05 Tel. (356) 66 44 88 Fax (356) 67 67 99 E-mail: <a href="mailto:gwrth@usa.net">gwrth@usa.net</a></p>	<p>EBIC Malaysia Level 7, Wisma Hong Leong 18 Jalan Perak 50450 Kuala Lumpur Tel. (60-3) 262 62 98 Fax (60-3) 262 61 98 E-mail: <a href="mailto:ebic_kl@mot.net.my">ebic_kl@mot.net.my</a></p>
<b>ESPAÑA</b>	<b>UNITED KINGDOM</b>	<b>MÉXICO</b>	
<p>Boletín Oficial del Estado Trabajos 27 E-28070 Madrid Tel. (34) 915 28 21 11 (Libros), 913 84 17 51 (Suscripc.) Fax (34) 915 28 21 (Libros), 913 84 17 51 (Suscripc.) E-mail: <a href="mailto:clientes@com.boe.es">clientes@com.boe.es</a> URL: <a href="http://www.boe.es">http://www.boe.es</a></p>	<p>THE Stationery Office Ltd International Sales Agency 51 Nine Elms Lane London SW8 4JH Tel. (44-171) 873 90 90 Fax (44-171) 873 84 03 E-mail: <a href="mailto:psa.enquiries@theso.co.uk">psa.enquiries@theso.co.uk</a> URL: <a href="http://www.the-stationery-office.co.uk">http://www.the-stationery-office.co.uk</a></p>	<p>Mundi Prensa Mexico, SA de CV Río Pánuco No 141 Colonia Cuernavaca MX-06200 Mexico, DF Tel. (525-2) 533 56 58 Fax (52-5) 514 67 99 E-mail: <a href="mailto:101545.2361@compuserve.com">101545.2361@compuserve.com</a></p>	
<b>FRANCIA</b>	<b>ISLAND</b>	<b>PHILIPPINES</b>	
<p>Journal officiel Service des publications des CE 26, rue Descartes F-75727 Paris Cedex 15 Tel. (33) 140 57 77 00 Fax (33) 140 57 77 00 URL: <a href="http://www.journal-officiel.gouv.fr">http://www.journal-officiel.gouv.fr</a></p>	<p>Bokabud Larusei Blöndal Skólastofnun Íslands Skólaþorðshús, 2 107 Reykjavík Tel. (354) 551 56 50 Fax (354) 552 56 50</p>	<p>EBIC Philippines 19th Floor, PS Bank Tower Sen. Gil Puyat Ave. cor. Tindalo St. Makati City Metro Manila Tel. (63-2) 759 66 80 Fax (63-2) 759 66 90 E-mail: <a href="mailto:ecppcm@global.com.ph">ecppcm@global.com.ph</a> URL: <a href="http://www.ecppcm.com.ph">http://www.ecppcm.com.ph</a></p>	
<b>IRELAND</b>	<b>NORGE</b>	<b>SRI LANKA</b>	
<p>Government Supplies Agency Publications Section 4.5 Howth Road Dublin 2 Tel. (353-1) 661 31 11 Fax (353-1) 475 27 60</p>	<p>Swets Norge AS Ostensjøveien 18 Boks 6512 Elterstad Bergen 5020 Tel. (47-22) 97 45 00 Fax (47-22) 97 45 45</p>	<p>EBIC Sri Lanka Trans Asia Hotel 115 Sir cchampalambam A. Gardiner Mawatha Colombo 2 Matale City Metro Manila Tel. (94-1) 074 71 50 78 Fax (94-1) 44 87 70 E-mail: <a href="mailto:abcsl@imin.com">abcsl@imin.com</a></p>	
<b>ITALIA</b>	<b>SWITZERLAND</b>	<b>THAILAND</b>	
<p>L'Isola SpA Via Duce di Calabria, 1/1 Casella postale 552 I-50129 Firenze Tel. (36-55) 48 63 Fax (36-55) 64 12 57 E-mail: <a href="mailto:liscosa@fbcc.it">liscosa@fbcc.it</a> URL: <a href="http://www.fbcc.it/liscosa">http://www.fbcc.it/liscosa</a></p>	<p>Europress Euromedia Ltd 59, 1030 Bratislava 93-10000 Bratislava Tel. (386-2) 980 37 66 Fax (386-2) 980 42 30 E-mail: <a href="mailto:Milena@lboxx.cz">Milena@lboxx.cz</a></p>	<p>EBIC Thailand 29 Vinitassa Building, 8th Floor Soi Charoen Ploenchit 10300 Bangkok Tel. (66-2) 655 06 27 Fax (66-2) 655 06 26 E-mail: <a href="mailto:abcba@ksc15.th.com">abcba@ksc15.th.com</a> URL: <a href="http://www.abcba.com">http://www.abcba.com</a></p>	
<b>LUXEMBOURG</b>	<b>CÉSKE REPUBLIKÁ</b>	<b>UNITED STATES OF AMERICA</b>	
<p>Messageries du livre SARL 5, rue Raiffeisen L-2411 Luxembourg Tel. (352) 40 10 20 Fax (352) 40 10 61 E-mail: <a href="mailto:mdu@mdu.lu">mdu@mdu.lu</a> URL: <a href="http://www.mdulu">http://www.mdulu</a></p>	<p>CYPRUS</p>	<p>Berman Associates 4611-F Assembly Drive Lanham, MD 20706 Tel. (1-800) 274 44 47 (toll free telephone) Fax (1-800) 865 55 00 (toll free fax) E-mail: <a href="mailto:query@berman.com">query@berman.com</a> URL: <a href="http://www.berman.com">http://www.berman.com</a></p>	
<b>NEDERLAND</b>	<b>ESTI</b>	<b>ANDERE LANDER/OTHER COUNTRIES/ AUTRES PAYS</b>	
<p>SOU Servicecentrum Uitgevers Christoffel Plantijnstraat 2 Postbus 20014 2500 EA Den Haag Tel. (31-70) 378 98 80 Fax (31-70) 99 77 63 E-mail: <a href="mailto:sdu@sdu.nl">sdu@sdu.nl</a> URL: <a href="http://www.sdu.nl">http://www.sdu.nl</a></p>	<p>Eesti Kaubandus-Tööstuskeskus (Estonian Chamber of Commerce and Industry) Toom-Kooli 17 EE-001 Tallinn Tel. (372) 645 00 44 Fax (372) 645 02 45 E-mail: <a href="mailto:env@koda.ee">env@koda.ee</a> URL: <a href="http://www.koda.ee">http://www.koda.ee</a></p>	<p>Blitte wenden Sie sich an ein Büro Ihrer Wahl/ Please contact the sales office of your choice/ Veuillez contacter l'adresseur au bureau de vente de votre choix</p>	
<b>ÖSTERREICH</b>	<b>GRÄZ</b>	<b>Office for Official Publications of the European Communities</b>	
<p>Manz'sche Verlags- und Universitätsbuchhandlung GmbH Kohlmarkt 16 A-1010 Wien Tel. (43-1) 53 16 11 00 Fax (43-1) 53 16 11 07 E-mail: <a href="mailto:bestellen@manz.co.at">bestellen@manz.co.at</a> URL: <a href="http://www.manz.at/index.htm">http://www.manz.at/index.htm</a></p>	<p>Mediatrade Ltd Pavila Hatzka 1 HR-10000 Zagreb Tel. (385-1) 481 94 11 Fax (385-1) 481 94 11</p>	<p>Office for Official Publications of the European Communities 2, rue Mercier L-2585 Luxembourg Tel. (352) 29 29-2425 Fax (352) 29 29-25 22 E-mail: <a href="mailto:info@opace.cec.be">info@opace.cec.be</a> URL: <a href="http://eur-op.eu.int">http://eur-op.eu.int</a></p>	

## NOTICE TO THE READER

*Information on European Commission publications in the areas of research and innovation can be obtained from:*

◆ **CORDIS, the Community R & D Information Service**

For more information, contact:

CORDIS Customer Service, BP 2373, L-1023 Luxembourg

Tel. (352) 40 10 12-2240; fax (352) 40 10 12-2248; e-mail: [helpdesk@cordis.lu](mailto:helpdesk@cordis.lu)  
or visit the website at <http://www.cordis.lu/>

◆ **Euroabstracts**

The European Commission's periodical on research publications,  
issued every two months. For more information, contact:

RTD help desk; European Commission, DG XIII, L-2920 Luxembourg

Fax (352) 43 01-32084; e-mail: [rtd-helpdesk@lux.dg13.cec.be](mailto:rtd-helpdesk@lux.dg13.cec.be)

CD-NA-18957-EN-C



OFFICE FOR OFFICIAL PUBLICATIONS  
OF THE EUROPEAN COMMUNITIES  
L-2985 Luxembourg

ISBN 92-828-5416-7



9 789282 854167